HIGH DENSITY ASTROPHYSICS

by

A.G.W. Cameron
W.D. Arnett
A. Gilbert
C.J. Hansen
J.W. Truran
S. Tsuruta

Table of Contents

1.1. Degenerate Matter (W.D. Arnett)

The study of such topics as white dwarfs and neutron stars requires a knowledge of the physics of ultradense matter. With this in mind we discuss the quantum statistics,* with emphasis upon the degenerate gas.

Fundamentals of Quantum Statistics

Consider a subsystem of a larger, macroscopic system, which, while small, is still macroscopic itself. It can be shown generally that the number of levels in a given finite interval of the energy spectrum of a macroscopic

---

* The derivation of the quantum statistical distributions given here follows the methods of Landau and Lifshitz (1958). A similar approach is that of Pauli (1926), which also may be found in Tolman (1938) and Chandrasekhar (1939). For a more detailed account of theoretical aspects, the above references are suggested. Besides this approach (which uses the "grand canonical ensemble") there are the more common "microcanonical" approaches of 1) finding the most probable distribution (Tolman, 1938) and 2) finding the mean distribution by the method of Darwin and Fowler (Sommerfeld, 1956).

body increases exponentially with the number of particles in the body,* hence the level spacing is an extraordinarily small number. This property will prove useful. Because no physical system is ever rigorously closed, some interactions will exist with the "outside." Even interactions which are so small that they have no other effect on the system will still appear large compared with the vanishingly small spacing between energy levels. Consequently, we consider our subsystem for times short enough that it is "quasi-closed," i.e., so that interactions with external systems have a minute effect. It is important to note that these interactions are the means by which the component subsystems of a larger body are brought to equilibrium with each other.

A quantum mechanical description based on incomplete information about a system is carried out by means of the "density matrix"**. The knowledge of the density matrix permits us to calculate the mean value of any variable of the system, and also the probabilities of the different values of these variables. We shall show how the density matrix can be introduced directly in the energy representation required for statistical applications.

---

* Landau and Lifshitz (1958) p. 28.

**Tolman (1938) has an excellent discussion of the density matrix in quantum statistics.

We consider a subsystem and define its "stationary states" as the states resulting if its interaction with its neighbors is ignored. Let $\psi_n(q)$ be the normalized wave functions (time-independent) of these states, where q stands for the coordinates of the subsystem and the index n for the set of all quantum numbers labelling the stationary states. E_n is the energy of these states. Assume that at some given time the subsystem is in some state completely described by a wave function ψ. Expanding in terms of the complete set,

$$\psi = \sum_n c_n \psi_n \qquad (1)$$

The mean value of an arbitrary quantity f is then

$$\bar{f} = \sum_n \sum_m c_n^* c_m f_{nm} \qquad (2)$$

where

$$f_{nm} = \int \psi_n^* \hat{f} \psi_m \, dq \qquad (3)$$

and $\hat{f}$ denotes the quantum mechanical operator corresponding to f.

The transition from a complete to an incomplete quantum mechanical description of a subsystem can, in a certain sense, be regarded as averaging over its different ψ states. As a result of such averaging the products $c_n^* c_m$ will give rise to quantities which we shall denote by w_{mn}, which form a double sequence (both indices vary), and which cannot be expressed as products of quantities forming a single sequence ($\langle c_n^* c_m \rangle_{av} \neq w_{mn}$). The mean is then

$$\bar{f} = \sum_m \sum_n w_{mn} f_{nm} \qquad (4)$$

The set of quantities w_{mn} forms the density matrix in the energy representation. If we consider the w_{nm} as matrix elements of some operator $\hat{w}$, then the sum in (4) will be a diagonal element of the matrix of the operator product, $\hat{w}\hat{f}$, and the mean value

$$\bar{f} = \sum_n (\hat{w}\hat{f})_{nn} = \mathrm{Tr}(\hat{w}\hat{f}) \qquad (5)$$

will be given by the trace (sum of the diagonal elements) of this operator. As the trace of an operator is known to be independent of the choice of the system of functions

in terms of which the elements are defined, this form of representation allows us to calculate with an arbitrary (subject to boundary conditions), complete, orthogonal, normalized set of wave functions. *

---

* If $\Psi = \sum_n c_n(t)\ \psi_n(q)$

we have

$$\frac{\partial \Psi}{\partial t} = \sum_n \frac{\partial C_n}{\partial t}\ \psi_n$$

but Schrödinger's equation is

$$\hat{H}\ \Psi(q,t) + \frac{\hbar}{i}\frac{\partial \Psi(q,t)}{\partial t} = 0$$

so that,

$$\sum_n \frac{\partial C_n}{\partial t}\ \psi_n = \frac{-i}{\hbar}\ \hat{H} \sum_m C_m\ \psi_m$$

or, on using the orthonormality of the $\psi_n(q)$'s,

$$\frac{\partial C_n}{\partial t} = \frac{i}{\hbar}\ H_{nm}\ C_m$$

where

$$H_{nm} = \int \psi_n^*\ \hat{H}\ \psi_m\ dq$$

Now, going to the average of macroscopic states Ψ which are possible from our limited knowledge,

$$w_{nm} = \overline{\overline{c_m^* c_n}}$$

where the double bar explicitly denotes both quantum mechanical and statisitical averaging. Then,

$$\frac{\partial w_{nm}}{\partial t} = \frac{i}{\hbar} \sum_k \left(H_{nk} w_{km} - w_{nk} H_{km} \right)$$

or, in operator language,

$$\dot{\hat{w}} = +\frac{i}{\hbar} [\hat{w}, \hat{H}]$$

By the definition of statistical equilibrium, the statistical distributions of the subsystems must be stationary, so $\hat{w}$ and $\hat{H}$ must commute. Hence the matrices of all the subsystems w_{nm} must be diagonal, and in this case

$$\bar{f} = \sum_n w_n f_{nn}$$

which involves only the diagonal elements of the f_{nm} matrix.

The probability that a system is in the n^{th} state is given by w_{nn}. Now,

$$w_n = w_{nn} > 0 \qquad (6)$$

always, and the normalization condition is now

$$\mathrm{Tr}(\hat{w}) = \sum_n w_n = 1 \qquad (7)$$

(corresponding to $\sum_n |c_n|^2 = 1$).

We note that the averages $\bar{f}$ defined in (4) have a double nature. First, they represent an average over the essential uncertainty of a quantum mechanical description, and second, they represent an average over the possible ψ's permitted by our incomplete knowledge of the system. Nevertheless, these two averaging processes are not separable, but occur simultaneously. In quantum statistics the density matrix plays the role that the distribution function does in classical statistics.

We now use the mathematical idealization of a closed system, for which we can construct a simple distribution function that suitably describes its statistical properties. This is called the "quantum microcanonical distribution." Bearing in mind the nearly continous

character of the energy spectra of macroscopic bodies, we say that a number of quantum states $d\Gamma$ "belong" to an infinitesimal energy interval dE.

Regarding the closed system as composed of subsystems whose interactions we neglect, the number $d\Gamma$ for the system is

$$d\Gamma = \prod_a{}' \, d\Gamma_a \qquad (8)$$

the permitted product of the number $d\Gamma_a$ for each subsystem "a" (such that the sum of the energies of the subsystems E lies in the proper range around the energy $E_{(o)}$ for the whole system). The probability that the system is in one of the states $d\Gamma$ is

$$dw = \text{const.}\ \delta(E-E_{(o)}) \prod_a{}' \, d\Gamma_a \qquad (9)$$

Now our original problem of finding the distribution function for a subsystem may be attacked by applying the microcanonical ensemble to the whole system. For convenience we now call the subsystem of interest the "body" while the rest of the whole system is called the "medium." For this two-part system of body and medium, (9) becomes

$$dw = \text{const.}\ \delta(E+E'-E_{(o)}) d\Gamma \, d\Gamma' \qquad (10)$$

where the primes refer to the medium and $E_{(o)}$ is the energy for the whole system (that is, $E_{(o)} = E+E'$).

Let $\Delta\Gamma'$ be the statistical weight of the macroscopic state of the medium and $\Delta E'$ denote the range of values for the energy of the medium corresponding to the range of quantum states $d\Gamma'$.

We wish to find the probability w_n that the whole system should be in a state in which the body is in some particular quantum state (with energy E_n), i.e., in a state described in a microscopic manner. To find this we replace $d\Gamma$ by unity, put $E = E_n$, and integrate (10) over $d\Gamma'$.

$$w_n = \text{const.}\int \delta(E_n+E'-E_{(o)})d\Gamma' \qquad (11)$$

Let $\Gamma'(E')$ be the total number of quantum states of the medium with energy less than or equal to E'. Since the integrand depends on E' alone (E_n, $E_{(o)}$ are parameters), we transform to integration over E' by using

$$d\Gamma' = \frac{d\Gamma'(E')}{dE'}\, dE' \qquad (12),$$

Now, the entropy of the medium may be defined by*

$$\frac{S'}{k} = \log \Delta\Gamma' \qquad (13)$$

---

* Landau and Lifshitz (1958), p. 23.

where $\Delta\Gamma'$ is the number of states in some region about the mean energy.

To evaluate (12) and (13) we note that the probability that the energy of any subsystem lies between some energy E and E+dE is just the product of the probability of a state $w_m = w(E_m)$ of energy E in this range and the number of such states $\frac{d\Gamma}{dE}\,dE$ in this range, where Γ and w are just the entities we have defined before. To normalize the probability,

$$\int w(E)\,\frac{d\Gamma(E)}{dE}\,dE = 1$$

$$= \int W(E)\,dE \qquad (14)$$

where the second equation defines W(E). Now, for a subsystem with many degrees of freedom, W(E) has a sharp maximum at $E = \bar{E}$, its average value. This allows us to define a "width" of the curve W(E) such that

$$W(\bar{E})\,\Delta E = 1 \qquad (15)$$

then

$$w(\bar{E})\,\Delta\Gamma = 1 \qquad (16)$$

where

$$\Delta\Gamma = \frac{d\Gamma(\bar{E})}{dE}\,\Delta E \qquad (17)$$

and $\Delta\Gamma$ is the "spread" of macroscopic states around $E = \bar{E}$.

From (17) and (13),

$$\frac{d\Gamma'}{dE'} = \frac{\Delta\Gamma'}{\Delta E'} = \frac{e^{S'(E')/k}}{\Delta E'} \qquad (18)$$

where $S'(E')$ is the entropy of the medium as a function of its energy, and $\Delta E'$ is also a function of E', in general. Thus, (11) gives

$$w_n - \text{const} \int \frac{e^{S'/k}}{\Delta E'} \delta(E'+E_n-E_{(o)})dE' \qquad (19)$$

and integrating,

$$w_n = \text{const} \left(\frac{e^{S'/k}}{\Delta E'}\right)_{E' = E_{(o)}-E_n} \qquad (20)$$

Since the body is small, E_n is small compared with $E_{(o)}$. The quantity $\Delta E'$ changes little with small changes in E', so we replace E' by $E_{(o)}$. In the exponential we expand $S'(E_{(o)}-E_n)$ in powers of E_n and keep the linear term

$$S'(E_{(o)}-E_n) = S'(E_{(o)}) - E_n \frac{dS'(E_{(o)})}{dE_{(o)}} \qquad (21)$$

but from thermodynamics

$$\left(\frac{\partial S'}{\partial E_{(o)}}\right)_V = \frac{1}{T} \qquad (22)$$

where T is the temperature of the system (in equilibrium the temperature of the body equals that of the medium).

So, finally, (20) becomes

$$w_n = A\, e^{-E_n/kT} \qquad (23)$$

where A is a normalization constant independent of E_n. (23) is called the "Gibbs distribution" or the "canonical distribution." Since (7)

$$\sum_m w_n = 1 \qquad (7)$$

we have

$$1/A = \sum_n e^{-E_n/kT} \qquad (24)$$

and the mean value of some f is now

$$\bar{f} = \sum_n w_n f_{nn}$$

$$= \frac{\sum_n f_{nn}\, e^{-E_n/kT}}{\sum_n e^{-E_n/kT}} \qquad (25)$$

So far we have implicitly assumed that the number of particles in the body is a given constant value. We now wish to generalize the Gibbs distribution to bodies with a variable number of particles. To be specific, we define a subsystem as the part of a system included in a specified volume, and N is the number of particles in that volume. We shall deal with bodies consisting of identical particles.*

* For generalization to systems of different particles, Landau and Lifshitz (1958), p.271.

The distribution function now depends not only on the energy of the quantum state, but also on the number N of the particles in the body, and clearly the energy levels E_{nN} themselves also vary with N. The probability that the body contains N particles and is at the same time in the n^{th} state is denoted by w_{nN}. (Do not confuse with the nondiagonal elements of the density matrix, eq. 4).)

We now use the same method as that by which the Gibbs distribution was obtained. The eutropy of the medium is now also a function of the N′ particles in it:

$$S' = S'(E',N') \qquad (26)$$

Writing

$$E' = E_{(o)} - E_{nN}$$

$$N' = N_{(o)} - N \qquad (27)$$

(N, the number of particles in the body is small compared to $N_{(o)}$, the number of particles in the whole closed system.)

Again regarding $\Delta E'$ as constant, 20) leads to

$$w_{nN} = \text{const.}\ \exp\left\{\frac{1}{k}\, S'(E_{(o)}-E_{nN},\ N_{(o)}-N)\right\} \qquad (28)$$

We again expand S' to linear terms. From thermodynamics,*

$$dE = TdS = PdV + \mu dN \qquad (29)$$

or

$$dS = \frac{dE}{T} + \frac{P}{T}dV - \frac{\mu}{T}dN$$

so that

$$\left(\frac{\partial S}{\partial E}\right)_{V,n} = \frac{1}{T} \qquad (30)$$

$$\left(\frac{\partial S}{\partial N}\right)_{E,V} = -\frac{\mu}{T} \qquad (31)$$

hence

$$S'(E_{(o)} - E_{mN},\ N_{(o)} - N)$$

$$\simeq S'(E_{(o)}, N_{(o)}) - \frac{E_{mN}}{T} + \frac{\mu N}{T} \qquad (32)$$

where the chemical potentials (μ) and the temperatures of the body and medium being equal at equilibrium. Then, the distribution functions are

$$w_{mN} = A\, e^{(\mu N - E_{mN})/kT} \qquad (33)$$

In order to evaluate A we wish to express the entropy in terms of the distribution function. We do this as follows.

---

* Landau and Litshitz (1958), eq. 24.5.

The distribution function must be an integral of the motion. In general, there are seven basic additive integrals of the motion: the energy, three components of linear momentum, and three components of angular momentum. The latter six can be made zero by an appropriate choice of coordinates. Therefore the logarithms of the distribution functions of the subsystems must be of the form

$$\log w_n = \alpha + \beta E_n \qquad (34)$$

if the subsystems are quasi-closed. Owing to the linearity of (34),

$$\log w(\bar{E}) = \alpha + \beta \bar{E} \qquad (35)$$

may be written

$$\log w(\bar{E}) = \overline{\log w(E_n)} \qquad (36)$$

but from (16)

$$w(\bar{E})\ \Delta\Gamma = 1$$

So (13) becomes

$$\frac{S}{k} = -\overline{\log w(E_n)} \qquad (37)$$

but, using the definition of mean value,

$$S = -k \sum_n w_n \log w_n \qquad (38)$$

and from (33) and (38),

$$S = -k \log A - \frac{\mu\bar{N}}{T} + \frac{\bar{E}}{T} \qquad (39)$$

so that

$$kT \log A = \bar{E} - TS - \mu\bar{N} \qquad (40)$$

but from thermodynamics

$$E - TS = F$$

and

$$F - \mu\bar{N} = \Omega \qquad (41)$$

where F and Ω are the free energy and the thermodynamic potential (as used by Laudau and Lifshitz(1958)).

$$w_{nN} = e^{(\Omega+\mu N-EnN)/kT} \qquad (42)$$

is the Gibbs distribution for a variable number of particles (grand canonical distribution). The normalization condition is now

$$\sum_N \sum_n w_{nN} = 1 \qquad (43)$$

or, using (42),

$$\Omega = -kT \log \sum_N \left[e^{\mu N/kT} \sum_n e^{-E_{nN}/kT} \right] \qquad (44)$$

which gives the potential Ω as a function of T, μ, and V (through E_n).

Applications of Quantum Statistics

As may be seen from (41),

$$N = -\left(\frac{\partial \Omega}{\partial \mu}\right)_{T,V} \qquad (45)$$

We will use this and (44) to derive the quantum statistical distributions. (44) is applicable even in the presence of exchange effects among the particles of the gas.*

Then, for the k^{th} state, with n_k particles and energy $n_k \epsilon_k$,

$$\Omega_k = -kT \log \sum_{n_k} \left(e^{(\mu-\epsilon_k)/kT}\right)^{n_k} \qquad (46)$$

For particles which obey the Pauli exclusion principle, the occupation numbers for each state can only be 1 or 0. Then

$$\Omega_k = -kT \log \left(1 + e^{(\mu-\epsilon_k)/kT}\right) \qquad (47)$$

and

$$\bar{n}_k = -\frac{\partial \Omega_k}{\partial \mu} = \frac{e^{(\mu-\epsilon_k)/kT}}{1+e^{(\mu-\epsilon_k)/kT}}$$

or

$$\bar{n}_k = \frac{1}{e^{(\epsilon_k-\mu)/kT} + 1} \qquad (48)$$

---

* Landau and Litshitz (1958), p.110.

This is the distribution function of a perfect gas obeying Fermi-Dirac statistics. Notice that for

$$e^{(\mu-\epsilon_k)/kT} \ll 1$$

it transforms to the Boltzmann distribution. The Fermi distribution is normalized by

$$\sum_k \frac{1}{e^{(\epsilon_k-\mu)/kT} + 1} = N \qquad (49)$$

where N is the total number of particles in the gas. Also,

$$\Omega = \sum_k \Omega_k = -kT \sum_k \log\left(1 + e^{(\mu-\epsilon_k)/kT}\right) \qquad (50)$$

For a perfect gas of particles described by a symmetrical set of wave functions, i.e., satisfying Bose-Einstein statistics, the occupation numbers may take on arbitrary values. Then

$$\Omega_k = -kT \log \sum_{n_k=0}^{\infty} \left(e^{(\mu-\epsilon_k)/kT}\right)^{n_k} \qquad (51)$$

The series converges only if $e^{(\mu-\epsilon_k)/kT} < 1$. Since this must hold for $e_k = 0$,

$$\mu < 0 \qquad (52)$$

That is, the chemical potential is negative for Bose-Einstein statistics. Using the geometric series,

$$\sum_{n=0}^{\infty} \gamma^n = (1-\gamma)^{-1},$$

$$\Omega_k = kT \log \left(1 - e^{(\mu-\epsilon_k)/kT}\right) \qquad (53)$$

and

$$\bar{n}_k = \frac{1}{e^{(\epsilon_k-\mu)/kT} - 1} \qquad (54)$$

Again, for $e^{(\mu-\epsilon_k)/kT} \ll 1$, this reduces to Boltzmann statistics. The total number of particles N is

$$N = \sum_k \frac{1}{e^{(\epsilon_k-\mu)/kT} - 1} \qquad (55)$$

and

$$\Omega = \sum_k \Omega_k = kT \sum_k \log\left(1 - e^{(\mu-\epsilon_k)/kT}\right) \qquad (56)$$

Now, the number of particles in an element of phase space $d^3p\, d^3q$ is obtained by multiplying the distribution (48) or (54) by*

$$g\, d\tau = g\, \frac{d^3p\, d^3q}{h^3} \qquad (57)$$

where

$$g = 2S + 1 \qquad (58)$$

and S is the spin of the particle.

---

* As shown by E.K. Brock, Phys. Rev. 51, 586, (1937), this also holds for particles obeying the Dirac equation.

That is,

$$dN = \bar{n}\, g\, d\tau \qquad (59)$$

By integrating over the volume element and denoting Fermi-Dirac statistics by a "+" and Bose-Einstein by a "-," we have

$$dN_{\pm}(p) = \frac{g\, V\, p^2\, d\, p}{2\pi^2 \hbar^3 \left(e^{(\epsilon-\mu)/kT} \pm 1\right)} \qquad (60)$$

If $\epsilon << mc^2$, then

$$\epsilon = \frac{p^2}{2m} \qquad (61)$$

and

$$dN_{\pm}(\epsilon) = \frac{gVm^{3/2}}{\sqrt{2}\pi^2 \hbar^3} \frac{\sqrt{\epsilon}\, d\epsilon}{e^{(\epsilon-\mu)/kT} \pm 1} \qquad (62)$$

consequently,

$$N_{\pm} = \frac{gVm^{3/2}}{\sqrt{2}\pi^2 \hbar^3} \int_o^{\infty} \frac{\epsilon^{1/2}\, d\epsilon}{e^{(\epsilon-\mu)/kT} \pm 1} \qquad (63)$$

which determines the chemical potential μ as a function of temperature T and density N/V. Transforming from summation to integration in (50) and (56), and integrating by parts

$$\Omega = -\frac{2}{3} \frac{gVm^{3/2}}{\sqrt{2}\pi^2 \hbar^3} \int_o^{\infty} \frac{\epsilon^{3/2}\, d\epsilon}{e^{(\epsilon-\mu)/kT} \pm 1} \qquad (64)$$

which, except for (-2/3) is the energy

$$E_{\pm} = \int_o^\infty \epsilon dN_{\pm}(\epsilon) = \frac{gVm^{3/2}}{\sqrt{2}\pi^2\hbar^3} \int_o^\infty \frac{\epsilon^{3/2}\, d\epsilon}{e^{(\epsilon-\mu)/kT} \pm 1} \qquad (65)$$

Since*

$$\Omega = -PV \qquad (66)$$

then

$$P_{\pm} = \frac{2}{3}\frac{E}{V}\pm \qquad (67)$$

which gives us the pressure. This is the well known relation for a gas with the polytropic index n = 1.5.

Equation (60) is also correct for a relativisitic gas ($E \gtrsim mc^2$) if we take

$$P = \frac{1}{c}\sqrt{w^2 - m^2c^4}$$

$$\epsilon = w - mc^2 \qquad (68)$$

where w is total relativisitc energy and ϵ is kinetic energy. Then

$$p^2dp = p\left(\frac{w}{c^2}dw\right)$$

$$= \frac{1}{c^3}\left(\epsilon^2 + 2mc^2\epsilon\right)^{1/2}\left(\epsilon + mc^2\right)d\epsilon$$

---

* Landau and Litshitz (1958), eq. 24.13.

since

$$w^2 = \epsilon^2 + 2mc^2\epsilon + m^2c^4$$

We choose to use p rather than e as our variable however, and if

$$x = \frac{p}{mc} \quad , \quad \mu' = \frac{\mu+mc^2}{mc^2}$$

$$\beta = \frac{mc^2}{kT} \quad , \quad y = \frac{w}{mc^2} \qquad (69)$$

then,

$$\frac{N_{\pm}}{V} = 4\pi g\left(\frac{mc}{h}\right)^3 \int_o^\infty \frac{x^2 dx}{\exp[\beta(y-\mu')] \pm 1} \qquad (70)$$

$$P_{\pm} = \left\{\frac{4\pi g m^4 c^5}{3h^3}\right\} \int_o^\infty \frac{x^4\, dx}{y[e^{\beta(y-\mu')} \pm 1]} \qquad (71)$$

$$\frac{E_{\pm}}{V} = \left\{\frac{4\pi g\, m^4 c^5}{3h^3}\right\} \int_o^\infty \frac{yx^2\, dx}{[e^{\beta(y-\mu)} \pm 1]} \qquad (72)$$

We now consider some limiting values for the parameters in the equations above. Recalling that for

$$e^{(\mu-\epsilon)/kT} << 1 \qquad (73)$$

the Bose-Einstein and Fermi-Dirac distributions transform to the Boltzmann distribution, so that for low densities and high temperatures the equation of state is that of an ideal gas for the nonrelativistic case.

In the relativistic case ($kT \gtrsim mc^2$) electron pair production is possible, and in the extreme limiting case $kT >> mc^2$, for low density of initial electrons,*

$$N_{e^-} = N_{e^+} = 0.183 \left(\frac{kT}{\hbar c}\right)^3 \qquad (74)$$

$$E_{e^-} = E_{e^+} = \frac{7\pi^2}{120} \frac{(kT)^4}{(\hbar c)^3} V \qquad (75)$$

and

$$P_{e^\pm} = \frac{1}{3} E_{e^\pm} / V \qquad (76)$$

where

$$P_{total} = P_{e^+} + P_{e^-} \qquad (77)$$

These relations are obtained from limiting forms of (70), (71), and (72).

The next limiting case we consider is that for $T \to 0$. The results are different for Fermi-Dirac and Bose-Einstein statistics.**

---

* Landau and Lifshitz (1958), p.325-6.

**Landau and Lifshitz (1958), p.168-71.

In the former case we first consider ($kT << mc^2$). Then as $T \to 0$, the expression

$$\frac{1}{e^{(\epsilon-\mu)/kT} + 1} = \begin{cases} 1 , & \epsilon < \mu \\ 0 , & \epsilon > \mu \end{cases} \qquad (78)$$

So (63) becomes

$$N = \frac{gV}{2\pi^2\hbar^3} \int_o^{p_o} p^2 dp = \frac{gVp_o^3}{6\pi^2\hbar^3} \qquad (79)$$

where for the limiting momentum p_o (corresponding to $e = \mu$) is

$$p_o = \left(\frac{6\pi^2}{g}\right)^{1/3} \left(\frac{N}{V}\right)^{1/3} \hbar \qquad (80)$$

and

$$\epsilon o = \frac{p_o^2}{2m} = \left(\frac{6\pi^2}{g}\right)^{2/3} \frac{\hbar^2}{2m} \left(\frac{N}{V}\right)^{2/3} \qquad (81)$$

Thus at the limit $T = 0$, the chemical potential μ corresponds to the Fermi energy of the particles.

Similarly,

$$E = \frac{3}{10} \left(\frac{6\pi^2}{g}\right)^{2/3} \frac{\hbar^2}{m} \left(\frac{N}{V}\right)^{2/3} N \qquad (82)$$

$$= \frac{2}{3} p \qquad (83)$$

The condition for the onset of degeneracy, i.e. that these relations be applicable, is that

$$kT \ll \epsilon_o \qquad (84)$$

A real degenerate electron gas is better approximated by an ideal degenerate gas as its density rises. To show this we consider a neutral ion-electron gas. The Coulomb interaction energy is of the order of

$$\frac{Ze^2}{a}$$

per electron, and

$$a \sim \left(\frac{ZV}{N}\right)^{1/3}$$

is of the order of the mean distance between electrons and nuclei. If this energy is small compared with the average kinetic energy per electron (of order ϵ_o) then the gas can be regarded as perfect. So.

$$\frac{Ze^2}{a} \ll \epsilon_o$$

or

$$\frac{N}{V} \gg \left(\frac{e^2 m}{\hbar^2}\right)^3 Z^2 \qquad (85)$$

which is better satisfied for higher densities.

We again consider an extremely degenerate gas, but in the ultra-relativistic limit, $kT >> mc^2$. Then (68) gives

$$w = pc, \quad w = \epsilon \tag{86}$$

Again we have

$$p_o = \left(\frac{6\pi^2}{g}\right)^{1/3} \left(\frac{N}{V}\right)^{1/3} \hbar \tag{87}$$

but

$$\epsilon_o = p_o c = \left(\frac{6\pi^2}{g}\right)^{1/3} \left(\frac{N}{V}\right)^{1/3} \hbar c \tag{88}$$

The total energy of the gas is

$$E = \frac{gcV}{2\pi^2\hbar^3} \int_o^{p_o} p^3 dp$$

$$= \frac{gcp_o^4}{8\pi^2\hbar^3} V \tag{89}$$

or

$$E = \frac{3}{4} \left(\frac{6\pi^2}{g}\right)^{1/3} \hbar c N \left(\frac{N}{V}\right)^{1/3} \tag{90}$$

and for an extreme relativistic gas

$$p = \frac{1}{3} \frac{E}{V}$$

holds, so that

$$p = \frac{1}{4}\left(\frac{6\pi^2}{g}\right)^{1/3} \hbar c \left(\frac{N}{V}\right)^{4/3} \qquad (91)$$

Let us briefly summarize these results. Figure (1) shows schematically the regions in which each of our approximations is valid. In the boundary zone between degeneracy and nondegeneracy, and also the boundary zone between relativistic and nonrelativisitc regions, numerical techniques must be applied to equations (70), (71), and (72).

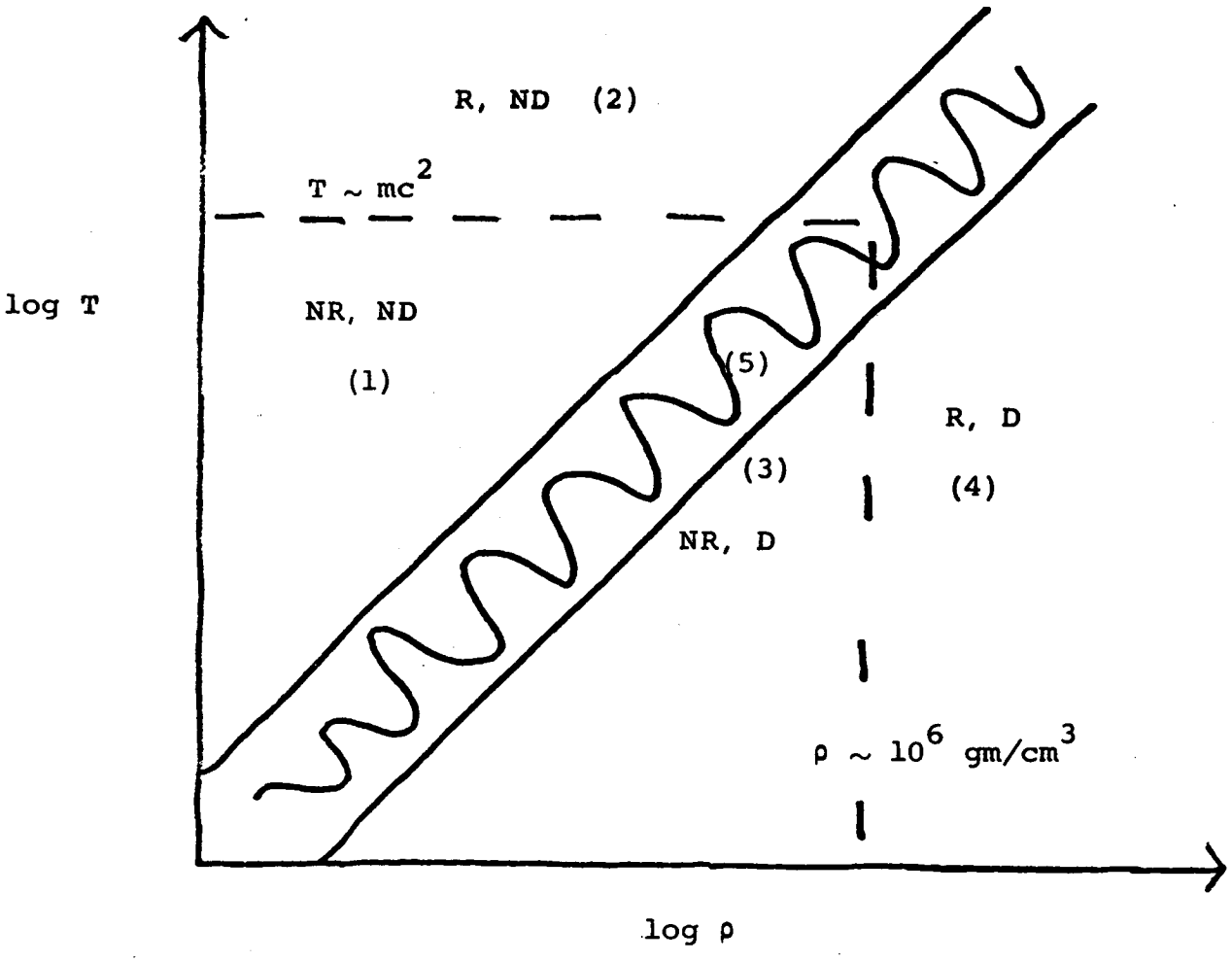

Region (1) - ideal gas law (nonrelativistic, nondegenerate)

Region (2) - pair production must be considered (relativistic, nondegenerate)

Region (3) - nonrelativistic degeneracy

Region (4) - relativistic degeneracy

Region (5) - border between degeneracy and nondegeneracy where the equation of state must be determined by numerical means.

Figure 1

Thermal Conductivity in a Degenerate Fermi Gas

This calculation was made by Mestel (1950) and Lee (1950). We follow Mestel's method. In calculating the thermal conductivity of electrons account must be taken of first-order deviations from the Fermi-Dirac distribution which arise partly from the temperature gradient of the star and partly from collisions between electrons and nuclei.

For a uniform temperature the Fermi-Dirac distribution function 48) may be rewritten as

$$f_o(\vec{v}) = \frac{1}{1+e^{(\epsilon-\mu)/kT}} \qquad 92)$$

where $\epsilon = \frac{1}{2} mv^2$; $v = |\vec{v}|$. 93)

$f_o(\vec{v})$ is independent of the direction of $\vec{v}$. With a temperature gradient $\frac{dT}{dx}$, the corresponding distribution $f(\vec{v})$ is slightly different from $f_o(\vec{v})$, and does depend on the direction of $\vec{v}$ as well as its magnitude. The particle current is then

$$I = \frac{gm^3}{h^3} \int v_x f(\vec{v}) d^3v \qquad 94)$$

and the energy flow is

$$Q = \frac{gm^3}{h^3} \int \epsilon v_x f(\vec{v}) d^3v \qquad (95)$$

where g=2 for electrons. The flow of electrons leads to an accumulation of space charge and the resulting field opposes the further drift. In equilibrium the electric field just compensates the effect of the temperature gradient. Hence the flow of electrons is zero:

$$I = 0 \qquad (96)$$

Also, the equilibrium state is characterized by the requirement that $f(\vec{v})$ is independent of time t. The temperature gradient, the electric field, and the collisions between the electrons and the nuclei tend to change $f(\vec{v})$. In equilibrium,

$$\left(\frac{\partial f}{\partial t}\right)_{\text{collisions}} + \left(\frac{\partial f}{\partial t}\right)_{\text{temp. grad.}} + \left(\frac{\partial f}{\partial t}\right)_{\text{E. field}} = 0 \qquad (97)$$

Equations (95), (96), and (97) lead to the required thermal conductivity.

In a star of given composition, μ, the chemical potential, depends on ρ and T. The equation of mechanical stability [illegible] relates ρ and T (with the equation of state) so that they are not independent variables. We regard ρ and μ as functions of T only. Then, with (92) we can show that

$$\frac{df_o(\epsilon)}{dx} = -\frac{\partial f_o(\epsilon)}{\partial \epsilon}\left(\frac{d\mu}{dT} + \frac{\epsilon-\mu}{T}\right)\frac{dT}{dx} \qquad (98)$$

We replace f by f_o in the second and third terms in (97). Then we have the results,

$$\left(\frac{\partial f}{\partial t}\right)_{\text{temp. grad}} = v_x \frac{\partial f_o}{\partial \epsilon}\left(\frac{d\mu}{dT} + \frac{\epsilon-\mu}{T}\right)\frac{dT}{dx} \qquad (99)$$

$$\left(\frac{\partial f}{\partial t}\right)_{E \text{ field}} = -ev_x F\frac{\partial f_o}{\partial \epsilon} \qquad (100)$$

where e is the electronic charge and F is the electric field in the x direction due to the effect of the temperature gradient. So,

$$\left(\frac{\partial f}{\partial t}\right)_{\text{coll.}} = v_x \frac{\partial f_o}{\partial \epsilon}\left[eF - \left(\frac{d\mu}{dT} + \frac{\epsilon-\mu}{T}\right)\frac{dT}{dx}\right] \qquad (101)$$

Now we obtain an expression for $\left(\frac{\partial f}{\partial t}\right)_{\text{coll.}}$ by considering collisions between electrons and nuclei. It will be assumed that the collisions are elastic, a good assumption if the nuclei are completely ionized. For simplicity we consider collisions between electrons and a particular nuclear species of atomic weight a, nuclear charge Z, mass M, and number density Na.

Let $P(\vec{v}, \vec{v}', \vec{V})d\vec{V}dw'$ be the probability per unit time of an electron of initial velocity $\vec{v}$ being scattered with velocity $\vec{v}'$ into the element of solid angle dw' by nuclei with velocities in the range $\vec{V}$ to $\vec{V} + d\vec{V}$.

From the nature of collisions,

$$P(\vec{v}, \vec{v}', \vec{V}) = P(\vec{v}', \vec{v}, \vec{V})$$

For elastic collisions, $|\vec{v}| = |\vec{v}'|$,

If we define $g(\vec{v})$ by

$$f(\vec{v}) = f_o(\vec{v}) + g(\vec{v}) \qquad (102)$$

then

$$\left(\frac{\partial f}{\partial t}\right)_{coll.} = \int dw'[g(\vec{v}) - g(\vec{v}) \,] \int P(\vec{v},\vec{v}',\vec{V})d\vec{V} \qquad (103)$$

If $\frac{dT}{dx} = 0$, the difference between $f(\vec{v})$ and $f_o(\vec{v})$ would disappear due to collisions in a relaxation time

$$\tau(\vec{v}) = -g(\vec{v}) / \left(\frac{\partial f}{\partial t}\right)_{coll.} \qquad (104)$$

An important feature of collision processes is that $\tau(\vec{v})$ must be effectively independent of the direction of $\vec{v}$.

Then (2.103) gives

$$\frac{1}{\tau(v)}\left(\frac{\partial f}{\partial t}\right)_{coll.} = \int dw' \left[\frac{\partial f(\vec{v})}{\partial t} - \frac{\partial f(\vec{v}')}{\partial t}\right]_{coll.} \int P(\vec{v},\vec{v}',\vec{V})d\vec{V} \qquad (105)$$

Using (2.101),

$$\frac{1}{\tau(v)} = \frac{1}{v_x} \int dw'(v_x - v_{x}) \int P(\vec{v},\vec{v}',\vec{V})d\vec{V} \qquad (106)$$

From the theory of collisions

$$P(\vec{v},\vec{v}',\vec{V}) = \frac{n_a e^4 Z^2}{m^2 |\vec{v}-\vec{V}|^3 (1-\cos\alpha)^2} \left(\frac{M}{2\pi kT}\right)^{3/2} e^{-\frac{MV^2}{2kT}} \qquad (107)$$

where α is the angle between $\vec{v} - \vec{V}$ and $\vec{v}' - \vec{V}$. Evaluation of (106) using (107) may be simplified by noting that the important contributions to (2.106) come when $(v/V) \div (M/m)^{1/2} >> 1$. Thus $|\vec{v} - \vec{V}| \to v^3$

$$\alpha \to \theta$$

where θ is the angle between $\vec{v}$ and $\vec{v}'$.

Then

$$\frac{1}{\tau(v)} = \frac{n_a e^4 Z^2}{m^2 v^3 v_x} \int dw' \frac{(v_x - v_x')}{(1-\cos\theta)^2} \qquad (108)$$

which can be reduced to

$$\frac{1}{\tau(v)} = \frac{4\pi n_\alpha e^4 Z^2 \Theta}{m^2 v^3} \qquad (109)$$

where

$$\Theta = \frac{1}{2}\int_{\theta_o}^{\pi} \frac{\sin\theta d\theta}{1-\cos\theta} = \frac{1}{2}\log\left(\frac{2}{1-\cos\theta_o}\right) \qquad (110)$$

and θ_o (the ratio of the de Broglie wavelength of the electron to the screening radius of the nucleus) is a "cut-off" angle from collision theory. Equations (101), (104), and (109) give the required solution for $g(\vec{v})$.

$$g(\vec{v}) = \frac{m^2 v^3 v_x}{4\pi n_a e^4 Z^2 \Theta} \frac{\partial f_o}{\partial \varepsilon} \left[eF - \left(\frac{d\mu}{dT} + \frac{\varepsilon-\mu}{T} \right) \frac{dT}{dx} \right] \qquad (111)$$

Using (111) we have from (94), (95) and (96) after some work,

$$Q = -C \int \varepsilon^4 \frac{\partial f_o}{\partial \varepsilon} \left[cF' - \frac{\varepsilon-\mu}{T} \frac{dT}{dx} \right] d\varepsilon \qquad (112)$$

$$0 = \int \varepsilon^3 \frac{\partial f_o}{\partial \varepsilon} \left[eF' - \frac{\varepsilon-\mu}{T} \frac{dT}{dx} \right] d\varepsilon \qquad (113)$$

where

$$eF' = eF - \frac{d\mu}{dT} \frac{dT}{dx}$$

and } (114)

$$C = \frac{16m}{3h^3 e^4 Z^2 n_a \Theta}$$

Introducing $y = (\varepsilon-\mu)/_{kT}$ and $\lambda = e^{\mu/kT}$ (112) and (113) become

$$Q = Ck^4 T^4 \int_{-\log\lambda}^{\infty} dy \, \frac{e^y (eF' - ky \frac{dT}{dx})}{(1+e^y)^2} (y+\log\lambda)^4 \qquad (115)$$

$$0 = \int_{-\log\lambda}^{\infty} \frac{dy \; e^y (eF' - ky \frac{dT}{dx})}{(1+e^y)} (y+\log\lambda)^3 \qquad (116)$$

Defining

$$K_p(\lambda) = \int_{-\log\lambda}^{\infty} \frac{x^p e^x dx}{(1+e^x)^2} \qquad (117)$$

we can reduce (115) and (116). We then eliminate the unknown F′ between the two. Then

$$Q = \nu \frac{dT}{dx} \qquad (118)$$

where the thermal conductivity is in terms of λ, i.e $e^{\mu/kT}$ and

$$\nu = \frac{BCk^5}{A} T^4 \qquad (119)$$

where

$$A = \log^3\lambda K_o(\lambda) + 3\log^2\lambda K_1(\lambda) + 3\log\lambda K_2(\lambda) + K_3(\lambda) \qquad (120)$$

$$B = \log^6\lambda(K_oK_2-K_1^2) + 3\log^5(K_oK_3-K_1K_2)$$
$$+ 3\log^4\lambda(K_1K_3-2K_2^2 + K_oK_4)$$
$$+ \log^3\lambda(K_oK_5 - 8K_2K_3 + 7K_1K_4)$$
$$+ 3\log^2\lambda(K_1K_5 - 2K_3^2 + K_2K_4)$$
$$+ 3\log\lambda(K_2K_5 - 3 4) + (K_3K_5 - K_4^2) \qquad (121)$$

when $\lambda \leq \frac{1}{50}$, two decimal accuracy can be obtained from

$$\nu = \frac{128mk^5T^4}{h^3e^4Z^2n_a@} \lambda$$

and similar accuracy from

$$\nu = C\frac{\pi^2}{3}k^5T^4\frac{(\log^6\lambda + \frac{11}{5}\pi^2\log^4\lambda + \frac{7}{5}\pi^4\log^2\lambda - \frac{49}{75}\pi^6}{\log\lambda(\log^2\lambda + \pi^2)}$$

when $\lambda \geq 200$.

In the limit of large $\frac{kT}{\epsilon_f}$ where ϵ_f is the fermi level,

$$\nu = \frac{C\pi^2}{3}k^5T^4\left(\frac{\epsilon_f}{kT}\right)^3\left(1 + 9.376\left(\frac{kT}{\epsilon_f}\right)^2\right)$$

with

$$\frac{\epsilon_f}{kT} = 2.996 * 10^5\left(\frac{m_H n_C}{T^{3/2}}\right)^{2/3}$$

$$= \left(\log^{3/2}\lambda + \frac{\pi^2}{8}\log^{-1/2}\lambda\right)^{2/3}$$

This formula gives second order accuracy for $\lambda \geq 300$.

Note that $\lambda \to \infty$ is the nondegenerate limit.

BIBLIOGRAPHY

Broch, E.K. (1937). Phys. Rev. 51, 586.

Chandrasekhar, S. (1939). "An Introduction to the Study of Stellar Structure." Republished by Dover Publications, New York, 1957.

Landau, L.D. and Lifshitz, E.M. (1958). "Statistical Physics." Addison-Wesley Publishing Co., Reading, Massachusetts.

Lee, T.D. (1950). Astrophysics Journal. 111, 625.

Mestel, L. (1950). Proc. Comb. Phil. Soc. 46, 331.

Pauli, W. (1926). Zs. f. Phys. 41, 81.

Schatzmann, E. (1958). "White Dwarfs." North-Holland Publishing Co., Amsterdam.

Sommerfeld, A. (1956). "Thermodynamics and Statistical Mechanics." Academic Press, New York.

Tolman, R.C. (1938). "The Principles of Statistical Mechanics." Oxford University Press, London.

Wrubel, M.H. (1958). Stellar interiors. Handbuch der Physik. 51, Springer-Verlag, Berlin.

2. THERMONUCLEAR REACTIONS IN MEDIUM AND HEAVY NUCLEI

J. W. TRURAN, C. J. HANSEN, AND A. G. W. CAMERON
Physics Department, Yale University, New Haven, Connecticut, and Institute for Space Studies, Goddard Space Flight Center, NASA, New York

AND

A. GILBERT
Physics Department, Columbia University, New York, and Institute for Space Studies, Goddard Space Flight Center, NASA, New York

Received October 1, 1965

ABSTRACT

A method is outlined by which thermonuclear reaction rates can be determined from the statistical properties of nuclei. Assuming that the contribution to the cross section of a given resonance is given by the Breit–Wigner single-level formula, the total rate is determined by integrating the product of the cross section, weighted by the nuclear level density, and the velocity over energy. The nuclear radiation widths were calculated on the assumption that electric-dipole transitions are dominant. The particle widths were determined by approximating the nuclear strength function by that value calculated for a black nucleus. Nuclear cross sections calculated in this manner are compared with experiment both for charged-particle reactions on lighter nuclei and for neutron-capture reactions proceeding on nuclei in the mass range $A > 60$. Good agreement is obtained in both cases.

I. INTRODUCTION

The methods employed in the calculation of thermonuclear reaction rates for reactions proceeding on light nuclei are well known (Salpeter 1952; Reeves and Salpeter 1959; Reeves 1964). At low excitations the nuclear levels are widely spaced and the reaction rates can be computed as a sum of the off-resonance contributions from these isolated resonances, where experimental values of the resonance parameters are available.

We have been concerned with the problem of calculating the formation of the iron peak elements in stellar interiors and with the production of heavy elements by neutron capture. For these nuclei, $A > 28$, there are many resonances in the energy range of interest for which experimental parameters are not available. Under these conditions it is necessary to compute the reaction rates from the known statistical properties of nuclei.

The determination of the reaction rates for nuclei in this mass range is the subject of this paper. The assumptions we have made and the methods employed in these calculations are outlined in Sections II to VII. In Section VIII the cross-section results obtained are compared with experiment for a variety of cases. Applications of these rate calculations to astrophysical problems will be reported in other papers.

II. THERMONUCLEAR REACTION RATES

In general, the number of reactions per unit volume per second, r, between two nuclear species with number densities n_1 and n_2 and masses m_1 and m_2 can be written in the form:

(2.1) $$r = n_1 n_2 \langle \sigma v \rangle .$$

Here $\langle \sigma v \rangle$ is an appropriate average of the product of the reaction cross section, $\sigma(v)$, and the relative velocity of the nuclei, v,

(2.2) $$\langle \sigma v \rangle = \frac{\int \sigma(v) v N(v) \mathrm{d}v}{\int N(v) \mathrm{d}v},$$

where $N(v)$ is the number density of nuclei having relative velocities v. Assuming that the velocity distributions of the two species are Maxwellian, the expression for $\langle \sigma v \rangle$ takes the form:

(2.3) $$\langle \sigma v \rangle = \left(\frac{8}{\pi \mu}\right)^{\frac{1}{2}} (kT)^{-3/2} \int_{E_t}^{\infty} E \sigma(E) \exp(-E/kT) \mathrm{d}E.$$

In this expression k is the Boltzmann constant, T is the temperature, E is the kinetic energy of relative motion, E_t is the threshold energy, and μ is the reduced mass

(2.4) $$\mu = m_1 m_2 / (m_1 + m_2).$$

The Breit–Wigner form of the cross section for the capture of particle a from a given state of the target nucleus to a given state of the compound nucleus near a resonance at energy E_r is

(2.5) $$\sigma(a, \gamma) = \pi \lambda\!\!\!^{-}_a{}^2 \frac{2J+1}{(2S_a+1)(2I+1)} \times \sum_{S=|I-S_a|}^{I+S_a} \sum_{l=|J-S|}^{J+S} \omega_l(\pi_a \pi_c) \frac{\Gamma_{al} \Gamma_\gamma}{(E_a - E_r)^2 + (\Gamma/2)^2}.$$

The corresponding cross section for a particle–particle reaction involving a as the incoming particle and b as the outgoing particle (leaving the residual nucleus in a definite state) is

(2.6) $$\sigma(a, b) = \pi \lambda\!\!\!^{-}_a{}^2 \frac{2J+1}{(2S_a+1)(2I+1)} \times \sum_{S=|I-S_a|}^{I+S_a} \sum_{S=|I'-S_b|}^{I'+S_b} \sum_{l=|J-S|}^{J+S} \sum_{l'=J-S'}^{J+S} \omega_l(\pi_a \pi_c) \omega_{l'}(\pi_b \pi_c) \frac{\Gamma_{al} \Gamma_{bl'}}{(E_a - E_r)^2 + (\Gamma/2)^2}.$$

J, I, I', S_a, S_b are the spins of the compound nucleus, the target, the residual nucleus, and the incoming and outgoing particles, respectively. $\lambda\!\!\!^{-}_a{}^2$ is the reduced de Broglie wavelength of the incoming particle. S, S' are the incoming and outgoing channel spins, which are vector sums of I and S_a (or I' and S_b). l, l' are the orbital angular momenta of the incoming and outgoing particles. π_a, π_b, π_c are the parities of the target nucleus, the residual nucleus, and the compound nucleus. Γ_{al} and Γ_{bl} are partial widths for decay of the compound nucleus by emission of particle a (or b) with orbital angular momentum l (or l'). Γ_γ is the partial width for gamma decay of the compound nucleus. Γ is the total width of the resonance, which is the sum of all partial widths. E_a is the energy of relative motion of the incoming particle. E_r is the energy of the

resonance for the incoming particle. Finally, $\omega_l(\pi_a\pi_c) = \frac{1}{2}[1 + (-1)^l\pi_a\pi_c]$ is a factor that ensures parity conservation, being 1 if $\pi_c = (-1)^l\pi_a$, and 0 if $\pi_c = (-1)^{l+1}\pi_a$.

The total width for decay of the compound nucleus by emission of particle a is

$$\Gamma_a = \sum_{S=|I-S_a|}^{I+S_a} \sum_{l=|J-S|}^{J+S} \omega_l(\pi_a\pi_c)\Gamma_{al}. \tag{2.7}$$

Thus, the single-level cross sections are simply

$$\sigma(a,\gamma) = \pi\lambda\!\!\!^{-}_a{}^2 g \frac{\Gamma_a\Gamma_\gamma}{(E_a - E_r)^2 + (\Gamma/2)^2}, \tag{2.8}$$

$$\sigma(a,b) = \pi\lambda\!\!\!^{-}_a{}^2 g \frac{\Gamma_a\Gamma_b}{(E_a - E_r)^2 + (\Gamma/2)^2}, \tag{2.9}$$

where

$$g = \frac{2J+1}{(2S_a+1)(2I+1)}. \tag{2.10}$$

For a narrow resonance, we assume that $\lambda\!\!\!^{-}_a$, Γ_a, Γ_b, and Γ_γ vary slowly over the resonance peak. The contribution of this resonance to the average cross section is therefore given by

$$\begin{aligned}\sigma(a,b) &\simeq \pi\lambda\!\!\!^{-}_a{}^2 g\Gamma_a\Gamma_b \int_{-\infty}^{\infty} \frac{1}{(E_a - E_r)^2 + (\Gamma/2)^2}\,dE_a \\ &= 2\pi^2 g\left(\lambda\!\!\!^{-}_a{}^2 \frac{\Gamma_a\Gamma_b}{\Gamma}\right)_{E_a=E_r},\end{aligned} \tag{2.11}$$

where, in order to extend the limits of integration from $-\infty$ to ∞, we have assumed that the contributions from the resonance tails are small.

The density of levels at an excitation U of the compound nucleus is denoted by $\rho(U, J, \pi)$. We assume that $\langle\sigma v\rangle$ can be written in terms of an averaged cross section given by $\sigma(a,b)\rho(U,J,\pi)$ integrated over energy for a given compound nuclear level (U, J, π). The total rate is then given as a sum over the possible spin and parity states of the compound nucleus:

$$\begin{aligned}\langle\sigma v\rangle = \frac{2.51\times10^{-13}}{(\mu T_9)^{3/2}} &\frac{1}{(2S_a+1)(2I+1)} \\ &\times \sum_{J,\pi}(2J+1)\int_{E_t}^{\infty} dE e^{-11.61E/T_9}\rho(U,J,\pi)\frac{\Gamma_a\Gamma_b}{\Gamma}\ \mathrm{cm^3 sec^{-1}},\end{aligned} \tag{2.12}$$

where μ is in a.m.u. and T_9 is the temperature in units of 10^9 °K. The corresponding expression for the rate for particle capture reactions is given by (2.12) with $\Gamma_b \to \Gamma_\gamma$. These are the general expressions evaluated by us in our determinations of the reaction rates.

We must now consider the approximations employed in the determination of the nuclear parameters contained in equation (2.12).

III. THE ATOMIC MASS FORMULA

We may write the nuclear mass excess in MeV on the ^{12}C scale of masses in the form (Cameron and Elkin 1965)

$$M - A = 8.07134A - 0.78261Z + E_{vs} + E_c + E_{ex} + S(Z, N) + P(Z, N),$$

where E_{vs} includes both volume and surface corrections, E_c is the Coulomb energy correction, E_{ex} is the exchange term, and $S(Z, N)$ and $P(Z, N)$ are the total shell and pairing corrections for protons and neutrons.

From a consideration of the abundance yields for the heavy uranium isotopes in the Mike fusion explosion of 1952 Cameron (1959) suggested that perhaps the neutron binding energies for the successive neutron-rich isotopes should not fall off as fast as is generally predicted by nuclear mass formulas. With regard to this question, consider the combined volume and volume symmetry energy in the form:

$$E_v = \alpha\left[1 - \frac{\beta}{\alpha}\frac{(A - 2Z)^2}{A^2}\right]^2 A. \tag{3.1}$$

The values of these coefficients were determined by Cameron (1957) to be:

$$\alpha = -17.0354 \text{ MeV},$$

$$\beta = -31.4506 \text{ MeV}.$$

This formula would then predict that the binding energy per nucleon will change from -17.0354 MeV for $A = 2Z$ to 14.4512 MeV for a pure neutron gas. Theory predicts, however, that a pure neutron gas should be only slightly unbound (Salpeter 1960).

Cameron and Elkin (1965) have suggested a form for the volume energy term that will reproduce the conventional results in the region $A \sim 2Z$, while simultaneously leaving pure neutron matter slightly bound, viz:

$$E_v = \alpha A \exp\left[-\frac{\beta}{\alpha}\frac{(A - 2Z)^2}{A^2}\right]. \tag{3.2}$$

This will have the effect of increasing the neutron binding energies for the neutron-rich isotopes far from the valley of beta stability. The fact that pure neutron matter is still slightly bound suggests that this correction has gone too far and that a more realistic extrapolation toward the neutron-rich region lies between these two extremes.

The shell and pairing energies employed in our calculations are those determined by Cameron and Elkin in this investigation. The neutron binding energies predicted by the conventional and exponential forms of the mass formula differ significantly. This problem will be considered in more detail in our discussion of the neutron-capture cross sections for the uranium isotopes.

IV. THE NUCLEAR LEVEL DENSITY

Perhaps the most critical factor in our determination of $\langle \sigma v \rangle$ is the nuclear level density. Gilbert and Cameron (1965) have recently examined this subject

in some detail. From a study of the known levels at low excitation energies and of the behavior of the level density in the vicinity of the neutron binding energy, they have determined parameters defining a fit to the observed level densities.

The original formulation of the statistical theory of nuclear level densities is due to Bethe (1937). In this theory the nucleus is considered to be a Fermi gas of two types of fermions. Treating the number of protons, the number of neutrons, the total energy, and the total magnetic quantum number as constants of the motion, we can define the grand canonical partition function for the system. Proceeding in this manner, Gilbert and Cameron (1965) arrived at the following expression for the density of states of all possible magnetic quantum numbers, M:

$$\omega(U) = \frac{\pi^{1/2} \exp[-2(aU)^{1/2}]}{12a^{1/4}U^{5/4}}. \tag{4.1}$$

In this expression

$$a = \tfrac{1}{6}\pi^2 g, \tag{4.2}$$

where g^{-1} is the single-particle level spacing,

$$U = E - U_0 \tag{4.3}$$

is the effective excitation energy, and U_0 is the Fermi energy.

$\omega(U)$ is the total density of states, including states degenerate in the magnetic quantum number M. We require, rather, an expression for the density of levels of given angular momentum J, parity π, and energy U. Following Bethe (1937), the density of levels of specified J can be written in the form:

$$\rho(U, J) \simeq \frac{\omega(U)}{(2\pi\sigma)^{1/2}} \frac{(2J+1)}{2\sigma^2} \exp[-(J+\tfrac{1}{2})^2/2\sigma^2]. \tag{4.4}$$

In the absence of experimental evidence favoring even or odd parity states, we shall assume that there is equal probability for either parity. The density of levels of spin J, parity π at an excitation energy U is thus given by

$$\rho(U, J, \pi) = \frac{1}{12} \frac{1}{(2)^{1/2}} \frac{e^{2(aU)^{1/2}}}{a^{1/4}U^{5/4}\sigma} \left\{ \frac{(2J+1)}{2\sigma^2} \exp[-(J+\tfrac{1}{2})^2/2\sigma^2] \right\} \{\tfrac{1}{2}\}. \tag{4.5}$$

In this expression σ is the spin-dependence parameter given by

$$\sigma^2 = g\langle m^2 \rangle t, \tag{4.6}$$

where t is the nuclear temperature

$$t = (U/a)^{\frac{1}{2}} \tag{4.7}$$

and $\langle m^2 \rangle$ is the mean-square single-particle magnetic quantum number. Jensen and Luttinger (1952) have demonstrated that the succession of shell-model states implies that

$$\langle m^2 \rangle \sim 0.146A^{2/3}, \tag{4.8}$$

with some fluctuations attributable to shell effects. Thus we find that

$$\sigma^2 = 0.0888\,(aU)^{1/2}A^{2/3}. \tag{4.9}$$

In this formula there are, in effect, two free parameters, a and U_0. It was assumed initially that U_0, the energy of the fully degenerate state, represented the ground state of the nucleus. a could then be determined from experimentally known neutron resonance spacings. However, it was found that there would be systematic differences in the values of a for neighboring even–even, odd-A, and odd–odd nuclei. Thus, a pairing correction is necessary. Such a correction is, in fact, supplied by the mass formula; if U_0 is taken to be the "pairing energy", it is found that these odd-even effects can be taken into account.

The treatment of the nucleus as a Fermi gas gives $a \propto A$. This would not allow us to account for the obvious shell effects in neutron resonance spacings. Gilbert and Cameron (1965) determined the following correlations for the parameter a: for undeformed nuclei

$$a/A = 0.00917S + 0.142\ (\mathrm{MeV}^{-1}) \tag{4.10a}$$

and for deformed nuclei

$$a/A = 0.00917S + 0.120\ (\mathrm{MeV}^{-1}). \tag{4.10b}$$

Here S is the total shell correction, the sum of the shell corrections for neutrons and protons. The shell and pairing corrections employed in these calculations are taken from Cameron and Elkin (1965) for the exponential form of the mass formula.

The Bethe formula is not expected to be valid at low excitation energies. Ericson (1959) has shown that the expression

$$\rho(E) = \{\exp[(E - E_0)/T]\}/T \tag{4.11}$$

provides a good fit to empirically determined nuclear levels over the first few MeV of excitation. The density of levels of specified angular momentum and parity is then given by

$$\rho(E, J, \pi) = \rho(E)\left\{\frac{(2J+1)}{2\sigma^2}\exp[-(J+\tfrac{1}{2})^2/2\sigma^2]\right\}\{\tfrac{1}{2}\}. \tag{4.12}$$

Gilbert and Cameron have shown that a reasonable and self-consistent description of the level density at any excitation can be obtained by using the Bethe formula at high energies, the Ericson form at low energies, and fitting the two tangentially. They give values of the parameters a, E_0, and T for nuclei for which experimental information is available. It was also found that the energy E_x at which the two formulas were fitted tangentially is given approximately by

$$E_x = 2.5 + (150/A) + U_0\ \mathrm{MeV}, \tag{4.13}$$

where U_0 is the pairing energy. If the nuclear levels are not known experimentally, the value of a may be obtained from equations (4.10), and T and E_0 are then determined by fitting the two density formulas at an energy E_x, determined from this expression.

V. RADIATION WIDTHS

As experimental determinations of the nuclear radiation widths are not available, it is necessary, for most of the nuclei of interest in our investigation, to calculate these widths by theoretical means. Only electric-dipole transition widths will be computed, since, in general, these contributions are dominant. Following Blatt and Weisskopf (1952), we can write the total radiation width for electric-dipole radiation from a level of energy E_a, spin J, and parity π in the form:

$$(5.1)\quad \Gamma_\gamma(E_a, J, \pi) = 0.296 \frac{A^{2/3}}{D_0} \sum_{J',\pi'} \frac{1}{\rho(E_a, J, \pi)} \int_0^{E_a} E^2 \rho(E_a - E, J', \pi) dE,$$

where D_0 is effectively a normalization factor, although it may be interpreted in some sense as the single-particle level spacing. Assuming an equality of the parity distributions and neglecting the exponential term in the angular-momentum dependence of the level density, the summation is performed over all allowed values of J',π' of the daughter levels consistent with electric-dipole selection rules ($\Delta J = \pm 1, 0$; not $0 \rightarrow 0$; parity change). This introduces a factor

$$\frac{[2(J+1)+1] + [2(J-1)+1] + [2J+1]}{(2J+1)} = \frac{6J+3}{2J+1} = 3$$

into the expression for the width; hence

$$(5.2)\quad \Gamma_\gamma(E_a, J, \pi) = \frac{0.89 A^{2/3}}{D_0} \frac{1}{\rho(E_a)} \int_0^{E_a} E^2 \rho(E_a - E) dE.$$

Employing the level density parameters from Gilbert and Cameron (1965), we have compared the widths calculated from this expression with experimental values for a large number of nuclei with $A > 40$, with the requirement that at least the value of Γ_γ for one level in the nucleus had been definitely established. These experimental values were taken from the Nuclear Data Sheets and from Hughes *et al.* (1960). The value of D_0 inferred from these calculations was $D_0 \simeq 230$ MeV. Calculations performed for $A \lesssim 40$ led to a value $D_0 \simeq 400$ MeV.

The ratio Γ_γ(calculated)/Γ_γ(experimental) from these calculations is plotted in Fig. 1. The experimental errors associated with the values of Γ_γ are generally $<30\%$. The dashed line in this figure is a "guide to the eye" for this ratio. The solid line corresponds to the optical model, deformed nucleus *s*-wave neutron-strength function due to Chase *et al.* (1958). The general behavior of these two curves is quite similar for $A \gtrsim 80$.

Cameron (1959) has suggested a possible explanation of this effect. The admixture of single-particle wave functions into the actual wave function in the region of the neutron binding energy is largest in the vicinity of the maxima of the neutron-strength functions. As the electric-dipole matrix elements are proportional to the degree of overlap of the wave functions of the initial and final states, which in turn is larger when the admixtures of single-particle wave

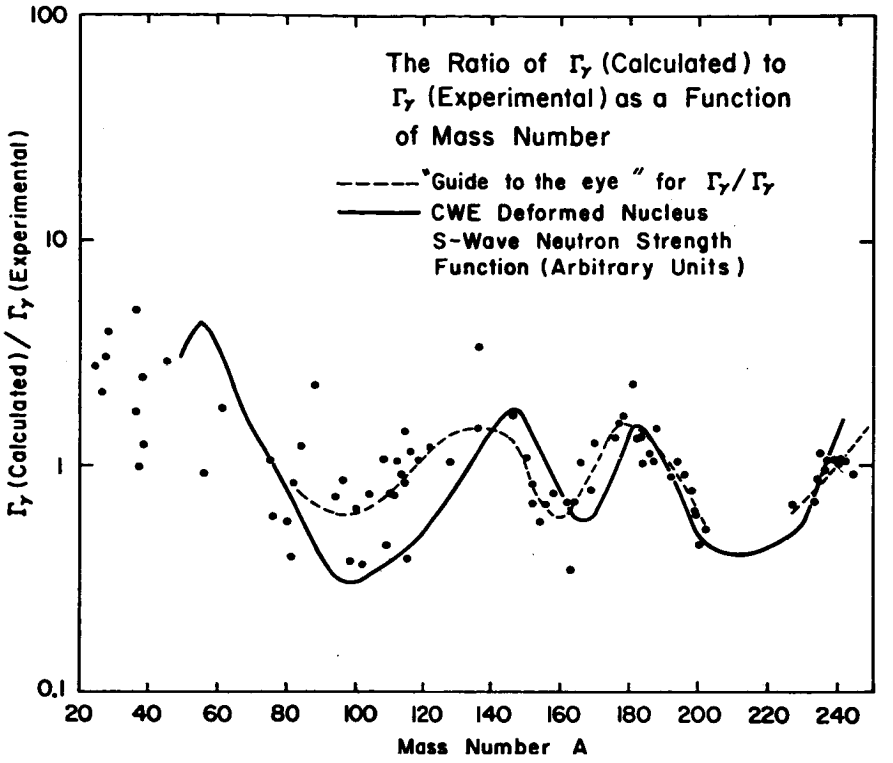

FIG. 1. The ratio of Γ_γ (calculated) to Γ_γ (experimental) is plotted as a function of mass number. The optical model, deformed nucleus *s*-wave neutron-strength function due to Chase *et al.* (1958) shows similar behavior.

functions into the initial states are larger, the values of Γ_γ for electric-dipole transitions following *s*-wave neutron capture might be expected to peak in the vicinity of the *s*-wave neutron function maxima.

VI. PARTICLE WIDTHS

From nuclear reaction theory, the particle widths can be written in the form:

$$\Gamma_l = 2P_l\gamma_l^2. \tag{6.1}$$

In this expression l specifies the value of the orbital angular momentum. P_l is the nuclear penetrability defined by

$$P_l = \rho/[F_l^2(\rho) + G_l^2(\rho)] \tag{6.2}$$

and

$$\rho = kR, \tag{6.3}$$

where R is the nuclear radius and $F_l(\rho)$ and $G_l(\rho)$ are the regular and irregular solutions of the Coulomb equation (Hull and Breit 1959).

The factor γ_l^2 is the reduced width for the particle channel and is dependent upon the behavior of the wave function within the nucleus. Generally a detailed knowledge of the form of the reduced width is not available. For *s*-wave neutrons the behavior of the strength function, defined by

$$S_l\langle R\gamma_l^2/D_l\rangle, \tag{6.4}$$

where R is the nuclear radius and D_l is the level spacing, has been studied extensively (Chase *et al.* 1958). Some evidence is available concerning the behavior of p- and d-wave neutron-strength functions and of s-wave proton-strength functions, but the results are far from complete.

We have assumed in these calculations that the strength functions for the various partial waves for protons, neutrons, and alpha particles can be approximated by the strength function predicted by a "black nucleus" model. On this model γ_l^2 can be written in the form:

$$\gamma_l^2 \simeq \frac{2 \times 10^{-14}}{R\rho(E, J, \pi)} . \tag{6.5}$$

In our calculations of reaction rates we have assumed the particle widths to be given by equation (6.1), with a reduced width as defined by equation (6.5). In this approximation the only dependence on the orbital angular momentum is through the penetration factors. The level densities are determined from the parameters presented by Gilbert and Cameron (1965). The nuclear radius is determined from an expression of the form

$$R = r_0(A_p^{1/3} + A_T^{1/3}), \tag{6.6}$$

where A_p and A_T are the mass numbers of the projectile and target nucleus respectively. This will be discussed in more detail in the subsequent sections.

VII. THE CALCULATION OF THE REACTION RATES

A computer code was prepared to calculate the reaction rates as a function of temperature, incorporating the various approximations outlined in the previous sections. Employing equation (2.12) for particle–particle reactions and the corresponding expression for particle-capture reactions, the contributions to the rate for ground-state interactions were computed. The summations were performed over all values of the channel spin and of the orbital angular momentum, l, consistent with the spin and parity of the compound nuclear state (J, π). Furthermore, summations were carried out over all integer and half-integer values of $J \leqslant 11/2$ for both parities.

The level densities employed in these calculations were determined from equations (4.5) and (4.12) and the level-density parameters tabulated by Gilbert and Cameron (1965). In our investigation of neutron-capture cross sections for comparison with the results of Macklin and Gibbons (1965), it was necessary in some cases to determine the level-density parameters from the pairing and shell corrections. This was also necessary in our study of neutron capture on uranium isotopes.

The radiation widths were calculated as a function of energy from equation (5.2). A value of $D_0 = 230$ was employed for mass number $A > 40$. For $A \leqslant 40$, $D_0 = 400$ provided a better fit to the data and was thus incorporated into our calculations.

The particle widths for protons, neutrons, and alpha particles were computed from equations (6.1) and (6.5). Insufficient experimental measurements were available in the energy range of interest to permit, generally, a more

refined determination of these widths. It is evident that large uncertainties can be assigned to these calculated values for a given orbital angular momentum. As even partial wave-strength functions tend to attain maxima near the minima of those of odd partial waves (as for instance in the case of *s*- and *p*-wave neutrons) it was felt that the resulting rates might be somewhat better than the uncertainties inherent in the individual widths.

The total widths are determined as a sum of the contributions from the radiation widths and the various particle widths. The contributions from the excited states are not included. Corrections due to particle-width fluctuations (Lane and Lynn 1957) are neglected, since these are small compared to uncertainties associated with level densities.

These various parameters were determined as a function of energy over a range defining the maximum contribution to the integrands of equation (2.12). A sufficient number of points were taken to allow for a good Simpson's Rule numerical integration. Any errors introduced by this method are far smaller than the uncertainties in the nuclear parameters employed.

VIII. COMPARISON OF RESULTS WITH EXPERIMENT

Where experimental determinations of cross sections or of individual resonance parameters were available, we have sought to determine the accuracy of our calculated values for $\langle \sigma v \rangle$. Four sources were available for this purpose. (*a*) Experimental determinations of (p, n) cross sections on nuclei from ^{37}Cl to ^{59}Co are available for proton energies below the threshold energy for neutron emission to the first excited state of the residual nucleus. (*b*) Experimental determinations of the individual resonance parameters are available for a number of alpha-particle and proton reactions on light nuclei. This allows a determination of the $\langle \sigma v \rangle$ as a sum over the contributions from individual resonances. (*c*) Average neutron-capture cross sections determined from experimental measurements and resonance parameters are available for a range of target mass number, $A = 54$ to 208. (*d*) The yield curve from the Mike fusion explosion suggests a slow decrease in the neutron-capture cross section with increasing mass number for heavy uranium isotopes. This behavior can be examined, employing the shell and pairing corrections and the neutron binding energies predicted by the exponential mass formula of Cameron and Elkin (1965).

(a) (p, n) Reaction Cross Sections Near Threshold

Johnson *et al.* (1958) have published experimental results for (p, n) reaction cross sections near threshold for a number of intermediate nuclei. We have computed these cross sections for proton energies below the threshold for neutron emission to the first excited state of the residual nucleus.

We assume that the cross section for capture proceeding through a compound nuclear state of spin J is given by the Breit–Wigner one-level formula. The cross section due to energy states of a specified spin–parity combination J^π is thus

$$\sigma(E, J, \pi) = \frac{4.065}{\mu E} g \frac{\Gamma_p \Gamma_n}{\Gamma} \rho(E, J, \pi), \tag{8.1}$$

where g is the statistical factor and μ is the reduced mass in a.m.u. The total cross section is determined by summing these contributions over all values of the spin and parity.

We have defined the nuclear radius to be of the form

$$R = r_0(A_p^{1/3} + A_T^{1/3}) \text{ fermis}, \tag{8.2}$$

where A_p and A_T are the mass numbers of the projectile and the target nucleus respectively. By this choice we have pictured the compound nuclear radius as a sum of the radii of the interacting particles. It is well known that there is no one expression for the nuclear radius that will fit all the experimental data (electron scattering, alpha decay, reaction cross sections, etc.). To the extent that any choice of a sharply defined nuclear radius is somewhat arbitrary, we have chosen to treat r_0 as a parameter in fitting our calculated cross sections to the experimental determinations.

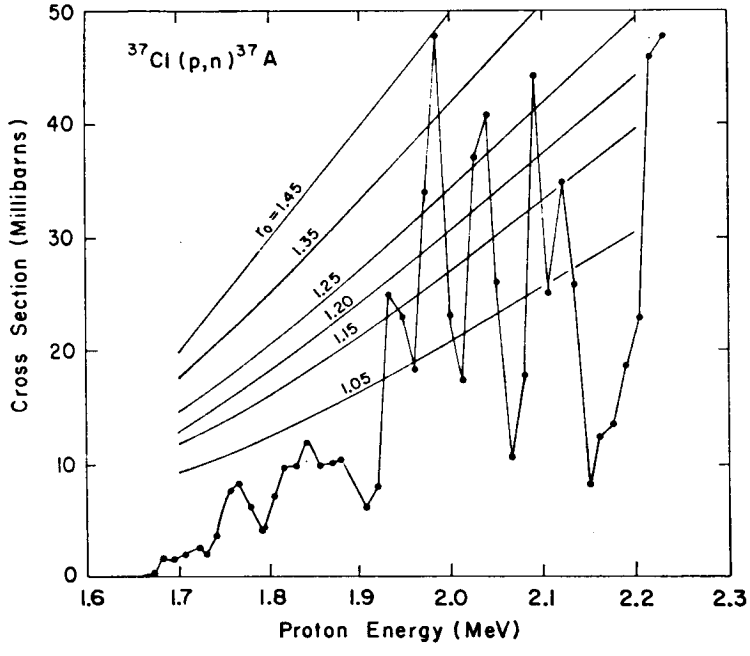

FIG. 2. The cross section for the reaction ^{37}Cl(p, n)^{37}A, calculated for several values of the radius parameter r_0, is compared to the experimental results due to Johnson *et al.* (1958).

The results of these comparisons are illustrated in Figs. 2 to 7. The experimental points are due to Johnson *et al.* The calculated cross sections are plotted as a function of energy below the excited-state threshold for a range of values of r_0. We conclude from these figures that the choice $r_0 = 1.20$ provides the best fit to the data. This is in good agreement with the square-well radius $R = 1.45(A_p + A_T)^{1/3}$ employed by Johnson *et al.* (1958) in their calculations of the proton strength functions.

(b) $\langle \sigma v \rangle$ Evaluated from Known Resonances for Light Nuclei

For a number of light nuclei, experimental determinations of the resonance parameters are available for a large number of levels in the energy region of interest. This should allow us to calculate with reasonable accuracy the values

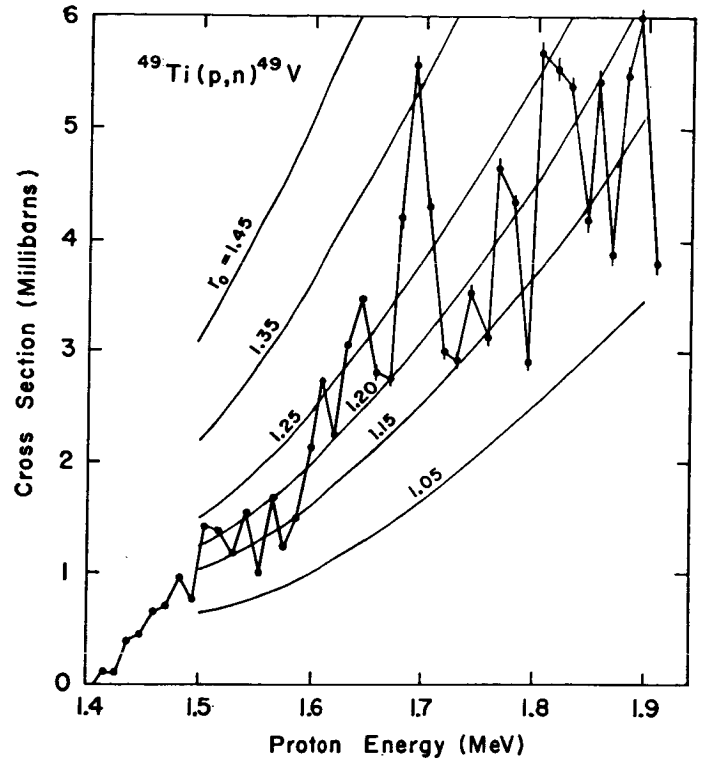

FIG. 3. The cross section for the reaction ^{49}Ti(p, n)^{49}V, calculated for several values of the radius parameter r_0, is compared to the experimental results due to Johnson *et al.* (1958).

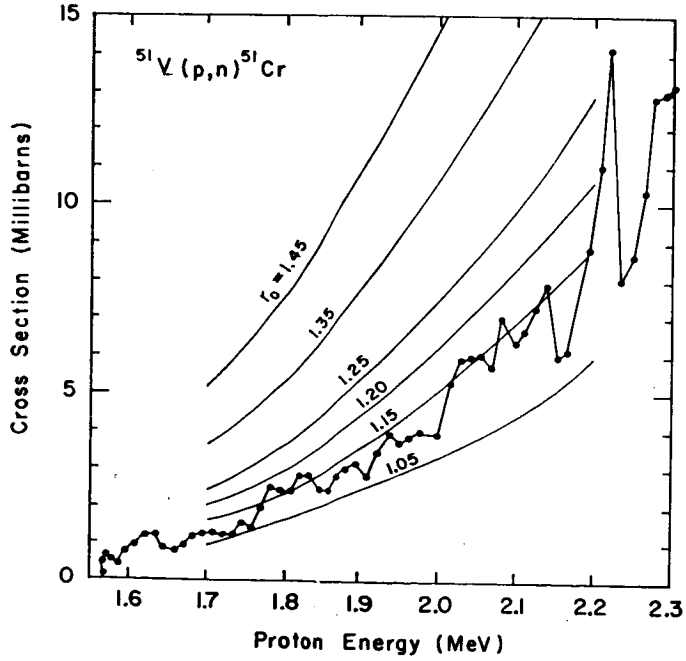

FIG. 4. The cross section for the reaction ^{51}V(p, n)^{51}Cr, calculated for several values of the radius parameter r_0, is compared to the experimental results due to Johnson *et al.* (1958).

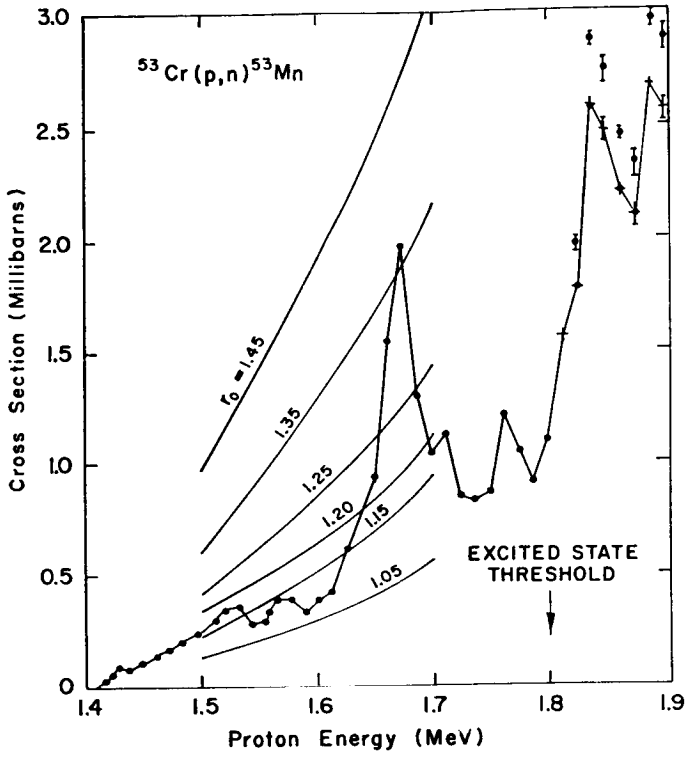

FIG. 5. The cross section for the reaction ^{53}Cr(p, n)^{53}Mn, calculated for several values of the radius parameter r_0, is compared to the experimental results due to Johnson *et al.* (1958).

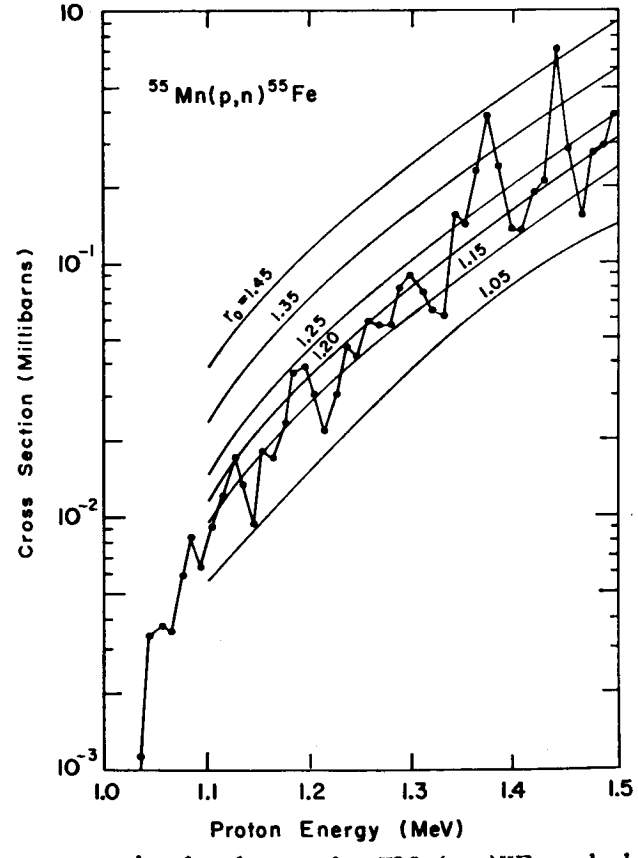

FIG. 6. The cross section for the reaction ^{55}Mn(p, n)^{55}Fe, calculated for several values of the radius parameter r_0, is compared to the experimental results due to Johnson *et al.* (1958).

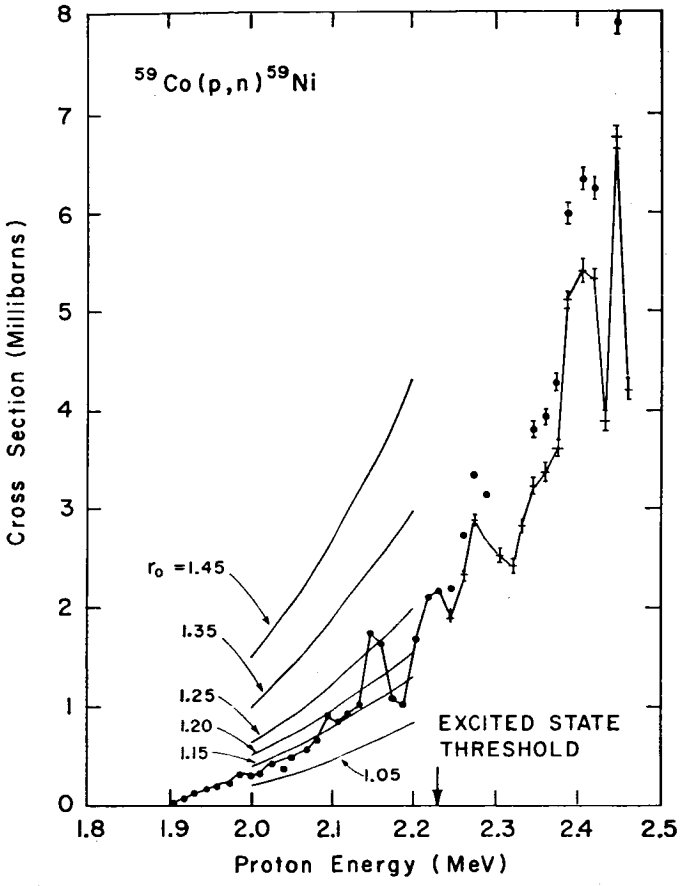

FIG. 7. The cross section for the reaction ^{59}Co(p, n)^{59}Fe, calculated for several values of the radius parameter r_0, is compared to the experimental results due to Johnson *et al.* (1958).

of $\langle \sigma v \rangle$ for these reactions. The total $\langle \sigma v \rangle$ is determined by summing over the contributions from the individual resonances as given by the equation

$$\langle \sigma v \rangle = \sum_r \left(\frac{32}{\mu}\right)^{1/2} \left(\frac{\pi}{kT}\right)^{3/2} \lambda_a^{\,2}(E_r)\, e^{-E_r/kT} \left(g\,\frac{\Gamma_\alpha \Gamma_\beta}{\Gamma}\right)_{E_r}. \tag{8.3}$$

Experimental determinations of $(g\Gamma_\alpha\Gamma_\beta/\Gamma)_{E_r}$ for eight reactions involving protons and alpha particles on light nuclei were reasonably complete in the appropriate energy range. These reactions are listed in Table I together with a statement of the number of resonances for which the relevant parameters are known, the energy range in which these resonances lie, and the reaction Q value. The ratios of the values of $\langle \sigma v \rangle$ determined by the general procedure outlined in the previous sections to $\langle \sigma v \rangle$ determined from experimental parameters are plotted as a function of temperature in Figs. 8 and 9 for two values of the nuclear radius parameter, $r_0 = 1.20$ and 1.45. The agreement is generally better for the choice $r_0 = 1.20$, inferred from our investigation of (p, n) reaction cross sections.

Discrepancies of a factor of two or three of our rates from the experimental values can readily be accounted for through the uncertainties in our values of the particle and radiation widths and in the level densities. Furthermore, the

TABLE I

Summary of experimental data on resonance parameters

Reaction	Number of resonances	Q (MeV)	Energy range of bombarding particle (MeV)	References
^{23}Na (p, γ)	22	11.693	0.25–1.45	Prosser *et al.* (1962)
^{26}Mg(p, γ)	120	8.272	0.3–3.0	Van der Leun and Endt (1963)
^{27}Al(p, γ)	61	11.581	0.2–2.2	Antoufiev *et al.* (1963)
^{30}Si(p, γ)	70	7.286	0.5–2.7	Van Rinsvelt (1964)
^{24}Mg(α, γ)	29	1.986	1.5–3.8	Smulders and Endt (1962); Weinman *et al.* (1964)
^{23}Na(p, α)	21	2.379	0.3–1.5	Kuperus *et al.* (1963); Fisher and Whaling (1963)
^{27}Al(p, α)	31	1.595	0.5–2.5	Andersen *et al.* (1963); Abuzeid *et al.* (1963)
^{31}P(p, α)	27	1.917	0.5–3.1	Kuperus *et al.* (1963)

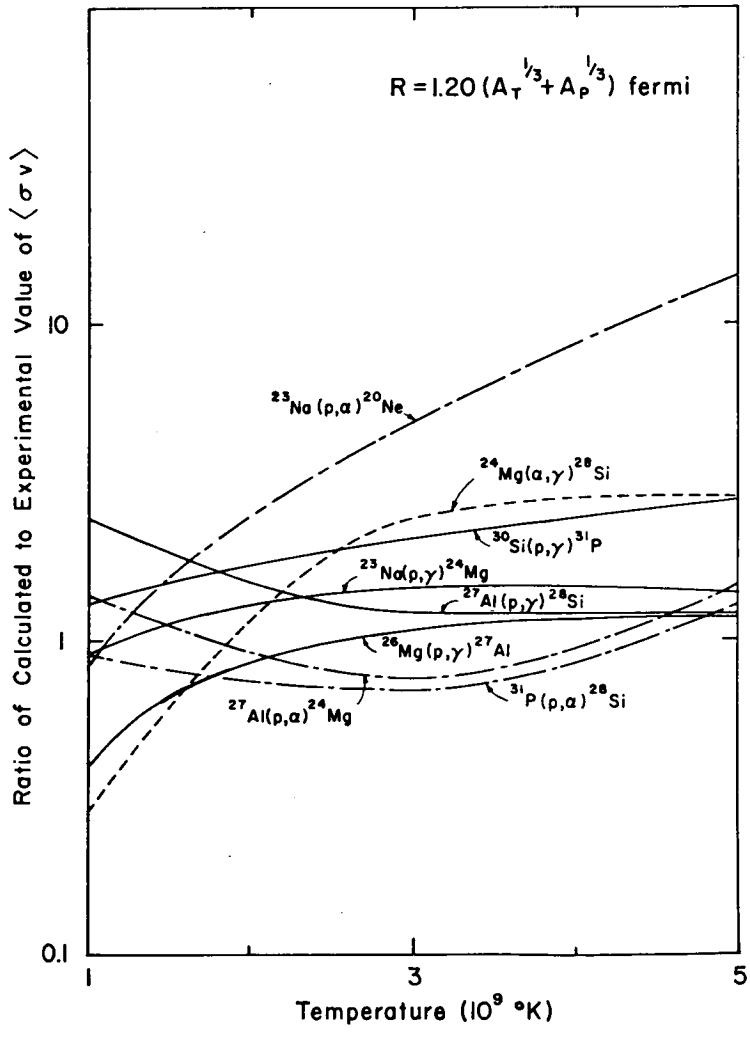

FIG. 8. The ratio of the reaction rates calculated by our procedure to the rates determined from experimental parameters is plotted as a function of temperature for a value of the radius parameter, $r_0 = 1.20$.

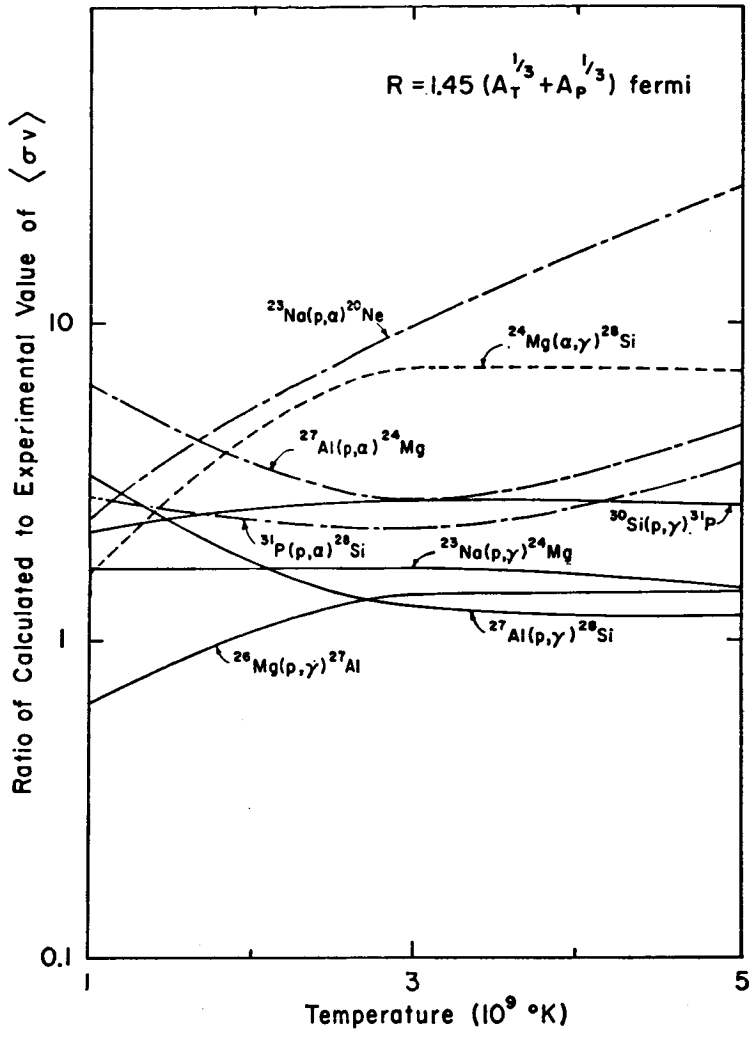

FIG. 9. The ratio of the reaction rates calculated by our procedure to the rates determined from experimental parameters is plotted as a function of temperature for a value of the radius parameter $r_0 = 1.45$.

uncertainties in the experimental values of $(g\Gamma_\alpha\Gamma_\beta/\Gamma)$ may contribute to the disagreement.

The large deviation of ^{23}Na(p, α) is due to the fact that there are large contributions to the integral from resonances at energies higher than the maximum energy of the experimental resonances. The other reactions give satisfactory results.

(c) Neutron-Capture Cross Sections

Macklin and Gibbons (1965) have recently published a rather extensive compilation of experimental determinations of neutron-capture cross sections in the energy range of importance to astrophysics. Their results afford a good check on the statistical methods employed in our calculations for a large number of nuclei.

Conveniently Macklin and Gibbons have transformed the experimental microscopic cross sections into effective cross sections for neutrons in a Maxwell

distribution. That is, by summing over the contributions from the individual neutron resonances they have determined the rates $\langle \sigma v \rangle$ in the usual form

$$\langle \sigma v \rangle = \frac{4}{(\pi)^{1/2}} \int_0^\infty \sigma \left(\frac{v}{v_T}\right)^3 \exp - \left(\frac{v}{v_T}\right)^2 dV, \tag{8.4}$$

where

$$v_T = (2kT/\mu)^{1/2} \tag{8.5}$$

is the most probable velocity in the Maxwell spectrum. The resulting cross sections are expressed in the form:

$$\langle \sigma \rangle = \langle \sigma v \rangle / v_T. \tag{8.6}$$

For purposes of comparison we have divided our calculated values of $\langle \sigma v \rangle$ by the most probable velocity. These comparisons were performed for an energy corresponding to $kT = 30$ keV and are displayed in Table II. The results of these calculations of $\langle \sigma v \rangle$ for neutrons are rather insensitive to the definition of the nuclear radius. The neutron width can be written in the form

$$\Gamma_l(U, J) = 2P_l \left[\frac{0.2}{R\rho(U, J)}\right], \tag{8.7}$$

where the radius R is in fermis. For neutrons $P_0 = \rho = kR$ and in our approximation the width is independent of the radius. For the case $l = 1$, $P_1 = \rho^3/(1 + \rho^2)$, where for $\rho > 1$ we still have $P_1/R \sim k$. Thus the discussion of the nuclear radius given in the previous sections is not relevant.

We have calculated cross sections both from known level-density parameters (Gilbert and Cameron 1965) and from nuclear parameters predicted by the exponential mass formula of Cameron and Elkin (1965). The agreement of these calculations with experiment is particularly good for those nuclei for which sufficient levels are known to permit a determination of the various level-density parameters. Generally the agreement is within a factor of two or three over a range in mass number A from 54 to 238.

(d) Interpretation of "Mike" Abundance Yields

Cameron (1959) has considered in some detail the results of the Mike fusion explosion of November, 1952. The large neutron flux released in this explosion resulted in the formation of heavy uranium isotopes by multiple neutron capture. The yield curve for these isotopes is displayed in Fig. 10. It is observed that the yields of both even and odd mass numbers are exponentially decreasing functions of the mass number, odd mass numbers being suppressed by approximately a factor of two. The general character of this curve, the constancy of successive product abundance ratios, suggests that the neutron-capture cross sections cannot fall off rapidly with increasing mass number.

This conclusion is not consistent with the prediction of conventional mass formulas that the neutron binding energies fall off rapidly with increasing mass number. It was this problem that led Cameron and Elkin (1965) to a re-evaluation of the mass formula, as discussed in a previous section. Employing

TABLE II

Cross sections $\langle\sigma v\rangle/V_T$ for neutron capture at $kT = 30$ keV. The results determined from known level-density parameters and those determined from the exponential mass formula are compared with the experimental values of Macklin and Gibbons (1965). The units are millibarns

Target nucleus	Experimental cross section	Cross section from exponential mass formula	$\frac{\sigma \text{ (exponential)}}{\sigma \text{(experimental)}}$	Cross section from known level-density parameters	$\frac{\sigma \text{(parameters)}}{\sigma \text{(experimental)}}$
^{54}Fe	33.8	38.9	1.15	45.1	1.33
^{56}Fe	15.1	19.1	1.26	28.0	1.85
^{57}Fe	61.0	33.7	0.55	56.2	0.921
^{59}Co	44	48.6	1.10	45.4	1.03
^{75}As	358	148.5	0.41	336	0.939
^{86}Sr	75	165.3	2.20		
^{87}Sr	108	324.7	3.00		
^{88}Sr	6.9	26.0	3.77		
^{91}Zr	59	142	2.41	142	2.41
^{92}Zr	34	48.1	1.41		
^{94}Zr	21	23.3	1.11		
^{96}Zr	41	15.7	0.383		
^{93}Nb	277	260.0	0.94	408	1.47
^{98}Mo	102	42.0	0.41	48.7	0.477
^{100}Mo	133	44.7	0.34	177	1.33
^{103}Rh	837	635.1	0.76	623	0.744
^{116}Sn	104	278	2.67	263	2.53
^{117}Sn	418	855	2.05	756	1.81
^{118}Sn	65	236	3.63	218	3.35
^{119}Sn	257	486	1.89	631	2.46
^{120}Sn	41	99.3	2.42		
^{127}I	737	783.6	1.06	911	1.24
^{133}Cs	462	824.5	1.78	761	1.65
^{139}La	45	80.5	1.79		
^{141}Pr	95	365.6	3.85	237	2.49
^{144}Sm	150	394	2.63		
^{147}Sm	1169	909	0.778	970	0.830
^{148}Sm	257	199	0.774	183	0.712
^{149}Sm	1617	864	0.534	1514	0.936
^{150}Sm	369	176	0.477	186	0.504
^{152}Sm	410	222	0.541		
^{154}Sm	325	148	0.455		
^{159}Tb	1908	1445	0.76	1309	0.686
^{165}Ho	1792	1190	0.66	1204	0.672
^{169}Tm	1298	1445	1.11	1325	1.02
^{175}Lu	1623	1874	1.15	1552	0.956
^{181}Ta	760	1411	1.86	1353	1.78
^{197}Au	605	997	1.65	894	1.47
^{204}Pb	110	62.4	0.57	69.3	0.630
^{206}Pb	9.6	17.4	1.81	17.1	1.78
^{207}Pb	8.7	9.25	1.06	12.0	1.381
^{209}Bi	12.1	8.14	0.67	7.03	0.58
^{232}Th	521	682	1.31	641	1.23
^{238}U	499	635	1.27	585	1.17

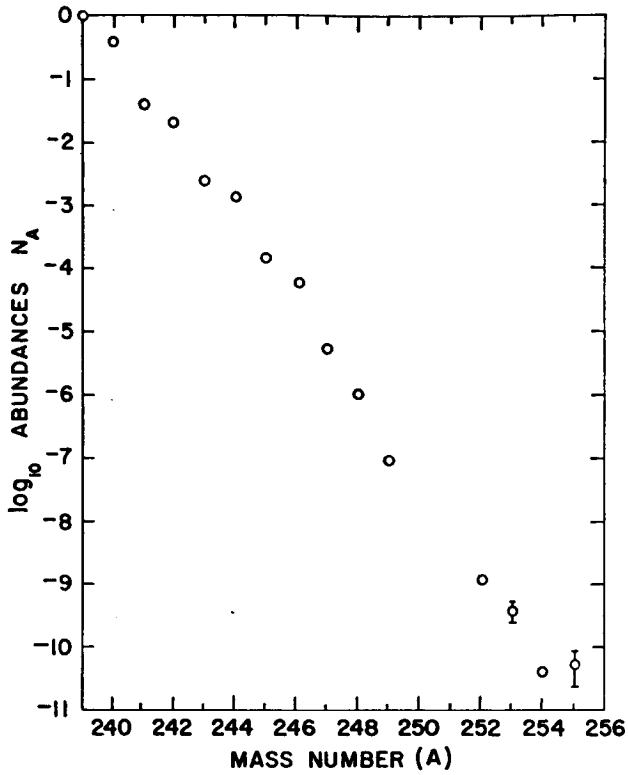

FIG. 10. The yield curve for the "Mike" thermonuclear explosion. The $\log_{10}$ of the abundance of the various nuclei is plotted as a function of mass number.

the shell and pairing corrections of Cameron and Elkin, the level densities can be determined by the method outlined in Section IV. Thus we can calculate the neutron-capture cross sections for the uranium isotopes employing the binding energies predicted by both the conventional form and the exponential form of the mass formula. The results of these calculations for a temperature corresponding to $kT = 20$ keV are displayed in Fig. 11. The velocity by which the calculated values of $\langle \sigma v \rangle$ have been divided corresponds to a neutron energy of 20 keV. In these calculations we have assumed that the total width is the sum of the neutron width and the radiation width, decay into other channels being negligible.

Returning to the yield curve, we note that for mass numbers above $A = 250$ there appears to be a reversal of the odd–even effect. Recently the yields resulting from the Par and Barbel tests have confirmed the existence of this effect (Bell 1965; Dorn and Hoff 1965). It has been suggested that this reversal is the result of the gain or loss of a proton earlier in the capture chain. Therefore, the neutron-capture cross sections for neptunium and protactinium have been calculated from the predictions of both mass formulas.

The cross sections for these isotopes exhibit the usual odd–even effect. Generally we observe that while the cross sections predicted by the conventional mass formula fall off by three or four orders of magnitude between mass numbers $A = 234$ and 264, the capture cross sections determined for the exponential form decrease by roughly a factor of ten. The errors in our numbers

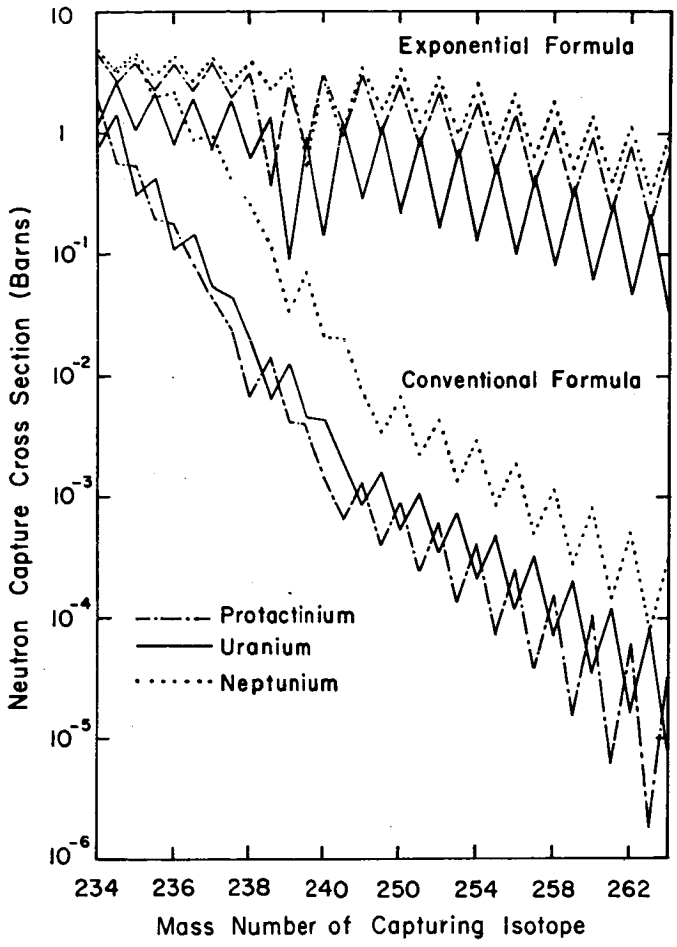

FIG. 11. The neutron-capture cross sections for protactinium, uranium, and neptunium isotopes, calculated from both the exponential and conventional mass-formula parameters, are plotted as a function of mass number. The energy at which these cross sections have been evaluated is 20 keV.

can be expected to be rather large, but the agreement with the capture cross section for ^{238}U from Hughes *et al.* (1960) is rather good: calculated $\sigma \sim 0.72$ barns, experimental $\sigma = 0.50$ barns. The observed slow decrease in the capture cross sections determined from the exponential mass-formula parameters is consistent with the behavior inferred from the yield curves.

The dip in our capture cross sections corresponding to neutron number 152 must be interpreted with caution. There is a gap in the Nilsson diagram for deformed nuclei at this point (Mottleson and Nilsson 1958) that predicts this effect for heavier nuclei on the valley of beta stability. However, as the mass-formula parameters were fitted to nuclei along the beta stable valley, the existence of this effect in our calculated cross sections for nuclei in the neutron-rich region must be interpreted with caution.

Ingley (1965) has recently determined values for the neutron-capture cross sections for a number of uranium isotopes from the results of the Par and Anacostia experiments. His results are plotted in Fig. 12, together with our calculated values for the neutron-capture cross sections, for a neutron energy

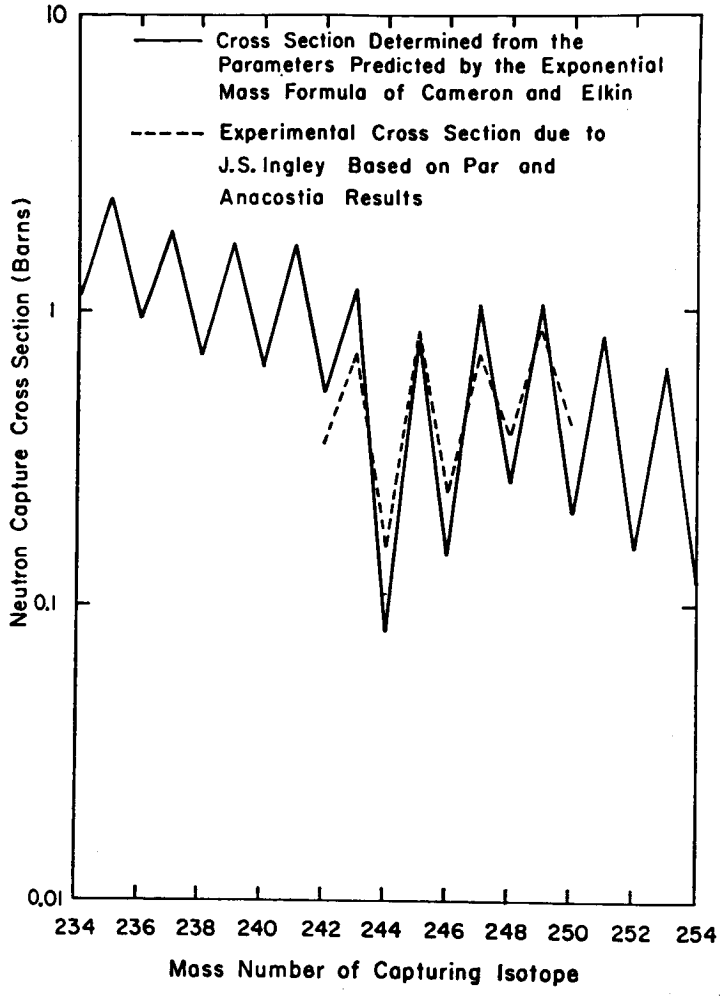

FIG. 12. The calculated values of the neutron-capture cross sections for the uranium isotopes are compared with experimental values inferred from the yields of the Par and Anacostia devices (Ingley 1965).

of 20 keV. The agreement is seen to be quite good. Furthermore, the same dip in the capture cross section at ^{244}U is evident in these results, suggesting that the Nilsson gap at neutron number 152 is present in the heavy uranium nuclei.

As future experiments of this nature may be performed, employing somewhat heavier target nuclei, we have calculated the cross sections predicted by the exponential mass-formula parameters for nuclei having $91 \leqslant Z \leqslant 98$ and $N \leqslant 186$, for a neutron energy of 20 keV. These results are presented in Table III. We have assumed a spin 5^+ for odd–odd nuclei, and $5/2^+$ for odd-A nuclei. Ground and first excited states of odd–odd nuclei tend to have a high spin in one case and a low spin in the other case. Level multiplicity effects on the capture process tend to favor high-spin states in the photon cascade process, and there is unlikely to be time for isomeric transitions to a low-spin ground state on the time scale of an underground multiple neutron-capture experiment.

These various comparisons between our calculated cross sections and the experimental data show in general that reaction and capture cross sections in

TABLE III

The neutron-capture cross sections at 20 keV are given for the neutron-rich isotopes of the elements $91 < Z < 98$

Mass number of target nucleus	Cross section (barns)							
	^{91}Pa	^{92}U	^{93}Np	^{94}Pu	^{95}Am	^{96}Cm	^{97}Bk	^{98}Cf
229	2.86							
230	4.40							
231	2.84							
232	4.19	1.41						
233	2.59	2.67	2.96					
234	4.00	1.11	4.28					
235	2.42	2.42	2.77					
236	3.48	0.953	4.11	1.42				
237	2.09	1.88	2.62	2.68	2.86			
238	3.37	0.716	3.70	1.22	4.17	1.41		
239	2.02	1.71	2.32	2.23	2.72	2.63	2.94	
240	3.34	0.660	3.59	0.960	3.79	1.22	4.22	
241	1.76	1.70	2.25	2.08	2.48	2.19	2.80	
242	2.72	0.536	3.54	0.885	3.72	0.975	3.90	1.27
243	0.338	1.22	2.01	2.04	2.40	2.05	2.62	2.22
244	2.15	0.0814	3.01	0.742	3.67	0.902	3.84	1.03
245	0.616	0.816	0.472	1.57	2.18	2.00	2.55	2.11
246	2.58	0.147	2.53	0.137	3.17	0.742	3.78	0.958
247	1.08	1.06	0.827	1.19	0.617	1.53	2.34	2.04
248	2.64	0.263	2.95	0.237	2.79	0.151	3.34	0.800
249	0.863	1.06	1.37	1.46	1.04	1.21	0.803	1.60
250	2.26	0.203	2.95	0.404	3.22	0.257	3.08	0.185
251	0.698	0.832	1.11	1.44	1.59	1.47	1.30	1.32
252	1.90	0.156	2.58	0.312	3.19	0.428	3.45	0.309
253	0.556	0.650	0.891	1.18	1.33	1.46	1.85	1.59
254	1.60	0.121	2.23	0.244	2.84	0.330	3.44	0.491
255	0.437	0.518	0.714	0.942	1.08	1.18	1.57	1.56
256	1.32	0.0932	1.92	0.192	2.47	0.257	3.10	0.385
257	0.346	0.400	0.573	0.747	0.884	0.938	1.31	1.29
258	1.07	0.0726	1.58	0.149	2.13	0.201	2.74	0.274
259	0.278	0.311	0.453	0.592	0.700	0.738	1.07	1.04
260	0.869	0.0561	1.29	0.117	1.79	0.155	2.39	0.232

TABLE III (*Concluded*)

Mass number of target nucleus	Cross section (barns)							
	^{91}Pa	^{92}U	^{93}Np	^{94}Pu	^{95}Am	^{96}Cm	^{97}Bk	^{98}Cf
261	0.218	0.245	0.362	0.464	0.564	0.570	0.871	0.819
262	0.710	0.0431	1.05	0.0903	1.47	0.121	2.03	0.180
263	0.174	0.188	0.286	0.373	0.450	0.449	0.706	0.644
264	0.574	0.0344	0.852	0.0706	1.22	0.0960	1.71	0.140
265	0.137	0.147	0.230	0.285	0.355	0.357	0.564	0.498
266	1.15	0.0274	0.700	0.0561	0.996	0.0743	1.41	0.110
267	0.240	0.322	0.185	0.230	0.283	0.275	0.444	0.394
268	0.629	0.0477	1.31	0.0443	0.816	0.0583	1.17	0.0862
269	0.154	0.171	0.279	0.453	0.228	0.214	0.359	0.307
270	0.371	0.0328	0.688	0.0700	1.41	0.0455	0.962	0.0676
271	0.0907	0.105	0.175	0.230	0.319	0.408	0.288	0.239
272	0.187	0.0209	0.393	0.0465	0.732	0.0683	1.53	0.0534
273	0.141	0.0556	0.0976	0.131	0.190	0.201	0.369	0.421
274	0.304	0.0302	0.186	0.0277	0.386	0.0427	0.778	0.0725
275	1.42×10^{-4}	0.0849	0.154	0.0661	0.101	0.107	0.211	0.201
276	3.59×10^{-3}	6.16×10^{-5}	0.305	0.0405	0.173	0.0247	0.397	0.0442
277	1.02×10^{-3}	9.33×10^{-4}	2.96×10^{-4}	0.102	0.162	0.0519	0.104	0.103
278		2.95×10^{-4}	5.04×10^{-3}	1.47×10^{-4}	0.286	0.0364	0.163	0.0244
279			1.84×10^{-3}	1.69×10^{-3}	5.31×10^{-4}	0.0812	0.174	0.0412
280				6.22×10^{-4}	6.79×10^{-3}	1.96×10^{-4}	0.284	0.0361
281					2.92×10^{-3}	1.73×10^{-3}	8.96×10^{-4}	0.0732
282						7.61×10^{-4}	9.09×10^{-3}	2.93×10^{-4}
283							4.58×10^{-3}	2.12×10^{-3}
284								1.03×10^{-3}

medium and heavy nuclei can be calculated using systematic nuclear parameters usually to within about a factor of three (the probable error seems to be about a factor of two). This accuracy is quite sufficient to provide a reliable basis for studies of thermonuclear reactions at unusually high stellar temperatures. A number of such calculations have been performed, the details of which will be reported in separate papers.

We wish to thank Drs. D. W. Dorn and J. S. Ingley for communicating to us the results of their cross-section analysis of the heavy uranium isotopes. The computer code for the Coulomb wave functions used in these calculations was developed by Mr. M. Halem and Miss F. Turnheim, to whom we are indebted.

REFERENCES

ABUZEID, M. A., ALY, F. M., ANTOUFIEV, Y. P., BARANIK, A. T., NOWER, T. M., and SOROKIN, P. V. 1963. Nucl. Phys. **45**, 123.
ANDERSON, S. L., HAUG, A., HOLTEBEKK, T., LONSJO, O., and NORDHAGAN, R. 1963. Norvegica, **1**, 1.
ANTOUFIEV. Y. P., EL NADI, L. M., DARWISH, D. A. E., BADAWAY, O. E., and SOROKIN, P. V. 1963. Nucl. Phys. **46**, 1.
BELL, G. I. 1965. Phys. Rev. **139**, 1207B.
BETHE, H. A. 1937. Rev. Mod. Phys. **9**, 69.
BLATT, J. M. and WEISSKOPF, V. F. 1952. Theoretical nuclear physics (Wiley, New York).
CAMERON, A. G. W. 1959. Can. J. Phys. **37**, 322.
CAMERON, A. G. W. and ELKIN, R. 1965. Can. J. Phys. **43**, 1288.
CHASE, D. M., WILETS, L., and EDMONDS, A. R. 1958. Phys. Rev. **110**, 1080.
DORN, D. W. and HOFF, R. W. 1965. Phys. Rev. Letters, **14**, 440.
ERICSON, T. 1959. Nucl. Phys. **11**, 481.
FISHER, T. R. and WHALING, W. 1963. Phys. Rev. **131**, 1723.
GILBERT, A. and CAMERON, A. G. W. 1965. Can. J. Phys. **43**, 1446.
HUGHES, D. H., MAGURNO, B. A., and BRUSSEL, M. K. 1960. Brookhaven Natl. Lab. Rept. BNL-325.
HULL, M. H. and BREIT, G. 1959. Handbuch der Physik, **41**, 408.
INGLEY, T. S. 1965. Private communication.
JENSEN, J. H. D. and LUTTINGER, J. M. 1952. Phys. Rev. **86**, 907.
JOHNSON, C. H., GALONSKY, A., and ULRECH, J. D. 1958. Phys. Rev. **109**, 1243.
KUPERUS, J., GLAUDEMANS, P. W. M., and ENDT, P. M. 1963. Physica, **29**, 1281.
LANE, A. M. and LYNN, J. E. 1957. Proc. Phys. Soc. (London) Ser. A, **70**, 557.
MACKLIN, R. L. and GIBBONS, J. H. 1965. Rev. Mod. Phys. **37**, 166.
MOTTLESON B. R. and NILSSON, S. G. 1959. Kgl. Danske Vidensk. Selskab, Mat.-fys. Skr. **1**, No. 8.
PROSSER, F. W., UNRUH, W. P., WILDENTHAL, B. H., and KRONE, R. W. 1962. Phys. Rev. **125**, 594.
REEVES, H. 1964. A review of nuclear energy generation in stars and some aspects of nucleosynthesis (Publications of the Institute for Space Studies, New York).
REEVES, H. and SALPETER, E. E. 1959. Phys. Rev. **116**, 1505.
RINSVELT, J. VAN. 1964. Physica, **30**, 59.
SALPETER, E. E. 1952. Phys. Rev. **88**. 547.
——— 1960. Ann. Phys. **11**, 393.
SMULDERS, P. J. M. and ENDT, P. M. 1962. Physica, **28**, 1093.
VAN DER LEUN, C. and ENDT, P. M. 1963. Physica, **29**, 990.
WEINMAN, J. A., MEYER-SCHUTZMEISTER, L., and LEE, L. L. 1964. Phys. Rev. **133**, B590.

3. THE APPROACH TO NUCLEAR STATISTICAL EQUILIBRIUM

J. W. TRURAN AND A. G. W. CAMERON

Physics Department, Yale University, New Haven, Connecticut and Institute for Space Studies, Goddard Space Flight Center, NASA, New York, New York

AND

A. GILBERT[1]

Physics Department, Columbia University, New York, New York and Institute for Space Studies, Goddard Space Flight Center, NASA, New York, New York

Received November 24, 1965

ABSTRACT

The transformation of a region composed initially of ^{28}Si to nuclei in the vicinity of the iron peak, which is thought to take place in the late stages of evolution of some stars, is considered in detail. In order to follow these nuclear transformations, a nuclear reaction network is established providing suitable reaction links connecting neighboring nuclei. A method of solution of the network equations is outlined. Thermonuclear reaction rates for all neutron, proton, and alpha-particle reactions involving the nuclei in this network have been determined from a consideration of the statistical properties of nuclei. The evolution of this silicon region has been followed in time for two cases: $T = 3 \times 10^9$ °K, $\rho = 10^6$ g cm^{-3} and $T = 5 \times 10^9$ °K, $\rho = 10^7$ g cm^{-3}. While both the observed solar and meteoritic abundances display a broad peak in the vicinity of iron, centered on ^{56}Fe, in these calculations ^{54}Fe is found to be the most abundant isotope in this mass range. Beta decays required to change the peak to ^{56}Fe are very slow. As the transformation $2\,^{28}\text{Si} \rightarrow {}^{54}\text{Fe} + 2\text{p}$ is endothermic by $\sim$1.3 MeV, these results suggest that the silicon-to-iron conversion may not comprise an exothermic nuclear burning stage of stellar evolution.

I. INTRODUCTION

The details of stellar evolution are quite well established through the hydrogen- and helium-burning phases (Hayashi *et al.* 1962). The sequence of nuclear-burning stages following helium burning is considered to be carbon burning, oxygen burning, and the buildup of the iron peak from the products of these reactions by an equilibrium process.

The destruction of ^{12}C can proceed at temperatures $T \geqslant 7 \times 10^8$ °K by the reaction $^{12}\text{C} + {}^{12}\text{C}$ (Cameron 1959*a*; Reeves and Salpeter 1959). At somewhat higher temperatures ($T \sim 10^9$ °K), oxygen burning by $^{16}\text{O} + {}^{16}\text{O}$ is also possible (Cameron 1959*b*; Reeves and Salpeter 1959). The details of these reactions are not well determined. Generally the reaction products should be nuclei with masses in the range $20 \leqslant A \leqslant 32$, particularly the alpha-particle nuclei ^{24}Mg, ^{28}Si, and ^{32}S. Of the nuclei in this region, ^{28}Si has the highest separation energies for protons and alpha particles. As the temperature is increased, ^{28}Si will be the last nucleus to be photodisintegrated, and will therefore accumulate. It can be assumed that the material consists mainly of ^{28}Si after carbon and oxygen burning have taken place, at temperatures $T \gtrsim 2 \times 10^9$ °K.

At temperatures $\gtrsim 3 \times 10^9$ °K the photodisintegration of silicon will proceed rapidly, releasing protons, neutrons, and alpha particles. The capture of

[1]Now at the Lawrence Radiation Laboratory, Berkeley, California.

these light particles on nuclei remaining in this region will result in the buildup of nuclei to the vicinity of iron. ^{56}Fe is favored in this instance by the fact that it has the maximum binding energy per nucleon. The iron-peak abundances observed in nature have usually been attributed to this equilibrium process (Burbidge *et al.* 1957). The general features of the iron peak can be reproduced reasonably well in this manner. The important consideration is whether the evolution of a presupernova star proceeds too rapidly to allow the silicon-to-iron conversion. This is a function of the extent to which neutrino energy losses will accelerate the evolution. From a consideration of the rate of energy loss by the pair annihilation process

$$e^- + e^+ \rightarrow \nu + \bar{\nu}$$

Stothers and Chiu (1962) have found the evolutionary time for $T = 3 \times 10^9$ °K and $\rho = 2 \times 10^6$ g cm^{-3} to be only 0.3 year. It is clear that an equilibrium process proceeding at an appreciably higher temperature is unlikely.

There is, however, another manner in which these iron-peak elements might be synthesized. The formation of a shock wave in the stellar core may result from the collapse of the core (Cameron 1963). If the shock is sufficiently energetic, it can propagate outward through the star, heating the medium through which it passes to temperatures $T \gtrsim 5 \times 10^9$ °K. The characteristics of these shock waves are currently under investigation (Colgate 1965; Arnett 1965).

At some point in its passage outward through the star, the strength of the shock may be sufficient to eject the regions above from the stellar gravitational potential. In order to determine whether this ejected material can contain significant amounts of iron-peak nuclei, we must know both the initial composition and the temperature–density history of the medium in the wake of the shock.

Colgate, Grasberger, and White (1961) have followed the dynamical implosion of a presupernova star of 10 solar masses ($10M_\odot$) through the formation of the shock wave. The mass ejected by the subsequent passage of the shock outward through the envelope was $1M_\odot$. The temperature and density of the medium at this point, immediately following the passage of the shock, were $T = 5 \times 10^9$ °K and $\rho = 1.3 \times 10^7$ g cm^{-3}. The temperature was found to remain above $\sim 5 \times 10^9$ °K for approximately 10^{-2} seconds, falling by an order of magnitude in the first second.

We are concerned with the general problem of the production of iron-peak elements in stellar interiors. We have followed the silicon-to-iron conversion for two temperatures, $T = 3$ and 5×10^9 °K, corresponding, respectively, to the conditions predicted for the medium following carbon and oxygen burning and to those predicted for the medium in the wake of the shock. A nuclear-reaction network is established, which provides suitable reaction links connecting the various nuclei in this region. This subject is discussed in Section V.

Reaction rates were determined as a function of temperature by the methods discussed in another paper by the authors (Truran *et al.* 1966) for all proton, neutron, and alpha-particle reactions involving the selected nuclei, as discussed in Section II. In Section III, the approximations involved in estimating

the nuclear beta-decay rates are outlined. The general conditions required for nuclear statistical equilibrium are presented in Section IV.

The results obtained for the evolution of a region composed initially of ^{28}Si at temperatures $T_9 = 3$ and 5 (T_9 is the temperature in units of 10^9 °K) are presented in Section VI. In Section VII, these results will be discussed with regard to the general problems of nucleosynthesis.

II. THERMONUCLEAR REACTION RATES

The number of reactions per unit volume per second, r, of two nuclear species with number densities n_1 and n_2 can be written in the form:

$$r = n_1 n_2 \langle \sigma v \rangle. \tag{2.1}$$

Here $\langle \sigma v \rangle$ is an appropriate average of the product of the reaction cross section, $\sigma(v)$, and the relative velocity of the nuclei, v,

$$\langle \sigma v \rangle = [\int \sigma(v) v N(v) \mathrm{d}v]/[\int N(v) \mathrm{d}v], \tag{2.2}$$

where $N(v)$ is the number density of nuclei having relative velocity v.

The determination of the rates $\langle \sigma v \rangle$ as a function of temperature was considered in detail in another paper by the authors (Truran *et al.* 1966). Assuming that the velocity distributions of the two species are Maxwellian, that the contribution to the cross section of a single narrow resonance is given by the Breit–Wigner single-level formula, and that there are many resonances in the energy range of interest, the total rate for a particle–particle reaction involving a as the incoming particle and b as the outgoing particle (leaving the residual nucleus in a definite state) is

$$\langle \sigma v \rangle_{a,b} = \frac{2.51 \times 10^{-13}}{(\mu T_9)^{3/2}} \frac{1}{(2S_a + 1)(2I + 1)} \times \sum_{J,\pi} (2J + 1) \int_{E_t}^{\infty} \mathrm{d}E \, \mathrm{e}^{-11.61/T_9} \rho(U, J, \pi) \frac{\Gamma_a \Gamma_b}{\Gamma} \mathrm{cm}^3 \, \mathrm{sec}^{-1}. \tag{2.3}$$

In this expression, E_t is the threshold energy for the reaction, μ is the reduced mass in a.m.u., T_9 is the temperature in units of 10^9 °K, Γ_a and Γ_b are the particle widths in MeV, Γ is the total width for the decay of a specified compound nuclear state (taken to be the sum of the proton, neutron, and alpha-particle widths and the nuclear radiation width), S_a is the spin of the incoming particle, I is the spin of the target nucleus, J and π are the spin and parity, respectively, of the compound nuclear state, and $\rho(U, J, \pi)$ is the level density of states of specified spin and parity at excitation U. The particle widths, Γ_a and Γ_b, contain summations over all values of orbital angular momentum and channel spin consistent with angular momentum and parity conservation. The corresponding expression for the rate for particle-capture reactions is given by equation (2.3) with $\Gamma_b \rightarrow \Gamma_\gamma$ (Γ_γ being the radiation width for the specified compound nuclear state (U, J, π)).

The rates employed in our network have been determined from these expressions: for particle–particle reactions, $r(a, b) = n_a N_T \langle \sigma v \rangle_{a,b}$, where N_T is

the number density of the target nuclei, and for particle-capture reactions, $r(a, \gamma) = n_a N_T \langle \sigma v \rangle_{a,\gamma}$. The rates for the inverse reactions can be determined from the condition of detailed balance. The validity of this condition is assured by the fact that summations have been performed over all spin orientations. In equilibrium, the forward and inverse rates will be equal:

$$r(a, b) = n_a N_T \langle \sigma v \rangle_{a,b} = n_b N_R \langle \sigma v \rangle_{b,a} = r(b, a), \tag{2.4}$$

where N_R is the number density of the residual nuclei. The rate for the inverse reaction can therefore be determined from the equations of nuclear statistical equilibrium:

$$\begin{aligned} \langle \sigma v \rangle_{b,a} &= \langle \sigma v \rangle_{a,b} \left(\frac{n_a N_T}{n_b N_R} \right)_{\text{equilibrium}} \\ &= \langle \sigma v \rangle_{a,b} \left(\frac{\mu_a}{\mu_b} \right)^{3/2} \frac{\omega_a \omega_T}{\omega_b \omega_R} \exp(-Q_{ab}/kT), \end{aligned} \tag{2.5}$$

where μ_a and μ_b are the reduced masses in the entrance and exit channels, ω_a, ω_b, ω_T, and ω_R are the nuclear partition functions

$$\omega = \sum_i (2I_i + 1) \exp(-E_i/kT), \tag{2.6}$$

and Q_{ab} is the energy difference

$$Q_{ab} = (M_R + M_b - M_T - M_a)C^2, \tag{2.7}$$

where the M's are the masses of the respective nuclei. The analogous expression for the photodisintegration rate is given by

$$\begin{aligned} \lambda &= \langle \sigma v \rangle_{a,\gamma} \left(\frac{n_a N_T}{N_R} \right)_{\text{equilibrium}} \\ &= \langle \sigma v \rangle_{a,\gamma} \left(\frac{2\pi k}{h^2} \right)^{3/2} (\mu_a T)^{3/2} \frac{\omega_a \omega_T}{\omega_R} \exp(-Q/kT), \end{aligned} \tag{2.8}$$

where k is the Boltzmann constant, h is Planck's constant, T is the temperature, and Q is given by

$$Q = (M_R - M_T - M_a)C^2. \tag{2.9}$$

The reaction rates employed in our calculations were determined from these equations, with the exception of those reactions for which sufficient experimental data were available for the individual resonance parameters. Experimental determinations of the reaction rates were therefore employed for the following reactions (Truran *et al.* 1966): $^{23}\text{Na}(p, \gamma)^{24}\text{Mg}$, $^{26}\text{Mg}(p, \gamma)^{27}\text{Al}$, $^{27}\text{Al}(p, \gamma)^{28}\text{Si}$, $^{30}\text{Si}(p, \gamma)^{31}\text{P}$, $^{24}\text{Mg}(\alpha, \gamma)^{28}\text{Si}$, $^{27}\text{Al}(p, \alpha)^{24}\text{Mg}$, and $^{31}\text{P}(p, \alpha)^{28}\text{Si}$. The rate for alpha-particle capture by ^{16}O has been determined by Cartledge *et al.* (1963) from the experimental results of Kuehner *et al.* (1961). We have calculated the $^{12}\text{C}(\alpha, \gamma)^{16}\text{O}$ rate from the data of Larson and Spear (1964).

For computing purposes, the reaction rates were fitted to the following expression:

$$\omega_T \langle \sigma v \rangle = \exp\left(F_1 + \frac{F_2}{T_9^{1/3}} + \frac{F_3}{T_9} \right) \Big/ T_9^{3/2}, \tag{2.10}$$

where ω_T is the partition function of the target nucleus and T_9 is the temperature in units of 10^9 °K. The fitting parameters F_1, F_2, and F_3 are presented in the Appendix. This fitting form is accurate to a few percent over a range in temperature $1 \leqslant T_9 \leqslant 9$. These errors are small compared to the uncertainties associated with the calculated values of the reaction rates.

The temperature dependence of the nuclear partition functions has been considered in our calculations:

$$\omega(A, Z, T) = \sum_i (2I_i + 1) \exp(-E_i/kT). \tag{2.11}$$

When both the energies and the spins are known for the lower levels, the contributions to the partition function can be computed exactly. At higher excitations the summation can be evaluated as an integral over energy of $(2I + 1)\exp(-E/kT)$ weighted by the nuclear level density. The resulting partition functions were fitted as a function of temperature to

$$\omega(A, Z, T_9) = G_1 + G_2 T_9^2 + G_3 T_9^3. \tag{2.12}$$

The parameters defining these fits for the nuclei included in our network are presented in the Appendix. The partition functions computed from this fit should be accurate to a few percent in the temperature range $1 \leqslant T_9 \leqslant 6$.

We have included the contributions from three additional reactions to the flows in the reaction network—the triple alpha reaction forming ^{12}C and two heavy-ion reactions, $^{12}C + {}^{12}C$ and $^{16}O + {}^{16}O$.

Cartledge *et al.* (1963) give the following expression for the rate of destruction of helium, per helium nucleus, due to the 7.65-MeV resonance level in ^{12}C:

$$P_\alpha = (\rho \chi_\alpha) \frac{5.92 \times 10^{-10}}{T_9^3} \times 10^{-1.89/T_9}. \tag{2.13}$$

In this expression χ_α is the mass fraction of alpha particles in the medium and ρ is the density in g cm^{-3}. The rate should be correct within a factor of two over the range $0.1 < T_9 < 5$. The resonance contribution from the 9.63-MeV level is roughly comparable to that for the 7.65-MeV level, but the uncertainty in this rate is large. Employing equation (2.13), we arrive at the following expression for the rate of formation of ^{12}C:

$$r_\alpha = \frac{n_\alpha^3}{3} \frac{2.53 \times 10^{-56}}{T_9^3} 10^{-1.89/T_9} \text{ cm}^{-3} \text{ sec}^{-1}, \tag{2.14}$$

where n_α is the alpha-particle number density. The rate of destruction of alpha particles is simply $3r_\alpha$. Assuming that detailed balancing holds, the rate of photodisintegration of ^{12}C can be determined from the statistical equilibrium equations to be

$$\lambda(^{12}C \rightarrow 3\alpha) = 3.67 \times 10^{12} e^{-88.81/T_9} \text{ sec}^{-1}. \tag{2.15}$$

Reeves (1964) has given the following expression for the number of reactions per carbon nucleus, P, for the reaction $^{12}C + {}^{12}C$ from an optical model analysis of the results of Vogt *et al.* (1964):

$$\log_{10}(P/\rho\chi_C) = 26.37 - \frac{36.55(1 + 0.07T_9)^{1/3}}{T_9^{1/3}} - \frac{2}{3}\log_{10}T_9. \tag{2.16}$$

Here χ_C is the fraction by mass of carbon. The major products of this reaction are (^{20}Ne + α + 4.619 MeV) and (^{23}Na + p + 2.230 MeV) in roughly equal amounts. The weak endothermic branching to (^{23}Mg + n) has not been considered in our computations. Reeves feels this rate is correct within a factor of three.

For the reaction ^{16}O + ^{16}O, the number of reactions per oxygen nucleus, P, is given by (Reeves 1964):

$$\log_{10}(P/\rho\chi_0) = 40.5 - 59.02\frac{(1 + 0.14T_9)^{1/3}}{T_9^{1/3}} - \frac{2}{3}\log_{10}T_9. \tag{2.17}$$

Experimental data for this reaction are quite limited. It is probable that protons and alpha particles have comparable yields, while neutrons have a somewhat smaller yield. In our computations we have assumed the products to be equal amounts of (^{31}P + p + 7.676 MeV) and (^{28}Si + α + 9.593 MeV).

The effects of electron screening on our reaction rates have been considered. It was found that for typical conditions—$T_9 \sim 5$, $\rho \sim 10^7$ g cm^{-3}—the rates are enhanced by factors of less than two. These are well within the uncertainties associated with our reaction-rate calculations.

The contributions of the excited states to the reaction rates have not been included. This effect can be important for nuclei with low-lying excited states. We have compensated in part for the neglect of these contributions by replacing the ground-state statistical factor, $2I + 1$, for the target nucleus by the total partition function. The errors associated with this approximation were found to be less than a factor of two in the worst cases.

III. BETA-DECAY RATES

The contributions of nuclear beta decays to the flows in the reaction network have been determined. For the beta decays of the ground states of unstable nuclei, there is experimental information available in the Nuclear Data Sheets. At high temperatures, however, the nuclear excited states, populated according to the Boltzmann factors, may have much greater beta-decay rates than does the ground state.

In general, the beta-decay rate λ is given by:

$$\lambda = Xf(Z, E). \tag{3.1}$$

The Fermi function, $f(Z, E)$, is a function of the final nuclear charge Z and the energy available for this transition; it contains the phase space of the electron (or positron) and the attraction (or repulsion) of the Coulomb field. The factor X contains the dependence on the nuclear matrix elements; its order of magnitude is determined by the changes of spin and parity between the initial and final states. For "allowed" transitions, the dominant transitions for most nuclei, the selection rules require a spin change of 0 or 1 and no parity change.

The product $f(Z, E)\tau_{\frac{1}{2}}$, where $\tau_{\frac{1}{2}}$ is the half-life for the decay, provides a convenient characterization of beta decays. For allowed transitions, it has been found experimentally that values of $\log_{10}(f(Z, E)\tau_{\frac{1}{2}})$ range from $\sim$4.5 to $\sim$6. In our calculations a value of $\log_{10}(f\tau) = 5.5$ was assumed. The beta-decay rates can then be determined from

$$\lambda = [\ln 2f(Z, E)]/(f(Z, E)\tau_{\frac{1}{2}}), \tag{3.2}$$

where we have taken values of $f(Z, E)$ from the graphs in Ajzenberg-Selove (1960).

The excited states of beta-decaying nuclei were taken from the Nuclear Data Sheets. The energies, spins, and parities of both parent and daughter nuclei are presented in Table I, together with the energy available for the decay, Q, and the calculated value of the rate, λ. In some instances, the positions of the excited states had to be guessed. For even–even nuclei, the energy

TABLE I

Level energies, spins, and parities for parent and daughter nuclei, energy release, and beta-decay rates calculated for $T = 3 \times 10^9$ °K

Parent			Daughter				
	E (keV)	J^π		E (keV)	J^π	Q (keV)	λ (sec^{-1})
^{36}Cl	1 164	1+	^{36}A	0	0+	1 164	2.2×10^{-4}
^{37}A	1 420	$\frac{1}{2}$+	^{37}Cl	0	3/2+	2 234	1.5×10^{-5}
^{39}A	1 520	3/2+	^{39}K	0	3/2+	2 085	3.5×10^{-4}
^{41}Ca	2 014	(3/2+)	^{41}K	0	3/2+	2 424	3.8×10^{-5}
^{44}Sc	68	1+	^{44}Ca	0	0+	3 716	2.4×10^{-4}
	146	(0+)				3 794	2.5×10^{-4}
^{44}Ti*	(1 500)	(2+)	^{44}Sc	0	2+	1 655	7×10^{-7}
				68	1+	1 587	5.5×10^{-7}
^{48}V	418	(1+)	^{48}Ti	0	0+	4 435	1.2×10^{-3}
^{50}V*	(320)	(1+)	^{50}Cr	0	0+	1 358	7×10^{-5}
^{48}Cr*	(1 000)	(2+)	^{48}V	306	(1+)	2 094	7×10^{-5}
				416	(2+)	1 984	4.5×10^{-5}
^{51}Cr	1 167	(5/2−)	^{51}V	0	7/2−	1 919	3.5×10^{-6}
^{52}Mn	548	1+	^{52}Cr	0	0+	5 251	3×10^{-3}
^{53}Mn	1 270	5/2−	^{53}Cr	0	3/2−	1 867	2.8×10^{-6}
^{54}Mn*	(365)	(1+)	^{54}Fe	0	0+	1 047	4.5×10^{-5}
^{52}Fe*	(1 200)	(2+)	^{52}Mn	383	2+	3 198	1.5×10^{-4}
				548	1+	3 032	1.1×10^{-4}
^{56}Co*	(827)	(1+)	^{56}Fe	0	0+	4 592	1.4×10^{-3}
^{56}Ni*	(1 800)	(2+)	^{56}Co	827	(1+)	3 097	1.4×10^{-4}

*The position of the parent state had to be guessed (see text).

of the first excited state (which presumably has $J^\pi = 2^+$) was estimated by comparison with neighboring nuclei. For odd-A or odd–odd nuclei, which generally have many excited states within a few hundred keV of the ground state, it was assumed that at least one state should have an allowed beta decay to the daughter nucleus.

The nuclei ^{43}Sc, ^{45}Ti, ^{47}V, ^{49}Cr, ^{51}Mn, ^{53}Fe, and ^{55}Co are not included in Table I because their ground states decay by allowed transitions; therefore, the excited states will add little to the decay rate.

The nuclei ^{25}Al, ^{29}P, ^{33}Cl, ^{37}K, and ^{41}Sc are not included in our reaction network, and must be treated somewhat differently. They are formed by

(p, γ) reactions proceeding on stable alpha-particle nuclei—^{24}Mg, ^{28}Si, ^{32}S, ^{36}A, and ^{40}Ca. Their proton binding energies are very low (<2.5 MeV), so that the corresponding photodisintegration times are $<10^{-8}$ second at $T = 3 \times 10^9$ °K. We assume that ^{25}Al is in equilibrium with ^{24}Mg + p and compute the abundance of ^{25}Al from the equations of equilibrium. The abundances of ^{29}P, ^{33}Cl, ^{37}K, and ^{41}Sc can be determined analogously. We can then calculate the rate of formation of the product nuclei ^{25}Mg, ^{29}Si, ^{33}S, ^{37}A, and ^{41}Ca.

Thermonuclear reaction rates, particularly the nuclear photodisintegration rates, increase rapidly with temperature. In contrast, the beta-decay rates are not very sensitive to changes in the temperature. We found the beta-decay contributions at $T = 5 \times 10^9$ °K to be negligible. We have, therefore, incorporated these rates into our relaxation calculation only for the case $T = 3 \times 10^9$ °K, as given in Table I. Even at this temperature, the influence of the beta decays on the resulting abundance distributions is minor.

IV. CONDITIONS FOR NUCLEAR STATISTICAL EQUILIBRIUM

At high temperatures and densities thermonuclear reactions will proceed rapidly, and an equilibrium can be established between the various nuclear species present in the medium. An understanding of this problem is essential to an understanding of the characteristics of our nuclear reaction network. Furthermore, we employ the defining equations for the number densities in equilibrium in our determinations of photodisintegration rates.

We shall now consider briefly the conditions that must be satisfied in order that nuclear statistical equilibrium may be realized.

(i) The energy of the system must be distributed statistically among the translational states of the particles. This condition will be satisfied provided that all types of particles experience many collisions per unit time. This will restrict us to temperatures above a few billion degrees. For protons at $T_9 \sim 4$ the collision cross section $\sigma \sim 10^{-16}$ cm^2. The number of collisions per second is then given by

$$\sigma v n \sim 10^{-16} v n,$$

where v and n are the proton velocity and number density, respectively. At these temperatures $v \sim 10^9$ cm/sec. The densities in which we are interested are of the order of 10^6 g/cc and about one part in 10^6 may consist of protons. Thus, $n \sim 10^{23}$ and the number of collisions per second is approximately 10^{16}. Similarly, for neutrons at this temperature $\sigma \sim 10^{-24}$ cm^2 and the number of collisions per second is $\sim 10^8$. In either case, the number of collisions is sufficient to guarantee a Maxwellian distribution over a wide range of energy. Furthermore, the usual expressions for the thermonuclear reaction rates should be valid insofar as they depend upon a Maxwellian distribution of velocities.

(ii) Nuclear statistical equilibrium demands that there be equilibrium between matter and radiation. This is necessary to ensure detailed balancing in the emission and absorption of radiation. We have employed the condition of detailed balancing in calculating photonuclear reaction rates. For our con-

ditions, it is sufficient to require that equilibrium be established for quanta with energies large compared to kT. This can be restated as a requirement that the amount of radiant energy produced per unit time per unit volume be large compared to the energy density in the same frequency range in the Planck distribution. The main source of high-energy photon emission will be bremsstrahlung collisions of free electrons and heavy charged particles. The time required to fill the upper end of the Planck spectrum by this mechanism, a measure of the time required to attain equilibrium, is roughly 10^{-12} second at $T \sim 4 \times 10^9$ °K (Hoyle 1946). Thus the condition that there be equilibrium between matter and radiation would seem to be well satisfied.

(iii) There must be suitable nuclear reaction chains connecting all pairs of nuclei. The reaction rates for each link in the chain must be sufficient to allow nuclear transformations to take place. The primary sources of neutrons, protons, and alpha particles are photodisintegrations of the nuclear species that are present. Our study of the photodisintegration rates suggests that equilibrium will be reached for temperatures $T \gtrsim 3 \times 10^9$ °K.

(iv) A condition of equilibrium (or detailed balance) involving weak interactions is not possible, since the mean free path of neutrinos exceeds the radius of the star and they can escape without interaction. There is, however, a possible steady-state condition in which the rate of neutrino emission is equal to the rate of antineutrino emission. We shall take this as our criterion for nuclear statistical equilibrium with respect to weak interactions.

V. THE NUCLEAR REACTION NETWORK

In our calculations a nuclear-reaction network containing 70 nuclear species was employed. All proton, neutron, and alpha-particle reaction links were included. In addition, we have considered the contributions of the reactions $^{12}C + {}^{12}C$, $^{16}O + {}^{16}O$, and $3\alpha \rightleftarrows {}^{12}C$ to the flows in the network.

The basic nuclear reaction network is illustrated in Fig. 1. For mass numbers $A < 23$ only the alpha-particle nuclei, ^{12}C, ^{16}O, and ^{20}Ne, have been included. Alpha capture is favored on these nuclei; (α, p) and (α, n) reactions are endothermic by several MeV. Above ^{24}Mg the choice of the nuclei included in the network is governed by our knowledge of the thermonuclear reaction rates.

We shall now establish the equations that define the evolution of our network. The rate of change of the number density, $N(A, Z, t)$, of a particular nuclear species is given by the rate of formation minus the rate of destruction for all the reaction links connecting this nucleus to its neighbors:

$$(5.1) \quad dN(A, Z, t)/dt = N(A+1, Z, t)\lambda_n - n_n(t)N(A, Z, t)\langle\sigma v\rangle_{n,\gamma} + n_n(t)N(A, Z+1, t)\langle\sigma v\rangle_{n,p} - n_p(t)N(A, Z, t)\langle\sigma v\rangle_{p,n} + \ldots .$$

The number densities of neutrons, protons, and alpha particles are denoted by n_n, n_p, and n_α. An expression of this form can be written for each of the 70 nuclear species included in the network and for protons, neutrons, and alpha particles.

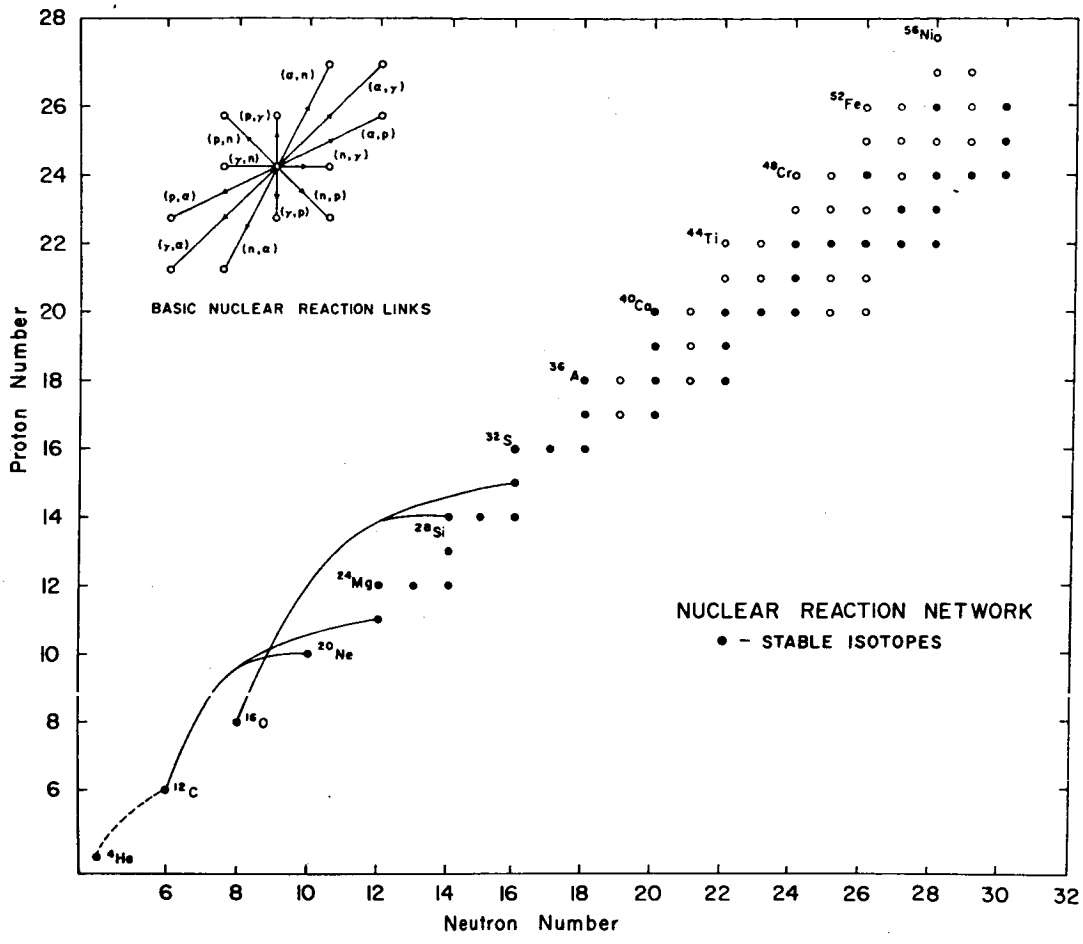

FIG. 1. Schematic of the nuclear reaction network employed in these calculations. Stable isotopes are designated by black dots; unstable isotopes by open circles.

A straightforward method of solution of these equations is available. The rates of change of the various nuclear abundances at time t can be determined from the number densities according to equation (5.1). The number densities at time $t + \Delta t$ are then given by

$$N(A, Z, t + \Delta t) = N(A, Z, t) + [\mathrm{d}N(A, Z, t)/\mathrm{d}t]\Delta t. \tag{5.2}$$

The number-density changes determined by this procedure are correct to first order only. This demands that the time intervals Δt be small compared with the typical reaction times in the network. A large amount of computing time would be required to follow the relaxation of the nuclear reaction network in this manner.

We have been able to increase the time intervals, hence to evolve the network more rapidly, by the use of the following method. We assume that the rate of change of a nuclear abundance at time t is given by the rate of change at time $t + \Delta t$:

$$\mathrm{d}N(A, Z, t)/\mathrm{d}t = [N(A + 1, Z, t) + \Delta N(A + 1, Z)]\lambda_{\mathrm{n}} - n_{\mathrm{n}}(t)[N(A, Z, t) + \Delta N(A, Z)]\langle\sigma v\rangle_{\mathrm{n},\gamma} + \ldots . \tag{5.3}$$

We have assumed that the number densities of neutrons, protons, and alpha particles are given by their values at time t. Writing the derivative in the form

$$\mathrm{d}N(A, Z, t)/\mathrm{d}t = \Delta N(A, Z)/\Delta t, \tag{5.4}$$

equations (5.3) become

$$\begin{aligned}\Delta N(A, Z)[-(1/\Delta t) - n_{\mathrm{n}}(t)\langle\sigma v\rangle_{\mathrm{n},\gamma} - n_{\mathrm{p}}(t)\langle\sigma v\rangle_{\mathrm{p,n}} + \ldots] \\ + \Delta N(A+1, Z)\lambda_{\mathrm{n}} + n_{\mathrm{n}}(t)\Delta N(A, Z+1)\langle\sigma v\rangle_{\mathrm{n,p}} + (\text{terms in other } \Delta N) \\ = N(A, Z, t)[n_{\mathrm{n}}(t)\langle\sigma v\rangle_{\mathrm{n},\gamma} + n_{\mathrm{p}}(t)\langle\sigma v\rangle_{\mathrm{p,n}} + \ldots] - N(A+1, Z, t)\lambda_{\mathrm{n}} + \ldots .\end{aligned} \tag{5.5}$$

The rates $\langle\sigma v\rangle$ and λ are a function only of the temperature. The number densities $n_{\mathrm{n}}(t)$, $N(A, Z, t)$, etc. are known from the previous time interval. If we choose a value of Δt, we are left with a system of linear equations that can be solved by matrix inversion for the number of density changes, $\Delta N(A, Z)$.

The new number densities are determined from the ΔN by

$$N(A, Z, t + \Delta t) = N(A, Z, t) + \Delta N(A, Z). \tag{5.6}$$

The number densities of neutrons, protons, and alpha particles are determined consistent with baryon conservation,

$$\begin{aligned}n_{\mathrm{n}}(t + \Delta t) = n_{\mathrm{n}}(t) + N(A+1, Z, t + \Delta t)\lambda_{\mathrm{n}} \\ - n_{\mathrm{n}}(t)N(A, Z, t + \Delta t)\langle\sigma v\rangle_{\mathrm{n},\gamma} \\ + n_{\mathrm{p}}(t)N(A, Z, t + \Delta t)\langle\sigma v\rangle_{\mathrm{p,n}} \\ - n_{\mathrm{n}}(t)N(A, Z+1, t + \Delta t)\langle\sigma v\rangle_{\mathrm{n,p}} + \ldots ,\end{aligned} \tag{5.7}$$

where all (n, γ), (p, n), and (α, n) reaction links are to be included.

This approach to the relaxation problem has allowed us to increase the time intervals typically several orders of magnitude over those demanded by the first-order method discussed previously. The value of the basic time interval Δt is generally a function both of the temperature and of the stage of evolution of the system. The photodisintegration rates are strongly temperature-sensitive, as is illustrated for ^{28}Si in Fig. 2. If we start with a region of pure silicon, the allowed time intervals are of the order of 10^{-6} of the mean lifetime for the silicon photodisintegrations.

An increase in the total flows in the network implies an increase in the numbers of neutrons, protons, and alpha particles emitted and absorbed in a time step. As the rates of emission and absorption of these particles approach equilibrium, the changes in number density will be computed as small differences between large numbers. Fluctuations in the number densities of these light particles can rapidly distort the evolution of the system. The following procedure has been incorporated, in our calculations, to ensure smooth variations in the number densities of protons, neutrons, and alpha particles.

We denote the total number of alpha particles emitted and absorbed in an interval by E and A respectively. (Analogous arguments can be employed for protons and neutrons.) The increase in the alpha-particle number density

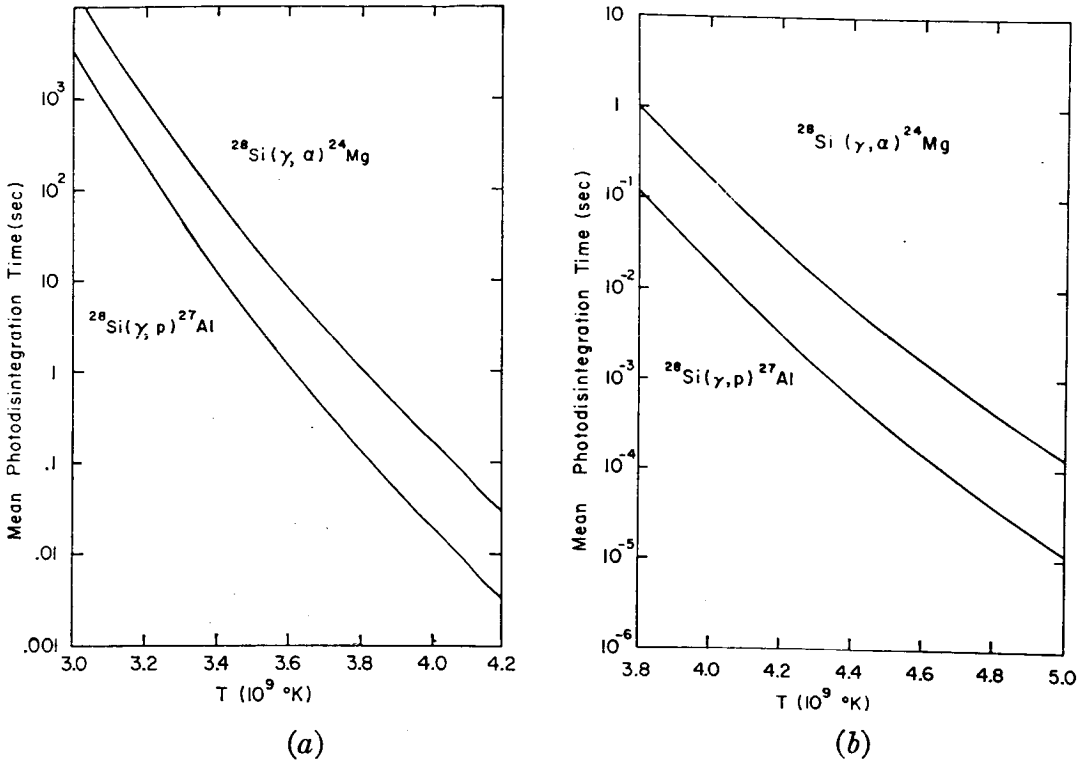

FIG. 2. The photodisintegration rates of ^{28}Si for protons and alpha particles plotted as a function of temperature. These results have been calculated as a sum over resonances for which the parameters are known.

in this interval is given by the difference, $E - A$. This establishes for this interval an excess of particles—a reservoir from which we wish to feed alpha particles smoothly into the system in the succeeding time step. The new alpha-particle number density is then given by

$$n_\alpha(t + \Delta t) = [(X(t) + E)/A]n_\alpha(t), \tag{6.1}$$

where the "excess"

$$X(t) = X(t - \Delta t) + E - A. \tag{6.2}$$

This expression demands that the new alpha-particle number density be sufficient both to maintain equilibrium in the next time interval between the rates of emission and absorption of alpha particles and to "absorb" the previously accumulated excess. It is evident that this approximation will be reasonable only when the rates of emission and absorption are closely in balance. If the excess is adjusted as particles are fed into the system, this procedure is strictly baryon-conserving.

Proceeding in the manner described above, we were able to follow the time evolution of the network. Attempts to extrapolate the number densities over long time intervals, based on the observed behavior of the system, were not successful. This was due to the difficulties associated with extrapolations of proton, neutron, and alpha-particle number densities. Slight errors in the extrapolated values were found to result in pronounced oscillations of the system, rendering the subsequent evolution untrustworthy.

VI. THE APPROACH TO EQUILIBRIUM

Assuming that the carbon- and oxygen-burning stages have gone to completion, the products ^{24}Mg, ^{28}Si, and ^{32}S should be the main components of the stellar core. ^{28}Si, having the largest separation energies for protons and alpha particles, is expected to be the major constituent of the medium for temperatures $T \sim 2$–3×10^9 °K. A further increase in the temperature will result in the photodisintegration of ^{28}Si into protons and alpha particles. These photodisintegration rates are plotted as a function of temperature in Fig. 2 (*a*) and (*b*).

Employing the nuclear reaction network defined in Section V, we have followed the thermonuclear processing of a region composed initially of pure ^{28}Si at temperatures $T = 3$ and 5×10^9 °K. The early stages of this evolution at $T_9 = 5$ are displayed in Fig. 3. The photodisintegration of silicon to alpha particles results in a rapid buildup of the products ^{24}Mg, ^{20}Ne, and ^{16}O. The subsequent capture of alpha particles on silicon in these early stages leads to a rapid rise in the abundance of ^{32}S. ^{12}C increases slowly in abundance

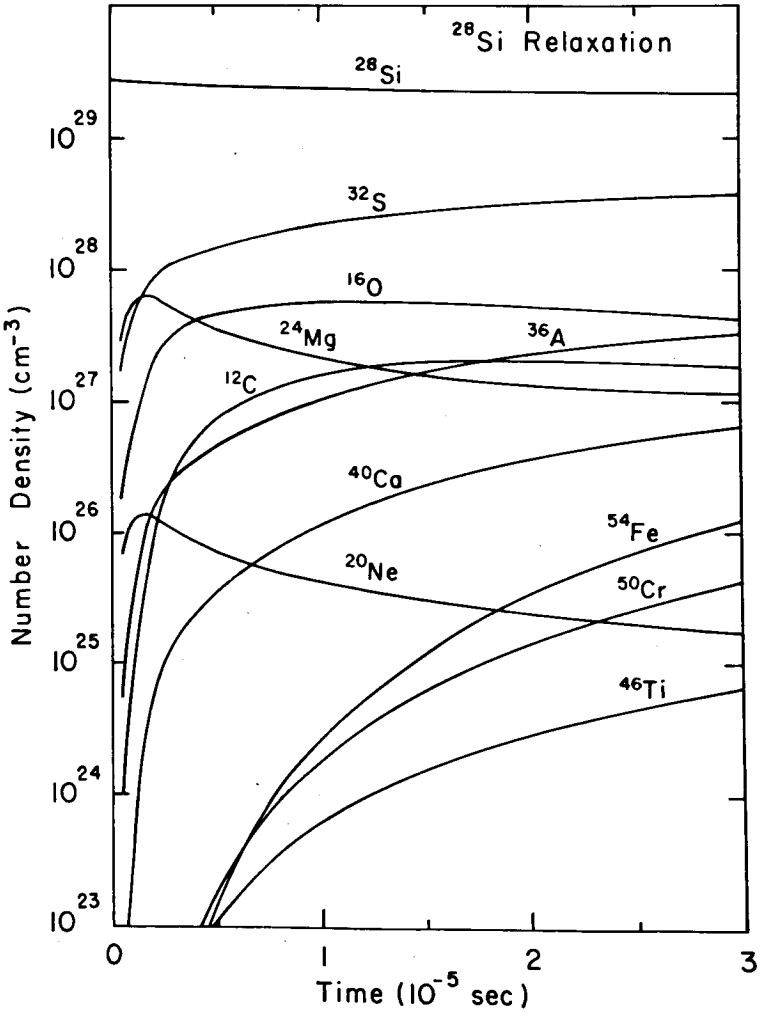

FIG. 3. The early stages of evolution of a region composed initially of pure ^{28}Si at a temperature $T_9 = 5$.

because of the relatively low value of the rate for $^{16}O(\gamma, \alpha)^{12}C$. As the rate of photodisintegration of silicon to protons is roughly an order of magnitude lower than the alpha-particle photodisintegration rate, the products ^{27}Al and ^{23}Na are produced in somewhat lower abundance. The alpha-particle nuclei are generally the most abundant products in their respective mass ranges through ^{40}Ca.

Figures 4 and 5 show the late stages of evolution of this silicon region. As the alpha-chain nuclei come into relative equilibrium with silicon, their abundances tend to decrease at a rate comparable with the rate of decrease of silicon. Our calculations were carried to the point at which computer

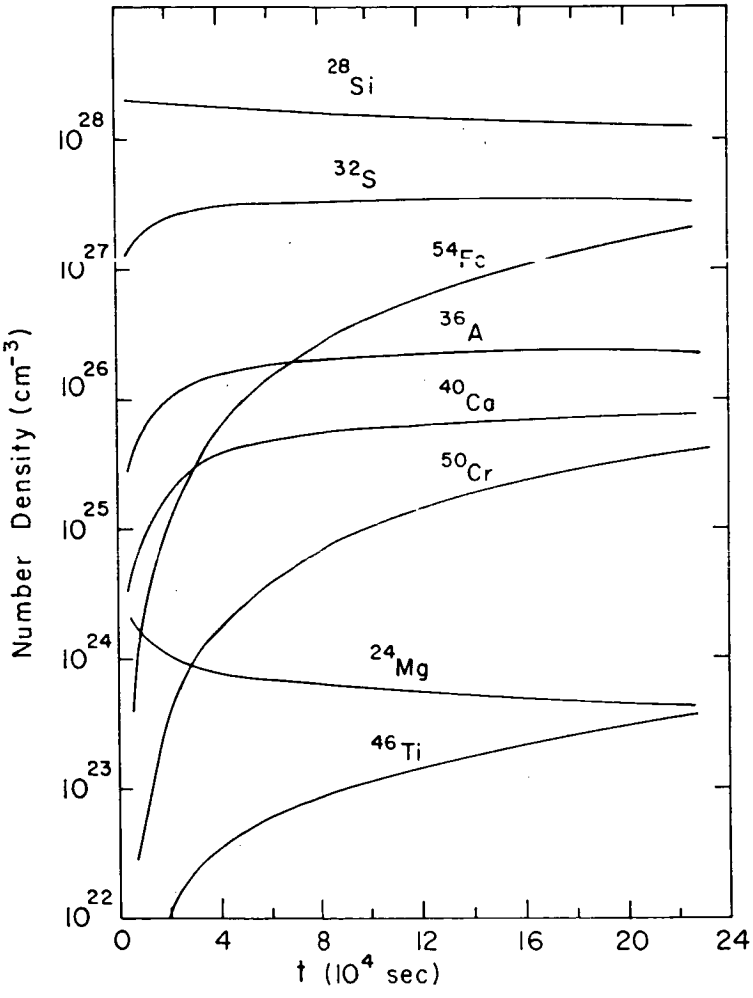

FIG. 4. The evolution of a region composed initially of pure ^{28}Si at a temperature $T_9=3$.

round-off errors rendered further results unreliable at about the 1% level of uncertainty. In both cases, the time scales of decrease of ^{28}Si are considerably longer than the nuclear photodisintegration times ($\lambda^{-1} \sim 1.4 \times 10^{-4}$, $T_9 = 5$; $\lambda^{-1} \sim 3 \times 10^3$, $T_9 = 3$).

The buildup of ^{24}Mg and ^{27}Al towards an effective equilibrium with ^{28}Si results in a decrease in the net rate of destruction of silicon. That is, as the

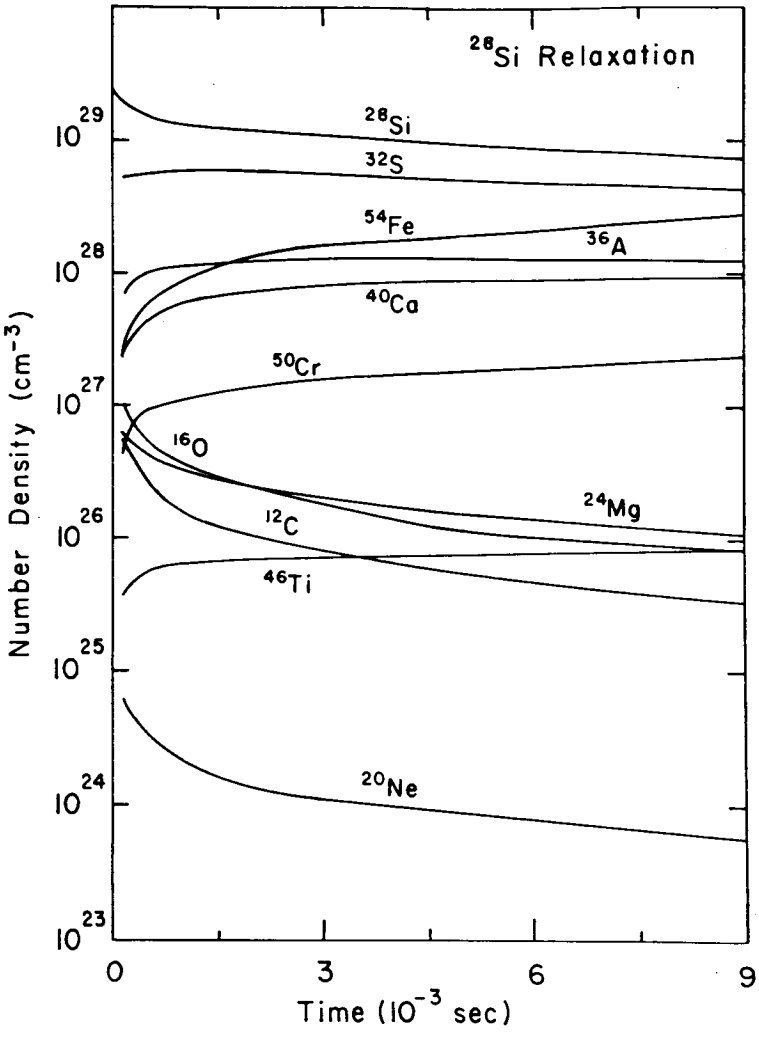

FIG. 5. The late stages of evolution for $T_9 = 5$.

rate of ^{24}Mg$(\alpha, \gamma)^{28}$Si becomes comparable with that of ^{28}Si$(\gamma, \alpha)^{24}$Mg, the net flow from silicon to ^{24}Mg will decrease. A measure of the effective rate of destruction of silicon is the ratio of the net flow down the chain from silicon to the total photodisintegration rate of silicon to form protons and alpha particles. These ratios are plotted in Figs. 6 and 7 as a function of the fraction of the initial silicon remaining in the medium.

The ratio of the net flow to the total photodisintegration rate is seen to decrease as the abundance of silicon decreases in time. This is a measure of the degree to which the forward and inverse reaction rates have come into equilibrium. The smoothness of this curve suggests that we might predict roughly the future behavior of the relaxation by an extrapolation of this dependence.

The dominant flows in the network are shown in Fig. 8. These flows generally support the arguments presented in this section. The net flow down the chain from ^{28}Si to alpha particles is evident in this picture. The flow from ^{12}C to alpha particles proceeds very slowly, owing to the slow rate of the

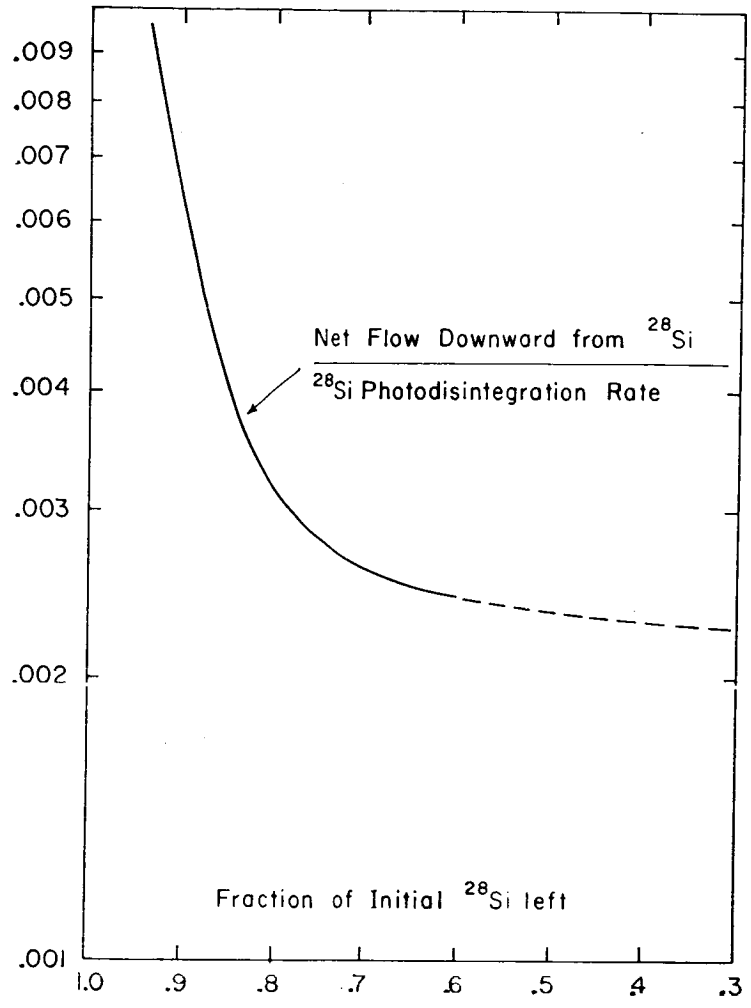

FIG. 6. The ratio of the net downward flow from ^{28}Si to the total ^{28}Si photodisintegration rate plotted as a function of the fraction of the initial ^{28}Si remaining in the medium for $T_9 = 3$.

$^{12}C(\gamma, 3\alpha)$ reaction. An equilibrium between ^{12}C and α particles is not established on the time scale of this relaxation. Above ^{28}Si the alpha-particle links contribute appreciably to the evolution through ^{36}A. Beyond this point (α,p), (p, γ), and (p, n) reactions carry the major flow toward the iron region.

The abundance distributions as a function of mass number at the end of our relaxation calculations are shown in Figs. 9 and 10. The general features of these distributions can be understood in terms of the nuclear-reaction-rate properties. The high abundances of protons and alpha particles at $T = 5 \times 10^9$ °K are the result of the rapid photodisintegration rates at these temperatures. This has resulted, as well, in relatively larger abundances of the alpha-particle nuclei below silicon. The break in the alpha-particle chain past ^{40}Ca, resulting in the production of the $\alpha + 2n$ nuclei ^{46}Ti, ^{50}Cr, and ^{54}Fe, is evident in both distributions. However, the strong peaking at these mass numbers ($A = 46$, 50, and 54) at 3×10^9 °K is not apparent at 5×10^9 °K, because of the fact that at the higher temperatures many more reaction links are providing significant contributions to the flows.

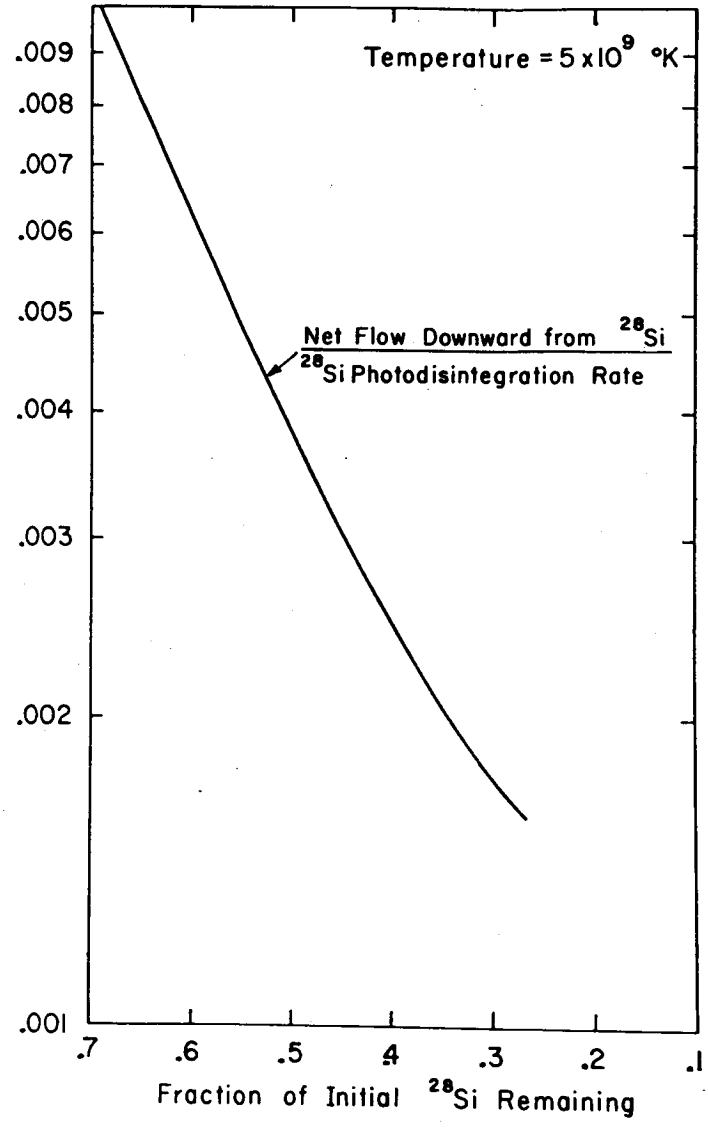

FIG. 7. The ratio of the net downward flow from ^{28}Si to the total ^{28}Si photodisintegration rate plotted as a function of the fraction of the initial ^{28}Si remaining in the medium for $T_9 = 5$.

VII. DISCUSSION OF RESULTS AND CONCLUSIONS

The results of these calculations have important implications regarding nucleosynthesis.

1. The governing rate for the silicon-to-iron conversion is the effective loss rate of ^{28}Si. This means that the time required for the silicon-to-iron conversion is not a sensitive function of the density. The buildup of nuclei in the vicinity of ^{28}Si results in the establishment of flows in opposition to the downward flows from silicon. As these abundances approach an equilibrium, the net flows out of ^{28}Si will decrease; hence the net rate of depletion of ^{28}Si will decrease. The ratios of the net flow downward from ^{28}Si to the total ^{28}Si photodisintegration rate (the sum of the proton and alpha-particle photodisintegration rates) are shown in Figs. 6 and 7 for the temperatures $T_9 = 3$ and 5, respectively.

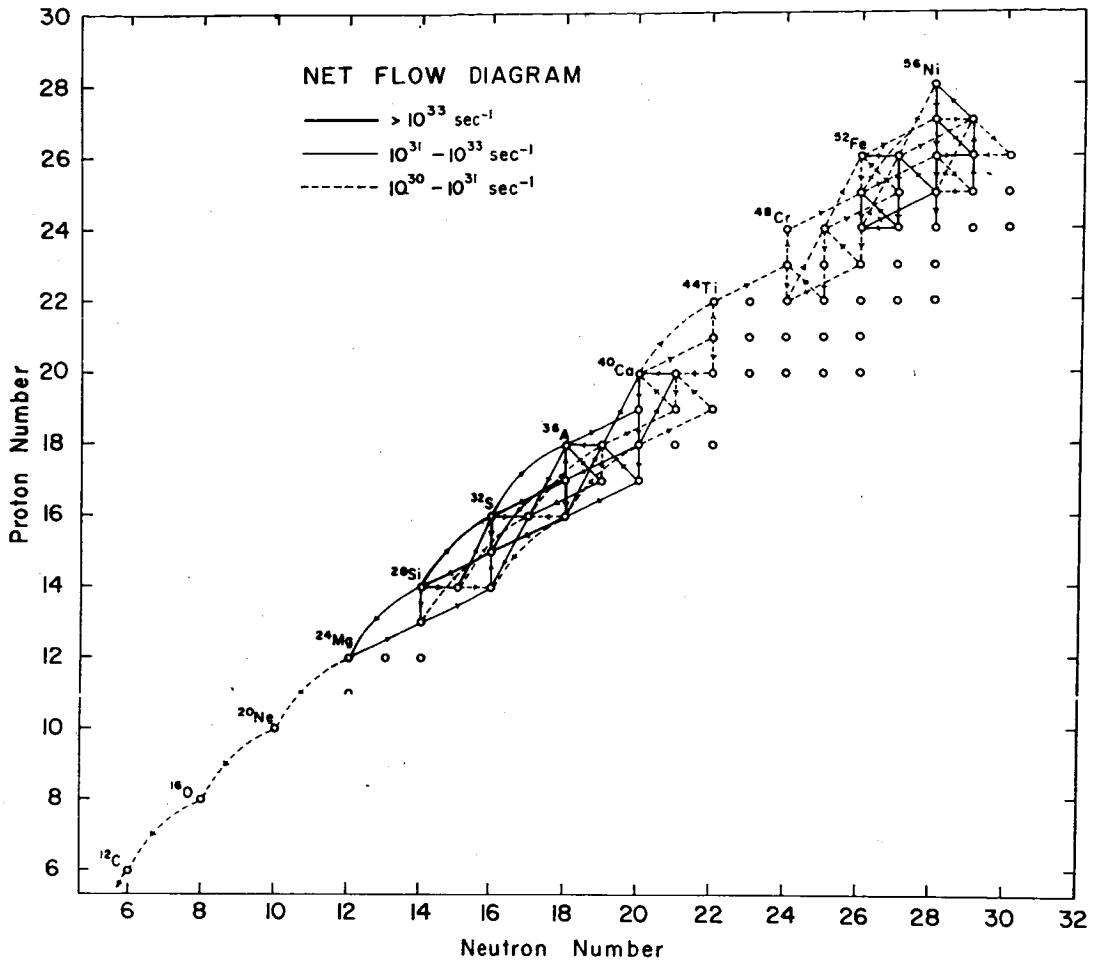

FIG. 8. The dominant net flows in the network are illustrated. The break in the alpha-particle chain past ^{44}Ti is evident in this diagram.

These figures differ somewhat because of the different character of the flows at the two temperatures. A reasonable generalization of these two cases might be that over a rather large range in the silicon abundance this ratio is typically 10^{-3} to 10^{-2}. This means that the time required for the ^{28}Si abundance to decrease to one half its initial value is roughly 100 to 1 000 times the photodisintegration half-life. This should allow a crude estimate of the time scale for the conversion of ^{28}Si to iron at a different temperature. The total ^{28}Si photodisintegration rate, taken to be the sum of the rates for (γ, p) and (γ, α) reactions, follows directly from the fitted values of $\langle \sigma v \rangle$ given in the Appendix and the equations of nuclear statistical equilibrium:

$$(7.1) \qquad \lambda = \lambda_p + \lambda_\alpha$$

$$= 1.13 \times 10^{10} \exp\left(18.18 - \frac{7.85}{T_9^{1/3}} - \frac{139.45}{T_9}\right)$$

$$+ 7.54 \times 10^{10} \exp\left(21.68 - \frac{21.77}{T_9^{1/3}} - \frac{121.73}{T_9}\right) \text{sec}^{-1}.$$

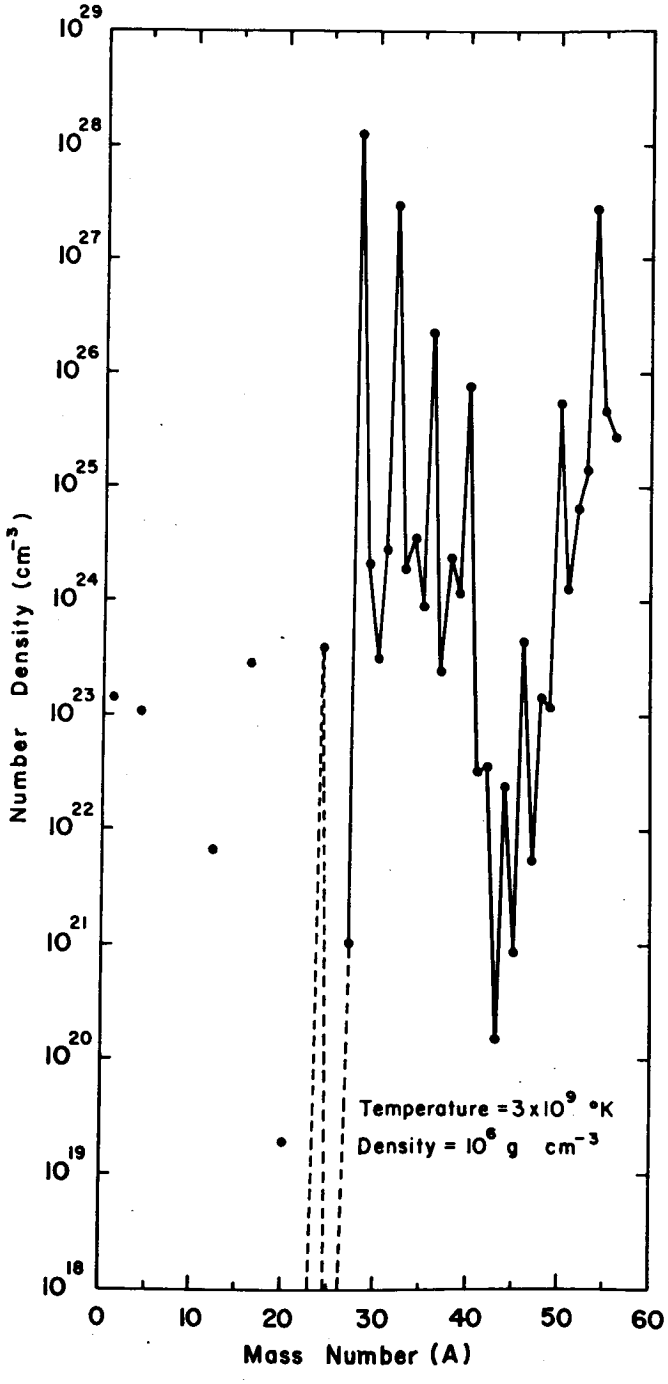

FIG. 9. The abundance distribution as a function of mass number at the end of the relaxation for $T = 3 \times 10^9$ °K.

2. Above ^{40}Ca, the most abundant nuclei (^{46}Ti, ^{50}Cr, ^{54}Fe) do not have equal numbers of neutrons and protons. This is not because of beta decay; such processes are quite ineffective, simply because beta-unstable nuclei do not build up to high enough abundances during the time scale of the relaxations considered here. It is, rather, a question of which reactions are energetically favorable.

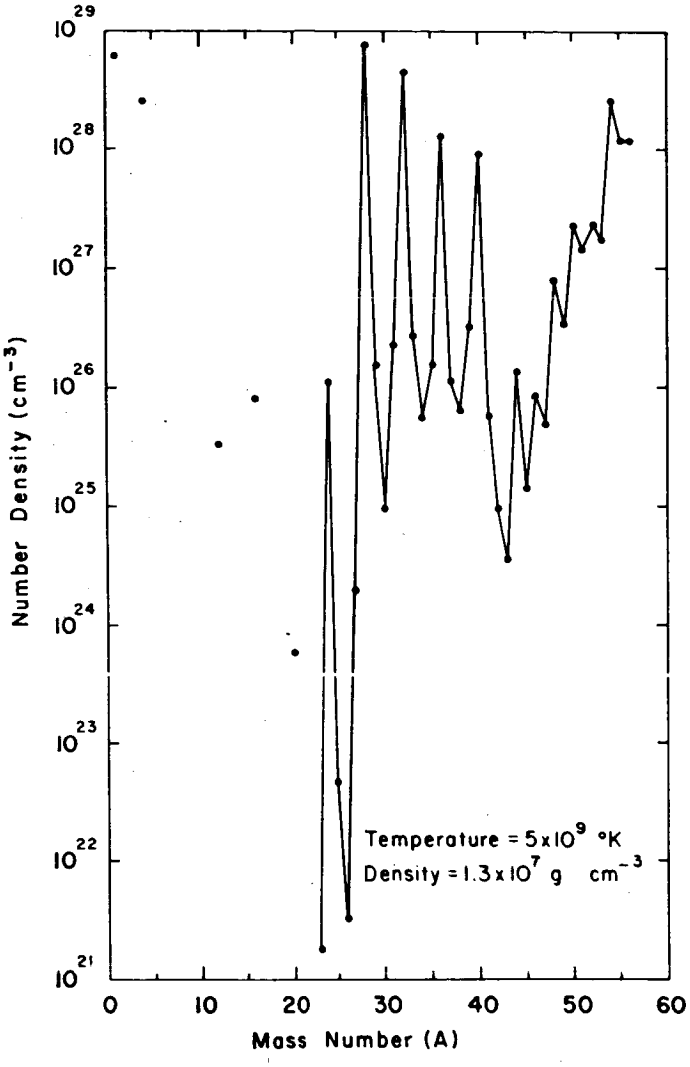

FIG. 10. The abundance distribution as a function of mass number at the end of the relaxation for $T = 5 \times 10^9$ °K.

Fowler and Hoyle (1964) have suggested a crude model in which ^{28}Si photodisintegrates by (γ, α) and captures the α particles to build nuclei with $N = Z$ up to ^{56}Ni. The present results suggest that this model is unrealistic; for instance, at $T_9 = 3$, ^{54}Fe is more abundant than any other nucleus with $A > 52$ by about two orders of magnitude. This becomes even clearer when the actual reaction rates across the various links in the network are considered, as has been illustrated in the diagram of the net flows (Fig. 8). Above ^{40}Ca it was found that the alpha-particle links did not carry the major flows. This can be explained by the rapid decrease of alpha penetrabilities with Z, at a given energy.

3. ^{54}Fe is the most abundant nucleus produced in the iron region. In the virtual absence of beta decays, this means that the overall reaction is not $2^{28}\text{Si} \rightarrow {}^{56}\text{Ni}$, which releases about 10 MeV per reaction, but $2^{28}\text{Si} \rightarrow {}^{54}\text{Fe} + 2\text{p}$,

which is actually endoenergetic by 1.3 MeV. The implication is that there is no exoenergetic reaction phase; nuclear reactions involved in the approach to equilibrium do not slow down the collapse of a star brought on by neutrino emission. The exact energy release depends somewhat on the composition of the material in the iron region, but if ^{54}Fe is the most abundant nucleus, the Si–Fe conversion can not be exothermic by much, if at all, and beta decays will not help the situation. It is true that if an electron or a positron is emitted it carries some of the energy release of the beta decay. However, there is also electron capture, which becomes important at high density. In fact, even normally stable nuclei can capture electrons when the electron Fermi energy becomes high. Fowler and Hoyle (1964) give a half-life of 4×10^4 seconds for electron capture at a temperature of 3.8×10^9 °K and a density of 3.1×10^6 g cm^{-3}. In this kind of reaction, the entire energy release goes into neutrinos.

4. It is evident that the iron peak observed in nature, centered on ^{56}Fe, cannot result from our calculations. However, the transformation of protons to neutrons at an early stage of this relaxation would result in the production of increased amounts of neutron-rich isotopes of the elements in the iron region.

Chiu (1965) has studied the presupernova stage of the evolution of a star in some detail. He finds that such stars will evolve to a high central density ($\rho \sim 10^{9\text{–}10}$ g cm^{-3}) at a central temperature $T \sim 3\text{–}4 \times 10^9$ °K. At these densities, electron capture on nuclei will proceed rapidly. In particular, the electron capture rates for ^{32}S and ^{32}P are $>10^{-1}$ sec^{-1}. In times of the order of 100 seconds, an appreciable amount of ^{32}S can be converted through ^{32}P to ^{32}Si. The processing of a region composed of ^{28}Si and a substantial amount of ^{32}Si by a shock wave of peak temperature $\sim 5 \times 10^9$ °K might result in the formation of an iron-abundance peak centered on ^{56}Fe.

5. The relaxation at 5×10^9 °K resulted in the production of large amounts of iron-peak nuclei ($\gtrsim$20% by mass) in $\sim 10^{-2}$ second. This is approximately the time for which the post-shock-wave temperature predicted by the model of Colgate *et al.* (1961) will remain $\gtrsim 5 \times 10^9$ °K. It is evident, therefore, that significant amounts of iron can be produced by the passage of the shock through a silicon region. A more detailed consideration of element formation in supernova shock waves will be presented in a future paper.

6. We were not able to follow the approach to equilibrium through its final stages in these calculations because of the accumulation of computer round-off errors. Several attempts were made, with little success, to extrapolate forward over long time intervals. The observation that ^{12}C is far out of equilibrium with respect to alpha particles, owing to the slow rate for the reaction $^{12}\text{C} \rightarrow 3\alpha$, provides a clue to what might perhaps be a better means of extrapolation.

In general, the abundance of a given nuclear species, i, in equilibrium is related to the number densities of free protons and neutrons by an equation of the form

$$N_i(A_i, Z_i) = n_n^{A_i - Z_i} n_p^{Z_i} f_i(T), \tag{7.2}$$

where A_i is the mass number, Z_i is the proton number, n_n and n_p are the free neutron and proton number densities, and $f_i(T)$ is a function of temperature alone for a specified nuclear species. In our calculations, an equilibrium between ^{12}C and alpha particles is not established on the time scale of the relaxations. However, the reactions involving the other nuclear constituents proceed rapidly, and the abundances of these nuclei should be in equilibrium with respect to the abundances of carbon, protons, and neutrons. For each of the 69 nuclei other than carbon we can then write the abundance in the form:

$$N_i(A_i, Z_i) = N(^{12}C)n_n^{A-Z-6}n_p^{Z-6}f_i(T). \tag{7.3}$$

The alpha-particle number density corresponds to equilibrium with neutrons and protons and is given by

$$n_\alpha = n_p^2 n_n^2 f_\alpha(T). \tag{7.4}$$

There are two further conditions to be imposed: mass conservation

$$n_n + n_p + 4n_\alpha + 12N(^{12}C) + \sum_i A_i N_i(A_i, Z_i) = N_0\rho, \tag{7.5}$$

where N_0 is Avogadro's number and ρ is the density, and the equality of the total numbers of protons and neutrons (demanded by an initial configuration of pure ^{28}Si in the absence of beta decays)

$$n_p + \sum_i Z_i N_i(A_i, Z_i) = n_n + \sum_i (A_i - Z_i)N_i(A_i, Z_i). \tag{7.6}$$

For a given temperature and density, equations (7.3), (7.4), (7.5), and (7.6) constitute 72 equations in 73 unknowns (n_n, n_p, n_α, the 69 $N_i(A_i, Z_i)$, and $N(^{12}C)$). These equations can be solved numerically for a specified value of $N(^{12}C)$. Assuming that the abundance of carbon varies smoothly in time, we can correlate the abundances determined in this manner, for an extrapolated ^{28}Si abundance, with the time, and follow the relaxation through to completion.

APPENDIX

For convenience in computing, both the reaction rates and the nuclear partition functions have been fitted to simple analytic expressions. The reaction rates are given as a function of temperature by

$$\omega_T\langle\sigma v\rangle = \exp\left(F_1 + \frac{F_2}{T_9^{1/3}} + \frac{F_3}{T_9}\right) \Big/ T_9^{3/2},$$

where ω_T is the nuclear partition function of the target nucleus and T_9 is the temperature in units of 10^9 °K. The fitting parameters F_1, F_2, and F_3 are presented in Table A.I together with the reaction Q value in MeV. This fitting form is accurate to a few percent over a range in temperature $1 \leqslant T_9 \leqslant 9$.

TABLE A.I

Reaction-rate fitting parameters

Target	Z, A	Reaction	$F1$	$F2$	$F3$	Q
6	12	(α, γ)	28.886	−44.288	2.685	7.148
8	16	(α, γ)	19.130	−29.163	5.266	4.730
10	20	(α, p)	20.800	−6.235	−32.278	−2.379
10	20	(α, γ)	20.949	−14.920	−10.388	9.314
11	23	(p, γ)	20.615	−12.223	−1.465	11.693
11	23	(α, p)	35.117	−31.057	−8.606	1.826
11	23	(α, γ)	26.452	−24.313	−10.081	10.098
12	24	(n, γ)	22.756	−13.717	2.219	7.331
12	24	(α, p)	25.140	−12.250	−25.717	−1.595
12	24	(α, γ)	21.678	−21.768	−5.992	9.986
12	25	(n, γ)	23.386	−11.347	2.266	11.101
12	25	(α, n)	36.293	−33.427	−8.869	2.655
12	25	(α, γ)	32.173	−38.069	−5.862	11.133
12	26	(p, γ)	24.917	−19.473	4.189	8.272
12	26	(α, n)	36.448	−36.189	−8.008	0.036
12	26	(α, γ)	31.857	−41.370	−4.561	10.646
13	27	(p, γ)	18.887	−7.846	−4.991	11.581
13	27	(α, p)	35.852	−33.833	−9.887	2.378
13	27	(α, γ)	29.939	−31.511	−10.038	9.664
14	28	(n, γ)	22.950	−13.639	2.215	8.478
14	28	(α, p)	24.302	−11.015	−31.673	−1.917
14	28	(α, γ)	22.272	−19.278	−14.563	6.946
14	29	(n, γ)	23.364	−12.410	1.659	10.610
14	29	(α, n)	36.965	−37.339	−10.903	−1.532
14	29	(α, γ)	33.244	−43.245	−1.821	7.110
14	30	(p, γ)	20.559	−12.761	−1.038	7.286
14	30	(α, n)	31.606	−21.709	−34.279	−3.504
14	30	(α, γ)	21.324	−15.280	−17.490	7.917
15	31	(p, γ)	22.786	−14.760	−1.653	8.862
15	31	(α, p)	38.135	−40.580	−10.080	0.631
15	31	(α, γ)	33.391	−43.095	−7.331	6.998
16	32	(n, γ)	23.606	−13.395	3.308	8.642
16	32	(α, p)	37.300	−39.335	−16.679	−1.866
16	32	(α, γ)	22.241	−23.386	−13.904	6.640
16	33	(n, γ)	23.949	−11.983	2.657	11.421
16	33	(α, p)	37.696	−37.433	−21.051	−1.931
16	33	(α, n)	36.823	−37.591	−14.891	−2.002
16	33	(α, γ)	28.291	−31.839	−10.221	6.792
16	34	(p, γ)	24.324	−18.557	−0.554	6.367
16	34	(α, p)	32.231	−27.244	−34.693	−3.030
16	34	(α, n)	29.874	−16.699	−50.131	−4.628
16	34	(α, γ)	23.172	−20.148	−17.953	7.213
17	35	(n, γ)	26.931	−16.562	5.266	8.577
17	35	(p, γ)	23.349	−15.318	−1.982	8.506
17	35	(α, p)	38.159	−41.075	−12.437	0.846
17	35	(α, γ)	30.977	−35.694	−13.002	7.213
17	36	(n, γ)	25.221	−13.187	2.818	10.322
17	36	(p, n)	33.513	−23.284	−2.692	−0.071
17	36	(p, γ)	26.018	−20.281	−1.564	8.723
17	36	(α, p)	40.911	−46.569	−14.562	−1.146
17	36	(α, n)	40.807	−45.855	−10.006	−1.364
17	36	(α, γ)	42.160	−63.784	3.176	6.434
17	37	(p, n)	31.944	−16.718	−15.134	−1.598
17	37	(p, γ)	22.502	−12.255	−4.366	10.243
17	37	(α, p)	35.538	−35.967	−18.691	−1.592
17	37	(α, n)	34.406	−26.755	−36.964	−3.888
17	37	(α, γ)	25.812	−22.913	−18.090	6.208
18	36	(n, γ)	22.028	−10.574	0.671	8.794
18	36	(α, p)	40.161	−47.669	−11.874	− 1.292

TABLE A.I (*continued*)

Target	*Z*, *A*	Reaction	*F*1	*F*2	*F*3	*Q*
18	36	(α, γ)	35.519	−56.702	2.335	7.044
18	37	(n, γ)	24.340	−13.007	2.195	11.841
18	37	(α, p)	39.315	−42.138	−22.793	−2.289
18	37	(α, n)	39.388	−44.208	−12.751	−1.750
18	37	(α, γ)	34.996	−47.394	−5.377	6.610
18	38	(n, γ)	24.426	−16.749	3.637	6.585
18	38	(p, γ)	25.160	−19.954	−0.944	6.367
18	38	(α, p)	33.658	−30.385	−45.966	−4.035
18	38	(α, n)	30.354	−16.868	−56.559	−5.231
18	38	(α, γ)	26.852	−26.238	−18.897	6.241
18	39	(n, γ)	26.324	−15.171	3.897	9.875
18	39	(p, n)	35.381	−26.114	−1.995	−0.218
18	39	(p, γ)	28.662	−24.400	0.741	7.580
18	39	(α, n)	39.819	−44.700	−12.053	−0.344
18	39	(α, γ)	39.104	−49.648	−8.727	7.586
18	40	(p, n)	30.660	−17.806	−22.305	−2.296
18	40	(p, γ)	23.572	−14.025	−4.718	7.800
18	40	(α, n)	37.875	−42.880	−16.799	−2.289
18	40	(α, γ)	30.801	−35.946	−13.065	8.847
19	39	(n, γ)	24.944	−13.425	3.828	7.798
19	39	(p, γ)	23.903	−16.507	−2.292	8.336
19	39	(α, p)	39.951	−46.127	−12.716	−0.126
19	39	(α, γ)	34.998	−43.839	−11.094	4.801
19	40	(n, γ)	26.152	−13.710	3.385	10.096
19	40	(p, n)	33.851	−25.340	−2.328	0.539
19	40	(p, γ)	27.221	−19.251	−2.324	8.899
19	40	(α, p)	43.114	−53.061	−8.162	0.006
19	40	(α, n)	38.698	−39.595	−23.649	−2.997
19	40	(α, γ)	45.510	−67.030	0.955	6.711
19	41	(p, n)	33.891	−23.189	−8.514	−1.196
19	41	(p, γ)	26.249	−18.540	−2.642	10.276
19	41	(α, p)	40.615	−50.470	−8.941	1.047
19	41	(α, n)	37.310	−35.844	−28.683	−3.384
19	41	(α, γ)	42.878	−58.180	−4.525	7.936
20	40	(n, γ)	24.209	−13.535	3.385	8.360
20	40	(α, p)	34.860	−32.672	−40.935	−3.535
20	40	(α, γ)	28.423	−30.598	−19.478	5.235
20	41	(n, γ)	26.657	−13.633	2.737	11.472
20	41	(α, p)	38.687	−40.708	−24.913	−2.188
20	41	(α, n)	36.919	−38.493	−25.183	−3.126
20	41	(α, γ)	34.206	−38.990	−14.782	6.290
20	42	(n, γ)	27.332	−18.498	5.682	7.930
20	42	(p, γ)	26.893	−23.329	−0.366	4.927
20	42	(α, p)	35.214	−36.768	−28.873	−2.341
20	42	(α, n)	31.452	−22.557	−53.207	−5.182
20	42	(α, γ)	32.546	−38.083	−16.013	8.008
20	43	(n, γ)	27.196	−14.004	3.443	11.136
20	43	(p, n)	31.610	−12.707	−33.277	−3.003
20	43	(p, γ)	27.586	−17.265	−4.467	6.705
20	43	(α, p)	40.984	−45.638	−19.867	−1.504
20	43	(α, n)	41.189	−49.292	−11.683	0.079
20	43	(α, γ)	43.166	−58.931	−5.006	8.966
20	44	(n, γ)	27.479	−19.555	4.908	7.420
20	44	(p, n)	30.025	−11.635	−49.970	−4.431
20	44	(p, γ)	28.944	−23.210	−1.951	6.889
20	44	(α, p)	40.085	−49.242	−24.342	−1.993
20	44	(α, n)	40.829	−50.019	−13.346	−2.170
20	44	(α, γ)	46.458	−72.229	3.870	9.450
20	45	(n, γ)	28.420	−16.389	3.727	10.400
20	45	(p, n)	36.581	−28.348	−2.143	−0.531
20	45	(p, γ)	36.711	−39.666	5.215	8.236
20	45	(α, n)	41.454	−48.636	−12.316	2.030

TABLE A.I (*continued*)

Target	Z, A	Reaction	$F1$	$F2$	$F3$	Q
20	45	(α, γ)	44.420	−59.274	−6.643	10.177
20	46	(p, n)	32.571	−22.435	−18.944	−2.165
20	46	(p, γ)	28.293	−19.825	−4.454	8.482
20	46	(α, n)	41.549	−51.914	−10.994	−0.223
20	46	(α, γ)	44.731	−65.673	−4.857	10.720
21	43	(n, γ)	28.573	−15.579	3.035	9.708
21	43	(p, γ)	28.466	−20.224	−3.286	8.770
21	43	(α, p)	41.136	−48.967	−13.660	3.082
21	43	(α, γ)	42.903	−54.515	−10.840	8.274
21	44	(n, γ)	29.930	−16.414	3.654	11.320
21	44	(p, n)	33.918	−24.704	−5.844	−0.938
21	44	(p, γ)	29.170	−22.507	−2.039	8.478
21	44	(α, p)	43.482	−54.142	−10.848	2.260
21	44	(α, n)	43.303	−53.835	−11.796	−1.435
21	44	(α, γ)	47.289	−66.163	−6.007	9.081
21	45	(n, γ)	28.042	−14.061	3.960	8.767
21	45	(p, n)	31.873	−13.952	−29.380	−2.841
21	45	(p, γ)	28.999	−17.889	−5.749	10.349
21	45	(α, p)	42.956	−56.445	−8.536	2.561
21	45	(α, n)	43.206	−51.564	−14.174	−2.239
21	45	(α, γ)	48.971	−71.721	0.450	9.314
21	46	(n, γ)	29.573	−15.399	4.897	10.647
21	46	(p, n)	34.499	−26.056	−3.303	1.583
21	46	(p, γ)	31.758	−23.904	−3.317	10.470
21	46	(α, p)	43.330	−54.256	−11.834	1.942
21	46	(α, n)	43.431	−53.413	−11.244	0.548
21	46	(α, γ)	47.333	−65.657	−7.068	9.885
21	47	(p, n)	36.643	−28.850	−2.347	−0.177
21	47	(p, γ)	36.540	−37.522	3.532	11.443
21	47	(α, p)	42.722	−52.655	−11.609	2.232
21	47	(α, n)	43.594	−53.878	−11.630	−0.763
21	47	(α, γ)	46.519	−63.375	−7.076	10.276
22	44	(n, γ)	25.334	−13.268	3.131	9.416
22	44	(α, p)	41.414	−53.304	−13.537	−0.497
22	44	(α, γ)	42.985	−66.003	−2.615	7.840
22	45	(n, γ)	29.571	−15.346	4.398	13.190
22	45	(α, p)	44.584	−56.112	−11.421	0.602
22	45	(α, n)	42.854	−55.564	−12.128	−1.578
22	45	(α, γ)	48.078	−69.704	−3.986	8.812
22	46	(n, γ)	27.295	−16.193	3.236	8.887
22	46	(p, γ)	30.080	−27.226	−0.462	5.192
22	46	(α, p)	41.293	−54.090	−14.195	−1.035
22	46	(α, n)	34.906	−33.793	−39.787	−4.378
22	46	(α, γ)	39.990	−58.221	−6.606	8.556
22	47	(n, γ)	28.494	−14.579	4.464	11.620
22	47	(p, n)	31.841	−13.694	−40.058	−3.695
22	47	(p, γ)	30.070	−20.843	−4.516	6.821
22	47	(α, p)	43.863	−56.021	−13.494	−0.585
22	47	(α, n)	42.571	−52.910	−12.905	−0.330
22	47	(α, γ)	46.689	−65.894	−5.159	8.919
22	48	(n, γ)	27.585	−17.711	3.995	8.147
22	48	(p, n)	30.698	−14.745	−53.345	−4.800
22	48	(p, γ)	29.909	−24.772	−2.526	6.753
22	48	(α, p)	43.512	−59.574	−12.582	−1.166
22	48	(α, n)	40.895	−50.971	−17.189	−2.701
22	48	(α, γ)	45.627	−71.632	1.257	9.350
22	49	(n, γ)	28.187	−15.201	3.400	10.943
22	49	(p, n)	35.150	−24.503	−8.837	−1.394
22	49	(p, γ)	32.025	−28.344	1.084	7.943
22	49	(α, n)	41.977	−50.744	−13.913	1.203
22	49	(α, γ)	43.400	−57.467	−10.545	9.146
22	50	(p, n)	32.579	−16.856	−29.983	−2.995
22	50	(p, γ)	30.736	−21.622	−4.430	8.044

TABLE A.I (*continued*)

Target	Z, A	Reaction	F1	F2	F3	Q
22	50	(α, n)	42.779	−55.509	−11.880	−1.792
22	50	(α, γ)	48.539	−77.661	1.879	7.930
23	47	(n, γ)	30.030	−16.588	4.432	10.516
23	47	(p, γ)	29.438	−21.618	−4.114	8.337
23	47	(α, p)	42.673	−53.592	−13.834	3.360
23	47	(α, γ)	44.452	−59.824	−10.916	8.650
23	48	(n, γ)	29.657	−14.509	2.750	11.553
23	48	(p, n)	33.447	−24.253	−18.726	−2.180
23	48	(p, γ)	30.525	−21.914	−4.431	8.210
23	48	(α, p)	44.890	−58.384	−11.069	2.098
23	48	(α, n)	44.499	−57.414	−12.774	−1.862
23	48	(α, γ)	48.046	−70.502	−5.975	8.663
23	49	(n, γ)	28.706	−14.222	4.286	9.337
23	49	(p, n)	32.021	−14.589	−35.031	−3.343
23	49	(p, γ)	29.287	−19.270	−5.919	9.591
23	49	(α, p)	43.186	−55.981	−11.859	2.597
23	49	(α, n)	42.924	−51.781	−19.256	−2.889
23	49	(α, γ)	47.342	−69.300	−3.337	9.160
23	50	(n, γ)	29.696	−17.184	5.541	11.039
23	50	(p, n)	35.606	−32.706	−2.936	0.255
23	50	(p, γ)	31.800	−24.409	−3.577	9.504
23	50	(α, p)	45.351	−63.162	−12.135	1.203
23	50	(α, n)	44.925	−58.491	−11.491	−0.177
23	50	(α, γ)	48.441	−71.816	−6.621	8.763
23	51	(p, n)	34.774	−23.454	−11.296	−1.535
23	51	(p, γ)	29.372	−22.816	−2.398	10.516
23	51	(α, p)	44.542	−62.581	−10.016	−0.115
23	51	(α, n)	44.353	−55.170	−14.165	−2.276
23	51	(α, γ)	51.171	−76.958	0.924	7.943
24	48	(n, γ)	27.790	−15.920	4.806	10.390
24	48	(α, p)	43.285	−58.536	−12.741	0.320
24	48	(α, γ)	45.248	−73.749	−2.209	7.680
24	49	(n, γ)	29.186	−15.481	4.564	12.934
24	49	(α, p)	45.617	−60.899	−11.538	0.454
24	49	(α, n)	42.479	−53.543	−18.036	−2.711
24	49	(α, γ)	47.535	−72.149	−2.254	7.729
24	50	(n, γ)	28.584	−17.941	5.222	9.249
24	50	(p, γ)	29.906	−27.910	−0.852	5.290
24	50	(α, p)	42.138	−56.484	−14.241	−0.432
24	50	(α, n)	33.871	−30.946	−51.649	−5.206
24	50	(α, γ)	42.988	−66.723	−4.712	8.414
24	51	(n, γ)	27.960	−12.910	3.101	12.051
24	51	(p, n)	31.954	−13.980	−42.545	−3.960
24	51	(p, γ)	29.320	−20.488	−5.389	6.565
24	51	(α, p)	44.695	−56.943	−15.820	−0.741
24	51	(α, n)	43.710	−57.640	−12.381	−0.836
24	51	(α, γ)	46.093	−67.512	−5.421	8.464
24	52	(n, γ)	27.576	−17.891	4.094	7.943
24	52	(p, n)	31.332	−19.023	−59.055	−5.486
24	52	(p, γ)	30.121	−26.832	−1.980	6.563
24	52	(α, p)	42.240	−55.659	−25.646	−2.572
24	52	(α, n)	39.768	−48.054	−25.145	−3.586
24	52	(α, γ)	47.172	−76.324	1.429	7.624
24	53	(n, γ)	28.527	−17.292	5.744	9.722
24	53	(p, n)	35.312	−27.081	−8.298	−1.380
24	53	(p, γ)	29.750	−25.077	−1.853	7.560
24	53	(α, n)	43.347	−55.635	−14.048	−0.319
24	53	(α, γ)	47.297	−68.922	−7.583	7.322
24	54	(p, n)	32.002	−20.648	−19.662	−2.161
24	54	(p, γ)	27.220	−19.152	−6.563	8.058
24	54	(α, n)	42.648	−56.067	−15.293	−2.400
24	54	(α, γ)	50.630	−81.361	2.613	7.648

TABLE A.I (*continued*)

Target	*Z*, *A*	Reaction	*F*1	*F*2	*F*3	*Q*
25	51	(n, γ)	29.357	−16.367	4.807	10.525
25	51	(p, γ)	27.794	−20.724	−4.680	7.360
25	51	(α, p)	44.010	−57.346	−14.423	3.130
25	51	(α, γ)	43.601	−60.899	−12.333	8.187
25	52	(n, γ)	29.147	−15.290	3.929	12.049
25	52	(p, n)	33.460	−26.583	−29.723	−3.165
25	52	(p, γ)	29.527	−23.421	−3.718	7.275
25	52	(α, p)	47.865	−70.201	−6.907	1.899
25	52	(α, n)	45.601	−61.088	−13.530	−2.344
25	52	(α, γ)	50.325	−81.042	0.532	7.757
25	53	(n, γ)	28.150	−14.433	4.590	8.940
25	53	(p, n)	31.701	−12.087	−54.129	−4.774
25	53	(p, γ)	29.191	−20.487	−5.868	8.846
25	53	(α, p)	44.395	−61.660	−10.663	1.061
25	53	(α, n)	39.975	−42.914	−34.548	−4.292
25	53	(α, γ)	47.521	−73.829	−1.681	7.055
25	54	(n, γ)	30.082	−16.128	4.272	10.219
25	54	(p, n)	36.003	−29.972	−3.791	−0.095
25	54	(p, γ)	32.111	−26.635	−3.474	9.205
25	54	(α, p)	45.723	−64.479	−12.343	−0.238
25	54	(α, n)	46.157	−61.025	−12.586	−1.885
25	54	(α, γ)	51.448	−80.605	−1.166	6.721
25	55	(p, n)	36.835	−30.501	−4.543	−1.014
25	55	(p, γ)	35.209	−35.834	2.734	10.196
25	55	(α, p)	45.839	−66.679	−9.124	−0.410
25	55	(α, n)	41.982	−49.861	−24.988	−3.498
25	55	(α, γ)	50.409	−75.130	−2.771	6.956
26	52	(n, γ)	27.563	−16.016	4.739	10.440
26	52	(α, p)	44.224	−62.475	−12.721	0.822
26	52	(α, γ)	43.673	−73.095	−5.205	8.085
26	53	(n, γ)	29.508	−16.027	3.137	13.620
26	53	(α, p)	47.160	−63.992	−12.138	0.486
26	53	(α, n)	44.876	−61.806	−14.857	−2.420
26	53	(α, γ)	48.865	−78.009	−3.132	7.815
26	54	(n, γ)	26.814	−14.734	2.857	9.300
26	54	(p, γ)	28.619	−26.215	−2.470	5.057
26	54	(α, p)	41.443	−55.124	−21.299	−1.791
26	54	(α, n)	32.173	−26.468	−59.767	−5.808
26	54	(α, γ)	35.537	−52.911	−13.483	6.411
26	55	(n, γ)	28.631	−15.690	4.893	11.210
26	55	(p, n)	31.468	−13.731	−46.759	−4.243
26	55	(p, γ)	28.125	−20.648	−5.963	5.858
26	55	(α, p)	42.834	−53.191	−30.095	−2.484
26	55	(α, n)	42.583	−54.923	−19.389	−2.889
26	55	(α, γ)	45.705	−68.924	−6.326	6.112
26	56	(n, γ)	28.643	−19.434	5.901	7.641
26	56	(p, n)	30.842	−15.056	−58.234	−5.353
26	56	(p, γ)	29.343	−26.214	−3.051	5.994
26	56	(α, p)	40.398	−51.186	−34.208	−3.240
26	56	(α, n)	34.875	−34.176	−47.394	−5.099
26	56	(α, γ)	33.967	−45.972	−18.730	6.290
26	57	(n, γ)	29.791	−18.991	4.633	10.048
26	57	(p, n)	34.425	−26.639	−11.855	−1.647
26	57	(p, γ)	28.054	−22.225	−4.893	6.959
26	57	(α, n)	44.592	−60.767	−13.926	−1.351
26	58	(p, n)	30.719	−15.946	−31.886	−3.088
26	58	(p, γ)	28.104	−20.361	−7.457	7.366
27	55	(n, γ)	27.976	−14.004	2.917	10.101
27	55	(p, γ)	26.345	−18.603	−6.311	7.263
27	55	(α, p)	45.312	−60.787	−15.087	1.354
27	56	(n, γ)	28.805	−14.792	4.445	11.347
27	56	(p, n)	32.916	−22.382	−27.906	−2.906
27	56	(p, γ)	27.925	−19.599	−6.651	7.329

TABLE A.I (*concluded*)

Target	Z, A	Reaction	$F1$	$F2$	$F3$	Q
27	56	(α, p)	44.865	−60.146	−15.443	0.254
27	57	(n, γ)	28.520	−15.094	4.015	8.606
27	57	(p, n)	31.871	−15.022	−44.090	−4.017
27	57	(p, γ)	28.128	−19.208	−7.296	8.202
27	57	(α, p)	41.060	−52.797	−19.468	0.297
27	58	(n, γ)	31.226	−17.751	5.098	10.454
27	58	(p, n)	36.441	−31.264	−4.127	−0.405
27	58	(p, γ)	34.754	−34.281	−0.820	8.596
27	59	(p, n)	34.613	−24.289	−15.019	−1.859
27	59	(p, γ)	30.200	−22.401	−6.081	9.530
28	56	(n, γ)	25.849	−14.455	3.603	10.235
28	57	(n, γ)	27.301	−14.368	2.682	12.219
28	58	(n, γ)	27.457	−15.783	3.839	9.001
28	59	(n, γ)	28.123	−14.279	3.565	11.389

The partition function for a nucleus (A, Z) is fitted as a function of temperature to

$$\omega(A, Z, T_9) \doteq G_1 + G_2 T_9^{\,2} + G_3 T_9^{\,3}.$$

The parameters G_1, G_2, and G_3 are presented in Table A.II. The partition functions computed from these fits should be accurate to a few percent over the temperature range $1 \leqslant T_9 \leqslant 6$.

TABLE A.II

Partition function parameters

	$G1$	$G2$	$G3$
^{12}C	1.000	0.	0.
^{16}O	1.000	0.	0.
^{20}Ne	1.005	−0.005	0.002
^{23}Na	3.890	0.176	−0.016
^{24}Mg	0.991	−0.001	0.002
^{25}Mg	5.895	0.043	0.002
^{26}Mg	1.010	−0.006	0.002
^{27}Al	5.922	0.022	0.002
^{28}Si	1.006	−0.004	0.001
^{29}Si	2.001	−0.007	0.004
^{30}Si	1.008	−0.004	0.001
^{31}P	1.997	−0.005	0.003
^{32}S	1.007	−0.003	0.001
^{33}S	3.981	0.003	0.003
^{34}S	1.009	−0.005	0.001
^{35}Cl	2.010	−0.010	0.004
^{36}Cl	4.845	0.049	0.005
^{37}Cl	4.007	−0.007	0.003
^{36}A	1.007	−0.004	0.001
^{37}A	4.020	−0.015	0.005
^{38}A	1.010	−0.005	0.001

TABLE A.II (*concluded*)

	$G1$	$G2$	$G3$
^{39}A	8.012	−0.017	0.008
^{40}A	1.024	−0.016	0.005
^{39}K	4.010	−0.005	0.001
^{40}K	14.329	0.173	−0.003
^{41}K	4.036	−0.039	0.017
^{40}Ca	1.002	−0.001	0.
^{41}Ca	8.049	−0.025	0.006
^{42}Ca	1.025	−0.015	0.005
^{43}Ca	7.914	0.244	−0.007
^{44}Ca	0.996	−0.008	0.005
^{45}Ca	9.417	0.211	−0.011
^{46}Ca	1.012	−0.011	0.004
^{43}Sc	7.843	0.118	0.002
^{44}Sc	8.065	0.842	−0.034
^{45}Sc	7.859	0.131	0.023
^{46}Sc	16.100	1.031	−0.064
^{47}Sc	7.972	−0.034	0.026
^{44}Ti	1.014	−0.010	0.004
^{45}Ti	12.888	0.070	0.010
^{46}Ti	0.927	0.021	0.002
^{47}Ti	8.156	0.299	−0.023
^{48}Ti	0.961	0.006	0.004
^{49}Ti	8.073	−0.044	0.013
^{50}Ti	1.014	−0.010	0.003
^{47}V	5.897	0.259	−0.004
^{48}V	8.942	0.325	0.006
^{49}V	12.108	0.329	−0.015
^{50}V	12.862	0.394	0.001
^{51}V	7.870	0.443	−0.033
^{48}Cr	0.960	0.006	0.004
^{49}Cr	5.877	0.038	0.010
^{50}Cr	0.894	0.038	0.001
^{51}Cr	7.892	0.018	0.014
^{52}Cr	1.033	−0.020	0.006
^{53}Cr	3.897	0.029	0.011
^{54}Cr	0.919	0.024	0.003
^{51}Mn	7.203	0.320	−0.031
^{52}Mn	12.873	0.211	0.004
^{53}Mn	7.994	0.198	−0.017
^{54}Mn	6.864	0.355	−0.003
^{55}Mn	8.832	0.285	−0.013
^{52}Fe	0.985	−0.001	0.003
^{53}Fe	8.023	−0.022	0.009
^{54}Fe	1.019	−0.013	0.005
^{55}Fe	3.587	0.298	−0.014
^{56}Fe	0.920	0.025	0.002
^{57}Fe	7.409	0.460	−0.026
^{58}Fe	0.928	0.019	0.006
^{55}Co	8.016	−0.017	0.007
^{56}Co	10.511	0.416	−0.027
^{57}Co	8.005	−0.010	0.005
^{58}Co	13.980	0.489	−0.015
^{59}Co	8.082	−0.081	0.033
^{56}Ni	1.015	−0.009	0.002
^{57}Ni	4.014	−0.016	0.007
^{58}Ni	1.023	−0.015	0.005
^{59}Ni	4.045	0.249	−0.005
^{60}Ni	1.029	−0.020	0.007

REFERENCES

ARNETT, D. 1966. Proc. Nucleosynthesis Conference, Institute for Space Studies, New York.

AJZENBERG-SELOVE, F. (*editor*). 1960. Nuclear spectroscopy (Academic Press, New York).

BURBIDGE, E. M., BURBIDGE, G. R., FOWLER, W. A., and HOYLE, F. 1957. Rev. Mod. Phys. **29**, 547.

CAMERON, A. G. W. 1959*a*. Astrophys. J. **130**, 429.

——— 1959*b*. Astrophys. J. **130**, 895.

——— 1963. Nuclear astrophysics (compilation of lectures given at Yale University).

CARTLEDGE, W. A., THIBAUDEAU, M., and REEVES, H. 1963. Helium thermonuclear reactions (Publications of the Institute for Space Studies, New York).

CHIU, H. Y. 1966. Presupernova evolution. *In* Stellar evolution, *edited by* R. F. Stein and A. G. W. Cameron (Plenum Press, N.Y., in press).

COLGATE, S. 1966. Proc. Nucleosynthesis Conference, Institute for Space Studies, New York.

COLGATE, S., GRASBERGER, W. H., and WHITE, R. H. 1961. Lawrence Radiation Laboratory, UCRL-6471.

FOWLER, W. A. and HOYLE, F. 1964. Astrophys. J. Suppl. **91**, 1.

HAYASHI, C., HOSHI, R., and SUGIMOTO, D. 1962. Progr. Theoret. Phys. Suppl. **22**, 1.

HOYLE, F. 1946. Monthly Notices Roy. Astron. Soc. **106**, 23.

KUEHNER, J. A., GOVE, H. E., LITHERLAND, A. E., CLARK, M. A., and ALMQUIST, E. 1961. Chalk River Rept. PD-317.

LARSON, J. D. and SPEAR, R. H. 1964. Nucl. Phys. **56**, 497.

REEVES, H. 1964. A review of nuclear energy generation in stars and some aspects of nucleosynthesis (Publications of the Institute for Space Studies, New York).

REEVES, H. and SALPETER, E. E. 1959. Phys. Rev. **116**, 1505.

STOTHERS, R. and CHIU, H. Y. 1962. Astrophys. J. **135**, 963.

TRURAN, J. W., HANSEN, C. J., CAMERON, A. G. W., and GILBERT, A. 1966. Can. J. Phys. **44**, 151.

VOGT, E. W., MCPHERSON, D., KUEHNER, J., and ALMQUIST, E. 1964. Phys. Rev. **136**, B99.

4. COMPOSITION OF MATTER IN NUCLEAR STATISTICAL EQUILIBRIUM AT HIGH DENSITIES

SACHIKO TSURUTA

Physics Department, Columbia University, New York, New York,
Institute for Space Studies, Goddard Space Flight Center, NASA, New York, New York,
and
Smithsonian Astrophysical Observatory, Cambridge, Massachusetts

AND

A. G. W. CAMERON

Institute for Space Studies, Goddard Space Flight Center, NASA, New York, New York

Received June 23, 1965

ABSTRACT

Various properties of dense matter in nuclear statistical equilibrium are studied for densities and temperatures in the range $10^6 \leqslant \rho \leqslant 10^{12}$ g/cm^3 and $2 \times 10^9 \leqslant T \leqslant 10^{10}$ °K. With increasing density the stability shifts to more and more neutron-rich nuclei. With increasing temperature the general tendency is that nuclei of smaller charge become more abundant, and the abundances of nuclei near a peak tend to become nearly as large as that of the peak nucleus. The shifting of the most stable region with change of density or temperature takes place rather abruptly from one neutron closed shell region to the next. For densities $\leqslant \sim 10^6$ g/cm^3, the ordinary iron group nuclei are most stable until the temperature becomes about 5×10^9 °K; for higher temperatures matter in equilibrium consists of almost pure helium. For higher density, this transition to a helium phase takes place at a somewhat higher temperature, and the equilibrium configuration for temperatures below the helium transition point shifts to the neutron-rich side of the valley of beta stability. When $T > 10^{10}$ °K, matter consists of almost pure neutrons at all densities. Rates of beta reactions and neutrino emission generally increase with increase of density and temperature. At a typical temperature of about 5×10^9 °K, the neutrino energy emission rate increases from about 2×10^{11} ergs/g sec at $\rho \sim 10^6$ g/cm^3 to about 2×10^{17} erg/g sec at $\rho \sim 3 \times 10^{11}$ g/cm^3.

INTRODUCTION

The course of stellar evolution is governed by a succession of nuclear reactions that take place in the stellar interior. After the exhaustion of one set of nuclear reactions, the temperature and density will tend to increase in the interior until the ashes of the previous set of reactions become the fuel of the next set. These nuclear reactions are generally quite sensitive functions of density and temperature.

The bulk of nuclear energy generation in stellar interiors comes from the conversion of hydrogen to helium. With increasing temperature, helium is converted in turn into carbon and oxygen. At temperatures of 1 to 2×10^9 °K, the carbon and oxygen ions react with themselves to form a profusion of nuclei in the range magnesium to sulphur. When the temperature reaches several billion degrees, these nuclei are further transformed into heavier nuclei. If the density of the matter does not exceed about 10^7 g/cm^3, the ordinary iron group nuclei are the most stable, until the temperature is raised to about

7×10^9 °K, at which point a conversion of the iron into helium nuclei takes place. For densities greater than about 10^7 g/cm^3, under conditions of nuclear statistical equilibrium the iron group nuclei will be replaced by other nuclei having a greater neutron to proton ratio. These nuclei no longer have the greatest nuclear binding energy per nucleon, but they are formed in conditions in which the electrons form a degenerate gas with a fairly high Fermi energy, and the system attains its minimum energy by minimizing the energy of the nuclei and the electrons together.

In order that the nuclei may be in nuclear statistical equilibrium, it is necessary that every nucleus be transformable into any other nucleus under consideration, and the radiation in the assembly must be in equilibrium with the matter. A discussion relevant to these questions have been given by Hoyle (1946). He showed that radiation must be in statistical equilibrium with matter to a high degree of validity at temperatures of several billion degrees. Current studies of nuclear reaction rates indicate that all known nuclei may be transformed into any other nucleus by nuclear reactions on a time scale of millions of years or less at temperatures of 2×10^9 °K or greater, and on time scales of a day or less at temperatures of 3.5×10^9 °K or greater (Gilbert, Truran, and Cameron 1966). The nuclear reactions concerned involve any combination of projectiles in and projectiles out for four types of projectiles: neutrons, protons, alpha particles, and photons.

In this paper we shall not be concerned with the details of the nuclear reactions responsible for achieving and maintaining nuclear statistical equilibrium, but rather we shall be concerned with determining what the actual abundances of nuclei in statistical equilibrium are, paying special attention to the highest densities. These considerations may apply to the stage of stellar evolution immediately preceding a supernova explosion, when temperatures of several billion degrees are expected to be attained in the interior of the star, and to the remnant of the explosion, which may be a neutron star.

The calculations are actually carried out for the case of beta-decay steady state, in which the assembly emits neutrinos and antineutrinos at the same rate. There may not be time for this condition to be reached in the presupernova configuration, but there is more likely to be time for it to be reached in the possible neutron star remnants. At any rate, it is necessary to specify some relation between the total number of neutrons and the total number of protons in the system, including those in the nuclei, and the condition of beta-decay steady state is a convenient condition to impose; it represents the state towards which the system must tend with time.

EQUATIONS OF NUCLEAR STATISTICAL EQUILIBRIUM

The abundance of a nucleus of atomic number Z and mass number A under statistical equilibrium is calculated from the relation (Burbidge, Burbidge, Fowler, and Hoyle 1957):

$$(1)\quad n(A, Z) = \omega(A, Z) \left(\frac{AMkT}{2\pi\hbar^2}\right)^{3/2} \left(\frac{2\pi\hbar^2}{MkT}\right)^{3A/2} \frac{n_n{}^{(A-Z)} n_p{}^{Z}}{2^A} \exp[Q(A, Z)/kT],$$

where n_p and n_n are the number densities of free protons and neutrons and $Q(A, Z)$ and $\omega(A, Z)$ are the binding energy and partition function of the nucleus (A, Z) respectively. The last quantities are defined as

$$\omega(A, Z) = \sum_r (2I_r + 1)\exp(-E_r/kT), \tag{2}$$

$$Q(A, Z) = c^2[(A - Z)M_n + ZM_p - M(A, Z)], \tag{3}$$

where I_r and E_r are the spin and the energy of the rth excited level, the summation being taken over all the excited states of the nucleus, and M_n, M_p, and $M(A, Z)$ are the masses of the neutron, hydrogen atom, and the atom (A, Z), respectively. The notation is that of Burbidge, Burbidge, Fowler, and Hoyle (1957). All atomic masses and transition energies used in the calculations of this paper were taken from the semiempirical mass formula of Cameron (1957) if they were not known experimentally (Everling, Konig, Mattauch, and Wapstra 1960).

Assuming that Q and ω are known, the only unknowns in equation (1) are T, n_p, and n_n. In our approach, the electron Fermi energy E_F and temperature T are selected as the free parameters. Therefore, we need relations connecting E_F to n_n and n_p. E_F is generally expressed in the form

$$E_F = E_F(n_e), \tag{4}$$

where n_e is the electron number density. For nonrelativistic and extremely relativistic electrons, this reduces to

$$E_F = (3\pi^2)^{2/3}\frac{\hbar^2}{2m_e}n_e^{2/3} \quad \text{(nonrelativistic)},$$
$$E_F = (3\pi^2)^{1/3}\hbar c n_e^{1/3} \quad \text{(relativistic)}. \tag{5}$$

The conservation of charge requires that n_e should be equal to the sum of all the positive-ion number densities times Z,

$$n_e = \sum_j Z_j n(A_j, Z_j). \tag{6}$$

The summation is taken over all the ions j of interest with $A \geqslant 1$ and $Z \geqslant 1$.

Under steady-state conditions, there are various photobeta processes connecting neighboring nuclei. These are beta decays originating in the statistically populated excited states of the nucleus as well as from its ground state (Cameron 1959). These beta processes are important in maintaining a balance between neutrons and protons (including bound nucleons as well as free ones). Under steady-state conditions the total number of electron emissions per unit time must be equal to the total number of the inverse processes (electron captures plus positron emissions per unit time):

$$\sum_i P^-(A_i, Z_i)n(A_i, Z_i) = \sum_k P^+(A_k, Z_k)n(A_k, Z_k), \tag{7}$$

where $P^{\pm}$ is the rate of a beta reaction per nucleus with the negative sign indicating electron emission and the positive sign indicating electron capture or positron emission. Because of the high densities involved in most of our calculations, we have neglected positron capture processes.

(8) $$P = \sum_i a_i \lambda_i$$

where

$$a_i = \frac{(2I_i + 1)}{\omega(A, Z)} \exp(-E_i/kT)$$

is the fractional population of an excited state with energy E_i, and λ is the decay constant. The summation is taken over all the nuclear energy levels.

The abundance of any nucleus of interest $n(A, Z)$ is then calculated by solving equations (1) through (8) for any given set of values of E_F and T. The total density of matter is obtained by the requirement for the conservation of mass:

(9) $$\rho = \sum_k A_k n(A_k, Z_k)/N_0,$$

where N_0 is Avogadro's number and the summation is taken over all nuclei k with $A \geqslant 1$ and $Z \geqslant 0$ which contribute appreciably to the total matter density.

LEVEL DENSITY RELATIONS

In the equilibrium abundance calculations outlined in the previous section, there are two places where summation over excited nuclear levels becomes necessary. One is in equation (2) for ω and the other is in equation (8) for P.

The nuclear level structure is fairly well known in the vicinity of 6 to 8 MeV through study of neutron resonances. In this and higher-energy regions the level spacing is sufficiently small so that conventional level density formulas are reasonably valid. Unfortunately, however, such formulas are not much help in the present problem, because the contribution to the summation in equation (7) is expected to be greatest from the intermediate levels around 3 to 6 MeV in the temperature range in which we shall be interested. A recent paper by Gilbert and Cameron (1965) shows how a composite nuclear level density formula may be constructed which is reasonably valid over the entire range of excitation energies. The results reported in this paper were obtained before the final form of the composite level density formula was ready, and so nuclear level densities were handled by approximate methods in the general spirit of the approach later developed in the paper by Gilbert and Cameron.

It was pointed out by Ericson (1960) that if the logarithm of the total number of nuclear levels below a given excitation energy is plotted versus that energy, a good straight-line relation is obtained:

(10) $$N = \exp[a(U - U_0)],$$

where N is the total number of states up to the excitation energy U, and a and U_0 are constants determined by the slope and the intercepts of the straight line drawn along the staircase diagram. Such graphs were plotted for various nuclei, and the staircase was seen to cluster closely about the straight line. Level structure thus shown in graphical form is distinct up to an excitation energy of about 3 to 6 MeV. Therefore, in general the line can be extrapolated

up to about 7 to 8 MeV, where conventional level density formulas start to become applicable (Gilbert and Cameron 1965).

This method provides us with a means for direct summation up to about 6 to 8 MeV, thus avoiding the use of level density formulas, which are poor approximations in the intermediate region of interest. In the present research, the summations were carried out in this way up to about 10 MeV and the levels were terminated there. The results indicated that this method is fairly reliable up to a temperature of 5×10^9 °K (that is, the contribution from states higher than 10 MeV can be neglected in this temperature region). But a serious deviation was noticed when the calculation was carried out at 10×10^9 °K.

In a preliminary analysis of data for nuclei up to the iron region it appeared that the constant a of equation (10) could be crudely represented by the following relations:

$$\begin{aligned} a &= 0.020A \text{ MeV}^{-1} \text{ for odd–odd nuclei,} \\ a &= 0.016A \text{ MeV}^{-1} \text{ for all except odd–odd nuclei.} \end{aligned} \tag{11}$$

In the work carried out here it was generally found that for any given density only about four nuclei would in general contribute appreciably to the beta-decay interactions. Consequently the level densities of only a very small number of such nuclei needed to be computed with any attempt at accuracy. Hence the logarithm of N was plotted against U for all nuclei with the same value of N or Z as the neutron-rich nucleus of interest. The plots made use of available experimental data such as those compiled in Landolt–Bornstein (1961). Then a straight line was drawn with the slope a obtained from equation (11) through the lower portions of the staircase diagram, and the intercept U_0 was obtained. This procedure seemed quite sufficient for the purpose of the present survey of the equilibrium abundances in nuclear statistical equilibrium at high densities.

BETA TRANSFORMATION RATES

The decay constant λ appearing in equation (8) is inversely proportional to the half-life t, and it may often be estimated in terms of the comparative half-life (ft), where f is the Fermi function. Equation (8) may then be written in the form

$$P = \sum_i \frac{(2I_i + 1)\ln 2[f_i/(ft)_i] \exp(-E_i/kT)}{\sum_j (2I_j + 1) \exp(-E_j/kT)}, \tag{12}$$

where the Fermi function is defined as

$$f = \int (W^2 - 1)^{1/2} W W_\nu^2 F(Z, W) S \, dW. \tag{13}$$

$F(Z, W)$ takes into account the Coulomb effect, the factor S conveniently includes all the modifications necessary to allow for the effect of the Pauli exclusion principle in the degenerate electron gas, W is the electron energy including the rest mass, and W_ν is the neutrino energy, both expressed in units

of mc^2. For any nucleus the transformation rate P from equation (12) requires an estimate of the Fermi function f_i, the (ft) value, and the spin I_i and energy E_i of each excited state i before the summation is taken.

For ordinary beta transformations the Fermi function f of equation (13) has been given to a fairly good approximation by Feenberg and Trigg (1950) for positron and electron emission, and by Major and Biedenharn (1954) for electron capture. Applications of these for nondegenerate matter at high temperatures were given by Cameron (1959). A more generalized consideration, including both nondegenerate and degenerate cases, was given by Bahcall (1964).

For temperatures in excess of 2×10^9 °K, all atoms are ionized and captures of bound electrons are negligible. Hence for such high temperatures the capture of continuum electrons and the emission of positrons constitute the inverse processes that must be balanced by electron emissions, as long as the density does not exceed about 10^7 g/cm^3. At higher densities the Pauli exclusion principle causes electron degeneracy, and electron emission rates are greatly reduced because of a lack of unoccupied electron states. Also, as the density is increased, the free capture rates are greatly enhanced because more electrons are present to be captured. However, the positron emission rates are hardly affected by the increase of density, and therefore at a sufficiently high density positron emission becomes negligible in comparison with continuum electron capture.

For completely degenerate matter equation (13) reduces, to a first-order approximation, to the following expressions:

(i) Electron capture:

$$(14a) \qquad f_c = \int_{W_x}^{W_F} (W^2 - 1)^{1/2} W (W + W_0)^2 F(Z, W)\, dW,$$

$$W_x = 1 \qquad \text{if } W_0 > -1,$$

$$W_x = |W_0| \qquad \text{if } W_0 < -1.$$

(ii) Electron emission:

$$(14b) \qquad f_{e^-} = \int_{W_F}^{W_0} (W^2 - 1)^{1/2} W (W_0 - W)^2 F(Z, W)\, dW.$$

Here W_F is the electron Fermi energy and W_0 is the threshold energy of the beta transition, both including the rest mass and expressed in units of mc^2. $W_0 > -1$ corresponds to the case where the nucleus in question undergoes positron emission in the laboratory or bound electron capture (exoergic). $W_0 < -1$ corresponds to the case where the nucleus is the product of electron emission and is stable under ordinary conditions in the absence of degeneracy (endoergic).

Equations (14) may be integrated to give the following results:

(i) Electron capture:

$$(15a) \quad f_c = \langle \bar{F} \rangle [\tfrac{1}{5} P_F^5 + \tfrac{1}{3} P_F^3 (1 + W_0^2) + \tfrac{1}{4} W_0 \{2 P_F W_F^3 - P_F W_F - \ln(P_F + W_F)\}$$

if $W_0 > -1$;

$$(15b)\quad f_c = \langle\bar{F}\rangle\{\tfrac{1}{5}(P_F^5 - P_0^5) + \tfrac{1}{3}(P_F^3 - P_0^3)(1 + W_0^2) - \tfrac{1}{4}|W_0|[2(P_F W_F^3 - P_0|W_0|^3) - (P_F W_F - P_0|W_0|) - \ln(P_F + W_F) + \ln(P_0 + |W_0|)]\}$$

if $W_0 < -1$.

(ii) Electron emission:

$$(16)\quad f_{e^-} = f^0(1 - \Delta/f^0),$$

$$\Delta/f^0 = I_1(P_F, W_0)/I_1(P_0, W_0),$$

$$I_1(x, y) = \tfrac{1}{5}x^5 + \tfrac{1}{3}x^3(1 + y^2) - \tfrac{1}{4}y\{2x(x^2 + 1)^{3/2} - x(x^2 + 1)^{1/2} - \ln(x + (x^2 + 1)^{1/2})\}.$$

Here $\langle\bar{F}\rangle = 2\pi\alpha Z$ if $Z > (2\pi\alpha)^{-1} \sim 23 (\alpha = 1/137)$,

$\langle\bar{F}\rangle = 1$ if $Z < (2\pi\alpha)^{-1}$,

$P_F^2 \equiv (W_F^2 - 1)$

and $P_0^2 \equiv (W_0^2 - 1)$.

f^0 is the electron emission Fermi function as given by Feenberg and Trigg (1950).

For extreme degeneracy, where the electrons become relativistic, and the approximation $P^2 = W^2 - 1 \sim = W^2$ applies, we obtain the simpler expressions:

(i) Electron capture:

$$(17a)\quad f_c = \tfrac{1}{5}\langle\bar{F}\rangle[(W_F^5 - 1) + \tfrac{5}{2}W_0(W_F^4 - 1) + \tfrac{5}{3}W_0^2(W_F^3 - 1)]$$

if $W_0 \gg -1$;

$$(17b)\quad f_c = \tfrac{1}{5}\langle\bar{F}\rangle[(W_F - |W_0|)^5 + \tfrac{5}{2}|W_0|(W_F - |W_0|)^4 + \tfrac{5}{3}|W_0|^2(W_F - |W_0|)^3]$$

if $W_0 \ll -1$.

(ii) Electron emission:

$$(18)\quad f_{e^-} = f^0(1 - \Delta/f^0),$$

$$\Delta/f^0 = D_1(W_F, W_0)/D_1(W_0, W_0)$$

where

$$D_1(x, y) \equiv \tfrac{1}{5}(x^5 - 1) - \tfrac{1}{2}(x^4 - 1)y + \tfrac{1}{3}(x^3 - 1)y^2.$$

It will be noticed that for a given beta transformation energy the Fermi function depends upon both the nuclear charge and the electron Fermi level. However, as will be indicated later, for a given Fermi energy the Fermi functions f are required for only a narrow range of Z, in the vicinity of the

abundance distribution. Preliminary determinations of the abundance distributions at higher densities were made in order to determine the relevant ranges of Z.

For a given temperature T and Fermi energy E_F, an approximate value of the matter density ρ may be obtained by guessing the mean molecular weight of the system per electron. Provided one additional constraint on the system is specified, the abundance distribution may then be calculated by adjusting the values of n_n and n_p in equation (1). The additional constraint chosen for the preliminary survey is that the most abundant nuclei in the system should be stable against beta transformation in the presence of the degenerate electrons corresponding to the chosen value of the electron Fermi energy.

This preliminary determination of the abundance distributions proved to be quite close to the one that was finally determined. On the basis of this survey the most probable values of Z were found to be 26, 28, 32, 28, both 28 and 40, and 38 for electron Fermi energies of 0, 5, 10, 15, 20, and 23 MeV. The two values of Z corresponding to $E_F = 20$ MeV were chosen because it appeared that there were two abundance peaks of comparable height at this Fermi energy. Fermi energies higher than 23 MeV were not chosen because the survey indicated that the system would have become largely composed of neutrons at such values of the Fermi energy. However, since it appeared that such nuclei as ^{3}H and ^{6}He might become important under these neutron-rich conditions, it was decided to calculate Fermi functions at higher electron Fermi energies for the case $Z = 0$.

Values of the Fermi function f for these various cases are plotted in Fig. 1 (for electron emission) and Fig. 2 (for endoergic electron capture). Exoergic electron capture is not shown because such transitions are not important in the region of high density. It is noteworthy that for high values of the electron Fermi energy the Fermi function may be very large for electron emission and capture processes. This indicates the likelihood that beta transitions of quite moderate energy may nevertheless take place extremely rapidly under conditions of very high density.

SPIN AND PARITY CONSIDERATIONS

The comparative half-life (ft) appearing in equation (12) is a measure of the inverse square of the matrix element $|M|$ and the strength of the interaction g:

$$(ft) = (\ln 2)/g^2|M|^2. \tag{19}$$

If the degree of forbiddenness of a beta transformation is known, then a typical value of (ft) may be assigned to it, although this may have a probable error of a factor 10. Since the great majority of the beta transformations involved in these calculations have not been measured experimentally, including all of the transitions between the excited nuclear states, it has been necessary to adopt this approach of assigning reasonable values to (ft) depending upon the degree of forbiddenness of the transition. The degree of forbiddenness of the transition, in turn, depends upon the spin change and whether or

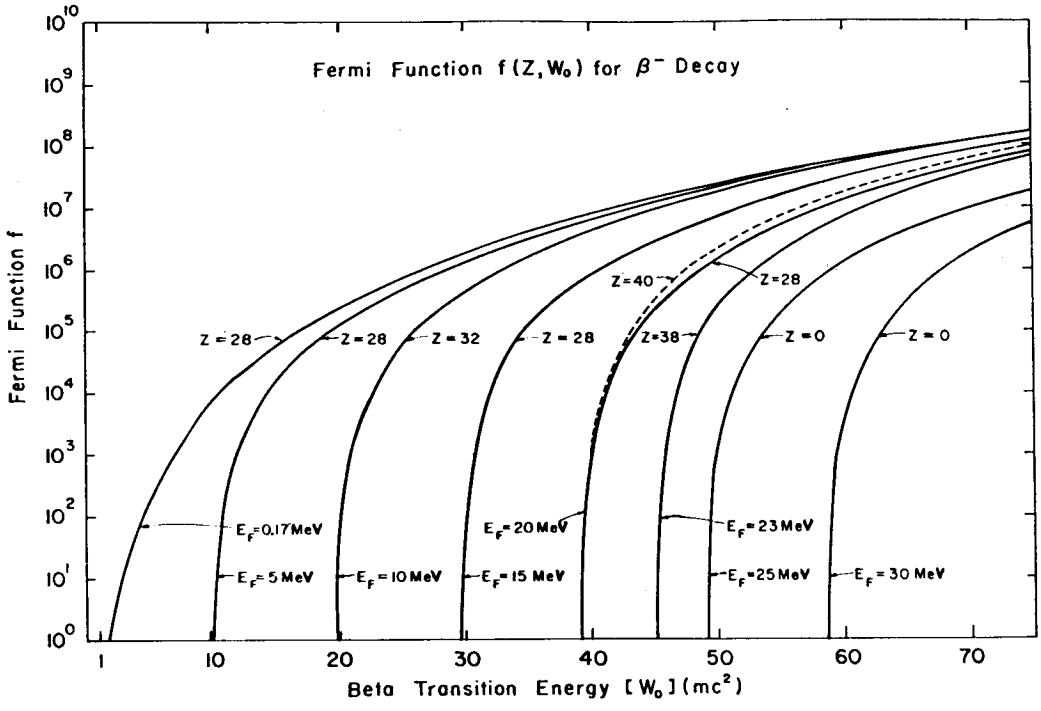

FIG. 1. Fermi function for electron emission plotted as a function of the transition energy for nuclear charges corresponding to nuclei in the vicinity of the maximum abundance at various Fermi energies.

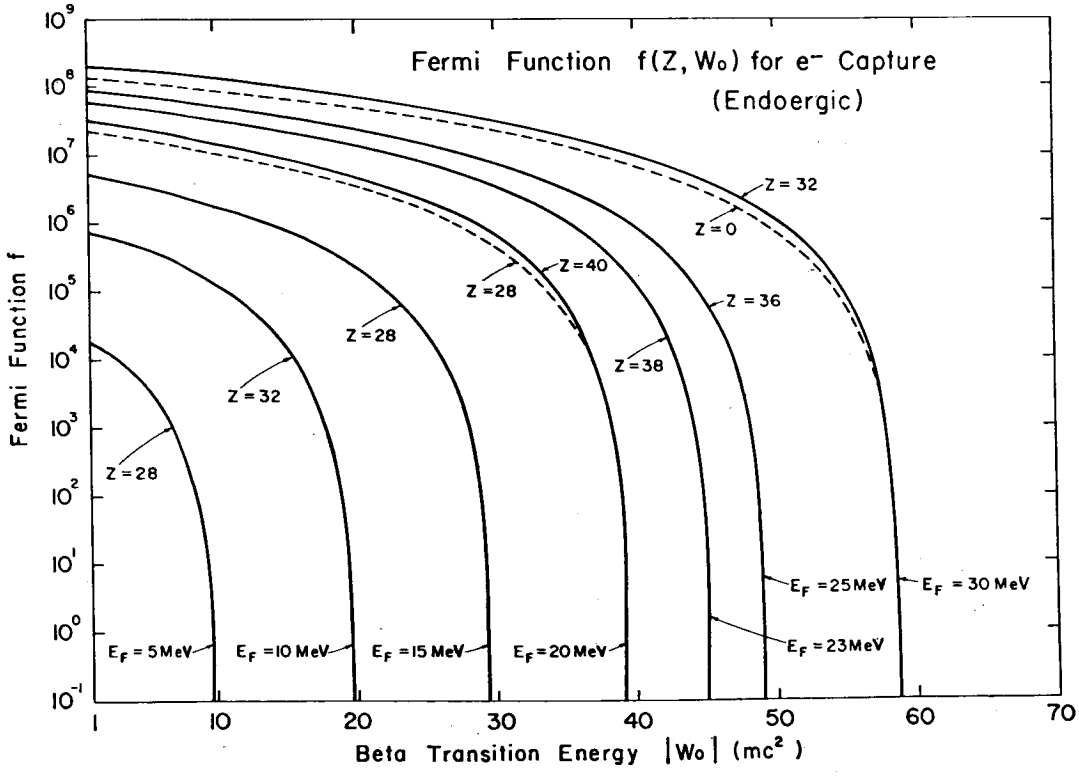

FIG. 2. Fermi function for electron capture plotted as a function of the transition energy for nuclear charges corresponding to nuclei in the vicinity of the maximum abundance at various Fermi energies.

not there is a parity change in the transition according to the well-known selection rules. However, since the spins and parities of the excited states involved in the nuclei of these considerations are not known either, it has been necessary to adopt a statistical approach to the assignment of these (ft) values.

For the nuclei under consideration here, the spin and parity of the ground state and of a few of the lowest excited states were estimated using the shell model and empirical data.

For each chosen value of the electron Fermi energy, the transition rates were estimated among four nuclei considered to be the most important in the assembly. Because of the considerable uncertainty in estimating the transformation rates between these nuclei, it was felt that the other nuclear transformations, which would be of less importance in any case, could be neglected. Table I shows the nuclei chosen in this way for each of the various

TABLE I

Assigned properties of the nuclei determined to be the most important participants in beta processes at various Fermi energies. If the spin–parity assignment does not correspond to the ground state, it is likely that it corresponds to a low lying excited state

Fermi energy (MeV)	Nuclei	Spin–parity	$\log_{10} ft$
0.17	^{55}Mn	5/2 −	5.5
	^{55}Fe	p 3/2 −	
	^{57}Co	f 7/2 −	6
	^{57}Fe	p 5/2 −	
5	^{65}Co	f 7/2 −	5.5
	^{65}Ni	f 5/2 −	
	^{67}Cu	p 3/2 −	4.5
	^{67}Ni	p 1/2 −	
10	^{81}Zn	d 5/2 +	6.5
	^{81}Ga	p 3/2 −	
	^{83}As	p 3/2 −	6.5
	^{83}Ge	d 5/2 +	
15	^{79}Ni	d 5/2 +	6.5
	^{79}Cu	p 3/2 −	
	^{81}Ga	p 3/2 −	6.5
	^{81}Zn	d 5/2 +	
20	^{123}Zr	f 7/2 −	7
	^{123}Nb	g 9/2 +	
	^{121}Nb	g 9/2 +	7.5
	^{121}Zr	h 11/2 −	
23	^{119}Rb	f 5/2 −	7
	^{119}Sr	d 3/2 +	
	^{121}Zr	d 3/2 +	6.5
	^{121}Y	p 1/2 −	

values of the electron Fermi energy for which calculations were done. It shows the spin and parity assigned to the ground state or a low-lying excited state of the nuclei and the value of (ft) that was estimated for the transitions between these states.

As indicated above, for the higher levels a statistical approach was used. The nuclear spin distribution is predicted to have the form (Bloch 1954; Hibdon 1959; Ericson 1960):

$$\rho(J) = \rho(0)[\exp(-J^2/(2C\tau)) - \exp(-(J+1)^2/(2C\tau))], \tag{20}$$

where $\rho(J)$ is the density of nuclear levels with spin J, $\rho(0)$ is the density of levels with zero spin, τ is the nuclear temperature, and C is a constant. Some authors use the symbol σ, which is related to this expression by

$$\sigma = (C\tau)^{1/2}.$$

σ is a parameter characterizing the distribution function and is a very slowly varying function of the excitation energy U through the nuclear temperature τ. Using the expression

$$C = (A^{5/3}B^2/55)\ \text{MeV}^{-1}, \qquad B = 0.55, \tag{21}$$

for the constant C, Hibdon (1959) concluded that $2C\tau = 6$ gives the best fit to the observations for ^{28}Al. In Huizenga and Vandenbosch (1960) and Vandenbosch and Huizenga (1960) it is shown that σ is about 2 to 5 for various nuclei with mass numbers in the range 80 to 200. The value of $2C\tau$ was estimated by using the value of C given by equation (21) and by obtaining τ through the use of the simplest level density expression as given by Blatt and Weisskopf (1950). As the energy of the excited level changes from about 1 to 10 MeV, $2C\tau$ varies from about 10 to 30 for A in the vicinity of 80, while it varies from about 13 to 36 in the vicinity of $A = 120$. These results are consistent with Huizenga's conclusion. A smaller value of $2C\tau$ would be expected for smaller mass numbers and hence these results are also consistent with Hibdon's conclusion.

The average spin of the excited states was computed through the expression

$$\langle J \rangle = \sum_{J_l=0}^{10} \left[J_l \rho(J_l) \Big/ \sum_{J_i=0}^{10} \rho(J_i) \right]. \tag{22}$$

The summation for J higher than 10 is not necessary because a sample calculation with $\sigma = 3$ shows that ρ is already negligible at $J = 7$, with a peak around $J = 2.3$.

It is evident that when the sum over beta transitions involving the higher excited states of a nucleus is performed, only the allowed transitions need to be taken into account. The contributions from the forbidden transitions are small compared with the uncertainties in the contributions from the allowed transitions. It was assumed that all allowed transitions have $\log ft = 5.5$. This value of $\log ft$ was used in equation (12) for all transitions involving the higher excited states of nuclei, but each such term was then multiplied by the probability that the combinations of spin and parity of the initial and final states of the transition should correspond to an allowed transition. This probability is given by the expression

$$(23)\qquad P_{\text{allowed}} = \sum_{J_j=0}^{10} \frac{1}{2}\left[\frac{\rho(J_j)}{\sum_{J_l=0}^{10}\rho(J_l)}\right]\left[\frac{\rho(J_j+1)+\rho(J_j)+\rho(J_j-1)}{\sum_{J_l=0}^{10}\rho(J_l)}\right];$$

$$\rho(J_j+1) = 0 \qquad \text{if } J_j = 10,$$

$$\rho(J_j-1) = 0 \qquad \text{if } J_j = 0.$$

The factor $\frac{1}{2}$ arises from the fact that both odd and even parities are about equally probable (Ericson 1960).

Evaluations of the expression in equation (23) show that there is about one chance in four that an arbitrary transition is allowed for the lower excited states of the nucleus up to a few MeV, while there is only about one chance in five or six that a transition between higher excited states in the vicinity of 6–8 MeV should be allowed. The variation is a consequence of the increase of average spin with excitation energy.

Typical results of the calculations for beta transition rates in a few of the key nuclei are shown in Fig. 3. The key nuclei are those given in Table I for

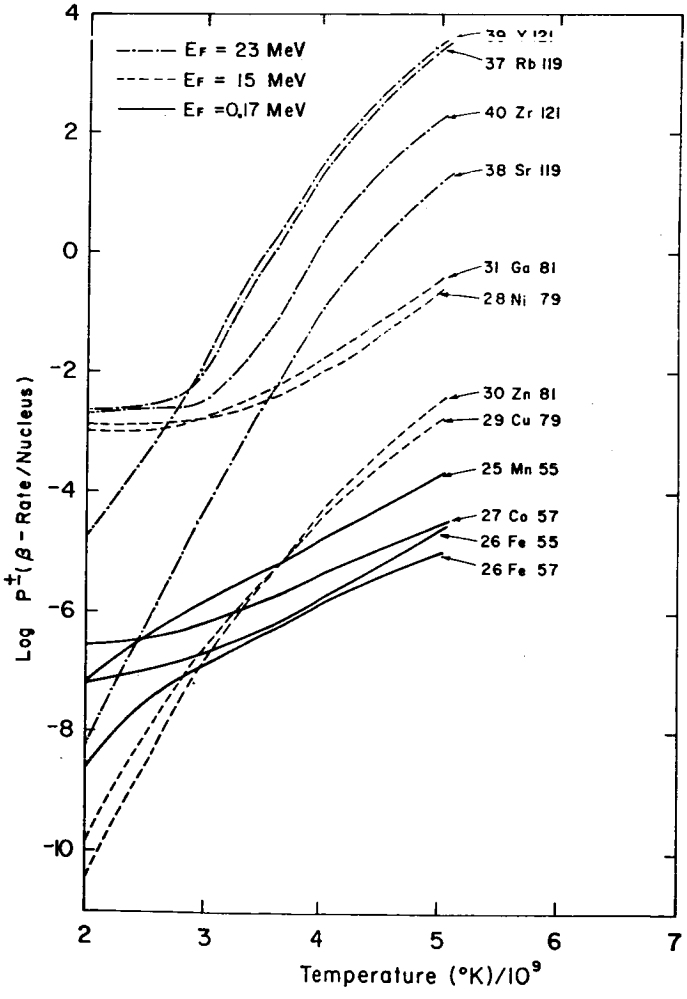

FIG. 3. Beta transition rates plotted as a function of temperature for the four key nuclei at three different Fermi energies.

the Fermi energies of 0.17, 15, and 23 MeV. It may be seen that the rates are very sensitive functions of both temperature and electron Fermi energy. At the higher Fermi energies and temperatures some of the nuclei may have beta-transition lifetimes in the range of milliseconds. The resulting neutrino emission rates can be very great, as is discussed later.

EQUILIBRIUM COMPOSITIONS

The final values of the equilibrium compositions were determined by adjustment of the values of n_p and n_n in equation (1) subject to the boundary conditions that the electron Fermi energy was specified and that the rate of neutrino emission from the material will be equal to the rate of antineutrino emission. The adjustment of free-particle number densities was carried out by an iterative procedure. It was found that the desired density could be approached to any degree of approximation desired by adjusting the product $n_p n_n$, and equality of the neutrino and antineutrino emission rates could be approached to any desired degree of approximation by adjusting the ratio n_p/n_n.

The final values of n_n and n_p/n_n are plotted as a function of density for several different temperatures in the Figs. 4 and 5. It may be observed that the material rapidly approaches a pure neutron gas in the density interval 10^{11} to 10^{12} g/cm^3.

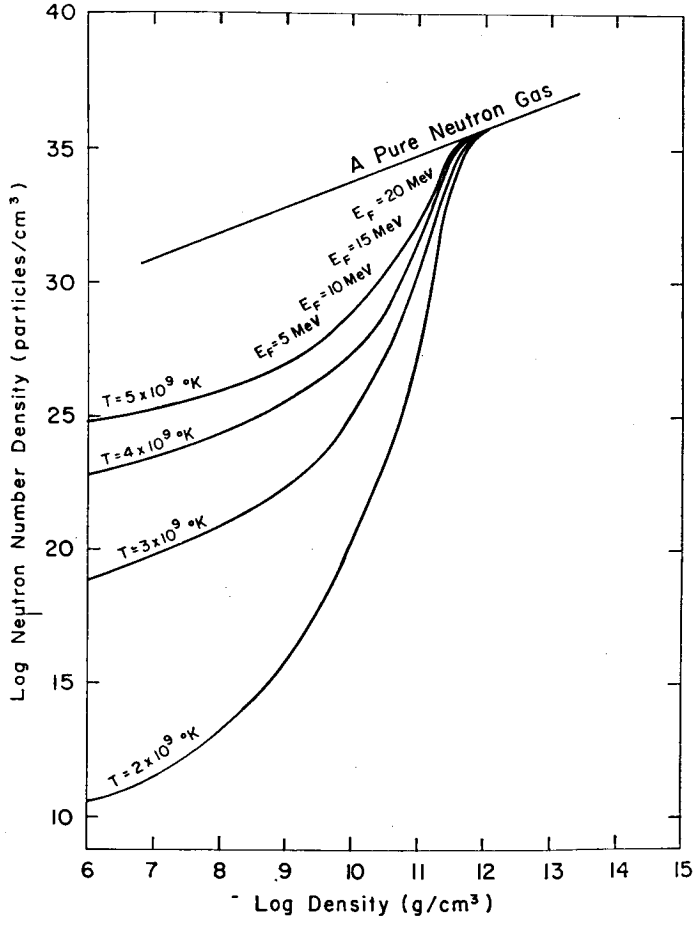

FIG. 4. Neutron number densities at several temperatures plotted as a function of the total matter density.

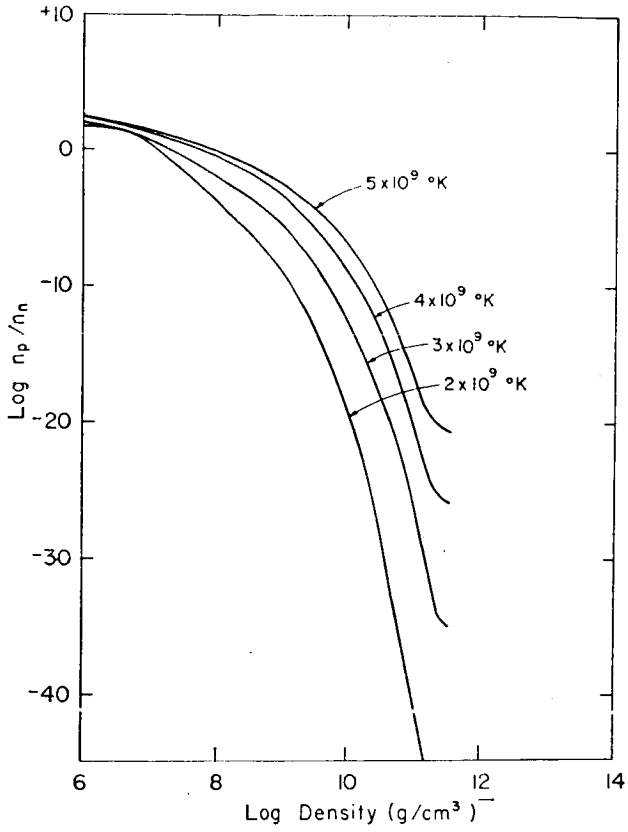

FIG. 5. Ratio of the number densities of free protons to free neutrons at various temperatures plotted as a function of matter density.

The equilibrium abundance distributions corresponding to a temperature of 5×10^9 °K are plotted for Fermi levels of 0.17, 5, 10, 15, 20, and 23 MeV in Figs. 6 through 11. The material density for each Fermi energy is also given in the figures. At the lowest Fermi energy, the equilibrium configuration is peaked at the nucleus ^{56}Fe, a well-known result. At 5 MeV the peak has become very broad, but for higher Fermi energies the abundance distribution is once again strongly peaked, and the peaks then remain for still higher densities. These narrow peaks at high density correspond to the influence of closed neutron shells upon the stability of nuclei. For Fermi levels of 10 and 15 MeV the most abundant nucleus has a closed shell of 50 neutrons. At 20 MeV the peak has slipped a little beyond 50 neutrons; the most abundant nucleus has 52 neutrons. However, it may be seen that another abundance peak centered about 82 neutrons has become almost as important as the peak at lower mass number. At 23 MeV this has indeed become the dominant peak and the most abundant nucleus has 82 neutrons.

Similar calculations were made at temperatures of 2, 3, and 4×10^9 °K and for the same values of E_F. The position of the abundance peaks remained unchanged at the lower temperatures, but the widths of the abundance distributions were much reduced. A comparison of the distributions at 5×10^9 °K and 2×10^9 °K for a Fermi energy of 10 MeV is shown in Fig. 12.

Our calculations done at a temperature of 10^{10} °K showed that the material had been broken down almost completely into individual nucleons at this

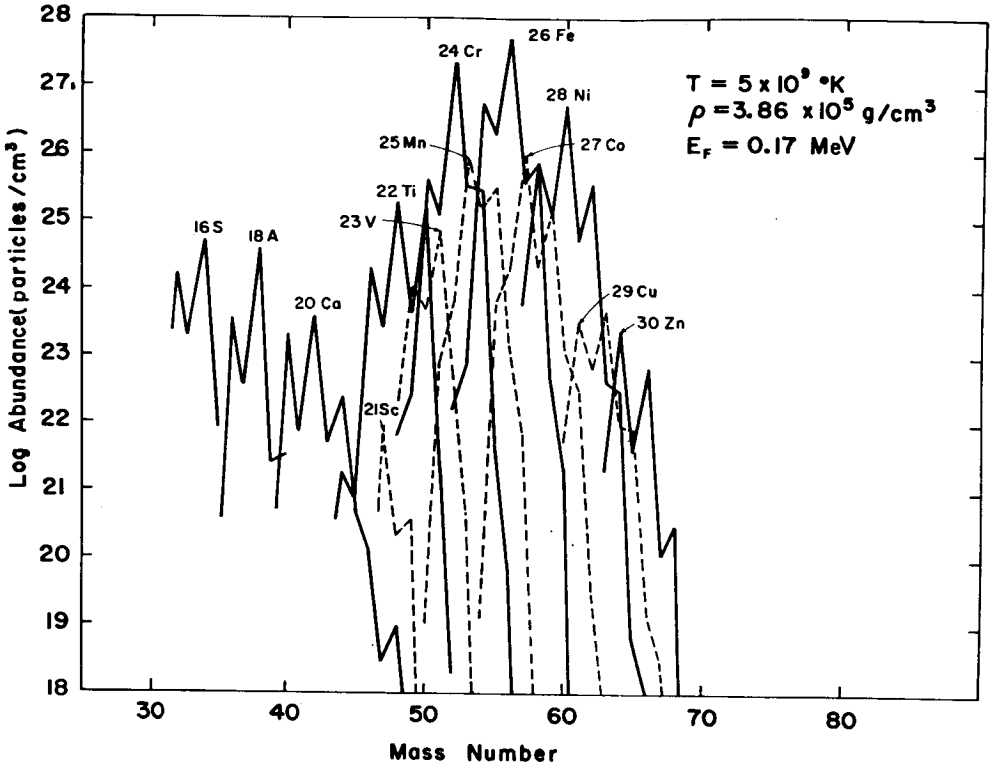

FIG. 6. Equilibrium abundances of nuclei at a Fermi energy of 0.17 MeV.

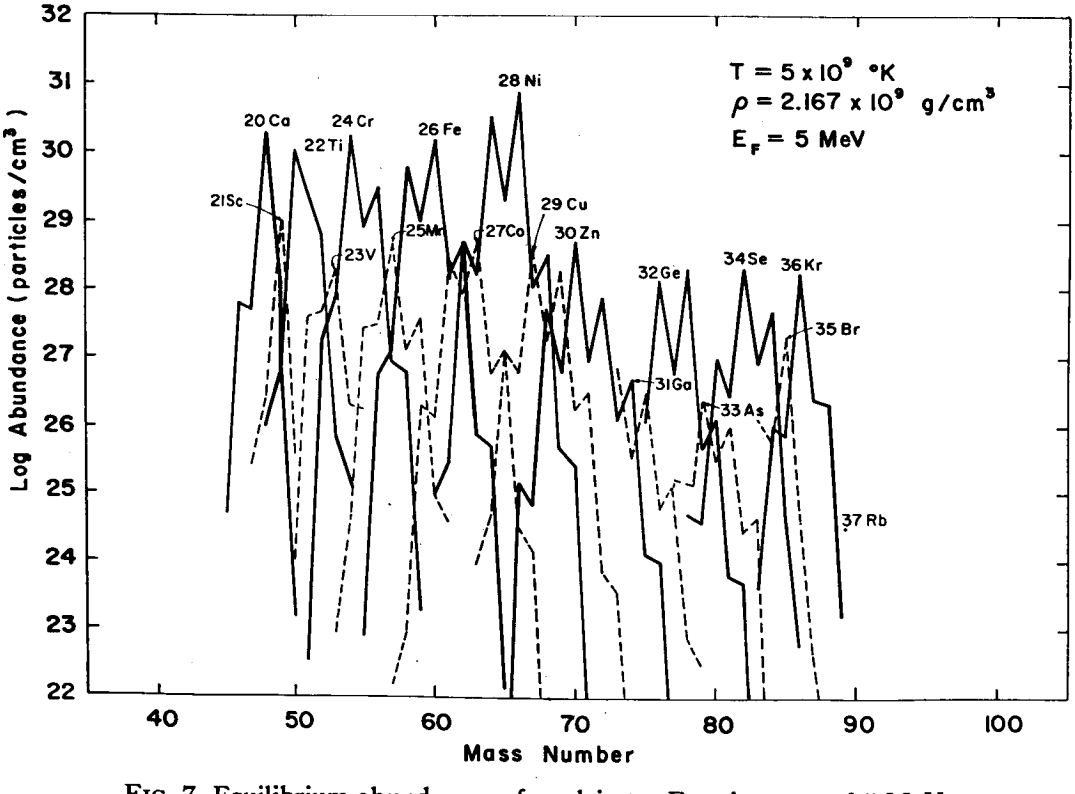

FIG. 7. Equilibrium abundances of nuclei at a Fermi energy of 5 MeV.

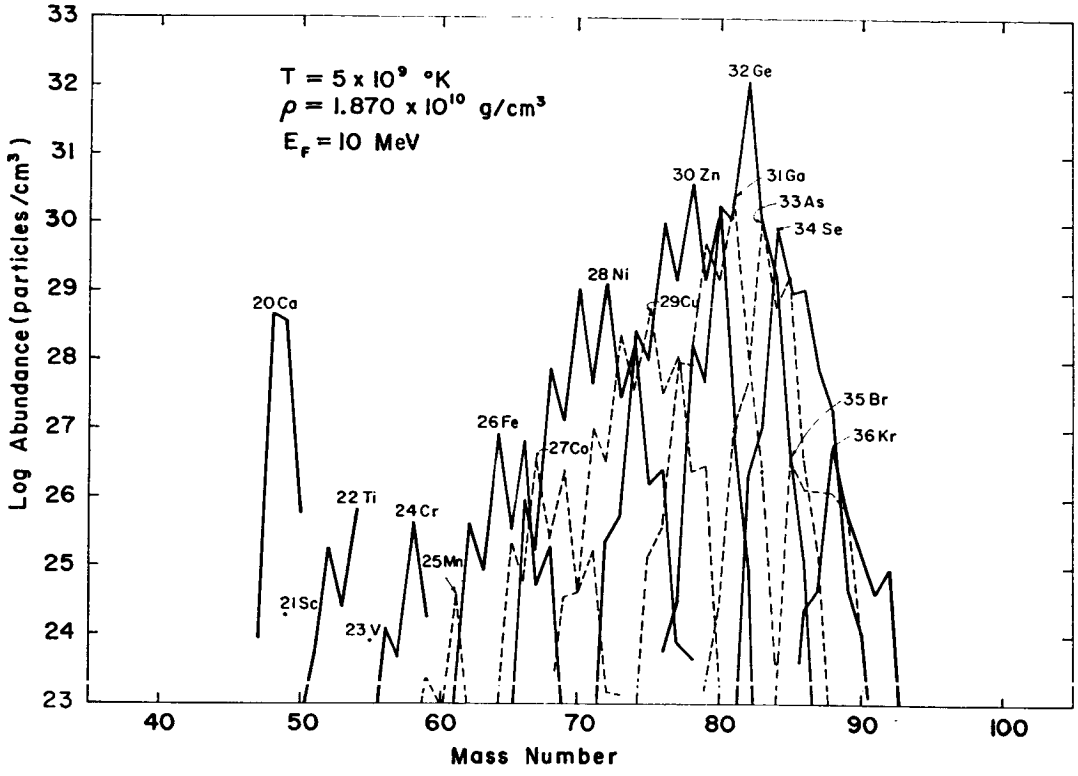

FIG. 8. Equilibrium abundances of nuclei at a Fermi energy of 10 MeV.

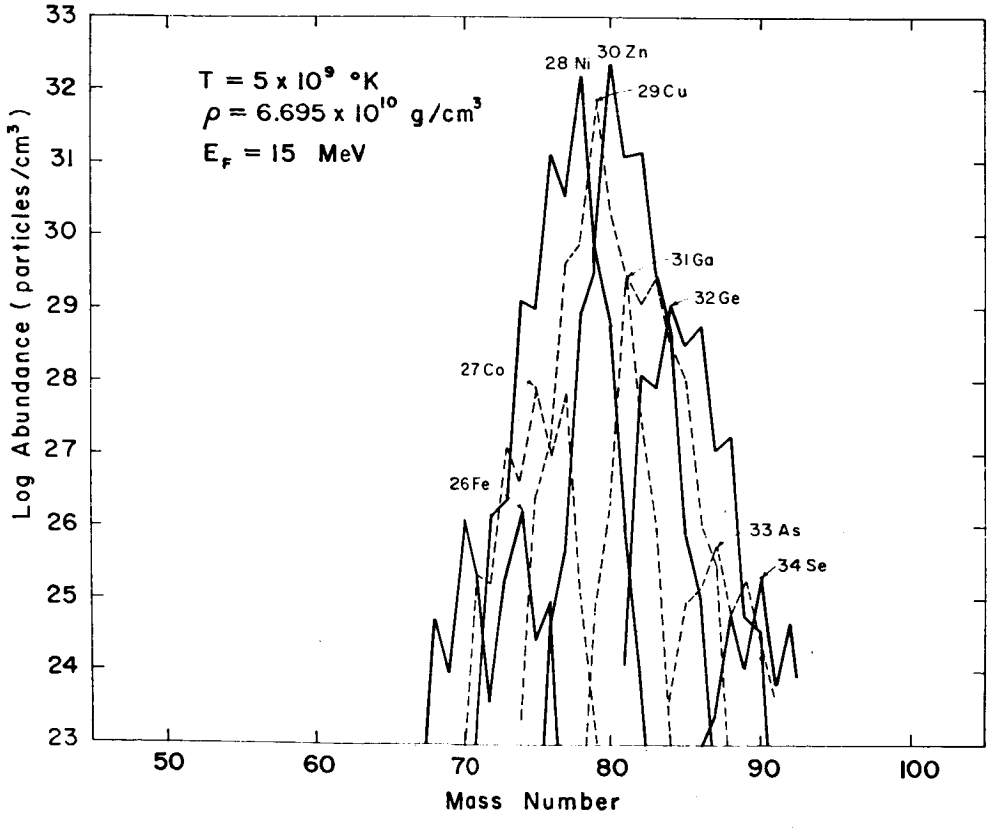

FIG. 9. Equilibrium abundances of nuclei at a Fermi energy of 15 MeV.

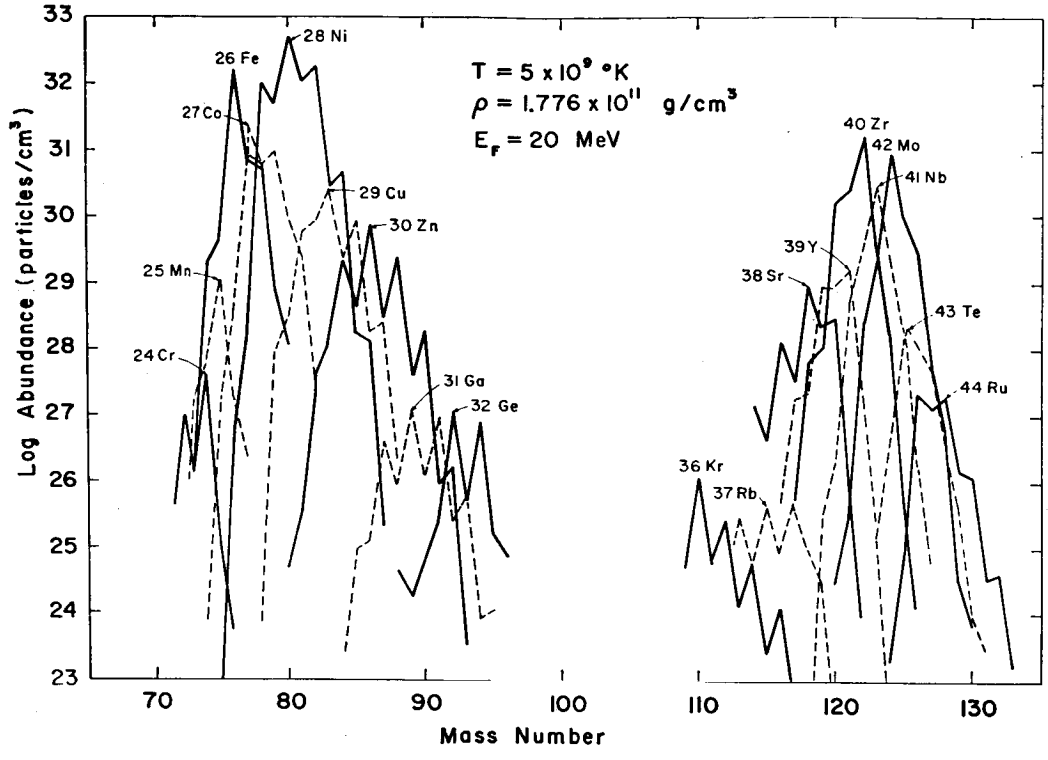

FIG. 10. Equilibrium abundances of nuclei at a Fermi energy of 20 MeV.

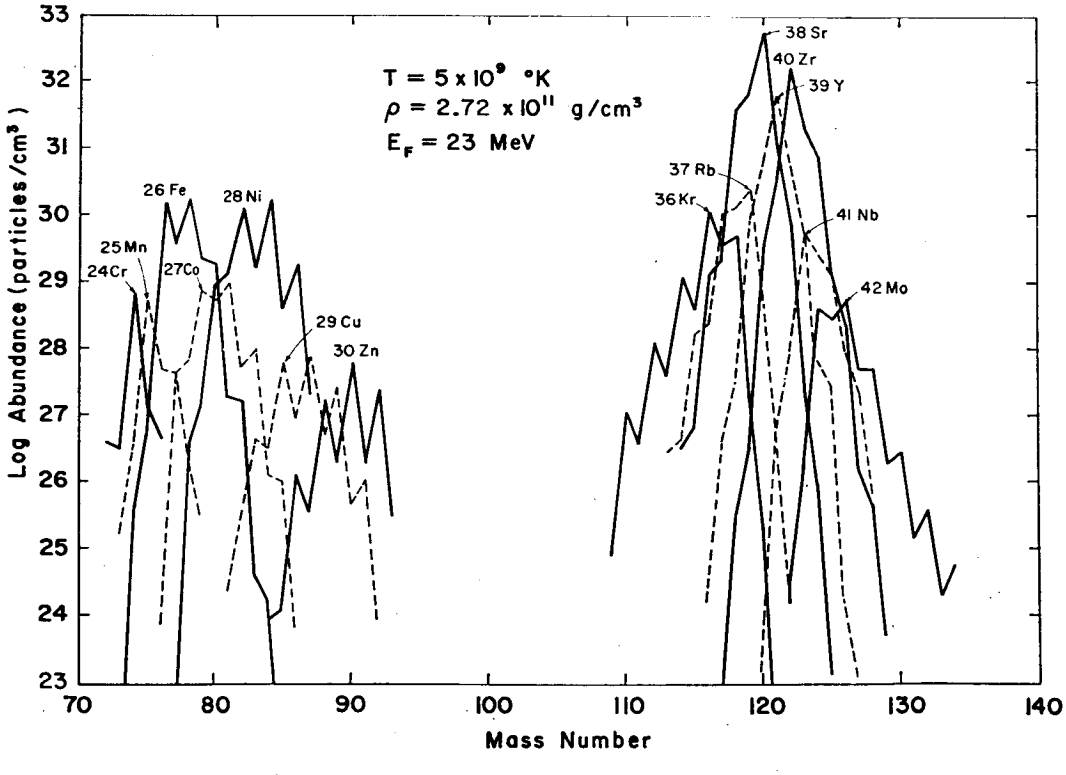

FIG. 11. Equilibrium abundances of nuclei at a Fermi energy of 23 MeV.

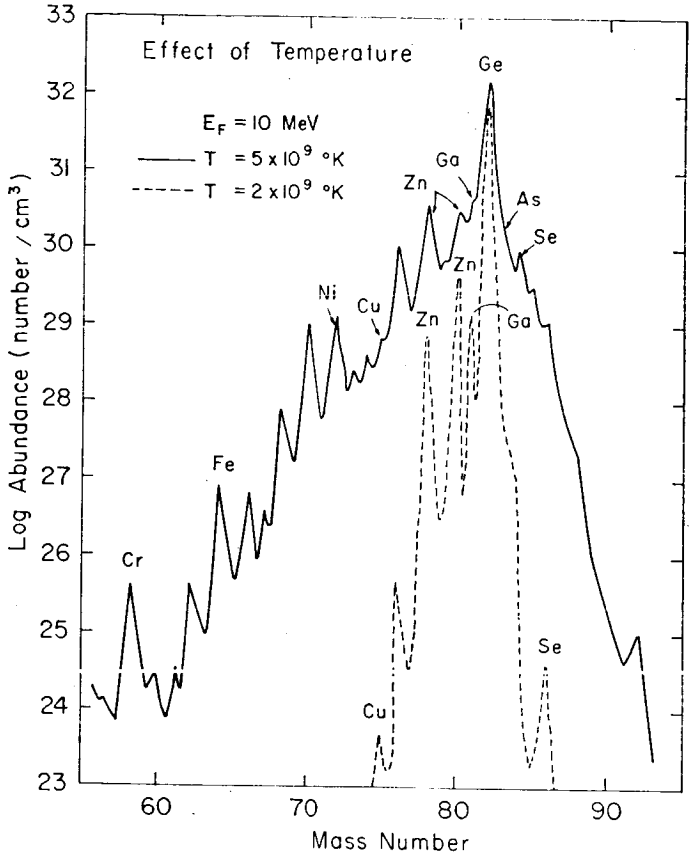

FIG. 12. The effect of temperature on the width of the abundance peak at a Fermi energy of 10 MeV.

temperature. For the higher densities, the composition was nearly that of a neutron gas, while at the lowest densities neutrons and protons were more nearly comparable.

One of the properties of the material required in the studies of dense matter is the mean molecular weight per electron, μ_e, defined as

$$\mu_e \equiv [\sum_k A_k n(A_k, Z_k)]/[\sum_i Z_i n(A_i, Z_i)], \tag{24}$$

where k is summed over all nuclei for $A \geqslant 1$ and $Z \geqslant 0$, and i is summed over all nuclei with $A \geqslant 1$ and $Z \geqslant 1$. Values of μ_e found at temperatures of 5×10^9 °K and 2×10^9 °K are listed in Table II. The difference in the mean molecular weight at the lowest density is due to the larger fraction of ^{4}He at

TABLE II

The mean molecular weight per electron for various Fermi energies and temperatures

	Fermi energy (MeV)						
T (°K)	0.17	5	10	15	20	23	25
5×10^9	2.08	2.375	2.563	2.720	2.985	3.06	7.158
2×10^9	2.16	2.362	2.563	2.677	2.848	3.138	5.970

the higher temperature. When the temperature increases above about 6×10^9 °K, at this small density, the composition of the system changes to favor ^{4}He. However, at high densities and high temperatures the abundance of ^{4}He is not important.

ENERGY LOSS RATES

In an assembly of nuclei in the statistical equilibrium, neutrinos and antineutrinos are produced continuously through the beta processes

$$\begin{aligned} &n(A, Z) + e^- \rightarrow n(A, Z-1) + \nu, \\ &n(A, Z) \rightarrow n(A, Z+1) + e^- + \bar{\nu}. \end{aligned} \tag{25}$$

For most of the systems that have been considered in which matter of composition such as that given in this paper would exist, the neutrinos and antineutrinos would be radiated away into space and would carry considerable amounts of energy with them. The rate of energy loss through these processes is

$$\begin{aligned} L_\nu &= \textstyle\sum_l U_l n(A_l, Z_l), \\ U_l &= \textstyle\sum_i (2I_i + 1)\lambda_i \omega_i \exp(-E_i/kT)/\omega(A_l, Z_l), \\ \lambda_i &= (\ln 2) f_i/(ft)_i, \end{aligned} \tag{26}$$

where U_l is the energy generation per second per nucleus, $n(A_l, Z_l)$ is the abundance of the nucleus l for the beta process in question, and $\lambda_i \omega_i$ is the average neutrino energy production per second per nucleus for the parent nucleus in an excited level i:

$$\omega_i = \int (W^2 - 1)^{1/2} W W_\nu^3 F(Z, W) S \, dW / \int (W^2 - 1)^{1/2} W W_\nu^2 F(Z, W) S \, dW. \tag{27}$$

The sum over l is carried out over all nuclei (A_l, Z_l) of interest, and the sum over i is carried out over all excited nuclear levels. The remaining symbols are those previously defined.

For complete electron degeneracy, the last expression becomes:

(i) Electron capture:

$$\omega_i = \int_{W_x}^{W_F} (W^2 - 1)^{1/2} W (W + W_0)^3 F(Z, W) \, dW/(f_c)_i; \tag{28a}$$

$$W_x = 1 \quad \text{if } W_0 > -1,$$

$$W_x = |W_0| \quad \text{if } W_0 < -1.$$

(ii) Electron emission:

$$\omega_i = \int_{W_F}^{W_0} (W^2 - 1)^{1/2} W (W_0 - W)^3 F(Z, W) \, dW/(f_{e^-})_i, \tag{28b}$$

where f_c and f_{e-} are given by equations (14a) and (14b).

These integrals reduce to the following approximate forms:

(i) Electron capture:

$$(29a)\quad \omega_i = \frac{5}{6}(W_F + W_0)\left[\frac{(1-y^6) - \frac{12}{5}x(1-y^5) + \frac{3}{2}x^2(1-y^4)}{(1-y^5) - \frac{5}{2}x(1-y^4) + \frac{5}{3}x^2(1-y^3)}\right],$$

where $x = W_0/(W_F + W_0)$,

$y = (1 + W_0)/(W_F + W_0)$, if $W_0 \gg -1$;

$$(29b)\quad \omega_i = \frac{5}{6}(W_F - |W_0|)\left[\frac{1 + \frac{12}{5}x + \frac{3}{2}x^2}{1 + \frac{5}{2}x + \frac{5}{3}x^2}\right],$$

where $x \equiv |W_0|/(W_F - |W_0|)$ if $W_0 \ll -1$.

(ii) Electron emission:

$$(30)\quad \omega_i = \frac{D_2(W_0, W_0)}{D_1(W_0, W_0)}\left[1 - \frac{D_2(W_F, W_0)}{D_2(W_0, W_0)}\right] \Big/ \left[1 - \frac{D_1(W_F, W_0)}{D_1(W_0, W_0)}\right],$$

where $D_1(x, y)$ is defined in equation (18), and

$$D_2(x, y) \equiv -\tfrac{1}{6}(x^6 - 1) + \tfrac{3}{5}(x^5 - 1)y - \tfrac{3}{4}(x^4 - 1)y^2 + \tfrac{1}{3}(x^3 - 1)y^3.$$

The total energy loss rate is the sum of the energy loss rates due to neutrinos and due to antineutrinos.

Energy loss rates were calculated from equations (26) to (30) for the key nuclei given in Table I. The total energy loss rates thus obtained are plotted as a function of temperature for a family of electron energies in Fig. 13. There is a striking dependence of the energy loss rates on the temperature and density. We shall designate the energy loss by these combined processes as the generalized URCA process.

There is a comparison between the generalized URCA process energy loss rates and those due to the plasma neutrino process (Adams, Ruderman, and Woo 1963; Inman and Ruderman 1964) in Fig. 14. It may be seen that above a temperature of 2 to 3 $\times$ 10^9 °K the nuclear URCA process exceeds the energy loss by the plasma process. Thus it is evident that the URCA process should be taken into account in detailed calculations of stellar evolution in which stellar material comes into the temperature and density range of interest to the calculations of this paper.

It must be emphasized that all the calculations reported in this paper are exploratory in character. They were carried out as part of a broader investigation of the properties of neutron stars, which will be reported in more detail in other papers. However, the interest in possible application of these calculations extends beyond the neutron star problem, and hence we have considered it desirable to give the various details that have been shown. If we were to repeat the calculations today we would use better values of nuclear masses (Cameron and Elkin 1965) and of nuclear level densities (Gilbert and Cameron 1965). The Fermi functions were calculated for the case of complete degeneracy; more accurate expressions could be used.

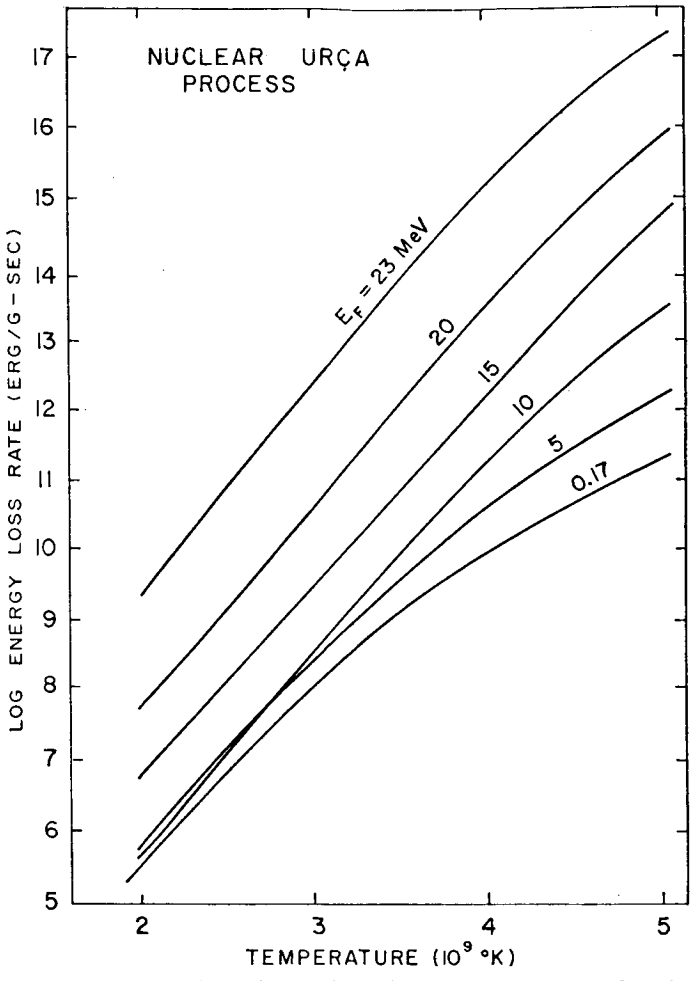

FIG. 13. Energy loss rates plotted as a function of temperature for the generalized nuclear URCA process for several Fermi energies.

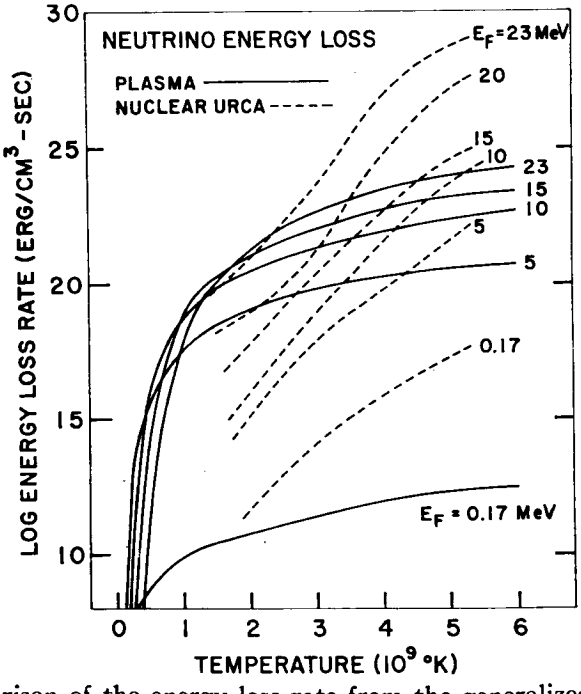

FIG. 14. Comparison of the energy loss rate from the generalized nuclear URCA process with that due to the emission of neutrino–antineutrino pairs by the plasma process plotted as a function of temperature for several Fermi energies.

REFERENCES

ADAMS, J. B., RUDERMAN, M. A., and WOO, C.-H. 1963. Phys. Rev. **129**, 1383.
BAHCALL, J. N. 1964. Astrophys. J. **139**, 318.
BLATT, J. M. and WEISSKOPF, V. F. 1960. Theoretical nuclear physics (John Wiley and Sons, New York).
BLOCH, C. 1954. Phys. Rev. **93**, 1094.
BURBIDGE, E. M., BURBIDGE, G. R., FOWLER, W. A., and HOYLE, F. 1957. Revs. Mod. Phys. **29**, 547.
CAMERON, A. G. W. 1957. Can. J. Phys. **35**, 1021.
——— 1959. Astrophys. J. **130**, 452.
CAMERON, A. G. W. and ELKIN, R. M. 1965. Can. J. Phys. **43**, 1288.
ERICSON, T. 1960. Advances in Phys. **10**, 425.
EVERLING, F., KONIG, L. A., MATTAUCH, J. H. E., and WAPSTRA, A. H. 1960. Nuclear Phys. **18**, 529.
FEENBERG, E. and TRIGG, G. 1950. Revs. Mod. Phys. **22**, 399.
GILBERT, A. and CAMERON, A. G. W. 1965. Can. J. Phys. **43**, 1446.
GILBERT, A., TRURAN, J. W., and CAMERON, A. G. W. 1966. To be published.
HIBDON, C. T. 1959. Phys. Rev. **114**, 179.
HOYLE, F. 1946. Monthly Notices Roy. Astron. Soc. **106**, 343.
HUIZENGA, J. R. and VANDENBOSCH, R. 1960. Phys. Rev. **120**, 1305.
INMAN, C. L. and RUDERMAN, M. A. 1964. Astrophys. J. **140**, 1025.
LANDOLT-BORNSTEIN. 1961. Numerical data and functional relationships in science and technology, vol. I: Energy Levels (Springer-Verlag, Berlin).
MAJOR, J. K. and BIEDENHARN, L. C. 1954. Revs. Mod. Phys. **26**, 321.
VANDENBOSCH, R. and HUIZENGA, J. R. 1960. Phys. Rev. **120**, 1313.

~~Appendix I~~

5. Composition of Matter Near Nuclear Density (C. J. Hansen)

A. Mixtures in Statistical Equilibrium

Several sections of these notes make use of the properties of mixtures of non-interacting particles in statistical equilibrium. These terms are used here in a specific way, i.e.:

1. A mixture of non-interacting particles consists of any combination of particle concentrations where individual contributions from any given type of particle to the variables pressure, energy, entropy and thermodynamic potential depend only on the concentration of that type of particle. Thus, for a mixture of electrons and positrons, the state of the system at any given time is to be described by treating electrons and positrons separately.

2. In a mixture in statistical equilibrium the thermodynamic potential Φ (see below) tends to a minimum for a fixed temperature and pressure.

3. If condition (2) is satisfied but there are energy losses from the system (neutrinos, photons, etc.), then it is assumed (or shown) that the composition of the system changes slowly compared to some chosen dynamic time scale. A special case of this is the system consisting of electrons, positrons and photons in equilibrium where pair annihilation into neutrino-antineutrino pairs is the only loss mechanism assumed. Since each pair carries off zero lepton number the composition cannot change in time except as the temperature drops due to energy loss.

4. It is always assumed that the chemical potentials (see below) of neutrinos and antineutrinos (of electronic or muonic kind) are equal. This, as will be shown, implies that their concentrations are equal. Rephrasing this, the assumption is that throughout the previous history of the system there has been no mechanism whereby one kind of neutrino has been stored in preference to another.* Thus, under the conditions of (3) this means that equal concentrations of neutrinos will persist for all times of interest.

B. Thermodynamic Condition for Equilibrium

To find the condition necessary for equilibrium we follow Landau and Lifshitz (1958) and express the thermodynamic potential Φ as a function of concentration (i.e., number density), temperature, and pressure,

$$\Phi = \Phi(T,P,N_i)$$

where i represents all of the constituents. A necessary condition for Φ to be a minimum, for fixed T and P, is that its total derivative vanish,

$$\frac{\partial \Phi}{\partial N_1} + \frac{\partial \Phi}{\partial N_2}\frac{\partial N_2}{\partial N_1} + \frac{\partial \Phi}{\partial N_3}\frac{\partial N_3}{\partial N_1} + \ldots = 0$$

where the subscripts on N range over all types of particles. Without loss of generality we will restrict this to three types of particles which can react according to

---

*This view would be unreasonable if it turned out that the universe contained a surplus of one kind of neutrino or another. Some arguments against this possibility are given in Wheeler et al (1965), chapt. 9.

$$A_1 + A_2 \leftrightarrow A_3 .$$

This fixes the rate of change of one number density with respect to another explicitly, i.e., $\partial N_1/\partial N_2 = 1$, $\partial N_1/\partial N_3 = -1$, etc., so that the equilibrium equation becomes

$$\frac{\partial \Phi}{\partial N_1} + \frac{\partial \Phi}{\partial N_2} - \frac{\partial \Phi}{\partial N_3} = 0$$

Defining the chemical potential μ (which <u>always</u> includes rest mass in this thesis)

$$\mu_i = \left(\frac{\partial \Phi}{\partial N_i}\right)_{T,P} ,$$

then,

$$\mu_1 + \mu_2 - \mu_3 = 0 .$$

The extension to more complex systems is straightforward.

Some examples appear later.

C. Calculation of Thermodynamic Quantities

For the physical conditions we encounter, quantum statistics are necessary to describe the state of the system. The relation between chemical potential and number density is given by the well known expression*

$$N = \frac{4\pi g}{h^3} \int_0^\infty \frac{p^2 dp}{\exp\left[(E-\mu)/kT\right] \pm 1}$$

*Eg., see Landau and Lifshitz (1958), chapter V or Chandrasekhar (1939), chapter X.

where g is the spin multiplicity g = 2S + 1, p the relativistic momentum and E the relativistic total energy

$$E^2 = (pc)^2 + (mc^2)^2 \ .$$

The plus (minus) sign in the denominator is for fermions (bosons). The Planck and Boltzmann constants are, respectively,

$$h = 6.625 \times 10^{-27} \text{ erg-sec},$$

$$k = 8.6167 \times 10^{-11} \text{ MeV}/^{\circ}\text{C}.$$

Defining the dimensionless variables

$$x = p/mc \ ,$$

$$y = E/mc^2 = (1 + x^2)^{1/2} \ ,$$

$$\beta = mc^2/kT \ ,$$

and $$u = \mu/mc^2$$

we have

$$N = 4\pi g \left(\frac{mc}{h}\right)^3 \int_0^{\infty} \frac{x^2 dx}{\exp\left[\beta(y-u)\right] \pm 1} \ .$$

Numerically, this becomes

$$N = g \left(\frac{m}{m_e}\right)^3 \frac{a_o}{2} \int_0^{\infty} \frac{x^2 dx}{\exp\left[\beta(y-u) \pm 1\right]}$$

where m_e is the electron mass and

$$a_o = 1.76 \times 10^{30} \text{ cm}^{-3} .$$

The corresponding expressions for pressure and total energy are

$$P = g \left(\frac{m}{m_e}\right)^4 \frac{a_1}{6} \int_o^\infty \frac{x^4}{y} \frac{dx}{\exp\left[\beta(y-u)\right] \pm 1} ,$$

$$E = g \left(\frac{m}{m_e}\right)^4 \frac{a_1}{2} \int_o^\infty \frac{yx^2 dx}{\exp\left[\beta(y-u)\right] \pm 1} ,$$

where

$$a_1 = \frac{8\pi m_e^4 c^5}{h^3} = 1.44 \times 10^{24} \text{ ergs/cm}^3 \text{ (or dynes/cm}^2\text{)} .$$

None of the above integrals are expressible in terms of elementary functions and must either be integrated numerically or suitable expansions must be found for limiting cases. For fermions, two limiting cases will be distinguished -- degenerate and non-degenerate. The latter is said to hold if $u \leq 0$ (with $T>0$) in which case (following Chandrasekhar, 1939) the Fermi-Dirac denominator may be expanded in powers of the exponential. The resulting integrals are directly expressible in terms of the modified Bessel functions K_n, and yield, for $u \leq 0$,

$$N = g \left(\frac{m}{m_e}\right)^3 \frac{a_o}{2} \sum_{n=1}^\infty (-1)^{n+1} \exp n\beta u \frac{K_2(n\beta)}{n\beta} ,$$

$$E = g\left(\frac{m}{m_e}\right)^4 \frac{a_1}{2} \sum_{n=1}^{\infty} (-1)^{n+1} \exp n\beta u \left[\frac{3K_2(n\beta)}{(n\beta)^2} + \frac{K_1(n\beta)}{n\beta}\right]$$

$$P = g\left(\frac{m}{m_e}\right)^4 \frac{a_1}{2} \sum_{n=1}^{\infty} (-1)^{n+1} \exp n\beta u \frac{K_2(n\beta)}{(n\beta)^2} .$$

(For computer application, the functions K_2 and K_1 are most easily evaluated using the polynomial approximations given in Abramowitz (1964), p. 378.)

The integrations for a degenerate fermion gas are more involved but the method of Sommerfeld* yields comparatively simple expansions which will be given here to three terms. Let x, the dimensionless Fermi momentum, have that value given for a completely degenerate gas (zero temperature), i.e.,

$$x = \left[\frac{6}{a_o g}\left(\frac{m_e}{m}\right)^3 N\right]^{1/3} .$$

Then,

$$N = g\left(\frac{m}{m_e}\right)^3 \frac{a_o}{6} x^3 \left[1 + \frac{\pi^2}{\beta^2}\frac{2x^2+1}{2x^4} + \frac{7\pi^4}{40\beta^4 x^8}\right] ,$$

$$E = g\left(\frac{m}{m_e}\right)^4 \frac{a_1}{16} g(x)\left[1 + \frac{4\pi^2}{3\beta^2 x}\frac{u_F(1+3x^2)}{g(x)} + \frac{7\pi^4}{15\beta^4 x^5}\frac{u_F(2x^4-x^2+1)}{g(x)}\right] ,$$

$$P = g\left(\frac{m}{m_e}\right)^4 \frac{a_1}{48} f(x)\left[1 + \frac{4\pi^2}{\beta^2}\frac{u_F x}{f(x)} + \frac{7\pi^4}{15\beta^4}\frac{u_F(2x^2-1)}{x^3 f(x)}\right] ,$$

---

*See Chandrasekhar (1939), p. 389.

where,

$$g(x) = u_F\, x(2x^2+1) - \ln (x+u_F),$$

$$f(x) = 8x^3 u_F - 3g(x) ,$$

and u_F is the dimensionless, degenerate total Fermi energy

$$u_F = (1+x^2)^{1/2} .$$

It is by means of these expansions that we determine whether the gas is degenerate -- the condition being that the second term in all expansions must be small compared to unity. The results will be accurate to within a fraction of a percent if the second term is ~ 0.05.

In the no man's land where $1 \geq u > 0$, or the gas is not degenerate according to the above oriterion, then the integrals must be done numerically.

D. Equilibrium Abundances for Electron-Positron-Radiation Mixtures

A particularly simple example of a mixture in equilibrium is that composed of electrons, positrons and radiation at high temperatures.* When $kT \sim m_e c^2$ ($T \sim 6 \times 10^{9}{}^{o}K$), pair annihilation and creation proceed at sufficiently rapid rates that chemical equilibrium for these reactions, i.e.,

$$e^+ + e^- \leftrightarrow \text{photons}$$

---

*Some of this discussion follows Landau and Lifshitz (1958), chapter XI, and Chiu (1961a).

is established. To see this we compute rough rates for the reactions. From second order perturbation theory the extreme relativistic cross sections for both pair creation and annihilation are approximately (Bjorken and Drell, 1964)

$$\sigma_{CM} \sim r_o^2 \pi \frac{m_e c^2}{E} ,$$

where the energy E refers to either photons or electrons, and r_o is the classical electron radius, $r_o^2 = 7.94 \times 10^{-26}$ cm^2. For $kT = mc^2$, the number density of black-body photons is $N_\gamma \sim 2 \times 10^{28}$ cm^{-3}. From the equilibrium calculation to be described below, the number density of electrons or positrons is $\sim 3 \times 10^{30}$ cm^{-3}. Without much error we assume all particles to have the energy kT and velocities close to c. Hence, the rate of pair creation is $\sigma c N_\gamma^2 \sim 10^{41}$ sec^{-1}cm^{-3} and for pair annihilation $\sim 10^{45}$ sec^{-1}cm^{-3}. The mean life per particle is then $\sim 10^{-15}$ sec. which is much shorter than any dynamic time scale we consider and is sufficient to guarantee equilibrium.

The condition for thermodynamic equilibrium requires that the sum of electron and positron chemical potentials equal some multiple of the chemical potential of the photon gas. However, since the photon number is a variable quantity, the photon chemical potential must be zero. Hence,

$$\mu_- + \mu_+ = 0.$$

If we generalize the problem to the case where there are N_o "permanent" electrons associated with ions in the gas, then charge

neutrality demands that

$$N_- - N_+ = N_o,$$

where N_- and N_+ are total numbers of electrons and positrons. For a given temperature and N_o, this equation and the relation $\mu_- = -\mu_+$ are sufficient to determine N_- and N_+ - or, as required in the first part of this thesis, μ_- can be found. Figure 1 shows the results of the latter calculation where ρ/μ_e is related to N_o by

$$\rho/\mu_e = 1.67 \times 10^{-24} N_o \text{ gms/cm}^3,$$

where ρ is the ion density of the medium (in gm/cm^3), and $\mu_e = (A/Z)_{avg}$, the mean molecular weight of the ionic electrons. T_9 is the temperature in units of 10^9 ^oK, and $u = \mu_-/mc^2$. N_- and N_+ are shown in Figure 2 where negative as well as positive values of $u = u_-$ are represented. (Notice that N is given in the "natural units" $a_o = 1.76 \times 10^{30}$ cm^{-3}.) This curve also illustrates the characteristics of an electron gas. For u less than zero the number density falls off as a negative exponential in u corresponding to a non-degenerate Maxwellian gas. For large positive u (degenerate region) it goes as the Fermi momentum cubed and relatively high temperatures are required to lift the degeneracy.

E. Equilibrium Mixtures for Neutron Stars

In order to compute neutron star compositions it will first

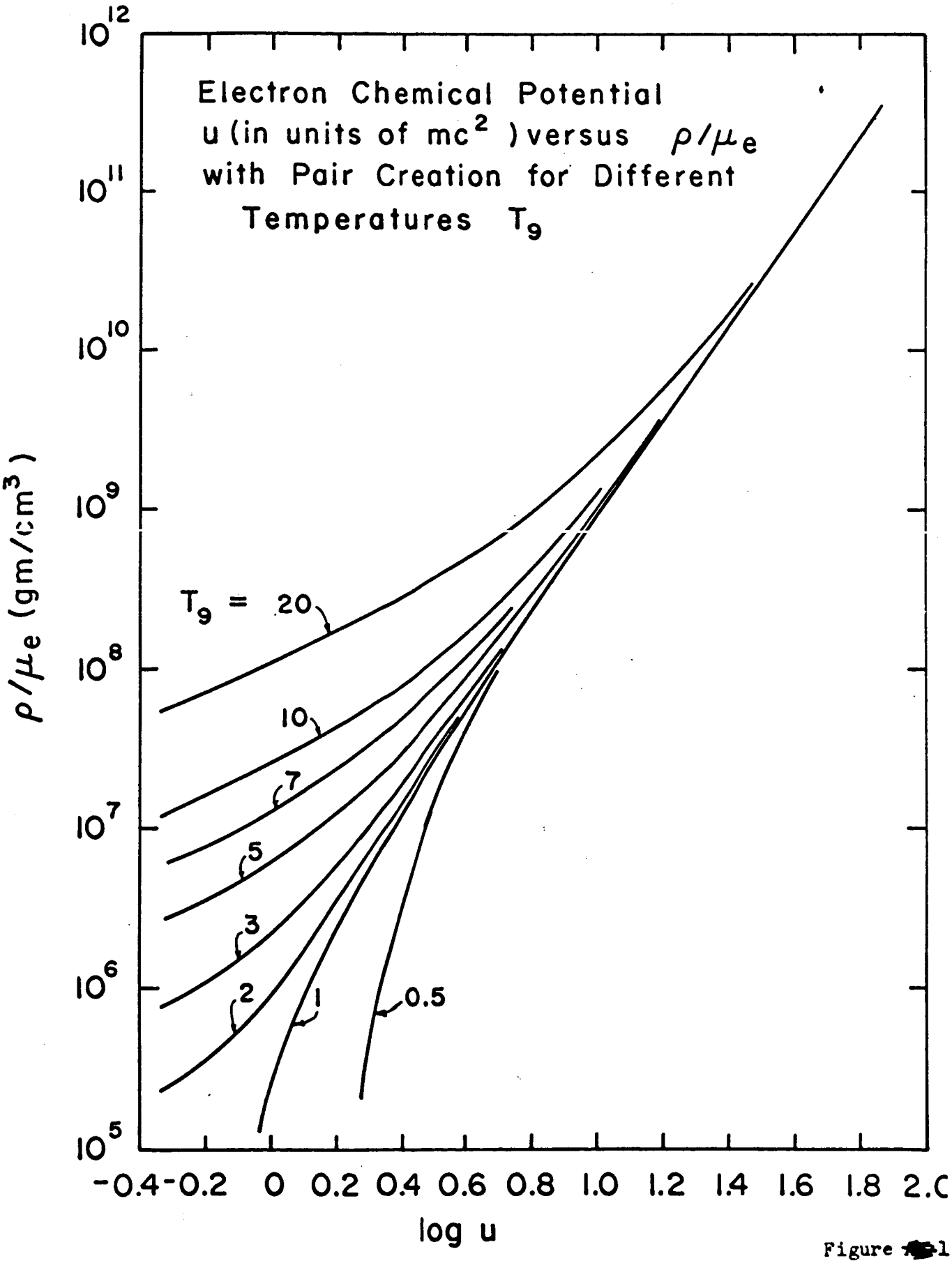
Electron Chemical Potential
u (in units of mc^2) versus ρ/μ_e
with Pair Creation for Different
Temperatures T_9
ρ/μ_e (gm/cm^3)
10^{12}
10^{11}
10^{10}
10^9
10^8
10^7
10^6
10^5
T_9 = 20
10
7
5
3
2
1
0.5
-0.4 -0.2 0 0.2 0.4 0.6 0.8 1.0 1.2 1.4 1.6 1.8 2.0
log u

Figure 1

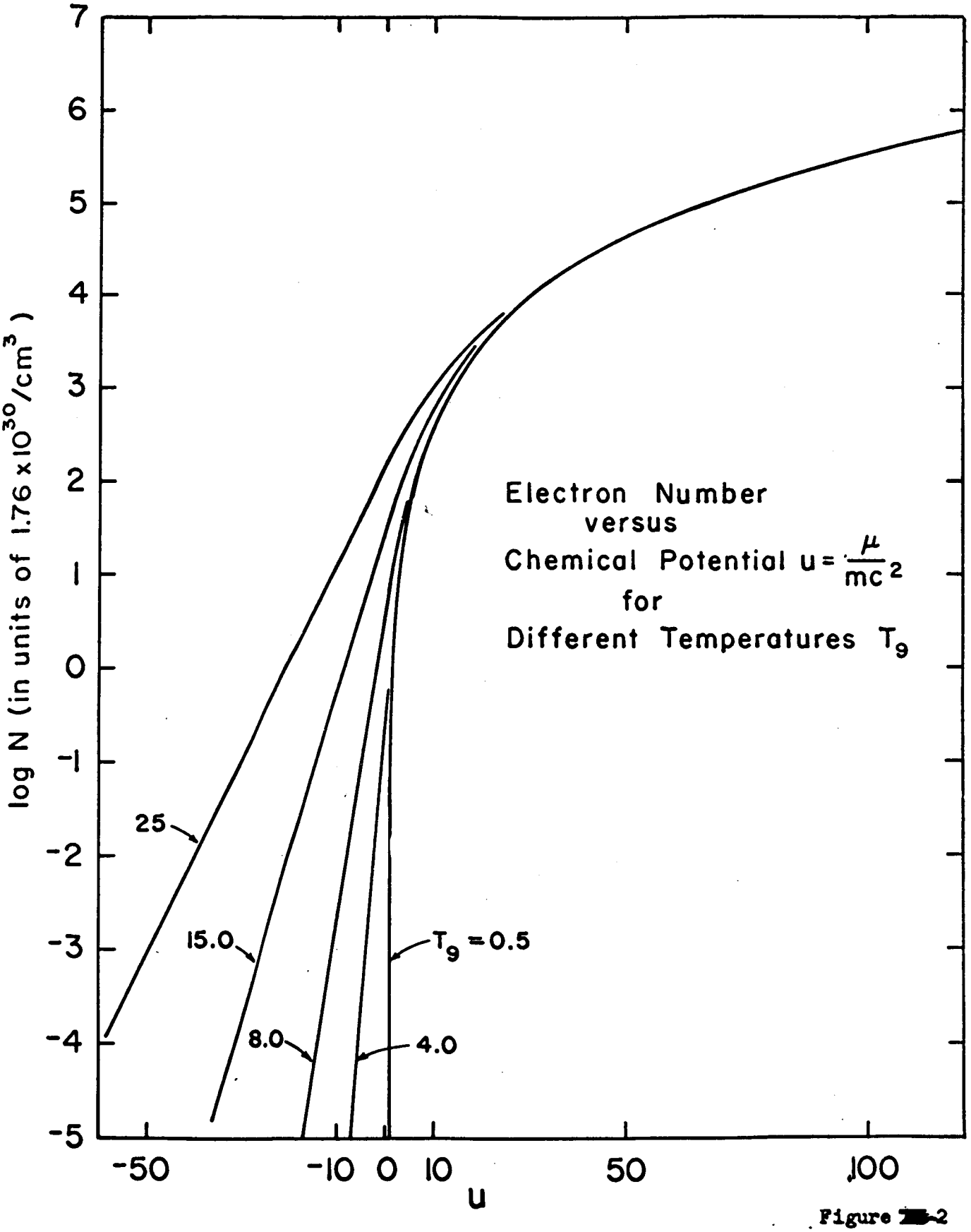
7
6
5
4
3
2
1
0
-1
-2
-3
-4
-5
log N (in units of 1.76 x 10^30/cm^3)
-50
-10
0
10
50
100
u
Electron Number
versus
Chemical Potential u = μ/mc^2
for
Different Temperatures T9
25
15.0
8.0
4.0
T9 = 0.5

Figure 2

be necessary to generalize the results of Section B.*

Consider a mixture composed of any set of elementary particles that satisfies the conditions of Section A. The thermodynamic potentials for a particular type of particle will be designated by φ_i. The total potential is then the sum of all φ_i,

$$\Phi = \Sigma\, \varphi_i(\text{baryons}) + \Sigma\, \varphi_i(\text{antibaryons}) + \Sigma\, \varphi_i(\text{leptons})$$

$$+ \Sigma\, \varphi_i(\text{antileptons}) + \Sigma\, \varphi_i(\text{mesons and antimesons}) + \Sigma\, \varphi_i(\text{photons}).$$

For equilibrium it is required that Φ be a minimum. This condition, however, does not determine the composition uniquely and so we impose the following natural restraints:

1. Baryon number, electronic lepton number, and muonic lepton number must all be conserved in processes leading to equilibrium.

2. The mixture must be electrically neutral.

These conditions are expressed by,

$$\Sigma\, N_i(\text{baryons}) - \Sigma\, N_i(\text{antibaryons}) = \text{constant} \equiv N(B),$$

$$\Sigma\, N_i(\text{electronic leptons}) - \Sigma\, N_i(\text{elec. antileptons}) = \text{constant} = N(e),$$

$$\Sigma\, N_i(\text{muonic leptons}) - \Sigma\, N_i(\text{muonic antileptons}) = \text{constant} = N(\mu),$$

$$\Sigma\, q_i N_i(\text{all particles}) = 0,$$

---

*The method to be outlined is essentially that of Ambartsumyan (1960) and Tsuruta (1964) except that their calculations are restricted to mixtures at zero temperature.

where q is the charge number of a specific type of particle, eq., q = - 1 for antiprotons, zero for neutrons, etc.

To incorporate these with the minimization of Φ we use the method of Lagrange multipliers and define

$$F = \Phi + a\,N(B) + b\,\Sigma qN + c\,N(e) + d\,N(\mu),$$

where a,b,c,d are coefficients to be determined. Since it is required that

$$\frac{\partial F}{\partial N_i} = 0, \text{ (i ranging over all types)},$$

it follows that

$\mu + bq + a = 0$	for	baryons
$\mu + bq - a = 0$	for	antibaryons
$\mu + bq + c = 0$	for	elec. leptons
$\mu + bq - c = 0$	for	elec. antileptons
$\mu + bq + d = 0$	for	muon leptons
$\mu + bq - d = 0$	for	muon antileptons
$\mu + bq = 0$	for	all mesons, photons

We assume that particles predominate over antiparticles so that it is convenient to express a and b in terms of proton and neutron chemical potentials. We obtain,

$$\mu = \mu_n(1-q) + q\mu_p \quad \text{for} \quad \text{baryons}$$
$$\mu = -\mu_n(1+q) + q\mu_p \quad \text{for} \quad \text{antibaryons}.$$

As is the case for all particles, the transformation particle

→ antiparticle implies q → -q, so the relation between particle and antiparticle μ's is

$$\mu \text{ (particle)} = -\mu \text{ (antiparticle)}.$$

It is for this reason that a large abundance of a particle implies a small abundance of its anti. (See eg., Figure AI-2)

Furthermore, we have,

$$c = -\mu(\nu_e) = \mu(\bar{\nu}_e)$$

$$d = -\mu(\nu_\mu) = \mu(\bar{\nu}_\mu)$$

where ν_e and ν_μ are electron and muon neutrinos. But by the application of condition (4) of Section A, $\mu(\nu) = \mu(\bar{\nu})$, or, $\mu(\nu_e) = \mu(\nu_\mu) = \mu(\bar{\nu}_e) = \mu(\bar{\nu}_\mu) = 0$*. Hence, $\mu = \mu_n - \mu_p$ for negative electrons or muons, and finally

$\mu = q(\mu_p - \mu_n)$ for mesons

$\mu = 0$ for photons (as in Section D).

The condition on μ for the boson mesons needs some clarification. Strictly speaking, a boson chemical potential cannot exceed the particle's rest mass energy, and will equal the rest mass energy only when the temperature is near or below the Bose-Einstein

---

*In terms of number density this means

$$N(\nu\text{'s of any kind}) = \left(\frac{kT}{hc}\right)^3 4\pi \sum_{n=1}^{\infty} (-1)^{n+1} \frac{2}{n^3} = 7.65\times10^{27}\, T_9^3 \text{ cm}^{-3}.$$

where $g = 1$ since the helicity has but one value for a given type of neutrino.

condensation temperature T_o. The latter quantity, for a π^- meson, which is the only one to be considered seriously, is related to the number density by

$$kT_o \text{ (MeV)} \simeq (N_\pi/4 \times 10^{34})^{2/3} .$$

In regions of interest, (i.e. where densities are less than $\sim 10^{17}$ gm/cm^3 and temperatures are less than $\sim 10^{10}$ ^oK), the condensation temperatures, for which $\mu_\pi = \mu_n - \mu_p \approx m_\pi c^2$ or N_π is comparable to other number densities, are much higher than 10^{10} ^oK implying that π^-'s may be considered degenerate. Thus, for $\mu_n - \mu_p \lesssim mc^2$, negligible numbers of π^- are present in the mixture.

The calculation of equilibrium concentrations proceeds as follows: for a given temperature the neutron density N_n is chosen, thus fixing μ_n. Iterative values of μ_p are then picked (each value yielding all the other particle number densities by application of the μ-equations) until charge neutrality is satisfied. The only difficulty in this procedure is that the iterative process is graphical and rather exhaustive tables of μ vs. N must be prepared beforehand.

For neutron star abundances the set of elementary particles given in Table 1 were chosen. Approximate masses, values of $g = 2 \times \text{spin} + 1$, and q were taken from Rosenfeld (1964).

No antiparticles were included because the condition $\mu = -\bar{\mu} \gg 0$ precluded any but negligible concentrations being present. The isospin quadruplet Δ_δ baryon (known also as $N^*_{3/2}$) was included

Table 1

Particle	Mass (MeV)	g	q
n	939.6	2	0
p	938.3	2	+1
Δ_δ^-	1238	4	-1
Δ_δ^o	1238	4	0
Δ_δ^+	1238	4	+1
Δ_δ^{++}	1238	4	+2
Λ^o	1115	2	0
$\Sigma^{+,o,-}$	1192	2,2,2	+1,0,-1
$\Xi^{+,o,-}$	1317	2,2	0,-1
e^-	0.511	2	-1
μ^-	105.7	2	-1
π^-	139.6	1	-1

because of its relatively low mass and high value of g.* Particles of mass greater than Ξ can only be created at densities greater than 10^{17} gm/cm^3 or at very high temperatures. This is a moot point, in a way, since the artificial nature of the non-interacting particle assumption probably makes itself evident at densities not too much greater than nuclear ($\sim 4 \times 10^{14}$ gm/cm^3).

Only two members of this quadruplet were included in the calculations of Ambartsumyan (1960) and Tsuruta (1964), namely Δ_δ^+ and Δ_δ^o which they called p and n*.

It has since come to my attention that a paper has been submitted for publication by B. M. Barker, M. S. Bhatia and G. Szamosi (University of Windsor, Ontario) in which they do a zero temperature calculation which includes 56 elementary particles. Their results for densities less than 10^{17} gm/cm^3 do not seem to differ from mine. They include a convenient table which lists the densities at which all the particles make their appearance.

In Figure 3 the particle abundances are shown for the range of densities of interest in neutron stars. These abundances are taken to be representative of temperatures from zero to $\sim 10^{10}$ °K. At higher temperatures the degenerate condition of the particles is relaxed and abundances will vary from those shown (especially at the lowest densities).

For densities up to about 6×10^{14} gm/cm^3 the mixture contains only neutrons, protons and electrons. At 6×10^{14} gm/cm^3 $\mu_n - \mu_p$ approaches the muon rest mass and so that particle makes its appearance. Beyond $\sim 10^{15}$ gm/cm^3 various heavy particles enter with Σ^- appearing first. It is interesting to note that these particles do not enter in order of increasing mass. In the case of Σ^- it is necessary to neutralize the positive charge produced by the increasing proton number density. It is energetically more economical to do this by producing one Σ^- rather than one more proton and two electrons because the proton and electron Fermi levels are very high. Thus Σ^- enters before the less massive Λ^o.

Figure 4 shows the run of equilibrium μ_n and μ_p with density. It is this curve which is used in the phase space calculation of the $(n,n) \rightarrow (n,p,e,\nu)$ reactions. This figure also indicates the approximate range of validity, in that calculation, of the assumption that the protons are degenerate. For example, at a density of $\sim 2 \times 10^{14}$ gm/cm^3 the proton Fermi kinetic energy is about 1.5 MeV indicating that degeneracy is lifted for temperatures greater than $\sim 10^{10}$ °K ($kT \sim .8$ MeV). The latter is taken as the upper limit on temperatures considered in neutron star calculations.

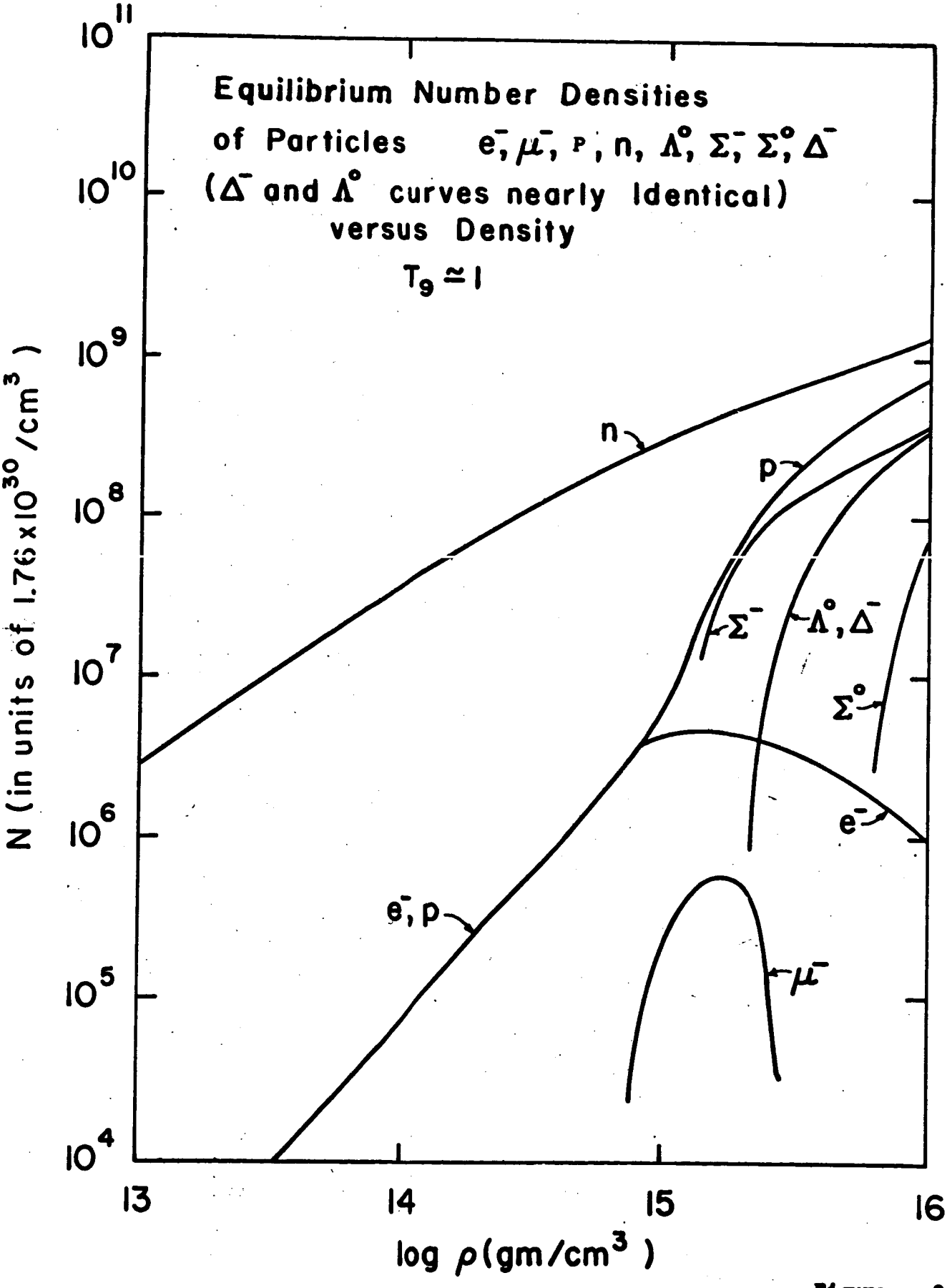
Equilibrium Number Densities
of Particles $e^-, \mu^-, p, n, \Lambda^\circ, \Sigma^-, \Sigma^\circ, \Delta^-$
(Δ^- and Λ° curves nearly Identical)
versus Density
$T_9 \simeq 1$
N (in units of 1.76×10^{30} /cm^3)
log ρ(gm/cm^3)
10^{11}
10^{10}
10^9
10^8
10^7
10^6
10^5
10^4
13
14
15
16
n
p
Σ^-
Λ°, Δ^-
Σ°
e^-
e^-, p
μ^-

Figure 3

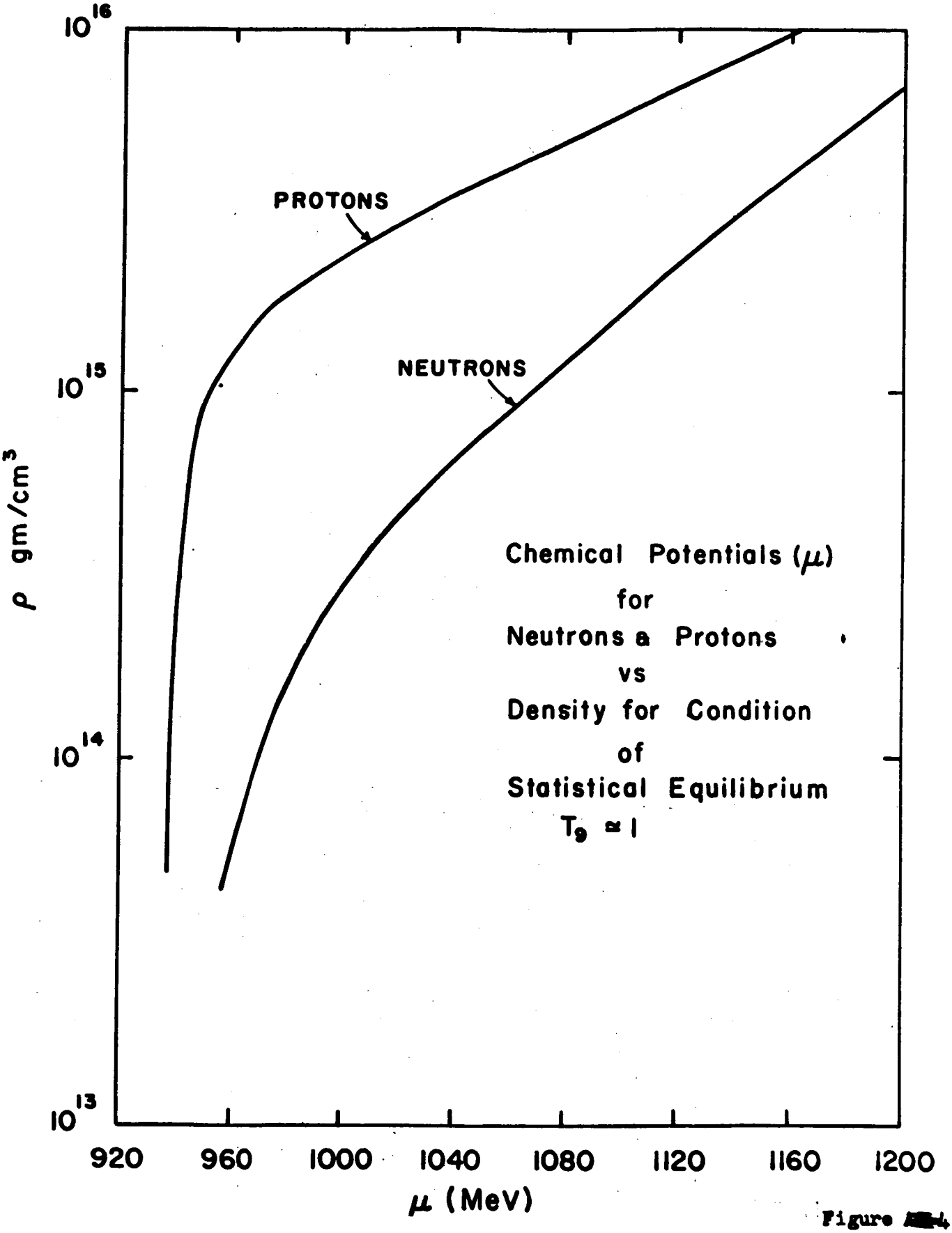
10^{16}
10^{15}
10^{14}
10^{13}
ρ gm/cm³
PROTONS
NEUTRONS
Chemical Potentials (μ)
for
Neutrons a Protons
vs
Density for Condition
of
Statistical Equilibrium
$T_9 \simeq 1$
920
960
1000
1040
1080
1120
1160
1200
μ (MeV)

Figure [illegible]4

For higher temperatures the method used in computing phase space integrals breaks down.

One additional equilibrium calculation was performed at the considerably higher temperature of 5.8×10^{11} ^{o}K (50 MeV kT) at the suggestion of D. Arnett who, in his thesis, points out the possibility that the implosion stage of a supernova explosion may occur at such a temperature. Of interest is the abundance of muons which give rise to muon neutrino losses. The characteristic time scale for this emission may be shorter than the hydrodynamic time scale of implosion and thus would affect the dynamics of the implosion considerably. Some results of this calculation are shown in Figures 5 and 6. As can be seen, the particle concentrations differ appreciably from the low temperature case. It will be an interesting exercise for the future to see what neutrino losses can be expected from such a mixture-provided a reasonable high temperature neutron star model can be constructed.

For references see page 433 et seq.

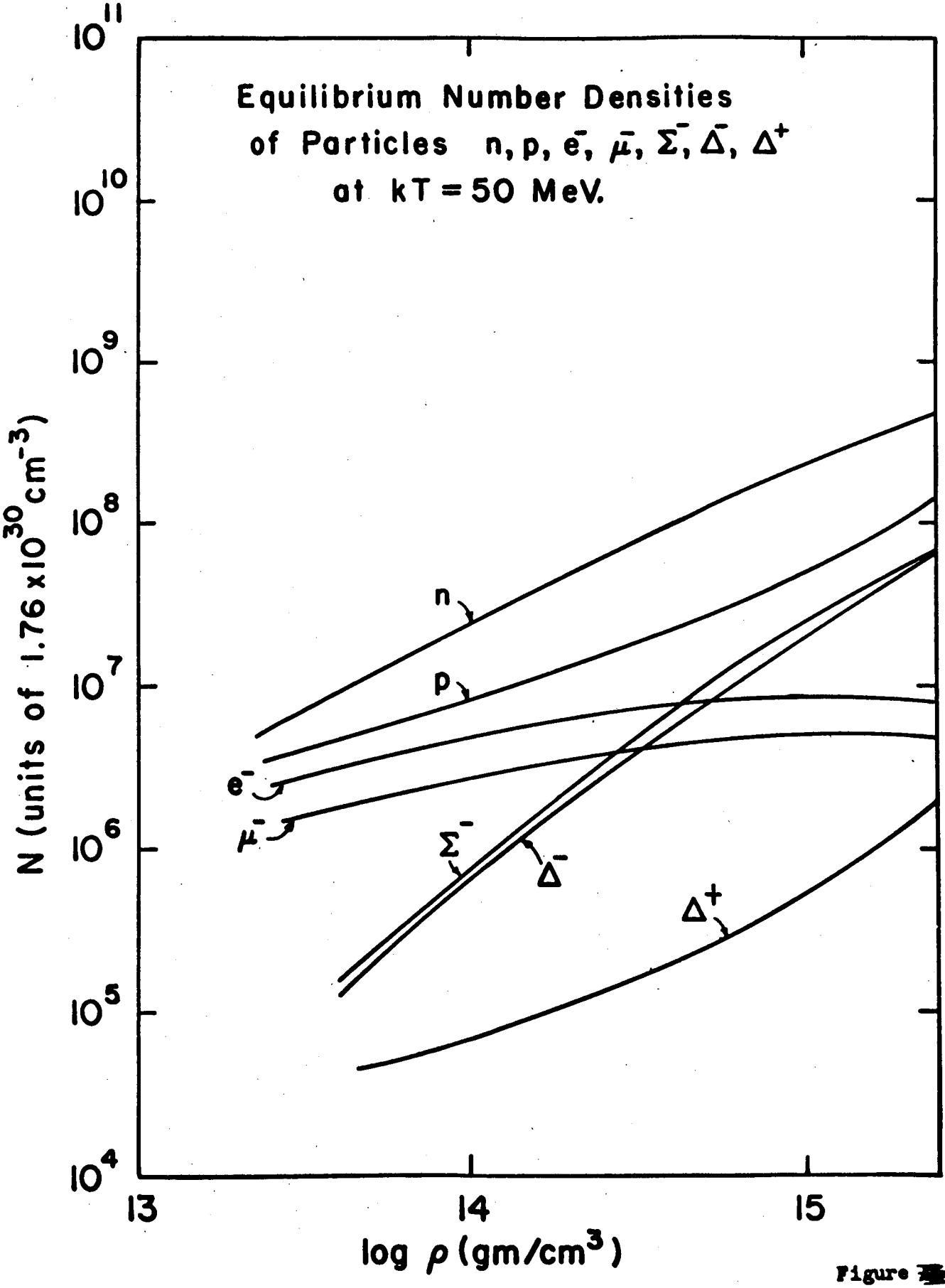
Equilibrium Number Densities
of Particles n, p, e⁻, μ⁻, Σ⁻, Δ⁻, Δ⁺
at kT = 50 MeV.
N (units of 1.76 x 10^30 cm^-3)
log ρ (gm/cm^3)
10^11
10^10
10^9
10^8
10^7
10^6
10^5
10^4
13
14
15
n
p
e⁻
μ⁻
Σ⁻
Δ⁻
Δ⁺

Figure 5

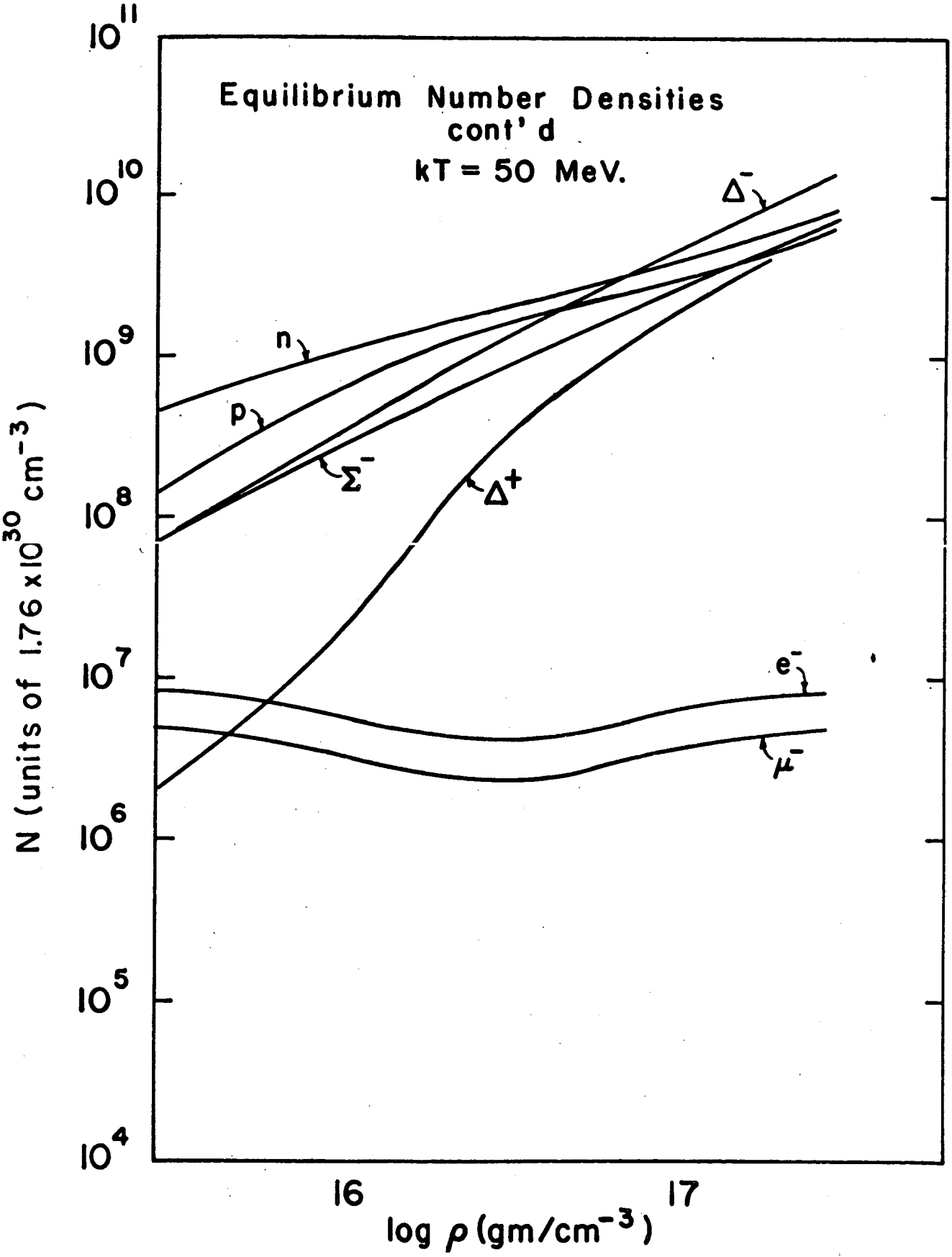
Equilibrium Number Densities
cont' d
kT = 50 MeV.
10^{11}
10^{10}
10^{9}
10^{8}
10^{7}
10^{6}
10^{5}
10^{4}
N (units of 1.76×10^{30} cm^{-3})
n
p
Σ^-
Δ^-
Δ^+
e^-
μ^-
16
17
log ρ (gm/cm^{-3})

Figure 6

6. Neutrino Loss Mechanisms (C.J. Hansen)

In this chapter we will discuss some neutrino loss mechanisms which might compete with either the nuclear URCA process or, under certain conditions, with neutrino emission via neutron-neutron scattering. Very little of the work reported is original but rather consists of extensions of other investigator's results to domains of higher temperature and densities.

A. Pair Annihilation

In the Feynmann and Gell-Mann (1958) theory of the Fermi interaction it is assumed that all such interactions have a universal form and a universal strength. The form is vector-minus-axial vector (V-A) where it is proposed that the vector part of the weak interaction current is conserved. This implies that by including pionic contributions to the current the vector part remains constant for nucleons upon renormalization.

We will assume that the Fermi interaction is a point interaction (range $\lesssim 4 \times 10^{-14}$ cm.) between four fermions - with no intermediate boson. Since the energies with which we are concerned are considerably less than the multi-BeV mass expected of the boson, the latter assumption should serve. Furthermore, we will restrict the form of the fermion current to be "maximum parity

---

*An excellent overall survey of neutrino loss mechanisms is given by Fowler and Hoyle (1964).

violating," viz.,*

$$J(\bar{a},b) = \frac{G^{1/2}}{2^{1/4}}\,\bar{a}\,\gamma_\mu(1-\gamma_5)b \equiv (\bar{a},b)$$

The total interaction current will consist of the terms (neglecting strange particles)

$$J = (\bar{e},\nu_e) + (\bar{n},p) + (\bar{\mu},\nu_\mu)$$

where the particle symbols represent the appropriate wave functions. The four fermion interactions arise from the various terms resulting from taking the product of J with its hermitian conjugate

$$J^* = (\bar{e},\nu_e)^* + (\bar{n},p)^* + (\bar{\mu},\nu_\mu)^* = (\bar{\nu}_e,e) + (\bar{p},n) + (\bar{\nu}_\mu,\mu).$$

Thus, the term $(\bar{e},\nu_e)(\bar{p},n)$ can represent neutrino capture on neutrons to give a proton and an electron (diagram a), or

---

*The methods and formalism of Bjorken and Drell (1964) will be used throughout this section. The metric is defined by $q\cdot p = q_\mu p^\mu = q_o p^o - \vec{q}\cdot\vec{p}$, i.e., diag. $g^{\mu\mu} = (1,-1,-1,-1)$, where $(x^o,x^1,x^2,x^3) = (t,x,y,z)$.

$$\gamma^o = \begin{pmatrix} 1 & 0 \\ 0 & -1 \end{pmatrix}, \quad \vec{\gamma} = \begin{pmatrix} 0 & \vec{\sigma} \\ -\vec{\sigma} & 0 \end{pmatrix}$$

, where $\vec{\sigma}$ are the Pauli matrices,

$$\sigma^1 = \begin{pmatrix} 0 & 1 \\ 1 & 0 \end{pmatrix}, \quad \sigma^2 = \begin{pmatrix} 0 & -i \\ i & 0 \end{pmatrix}, \quad \sigma^3 = \begin{pmatrix} 1 & 0 \\ 0 & -1 \end{pmatrix}.$$

$\gamma^5 = i\gamma^o\gamma^1\gamma^2\gamma^3 = \gamma_5$, $\gamma_\mu = \bar{\gamma}_\mu = \gamma^o\gamma^*\gamma^o$, (* = hermtian conjugate)

The weak coupling constant is taken to be $G = (1.01\pm.01)\times10^{-5}/m_p^2$, where m_p is the proton mass. We will use the units $\hbar = c = 1$, with $m_e = 9.11\times10^{-28}$ gm $= 0.511$ MeV $= (3.86\times10^{-11}\text{cm})^{-1}$ $= (1.288 \times 10^{-21}\text{sec})^{-1}$.

ordinary beta-decay of the neutron (diagram b), etc.

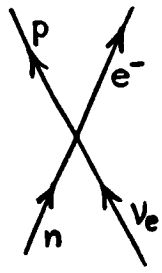

(a)

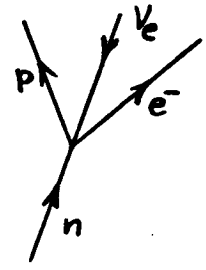

(b)

The rest of the cross terms are permutations of the experimentally verified reactions $(\bar{\nu}_\mu,\mu)(\bar{e},\nu_e)$($\mu^-$-decay) and $(\bar{\nu}_\mu,\mu)(\bar{n},p)$($\mu^-$ capture). The square terms are not so familiar, eg., consider $(\bar{e},\nu)(\bar{\nu},e)$, one of whose reactions is

$$e^+ + e^- \rightarrow \nu + \bar{\nu} \ ,$$

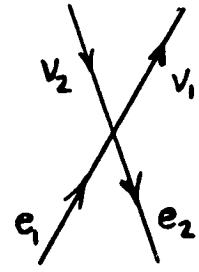

This reaction was first suggested to be of astrophysical importance by Pontecorvo (1959). It is unlikely that this reaction will be observed in the laboratory because of the extremely small probability that the neutrino decay mode will occur rather than straight pair annihilation into photons, since the comparative rates of decay go as the squared ratio of the weak to electromagnetic coupling constants

$$\left(\frac{m_p^2 G}{\alpha}\right)^2 \sim 10^{-21} \ .$$

The cross section for pair annihilation has been obtained by Chiu and Morrison (1960) who state that in the center of mass

$$\sigma = \sigma_0[(E_T^2-1)/v] \ .$$

E_T is the sum of electron and positron energies (including rest mass in units of mc^2), v is their relative velocity and

$$\sigma_0 = \frac{G^2m^2}{3\pi} = 1.5 \times 10^{-45} \text{ cm}^2 \ .$$

The derivation of this cross section is perhaps the simplest of the four fermion interactions and is given here in abbreviated form since it does not seem to appear in the literature.

We shall denote the electron (positron) four-momentum by p_1 (by p_2) and the neutrino (antineutrino) momentum by k_1 (by k_2). The matrix element corresponding to $(\bar{e}_2,\nu_2)(\bar{\nu}_1,e_1)$ is

$$M = \frac{G}{2^{1/2}} [\bar{e}(p_2)\gamma_\mu(1-\gamma_5)\nu(k_2)][\bar{\nu}(k_1)\gamma^\mu(1-\gamma_5)e(p_1)] \ ,$$

where summation over μ is implied. We assume that the electrons are unpolarized and the final neutrino spins are unobserved. Hence we average over incident spins and sum over final spins in computing $|M|^2$ using the projection operator

$$\Lambda = \frac{\gamma\cdot p+m}{2m} = \sum_{\text{spins}} u(p)\ \bar{u}(p) \ .$$

(The neutrino mass ℓ is assumed to be non-zero until the end of the calculation at which point it will be set to zero.) Performing the spin sums and averages we find,

$$|M|^2 = \frac{G^2}{8} \mathrm{Tr}\left[\frac{\gamma\cdot k_1+\ell}{2\ell}\,\gamma^\mu(1-\gamma_5)\,\frac{\gamma\cdot p_1+m}{2m}\,\gamma^\nu(1-\gamma_5)\right]$$

$$\times\ \mathrm{Tr}\left[\frac{\gamma\cdot p_2+m}{2m}\,\gamma_\mu(1-\gamma_5)\,\frac{\gamma\cdot k_2+\ell}{2\ell}\,\gamma_\nu(1-\gamma_5)\right] .$$

Using elementary properties of the traces of γ-matrices each trace can be reduced to the form

$$\mathrm{Tr}[(\gamma\cdot p_2+m)\gamma_\mu(1-\gamma_5)(\gamma\cdot k_2+\ell)\gamma_\nu(1-\gamma_5)]$$

$$= 2\ \mathrm{Tr}[\gamma_\nu(1-\gamma_5)\gamma\cdot p_2\gamma_\mu\gamma\cdot k_2] .$$

Thus,

$$|M|^2 = \frac{G^2}{2(2m)^2(2\ell)^2}\Big\{\mathrm{Tr}[\gamma^\nu\gamma\cdot k_1\gamma^\mu\gamma\cdot p_1]\ \mathrm{Tr}[\gamma_\nu\gamma\cdot p_2\gamma_\mu\gamma\cdot k_2]$$

$$- \mathrm{Tr}[\gamma^\nu\gamma_5\gamma\cdot k_1\gamma^\mu\gamma\cdot p_1]\quad \mathrm{Tr}[\gamma_\nu\gamma\cdot p_2\gamma_\mu\gamma\cdot k_2]$$

$$- \mathrm{Tr}[\gamma^\nu\gamma\cdot k_1\gamma^\mu\gamma\cdot p_1]\ \mathrm{Tr}[\gamma_\nu\gamma_5\gamma\cdot p_2\gamma_\mu\gamma\cdot k_2]$$

$$+ \mathrm{Tr}[\gamma^\nu\gamma_5\gamma\cdot k_1\gamma^\mu\gamma\cdot p_1]\ \mathrm{Tr}[\gamma_\nu\gamma_5\gamma\cdot p_2\gamma_\mu\gamma\cdot k_2]\Big\}$$

With the aid of the trace theorems*

$$\mathrm{Tr}[\gamma^\nu\gamma\cdot k_1\gamma^\mu\gamma\cdot p_1]\ \mathrm{Tr}[\gamma_\nu\gamma\cdot p_2\gamma_\mu\gamma\cdot k_2\gamma_5] = 0$$

---

*Bjorken and Drell (1964), p. 262, for example.

$$\mathrm{Tr}[\gamma^{\nu}\gamma\cdot k_1\gamma^{\mu}\gamma\cdot p_1]\ \mathrm{Tr}[\gamma_{\nu}\gamma\cdot p_2\gamma_{\mu}\gamma\cdot k_2] =$$

$$= 32[k_1\cdot p_2\ k_2\cdot p_1 + k_1\cdot k_2\ p_1\cdot p_2]$$

$$\mathrm{Tr}[\gamma^{\nu}\gamma\cdot k_1\gamma^{\mu}\gamma\cdot p_1\gamma_5]\ \mathrm{Tr}[\gamma_{\nu}\gamma\cdot p_2\gamma_{\mu}\gamma\cdot k_2\gamma_5] =$$

$$= 32[k_1\cdot p_2\ k_2\cdot p_1 - k_1\cdot k_2\ p_1\cdot p_2]\ ,$$

we finally arrive at

$$|M|^2 = \frac{32G^2}{(2m)^2(2\ell)^2}\ k_1\cdot p_2\ k_2\cdot p_1\ .$$

The general expression for the cross section is

$$d\sigma = \frac{|M|^2}{|\vec{v}|}\frac{d^3k_1}{(2\pi)^3}\frac{d^3k_2}{(2\pi)^3}\frac{m^2\ell^2\ (2\pi)^4\ \delta(p_1+p_2-k_1-k_2)}{E(k_1)E(k_2)E(p_1)E(p_2)}$$

where, the E's are the total energies of the respective particles, and $\vec{v}$ is the relative velocity of the electron and positron. Thus,

$$d\sigma = \frac{32G^2}{|\vec{v}|}\frac{k_1\cdot p_2\ k_2\cdot p_1}{2E(k_1)2E(k_2)2E(p_1)2E(p_2)}\frac{d^3k_1}{(2\pi)^3}\ \frac{d^3k_2}{(2\pi)^3}\ (2\pi)^4\delta(p_1+p_2-k_1-k_2).$$

We now use the integral*

---

*See Källén (1964), p. 381, for derivations including the case where both exit particles have non-zero mass.

$$I^{\alpha\beta} = \int \frac{d^3k_1}{2E(k_1)} \frac{d^3k_2}{2E(k_2)} k_1^\alpha k_2^\beta \delta(Q-k_1-k_2) = \frac{\pi}{24}\left[g^{\alpha\beta}Q^2+2Q^\alpha Q^\beta\right] ,$$

where $Q = p_1+p_2$. Therefore,

$$p_{1\alpha}p_{2\beta} I^{\alpha\beta} = \frac{\pi}{12}\left[m^4+3m^2(p_1\cdot p_2)+2(p_1\cdot p_2)^2\right] ,$$

and

$$\sigma = \frac{G^2}{6\pi|\vec{v}|E_1E_2}\left[m^4+3m^2(p_1\cdot p_2)+2(p_1\cdot p_2)^2\right] .$$

In the center of mass

$$p_1\cdot p_2 = 2E_1E_2 - m^2$$

so that

$$\sigma(cm) = \frac{G^2m^2}{3\pi v}\left(E_T^2 - 1\right) .$$

as required, where $E_T = (E_1+E_2)/m$. Numerically,

$$\sigma_o = \frac{G^2m^2}{3\pi} = \left[\frac{1.01\times10^{-5}m}{m^2\left(\frac{m_p}{m}^2\right)}\right]^2 \frac{1}{3\pi} = \frac{0.96\times10^{-24}}{m^2} = 1.5\times10^{-45}cm^2.$$

To compute the neutrino energy loss rate L_ν, $\sigma v(E_1+E_2)$ is to be weighted by the product of electron and positron number density distributions, and then integrated over all incident

momenta, i.e.,

$$L_\nu = \iint (E_1+E_2)\sigma v\, N_1(p_1)\, N_2(p_2)\, dp_1 dp_2$$

Chiu (1961a)* has recast this expression into the form

$$L_\nu = \Big[8\langle E_+\rangle\langle E_-^2\rangle + 7N_+\langle E_-\rangle - 2\langle E_-^2\rangle\langle 1/E_+\rangle + 5N_-\langle 1/E_+\rangle$$

$$+ 8\langle E_-\rangle\langle E_+^2\rangle + 7N_-\langle E_+\rangle - \quad - 2\langle E_+^2\rangle\langle 1/E_-\rangle + 5N_+\langle 1/E_-\rangle\Big]$$

(in units of 1.88×10^{19} ergs/cm^3-sec),

where a plus (minus) subscript refers to positrons (electrons). The various quantities are given in terms of the dimensionless Fermi integrals**

$$N = \int_0^\infty \frac{x^2 dx}{1 + \exp[\beta(y-u)]} ,$$

$$\langle E^n\rangle = \int_0^\infty \frac{y^n x^2 dx}{1 + \exp[\beta(y-u)]} .$$

The relation between the dimensionless chemical potentials $u = \mu/mc^2$ for electrons and positrons in equilibrium with radiation

---

*Note that the expression for σ_o given in this paper (eq. 2) is incorrect. Numerically, however, his result is correct. See also Chiu and Stabler (1961) for an earlier attempt at L_ν.

**See ~~Appendix I~~ Chapter 5, Section C for notation and methods of calculation.

is (from Chapter 5, Section D)

$$u(\text{electron}) = -u(\text{positron}).$$

For a fixed temperature and N_o (number density of electrons associated with ions), L_ν is then uniquely determined. Chiu (1961a) has calculated loss rates for ranges of temperature and density $.5 \lesssim T_9 \lesssim 10$, $2 \times 10^3 \lesssim (\rho/\mu_e = 1.67 \times 10^{-24} N_o) \lesssim 10^9$ gm/cm^3. I have extended these calculations up to $T_9 \sim 50$ and $\rho/\mu_e = 10^{12}$ gm/cm^3 to serve as comparisons for loss rates computed in the main body of the thesis. The results are incorporated in Figure 1.

To facilitate computation the following expansions were derived in the same way as those given in Chapter 5, Sect. C:

1. "Degenerate" electrons

$$\langle E^2 \rangle = j(x)\left[1 + \frac{\pi^2}{6}\frac{(1+x^2)(4x^2+1)}{\beta^2 x j(x)} + \frac{7\pi^4}{120 x^5 \beta^4}\frac{(8x^6+4x^4-x^2+1)}{j(x)}\right]$$

$$j(x) = x^3\left[\frac{1}{3} + \frac{x^2}{5}\right],$$

$$\langle E^{-1} \rangle = \frac{h(x)}{2}\left[1 + \frac{\pi^2}{3\beta^2}\frac{(1+x^2)^{1/2}}{x h(x)} + \frac{7\pi^4}{60\beta^4}\frac{(1+x^2)^{1/2}}{x^5\, h(x)}\right],$$

$$h(x) = g(x) - 2x^3(1+x^2)^{1/2}$$

2. Positrons and "non-degenerate" electrons

$$\langle E^2 \rangle = \sum_{n=1}^{\infty} (-1)^{n+1} \exp n\beta u \left\{ \left[\frac{12}{(n\beta)^2} + 1 \right] \frac{K_2(n\beta)}{n\beta} + \frac{3K_1(n\beta)}{(n\beta)^2} \right\} ,$$

$$\langle E^{-1} \rangle = \frac{1}{2} \sum_{n=1}^{\infty} (-1)^{n+1} \exp n\beta u \left[K_2(n\beta) - K_o(n\beta) \right] .$$

B. Plasmon Neutrinos

A well known result from both classical radiation theory and quantum electrodynamics is that a free photon cannot create electron-positron pairs because energy and momentum cannot both be conserved. This also follows from the form of the dispersion relation $\omega^2 \leq k^2 c^2$ where ω is the photon angular frequency and k is the wave number.

In a plasma, however, the dielectric constant results in a dispersion relation for electromagnetic waves of the form

$$\omega^2 \simeq \omega_o^2 + k^2 c^2 ,$$

where ω_o is the plasma frequency. Such waves, when quantized, behave as relativistic particles (plasmons) of mass $\hbar\omega_o/c^2$ which possibly can decay into electron-positron or neutrino pairs. Adams, et al (1963) and Inman and Ruderman (1964) have calculated the rate of neutrino energy loss due to transverse and longitudinal plasmon decays.* What follows is a transcription of their results

*Zaidi (to be published in Nuovo Cimento) has pointed out that the latter two references contain an error which has been propagated through this thesis. As a result, all rates to be derived should be decreased by a factor of four. See also Inman and Ruderman (1966).

into convenient numerical form:

Define

$$x = \frac{3.345\times10^{-4}\ (\frac{\rho}{\mu_e})^{1/2}}{T_9[1 + 1.0177\times10^{-4}\ (\frac{\rho}{\mu_e})^{2/3}]^{1/4}},$$

$$y = 0.1686\ T_9 x\ ,$$

with ρ/μ_e in gm/cm^3. For transverse plasmons the energy loss rate is

$$L_t = 1.228 \times 10^{22}\ y^9\ F(x)\ ergs/cm^3\text{-}sec\ ,$$

where for $x \leq 0.5$

$$F(x) = \frac{2.40412}{x^3} + \frac{1}{x}[0.5 \ln x - 0.59655] + \frac{1}{96}x(\ln x - 2.8509),$$

and for $x \geq 0.5$,

$$F(x) = \sum_{n=1}^{\infty} \frac{K_2(nx)}{nx}\ .$$

For longitudinal plasmons,

$$L_\ell = 3.15 \times 10^{20}\ y^9 (e^x - 1)^{-1}\ ergs/cm^3\text{-}sec.$$

C. Photoneutrinos

This process is the scattering of electrons by photons to yield neutrino pairs, i.e.,

$$\gamma + e^- \rightarrow e^- + \nu + \bar{\nu} \ .$$

The energy loss rate has been calculated by Chiu and Stabler (1961) (with a correction by Ritus, 1962) in various limits of degeneracy to be,

1. Relativistic, non-degenerate (R-ND)

$$L \simeq 2.51 \times 10^8 \ T_9^6 \ (\log_{10} T_9 + 0.6)(\rho/\mu_e) \ \text{erg/cm}^3\text{-sec}$$

2. Non-relativistic, non-degenerate (NR-ND)

$$L \simeq 10^8 \ T_9^8 \ (\rho/\mu_e) \ \text{ergs/cm}^3\text{-sec}$$

3. Non-relativistic, degenerate (NR-D)

$$L \simeq 3.9 \times 10^{10} \ T_9^9 \ (\rho/\mu_e)^{2/3} \ \text{ergs/cm}^3\text{-sec}$$

4. Relativistic, degenerate (R-D)

$$L \simeq 6.3 \times 10^6 \ \left(\frac{mc^2}{E_F}\right) \ T_9^7 \ (1+5T_9^2) \ \text{ergs/cm}^3\text{-sec} \ ,$$

where E_F is the electron Fermi level.

In the ranges $10^5 \lesssim (\rho/\mu_e) \lesssim 10^{12}$, $0.1 \lesssim T_9 \lesssim 50$ only the (R-ND) and (R-D) cases are of interest. A useful boundary in the (ρ/μ_e)-T_9 plane is the line where the energy loss rates are equal for the two cases, i.e.,

$$\left(\frac{\rho}{\mu_e}\right) \simeq 2 \times 10^5 \ T_9^{2.54} \ .$$

The total loss rate for the combined processes of pair annihilation, photoneutrino and plasmon decay is shown in Figure [redacted]1. The quantity q* is defined as the loss rate in ergs/cm^3-sec divided by ρ/μ_e. The conditions under which one or the other of the three mechanisms dominate is shown in Figure AII-2.

Loss mechanisms which have not been discussed, and are probably not as important as the above, are:

1. $\gamma + \gamma \rightarrow \bar{\nu} + \nu$, discussed by Matinyan and Tailosani (1962)*

2. $\gamma + \gamma \rightarrow \gamma + \nu + \bar{\nu}$, Van Hieu and Shabalin (1963).

3. $\gamma + (Z,A) \rightarrow (Z,A) + \nu + \bar{\nu}$, photon scattering in the field of a nucleus, Rosenberg (1963).

4. Neutrino bremsstrahlung -- the same process as ordinary bremsstrahlung except that neutrino pairs are emitted instead of photons. This might be important for neutron stars if the density of scattering centers is high. Ruderman and Festa are working on this at present. (From a private communication to S. Tsuruta and A. G. W. Cameron.)

---

*Gell-Mann (1961) has shown that this reaction cannot occur if the weak interaction is strictly local.

For references see page 433 et seq

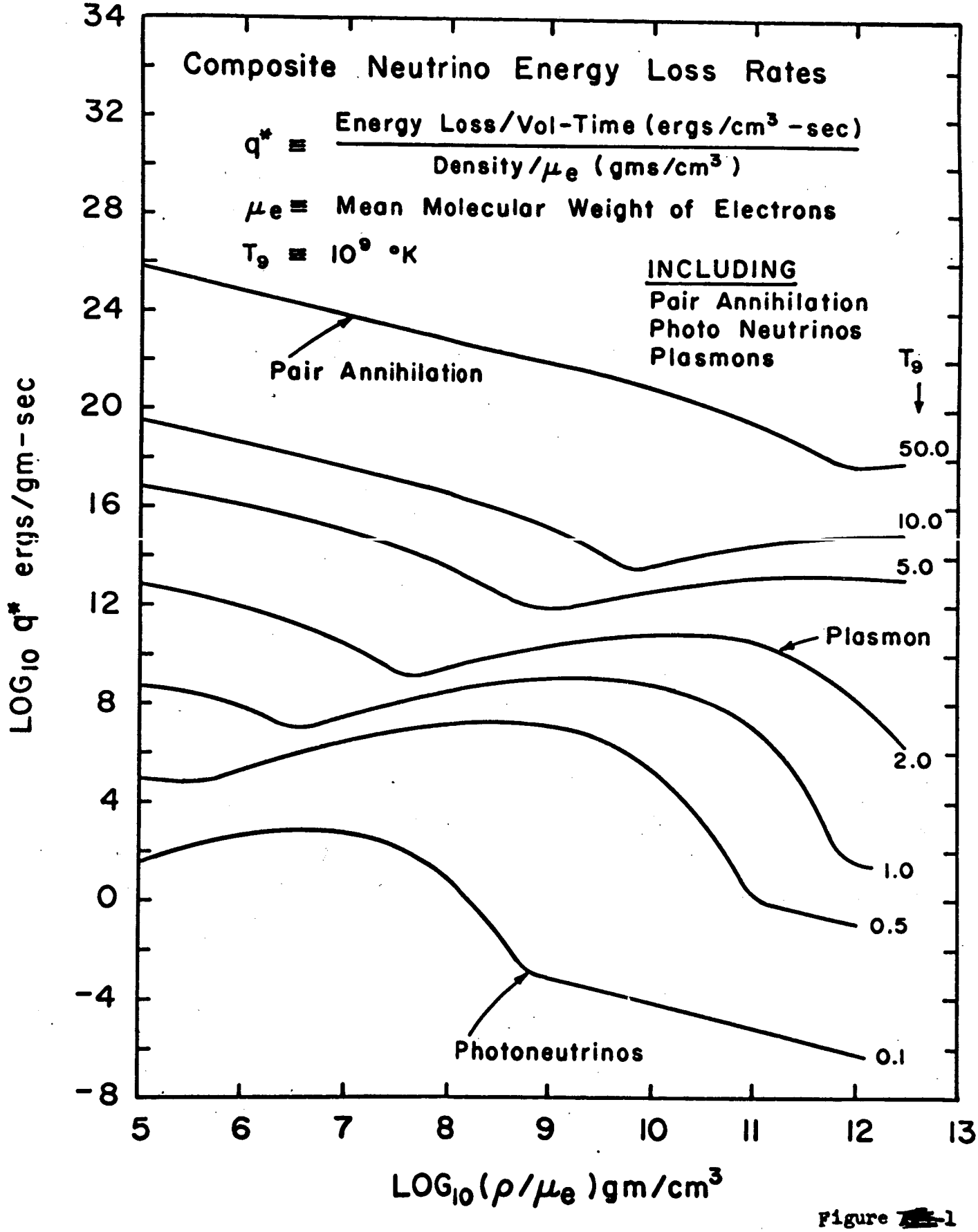
Composite Neutrino Energy Loss Rates
$q^* \equiv$ Energy Loss/Vol-Time (ergs/cm^3 -sec) / Density/μ_e (gms/cm^3)
$\mu_e \equiv$ Mean Molecular Weight of Electrons
$T_9 \equiv 10^9$ °K
INCLUDING
Pair Annihilation
Photo Neutrinos
Plasmons
T_9
Pair Annihilation
50.0
10.0
5.0
Plasmon
2.0
1.0
0.5
Photoneutrinos
0.1
LOG_{10} q^* ergs/gm-sec
$LOG_{10}(\rho/\mu_e)$ gm/cm^3
34
32
28
24
20
16
12
8
4
0
-4
-8
5
6
7
8
9
10
11
12
13

Figure 7-1

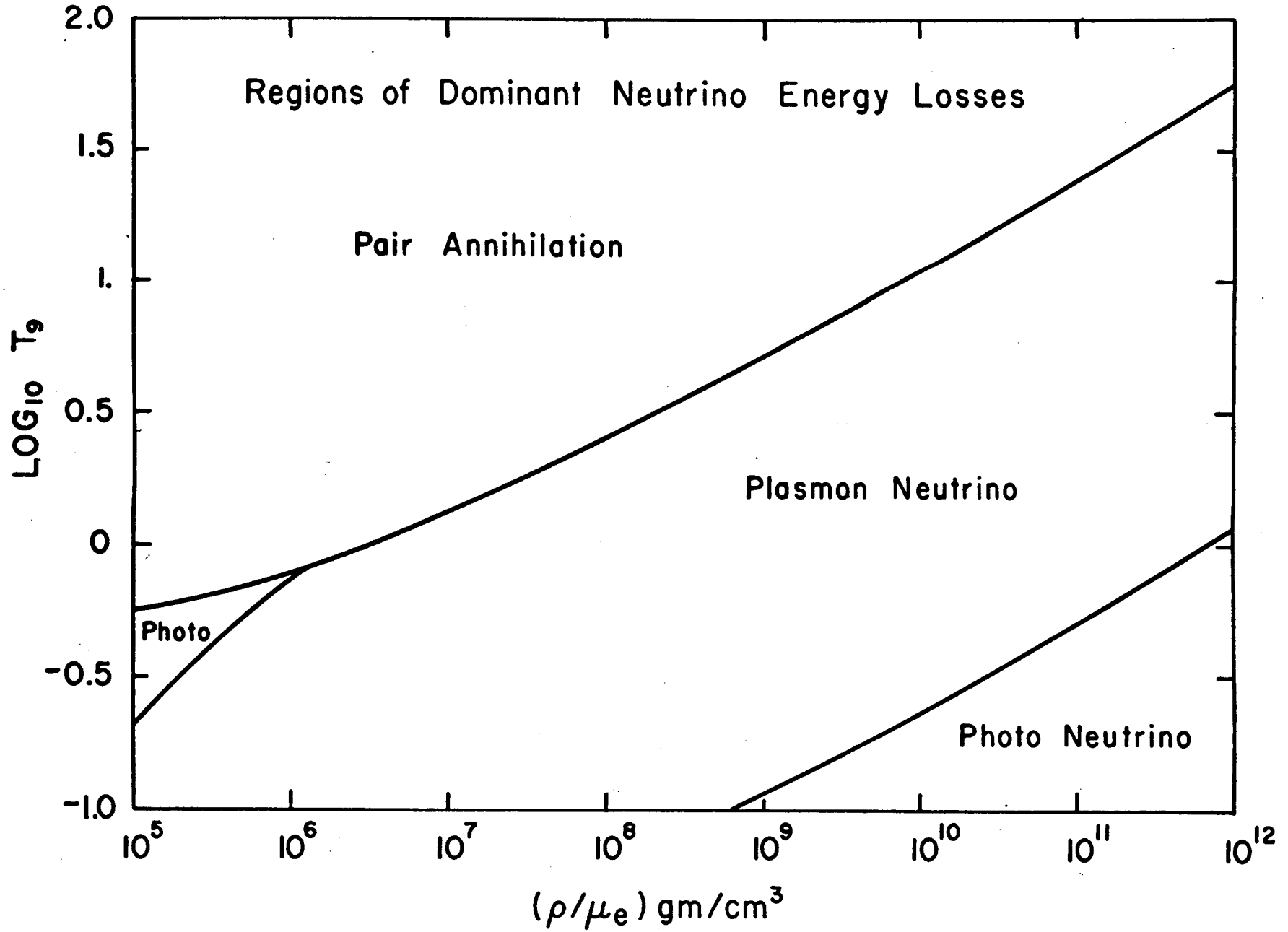
Regions of Dominant Neutrino Energy Losses
Pair Annihilation
Plasmon Neutrino
Photo
Photo Neutrino
LOG10 T9
2.0
1.5
1.
0.5
0
-0.5
-1.0
10^5
10^6
10^7
10^8
10^9
10^10
10^11
10^12
(ρ/μe) gm/cm^3

Figure. 2

7. The Supernova Process (W.D. Arnett)

Abstract

The behavior of a massive star during its final catastrophic stages of evolution has been investigated theoretically, with particular emphasis upon the effect of electron-type neutrino interactions. The methods of numerical hydrodynamics, with coupled energy transfer in the diffusion approximation, were used. Gravitational collapse initiated by electron-capture and by thermal disintegration of nuclei in the stellar center is examined, and the subsequent behavior does not depend sensitively upon which process causes the collapse.

As the density and temperature of the collapsing stellar core increase, the material becomes opaque to electron-type neutrinos and energy is transferred by these neutrinos to regions of the star less tightly bound by gravity. Ejection of the outer layers of the star can result. This phenomena has been identified with supernovae.

Uncertainty concerning the equation of state of a hot, dense nucleon gas causes uncertainty in the temperature of the collapsing matter. This affects the rate of energy transfer by electron-type neutrinos and the rate of energy lost to the star by muon-type neutrinos.

The effects of general relativity do not appear to become important in the core until after the ejection of the outer layers.

Introduction

The behavior of a massive star during its final catastrophic evolution has been investigated theoretically, with particular emphasis upon the effect of electron-type neutrino interactions. Colgate and White (1964) have suggested that the gravitational collapse of such a star may be partially reversed by a combination of shock phenomena and energy transfer by neutrino diffusion from a hot, ultra-dense core. The resulting ejection of hot matter has been identified with supernovae. The Von Neuman-Richtmeyer pseudo-viscosity method of numerical hydrodynamics, coupled with energy transfer in the diffusion approximation, has been used to investigate this hypothesis.

In section I the physical processes involved in the collapse, and the gravitational stability of a massive star are discussed. In particular, the problems of constructing an equation of state and determining the energy transfer by neutrinos under the extreme densities and temperatures to be encountered are considered. Following this, section II develops the initial models and presents their subsequent histories. Three methods of treating neutrino energy transfer - (1) no energy loss, (2) energy loss by electron pair-annihilation and plasmon decay neutrinos, and (3) thermal diffusion of neutrinos - are presented, and the results contrasted.

The effect of initial structure upon subsequent history is examined. The behavior of these models is compared with the work of Colgate and White (1964).

Section III contains an examination of the implications of the calculations reported in II, and section IV is a critique of the methods employed in the calculations. Details of the numerical techniques of hydrodynamics and energy transfer are presented in an appendix.

1. Physical Processes

In order to maintain its luminosity a star may derive energy from two sources: thermonuclear reactions and gravitational contraction. In the latter case the star converts its gravitational potential energy into kinetic energy of gas particles on such a slow time scale that hydrostatic equilibrium is approximately satisfied. No nuclear fuel can last indefinitely, so one expects that eventually the star will contract to higher densities. At these higher densities the Pauli exclusion principle can become operative and contribute to the pressure. However Chandrasekhar (1939) has shown that for electrons the maximum mass of a body supporting itself by degeneracy pressure is less than 1.5 solar masses.* If the mass of a star is less than the Chandrasekhar limit, it may radiate away its remaining thermal energy and settle down as a white dwarf. For more massive stars the situation is not so simple.

A massive star spends most of its life burning hydrogen and helium.** Helium-burning produces oxygen and perhaps some carbon (Deinzer (1964)). Fowler and Hoyle (1964) have discussed in detail the nuclear reactions occurring in subsequent evolution.

---

* For pure hydrogen the limit is higher, (see Chandrasekhar (1939), p. 423) but a pure hydrogen star is unrealistic when the Fermi energy of electrons is higher than the beta-decay energy of the neutron.

** See Hayashi (1962), Hofmeister (1964), and Stothers (1965).

After carbon-burning (temperature~8×10^8 ^oK) neutrino production by plasmon decay and electron-positron pair-annihilation robs the star of significant amounts of energy. This speeds the evolution of the star. Chiu (1964) has calculated some models of pre-supernova stars including this effect.

There are at least two mechanisms by which the star can be robbed of internal energy faster than it can replace the lost energy by quasi-static gravitational contraction. They are thermal disintegration of nuclei and electron-capture. When these mechanisms operate, the star will collapse, falling almost freely in its own gravitational field. Which process will actually trigger the collapse depends on the details of pre-implosion evolution.

A. Thermal Disintegration of Nuclei

For temperatures greater than $T = 4 \times 10^9$ ^oK and densities the order of or greater than $\rho = 10^6$ gm/cm^3 a wide variety of nuclear reactions can occur. A calculation of these rates requires an accurate knowledge of the initial nuclear composition of the matter, a large collection of nuclear parameters,* and considerable effort. It is beyond the scope of this work to justify a pre-supernova model involving such a calculation.

---

* See Truran, Hansen, Cameron, and Gilbert (1965), for instance.

If the reactions are fast enough, the problem may be treated by the methods of statistical equilibrium. Insofar as the equation of state is concerned, the only changes of interest are those which are strongly endoergic or exoergic. The photodisintegration of ^{56}Fe matter in the implosion has been discussed by Fowler and Hoyle (1964). They find that for temperatures $T \geq 7.10^9\ ^oK$ that the photodisintegration time is $t \sim 10^{-6}$ second --- which is no larger than the most restrictive hydrodynamic time scale. Hoyle and Fowler note that the equilibrium composition for ^{56}Fe matter changes to essentially pure ^4He in a region of width

$$\Delta T \sim 1 \times 10^9\ ^oK$$

about the density-temperature curve corresponding to an equilibrium concentration of half ^{56}Fe, and half ^4He and neutrons, i.e., the curve

$$\log \rho = 11.62 + 1.5 \log T_9 - \frac{39.17}{T_9}$$

where T_9 means temperature in units of one billion degrees, logarithms are to the base 10 and density ρ is in gm/cm^3. This may be approximated by the expression

$$T_9/6.0 = (\rho/1.82 \times 10^6\ gm/cm^3)^{0.081}.$$

For somewhat higher temperatures photodisintegration of alpha particles is expected.

$$^4He \rightarrow 2p + 2n$$

In this case the transition region is approximated by

$$T/(12\times10^9\ {}^{o}K) = (\rho/(10^8\ gm/cm^3)\ )^{0.13}$$

Now the energy required to produce the reaction

$$^{56}Fe \rightarrow 13\ ^{4}He + 4n$$

is

$$Q(Fe,\alpha) = -2.1\times10^{18}\ erg/gm$$

and for

$$^{4}He \rightarrow 2p + 2n$$

is

$$Q(\alpha,np) = -6.8\times10^{18}\ erg/gm$$

These values will be roughly correct even if the composition is not ^{56}Fe, but some other stable nuclide. Subsequent results will not depend sensitively upon this choice.

B. Electron-capture

Consider a nucleus (Z,A) which is stable against beta-decay on earth. It may be a product of some reaction represented by

(1) $$(Z-1,A) \rightarrow (Z,A) + e^- + \bar{\nu}.$$

Under stellar conditions of extreme density, an endothermic reaction of the form

(2) $$(Z,A) + e^- \rightarrow (Z-1,A) + \nu$$

can occur in which the terrestrially stable nucleus (Z,A) is induced to capture a continuum electron from the surrounding plasma.

Bahcall (1964c) has investigated this process and finds that for allowed decays, the half-life for the process (2) in a stellar interior is related to the half-life for the decay (1) on earth by

$$(\tau_{1/2})_{star} = (f\tau_{1/2})_{lab} K^{-1}$$

where f is the usual function used in the comparative half life, i.e.,

$$f(\pm Z,W) = \int_0^{p_{max}} dp\ p^2\ F(\pm Z,W)$$

and p is electron momentum, W is relativistic electron energy, q is the neutrino momentum and $F(\pm Z,W)$ is the Fermi function. Now

$$K = \int_{p_{threshold}}^{\infty} dp\ p^2\ q^2\ F(Z,W)/(1+e^{(W-\mu)/kT})$$

(where μ is the relativistic chemical potential) is the appropriate generalization of $f(+Z,W)$ for reaction (2). The range of integration now extends from the electron momentum corresponding to the threshold energy of (2) to all higher energies. The correct weighing factor for a Fermi-Dirac distribution of electrons,

$$(1 + \exp[\ (W-\mu)/kT]\ )^{-1},$$

is included. The integral K will be large compared to $f(+Z,W)$ when the electron distribution is such that energy levels with

$$W \geq W_{threshold}$$

for the capture reaction, are well populated. This can occur in

the nondegenerate case when

(3) $$kT \gtrsim W_{threshold}$$

and in the degenerate case when

(4) $$W_{Fermi} \gtrsim W_{threshold}$$

Taking $W_{threshold}$ to be the order of nucleon binding energy in the nuclear potential should give an estimate of the thermodynamic conditions under which induced electron capture will begin to occur. If we take the threshold for the electron capture to be

$$W_{threshold} \sim 8 \text{ MeV},$$

then for a nondegenerate gas, the condition (3) implies that the temperature is

$$T \gtrsim 10^{11} \, ^{o}K,$$

but thermal disintegration discussed in the previous section will have already disrupted the nuclei at much lower temperatures. Using (4) gives a condition* on the density ρ

$$\frac{\rho}{\mu_e} \gtrsim 10^{9} \text{ gm/cm}^3.$$

* The quantity μ has its usual astrophysical definition of average atomic weight per free particle ($\mu_e = A/(Z + 1)$ for a completely ionized gas).

Beyond this density nuclei will capture high energy electrons from the top of the Fermi sea. The alpha particle, ^4He, will be extremely resistent to electron capture because there is no stable nucleus with Z = 1, A = 4, whereas the α particle is tightly bound. The threshold for electron capture on ^4He will be of the order of the energy needed to disintegrate the nucleons, i.e., about 30 MeV for complete disruption, but the reaction of most importance is probably

$$^4He + e^- \rightarrow {}^3H + n + \nu_e$$

which requires about 21 MeV. A value for the electron Fermi energy of 30 MeV corresponds to a density of the order of

$$\frac{\rho}{\mu_e} \sim 2 \times 10^{11} \text{ gm/cm}^3$$

As the density rises, so that the Fermi energy becomes greater than the threshold energy, the continuum electron capture rates increase until an assembly composed predominantly of neutrons is formed.

C. Stability Against Continued Implosion

Once the implosion begins it cannot be stopped until the pressure is again large enough to provide mechanical support for the configuration. Chandrasekhar (1939) has shown that the boundary for mechanical stability of a self-gravitating mass is

the $\gamma = 4/3$ adiabat. That is, if upon compression the change in pressure and density of the material can be represented by

$$\gamma = d(\log P)/d(\log \rho)$$

then for $\gamma > 4/3$ the material is stable, but for $\gamma < 4/3$ the material is unstable toward continued contraction.* As particles become relativistic the relation between energy and momentum changes from

$$\epsilon = \frac{p^2}{2m}$$

to

$$\epsilon = pc$$

in the extreme relativistic case. The corresponding relations for a gas of such particles are

nonrel.	rel.
$E = \frac{3}{2} PV$	$E = 3 PV$
$\gamma = 5/3$	$\gamma = 4/3$

*Actually the criteria are somewhat more complicated, dealing with pressure averages of γ. F. Dyson, "Hydrostatic Instability of a Star," unpublished.

where E is the energy density per unit mass, P the pressure and $V = 1/\rho$ the specific volume. Thus, as the temperature (or the Fermi energy) increases we expect the effective adiabatic exponent of the gas, γ , to approach four-thirds. At what temperature this occurs depends upon the rest mass of the gas particles (photons, having zero rest mass are always relativistic, electrons become relativistic for $T \sim 6 \times 10^9$ ^oK, while nucleons require $T \sim 1.2 \times 10^{13}$ ^oK). Large amounts of energy are removed from the star by neutrino emission. Both the processes of electron-capture and thermal disintegration of nuclei require large amounts of energy to proceed; in both cases this energy is at least of the order of nuclear binding energy. In view of these large energy requirements, the material is expected to become degenerate even if it was not originally so.

The problem of stability against continued collapse is then reduced to whether a cold, dense neutron gas can give a pressure contribution which increases with density faster than $\gamma = 4/3$. From investigation of the properties of nuclear matter such a contribution is found.

D. The Equation of State

At densities of the order of or less than nuclear densities ($\rho \lesssim 3 \times 10^{14}$ gm/cm^3) the attractive nuclear potential lowers

the pressure below that expected for a degenerate, noninteracting gas of fermions. The nuclear potential becomes strongly repulsive at higher densities, and raises the pressure above that expected for a noninteracting gas, but the exact details of nuclear potentials in this range (greater than nuclear density) is not well known. From the several forms of the nuclear potential discussed by Tsuruta (1964), it appears that there will be a pressure term of the form

$$P \sim \rho^{\gamma}$$

where

$$\gamma \gtrsim 2$$

These results for the equation of state are based on the assumption that the nucleons may represent a noninteracting, degenerate gas of Fermi particles in a common potential well.

Bahcall and Wolf (1965) have attempted to determine the effect of nucleon-nucleon interactions more accurately by using the "independent-pair" model of Gomes, Walecka and Weisskopf (1958). This technique is valid only if the nucleons are highly degenerate. Unfortunately it is necessary to know the equation of state for nondegenerate and semi-degenerate nucleon matter. In view of the uncertainties involved in any nuclear equation of state and the numerical limitations of this investigation, and extremely simple form for nuclear pressure at high density and temperature was chosen: The nucleons were assumed to be a gas of noninteracting,

free Fermi particles. This reproduces the correct general character in the limits of complete degeneracy and of high temperature, low density. In order to avoid excessive use of computer time, the equation of state was constructed from a composite of analytic terms.

In addition to the nucleon pressure terms discussed above, black-body radiation pressure and electron pressure (including relativistic degeneracy) were taken into account. Thus the approximate expression for the pressure is

$$P = R\left(\frac{\rho}{\mu_n}\right)T + K_n\left(\frac{\rho}{\mu_n}\right)^{5/3}$$

$$+R\left(\frac{\rho}{\mu_e}\right)T + K_e\left(\frac{\rho}{\mu_e}\right)^{4/3} + \frac{aT^4}{3}$$

where R is the gas constant, the constants K_e and K_n are

$$K_e = 1.201 \times 10^{15} \text{ dynes cm}^{-2}$$

$$K_n = 5.226 \times 10^{9} \text{ dynes cm}^{-2}$$

if the density ρ has units gm cm^{-3}, T is the temperature, and the number density of the $i^{\underline{th}}$ type of particle (n = neutron, e = electron) is

$$N_i \sim \frac{\rho}{\mu_i} N_a$$

where N_a is Avagadro's number. The number density of neutrons is negligible before electron capture occurs. Electron-pair

creation does not affect the equation of state for large electron number density. The energy density corresponding to this pressure has the simple form

$$E = \sum_i \frac{P_i V}{(\gamma_i - 1)}$$

where $\gamma = 4/3$ for the relativistic particles and $\gamma = 5/3$ for nonrelativistic ones.

Electron capture reactions were accounted for as follows: Since the expression

$$\frac{\rho}{\mu_e} = \frac{1}{V \mu_e} \sim n_e$$

is proportional to the number density of electrons, smoothly changing μ_e provides a convenient way to reduce the electron pressure of the system. When the relativistic electron Fermi energy E_f,

$$\frac{E_f}{m_e c^2} \approx \left(\frac{\rho_6}{\mu_e}\right)^{1/3}$$

where ρ_6 is density in units of 10^6 gm/cm^3, reaches a given level, the number density of electrons is held constant until the degenerate nucleon pressure becomes more important. That this agrees with other estimates may be seen in Figure (1). Two parameters are involved: the Fermi energy at which captures are supposed to occur, and the factor by which the electron number density is decreased.

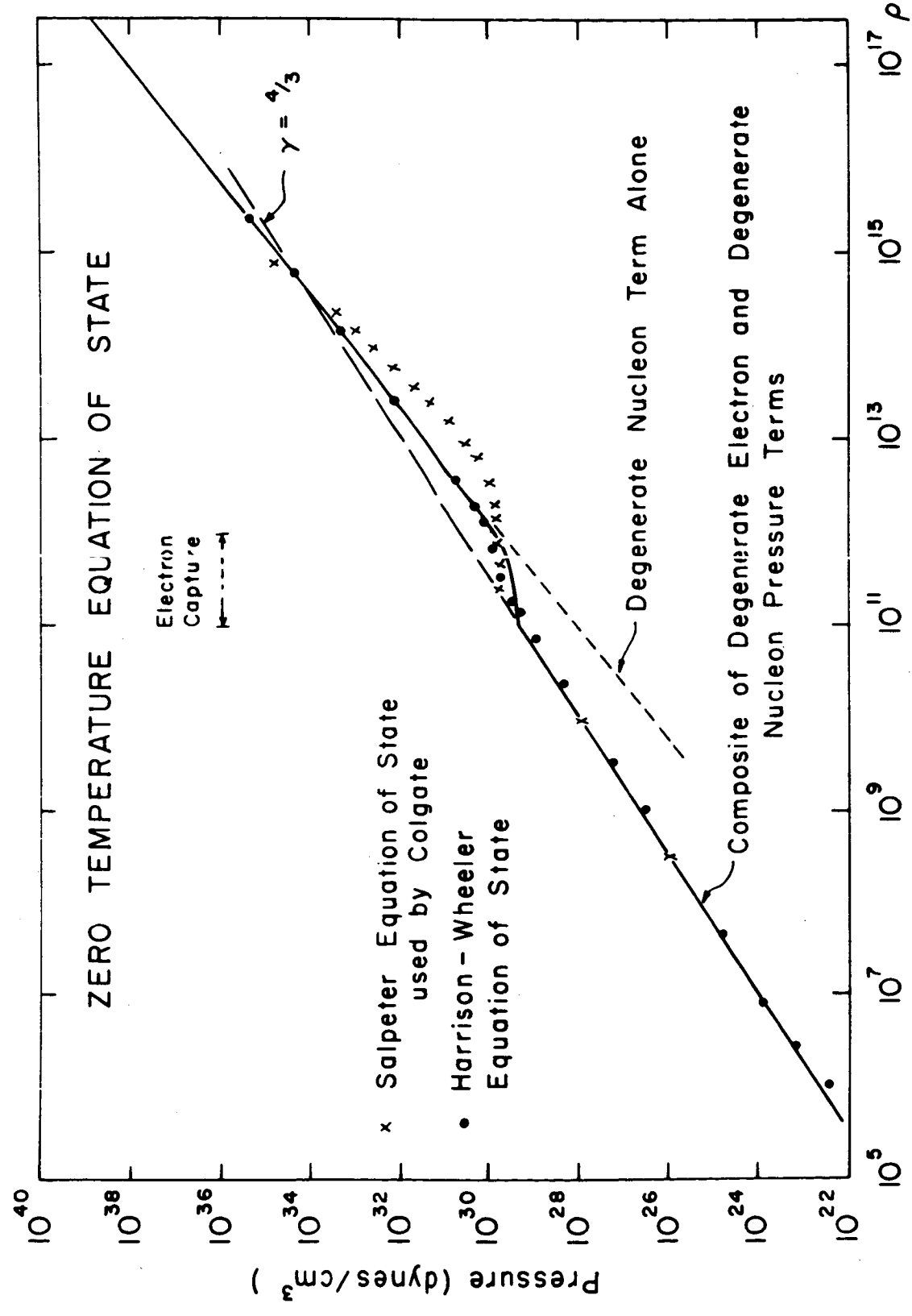
ZERO TEMPERATURE EQUATION OF STATE
Electron Capture
$\gamma = 4/3$
× Salpeter Equation of State used by Colgate
• Harrison-Wheeler Equation of State
Degenerate Nucleon Term Alone
Composite of Degenerate Electron and Degenerate Nucleon Pressure Terms
Pressure (dynes/cm^2)
Density (g/cm^3)
10^{40}
10^{38}
10^{36}
10^{34}
10^{32}
10^{30}
10^{28}
10^{26}
10^{24}
10^{22}
10^5
10^7
10^9
10^{11}
10^{13}
10^{15}
10^{17} ρ

Fig. 1

Actually the onset of electron capture reactions is a gradual process, beginning at densities as low as 10^9 gm/cm^3. Figure (1) shows that the Harrison-Wheeler* equation of state gives a slightly lower pressure than expected from a relativistic electron gas at densities from about 10^9 to 10^{11} gm/cm^3 because of electron capture. Tsuruta (1964) finds that the equilibrium abundance peak of zero temperature matter shifts from ^{56}Fe at low density ($\sim 10^7$ gm/cm^3) to very neutron-rich heavy nuclei at higher density ($\gtrsim 10^{11}$ gm/cm^3) due to electron capture. The effect of this is to initiate a contraction in a pre-supernova star at much lower densities than might be expected otherwise. The assumption of a sharp electron capture threshold is unrealistic, but is probably a minor source of error. In the calculations to be reported, electron capture was assumed to occur rapidly when the Fermi energy was slightly above the 21 MeV or so necessary to drive the reaction

$$^4\text{He} + e^- \rightarrow {}^3\text{H} + n$$

that is, for $\rho \sim 10^{11}$ gm/cm^3.

---

* Harrison, B. K., et al, 1965, chapter 10.

As Figure (1) shows, a zero-temperature body undergoing quasi-static gravitational contraction will encounter a pressure deficit at densities above $\rho \sim 10^{11}$ gm/cm^3. The equation of state does not compensate for this pressure loss relative to a $\gamma = 4/3$ adiabat until the density is about 10^{15} gm/cm^3. This is accomplished here by approximating the complicated equation of state for nuclear matter by that of a noninteracting non-relativistic Fermi gas. In the region where the pressure deficit occurs, $10^{11} < \rho < 10^{15}$ gm/cm^3, the detailed nature of the equation of state is relatively unimportant because the supernova core is falling in freely to higher densities and is not affected by the nucleon pressure contribution. In this region Tsuruta's equation of state gives pressures between those of the Harrison-Wheeler and the Salpeter equation of state, except when a nuclear hard-core term begins to dominate the equation of state. It should be emphasized that the zero-temperature equation of state is only a convenient limiting case, and that finite temperature effects are important in supernovae collapse.

E. Neutrinos and Energy Transfer

The effectiveness of a given mechanism for energy transfer depends on the rate at which energy can be put into the given mode, and on the speed with which the given mode moves this energy. Energy transfer in stars is generally accomplished by photon

diffusion, or in some cases by convective mass motion or conduction by degenerate electrons (see Schwarzschild, 1958). Using the Thomson cross-section for the electron, the photon mean free path is roughly

$$\lambda \text{ photon} \sim \frac{1}{N_e \sigma_{th}} \sim \frac{1}{\rho} \text{ cm.}$$

where N_e is the electron number density per unit volume, σ_{th} is the Thomson cross-section, and ρ is the density in gm/cm^3. For the core of a star with a central density of, say, 10^6 gm/cm^3, the time for a photon to diffuse through even ten kilometers of matter is

$$\tau_{\text{ph.dif.}} \sim \frac{\Delta R^2}{\lambda c} \sim 10 \text{ years.}$$

The universal theory of weak interactions* of Feynman and Gell-Mann (1958) predicts a large number of processes that result in the formation of neutrino-antineutrino pairs. The emission of a neutrino pair is much less probable than the emission of a photon so that the process is not generally observable in the laboratory. Once formed, however, the neutrino pair is virtually certain to escape from a normal star ($\rho_{\text{central}} \ll 10^{11}$ gm/cm^3). For temperatures less than several billion degrees, the cross-section for neutrinos and antineutrinos is roughly

$$\sigma \sim 10^{-44} \text{ cm}^2.$$

so that the mean free path is

$$\text{neutrino} \sim \frac{10^{20}}{\rho} \text{ cm.}$$

---

*Or any theory which predicts coupling of terms of the form $(\bar{\nu}e)(\bar{e}\nu)$.

which is roughly 100 light years for the density of the sun. Thus, excluding extreme conditions, the production of neutrinos acts as an instantaneous local energy sink for the star.

1. Energy Loss by Neutrino Escape.

Chiu (1961) has calculated the energy loss rate due to the process

$$e^+ + e^- \rightarrow \bar{\nu} + \nu$$

for stellar material in the temperature range (0.5 to 10) x 10^9 ^oK and densities (0 to 10^9 gm/cm^3). In much of this range the electrons are partially degenerate and numerical eveluation of integrals was necessary. Analytic forms for limiting cases have been presented by Chiu and Stabler* (1961).

For

$$mc^2 \ll kT$$

and

$$E_{Fermi} \lesssim kT$$

the energy loss rate is

$$Q = 4.3 \times 10^{15} \frac{(T_9)}{\rho} \text{ ergs/gm/sec}$$

where ρ is in gm/cm^3 and T_9 is the temperature in units of 10^9 ^oK.

---

* See Ritus (1962) for a numerical correction of the photoneutrino rates in this paper.

This approximation is inaccurate when temperatures are about 3×10^9 °K or below, but the energy loss rates are then too small to affect the hydrodynamic calculation. The approximation is also invalid when degeneracy is pronounced, but then the plasmon-neutrino loss rate is larger, so that the numerical error is negligible.

The production of neutrino pairs by coherent electron excitations (transverse plasmons) in a hot, partially degenerate relativistic plasma has been calculated* by Adams, Ruderman and Woo (1963), and extended by Inman and Ruderman (1964). Neutrino-pair emission by collective electron modes, especially transverse plasma excitations, is found to be the main mechanism for neutrino radiation by a dense plasma when electron-positron production is small either because the temperature is too low or degeneracy suppresses it. Chiu (1964) gives an analytical approximation for the plasma neutrino process:

$$Q = -1.1 \quad (T_9)^3 \quad \rho \text{ erg/gm/sec.}$$

where the usual notation is employed. This is valid for

$$x \leq 1$$

where x is given by

$$x = 0.237(1 + 0.6413(\rho_6)^{2/3})^{-1/4} \quad (\rho_6)^{1/2}$$

if

$$\rho_6 \gg 1$$

---

* Zaidi has recently indicated that this rate is too large by a factor of 4 (to be published).

The density ρ_6 has units of 10^6 gm/cm^3. Actually numerical evaluation of the pair annihilation, plasma and photoneutrino rates by Hansen (1964) indicates that this approximation is reasonably good (factor of 2) for densities as high as 10^{11} gm/cm^3 or so if the temperature is $T \leq 10^{10}$ ^oK. Again, errors in small energy-loss rates are negligible from a hydrodynamic point of view. For temperatures much higher than this the pair annihilation rate is dominant, so that the approximation is reasonable in the region in which it is the primary energy loss mechanism.

The plasmon-decay and the pair-annihilation energy loss rates are of interest for two reasons. First, they may be important in cooling shock-ejected matter whose density is less than $\rho \sim 10^{11}$ gm/cm^3. Also, for higher densities other neutrino processes will probably dominate, but these processes nevertheless provide a convenient estimate of the minimum possible energy loss rate which is not plagued by the uncertainties* in the effect of strong interactions.

2. Neutrino Opacity.

The interactions of neutrinos and antineutrinos in dense matter have been discussed by Bahcall (1964a), Bahcall and Frautschi (1964b) and Euwema (1964). Euwema calculates the inhibiting factor for effects of the exclusion principle on neutrino absorption.

* See Bahcall and Wolf (1965) for example.

Negligible temperature and completely noninteracting particles which filled all states below the Fermi level and none above, were assumed. Bahcall and Frautschi have considered neutrino-lepton scattering and neutrino-nucleon interactions generally. In particular, Bahcall (1964a) has suggested that neutrino-electron scattering

$$\nu_\beta + e^- \rightarrow \nu_\beta' + e^{-\prime}$$

$$\bar{\nu}_\beta + e^- \rightarrow \bar{\nu}_\beta' + e^{-\prime}$$

is the most important neutrino process for energy deposition in the supernova model of Colgate and White (1964).

a) Nondegenerate gas.

For a nondegenerate gas of electrons, the total cross-section averaged over the initial electron distribution is

$$(\sigma)_{\omega,p} = \left[4\pi^3 n_e \left(\frac{\hbar}{mc}\right)^3 \right]^{-1} \int d^3p \left[1 + e^{(W-\mu)/kT}\right]^{-1} \sigma(p_\alpha, \omega_\alpha)$$

where $\sigma(p_\alpha, \omega_\alpha)$ for neutrino-electron scattering is

$$\sigma(p_\alpha, \omega_\alpha) = \sigma_o (p_\alpha \cdot \omega_\alpha)^2 / (1 + 2p_\alpha \cdot \omega_\alpha)$$

and for antineutrino electron scattering is

$$\sigma(p_\alpha, \omega_\alpha) = \sigma_o \left(\frac{p_\alpha \cdot \omega_\alpha}{6}\right) \left[1 - (1 + 2p_\alpha \cdot \omega_\alpha)^{-3}\right]$$

where n_e is the electron number density per unit volume, p is the electron momentum, W the total electron energy, p_α the dimensionless

four-momentum of the electron, ω_α the corresponding four-momentum for the neutrino, and μ the chemical potential of the electrons. The constant σ_o is

$$\sigma_o = \frac{4}{\pi} \left(\frac{\hbar}{m_e c}\right)^{-4} \left(\frac{G}{m_e c^2}\right)^2$$

$$\approx 1.7 \times 10^{-44} \text{ cm}^2.$$

In the case $kT >> m_e c^2$, the thermal motion of the electrons produces a large center-of-mass energy and hence causes the cross-section to exceed greatly the cross-sections for electrons at rest. In this limit Bahcall finds, for neutrino energies $E_\nu >> m_e c^2$, that

$$(\sigma)_{\omega,T} \simeq 3.2 \, (kT/m_e c^2) \, \frac{\sigma_o \omega}{2}$$

for the neutrino, and for the antineutrino

$$\frac{\sigma_o \omega}{2} \rightarrow \frac{\sigma_o \omega}{6}.$$

Bahcall gives the following form for the neutrino energy loss per scatter

$$\frac{(\omega - \omega')_{av.}}{\omega} \approx \frac{1}{2} \left[1 - \frac{4kT}{\omega m_e c^2}\right]$$

where ω is the dimensionless neutrino energy and the prime refers to the quantity after collision. This approximation requires

$$\omega >> 1 \text{ and } kT >> m_e c^2$$

For sufficiently high electron temperatures, the neutrinos gain more energy per collision on the average than they lose.

b) Degenerate Gas.

In a degenerate electron gas both the initial electron distribution and the prior occupation of final electron states must be considered. Bahcall (1964a) gives the general expression for neutrino-electron scattering as

$$\sigma_\omega = \frac{\sigma_o}{4\pi}\left[4\pi^3 n_e \left(\frac{\hbar}{m_e c^2}\right)^3\right]^{-2} \iiint\left[d^3p\,\frac{d^3p'\,d^3\omega'}{\epsilon'\omega'}\right.$$

$$\left. S(\epsilon)[1 - S(\epsilon')](P'_\alpha \quad \omega'_\alpha) \quad \delta^{(4)}(P_\alpha+\omega_\alpha-P'_\alpha-\omega'_\alpha)\right]$$

where ϵ is the dimensionless electron total energy and the other notation is as before, except for

$$S(x) \equiv [1 + \exp([x-\mu]/kT)]^{-1}$$

where μ is the electron chemical potential. For a completely degenerate gas,

$$S(\epsilon) = 1 \text{ for } \epsilon < E_f$$

$$= 0 \text{ for } \epsilon > E_f$$

where E_f is the total Fermi energy. Bahcall estimates

$$\sigma(\omega', E_f) \approx \begin{cases} \sigma_o \omega^2 & \omega << E_f \\ \sigma_o E_f \omega & \omega >> E_f \end{cases}$$

and for antineutrino scattering the results are multiplied by 1/3.

The results of Bahcall and Frautschi (1964b) indicate that for

$$N_e > 10^{-2} N_n$$

that is, for the electron number density more than 1% of the nucleon number density, neutrino-nucleon scattering is less than neutrino-electron scattering, and will be neglected.

The situation is not clear concerning neutrino absorption by nucleons. In the "low" density domain ($\rho < 3 \times 10^{14}$ gm/cm^3) nucleons not bound in nuclei will display the cross-section

$$\sigma(\omega) \approx \sigma_o \omega^2$$

for neutrinos with energy much larger than $m_e c^2 \sim 0.5$ MeV. For lower energies the behavior is more complicated, with the reaction

$$\bar{\nu} + p \rightarrow n + e^+$$

having a threshold while the reaction

$$\nu + n \rightarrow p + e^-$$

does not. For densities greater than or the order of nuclear density ($\rho \gtrsim 3 \times 10^{14}$ gm/cm^3) the previously mentioned uncertainty with the equation of state may affect the neutrino absorption cross-section by changing the threshold energy or by reducing the phase space available to nucleons in the exit channel. In any case, the extinction cross-section for neutrinos is at least as large as that predicted by neutrino-electron scattering alone, and may be larger. If the number density of electrons becomes considerably less than that of nucleons, then the neutrino opacity of the material cannot be represented, even approximately, without knowing the neutrino-nucleon interaction cross-sections. Thus the equation of

state problem is again encountered. The opacities used in the calculations presented here are due to neutrino-electron scattering.

3. Energy Transfer by Neutrinos.

In this investigation neutrinos were assumed to transfer energy by thermal diffusion. Although tested numerical techniques for time-dependent transfer problems are available (Richtmyer, 1957) it appears that any reasonably accurate transport treatment requires too much machine time for an exploratory calculation. In addition, other approximations, such as neglect of general relativity, make a detailed study of the coupled problem inappropriate at this time. Consequently energy transfer by neutrinos was treated in the thermal diffusion approximation* with the hope that the accuracy would be on the level attained by other aspects of the calculation.

The thermal diffusion approximation assumes that the diffusing energy carriers (usually photons, but in this case electron-type neutrinos and their anti-particles) are in thermal equilibrium with the medium through which they move. The anisotropy which drives the energy transfer is assumed to be a perturbation on a generally isotropic distribution of carriers. The assumption of thermal equilibrium avoids detailed consideration of the processes of neutrino formation, a neglect which greatly simplifies the problem.

---

* The approach in this section follows that of Frank-Kamenetskii (1962) for photons.

The first law of thermodynamics can now be expressed as

$$dE = (\dot{s} - \frac{\partial L}{\partial M}) \, dt - PdV$$

where E is energy density, $\dot{s}$ the rate at which thermal energy is added to the medium, P is the pressure, and V is the specific volume. Assuming spherical geometry, the mass M satisfies the equation

$$dM = 4 \pi \rho \, r^2 \, d \, r$$

where $\rho = 1/V$ is the density and r is the radius of the spherical element under consideration. The luminosity L is given by the usual expression

$$L = (4\pi r^2)^2 \frac{ac}{3\bar{K}} \frac{d(T^4)}{dM}$$

where a is the radiation constant, c the velocity of light, T the temperature and $\bar{K}$ the Rosseland mean opacity

$$\bar{K} = \frac{1}{\rho \bar{\ell}}$$

where $\bar{\ell}$ is the corresponding mean free path. Notice that for simplicity we have assumed that the neutrino and anti-neutrinos may be described by a single "black-body" Fermi gas, that is, the chemical potentials of the neutrinos and antineutrinos are zero. Using Bahcall's (1964) limiting forms for the electron-neutrino (antineutrino) cross-sections, the Rosseland mean opacities can be evaluated analytically*

---

* L.D. Landau and E.M. Lifshitz (1958) Statistical Physics.

for a "black-body" Fermi distribution. However it is sufficiently accurate to replace the neutrino energy by an average value

$$< \mathcal{E}_{\nu} > \sim 3kT$$

so that

$$_{o}\bar{K} = N_{e} \sigma_{o} (3kT)^{2}$$

where the quantities have been defined previously.

It is interesting to note that the integrated neutrino-electron scattering cross-section for a degenerate electron gas is nonzero even if the neutrino energy ω is less than the electron Fermi energy ϵ_{f},

$$< \sigma > \simeq \sigma_{o} \omega^{2} \text{ for } \omega << \epsilon_{f}$$

This means that there is no completely transparent window even for low energy neutrinos ($m_{e}c^{2} << \omega << \epsilon_{f}$). Very low energy neutrinos ($\omega \leq m_{e}c^{2}$) are expected to transfer little energy on short time scales.

The approximation of thermally diffusing neutrinos will be valid only if the neutrino mean free path is shorter than the distance in which the macroscopic variables change. That this condition may be satisfied can be seen as follows. For a density greater than

$$\rho \sim 10^{11} \text{ gm/cm}^{3}$$

the electron Fermi energy never falls below about 30 MeV, so that the electron number density is at least $N_e \sim 10^{35}$ cm^{-3}. Detailed numerical calculations show that the macroscopic variables change little over distances of the order of

$$\Delta X < 2 \times 10^6 \text{ cm.}$$

If the mean free path for a neutrino must satisfy the relation

$$\bar{\ell} \gtrsim \Delta X$$

then the average neutrino energy must be

$$\bar{\epsilon} \gtrsim (\Delta X \quad N_e \quad \sigma_o)^{-\frac{1}{2}} \sim 8 \text{ MeV}$$

If a thermal distribution is assumed, $\bar{\epsilon} \sim 3kT$, so that the temperature must be greater than

$$T \sim 36 \times 10^9 \text{ }^oK.$$

Temperatures far in excess of this are encountered. Eventually this condition breaks down at lower densities, and a "luminous surface" for neutrinos is formed, beyond which the neutrinos almost certainly escape the star without interaction. In this region the energy deposited by the incident neutrino flux and that lost by neutrinos escaping were taken into account in determining the boundary condition. Because of the rapid transition from neutrino-opaque to neutrino-transparent condition, the calculation appears to be insensitive to exact form used.

III. Hydrodynamic Calculations of Stellar Collapse.

A. Initial Models.

Models for stars just prior to supernova implosion have been suggested by Fowler and Hoyle, (1964), and by Chiu (1964). It appears that the essential differences are: (1) Chiu's model is much more centrally condensed, with a higher central density, and (2) because the central temperatures are roughly the same, the center of Chiu's model lies on a lower adiabat. The model suggested by Chiu has electron degeneracy in the core while that of Fowler and Hoyle is nondegenerate, at least until endoergic nuclear reactions become significant. Figures (2) and (3) illustrate the two approximate models chosen to reproduce these characteristics. An n = 3 polytrope, that is, a gravitating gas sphere in hydrostatic equilibrium for which the pressure and density are related by

$$\rho \sim p^{4/3}$$

was chosen to represent the Fowler-Hoyle model. The mass was ten times that of the sun and the initial radius was $R = 10^{10}$cm.

The Chiu model was approximated by an isothermal core of 1.435 $M_\odot$ and a $\gamma = 5/3$ envelope giving a total mass of 1.952 $M_\odot$. This model might correspond to the centrally-condensed core of a more massive star with giant structure,

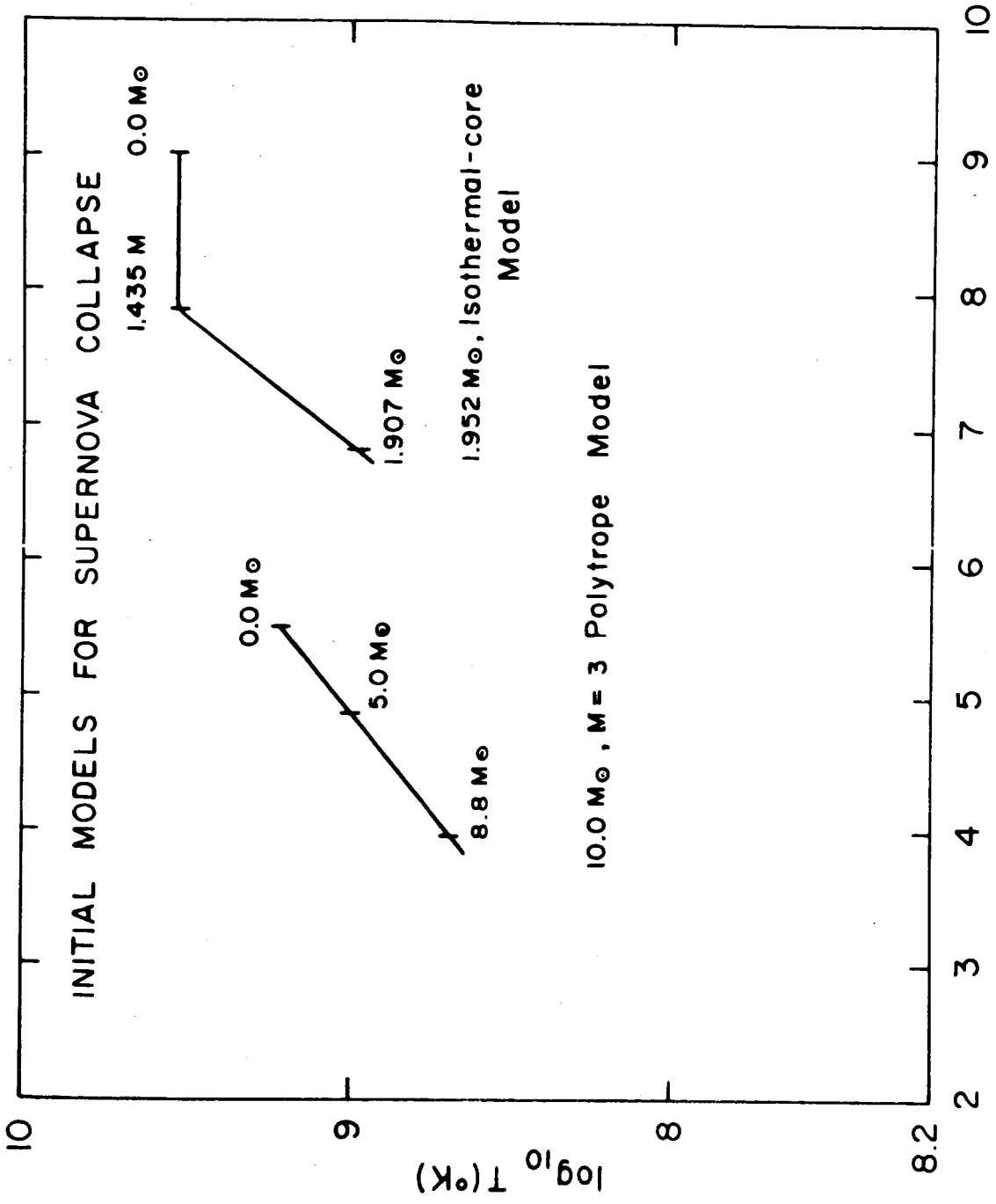
INITIAL MODELS FOR SUPERNOVA COLLAPSE
1.435 M⊙
0.0 M⊙
1.907 M⊙
1.952 M⊙, Isothermal-core Model
0.0 M⊙
5.0 M⊙
8.8 M⊙
10.0 M⊙, M = 3 Polytrope Model
log10 T(°K)
log10 ρ(gm/cm3)
10
9
8
8.2
2
3
4
5
6
7
8
9
10

Fig. 2

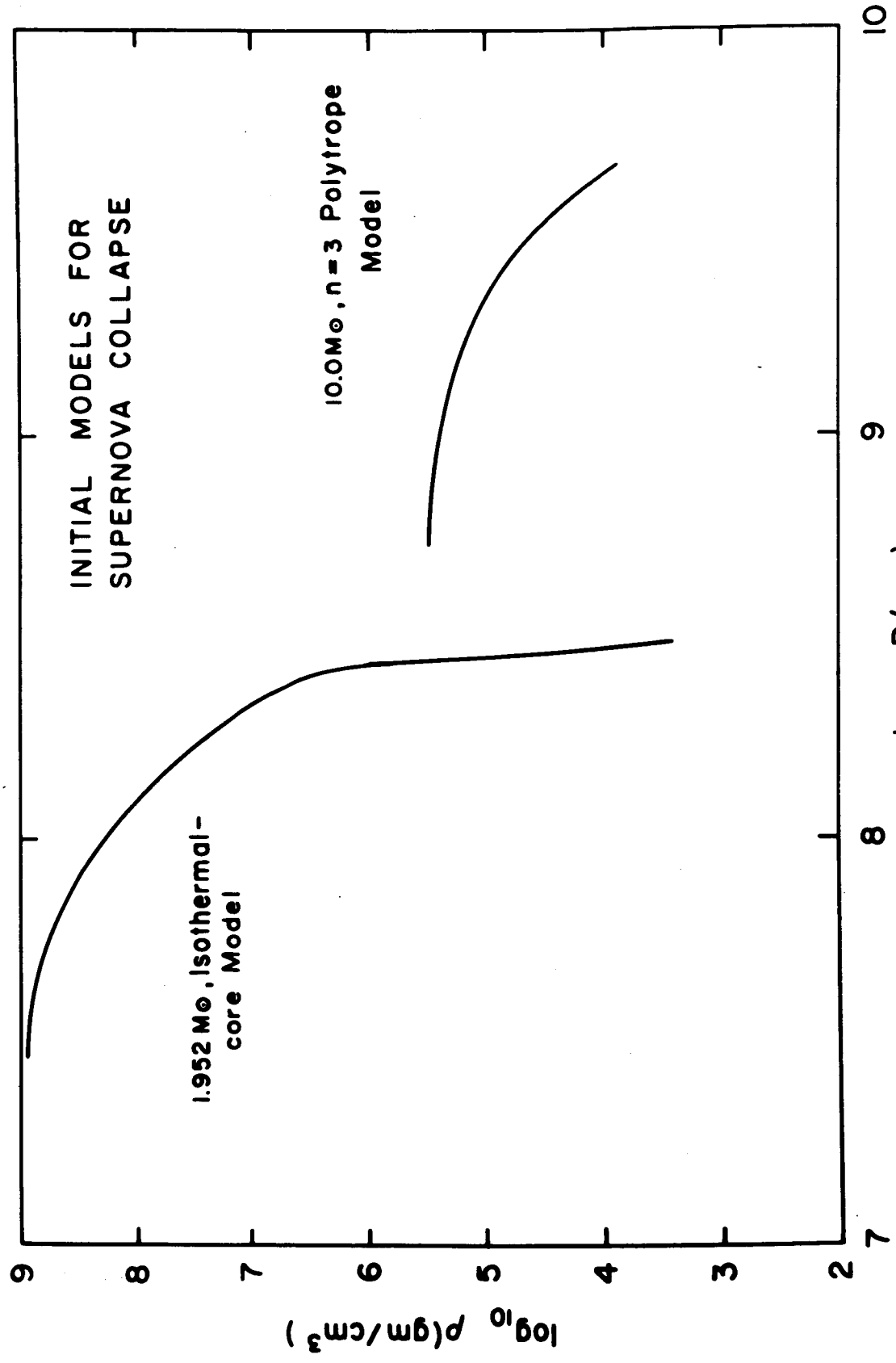
INITIAL MODELS FOR
SUPERNOVA COLLAPSE
10.0M⊙, n=3 Polytrope
Model
1.952 M⊙, Isothermal-
core Model
log10 R(cm)
log10 ρ(gm/cm³)
10
9
8
7
6
5
4
3
2

Fig. 3

the extensive envelope being neglected. Although this is not as centrally condensed as the model with a positive temperature gradient in the core which Chiu first suggested, it does give a highly condensed structure and is in sufficient contrast with the Fowler-Hoyle model.

B. Dynamical History of $10M_\odot$ Pre-supernova Models of Polytropic Structure.

In order to clarify the effects of neutrino energy transfer, the following models are to be presented: (1) the "no-neutrino" model in which all neutrino energy transfer is ignored, (2) "neutrino sink" model in which all neutrinos, once formed, are assumed to escape the star without interaction, (3) "neutrino diffusion" model in which diffusive energy transfer by neutrinos at high densities and temperatures may occur. The choice of a $10M_\odot$ polytrope of index 3 allowed comparison with the results of Colgate and White (1964). The initial evolution of all three models ($10M_\odot$ polytropes of index 3), was identical, following the path ABC in Figure (4); consequently this part of the evolution will be discussed only once.

Figure (4) illustrates the history of one representative zone, ($M_r = 1.5M_\odot$) falling into the core, of the models just discussed. The contraction was initiated by introducing a

EVOLUTION OF REPRESENTATIVE
ZONE (M_r = 1.5 $M_\odot$) FOR THREE
ENERGY TRANSFER ASSUMPTIONS
"STABILITY BOUNDARY"
X "No Neutrinos"
● "Neutrino Sink"
▲ "Neutrino Diffusion
A
B
C
D
E
F
G
H
K
L
LOG_{10}(TEMPERATURE-°K)
LOG_{10}(DENSITY-GM/CM^3)
12
11
10
9
4
5
6
7
8
9
10
11
12
13
14
15
16

Fig. 4

small energy sink to evolve the model. This was done by uniformly increasing the combination pair-annihilation and plasmon neutrino rates throughout the model until it contracted to the collapse point, slow enough to follow a $\gamma = 4/3$ adiabat more or less, but fast enough to do so without using too much computing time. The stability condition (Appendix equation C. 1) on the hydrodynamic difference equations is unduly restrictive for the quasi-static evolution of hydrostatic models, so that this accelerated contraction was necessary. So long as the configuration follows the correct path in the pressure-temperature plane for pre-collapse, and at the point of collapse has negligible kinetic energy, this approximation is valid. This part of the evolution carried the zone along the path AB.

The evolution along the path BC represents the evolution of the material through the Fe-He phase change. At point B energy is removed by endoergic nuclear reactions so that the zones begin to fall inward rapidly. At point C the conversion of the iron-peak nuclei to helium and nucleons is nearly complete. In order to keep the amount of data manageable, quantities were printed out every 200 time cycles of the hydrodynamic calculation. The evolution was so rapid at this

point that the accurate position at which the transition was completed is not known, but it is probably as drawn in Figure (4).

1. "No-neutrino" model.

The evolution from C to D in Figure (4) may be explained as follows. The implosion proceeds until the nucleon terms in the equation of state provide sufficient pressure to halt the infalling material. When neutrino energy loss is neglected, the following artificial situation develops. When the electron Fermi energy rises sufficiently to cause inverse beta-decay, the number density of electrons does not rise much with an increase in density, and hence the pressure contribution due to electrons does not rise either. The free nucleons which are formed do contribute an ideal gas term to the pressure (in this model). Since neutrino energy loss is neglected in this model, the material falling upon the initial $0.5M_{\odot}$ core is shock-heated to high temperatures.

The path CD describes the thermodynamic history of the zone as it encounters this stationary core shock. The kinetic energy which the zone gained upon falling to this density was converted to thermal energy of an ideal nucleon gas. This may be seen from the following estimates:

Change in potential energy upon contraction	$\sim -5.3 \times 10^{52}$ ergs
Change in thermal energy necessary to support the core material hydrostatically	$\sim 4.2 \times 10^{52}$ "
Energy lost in photodisintegration of nuclei	$\sim 1.0 \times 10^{52}$ "
Energy left to form an over-pressure and mass ejection	$\lesssim 0.1 \times 10^{52}$ "

The energy available to form an overpressure is negligible as far as an explosion of the model is concerned. In fact the core continued to adjust itself as overlying layers continued to rain down, and the implosion was not reversed. During this period the zone plotted in Figure (4) evolved along path DE. The calculation was terminated when a core of about three solar masses was formed; at this point there was no indication of any possibility of mass ejection. Although the histories of only "representative" zones are given in the Figures, statements of results (as here with the absence of mass ejection) are based on examination of the behavior of all zones in the model.

During a homologous contraction (or expansion) every mass zone of hydrostatic gas mass has its pressure related to its density by

$$P = P_o \left(\frac{\rho}{\rho_o}\right)^{4/3}$$

where P_o is the pressure and ρ_o the density of this zone for some reference configuration. This relationship defines the path in the pressure-density plane upon which the mass zone must lie for hydrostatic configurations (which are homologous to the reference configuration). When the gravitational acceleration

$$g(r) = - \frac{G M_r(r)}{r^2}$$

is linear in the radius r, a gas sphere in free-fall contracts homologously. This occurs when

$$M(r) \sim r^3$$

or equivalently, when the density is constant.

$$\rho = \text{constant}.$$

For a density which decreases with radius, the outer zones of the gas sphere must be accelerated less than would be necessary for homologous contraction, and "left behind". The innermost zones of a gas cloud freely falling under its own gravity tend to fall homologously, leaving behind those zones which do not. Thus the relation $P \sim \rho^{4/3}$ defines a locus of hydrostatic configurations for the imploding core (and for the whole star model in so far as the homology requirement is satisfied). This curve in the P-ρ plane, and its corresponding curve in the ρ-T plane, define a sort of

stability boundary, such that if the pressure predicted by this relation is greater than the model actually has for a given density, then the core is unstable toward contraction and cannot be static. The dashed line in Figure (4) defines such a boundary. Note that the evolutionary path of the "no-neutrino" model does not cross this line, although at point E the zone shown is a part of a quasi-static core of $3M_{\odot}$ and the stability boundary is approached. By this time the structure of the core is by no means a scaled-down version of the structure of the same matter in the initial hydrostatic model. Although the homology requirement for the use of the stability boundary is violated, in fact there is no evidence that any significant reversal of implosion or mass ejection is likely. For smaller mass cores, it will be seen that the stability boundary concept is useful.

2. "Neutrino Sink" Model.

The "neutrino sink" model differs from the "no-neutrino" model just described through the inclusion of an energy loss rate of the form:

$$Q = -4.3 \times 10^{15} \frac{(T_9)^9}{\rho} - 1.1 (T_9^3) \rho \text{ erg/gm/sec}$$

This is the sum of approximate forms for electron pair-annihilation and plasmon decay neutrino loss processes

mentioned earlier. It is not maintained that this expression is the correct form to use. Quite the contrary, other processes such as the URCA process for nucleons are probably more important. What is important is that the neutrino energy production rate is almost certainly as large as this. If it is assumed arbitrarily that all neutrinos, once formed, escape from the model, then this energy loss rate is a lower limit.

What is the purpose of such an artificial model? Simply this: it shows that for this comparatively mild energy loss rate, there is no reversal of implosion, no mass ejection, but just the accumulation of a degenerate core of ever-increasing size when neutrino diffusion is neglected. This is shown in Figure (4), where this "neutrino sink" model follows the path CFG. In the segment CF the graphed zone encounters a stationary core shock, in which the infalling zones are slowed and become part of the core. For this model, the neutrino energy loss rate keeps the temperature much lower than was the case for the "no-neutrino" model. This causes the core to form at a much higher density than was the case in the "no-neutrino" model. This means that more gravitational potential energy has been released, but is

lost from the star. The continued loss of energy allows the core to evolve slowly to higher densities, along the path FG. The irregularities in the path along FG correspond to oscillations* of the core, perturbed by the continued infall of matter. The matter is quite degenerate at this point, so that temperature has little effect on the equation of state. Notice that the evolutionary path CFG never comes near the "stability boundary".

3. "Neutrino Diffusion" Model.

Neutrino opacity and the approximations involved in the assumption of diffusive energy transfer have been discussed. In this model the possibility of energy transfer by the diffusion of neutrinos is considered. It should be emphasized that the neutrinos were assumed to be in thermal equilibrium with the other particles in order to avoid a kinematic calculation.

The temperatures shown in Figure (4) are unreasonably high because of the approximate nature of the equation of state. In particular, the thermal contribution of the nucleons to the pressure was underestimated. The neutrino opacity depends sensitively upon the average neutrino energy,

---

* These oscillations may be due to the finite size of the mass zones as well as to the excitation of actual physical oscillations.

which depends upon the temperature. Because of this overestimate of the temperature, the collapse of a model using the electron-neutrino scattering opacity behaved much like the previously discussed "no-neutrino" model, that is, a hot core was formed, but there was no mass ejection. In order to examine the effects of neutrino energy transfer, the opacity in the core was kept low enough so that the energy transfer time scale was of the order of the hydrodynamic time scale. This affects only the zones of higher density,

$$\rho \gtrsim 10^{12} \text{ gm/cm}^3,$$

so that opacity in the crucial region in which the infall of the matter is reversed, is just that for neutrino-electron scattering, with average neutrino energy $E \sim 3kT$. A report on investigation of the validity of this assumption for the opacity at high densities is currently being prepared for publication.

The "neutrino diffusion" model was calculated in exactly the same manner as the "neutrino sink" model until the neutrino mean free path became short compared with the dimension of the star. At this point the transfer of energy by neutrino diffusion was calculated, and some results are indicated in Figure (4). The path CD is identical with the

"no-neutrino" case, but the temperature continues to rise rapidly as DH shows.

That this shock heating is more pronounced than in the "no-neutrino" model is quite important. Why this is the case may be seen as follows. Neutrino diffusion removes energy from the core. Before the neutrino diffusion is initiated, neutrinos are unhindered as they escape the core, again removing energy. This loss of energy prevents the temperature from rising rapidly, so that it is nucleon degeneracy pressure rather than thermal pressure which halts the infall of the core. This means that the core will have a much greater density than in the case of the "no-neutrino" model, which in turn implies that more potential energy is released by the contraction. Hence more energy is available for expelling matter.

The situation is now unstable in the following sense. If the infalling matter supplies kinetic energy to the core faster than this energy can be removed by neutrino diffusion, the temperature will rise. Because the neutrino interaction cross-sections are roughly proportional to the square of the neutrino energy, and because at higher temperatures neutrinos are formed with higher energies, the opacity

increases. The transfer of energy by neutrinos then decreases, and the temperature rises still more. Thus the medium may become opaque if the inflow of kinetic energy is sufficiently high.

The greater potential energy released in the "neutrino diffusion" model is now available for reversing the implosion of the outer layers. A neutrino diffusion wave sweeps out of the core, leaving the matter behind it opaque. The zone shown in Figure (4) is heated so that the path DH lies well above the stability boundary. Along the path HKL, this zone falls into the core. The path KL shows the core adjusting itself while overlying matter is ejected. Figure (5) shows the curve already shown on Figure (4) as CDHKL but is now labeled MNOP. The new curve on Figure (5), DEF, corresponds to the zone with an interior mass

$$M_r = 2.0\ M_\odot$$

and which is ejected from the star. The path DE corresponds to the heating of the zone by the neutrino diffusion shock wave, and EF is the subsequent expansion of the zone as it leaves the star. The remnant core mass was 1.8 $M_\odot$.

C. Comparison With the Results of Colgate and White.

Although the hydrodynamics of supernova envelopes has

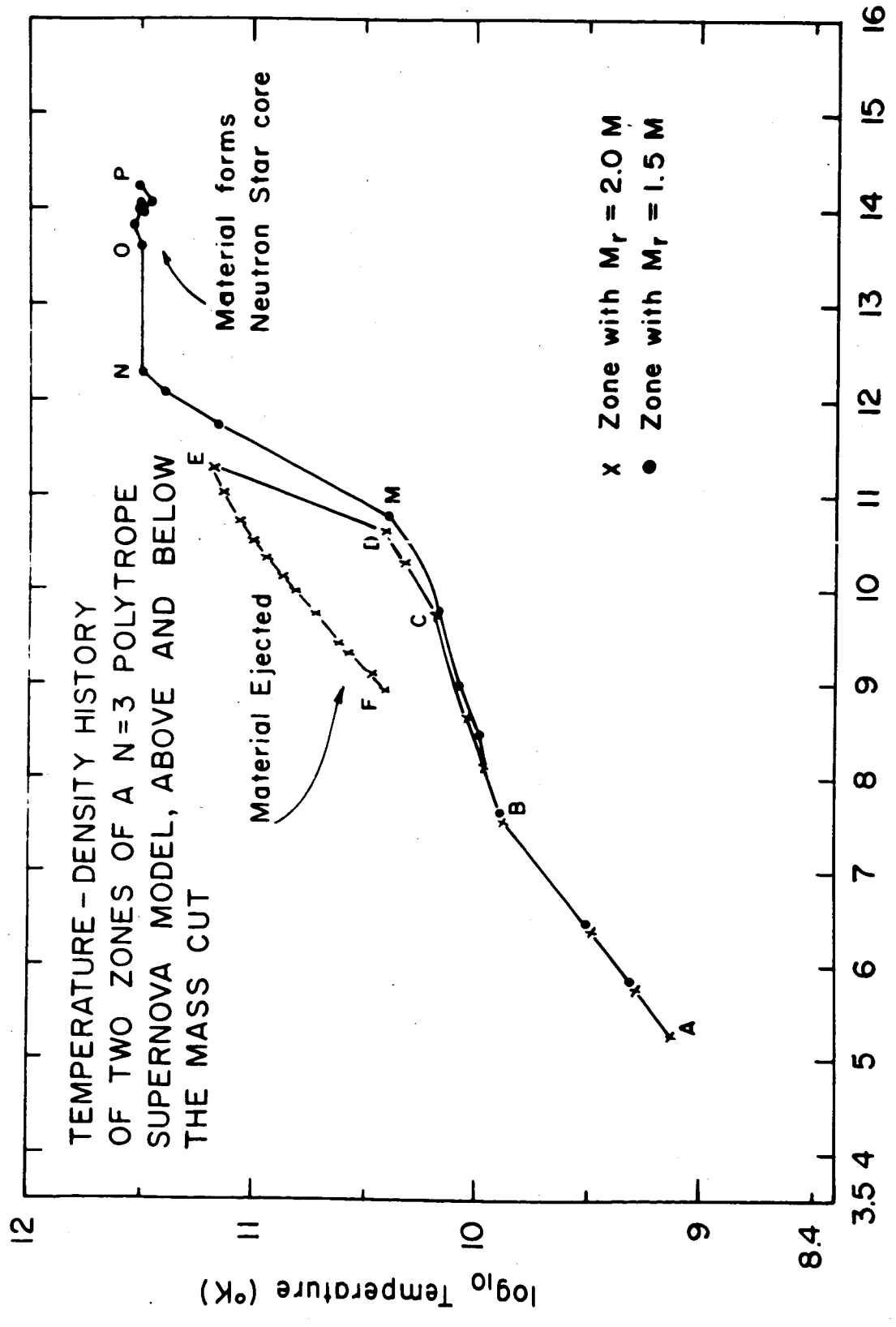
TEMPERATURE-DENSITY HISTORY
OF TWO ZONES OF A N=3 POLYTROPE
SUPERNOVA MODEL, ABOVE AND BELOW
THE MASS CUT
Material forms
Neutron Star core
Material Ejected
x Zone with M_r = 2.0 M
• Zone with M_r = 1.5 M
A
B
C
D
E
F
M
N
O
P
$\log_{10}$ Temperature (°K)
$\log_{10}$ Density (gm/cm^3)
12
11
10
9
8.4
3.5 4 5 6 7 8 9 10 11 12 13 14 15 16

Fig. 5

received much attention, the only previously published investigations (of which the author is aware) of the initial instability and subsequent dynamical history of supernova interiors are those of Colgate and his collaborators. A review of these investigations by Colgate and White (1964) describes some of their more recent results and is the primary source for the following description of their work. In particular, the evolution of type II supernova models was followed by means of a numerical hydrodynamic computer code from the onset of gravitational collapse to the reversal of the infall of the core (due to terms in the equation of state corresponding to a nucleon hard-core potential). The loss of neutrinos emitted in inverse beta-decays cools the core during implosion. This loss rate is approximated by a simple analytic form; a more exact analysis would involve the evaluation of Fermi-Dirac integrals because the material becomes degenerate. A partial deposition of this neutrino flux in the stellar envelope and the shock wave reflected upon the formation of a neutron star core provide sufficient energy to eject $\sim$ 80% of the mass of a 10 solar mass star. To simulate the emission and deposition of neutrinos from the shock wave formed by the infalling material raining

down upon the quasi-static core, half of the emitted energy was deposited in the matter external to the core shock. This deposition was initiated only when the core shock was formed and was turned off when the rarefaction due to expansion terminated the core shock. The time-dependent energy sink term, integrated over the core, is

$$\dot{s} = \int_o^M \left(\frac{dE_\nu}{dt} \right) dM$$

where the factor in parenthesis is just an analytic approximation to the inverse beta-decay neutrino loss rate, i.e.

$$\frac{dE_\nu}{dt} = - 0.1 \; T \; \rho^{5/3} \text{ erg/gm/sec}$$

where ρ is the density in grams/cm^3 and T the temperature in KeV. The rate of neutrino energy deposition that was used, in units of ergs/gm/sec, is

$$\left(\frac{dE_\nu}{dt}\right)_{\text{deposited}} = \frac{\dot{s}K}{4\pi r^2} \exp \left(-K \int_{r_{shock}}^{r} \rho \, dr\right)$$

for

$$r \geq r_{shock}$$

and where

$$K = \ln 2 / \left(\int_{r_{shock}}^{\infty} \rho \, dr \right.$$

The test for initial equilibrium proceeded for a real time of 30 seconds for a $10M_{\odot}$ polytrope of index 3 taken to be the model of a pre-supernova star. This model was inspired by considerations of Fowler and Hoyle (1964). The instability was initiated by removing 1% of the internal energy. The core formed cold with 5% of the mass of the star; after the implosion was reversed in the innermost mass zones a shock formed and neutrino deposition of energy was initiated. In this case $2M_{\odot}$ accumulated in the core before sufficient heat was deposited to reverse the implosion of the outer layers and create an explosion.

Colgate and White (1964) also discuss some calculations involving initial models of 2.0 and 1.5 solar masses. These models evolved on such a low adiabat that, rather than pass through Fe-He phase transition, they were brought to dynamic implosion by rapid electron capture (inverse beta-decay) at a density above 2×10^{11} gm/cm^3. The subsequent core formation, shock wave, neutrino emission and deposition, and finally explosion followed as in the $10M_{\odot}$ case. The expansion velocities and residual core mass were lower, but not drastically so.

Figure (6) compares the result of the "neutrino diffusion"

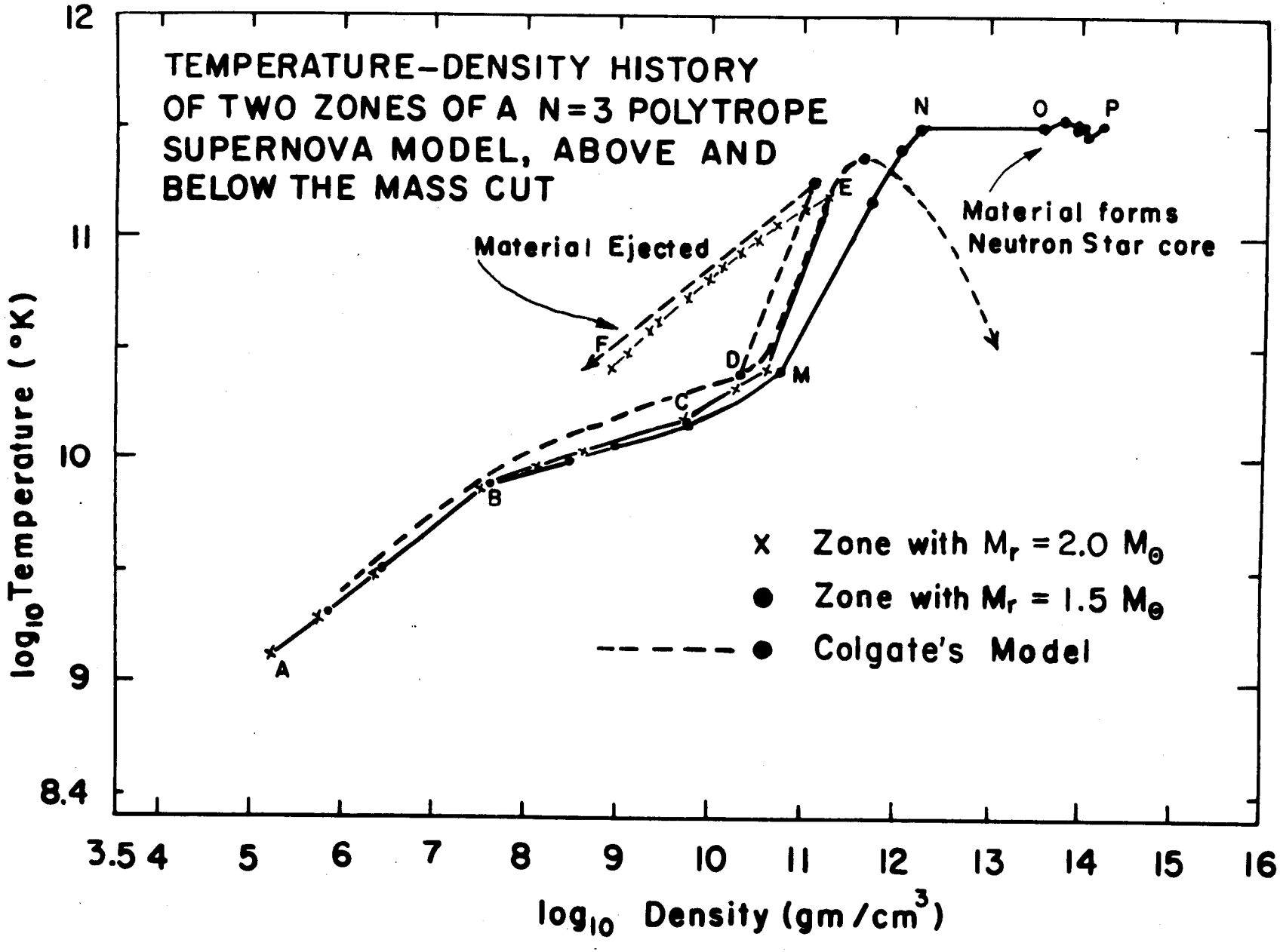
TEMPERATURE–DENSITY HISTORY
OF TWO ZONES OF A N=3 POLYTROPE
SUPERNOVA MODEL, ABOVE AND
BELOW THE MASS CUT
Material Ejected
Material forms
Neutron Star core
A
B
C
D
E
F
M
N
O
P
x Zone with $M_r = 2.0\ M_\odot$
● Zone with $M_r = 1.5\ M_\odot$
Colgate's Model
$\log_{10}$ Temperature (°K)
$\log_{10}$ Density (gm/cm^3)
12
11
10
9
8.4
3.5 4 5 6 7 8 9 10 11 12 13 14 15 16

Fig. 6

model to the results of Colgate and White (1964). Although the data for the plot of Colgate's model were taken somewhat crudely from graphs, there seem to be three differences. This first concerns the Fe-He phase change region BCD which lies on a lower curve for the diffusion model. This does not affect the dynamics much since both models are in free-fall at this point. Considering the widely different methods used in treating this phenomenon, the difference in the two paths is not surprising. The second point is that Colgate's sudden heating (path DE and MN in the diffusion model) seems to occur at lower densities. This is thought to be attributable to Colgate's technique of depositing energy. The last difference is the rapid cooling of the core as shown by Colgate's model. Colgate's energy transfer technique probably is inaccurate at this point; this cooling occurs after the mass ejection so that its effect upon other aspects of the supernova phenomena is small. Also, the diffusion approximation will incorrectly predict the energy loss rate as the distribution function for neutrinos departs from its form for thermal equilibrium. The problem of core cooling would be properly handled only by a detailed transfer calculation.

D. Effect of Pre-collapse Structure.

Figure (7) illustrates the history of two representative zones of the centrally-condensed pre-supernova model described previously. This model was evolved slowly along a path

$$\rho \sim T^3$$

until electron capture instigated collapse. This phase, similar to the evolution of the $10M_\odot$ polytrope model before the Fe-He phase transition, is shown in Figure (7) as the paths AB and MN. By the time these zones had reached the vicinity of points B and N, the core had "bounced" and the neutrino diffusion wave was moving outward.

The effect of this diffusion "wave" may be seen in Figure (7). Consider the zone with 0.98 $M_\odot$ underneath it first. Along path NP there is a wiggle which was caused by initiating the diffusion calculation and has no significance. During this time the diffusion wave has not yet reached the zone. Path PQ shows the heating of this zone as it, falling in, encounters the diffusion wave sweeping outward. During the time the zone moves from Q to R it is inside the neutrino emitting surface. It falls on the core at point R, and evolves slowly from this point on. Further evolution is due to "slow" energy loss by neutrino diffusion (the time

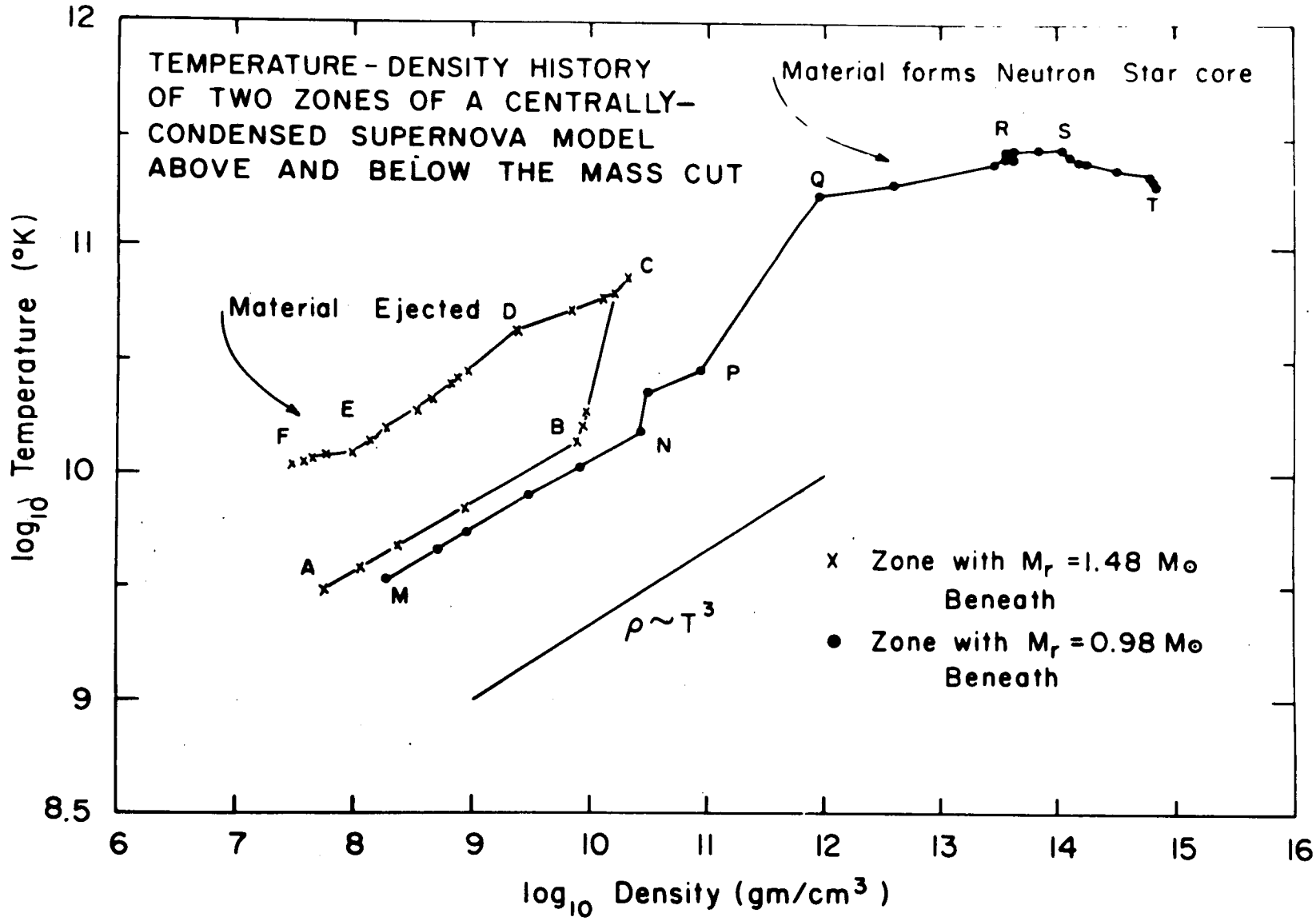
TEMPERATURE - DENSITY HISTORY
OF TWO ZONES OF A CENTRALLY-
CONDENSED SUPERNOVA MODEL
ABOVE AND BELOW THE MASS CUT
Material forms Neutron Star core
Material Ejected
A
B
C
D
E
F
M
N
P
Q
R
S
T
ρ ~ T³
x Zone with M_r = 1.48 M⊙ Beneath
• Zone with M_r = 0.98 M⊙ Beneath
log10 Temperature (°K)
log10 Density (gm/cm³)
12
11
10
9
8.5
6
7
8
9
10
11
12
13
14
15
16

Fig. 7

involved between R and T is $t \geq 10^{-3}$ sec).

The ejected zone ($M_r = 1.48\ M_\odot$) encounters a combination of shock heating and neutrino diffusive heating along the path BC. At C, the peak temperature for this zone, expansion begins. Along CD there is some heating due to acceleration of lower zones, but along path DE the pair-annihilation neutrino energy losses make the path slightly steeper than $\rho \sim T^3$. At point E, the thermally decomposed nuclei begin to recombine by exoergic reactions. This causes the temperature to drop off more slowly along path EF. At this point the calculation was terminated.

The similarities and differences in the two structurally different models are summarized in Table I. The "velocity of ejected matter" quoted in Table I means the average velocity of that matter behind the ejection shock wave at the conclusion of the calculation. The velocity corresponding to the observed expansion velocities of supernova remnants should be less because an envelope of several solar masses still lies outside the ejection shock. Extension of these calculations to this asymptotic ejection velocity is contemplated.

The more violent ejection of matter from the centrally

condensed model is to some extent due to nuclear recombination late* in the expansion. The similarities are more striking than the differences. These two widely differing models, brought to collapse by different mechanisms, nevertheless have surprisingly similar characteristics. The remnant core mass seems to be higher for the less condensed model; this might be expected because the mass of the sphere inside which the gravitational acceleration,

$$g(r) = \frac{GM(r)}{r^2}$$

is nearly linear, is smaller in the more condensed model. This determines the mass of the material which halts its contraction as a unit; this material collapses approximately as a uniform density sphere would.

E. Comparison of Calculations and Observations.

Because of the low frequency of occurrence of supernova outbursts (about 1/century/galaxy) observational information is meager. Zwicky (1956) gives a history of supernova observations. More recent accounts by Shklovski (1960) and Minkowski (1964) make it reasonable to identify type II supernovae with the catastrophic disintegration of a massive

---

* The polytrope model was not followed this far.

star ($M>>M_{\odot}$). Table II contains a summary of some characteristic properties of supernovae type II. Details concerning the optical spectra and light curves, which are not investigated here, may be found in the references mentioned above.

Comparing Tables I and II, it will be seen that there is reasonable agreement between the observational evidence and theoretical predictions. The visual magnitude expected from the theoretical models has not been estimated, but the kinetic energy of ejected mass is appropriate. The velocity of ejection appears larger than observed, but in fact the asymptotic value of the velocity will be lower, especially if the star has an extensive envelope as has been assumed. This comment applies to the condensed model, in particular, which is envisaged as having a large envelope.

IV. Interpretation of the Results of the Model Calculations.

A. Peak Temperature and Muon Neutrino Energy Loss. Muon neutrinos do not have the same interaction cross-sections as electron neutrinos. Unfortunately the opacity for mu neutrinos in a hot, dense medium like a supernova core is not as well investigated as for electron neutrinos. It appears that neutrino production by muon-pair annihilation will dominate production from simple muon decay, for higher temperatures at least, as will be shown by the following argument.

Some rough estimates of the muon neutrino energy loss rates may be made as follows. The number density of fermion pairs,

neglecting any decay modes, is given by

$$N = \frac{2}{h^3} \int_0^\infty \frac{d^3 p_\pm}{1 + \exp\left[(\mathcal{E}_\pm \pm \mu)/kT\right]}$$

Assume that the muons are nondegenerate and that the number densities of μ_+ and μ_- are equal. Then, since*

$$\exp\left[(\mathcal{E}_\pm \pm \mu)/kt\right. >> 1$$

where the maximum of the integrand occurs, then

$$N_p = \left(\frac{mc}{\hbar}\right)^3 \frac{1}{\pi^2} f(\beta)$$

where N_p is the number density of muon pairs, mc^2 is the rest energy of the muon, and

$$f(\rho) = \int_0^\infty \exp\left[-\beta(1+x^2)^{1/2}\right] x^2 \, dx$$

$$\beta = \frac{mc^2}{kT} .$$

For large β, that is, $kT << mc^2$,

$$f(\beta) \approx \sqrt{\pi/2} \frac{e^{-\beta}}{\beta^{3/2}}$$

so that

$$N_p \sim \frac{10^{38}}{3.2} \frac{e^{-\beta}}{\beta^{3/2}}$$

The rate of neutrino energy loss at high enough temperatures by muon decay is roughly

$$\dot{s} \sim - 2N_p \bar{\mathcal{E}}/(\rho\tau) \text{erg/gm/sec}$$

---

* Chiu and Stabler (1961) present this approximation for electrons.

where $\bar{\epsilon}$ is some average energy of the emitted neutrino, ρ the matter density, and τ the half life of the muon. Assuming equipartition of energy, $\bar{\epsilon}$ might be of the order of 35 MeV.

Using the same approximations of nondegeneracy and $kT << mc^2$, Chiu and Stabler give the approximate pair annihilation energy loss rate

$$\dot{s}_e = -4.8 \times 10^{18} \frac{T_9^3}{\rho} e^{-(2m_e c^2/kT)} \quad \text{ergs/gm/sec}$$

Correcting this for the heavier mass muon,

$$\dot{s}_\mu \sim \left(\frac{m_\mu}{m_e}\right)^9 \dot{s}_e$$

$$\approx 3 \times 10^{32} \frac{T_9^3}{\rho} e^{-(2400/T_9)}$$

Neglecting the effect of muon decay on the number of muon pairs formed in equilibrium with radiation may be justified as follows. The characteristic time for muon deacy is 2×10^{-6} seconds. Taking $kT << m_\mu c^2$ the muon pair annihilation cross-section has roughly the same magnitude as

$$\sigma \sim \frac{8\pi}{3} \left(\frac{e^2}{m_\mu c^2}\right)$$

$$\sim 10^{-29} \text{ cm}^2$$

So that the mean reaction time is

$$\tau_r \sim \frac{1}{N \sigma v}$$

which for $T_9 = 120$ gives

$$\tau_r \sim 10^{-13} \text{ sec}$$

so that

$$\tau_r \ll \tau_{\text{decay}}$$

and this implies that muon decay does not greatly alter the muon number density. Some estimates for the energy loss rates by muon type neutrinos are given in Table III.

The energy loss rates have units erg/gm/sec and are all evaluated at a density of 10^{12} gm/cm^3. The relaxation times for these rates, if they proceed unimpeded are given in Table IV.

In the last case the energy loss by neutrinos emitted by muon decay is dominant, but the time scale for cooling is then longer than the characteristic collapse and mass ejection time scale. From these rough estimates it might be expected that the temperatures for the n=3 polytrope model, Figure (5), are artificially high. The muon-neutrino energy loss is probably not so large for the isothermal model. It is not convincing to estimate what effect muon neutrinos will play in supernova explosions without a careful analysis of all possible reactions, both for neutrino production and neutrino opacity, and a careful estimate of the temperature. It does appear that larger remnant cores might be expected with the inclusion of muon-type neutrino energy loss, but little more can be said at this time.

B. Electron Neutrino Luminosity and Detectability. The immense energy radiated by neutrinos that the previous models predict, and the high temperature of the emission surface, suggest that it might be possible to detect supernovas by their neutrino flux. Dr. Raymond Davis, Jr.* of

---

* R. Davis, Jr. (1965).

Brookhaven has kindly provided information about his detector with which to evaluate this possibility.

If a detector contains N absorbers, then the fraction of the total integrated neutrino flux absorbed in the detector is

$$f = \frac{N\sigma}{4\pi R^2}$$

where σ is the interaction cross-section and R is the distance of the source. The total integrated flux is roughly

$$F = \frac{E_{tot.}}{3kT}.$$

where $E_{tot.}$ is the total energy emitted in the form of neutrinos (only electron neutrinos are considered because of the uncertainty in the muon reaction rates), and T is the temperature of the zone just inside the neutrino emission surface.

For kT ~ 10 MeV, and

$$E_{tot.} \sim 10^{53} \text{ ergs}$$

$$N \sim 2 \times 10^{30} \ Cl^{37} \text{ atoms}$$

$$\sigma \sim 7 \times 10^{-41} \text{ cm}^2,$$

where the cross-section is for the reaction

$$\nu + Cl^{37} = e^- + A^{37},$$

and for a minimum detectable signal of 100 counts,

$$R \sim 1.5 \times 10^{22} \text{ cm}$$

$$\sim 5 \text{ kpc.}$$

the maximum source distance is 5 kiloparsecs. According to Allen*, the diameter of the Galaxy is

$$D \sim 25 \text{ kpc.}$$

Recalling the supernova rate quoted earlier, one per century per galaxy, it appears that no burst of electron neutrinos is likely to have produced a detectable signal since suitable detectors have been operating.

C. General Relativity and Core Collapse.

In order to check the neglect of general relativity, the Schwarzschild radius

$$r_s = \frac{2\,GM}{c^2} \sim 0.3 \times 10^6 \left(\frac{M}{M_\odot}\right) \text{ cm.}$$

is compared to the radius of the dense core.

	Condensed Model	n = 3 polytrope model
r_s/r core	0.22	0.38

As anticipated the general relativistic effects are becoming important, especially for the n = 3 polytrope model. These effects will be more pronounced in the core. The mass ejection, occurring before such high densities are reached

---

* Allen (1963), p. 267.

(r_s/r_{core} for the n = 3 polytrope is then only ~ 0.16), will be less sensitive to this effect. However, the bounce point for the core collapse, where the infall is halted, is somewhat dependent on both the nuclear equation of state and the temperature of the infalling matter. Careful investigation with general relativistic hydrodynamic equations is needed to confirm that neglect of general relativity is reasonable until after mass ejection.

V. Critique of Calculational Method.

Approximating the transfer of energy by neutrinos by a model of diffusing neutrinos in local thermodynamic equilibrium is probably correct in a rough sense, but while it may be on firmer theoretical ground than the intuitive approach of Colgate and White (1964), it leaves much to be desired. On the other hand, the solution of a transport equation coupled with hydrodynamic motion poses extremely difficult computational problems.

The shock width in Figure (5), path MN, and in Figure (7), path PQ, stretches over a density range of more than a power of ten. Direct examination of the numerical results of the calculation reveal that in general the width of the shock zone is smeared over too wide a

region due to the lack of an adequately fine zoning mesh. Unfortunately, the present generation of computers is too slow to make the use of models with more zones feasible. The computing time goes as the square of the number of mass zones in the model, so that this limitation is difficult to overcome.

By the similarity in energy release and core size as obtained by the polytrope of index 3 and the isothermal model, it appears that the interior dynamics of supernova are relatively insensitive to the structure of the pre-supernova model. This does not mean that the existence of an extensive envelope such as found in massive red giants might not affect the velocity of ejection and the peak shock temperature in the matter ejected. It does mean that the implosion and "bounce" of the core, as well as the neutrino energy transfer process are insensitive to initial structure. The interior dynamics is much the same for the two models presented.

Summary

The calculations reported here indicate that it is possible to construct reasonable models of supernova by assuming energy to transferred by electron-type neutrinos during stellar collapse. Whether or not considerable mass

ejection by this process actually occurs depends critically upon the average neutrino energy and the opacity for neutrinos in regions of high density ($\rho \geq 10^{12}$ gm/cm^3). Unfortunately these quantities remain uncertain. Because of the temperature uncertainty, the emission rate of muon-type neutrinos is also unknown. Even the relatively low estimates of energy loss rates made for muon-decay (neutrinos from pion-decay may be more important) indicate that muon-type neutrino processes will be of paramount importance at the higher temperatures.

Appendix on Numerical Methods

Because the techniques used in this research are not as yet well known to most physicists and astronomers, a brief summary is presented here. The equations of hydrodynamics may be written as follows:

1) mass conservation

$$dM_R = 4\pi R^2 \rho dR,$$

2) momentum conservation

$$\frac{dU}{dt} = -\frac{GM_R}{R^2} - 4\pi R^2 \frac{dP}{dM},$$

3) energy conservation

$$dE = \dot{s}\, dt - PdV,$$

but using

$$dE = \left(\frac{\partial E}{\partial V}\right)_T dV + \left(\frac{\partial E}{\partial T}\right)_V dT$$

gives

$$dT = \frac{1}{\left(\frac{\partial E}{\partial T}\right)_V} \left(\dot{s}\, dt - \left(P + \left(\frac{\partial E}{\partial V}\right)_T\right) dV\right),$$

4) equation of state as a function of temperature T and specific volume V

$$P \equiv P(v,T),$$

$$\left(\frac{\partial E}{\partial T}\right)_V \equiv ET(V,T),$$

$$\left(\frac{\partial E}{\partial V}\right)_T \equiv EV(V,T).$$

In these equations M_R is the mass interior to some radius R, $\rho = 1/V$ is the density, U is the velocity of Lagrangian mass element at R, E is the internal energy per unit mass, $\dot{s}$ the rate of addition of energy per unit mass, and P is the pressure.

A. Difference Equations. As they stand, the fluid dynamic equations are highly nonlinear. Because of this difficulty only a few analytic solutions are available, and all of rather limited applicability. For other cases one is usually forced to some sort of approximation technique which is often as complex as numerical solution, and which may tend to obscure the physical situation. Even the approximation techniques are generally restirctive. In view of these problems it is often the case that numerical solution difference equations is preferable. At first we neglect radiative transfer of energy. Neutrino energy transfer will be treated subsequently.

The star will be divided into concentric spherical shells by J boundaries numbered 1, 2, 3,...J (from the center outward). Quantities associated with the zone boundaries will be subscripted j; those associated with zone centers

are subscripted j + 1/2. Time centering is indicated by a superscript n in a like manner.

After using some simpler forms, difference equations quite similar to those of Colgate and White (1964) were adopted. Although they have been presented in the above reference, the equations are discussed here for completeness.

The initial configuration is input. The position and velocity of each boundary

$$R_j^1$$

$$j = 1, \ldots JJ$$

$$U_j^1$$

where JJ is the number of boundaries, the pressure, specific volume and temperature of each zone

$$P_{j+1/2}^1$$

$$V_{j+1/2}^1$$

$$T_{j+1/2}^1$$

must be specified. The mass of each zone may be calculated from

$$DM_{j+1/2}^1 = \frac{4\pi}{3}\left(R_{j+1}^1\right)^3 - \left(R_j^1\right)^3 / V_{j+1/2}^1 \qquad \text{A.1}$$

The effective mass of a zone as seen from a boundary is the simple average

$$DM_j^1 = \tfrac{1}{2}\left(DM_{j+1/2}^1 + DM_{j-1/2}^1\right)$$

A.2

which assumes that the zone masses differ little. In practice it was found that results were often better when neighboring zone masses were the same or changed by a small constant fraction. The total mass inside a boundary j+1 is

$$XM_{j+1}^1 = XM_j^1 + DM_{j+1/2}^1$$

A.3

In the Lagrangian system mass is necessarily conserved until the zoning is changed. When a system changes drastically it is sometimes possible to shorten the time required for a calculation by rezoning the configuration, but otherwise the zone masses remain the same.

The equation for momentum conservation, may be written as

$$U_j^{n+1/2} = U_j^{n-1/2} - (R_j^n)^2\left[P_{j+1/2}^n - P_{j-1/2}^n + Q_{j+1/2}^{n-1/2} - Q_{j-1/2}^{n-1/2}\right]\Delta t^n/DM_j$$

A.4

$$- \frac{G\ XM_j}{(R_j^n)^2}\ \Delta t^n$$

where the fluid velocity is

$$U \equiv \frac{dR}{dt}$$

so

$$R_j^{n+1} = R_j^n + U_j^{n+1/2} \Delta t^{n+1/2}$$

A.5

From this the specific volume can be updated by

$$V_{j+1/2}^{n+1} = \frac{1}{3} \frac{(R_{j+1}^{n+1})^3 - (R_j^{n+1})^3}{DM_{j+1/2}}$$

A.6

which reflects mass conservation. The specific volume evaluated at the same point in time as the fluid velocity U, that is at n+1/2, will be useful.

$$V_{j+1/2}^{n+1/2} = \tfrac{1}{2} (V_{j+1/2}^{n+1} + V_{j+1/2}^{n})$$

A.7

At this point a linear extrapolation in time is made for the new temperature at point n+1/2. Initially

$$T_{j+1/2}^{3/2} = T_{j+1/2}^{1}$$

but afterward

$$T_{j+1/2}^{n+1/2} = T_{j+1/2}^{n} + \frac{1}{2} \frac{\Delta t^{n+1/2}}{\Delta t^{n-1/2}} (T_{j+1/2}^{n} - T_{j+1/2}^{n-1})$$

A.8

This will be used to determine the temperature at the epoch n+1.

Evaluating the equation of state at time step n+1/2 gives

$$P_{j+1/2}^{n+1/2} = P(T_{j+1/2}^{n+1/2}, \quad V_{j+1/2}^{n+1/2}),$$

A.9

$$\left(\frac{\partial E}{\partial T}\right|_{V}^{n+1/2}{}_{j+1/2} = ET \ (T_{j+1/2}^{n+1/2}, \quad V_{j+1/2}^{n+1/2}),$$

A.10

$$\left(\frac{\partial E}{\partial V}\right|_{T}^{n+1/2}{}_{j+1/2} = EV \quad (T_{j+1/2}^{n+1/2}, \quad V_{j+1/2}^{n+1/2}).$$

A.11

The quantity Q in the momentum conservation difference equation is the so-called pseudo-viscosity term which stabilizes this set of difference equations. When zone boundaries approach rapidly it supplies a large pressure to prevent them from crossing. In a shock the pseudo-viscosity term converts kinetic energy of zone motion into thermal energy, and is negligible elsewhere. The form used is

$$Q_{j+1/2}^{n+1/2} = 2 \ (U_{j+1}^{N+1/2} - U_{j}^{n+1/2})/V_{j+1/2}^{n+1/2} \quad \text{if} \quad V_{j+1/2}^{n+1} < V_{j+1/2}^{n}$$

$$\text{and} \quad U_{j+1}^{n+1/2} < U_{j}^{n+1/2}$$

$$= 0 \quad \text{otherwise},$$

A.12

which is zero on expansion.

The energy conservation equation becomes

$$T^{n+1}_{j+1/2} = T^{n}_{j+1/2} + \frac{1}{ET^{n+1/2}_{j+1/2}} \left[- (P^{n+1/2}_{j+1/2} + Q^{n+1/2}_{j+1/2} + EV^{n+1/2}_{J+1/2}) \right.$$

$$\left. * \ (V^{n+1}_{j+1/2} - V^{n}_{j+1/2}) + \dot{s}^{n+1/2}_{j+1/2} \ \Delta t^{n+1/2} \right]$$

A.13

Although the energy source term $\dot{s}$ has not been specified, a form for it could have been evaluated at epoch n+1/2 along with (A.9) for instance.

B. Pseudo-viscosity Technique. The pseudo-viscosity technique for treating hydrodynamic shocks is due to Von Neumann and Richtmyer (1950). There are few* references to it in the literature although it seems to be arousing some interest among astrophysicists.

Attempts to solve the equations of fluid motion by numerical procedures are greatly complicated by the presence of shocks. Mathematically the shocks are represented by surfaces upon which the temperature, density, pressure and fluid velocity are discontinous. The partial differential equations governing the motion require boundary conditions connecting the values of

---

* The author found Richtmyer (1957), Fromm (1961), Henyey (1959), Christy (1964) and Colgate and White (1964) most useful.

these quantities on each side of the shock surface. The Rankine-Hugoniot relations, i.e., local conservation of mass, momentum and energy by the fluid, supply the necessary restrictions, but are difficult to apply during a calculation because the shock surface moves relative to the mesh points in space-time which are used for the numerical work. The nonlinearity of both the differential equations and the boundary conditions does not simplify the problem. The motion of the shock surfaces is not known in advance but is determined by the differential equations and the boundary conditions themselves.

The method of Von Neumann and Richtmyer automatically treats shocks and avoids the necessity for pre-knowledge of shock motion by utilizing the effects dissipative mechanisms (such as radiation, viscosity, and heat condiction) upon shocks. When viscosity is considered, the mathematical shock discontinuity becomes a thin layer in which the pressure, density, fluid velocity and temperature vary rapidly but continuously. By introducing an artificial dissipative mechanism to spread this shock layer over a few mesh points, the difference equations approximating the equations of fluid motion can be used throughout the calculation, as if no shocks were present.

In the numerical results the shocks appear as rapid changes in the variables, almost discontinuities, which have very nearly the correct speed and across which the pressure, temperature, and density have very nearly the correct changes.

In an actual physical problem the dissipative mechanisms are generally much smaller than the artificially introduced viscosity term. The limit on computational reproduction of a physical situation is that the zone size be smaller than the smallest dimension of interest. The quadratic dependence of (Q) on the velocity difference insures that this form for the artificial viscosity is small except in the shock region. Note that the 1/V dependence gives an increasing pseudo-viscosity for large compression.

C. Stability of the Difference Equations. For a more complete discussion of the stability of finite difference approximations the reader is referred to Von Neumann and Richtmyer (1950), Fromm (1961) and Richtmyer (1957). To clarify the meaning of stability, consider the exact solution $\Psi(r,t)$ to the one-dimensional differential equations of fluid dynamics for some specified initial-value problem. Let Ψ_j^n be the corresponding solution to a system of difference equations which approximate these differential equations.

The error of the approximation is then

$$|\Psi_j^n - \Psi(r=j\Delta r,\ t=n_\Delta t)|$$

Suppose that this error is small enough at some time t, and consider some small perturbation $\delta\Psi$. Does this perturbation grow with time? If so the difference scheme is obviously unacceptable as an approximation to $\Psi(r,t)$.

The criterion for stability against such small perturbations, for a set of difference equations such as presented here, is that the time step for integration Δt satisfy

$$\Delta t < \frac{\Delta x_{j+1/2}}{v_s} \qquad \text{C.1}$$

where Δx is a zon width and v_s is the local sound velocity. This must be true for each zone. There is a simple physical interpretation for this restriction. Neglecting any sort of radiative transfer and considering only gasdynamic effects, the minimum time for material at zone boundary j to communicate with material at zone boundary j+1 is just the sound traversal time t_s

$$t_s = \frac{x_{j+1} - x_j}{v_s} = \frac{\Delta x_{j+1/2}}{v_s}$$

The requirement

$$\Delta t < t_s$$

is simply that conditions at boundary j+1, say, at time epoch n+1 be physically independent of what transpires at boundary j at the same epoch n+1. Most physicists are more familiar with the analagous situation in relativity where the velocity of light plays the part here taken by the sound velocity. Although such a restriction is mathematically required of difference equations such as these, this restriction is physically necessary only when gasdynamic motions having velocities of the order or greater than the sound velocity are encounteed. If this is not the case a different set of difference equations might be developed which had a less stringent requirement* on the integration time step.

For a complex problem in which there are drastic changes from the initial configuration, considerable computational time may be saved by choosing the integration time step Δt as the maximum value consistent with the stability requirement (C.1). In the supernova problem it was discovered that this requirement, while necessary, was not sufficient to reproduce the physical situation faithfully. In the adiabatic contraction of a gravitating uniform sphere, it was found that the analytic solution was not successfully

---

* See Henyey (1959) for example.

approximated unless some restriction like the following was used:

$$\Delta V^{n+1/2} \leq 0.02\ V^{n},$$

so that the fractional change in specific volume was only a few percent. Colgate and White (1964) use the following simple and effective restriction on the time interval.

$$\Delta t^{n+3/2} \leq \frac{0.02 * V^{n}_{j+1/2} * \Delta t^{n+1/2}}{|V^{n}_{j+1/2} - V^{n-1}_{j+1/2}|} \qquad \text{C.2}$$

In the difference form for the energy equation, an energy source term $\dot{s}$ appears. This allows energy to be added or removed locally, although as written does not explicitly account for energy transfer between zones. When energy is suddenly added or lost instabilities often result. Now the energy density E of a fluid may be written as

$$E = \frac{1}{\gamma - 1}\ PV$$

where P is the pressure, V the specific volume, and γ the "ratio of specific heats" which is constant for an ideal gas. Generally γ is a slowly varying function. With this in mind, the following time interval restriction was used

$$\Delta t^{n+3/2} \leq \frac{0.02\ P^{n}_{j+1/2}\ V^{n}_{j+1/2}\ \Delta t^{n+1/2}}{|P^{n}_{j+1/2}\ V^{n}_{j+1/2} - P^{n-1}_{j+1/2}\ V^{n-1}_{j+1/2}|}$$

C.3

and found to be adequate.

Using these three restrictions on the time step, the new time interval can be calculated. The sound velocity was found to be adequately represented by the simple approximation

$$v_s \approx \sqrt{2PV}$$

The time intervals $\Delta t^{3/2}$ and $\Delta t^{1/2}$ are input. Then Δt^{n}, which is needed in (A.4), the momentum conservation equation, is

$$\Delta t^{n} = \frac{1}{2}\ (\Delta t^{n+1/2} + \Delta t^{n-1/2})$$

C.4

This procedure allows a small, conservative estimate of the time interval to be input which insures that the stability requirements are not violated. The scheme then chooses the optimum time interval and rapidly approaches it. It is noted in passing that the reason for centering these difference equations in time* is to allow this calculated time step scheme to be used accurately with varying time steps.

---

* Only the pseudo-viscosity Q in (A.13) is not centered in time, a condition mitigated by the fact that Q is not a physical but a computational quantity, and that computations using this Q are accurate.

D. Boundary Conditions. In the supernova problem the interior boundary was taken to be at the origin, so by symmetry

$$R_1^n = 0$$

$$U_1^n = 0$$

for all time. This was not necessary; the inner boundary could have been at some distance R from the center of the star, acting as a spherical piston with velocity

$$U_1^n = f(t^n)$$

which in general varies in time.* There are difficulties associated with zones near a piston in this sort of scheme, however, and care should be taken.

Having specified the center of the star as the inner boundary, symmetry assures that pressure, temperature and specific volume are continuous through the origin and no inner boundary condition need be specified. The outer boundary is free to move, however,

$$U_{JJ}^n \neq 0$$

in general, so that its motion will be determined by the pressure (and artificial viscous pressure) at JJ+1/2. These are not calculated and must be imposed. If

* Christy, R. (1964).

$$P^{n}_{JJ+1/2} = - P^{n}_{JJ-1/2}$$

$$Q^{n-1/2}_{JJ+1/2} = - Q^{n-1/2}_{JJ-1/2}$$

D.1

then the total calculational pressure (P+Q) will be zero at JJ. This boundary condition was used. In this particular problem the motion of the inner regions was most interesting so that the choice of surface boundary condition did not happen to be critical.

E. Analytic Checks of Numerical Results. In order to test the validity of the numerical techniques employed, several problems for which exact analytic solutions exist were calculated. Some of these results are to be found in Colgate and White (1964), and they are reproduced in the author's thesis both as an argument for the validity of these particular difference equations and because they provide insight into the technique. The problems for which checks were made are: (1) a strong, plane shock propagating through an ideal gas with $\gamma = 5/3$ and density decreasing with the -7/4 power of the distance, (2) a strong spherical blast wave in an ideal gas with a density

$$\rho \sim R^{-n},$$

(3) the adiabatic collapse of an ideal gas sphere of uniform density, and (4) the hydrodynamic motion (or lack of it) of a gravitating gas sphere in hydrostatic equilibrium.* There is excellent agreement between the numerical and analytical solutions in all four cases.

F. Radiative Energy Transfer. If the diffusion approximation is valid the change in energy density due to sources and time-dependence can only affect lengths large compared to the mean free path. Then, for conservation of energy,

$$\frac{\partial E}{\partial t} + v\nabla E = \dot{s} - \frac{1}{\rho} \nabla \cdot \vec{J}$$

where $\dot{s}$ is the energy generation rate (per unit mass) due to sources, E the energy density per unit mass, v the velocity of the source, ρ the mass density, and $\vec{J}$ the energy flux. If source motion can be neglected, and macroscopic changes occur on a time scale much larger than the mean free time for the diffusing particles, then

$$\rho \dot{s} = - \nabla \cdot \left(\frac{\lambda_c}{3} \frac{dE}{dT} \Delta T\right)$$

Assuming sperical symmetry, this may be rewritten as

$$D \frac{dT}{dR} = - \frac{L(r)}{4\pi R^2}$$

where r is the radial coordinate and

---

* The exact solutions for (1), (2) and (3) are to be found in Burgers (1949), Sedov (1959), and Colgate and White (1964), respectively.

$$L(R) = \int_0^r 4\pi R^2 \, \dot{s} \, \rho \, dR$$

$$D = \frac{\bar{l}c}{3} \frac{dE}{dT}$$

which are the standard forms for radiative diffusion used in quasi-static stellar models.

If macroscopic changes occur fast enough so that work done by pressure forces PdV must be included in the energy conservation equation, then

$$dE = \dot{s} \, dt + \frac{1}{R^2 \rho} \frac{\partial}{\partial R} \left(R^2 \frac{\bar{l}c}{3} \frac{\partial (aT^4)}{\partial R} \right) dt - PdV$$

where spherical symmetry is assumed, V is the specific volume and a is the radiation constant.* Using $dM = 4\pi\rho R^2 dR$,

$$dE = \left(\dot{s} - \frac{\partial L}{\partial M} \right) dt - PdV$$

where

$$L = - (4\pi R^2)^2 \frac{ac}{3\bar{k}} \frac{d(T^4)}{dM}$$

F.1

and

$$\bar{k} = \frac{1}{\rho \bar{l}}$$

F.2

is the Rosseland mean opacity. Rewriting the energy conservation equation in terms of the temperature T gives

$$dT = \left[\left(\dot{s} - \frac{\partial L}{\partial M} \right) dt - \left(P + \frac{\partial E}{\partial V}\bigg|_T \right) dV \right] / \left(\frac{\partial E}{\partial T}\bigg|_V \right),$$

F.3

---

* For electron-type neutrinos and antineutrinos in thermal equilibrium and in equal abundance, the radiation constant is a(neutrinos) $\approx \frac{7}{8}$ a(photons).

where $(\frac{\partial L}{\partial M})dt$ is the energy lost by diffusive transfer, PdV is the work extracted by macroscopic motion, and $\dot{s}$ is the energy gain by other mechanisms.

G. Difference Equations and Boundary Conditions For Radiative Transfer. Equations (F.1), (F.2) and (F.3) may be incorporated into the hydrodynamic difference equations discussed in the previous section. Comparing (F.3) with our earlier energy conservation equation suggests the following difference equation, by analogy with (A.13),

$$T_{j+1/2}^{n+1} = T_{j+1/2}^{n} + \frac{1}{ET_{j+1/2}^{n+1/2}} \Big[- (P_{j+1/2}^{n+1/2} + Q_{j+1/2}^{n+1/2} + EV_{j+1/2}^{n+1/2}) \, (V_{j+1/2}^{n+1} - V_{j+1/2}^{n}) + (\dot{s}_{j+1/2}^{n+1/2} - \frac{(AL_{j+1}^{n+1/2} - AL_{j}^{n+1/2})}{DM_{j+1/2}}) \, \Delta t^{n+1/2} \Big]$$

G.1

But then (F.1) becomes

$$AL_{j}^{n+1/2} = - \frac{16\pi^2 ac}{3} (R_{j}^{n+1/2})^4 \frac{(T_{j+1/2}^{n+1/2})^4 - (T_{j-1/2}^{n+1/2})^4}{(DM * AK)_{j}^{n+1/2}}$$

G.2

where

$$(DM * AK)_{j}^{n+1/2} = \frac{1}{2} (DM_{j+1/2} \, AK_{j+1/2}^{n+1/2} + DM_{j-1/2} \, AK_{j-1/2}^{n+1/2})$$

G.3

and (F.2) becomes

$$AK_{j+1/2}^{n+1/2} = AK\ (T_{j+1/2}^{n+1/2},\ V_{j+1/2}^{n+1/2})$$

G.4

The term $AL_{j+1}^{n+1/2}$ involves quantities evaluated at space points j-1/2, j. and j+1/2. The latter will not have been evaluated when $T_{j+1/2}^{n+1}$ is to be calculated from (G.1), if the method of sweeping through the space-time mesh described previously is used. The difficulty may be avoided by evaluating

$$U_2^{n+1/2},\ R_2^{n+1},\ V_{3/2}^{n+1},\ V_{3/2}^{n+1/2},\ T_{3/2}^{n+1/2} \quad \text{and}$$

$$P_{3/2}^{n+1/2},\ ET_{3/2}^{n+1/2},\ EV_{3/2}^{n+1/2},\ AK_{3/2}^{n+1/2},\ AL_{3/2}^{n+1/2}$$

G.5

initially, and then sweeping the mesh as shown in Table V.

The quantities listed in (G.5) may be determined from equations given previously, with the exception of the luminosity AL at the inner boundary. If this boundary is the center of the star, i.e., $R_1^n = 0$ for all time n, then by symmetry

$$AL_1^n = 0 \qquad \text{G.6}$$

for all n also.

Another boundary condition must be imposed on diffusive energy transfer. Christy (1964) has proposed that this be accomplished by requiring that the surface boundary condition for the time-dependent problem be consistent with that for the time-independent diffusion equation. For a static, gray atmosphere, the solution of the equation of transfer for photons is

$$T^4 = \frac{3}{4} T_e^4 [\tau + q(\tau)]$$

where τ is the optical depth and $q(\tau)$ is a slowly-varying function. The diffusion approximation for the same problem gives

$$T^4 = \frac{3}{4} T_e^4 [\tau + c]$$

where c is some constant. If c = 2/3 then

$$\left.\frac{\partial (T^4)}{\partial \tau}\right|_{\text{Surface}} = \frac{3}{4} T_e^4 = \frac{3}{2} \left. T^4 \right|_{\text{Surface}}$$

If the effective temperature T_e of the surface is known, the problem is determined. This may be expressed as

$$\left.\frac{\partial(\log T^4)}{\partial \tau}\right|_{\text{Surface}} = \frac{3}{2}$$

but to apply this expression it is necessary to know where the surface is.

In order to avoid prejudging the calculation, a different approach was taken to determine the surface boundary condition.

When the mean free paths per zone reached a certain small fraction X, a simple energy transfer calculation was made. The incident flux upon zone j+1/2 was obtained from the luminosity at boundary j while the opacity of zone j+1/2 was determined by the temperature of this flux, i.e., the temperature of zone j-1/2. This gave the energy deposited while the neutrino loss rates discussed in chapter III gave the energy emitted by the zone j+1/2. Using (A.13) with the change

$$\dot{s}^{n+1/2}_{j+1/2} \rightarrow \Delta E^{n+1/2}_{j+1/2}$$

where $\Delta E^{n+1/2}_{j+1/2}$ is the net energy deposited by neutrinos, the temperature of zone j+1/2 in the emission surface was determined. In practice the transition from opaque to trans-

parent was so abrupt that the calculation was not sensitive to any sort of reasonable boundary condition of either of the types just mentioned. Outside the emission surface the uncoupled hydrodynamic scheme was used, without any diffusive energy transfer.

H. Stability of the Difference Equations With Radiative Transfer. Richtmyer (1957) has discussed the stability of finite difference approximations to the diffusion equation in some detail. The discussion in this section is therefore limited to those aspects of stability of immediate interest. A complete treatment of the stability of a nonlinear diffusion equation coupled with the equations of hydrodynamics would be extremely complex. It appears that in practice the restrictions necessary for a linear, uncoupled diffusion problem can be suitably generalized for more complex systems.

The simple form of the diffusion equation is

$$\frac{\partial C}{\partial t} = D \frac{\partial^2 C}{\partial x^2}$$

in one dimension, where C is the concentration of whatever is diffusing, t the time, x the spatial coordinate and D the diffusion coefficient. Perhaps one of the simplest difference approximations is

$$\frac{c_j^{n+1} - c_j^n}{\Delta t^{n+1/2}} = D_j^{n+1/2} \quad \frac{c_{j+1}^n - 2c_j^n + c_{j-1}^n}{(\Delta x^2)_j^n}$$

where the subscripts and superscripts have the same meaning as before, and

$$(\Delta x^2)_j^n = (\Delta x_{j+1/2}^n + \Delta x_{j-1/2}^n)^{2/4}$$

For stability it is necessary that*

$$\frac{2D\Delta t}{(\Delta x)^2} \leq 1$$

H.1

for all j and n. This expression may be used to determine the time step $\Delta t^{n+3/2}$ at the next epoch. In particular, for the coupled problem, (H.1) gives

$$\Delta t^{n+3/2} = \frac{ET_{j-1/2}^{n+1/2} \; AK_{j-1/2}^{n+1/2} \; (R_j^{n+1} - R_{j-1}^{n+1})^2}{2(V_{j-1/2}^{n+1/2})^2 \quad (T_{j-1/2}^{n+1/2})^3} \times \text{const.}$$

H.2

which worked quite well when the minimum value for j = 1,. . . JJ was taken.

---

* See Richtmyer 1957, chapters 1 and 6.

TABLE I

	Condensed model	n = 3 polytrope model
escape velocity for ejected matter	$\sim 1.4 \times 10^{8}$ cm/sec	$\sim 4 \times 10^{8}$ cm/sec
"velocity of ejected matter"	$\sim 7 \times 10^{9}$ cm/sec	$\sim 10^{9}$ cm/sec
mass of remnant core	1.2 $M_{\odot}$	1.8 $M_{\odot}$
radius of core	1.6×10^{6} cm	1.4×10^{6} cm
kinetic energy of ejected mass	$\geq 4 \times 10^{52}$ ergs	$\geq 1.4 \times 10^{52}$ ergs
energy of emitted electron neutrinos	$\sim 7 \times 10^{52}$ ergs	$\sim 6 \times 10^{52}$ ergs

T A B L E II

total light emitted	<< kinetic energy	
intrinsic maximum visual magnitude	-17.5	
mass ejected	≥ 5	$M_\odot$
velocity of ejection	$\sim 7 \times 10^8$	cm/sec
kinetic energy of ejected mass	$\geq 10^{52}$	ergs

TABLE III

T_9	$(-\dot{s}_{\text{decay}})$	$(-\dot{s}_{\text{pair-annih.}})$	$(-\dot{s}_{\text{tables}})$ *
360	5×10^{24}	3×10^{25}	1.4×10^{26}
240	3.7×10^{22}	4×10^{23}	8×10^{23}
120	1.3×10^{21}	5×10^{18}	2.6×10^{18}

* These values are derived from the Chiu (1961) tables of electron pair-annihilation neutrino rates.

TABLE IV

T_9	τ
360	10^{-6} sec
240	1.4×10^{-4} sec
120	10^{-2} sec

TABLE V

quantity	time epoch	space point
U	n+1/2	j+1
R	n+1	j+1
V	n+1	j+1/2
	n+1/2	j+1/2
T	n+1/2	j+1/2
P	n+1/2	j+1/2
ET	n+1/2	j+1/2
EV	n+1/2	j+1/2
AK	n+1/2	j+1/2
AL	n+1/2	j
T	n+1	j-1/2
P	n+1	j-1/2

References

Adams, J. B., M. A. Ruderman, and C. H. Woo. 1963. Phys. Rev. 129, 1383.

Allen, C. W. 1963. Astrophysical Quantities, 2nd ed., The Athlone Press.

Bahcall, J. N. 1964a. Phys. Rev. 136, B1164.

Bahcall, J. N. and S. C. Frautschi. 1964b. Phys. Rev. 136, B1547.

Bahcall, J. N. 1964c. Astrophys. J. 139, 318.

Bahcall, J. N. and R. A. Wolf. 1965. Phys. Rev. Letters 14, 343.

Burgers, J. M. and W. P. Robbertse. 1949. Proc. Koninkl. Ned. Akad. Wetenschap. 52, 1067.

Chandrasekhar, S. 1939. An Introduction to the Study of Stellar Structure, reprinted by Dover Publications, Inc., 1957.

Chiu, H. Y. and R. C. Stabler. 1961. Phys. Rev. 122, 1317.

Chiu, H. Y. 1961. Phys. Rev. 123, 1040.

Chiu, H. Y. 1964. NASA Stellar Evolution Conference held at Institute for Space Studies, in press.

Christy, R. 1964. Rev. Mod. Phys. 36, 555.

Colgate, S. A. and R. H. White. 1964. "The Hydrodynamic Behavior of Supernovae Explosions," UCRL-7777. To be published in the Astrophys. J., 1966.

Davis, R., Jr. 1965. Private communication to A. G. W. Cameron.

Deinzer, W., E. Salpeter. 1964. Astrophys. J. 140, 499.

Dyson, F. "Hydrostatic Instability of a Star," unpublished.

Euwema, R. N. 1964. Phys. Rev. 133, B1046.

Feynman, R. P. and M Gell-Mann. 1958. Phys. Rev. 109, 193.

Frank-Kamenetskii, D. 1962. Physical Processes in Stellar Interiors, Office of Technical Services, U. S. Department of Commerce, Washington 25, D. C., translation from the Russian.

Fowler, W. A. and F. Hoyle. 1964. "Neutrino Processes and Pair Formation in Massive Stars and Supernovae" J. Supplement 91, vol. IX, 201.

Gomes, L. C., J. D. Walecka, and V. F. Weisskopf. 1958. Ann. Phys. 3, 241.

Hansen, C. 1964. unpublished.

Harrison, B., K. Thorne, M. Wakano and J. A. Wheeler. 1965. Gravitational Theory and Gravitational Collapse, University of Chicago Press, Chicago, Ill.

Hayashi, C., R. Hoshi and D. Sugimoto. 1962. Progress of Theoretical Physics, Supplement 22.

Henyey, L. L., L. Wilets, K. H. Bohm, R. LeLevier, and R. D. Levee. 1959. Astrophys. J. 129, 628.

Hofmeister, E., R. Kippenhahn and A. Weigert. 1964. Zeitschrift für Astrophysik 60, 57.

Inman, C. L. and M. A. Ruderman. 1964. Astrophys. J. 140, 1025.

Landau, L. D. and E. M. Lifshitz. 1958. Statistical Physics, Addison-Wesley Publishing Co., Reading, Mass.

Minkowski, R. 1964. Annual Review of Astronomy and Astrophysics, 2, 247.

Richtmyer, R. D. 1957. Difference Methods for Initial Value Problems, Interscience Publishers, Inc., New York.

Ritus, V. I. 1962. Soviet Physics - JETP 14, 915.

Schwarzschild, M. 1958. Structure and Evolution of the Stars, Princeton University Press, Princeton, N. J.

Sedov, L. I. 1959. Similarity and Dimensional Methods in Mechanics, Academic Press, New York.

Shklovskii, I. S. 1960. Soviet Astronomy - AJ V, 355.

Stothers, R. 1966. Astrophys. J. 143, 91.

Truran, J. W., C. J. Hansen, A. G. W. Cameron and A. Gilbert. 1966. Can. J. Phys. 44, 151.

Tsuruta, S. 1964. Ph. D. Thesis, Columbia University.

Von Neumann, J. and R. D. Richtmyer. 1950. Journal of Applied Physics 21, 232.

Figure Captions

Figure 1. Zero temperature equation at State.

Figure 2. Comparison of the structure of isothermal-core and polytrope of index 3 models in the temperature - density plane.

Figure 3. Comparison of the structure of isothermal-core and polytrope of index 3 models in the radius - density plane.

Figure 4. Evolutionary history of $M_r = 1.5\ M_\odot$ zone of $10\ M_\odot$ polytrope of index 3, for three different treatments of neutrino energy transfer.

Figure 5. Evolutionary history of two representative mass zones of a $10\ M_\odot$ polytrope of index 3 initial model, with neutrino energy transfer treated in the diffusion approximation.

Figure 6. Comparison with the calculations of Colgate and White.

Figure 7. Temperature-density history of two representative zones of the isothermal-core initial model, with energy transfer by neutrinos in the diffusion approximation.

Table Captions

Table I. Comparison of centrally-condensed and polytropic models.

Table II. Observed characteristics of type II supernovae.

Table III. Estimates of energy loss in ergs/gm/sec due to muon-type neutrinos formed by muon-decay and muon pair-annihilation (density is $\rho = 10^{12}$ gm/cm^3).

Table IV. Relaxation time for cooling due to muon-type neutrino escape at high temperature (density is $\rho = 10^{12}$ gm/cm^3).

Table V. Space-time points at which quantities appearing in the coupled difference equations of hydrodynamics and diffusive energy transfer are evaluated.

8. White Dwarf Stars.

In this ~~chapter~~ ~~section~~ we will start to discuss the properties of stars whose interiors are composed of matter in the degenerate state. The first to be considered will be stars whose internal pressures derive from the presence of degenerate electrons.

The pressure of a degenerate electron gas at zero temperature is characterized by a function f(x) such that

$$p = A\, f(x)$$

where x is the Fermi momentum in units of mc,

$$f(x) = x(2x^2 - 3)\,(x^2 + 1)^{\frac{1}{2}} + 3\,\sinh^{-1} x$$

and

$$A = \frac{\pi m^4 c^5}{3h^3} = 6.01 \times 10^{22}$$

We may relate x to the density by

$$\rho = n\mu_e\, H = Bx^3$$

where

$$B = \frac{8\pi m^3 c^3 \mu_e H}{3h^3} = 9.82 \times 10^5\ \mu_e$$

H is the hydrogen atom mass, n is the electron number density, and μ_e is defined by the equation for ρ and is the mean molecular weight per electron.

We recall the asymptotic forms

$$f(x) \sim \frac{8}{5}x^5 - \frac{4}{7}x^7 + \frac{1}{3}x^9 - \frac{5}{22}x^{11} + \ldots \quad (x \to 0)$$

$$f(x) \sim 2x^4 - 3x^2 + \ldots \quad (x \to \infty)$$

We wish to find the stellar structure corresponding to the above equation of state. We recall,

$$\frac{dM(r)}{dr} = 4\pi r^2 \rho,$$

$$\frac{dp}{dr} = \frac{-GM(r)}{r^2}\rho$$

so that

$$\frac{1}{r^2}\frac{d}{dr}\left(\frac{r^2}{\rho}\frac{dp}{dr}\right) = -4\pi G\rho$$

Substitution of ρ and p for the electron gas yields

$$\frac{A}{B}\frac{1}{r^2}\frac{d}{dr}\left(\frac{r^2}{x^3}\frac{df(x)}{dr}\right) = -4\pi GBx^3$$

where

$$\frac{df(x)}{dr} = \frac{8x^4}{(x^2+1)^{\frac{1}{2}}}\frac{dx}{dr}$$

or

$$\frac{1}{x^3}\frac{df(x)}{dr} = \frac{8x}{(x^2+1)^{\frac{1}{2}}}\frac{dx}{dr} = 8\frac{d\sqrt{x^2+1}}{dr}$$

Thus,

$$\frac{1}{r^2}\frac{d}{dr}\left(r^2\frac{d\sqrt{x^2+1}}{dr}\right) = -\frac{\pi GB^2x^3}{2A}$$

Transforming by $y^2 = x^2 + 1$ yields

$$\frac{1}{r^2}\frac{d}{dr}\left(r^2\frac{dy}{dr}\right) = -\frac{\pi G B^2 (y^2 - 1)^{3/2}}{2A}$$

We define the boundary conditions at the center by $x \to x_o$, $y \to y_o$ as $r \to 0$. Finally, by means of the transformation

$$\eta = r/\alpha \ , \ \Phi = y/y_o$$

with

$$\alpha = \left(\frac{2A}{\pi G}\right)^{\frac{1}{2}} \frac{1}{By_o}$$

we find

$$\frac{1}{\eta^2}\frac{d}{d\eta}\left(\eta^2\frac{d\Phi}{d\eta}\right) = -\left(\Phi^2 - \frac{1}{y_o^2}\right)^{3/2}$$

where the boundary conditions are taken as

$$\Phi \to 1, \ \frac{d\Phi}{dr} \to 0 \quad \text{as } \eta \to 0,$$

and for the surface, take $y = \eta_1$ at which $x \to 0$ so that

$$\Phi(\eta_1) = 1/y_o .$$

In general, the density is given by

$$\rho = \rho_o \frac{y_o^3}{(y_o^2 - 1)^{3/2}}\left(\Phi^2 - \frac{1}{y_o^2}\right)^{3/2}$$

where $\rho_o = Bx_o^3 = B(y_o^2 - 1)^{3/2}$ and is the central density.

If Φ is the gravitational potential then

$$\frac{d\Phi}{dr} = \frac{GM(r)}{r^2} = -\frac{1}{\rho}\frac{dp}{dr} .$$

For the degenerate equation of state

$$\frac{d\Phi}{dr} = -\frac{8A}{B} y_o \frac{d\phi}{dr} \quad \text{so that}$$

$$\Phi = -\frac{8A}{B} y_o \phi + \text{constant.}$$

Since $\Phi \to 0$ as $r \to \infty$, the constant is

$$\frac{8A}{B} - \frac{GM}{R} . \quad \text{Thus,}$$

$$\Phi = -\frac{8A}{B} y_o \left(\phi - \frac{1}{y_o}\right) - \frac{GM}{R} , \quad (r \le R).$$

The mass inside any point is

$$M(\eta) = 4\pi \int_o^\eta \rho r^2 dr = 4\pi \alpha^3 \int_o^\eta \rho \eta^2 \, d\eta$$

$$= 4\pi \rho_o \frac{\alpha^3 y_o^3}{(y_o^2 - 1)^{3/2}} \int_o^\eta \left(\phi^2 - \frac{1}{y_o^2}\right)^{3/2} \eta^2 d\eta$$

$$= -4\pi \rho_o \frac{\alpha^3 y_o^3}{(y_o^2 - 1)^{3/2}} \eta^2 \frac{d\Phi}{d\eta}$$

$$= -4\pi \left(\frac{2A}{\pi G}\right)^{3/2} \frac{1}{B^2} \eta^2 \frac{d\Phi}{d\eta}$$

The total mass is then

$$M = -4\pi \left(\frac{2A}{\pi G}\right)^{3/2} \frac{1}{B^2} \left(\eta^2 \frac{d\Phi}{d\eta}\right)_{\eta = \eta_1}$$

For the case of high central densities ($y \to \infty$), the differential equation becomes

$$\frac{1}{\eta^2} \frac{d}{d\eta} \left(\eta^2 \frac{d\Phi}{d\eta}\right) = -\Phi^3$$

If we recall the form of the Lane-Emden equation, viz.,

$$\frac{1}{\xi^2} \frac{d}{d\xi} \left(\xi^2 \frac{d\theta}{d\xi}\right) = -\theta^n$$

then we see that our configuration approaches a Lane-Emden polytrope of index 3. We note also that the radius scale factor $\alpha \to 0$ implying that the stellar radius approaches zero. At the same time the mass approaches

$$M \to -4\pi \left(\frac{2A}{\pi G}\right)^{3/2} \frac{1}{B^2} \left(\xi^2 \frac{d\theta}{d\xi}\right)_{\xi} = \xi(\theta_3)$$

where θ_3 is the index 3 solution. This implies a limiting mass M_3 given by

$$M_3 = \frac{5.75}{\mu_e^2} M_\odot$$

For small central densities one can show that the configuration approaches a polytrope of index 1.5. Hence the density distribution will lie between those of polytropes of index 1.5 and 3.

To compute the internal energy of the configuration we use the relation between total kinetic energy and Fermi momentum given by

$$U_{kin} = \frac{\pi m^4 c^5}{3h^3} g(x), \text{ where}$$

$$g(x) = 8x^3 \left[(x^2 + 1)^{\frac{1}{2}} - 1\right] - f(x)$$

Hence, the total kinetic energy for the configuration is found from

$$U = A \int_o^R \left\{8x^3 \left[(1 + x^2)^{\frac{1}{2}} - 1\right] - f(x) \right\} dV$$

$$= \frac{8A}{B} \int_o^R \rho \left[(1 + x^2)^{\frac{1}{2}} - 1\right] dV - \int_o^\infty Pdv$$

The corresponding equation for the total potential energy is

$$-\Omega = G \int_o^\infty \frac{M(r)dM(r)}{r} = -\frac{1}{2} \int_o^R \Phi \, dM(r)$$

$$= G \int_o^R 4\pi\rho r M(r) dr = -4\pi \int_o^R \frac{dp}{dr} r^3 \, dr$$

Integrating by parts yeilds

$$-\Omega = 12\pi \int_o^R Pr^2 \, dr = 3 \int_o^R Pdv$$

From U we also have

$$\int_0^R P\left[(1+x^2)^{\frac{1}{2}} - 1\right]dV = \int_0^R \left[(1+x^2) - 1\right] dM(r)$$

$$= y_0 \int_0^R \left(\frac{\Phi}{} - \frac{1}{y_0}\right) dM(r)$$

Hence

$$U = \frac{8A}{B} y_0 \int_0^R \left(\frac{\Phi}{} - \frac{1}{y_0}\right) dM(r) + \frac{\Omega}{3}$$

$$= - \int_0^R \left(\frac{GM}{R}\right) dM(r) + \frac{\Omega}{3}$$

$$= - \frac{5}{3}\Omega - \frac{GM^2}{R}$$

The total energy E is

$$E = U + \Omega = - \frac{2}{3}\Omega - \frac{GM^2}{R}$$

For a polytrope of $n = 1.5$, $\Omega = - \frac{6}{7}\frac{GM^2}{R}$

and

$$U = - \frac{1}{2}\Omega$$

For $n = 3$,

$$\Omega = - 3GM^2/2R \text{ and } U = - \Omega$$

For the index 3 solution for the total mass we note that for a reasonable composition with $\mu_e = 2$, M_3 has an upper limit of about $1.4M_\odot$. This is the so-called Chandrasekhar limit for such objects. More refined calculations bring this down to about $1.2M_\odot$.

As the central density of a white dwarf star approaches very high values, new physical phenomena come in which cause a departure from the asymptotic approach to this limiting mass. One modification arises from the need to use the general relativistic equation of hydrostatic equilibrium. Much more important is the increase of the mean molecular weight at the center owing to electron capture on all nuclei which occurs for high electron Fermi energies. This decreases the value of the limiting mass and eventually induces an instability in the models. As will be seen later, beyond a little more than 10^9 gm./cm.^{3} central density there are no longer any stable degenerate stars owing their stability to electron degeneracy. A new set of stable models becomes possible in the region of nucleon degeneracy.

For further details see S. Chandrasekhar, An Introduction to the Study of Stellar Structure (U. of Chicago Press, 1939).

9.

NEUTRON STAR MODELS

by

Sachiko Tsuruta

Smithsonian Astrophysical Observatory
Cambridge, Massachusetts

Physics Department, Columbia University
New York, New York

and

Institute for Space Studies
Goddard Space Flight Center, NASA
New York, New York

and

A.G.W. Cameron

Institute for Space Studies
Goddard Space Flight Center, NASA
New York, New York

ABSTRACT

Two composite equations of state have been used in the investigation of the structure of neutron (or hyperon or baryon) stars. These have been based upon two forms of the neutron-neutron potential suggested by Levinger and Simmons. In one form repulsive forces come in quickly at greater than nuclear densities; in the other form the repulsive forces come in slowly. In the former case the maximum stable mass of a neutron star is about two solar masses; whereas in the latter case it is only about one solar mass. This probably represents a measure of the basic uncertainty in the properties of neutron star models due to our lack of knowledge of nuclear forces. The maximum central density of a stable configuration is similarly uncertain; this density probably lies in the range 10^{15} to 10^{16} grams/cm^3. Details of many of the neutron star models calculated are summarized and discussed.

INTRODUCTION

The problem of the properties of highly condensed matter has a long history. The first important contributions came as early as in the period of 1930-40, from Chandrasekhar (1935, 1939), Landau (1932), Oppenheimer and Serber (1938), Oppenheimer and Volkoff (1939), and others. For a degenerate body under gravitational attraction there may exist two possible equilibrium states, the less condensed state composed of electrons and nuclei, and the more compressed state of neutronic or baryonic configuration. The "electron-nuclear" state corresponds to the observed white dwarf stars. It was suggested (Zwicky 1938, 1939, and 1958) that the more condensed state of nuclear density might be physically realized in a form of a neutron star formed as the result of a supernova explosion, at the last stage of evolution of a sufficiently massive star. This view was somewhat neglected for a long time. However, there has recently arisen a possibility that a neutron star formed as a remnant of a supernova explosion may directly or indirectly be responsible for some of the celestial x-ray sources now known to exist (Chiu 1964, Chiu and Salpeter 1964, Morton 1964, Tsuruta 1964, Cameron 1965, and others), and the importance of the study of highly condensed matter has been greatly increased. Even aside from the problem of observing

these stars, the study of degenerate stars is important in itself as a fundamental problem in physics. J.A. Wheeler and his collaborators have been pursuing the problem of degenerate stars since 1958 in connection with gravitation theory and gravitational collapse. The best collection of their work is found in Harrison, Thorne, Wakano and Wheeler (1965). Some other recent contributions to this problem are those of Cameron (1959), Amburtsumyan and Saakyan (1960, 1962, a,b), Sahakian and Vartaman (1963), and Misner and Zapolsky (1964).

In considerations of neutron stars the greatest uncertainty is caused by lack of knowledge of high energy physics, and, for this reason, the interaction forces between neutrons were usually neglected in most of the previous work. However, the typical density in neutron stars is as high as $\sim 10^{15}$ gm/cm^3 or more, for which the nuclear forces between the constituent particles are far too important to be neglected. It should be emphasized that an exact knowledge of the nuclear forces near and just above nuclear densities (around $10^{14} \leq \rho \leq 10^{16}$ gm/cm^3) is required to determine the quantitative properties of the models not only in this range but also for far denser configurations. It is likely that denser matter, $\rho > 10^{16}$ gm/cm^3, should follow a simple asymptotic equation of state of the polytropic form $P = cn^{\gamma} = (\gamma-1)\epsilon$, with the value of γ properly chosen (where P is the pressure, c is a constant, γ is the adiabatic exponent

and ϵ is the energy density), but the important question is: to what nuclear equation of state should this be joined in the lower density region near the surface? Some efforts have been made in recent years to take into account these nuclear forces by Cameron (1959), Amburtsumyan and Saskaan (1962a) and others. In this paper we explore this problem in more detail.

For this purpose, we have chosen two possible forms of the nuclear interaction between neutrons as suggested by Levinger and Simmons (1961). The possible application of these nuclear potentials to the problem of neutron stars was proposed by Salpeter (1963). These potentials are consistant with our knowledge of nuclear forces in the vicinity of normal nuclear densities, if we assume charge independence of these forces. However, the uncertainty is increased as the density goes higher. Hence, the difference in the models constructed by the use of these two different nuclear potentials may give an indication of the uncertainty due to the lack of knowledge in this field.

In a physically realistic equation of state the pressure is not allowed to become indefinitely large. Therefore, either one of the possible pressure saturation conditions $P \leq \epsilon/3$ (Landau and Lifshitz 1959) or $P \leq \epsilon$ (Zel'dovich 1962) were applied in our models. In our composite equation of state the equilibrium composition of degenerate matter was used. For

densities lower than about 3×10^{11} gm/cm^3 matter consists of degenerate electrons and various heavy nuclei. The most abundant nucleus changes from iron to more neutron-rich nuclei with increasing density (Tsuruta and Cameron 1965). For densities higher than this, heavy ions gradually disolve into neutrons. The system then consists of neutrons, protons and electrons in equilibrium. Near and above 10^{15} gm/cm^3, mesons and other baryons appear. The threshold density at which these new particles appear is quite uncertain due to the lack of knowledge of the interaction forces between the strongly interacting particles. However, as will be shown later, the effect of the possible change of composition due to the shifting of the threshold energy for the appearance of these particles is very small. At the present stage, we are very ignorant concerning the quantitative nature of the strong interaction forces between hyperons, but we know that these forces are of the same nature as the nuclear forces which are responsible for the binding of nucleons together in a nucleus. Hence it was assumed that the same Levinger-Simmons type nuclear potentials were experienced by all the nucleons and hyperons which are present in the assembly.

This paper is confined to cold models of degenerate stars. The cooling of such stars will be treated in a separate paper.

HYPERONIC MIXTURES

When densities exceed about 3×10^{11} gm/cm^3, all heavy ions become unstable against disintegration to neutrons by means of electron capture, and matter consists mainly of neutrons. These neutrons are, however, unstable against decay to protons and electrons by 0.783 Mev, the neutron-hydrogen mass difference, and the neutron gas is always contaminated with protons and electrons. When the Fermi energy of the electrons reaches the rest mass of the muon, 106 Mev, neutrons can be transformed into protons and negative muons. With further increase of energy, various kinds of hyperons are created. Some of the many possible hyperon production reactions are:

$$2n \rightarrow p+\Sigma^-, \quad 2n \rightarrow 2\Lambda, \quad 2n \rightarrow p+\Xi^-, \quad 2p \rightarrow 2\Sigma^+,$$
$$2\Lambda \rightarrow 2\Sigma^0, \quad 2\Lambda \rightarrow 2\Xi^0, \quad n+\Lambda \rightarrow p+\Xi^- \quad . \qquad (1)$$

We note that in these reactions strangeness is not conserved. The time scale of processes like (1) is on the order of 10^{-9} sec, which is long compared with nuclear time scales but extremely short from the astronomical point of view. Even though faster reactions exist, the above examples are fast enough to maintain equilibrium. Consequently we can safely assume that thermodynamic equilibrium is maintained throughout.

The densities at which these meson and hyperon transformations take place are above nuclear densities, and all the constituent baryons and leptons become highly degenerate soon after creation at the threshold energy. Even when the temperature is as high as 5×10^9 °K (a typical maximum temperature of interest in the problem of neutron stars) their degeneracy is so high that the cold matter approximation is fully justified. (For instance, at $T = 5 \times 10^9$ °K and $\rho = 10^{15}$ gm/cm^3, the ratio of neutron Fermi energy to kT is about 400). Therefore, we can assume that all the constituent particles are in their lowest energy states.

Some years ago we had a rather tidy list of about 30 so-called "elementary" particles. Today 60 to 70 more have been added. The first problem we face is to determine which of this profusion of particles survive as the authentic components of our baryon gas in our range of interest. First of all, positrons, photons, neutrinos, positive muons and pions, and K mesons are all absent at zero temperatures because nothing prevents their decay and annihilation. On the other hand, stability is established among hyperons, nucleons, negative muons and electrons, because the decay products of these particles find no unoccupied place in phase space due to the complete degeneracy of baryons and electrons and the Pauli exclusion principle. The stability of

negative pions is established through the high degeneracy of negative muons at very high densities. The presence of the newly discovered particles is restricted due to the fact that most of these particles are heavier states of familiar mesons, nucleons, and hyperons, and that the upper limit of density of interest to us is about 10^{16} gm/cm^3. This is because the equation of state for densities higher than this value becomes independent of the kind and the concentration of particles present as explained in the next section. Consequently, the following thirteen particles were selected as sufficient for our investigation, following Ambartsumyan and Saakyan (1960):

$$e^-,\ \mu^-,\ p,\ p^*,\ n,\ n^*,\ \Lambda,\ \Sigma^o,\ \Sigma^+,\ \Sigma^-,\ \Xi^o,\ \Xi^-,\ \pi^- \qquad (2)$$

n* and p* are isobars of neutrons and protons in the first excited states, now called delta particles.

The concentration and the threshold energy of the appearance of each of these particles are determined by minimizing the total energy subject to the constraints of conservation of charge and baryon number. The results may be expressed as:

$$E_b^+ + E_e = E_b^- - E_e = E_b^0 \qquad (3a)$$

$$E_\ell^- = E_e = E_\pi^- \qquad (3b)$$

$$\Sigma\ n_b = n \qquad (3c)$$

$$\sum_b n_b^+ - \sum_b n_b^- - \sum_\ell n_\ell^- - n_\pi^- - n_e = 0 \qquad (3d)$$

where E and n represent the total energy and total number density. The superscripts +, -, and 0 refer to individual positive, negative, and neutral particles, and the subscripts b, ℓ, π and e refer to baryons, leptons excluding electrons, pions, and electrons. The first two equations correspond to thermodynamic equilibrium and the last two equations represent the conservation of baryon number and the conservation of electric charge, respectively. In a macroscopic medium consisting of sub-atomic particles, only the average potential energy of the particle is worth mentioning, as it represents the interaction of one particle with all the others. In such a case, the total energy E_k of completely degenerate fermions k can be expressed as

$$E_k = \left[M_k{}^2 c^4 + \left(p_k^F\right)^2 c^2\right]^{1/2} + V_k \qquad (4)$$

where

$$p_k^F = \left(\frac{6\pi^2}{a_k}\right)^{1/3} \hbar\, n_k{}^{1/3}$$

is the Fermi momentum, M_k is the mass, and V_k is the average interaction potential of the particles k. (a_k is as defined in (5)). The first two terms represent the chemical potential. For completely degenerate bosons the chemical potential is just the rest mass of the particle. The present state of the theory of elementary particles is so far in no position to give any definite information on the inter-

action potentials of strongly interacting particles for densities substantially exceeding nuclear density. Hence, at present we do not know how to improve upon the simple assumption that all baryons interact identically (that is, V_k for all baryons are equal). We neglect V_k in calculating the composition of the medium, but not its pressure. Interaction potentials of leptons can always be neglected in the problem of neutron stars (Salpeter, 1961). The concentration n_k of the particles k in a hyperonic mixture may then be found from

$$n_k = \frac{1}{2} a_k n_i \left[1-(A_k^i/n_i)^{2/3}\right]^{3/2} \qquad (5)$$

where

$$A_k^i = \frac{1}{3\pi^2 \lambda_k^3} \left[1-(M_i/M_k)^2\right]^{3/2}$$

$\lambda_k = \hbar/(M_k c)$, M_k is the mass of a particle k,

$a_k = 2I_k + 1$, I_k = the spin of the particle k,

[$I_k = 3/2$ for n* and P*, $I_k = \frac{1}{2}$ for others in (2)]

$i = e^-$ when $k = \mu^-$

$i = n$ when $k = \Lambda$, Σ^o, Ξ^o or n*,

$i = P$ when $k = \Sigma^+$ or P*, and

$i = \Sigma^-$ when $k = \Xi^-$.

When $n_i \leq A_k^i$ no particles k exist and therefore A_k^i is the threshold number density of the particles i for the creation of particles k. The numbers of muons are expressed in terms of electron numbers, the numbers of the positively charged baryons are expressed in terms of proton numbers, those of negatively charged baryons Ξ^- are expressed in terms of Σ^-, and the numbers of neutral baryons are expressed in terms of neutrons. Hence equations (5) give the concentration of all particles k as a function of neutron number density n_n, if the number densities of electrons, protons and Σ^-, n_e, n_p, and n_{Σ^-}, are known as a function of n_n. These are determined from

$$E_p + E_e = E_n$$

$$E_{\Sigma^-} - E_e = E_n \qquad (6)$$

and the last two equations in (3). This problem was solved by an iterative procedure. Once the concentrations of the constituent particles are known, the total density of matter is found from

$$\rho = \sum_k n_k M_k \qquad (7)$$

where the summation is taken over all particles k which are present.

When the threshold energies of electrons and negative muons exceed the rest mass of negative pions it is more economical energetically if e^- and μ^- are converted to π^-. In this case,

the number densities of e^- and μ^- stay constant with further increase in total density, at the values

$$n_e = 1.2 \times 10^{37}\ cm^{-3} = (3\pi^2 \lambda\!\!\!^{-}_{\pi}{}^3)^{-1}$$

$$n_\mu = 3.36 \times 10^{36}\ cm^{-3} = \frac{c^3}{3\pi^2}\,(m_\pi{}^2 - m_\mu{}^2)^{3/2}/\hbar^3 \ . \qquad (8)$$

This is because all the excess electrons and μ^- above the threshold value are converted to π^- in a higher density region.

When the electron threshold energy is lower than the muon rest energy, but when the sum of the proton and electron theshold energies is larger than the neutron rest energy, the abundance equations take the simpler form:

$$n_p = n_e = n_o \chi^{-3}\{[1+\alpha\chi/\pi + \chi^2 (n_n/n_o)^{2/3}]^{1/2} - 1\}^3$$

with

$$\alpha = (M_n - M_p)/m_e = 2.54; \quad \chi = 2\pi m_e/M_p,$$
$$n_o = 8(m_e c/\hbar)^3 = 8/\lambda\!\!\!^{-}_e{}^3 \qquad (9)$$

and

$$\rho = M_p n_p + M_n n_n$$

For densities lower than $\sim 3 \times 10^{11}$ gm/cm^3, the equilibrium nuclear abundances of various heavy nuclei as calculated by Tsuruta and Cameron (1965) apply.

The results are summarized in Figure 1. The number densities of various baryons k are plotted as functions of the total density ρ. For $\rho \leq 10^{15}$ gm/cm^3 the total baryon number density and nuetron number density practically coincide. For $\rho \geq 3 \times 10^{15}$ gm/cm^3 the rapid rise in the densities of other baryons depresses the neutron density considerably below the total baryon density. For densities higher than about 5×10^{16} gm/cm^3 the concentrations of all kinds of baryons are about $10^{39} - 10^{40}$ cm^{-3} and they are all of the same order of magnitude. The electrons and μ^- densities exhibit a sudden drop a little above $\rho = 10^{15}$ gm/cm^3, where the Σ^- hyperons appear. n_e and n_μ become constant around $\rho = 10^{17}$ gm/cm^3, due to the creation of π^- mesons.

It may be worthwhile to note that the order in which the particles appear is not in the order of increasing masses. For instance, Σ^- is heavier than Λ, but Σ^- begins to appear at lower densities than Λ. The reason is that the Σ^- hyperons have to neutralize the positive charge of the protons whose concentration increases with increasing n_n, and starting from a certain point the production of Σ^- is energetically more economical than that of one new proton and two new electrons. A similar argument explains why the Ξ^- hyperons appear at lower densities than the Σ^+ hyperons which are lighter than Ξ^-. For $\rho \geq 1.4 \times 10^{17}$ gm/cm^3 the π^- density increases so rapidly with further increase in density thatit soon becomes of the order of the densities of the

other members of the mixture.

The general results for the whole region are shown in Figure 2. In order to avoid overcrowding, the hyperons in this graph have been grouped together in a strip. The rise of the densities of these particles is so rapid right after the thresholds have been crossed that the effect of nondegeneracy can safely be neglected. The neutron Fermi energy is about 510 Mev when $n_n \sim 6 \times 10^{38}$ cm^{-3}. All through the region of the hyperon phase the electron number densities are roughly two to three orders of magnitude lower and the μ^- meson number densities are about three to four orders of magnitude lower than the neutron number densities.

Recently, Bahcall and Wolf (1965) raised the question of the presence of pions even near normal nuclear densities ($\sim 4 \times 10^{14}$ gm/cm^3). This is possible only if pions have a sufficiently small effective mass. If protons and neutrons were present with equal abundance, this might be realized. However, both Bahcall and Ruderman, through recent private communications, indicated to one of us (Cameron) their expectations that, under the conditions in which pions may be present in a neutron star (where n_p/n_n is quite small), there will be a predominantly repulsive interaction between the pions and neutrons. This would raise rather than lower the effective mass of the pions, which makes it very

unlikely that pions will be present in neutron stars.

COMPOSITE EQUATION OF STATE

As we go outward from the center of a neutron star, the density decreases from the central value. If the central density is higher than about 10^{15} gm/cm^3, we will have a mixture of hyperons, nucleons, mesons and electrons in the central region, neutron-dominated intermediate layers (with a small admixture of protons and electrons), and outermost layers of electrons and heavy ions. In this section we consider how the pressure depends on density in these complex layers. The equation of state is most conveniently expressed as:

$$P = P_{KE} + P_{PE}; \qquad \epsilon = \epsilon_{KE} + \epsilon_{PE} \tag{10}$$

where P is the total pressure, ϵ is the total energy density and the subscripts KE and PE stand for the kinetic and potential terms, respectively. The kinetic parts are expressed as

$$\epsilon_{KE} = K_n \sum_k \left(\frac{M_k}{M_n}\right)^4 \frac{a_k}{2} (\sinh t_k - \cdots)$$

$$P_{KE} = \frac{K_n}{3} \sum_k \left(\frac{M_k}{M_n}\right)^4 \frac{a_k}{2} (\sinh t_k - 8 \sinh \frac{t_k}{2} + 3t_k) \tag{11}$$

where the summation is taken over all particles in (2) which are present, and

$$K_n = M_n^4 c^5/(32\pi^2\hbar^3) = 5.117 \times 10^{35} \text{ dynes/cm}^2$$

$$a_k = (2I_k+1) \quad \text{as given in Equation (5)}$$

$$t_k = 4 \sinh^{-1}\left[\left(\frac{6\pi^2}{a_k}\right)^{1/3} \frac{\hbar}{M_k c} n_k^{1/3}\right] \tag{12}$$

and the remaining notation is that given in the last section. Each term in Equation (11) corresponds to the partial pressure or partial energy density (including rest mass energy) of completely degenerate fermions k of a particular kind, and applies to both non-relativistic and relativistic particles.

At the present time, the behavior of nuclear forces in the high energy region is not well known. However, various models of nuclear potential near the region of nuclear density have been constructed by different authors (Brueckner and Gammel 1958; Brueckner, Gammel, and Kubis 1960; Sood and Moszkowski 1960; de Swart and Dullemond 1961; Serber 1964; and others). In this paper, the neutron-neutron potentials as introduced by Levinger and Simmons (1961) were utilized.

Levinger and Simmons introduced three forms of potential designated V_α, V_β, and V_γ, but due to the poor fit in our region of most interest, V_α was not used in this paper. The V_β is a square well potential with a tail of the Yukawa type, and the V_γ is a complicated combination of exponentially decreasing

terms which in effect give rise to the same kind of properties as V_β. Both potentials V_β and V_γ are well behaved, velocity-dependent, and, with the assumption of charge independence, are well fitted to the ^1S and ^1D phase shifts from 20 to 340 Mev. They are utilized in this paper. They consist of static and velocity-dependent parts of the ordinary and exchange integrals. The ordinary static term V_o and the ordinary velocity-dependent term ω_o are given in the analytic forms $-\alpha k_f^3$ and βk_f^5, respectively, where α and β are positive constants (which are different for V_β and V_γ, and k_f is the Fermi wave number, which is related to number density by

$$n = k_f^3/(3\pi^2). \tag{13}$$

On the other hand, the exchange terms V_e (ordinary) and ω_e (velocity-dependent) depend on k_f in a complicated way. Therefore, the potential terms of the equations of state are conveniently expressed as:

$$\epsilon_{PE} = nV(n) = (-\alpha k_f^3 + \beta k_f^5 + 0.7V_e - 2\omega_e)cn \text{ ergs/cm}^3$$

$$P_{PE} = n^2 \frac{\partial V(n)}{\partial n} = \left[\frac{n}{3}\left(-3\alpha k_f^3 + 5\beta k_f^5\right) + n^2\left(0.7\frac{\partial V_e}{\partial n} - 2\frac{\partial \omega_e}{\partial n}\right)\right]c \text{ dynes/cm}^2 \tag{14}$$

where V(n) is the Levinger-Simmons potential energy per particle,

and

$$c = 1.602 \times 10^{-6} \text{ ergs/Mev}$$

$$\alpha = 1.3a_1, \quad \beta = 4a_2$$

$$a_1 = 3.02, \quad a_2 = 0.045 \text{ for } V_\beta \text{ (Mev)}$$

$$a_1 = 4.02, \quad a_2 = 0.28 \text{ for } V_\gamma \text{ (Mev)} \qquad (15)$$

The total baryon number density n is

$$n = \sum_b n_b \quad \text{(b denotes all baryons which are present).} \qquad (16)$$

n_b is related to t_b through the last equation in (12). V_e and ω_e were determined numerically in the region $0 \leq k_f \leq 2$ (Levinger and Simmons 1961). These values were plotted against k_f and the slopes have been used to determine $\frac{\partial V_e}{\partial n}$ and $\frac{\partial \omega_e}{\partial n}$. For $k_f > 2$, the results were extrapolated. This procedure is justified because V_e and ω_e are negligible for $k_f \gtrsim 3$, as compared with the other terms. (k_f is expressed in f^{-1}, where f is in fermis, 10^{-13} cm.)

The total energy per particle is plotted against density in Figure 3, for the Levinger-Simmons V_β and V_γ potentials, the Skyrme potential and Salpeter's potential. For $10^{13} < \rho < 10^{15}$ gm/cm^3, the potentials are attractive and the total energy is less than the case for the noninteracting particles. For $\rho > 10^{15}$ gm/cm^3, the repulsive terms become dominant. In most of the region of

attractive potential V_γ is somewhat lower than V_β, but the repulsive term of V_γ is much larger than that of the V_β. Nuclear potentials are negligible for $\rho < 10^{13}$ gm/cm^3.

In the above equations, the potential terms were expressed as functions of total baryon number density. This implies that we have applied these potential interactions between baryons without distinction as to the type of baryon. At the present time general baryon interaction potentials are not known properly, so the use of V_β and V_γ in this way corresponds to slowly and rapidly increasing repulsive terms among baryons at high densities.

At densities less than or equal to nuclear density, the character of nuclear forces is reasonably well known and is given to a rough approximation by either of the two potentials adopted here, and the composition of the matter is mostly neutrons, for which the potentials were originally constructed. At much greater than nuclear density many different types of baryons are present, and the rapidity with which nuclear forces turn repulsive is very speculative. Therefore, the two potentials V_β and V_γ tend to span a range of possible behavior of the nuclear forces at high densities and the differences in the neutron star models which result from the adoption of one or the other of these potentials will give an indication of the uncertainty due to lack of knowledge in this field.

In the above equations of state, bosons are not included, because the only bosons considered and listed in (2) are negative pions, which are most unlikely to exist at densities below about 10^{17} gm/cm^3, while the equation of state becomes independent of composition and the above Levinger-Simmons type equations of state cease to be valid long before such high densities are reached. This restriction is imposed due to two reasons. One is that in the case of a perfect fluid there is a relativistic limitation on the pressure that it cannot exceed one-third of the proper energy density (Landau and Lifshitz 1959). The other more general restriction which may apply in a fluid with anisotropic properties is that the pressure cannot exceed the energy density (Zel'dovich 1962). If this were to be violated the speed of sound would exceed the speed of light in the medium. Accordingly, the Levinger-Simmons equations of state were cut off with one of these pressure saturation conditions at the high density limit.

In order to determine the composite equation of state as described above, we must know the equilibrium composition as a function of density. To examine this problem, let us go back to Figure 2. In region (I) the nuclear abundances as calculated in a separate paper (Tsuruta and Cameron 1965) are valid. In the higher density region marked (III) the hyperonic mixture as obtained in the last section applies. Care may have to be taken in dealing

with the intermediate region marked (II). When the density is about 3×10^{11} gm/cm^3 (the point marked (a) in Figure 2) the electron Fermi energy is about 23 Mev and nuclei such as ^{120}Sr will coexist with free neutrons. By the time we arrive at the border (b), where the density is about 8×10^{13} gm/cm^3, all the heavy nuclei are expected to have disappeared, leaving neutrons, protons and electrons in equilibrium. The exact behavior of the transition in this region is quite complicated, but the same principles, the conservation of total energy, charge and number of particles, control the equilibrium in this region. To prevent a discontinuous change in the ion number densities, it was assumed that the average charge $\bar{Z}$ changes from 38 to 1 in a smooth way from point (a) to point (b). Then, the average ionic charge is expressed as:

$$\bar{Z}(\rho) = 1 + 37\ \chi(\rho) \qquad (17)$$

where

$$\chi(\rho) = \frac{(\rho_2 - \rho)}{(\rho_2 - \rho_1)} \qquad \text{for} \qquad \rho_1 \leq \rho \leq \rho_2 \ .$$

ρ_1 is the density at (a), and ρ_2 is the density at (b).

Strictly speaking electron density increases slightly as we go from (a) to (b) with an increase of neutron density, but this rise is negligible and not appreciable in Figure 2. This is because the major part of the extra energy density as we go from (a) to

(b) goes to neutron density. Figure 2 also indicates that there is a rise in the total ion number density as the average ionic charge changes from 38 to 1.

In the lower density region $\rho \leq 8 \times 10^{13}$ gm/cm^3 it is more convenient if the matter density ρ, as defined below, is used as a free parameter.

$$\rho = \sum_k \left\{\left[n_n + (A-Z) n_k(A,Z)\right] m_n + \left[n_p + Z n_k(A,Z)\right] m_p\right\} + n_e m_e \qquad (18)$$

k represents all nuclei of appreciable abundance. Then the energy density is expressed as

$$\epsilon = \epsilon_{KE} + \epsilon_{PE} + \rho - n_n m_n - n_p m_p - n_e m_e$$

The rest mass density of p,e,n must be subtracted because both ϵ_{KE} and ρ include them. ϵ_{KE} is given by (11) with k = n,p,e; ϵ_{PE} is given by (14) with $n = n_n + n_p$. The abundances of different particles as a function of density were taken from Tsuruta and Cameron (1965). The expressions for pressure in Equations (10) - (16) are valid in this region with k = n,p,e and $n = n_n + n_p$. The contribution of interactions between electrons is always negligible in the problem of neutron stars (Salpeter 1961) and hence such terms are not included in the above equations. In this low density region the main contributor to pressure is electrons or neutrons. The effect of the presence of heavy nuclei appears in

the density but not in the pressure.

For the region $\rho > 8 \times 10^{13}$ gm/cm^3 the composite equations of state as described above are most easily solved by choosing t_n, the relativistic parameter for neutrons as defined in Equation (12), as our free parameter.

The solid curves in Figure 4 represent the final composite equations of state of type V_β and V_γ. The nearly straight line in the lower density region corresponds to the electron-nucleus configuration. Even though it is not apparent from the graph, this line is found to be slightly bent downward if we examine it more carefully, which is due to the decrease of Z/A with the increase in density in this region. In high density regions ($\rho > 10^{16}$ gm/cm^3) the asymptotic equation $P = \epsilon$ is seen to be approached. The difference between the two potentials V_β and V_γ is apparent in the most interesting region of $10^{13} \leq \rho \leq 10^{16}$ gm/cm^3.

GENERAL RELATIVISTIC EQUATIONS OF HYDROSTATIC EQUILIBRIUM

The most general static line element exhibiting spherical symmetry may be expressed in the following form (Tolman 1934):

$$ds^2 = -e^{\lambda(r)}\, dr^2 - r^2 d\theta^2 - r^2 \sin^2\theta\, d\varphi^2 + e^{\nu(r)} dt^2 \qquad (19)$$

For this line element and with the assumption that the matter supports no transverse stresses and has no mass motion, the general

relativistic equations of hydrostatic equilibrium are expressed as (Oppenheimer and Volkoff 1939):

$$\frac{dU(r)}{dr} = 4\pi\epsilon r^2 \tag{20}$$

$$\frac{dP}{dr} = -\frac{(P+\epsilon)}{r(r-2U(r))}(4\pi r^3 P+U(r)) \tag{21}$$

where P is the pressure and ϵ is the macroscopic energy density both measured in proper coordinates, and U(r) is the gravitational mass contained within a sphere of radius r. The gravitational mass of the star, M, is obtained by integrating (20) from the center to R, the radius of the star, where P = 0.

In this section, we use the following system of units unless otherwise stated: the units for which

$$c = G = 1$$

(c is the velocity of light and G is the gravitational constant), and

$$\left(\frac{M_n^4 c^5}{32\pi^2 \hbar^3}\right) = K_n = 1/4\pi$$

The quantities in this system of units are converted to those in cgs units by multiplying them by the following conversion factors:

length: $r_o = 2\sqrt{2\pi}\left(\frac{\hbar}{M_n c}\right)^{3/2}\frac{c}{\sqrt{GM_n}} = 1.37 \times 10^6 \text{ cm} = 13.7 \text{ km} \sim 10^{-5} R_\odot$

mass: $m_o = r_o c^2/G = 1.85 \times 10^{34} \text{ gm} = 9.29 M_\odot$

pressure: $P_o = (M_n^4 c^5/32\pi^2\hbar^3)4\pi = 6.46 \times 10^{36} \text{ dynes/cm}^2$

density: $\rho_o = P_o/c^2 = 7.15 \times 10^{15} \text{ gm/cm}^3$

The gravitational mass M as defined earlier is the mass of the star as perceived by a distant observer. This differs from the proper mass, which is the mass the star would have if its particles were dispersed to infinity. The proper distance and proper time intervals in a gravitational field are determined from:

$$dr_p = \sqrt{-g_{rr}}\, dr \tag{22}$$

where

$$-g_{rr}(r) = e^{\lambda(r)} = \left(1 - \frac{2M}{r}\right)^{-1} \qquad \text{if } r \geq R$$

$$g_{44}(r) = e^{\nu(r)} = \left(1 - \frac{2M}{r}\right)$$

$$-g_{rr}(r) = \left(1 - \frac{2U(r)}{r}\right)^{-1} \qquad \text{if } r < R$$

$$g_{44}(r) = \left(1 - \frac{2M}{R}\right)\left(\frac{\mu_s}{\mu(r)}\right)^2$$

(23)

where μ_s is the chemical potential at the surface and $\mu(r)$ is the chemical potential at distance r, which can be expressed as:

$$\mu_s = M(56,26)/56$$

$$\mu(r) = (P + \epsilon)/n \tag{24}$$

M(56,26) is the mass of a free atom of ^{56}Fe, and n is the total baryon number density. The proper mass M_p is obtained by integrating the following differential equation:

$$\frac{dM_p}{dr} = 4\pi\rho r^2 \left(\frac{r}{r-2U(r)}\right)^{1/2} \tag{25}$$

ρ is the matter density as defined by Equation (7) or (18). The total binding energy in mass units M_B is obtained by integrating the following:

$$\frac{dM_B}{dr} = 4\pi r^2 \left[\rho\left(\frac{r}{r-2U(r)}\right)^{1/2} - \epsilon\right] \tag{26}$$

It is evident that the solution of the differential equations (20), (21), (25), and (26) depends only on the equation of state and on the boundary conditions at the center.

Examining the expression of the line element in Equations (19) and (23) we note that the following inequality must be fulfilled for any real solutions:

$$R > R_G = 2GM/c^2 = 2.94\ (M/M_\odot)\ \text{in units of km.} \tag{27}$$

The limiting radius R_G is called the "gravitational radius". When $R = R_G$, a singularity occurs. This singularity is called the Schwarzschild singularity. On this surface, the time metric vanishes, the curvature of space becomes infinite and no light emitted from this surface will reach us. Hence, we will face a serious problem if the solution of the above equilibrium equations gives rise to a radius less than or equal to the gravitational radius.

In the problem of neutron stars, another interesting quantity is the gravitational red shift which is obtained from:

$$\varphi = \frac{\Delta\lambda}{\lambda} = \frac{GM}{Rc^2} = \frac{1.47\ (M/M_\odot)}{R(\text{km})} = \frac{R_G}{2R} \tag{28}$$

RESULTS

The equilibrium equations (20), (21), (25), and (26) have been integrated numerically with the aid of the 7094 computer, for each of about 120 initial values of central density in the range $10^6 \leqslant \varepsilon^c \leqslant 10^{26}$ gm/cm^3, for each of the composite equations of state of type V_β and V_γ with the pressure saturation condition $P \leq \varepsilon$. Additional integrations were carried out for the same

composite equations of state but with a different pressure saturation condition, $P \leq \epsilon/3$. The integrations were terminated at the point where $\log \epsilon = 0$. (ϵ^c is the central energy density.)

The characteristic features of the resulting models of the type V_β and V_γ with the asymptotic equation of state $P = \epsilon$ are given in Tables 1 and 2. Similar results were obtained for these models with the restriction $P \leq \epsilon/3$. The gravitational and proper masses of these models (both with $P \leq \epsilon$ and $P \leq \epsilon/3$) are plotted as functions of the central matter density ρ^c in Figure 5. The points where the respective form of the asymptotic equations of state start to become applicable are marked by crosses. It is clear that the individuality of the constituent particles becomes indistinguishable for $\rho^c \geq 10^{16}$ gm/cm^3. The models lying along the lower branch of the principal mass peak are stable, while the models beyond this point are unstable (Tsuruta 1965, Harrison, Thorne, Wakano and Wheeler 1965). Hence, the effect of the pressure saturation condition $P \leq \epsilon$ or $P \leq \epsilon/3$ is negligible for most of the stable neutron stars. However, different assumptions of the pressure saturation condition give rise to a small shift in the values of mass, radius, etc., for models near and above the principal mass peak. A small local mass peak is observed in the intermediate region between the regions of white dwarfs and neutron stars. This is the region where we assumed a smooth but crude

dissolution of ions into nucleons. The reality of this small peak is questionable and requires further investigation. We conveniently use the expression "pressure saturation condition" to refer to the phenomenon that the pressure is not allowed to go beyond certain limits which are functions of energy density. "Ideal" gas models refer to models consisting of non-interacting particles, and "real" gas models refer to the models for which some interaction potential between baryons is assumed.

The mass-radius relation for the entire range of central density is shown in Figure 6. The portion marked (I) belongs to the white dwarf region. Around the region marked (II) lie a series of models in the intermediate region where inverse beta processes change the equilibrium composition rapidly with change of density. Around the region marked (III) lie neutron and hyperon stars. The solid curves represent our "real" gas models of V_β and V_γ type, and the dashed curve marked (a) and that marked (b) represent the "ideal" gas and "real" gas models constructed by Ambartsumyan and Saakyan (1962a), respectively. The masses are significantly increased when the nuclear forces are taken into account. In the absence of nuclear forces, the maximum mass of neutron stars is only about 0.67 of the mass of the sun, while it can be as large as twice the solar mass in the presence of nuclear forces.

The radius of the models of type V_β and V_γ is plotted as a function of central energy density in Figure 7. At the points

marked D, the models are as large as some of white dwarfs. The density at the center of these models is about $4 \sim 7 \times 10^{13}$ gm/cm^3. These models have the interesting configuration of a small central core of neutrons (with small concentration of electrons and protons) surrounded by huge envelopes consisting of electrons and heavy nuclei, whose exact composition changes from layer to layer as we approach the surface. We shall call these envelopes "electron-nucleus" envelopes. The possible existence of these extended envelopes of electrons and heavy ions was first suggested by Hamada and Salpeter (1961) and is confirmed in this paper. Other points marked by crosses and letter symbols are some of the critical points as defined in Table 3. The radius-central density relation in the region of neutron and hyperon stars is shown in an enlarged scale in Figure 8. The "ideal" gas models are also shown for comparison. We note that the effect of the presence of nuclear forces on stellar radius is not so significant as that on mass.

We have observed in earlier figures various critical points where major and minor maxima and minima in masses and radius occurred. These points are marked by letter symbols A,B C, etc., in the order of increasing density, in Figure 9. The nature and characteristic features of each critical point are summarized in Table 3. One of the most interesting properties of cold dense stars is that the stellar parameters such as mass, total baryon number, radius,

binding energy, components of metric tensor, etc., exhibit damped oscillations as functions of central density of the star. To examine the behavior of these oscillations more closely, the amplitude fall-off factor and the peak-to-trough separations for each critical point of the oscillation of mass at sufficiently high densities were calculated for our models of the V_β and V_γ type with the asymptotic equation of state $P = \epsilon$. These values are listed in the last two columns of Table 3. Theoretical values of these quantities were predicted by Harrison, Thorne, Wakano and Wheeler (1965) to be

$$\text{Amplitude fall-off factor} = \exp(\pi\alpha/\beta) = 3.95 \text{ for } \gamma = 4/3 (P = \epsilon/3) \text{ and } = 6.147 \text{ for } \gamma = 2 (P = \epsilon) \tag{29}$$

and

$$\Delta \log_{10} \epsilon^c = 2 \times 0.4343\, \pi/\beta = 1.59 \text{ for } \gamma = 4/3 (P = \epsilon/3) \text{ and } = 1.578 \text{ for } \gamma = 2 (P = \epsilon), \tag{30}$$

where

$$\alpha = \frac{3}{2} - \left(\frac{1}{\gamma}\right)$$

$$\beta = \left[-\left(\frac{9}{\gamma^2}\right) + \left(\frac{11}{\gamma}\right) - \frac{1}{4} \right]^{1/2}, \quad \gamma = \text{the adiabatic exponent} \tag{31}$$

At sufficiently high densities the approximation $P = \epsilon$ should be valid for our real gas models of V_β and V_γ shown in Table 3. The agreement between our results and the theoretical values in Equations (29) and (30) is quite satisfactory within the estimated order of accuracy. Figure 9 shows the damped oscillations of radius and mass for the V_γ models with $P \leq \epsilon$. We see that the oscillation of radius is somewhat out of phase with the oscillation of mass.

To show the effect of having a composite hyperonic mixture, the composite models and models calculated for a pure neutron configuration are drawn together in Figure 10. The presence of other subatomic particles lowers the partial pressure of the neutrons, and, consequently, smaller stellar masses are expected for the resulting composite models than for the pure neutron stars. This effect of composition, however, is seen to be very small as compared with some other effects such as the effect of nuclear forces.

The internal distribution of matter is shown in Figure 11 for six models of interest. Their properties are given in Table 4. The models marked (1) contain about 0.2 solar mass and consist of large but condensed cores of neutrons surrounded by large envelopes of electrons and nuclei. The envelopes are about 1/3 in width of the total stellar radius. However, such envelopes

quickly diminish for slightly denser stars of $\sim 4 \times 10^{14}$ gm/cm^3 and they are never important for models with higher densities. The internal distribution of matter for stars denser than this is almost constant until the density goes beyond $\varepsilon^c \sim 10^{17}$ gm/cm^3. For higher densities matter starts to accumulate near the center and the deviation from homogeneity becomes serious. For models with $\varepsilon^c \geq 10^{18}$ gm/cm^3 the additional density appears only at the center, leaving the rest of the interior practically intact. For instance, the model of $\varepsilon^c \sim 10^{19}$ gm/cm^3 and that of $\varepsilon^c \sim 10^{24}$ gm/cm^3 with the same equation of state have practically the same internal and external structure, except at the center.

The internal distributions of various stellar parameters are given in Table 5, for two models of type V_γ, the one lying just below and the other just above the principle neutron mass peak. It is interesting to note that the binding energy is negative in the central core but it becomes positive in the outer layers. The internal distribution of the radial and time metrics - $g_{rr}(r)$ and $g_{44}(r)$ for "ideal" gas models were studied by Ambartsumyan and Saakyan (1962b). By comparing their results with our results for the "real" gas models shown in Tables 1, 2, and 5, it is obvious that the non-Euclidean nature of space is more strongly pronounced both in the interior and on the surface when nuclear forces are taken into account.

When the central density of neutron stars is higher than ordinary nuclear densities but is less than about 10^{15} gm/cm^3, they are generally composed of a condensed neutron-dominant core surrounded by thin or negligible envelopes of electron-nuclear configuration. These stars were called neutron star models in our discussion. The stars of densities higher than this consist of a condensed hyperon-dominant core surrounded by thin neutron dominant outer layers. These are called hyperon stars in this paper. The electron-nuclear envelopes are always negligible for these hyperon stars.

DISCUSSION

It may be noted that some of the characteristics of dense stars depend greatly not only on the presence of nuclear forces but also on the exact form of these forces. For instance, both the radii and masses of the V_γ type models of dense neutron and hyperon stars are about twice as large as the corresponding values of the V_β type models. It is most desirable to further improve the nuclear equation of state in the critical region of $10^{14.5} \leqslant \rho \leqslant 10^{16.5}$ gm/cm^3.

It is gratifying that the effect of the exact composition of the hyperonic mixture is so small. Even if the threshold density of the appearance of some of the mesons and hyperons is shifted to as low as ordinary nuclear density, the resulting change of

composition will not seriously affect the major properties of cold models of neutron and hyperon stars reported in this paper unless there is a large accompanying change in the interaction potentials.

There are certain physical variables whose values are greatly affected by the presence of nuclear forces but are relatively insensitive to the exact form of the nuclear potential. These are the variables which depend on the ratio of mass to radius. For instance, the red shifts of both the V_β and V_γ type models are about two to three times as large as the corresponding values for the "ideal" gas models. The maximum red shift and the largest departure from Euclidean space are noted at a point just above the principal mass peak of the neutron stars (point F in Figures 6 and 9). At this point, the red shift of both the V_β and V_γ type model is about 0.32 while that of the "ideal" gas model is only about 0.15. The non-Euclidean nature of space is enhanced by a factor of 2 when either the V_β or V_γ type nuclear potential is included. However, the departure from the Euclidean characteristics is not large enough to produce a Schwarzschild singularity for all the models constructed in this paper. (See Equation (28) and Tables 1 and 2.)

A complicated effect of nuclear forces appears in the property of binding energy. When the constituent baryons become relativistic the binding energy, which is the proper mass minus gravitational

mass, becomes negative if nuclear forces are neglected (Tsuruta 1964, Misner and Zapolsky 1964). The same argument does not necessarily apply when the interaction forces enter. Depending on the different assumptions of the nuclear forces, the negative binding may or may not occur. For instance, the binding energy becomes negative for sufficiently dense models of "real" gases constructed by Ambartsumyan and Saakyan (1962b), but all the other nuclear models we have studied (the Levinger-Simmons V_β and V_γ type, and Skyrme type potentials) fail to give negative binding energies for relativistic baryons.

It is interesting to note, however, that a small negative binding of about 1% of the stellar mass occurs in the lower density regions of $10^{12} \leqslant \epsilon^c < 8 - 9 \times 10^{13}$ gm/cm^3, below the nuclear densities. This is caused by the presence of relativistic electrons. At these densities the concentration of neutrons is not sufficiently large to overcome the effect of relativistic electrons.

Some of the properties of cold degenerate stars seem to be independent of the type of equation of state to be adopted. The gravitational mass, the proper mass (or total baryon number) and the binding energy exhibit damped oscillations in phase with each other as functions of central density. Hence the point of tightest binding is also the point of maximum mass and maximum baryon number. We have seen that the stellar radius also oscillates as a function

of central density but the oscillation is partly out of phase with the oscillations of the masses. Other interesting variables, the components of the metric tensor and the red shift, also show similar damped oscillations as the central density is increased. Their oscillations are in phase with each other but are not in phase with the oscillations of either the radius or the mass. These properties are found to be common to all different types of equation of state studied by us.

It may be noted that in the models of mass less than about $0.2M_{\odot}$, the binding energy is much less than 1% of the total mass (Table 1 and 2). Such models are energetically unstable against transformation into iron white dwarfs (Cameron 1959). We have noted that the models lying above the principal mass peak (point F) are dynamically unstable. Hence the stable neutron stars, if observable, are expected to lie in the small range of density corresponding to the region $0.2M_{\odot} \leqslant M \leqslant 2M_{\odot}$. The binding energy is only about 1% of the total stellar mass for the lightest of the stable neutron stars but at the mass peak it is as large as about 20% of the observable mass.

Another outcome which may well be noted is the possible importance of the "electron-nucleus" envelopes in some of the lightest stable neutron stars. The most extended envelopes were seen to occur in unstable regions, but it was shown that some of the

stable neutron stars could have quite an extended envelope also, almost as large as the neutron core itself. The mass contained in such envelopes is negligible. Therefore, any physical variables which depend on radius can be greatly affected by the presence of these envelopes. Red shift is an important stellar parameter in the problem of observation. By neglecting the envelopes of electrons and heavy nuclei, about 50% error in the value of red shift could occur for some of the lightest stable neutron stars.

References

Ambartsumyan, V.A. and Saakyan, G.S. 1960. Soviet Astronomy, 4, 187.

_____ 1962a. Soviet Astronomy, 5, 601.

_____ 1962b. Soviet Astronomy, 5, 779.

Bahcall, J.N. and Wolf, R.A. 1965. Phys. Rev. Lett., 14, 343.

Brueckner, K.A. and Gammel, J.L. 1958. Phys. Rev., 109, 1023.

Brueckner, K.A., Gammel, J.L., and Kubis, J.T. 1060. Phys. Rev., 118, 1095.

Cameron, A.G.W. 1959. Astrophys. J. 130, 884.

_____ 1965. Nature, 205, 787.

Chandrasekhar, S. 1935. Monthly Notices of Roy. Astronom. Soc., 95, 207.

_____ 1939. Introduction to the study of stellar structure (Univ. of Chicago Press, Chicago).

Chiu, H.Y. 1964. Annals of Phys., 26, 364.

Chiu, H.Y. and Salpeter, E.E. 1964. Phys. Rev. Lett., 12, 412.

Hamada, T. and Salpeter, E.E. 1961. Astrophys. J., 134, 683.

Harrison, B.K., Thorne, K.S., Wakano, M., and Wheeler, J.A. 1965. Gravitation theory and gravitational collapse (Univ. of Chicago Press, Chicago).

Landau, L.D. 1932. Physik. Zeits. Sowjetunion, 1, 285.

Landau, L.D. and Lifshitz, E. 1959. The classical theory of fields (Addison-Wesley Pub. Co., Reading, Mass.).

Levinger, J.S. and Simmons, L.M. 1961. Phys. Rev., 124, 916.

Misner, C.W. and Zapolsky, H.S. 1964. Phys. Rev. Lett., 12, 635.

Morton, D.C. 1964. Nature, 201, 1308.

Oppenheimer, J.R. and Serber, R. 1938. Phys. Rev., 54, 540.

Oppenheimer, J.R. and Volkoff, G.M. 1939. Phys. Rev., 55, 374.

Sahakian, G.S. and Vartaman, Yu. L. 1963. Nuovo Cimento, 30, 82.

Salpeter, E.E. 1961. Astrophys. J., 134, 669.

_____ 1963. Presented at the First Texas Symposium on Relativistic Astrophysics. Also see Ch. VI #32 of I. Robinson, A. Schild, and E.L. Schucking's Quasi-stellar sources and gravitational collapse 1965. (Univ. of Chicago Press, Chicago).

Serber, R. 1964. Revs. Modern Phys., 36, 649.

Sood, P.C. and Moszkowski, S.A. 1960. Nucl. Phys., 21, 582.

de Swart, J. and Dullemond, C. 1961. Bull. Am. Phys. Soc., 6, 269.

Tolman, R.C. 1934. Relativity, thermodynamics, and cosmology (Clarendon Press, Oxford).

Tsuruta, S. 1964. Thesis, Columbia University.

_____ 1965. Nature, 207, 470.

Tsuruta, S. and Cameron, A.G.W. 1965. Can. J. Phys., 43, 2056.

Zel'Dovich, Ya. B. 1962. Soviet Physics JETP, 14, 1143.

Zwicky, F. 1938. Astrophys. J., 88, 522.

_____ 1939. Phys. Rev. 55, 726.

_____ 1958. Handbuck der Physik, (Springer-Verlag, Berlin) 51, 766.

TABLE CAPTIONS

Table 1: Characterisitics of Composite Models of Degenerate Stars with the Nuclear Potential V_β and the Asymptotic Equation of State $P = \epsilon$; P^c is the central pressure in dynes/cm^2, $P_o = (M_n^4 c^5/32\pi^2\hbar^3)4\pi = 6.46 \times 10^{36}$ dynes/cm^2, ϵ^c is the total energy density at the center and ρ^c is the total matter density at the center in gm/cm^3, R is the coordinate radius of the star, M, M_p, and M_B are the gravitational and proper mass and the binding energy in mass units, $M_\odot$ is the mass of the sun, t_n^c is the relativistic parameter for neutrons at the center, $g_{44}(R)$ is the time metric and $-g_{rr}(R)$ is the radial metric at the surface.

Table 2: Characterisitics of Composite Models of Degenerate Stars with the Nuclear Potential V_γ and the Asymptotic Equation of State $P = \epsilon$; the notation is that introduced in Table 1.

Table 3: Properties of Critical Points; the letters A, B, C, etc., denote the various critical points in order of increasing central density of the models ; MAX. 1, etc., means the first maximum point, etc.; MIN. 2, etc., means the second minimum point, etc.; the capital letters in ( ) stand for the names of the persons who recognized or identified these points first (C = Cameron, H = Harrison, L = Landau, M = Misner, O = Oppenheimer, HS = Hamada and Salpeter, T = Tsuruta, V = Volkoff, WW = Wakano and Wheeler, and Z = Zapolsky); the

models HTWW are models constructed by Harrison, Thorne, Wakano and Wheeler; IDEAL means the models with no nuclear interactions, ($\Delta M_{n-1}/\Delta M_n$) stands for the amplitude fall-off factor, and (ΔLOG ϵ^c) means the peak-to-trough separation in the LOG ϵ^c vs $M/M_\odot$ plane. Remaining notation is that introduced in Table 1. The second and third columns explain the nature of the critical points designated A, B, C, etc., the 4th column explains the type of model for which the calculations in the last 5 columns were made, and the last 5 columns give the characteristic properties at these points.

Table 4: This table gives the properties of the models used in Figure 11. The notation is that introduced in Table 1.

Table 5: Internal Distribution of Various Stellar Parameters for two models of the V_γ type. The model (A) is slightly less dense and the model (B) is slightly denser than the configuration of maximum mass. r is the radial distance from the center, $\epsilon(r)$, $t_n(r)$, $-g_{rr}(r)$, and $g_{44}(r)$ are the energy density, relativistic parameter for neutrons, the radial and time metrics, all at the point r from the center. $U(r)/M_\odot$ and $M_p(r)/M_\odot$ are the gravitational and proper mass of matter in solar mass units contained within the radius r, and

$$M_B(r) = M_p(r) - U(r)$$

TABLE 1

p^c/p_o	LOG ε^c (gm/cm^3)	LOG ρ^c (gm/cm^3)	R(km)	$M/M_\odot$	$M_p/M_\odot$	$M_B/M_\odot$	t_n^c	$g_{44}(R)$	$-g_{rr}(R)$	RED SHIFT
10^{-13}	6.95173	6.95167	6.782×10^{3}	0.66838	0.67001	0.00163	0	0.9997	1.0003	1.45×10^{-4}
5×10^{-12}	8.16160	8.16135	3.721×10^{3}	1.03641	1.03827	0.00186	0	0.9992	1.0008	4.09×10^{-4}
10^{-10}	9.15375	9.15318	2.185×10^{3}	1.13933	1.14079	0.00146	0	0.9985	1.0015	7.66×10^{-4}
2.5×10^{-9}	10.2786	10.2774	1.217×10^{3}	0.92016	0.92067	0.00051	0	0.9978	1.0022	1.11×10^{-3}
2.5×10^{-8}	11.0854	11.0836	7.627×10^{2}	0.72631	0.72655	0.00024	0	0.9972	1.0028	1.40×10^{-3}
2.5×10^{-7}	12.3145	12.3109	7.113×10^{2}	0.62594	0.62544	-0.00050	0.2661	0.9974	1.0026	1.29×10^{-3}
2.5×10^{-6}	12.9881	12.9836	1.256×10^{3}	0.62290	0.62176	-0.00114	0.4621	0.9985	1.0015	7.29×10^{-4}
10^{-5}	13.3880	13.3824	2.283×10^{3}	0.67250	0.67145	-0.00104	0.6299	0.9991	1.0009	4.32×10^{-4}
2.2×10^{-5}	13.6147	13.6084	4.193×10^{3}	0.40163	0.40108	-0.00055	0.7490	0.9997	1.0003	1.41×10^{-4}
10^{-4}	14.0439	14.0360	53.00	0.12848	0.12856	0.00008	1.0358	0.9929	1.0072	0.00356
8×10^{-4}	14.5587	14.5456	17.37	0.20809	0.21000	0.00191	1.510	0.9648	1.0365	0.01762
4×10^{-3}	14.9626	14.9404	11.66	0.33606	0.34380	0.00774	2.003	0.915	1.0929	0.0425
2×10^{-2}	15.3844	15.3607	8.829	0.44673	0.46737	0.02064	2.443	0.8512	1.173	0.0744
7×10^{-2}	15.6042	15.5748	6.977	0.62085	0.68233	0.06148	2.613	0.738	1.354	0.131
2×10^{-1}	15.7810	15.7322	6.022	0.82269	0.96081	0.13812	2.749	0.598	1.6704	0.201
7×10^{-1}	16.0216	15.9174	5.184	0.96627	1.19409	0.22782	2.932	0.452	2.211	0.274
4×10^{0}	16.4631	16.1847	4.261	0.91218	1.10643	0.18715	3.1983	0.372	2.688	0.314
2×10^{1}	17.1556	16.5014	3.898	0.78682	0.89163	0.10481	3.5547	0.406	2.459	0.297
2×10^{2}	18.1556	16.8936	4.046	0.75035	0.82474	0.07439	4.089	0.4548	2.201	0.2726
2×10^{3}	19.1556	17.2676	4.086	0.77491	0.86534	0.09043	4.742	0.4424	2.260	0.2788
2×10^{4}	20.1556	17.6391	4.059	0.77210	0.86071	0.08861	5.527	0.4408	2.269	0.2796
2×10^{5}	21.1556	18.0115	4.051	0.77040	0.85806	0.08766	6.4317	0.4408	2.269	0.2796
2×10^{6}	22.1556	18.3847	4.0533	0.77107	0.85938	0.08831	7.4257	0.4408	2.269	0.2796
2×10^{7}	23.1556	18.7586	4.05253	0.771024	0.858841	0.087817	8.4805	0.4406	2.270	0.2797
2×10^{8}	24.1556	19.1329	4.05255	0.770956	0.858720	0.087764	9.5737	0.4406	2.270	0.2797
2×10^{9}	25.1556	19.5074	4.05265	0.771029	0.858255	0.087226	10.6905	0.4406	2.270	0.2797
4×10^{9}	25.4566	19.6202	4.05265	0.771031	0.858259	0.087228	11.030	0.4406	2.270	0.2797

TABLE 2

p^c/p_o	LOG ϵ^c (gm/cm^3)	LOG ρ^c (gm/cm^3)	R(km)	$M/M_\odot$	$M_p/M_\odot$	$M_B/M_\odot$	M_B/M (%)	t_n^c	$g_{44}(R)$	$-g_{rr}(R)$	RED SHIFT
1×10^{-14}	6.28406	6.28403	9.101×10^3	0.42483	0.42599	0.00116	0.2738	0	0.9999	1.0001	6.85×10^{-5}
1×10^{-12}	7.65431	7.65416	4.842×10^3	0.90802	0.90988	0.00186	0.2048	0	0.9994	1.0006	2.76×10^{-4}
6×10^{-11}	8.97596	8.97546	2.387×10^3	1.14596	1.14761	0.00165	0.144	0	0.9986	1.0014	7.06×10^{-4}
6×10^{-10}	9.77921	9.77836	1.591×10^3	1.03860	1.03942	0.00082	0.078	0	0.9981	1.0019	9.59×10^{-4}
6×10^{-9}	10.5852	10.5839	1.024×10^2	0.84461	0.84499	0.00038	0.045	0	0.9976	1.0024	1.21×10^{-3}
6×10^{-8}	11.3924	11.3902	6.314×10^2	0.65904	0.65923	0.00019	0.0288	0	0.9969	1.0031	1.531×10^{-3}
2×10^{-7}	12.2363	12.2328	6.857×10^2	0.63057	0.63022	-0.00035	-0.0555	0.2482	0.9973	1.0027	1.351×10^{-3}
2×10^{-6}	12.9685	12.9641	1.076×10^3	0.63119	0.63013	-0.00106	-0.168	0.4550	0.9982	1.0018	8.64×10^{-4}
10^{-5}	13.4482	13.4428	1.776×10^3	0.71074	0.70960	-0.00114	-0.1605	0.6598	0.9988	1.0012	5.88×10^{-4}
3.7×10^{-5}	13.8117	13.8052	4.246×10^3	0.54908	0.54858	-0.00050	-0.0911	0.8702	0.9997	1.0003	1.291×10^{-4}
10^{-4}	14.0566	14.0495	62.28	0.10583	0.10595	0.00012	0.1135	1.046	0.995	1.0050	2.50×10^{-3}
5×10^{-4}	14.3779	14.3678	17.78	0.20033	0.20234	0.00201	1.001	1.326	0.967	1.034	0.0166
5×10^{-3}	14.7461	14.7251	12.55	0.76612	0.80792	0.04180	5.46	1.720	0.802	1.247	0.0989
2.5×10^{-2}	15.0358	14.9867	11.90	1.49104	1.66813	0.17709	11.88	2.069	0.631	1.581	0.1844
2×10^{-1}	15.4728	15.3369	9.940	1.95294	2.31678	0.36384	18.60		0.421	2.374	0.2896
5×10^{-1}	15.7040	15.4906	8.942	1.88475	2.22228	0.33753	17.91	2.546	0.380	2.628	0.3101
10^0	15.9015	15.6061	8.273	1.77553	2.05128	0.27575	15.49	2.639	0.368	2.719	0.3158
5×10^0	16.5535	15.9218	7.488	1.51917	1.62528	0.10611	7.00	2.936	0.404	2.476	0.2981
5×10^1	17.5535	16.3348	7.769	1.44985	1.50706	0.05721	3.94	3.360	0.4512	2.215	0.2744
5×10^2	18.5535	16.7237	7.875	1.49956	1.58278	0.08322	5.55	3.840	0.440	2.271	0.280
5×10^3	19.5535	17.1055	7.812	1.49311	1.57391	0.08080	5.401	4.442	0.438	2.283	0.2810
5×10^4	20.5535	17.4825	7.817	1.48981	1.56864	0.07883	5.247	5.180	0.4396	2.275	0.2802
5×10^5	21.5535	17.8583	7.803	1.49134	1.57083	0.07949	5.2322	6.047	0.438	2.283	0.2810
5×10^6	22.5535	18.2336	7.801	1.49129	1.57076	0.07947	5.2310	7.015	0.438	2.283	0.2810
5×10^7	23.5535	18.6087	7.80088	1.49116	1.57054	0.07938	5.2314	8.052	0.438	2.283	0.2810
5×10^8	24.5535	18.9836	7.80105	1.49120	1.57060	0.07940	5.2325	9.134	0.438	2.283	0.2810
5×10^9	25.5535	19.3585	7.80100	1.49120	1.57060	0.07940	5.2325	10.244	0.438	2.283	0.2810

TABLE 3

PROPERTIES OF CRITICAL POINTS

POINT	EXPLANATION		MODEL	LOG ϵ^c (gm/cm^3)	R (km)	$M/M_\odot$	$\frac{\Delta M_{n-1}}{\Delta M_n}$	Δ LOG ϵ^c (gm/cm^3)
	MASS	COMMENT (NOTATION)						
		WHITE DWARF	V_γ	8.95	2.34×10^3	1.15		
A	MAX. 1	MASS PEAK	V_β	8.95	2.34×10^3	1.15		
		(L-HWW)	HTWW	8.4	3.5×10^3	1.2		
		LOCAL	V_γ	12.675	8.3×10^2	0.622		
B	MIN. 1	(TC1)	V_β	12.76	9.6×10^2	0.612		
		LOCAL	V_γ	13.65	2.45×10^3	0.754		
C	MAX. 2	(TC2)	V_β	13.38	2.25×10^3	0.673		
		LARGEST	V_γ	13.856	5.2×10^3	0.3		
D		ENVELOPE	V_β	13.64	4.55×10^3	0.272		
		(HS-TC)	HTWW	13.17	3×10^3	0.38		
		NEUTRON STAR	V_γ	13.925	280	0.095		
E	MIN. 2	MAIN TROUGH	V_β	13.75	260	0.113		
		(HWW)	HTWW	13.3	225	0.18		
		NEUTRON STAR	V_γ	15.48	9.88	1.953		
F	MAX. 3	PRINCIPAL PEAK	V_β	16.05	5.103	0.973		
		(LOV)	IDEAL	15.59	9.25	0.712		
		NEUTRON STAR	V_γ	17.253	7.638	1.43582	8	1.601
G	MIN. 3	SECOND TROUGH	V_β	17.854	3.973	0.738	6.12	1.80
		(MZ-TC1)						
		NEUTRON STAR	V_γ	18.854	7.828	1.50017	6.16	1.552
H	MAX. 4	SECOND PEAK	V_β	19.456	4.065	0.7765	6.07	1.602
		(MZ-TC2)						

TABLE 3 (continued)

PROPERTIES OF CRITICAL POINTS

POINT	EXPLANATION: MASS	EXPLANATION: COMMENT (NOTATION)	MODEL	LOG ε^c (gm/cm^3)	R (km)	$M/M_\odot$	$\frac{\Delta M_{n-1}}{\Delta M_n}$	Δ LOG ε^c (gm/cm^3)
I	MIN. 4	NEUTRON STAR THIRD TROUGH (H-TC)	V_γ V_β	20.406 21.004	7.807 4.050	1.48976 0.77015	6.2 6.47	1.549 1.548
J	MAX. 5	NEUTRON STAR THIRD PEAK (TC3)	V_γ V_β	21.955 22.554	7.8016 4.0529	1.49144 0.77114	6 6	1.599 1.550
K	MIN. 5	NEUTRON STAR 4th TROUGH (TC4)	V_γ V_β	23.554 24.154	7.8009 4.0525	1.49116 0.77096	7	1.600 1.600
L	MAX. 6	NEUTRON STAR 4th PEAK (TC5)	V_γ V_β	25.154 25.734	7.80103 4.05265	1.49120 0.77103		1.6 1.58

TABLE 4

	V_β (1)	V_β (2)	V_β (3)	V_γ (1)	V_γ (2)	V_γ (3)
$M/M_\odot$	0.1996	0.9663	0.7710	0.2003	1.9529	1.4912
R(km)	18.219	5.1842	4.063	17.79	9.940	7.801
LOG ε^c	14.5262	16.0216	23.8546	14.3779	15.4728	23.8546
LOG ρ^c	14.5137	15.9174	19.0202	14.3678	15.3369	18.7216
t_n^c	1.476	2.932	9.242	1.326	2.422	8.374
p^c/p_o	7×10^{-4}	0.7	10^8	5×10^{-4}	0.2	10^8

TABLE 5

INTERNAL DISTRIBUTION

	r(km)	LOG $\epsilon(r)$ (gm/cm^3)	$U(r)/M_\odot$	$M_p(r)/M_\odot$	$M_B(r)/M_\odot$	$-g_{rr}(r)$	$g_{44}(r)$	$t_n(r)$
MODEL (A) V_γ	0	15.1683	0	0	0	1.0000	0.2535	2.25
	1.027	15.164	3.3585×10^{-3}	2.6071×10^{-3}	-7.514×10^{-4}	1.0097	0.2557	2.24
	1.986	15.152	2.3889×10^{-2}	1.8894×10^{-2}	-4.995×10^{-3}	1.0368	0.2616	2.23
	2.984	15.132	7.8235×10^{-2}	7.0328×10^{-2}	-7.907×10^{-3}	1.0838	0.2718	2.20
	4.029	15.101	0.18423	0.16646	-0.01777	1.1559	0.2874	2.16
	4.987	15.062	0.33250	0.31203	-0.02047	1.2448	0.3064	2.11
	5.999	15.010	0.54263	0.52955	-0.01308	1.3638	0.3319	2.05
	7.005	14.941	0.79775	0.81098	0.01323	1.5058	0.3632	1.96
	8.007	14.851	1.0809	1.1452	0.0643	1.6615	0.4001	1.85
	9.003	14.727	1.3637	1.5016	0.1379	1.8076	0.4419	1.70
	10.000	14.539	1.6142	1.8347	0.2205	1.9087	0.4855	1.49
	11.000	13.466	1.7537	2.0254	0.2717	1.8876	0.5295	0.67
	11.2	0	1.7552	2.0275	0.2723	1.86	0.538	0
MODEL (B) V_γ	0	15.7001	0	0	0	1.0000	0.0429	2.88
	1.061	15.682	1.2364×10^{-2}	6.7476×10^{-3}	-5.616×10^{-3}	1.0356	0.0453	2.86
	2.089	15.632	0.08795	0.05195	-0.03600	1.1418	0.0527	2.80
	3.018	15.561	0.23955	0.16876	-0.07079	1.3056	0.0650	2.72
	4.002	15.463	0.48911	0.37571	-0.1134	1.5637	0.0859	2.61
	5.010	15.340	0.81651	0.69958	-0.1169	1.9258	0.1188	2.46
	6.008	15.193	1.1725	1.1232	-0.0493	2.3564	0.1661	2.28
	7.006	15.007	1.5133	1.6020	0.0887	2.7554	0.2293	2.04
	8.002	14.728	1.7850	2.0325	0.2475	2.9235	0.3040	1.70
	8.91	0	1.901	2.226	0.325	2.702	0.371	0

FIGURE CAPTIONS

Figure 1: Number densities in cm^{-3} of various sub-atomic particles as functions of total matter density in gm/cm^3. The symbols n, p, Λ, Σ^-, Σ^o, Σ^+, Ξ^-, Ξ^o, e, μ^-, n* and p* stand for neutrons, protons, hyperons corresponding to their respective symbols, electrons, negative muons, and neutrons and protons in the first excited state.

Figure 2: The composition distribution used in our composite equation of state. The partial number densities of various constituent particles (in units of cm^{-3}) are plotted as functions of total matter density (in gm/cm^3).

Figure 3: Energy in Mev/particle is plotted against density in gm/cm^3, for various nuclear potentials and for non-interacting particles.

Figure 4: Pressure is plotted against energy density for the composite equations of state of type V_β and V_γ, with the asymptotic equation of state $P = \epsilon$.

Figure 5: The gravitational and proper masses of the models of type V_β and V_γ with the asymptotic equation of state of either $P = \epsilon$ or $P = \epsilon/3$. The points at which the composite equations of state switch over to the asymptotic equations of state are shown by crosses.

Figure 6: The mass-radius relation of the composite models of the type V_β and V_γ with the pressure saturation condition $P < \epsilon$ (solid curves). The points A, B, C, etc., are the critical points as explained in Table 3. The regions (I), (II), and (III) are the regions of white dwarfs, the intermediate regions, and the regions of neutron and hyperon stars. The dashed curves are the "ideal" gas models (a) and "real" gas models (b) constructed by Amburtsumyan and Saakyan (1962a).

Figure 7: The relation between the radius and central energy density for the composite models of the V_β and V_γ type. Some of the critical points in low density regions are shown by crosses and the corresponding letter symbols as introduced in Table 3.

Figure 8: The relation between the radius and the central energy density in the region of neutron stars is shown in detail. For comparison, the models of "ideal" gases are shown as a dashed curve, together with the "real" gas models of the V_β and V_γ type (solid curves).

Figure 9: The damped oscillations of the gravitational mass and radius as functions of central energy density. The regions (I), (II), and (III) are those defined in Figure 6. The points A, B, C, etc., stand for the critical points explained in Table 3. The peaks and troughs of mass and radius are shown by the respective marks.

Figure 10: The effect of the presence of hyperons. The models of the V_β and V_γ type are shown both for the configuration of pure neutrons (dashed curves) and for the baryonic mixtures (solid curves).

Figure 11: Internal distribution of energy density for 6 models whose characteristic properties are listed in Table 4. The solid curves represent the V_γ type models and the dashed curves represent the V_β type models. These were selected from (1) the region of the lightest stable neutron stars, (2) the region near the principal mass peak (point F in Figure 9), and (3) the region of superdense stars with $\varepsilon^c \sim 10^{24}$ gm/cm^3.

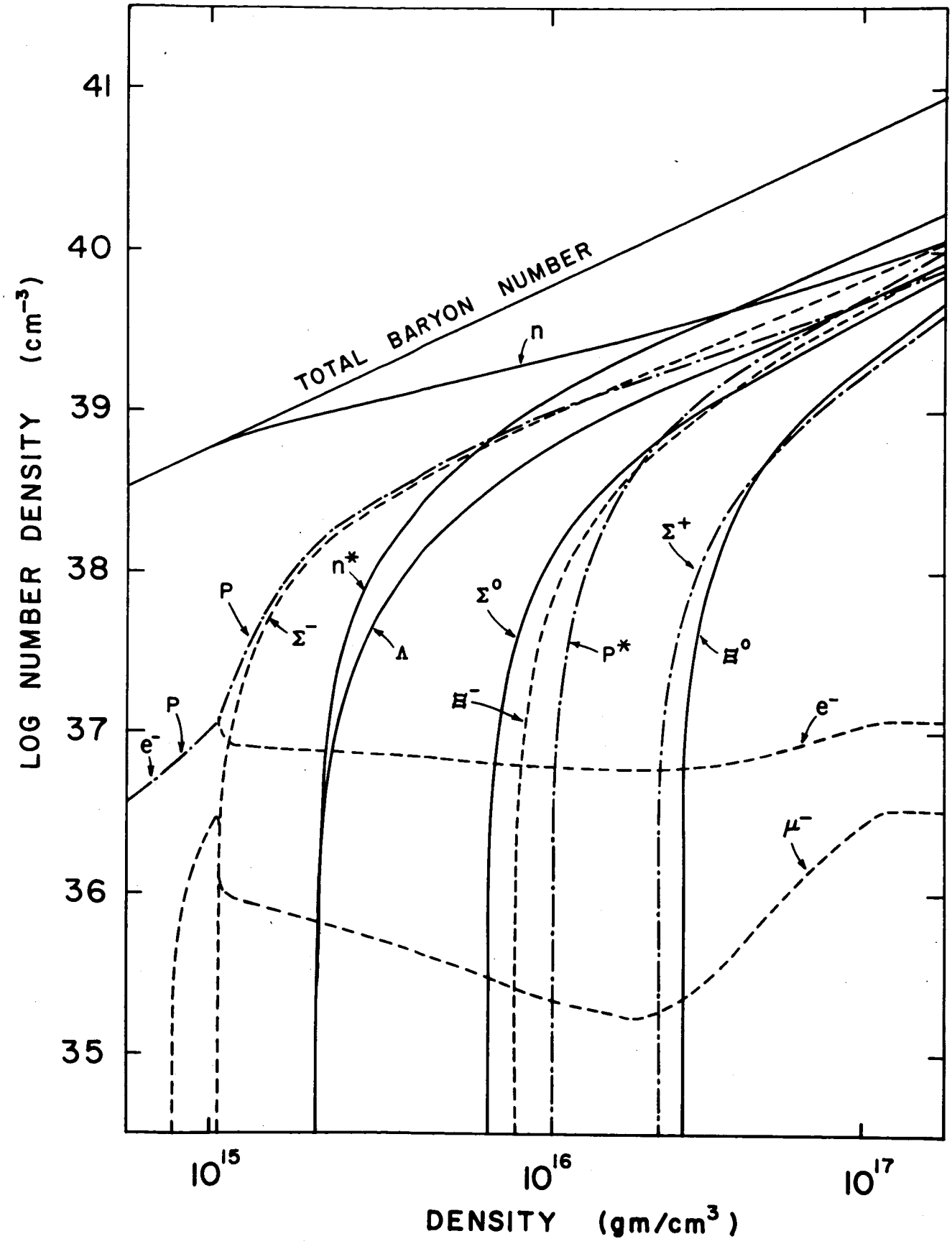
41
40
39
38
37
36
35
LOG NUMBER DENSITY (cm⁻³)
TOTAL BARYON NUMBER
n
n*
P
Σ⁻
Λ
Σ⁰
P*
Ξ⁻
Σ⁺
Ξ⁰
e⁻
μ⁻
10¹⁵
10¹⁶
10¹⁷
DENSITY (gm/cm³)

Fig. 1

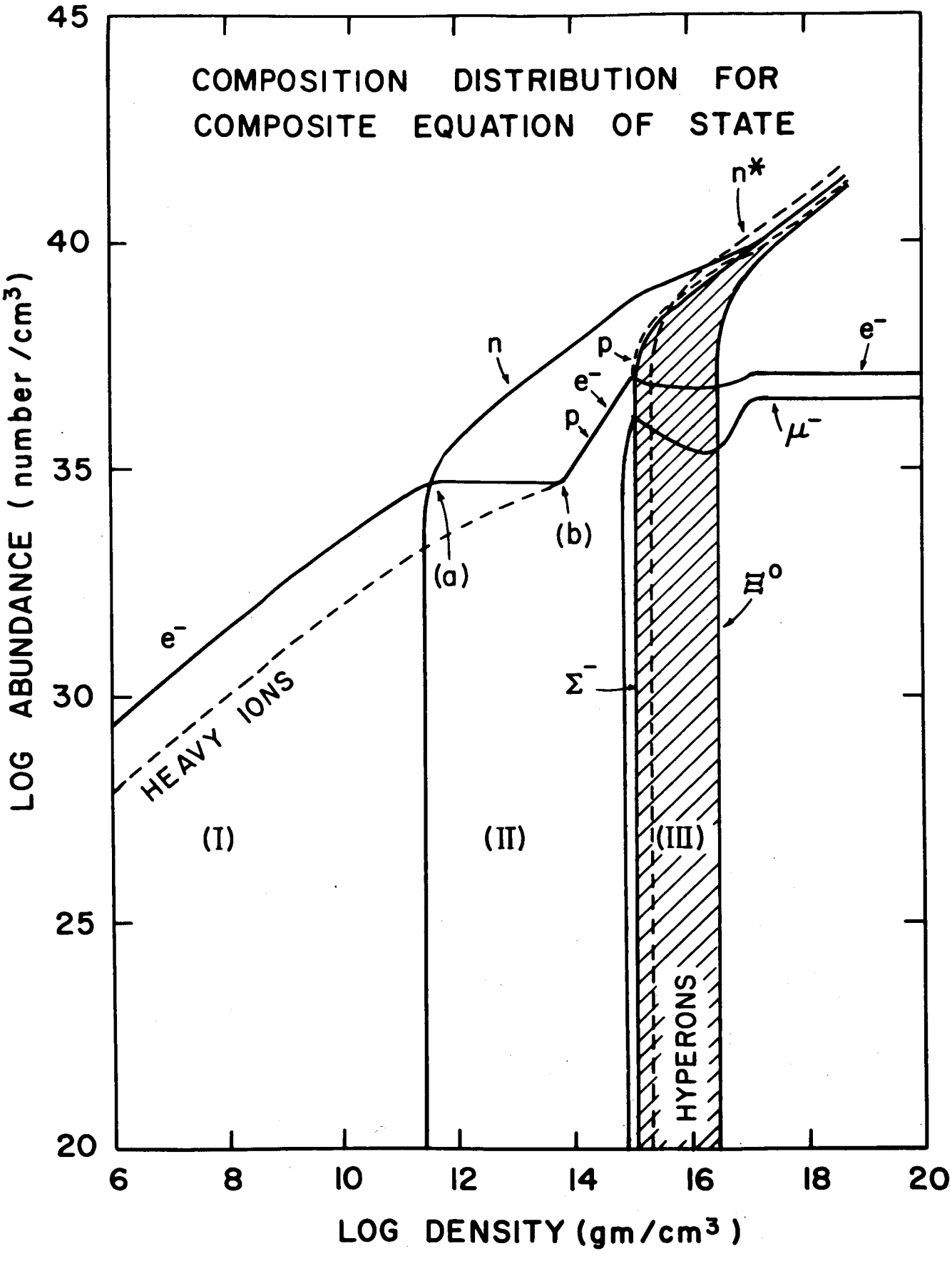
COMPOSITION DISTRIBUTION FOR
COMPOSITE EQUATION OF STATE
LOG ABUNDANCE (number /cm³)
LOG DENSITY (gm/cm³)
45
40
35
30
25
20
6
8
10
12
14
16
18
20
n*
n
p
e⁻
p
e⁻
μ⁻
(a)
(b)
Ξ⁰
Σ⁻
e⁻
HEAVY IONS
(I)
(II)
(III)
HYPERONS

Fig. 2

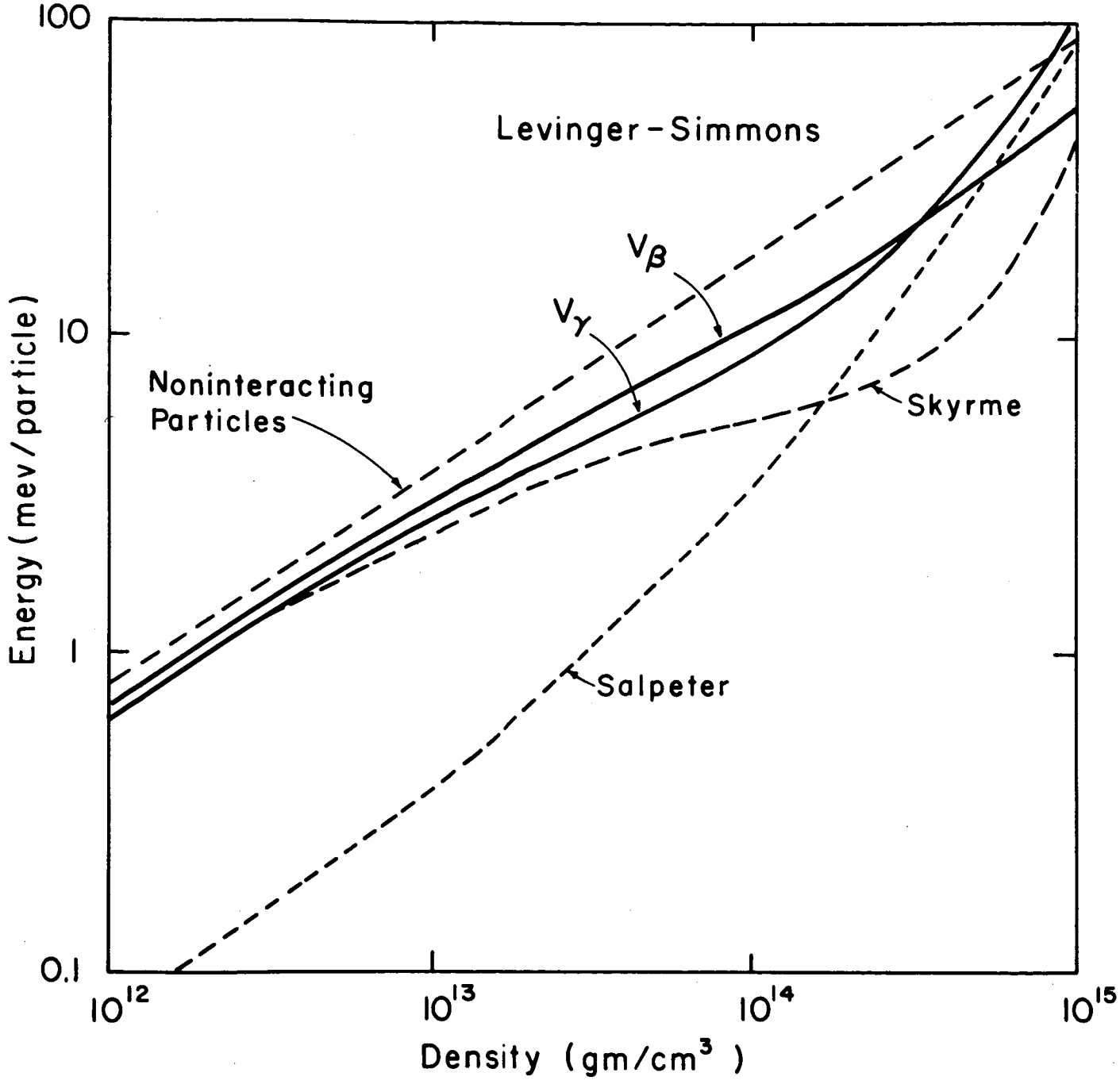
100
10
1
0.1
Energy (mev/particle)
Levinger-Simmons
V_β
V_γ
Noninteracting
Particles
Skyrme
Salpeter
10^{12}
10^{13}
10^{14}
10^{15}
Density (gm/cm^3)

Fig. 3

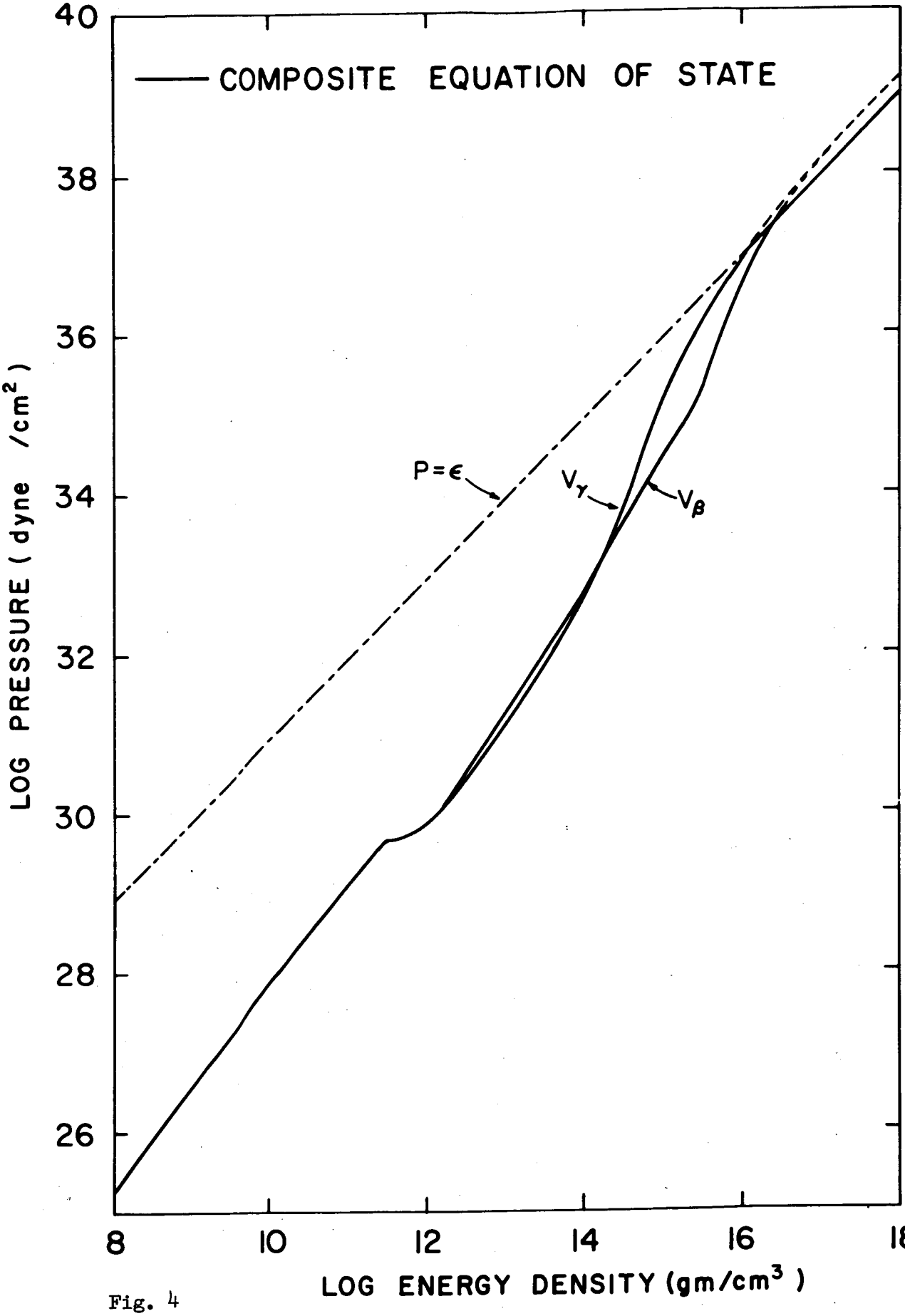
COMPOSITE EQUATION OF STATE
P=ε
V_γ
V_β
LOG PRESSURE (dyne /cm²)
LOG ENERGY DENSITY (gm/cm³)
40
38
36
34
32
30
28
26
8
10
12
14
16
18

Fig. 4

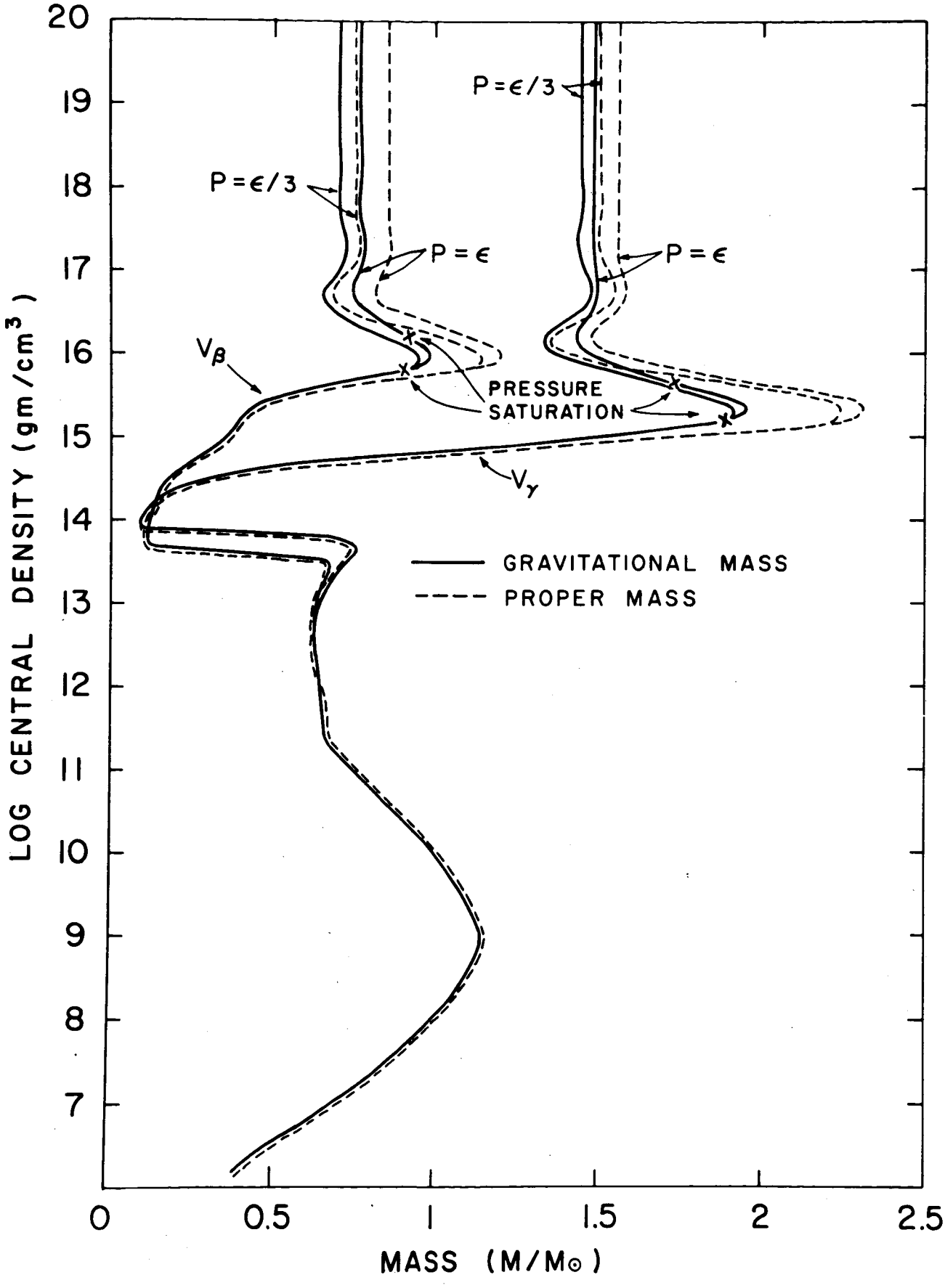
20
19
18
17
16
15
14
13
12
11
10
9
8
7
LOG CENTRAL DENSITY (gm/cm³)
P=ϵ/3
P=ϵ/3
P=ϵ
P=ϵ
Vβ
PRESSURE SATURATION
Vγ
GRAVITATIONAL MASS
PROPER MASS
0
0.5
1
1.5
2
2.5
MASS (M/M⊙)

Fig. 5

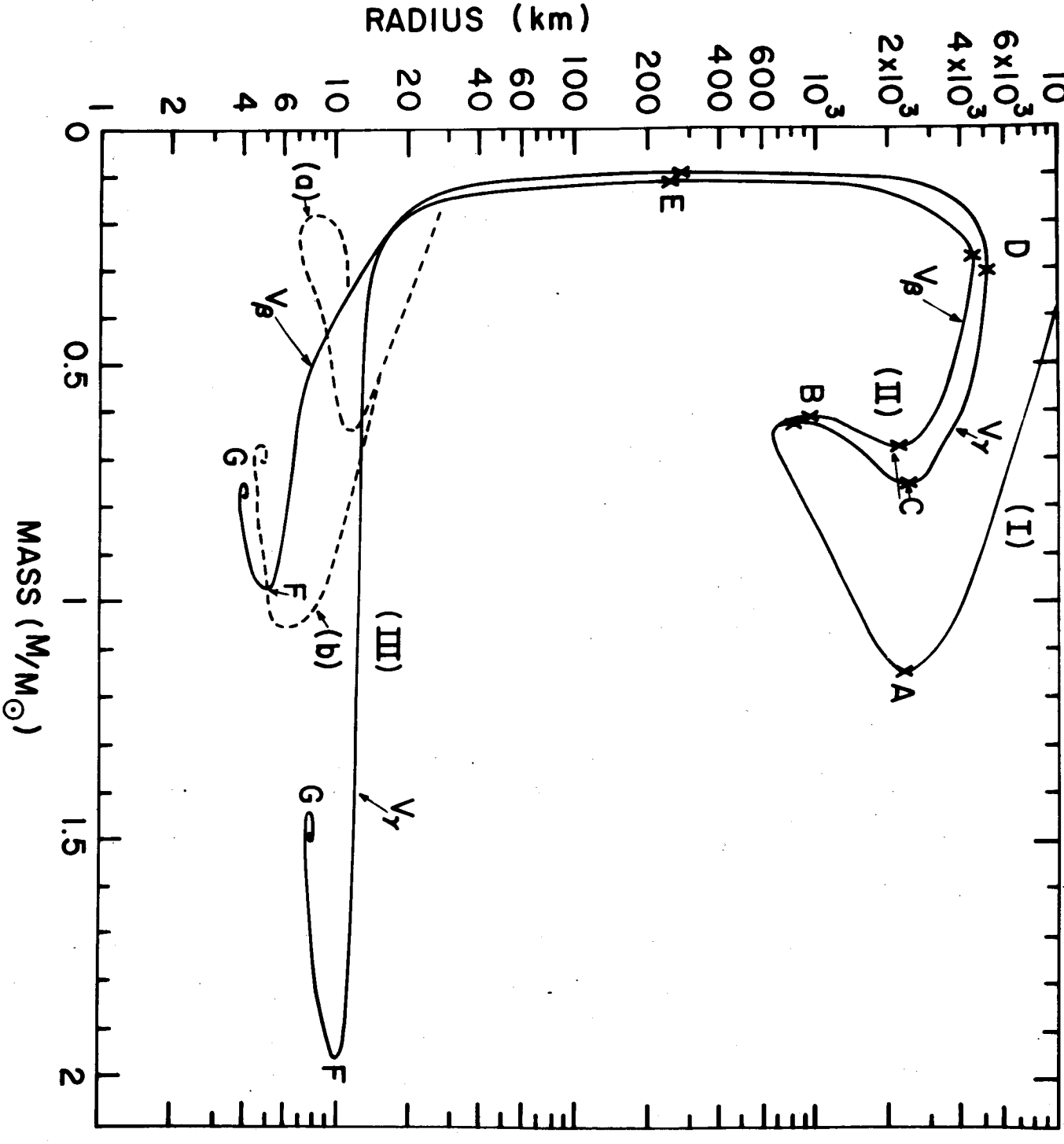
RADIUS (km)
1
2
4
6
10
20
40
60
100
200
400
600
10^3
2×10^3
4×10^3
6×10^3
10^4
0
0.5
1
1.5
2
MASS ($M/M_\odot$)
A
B
C
D
E
F
G
(a)
(b)
(I)
(II)
(III)
V_β
V_γ

Fig. 6

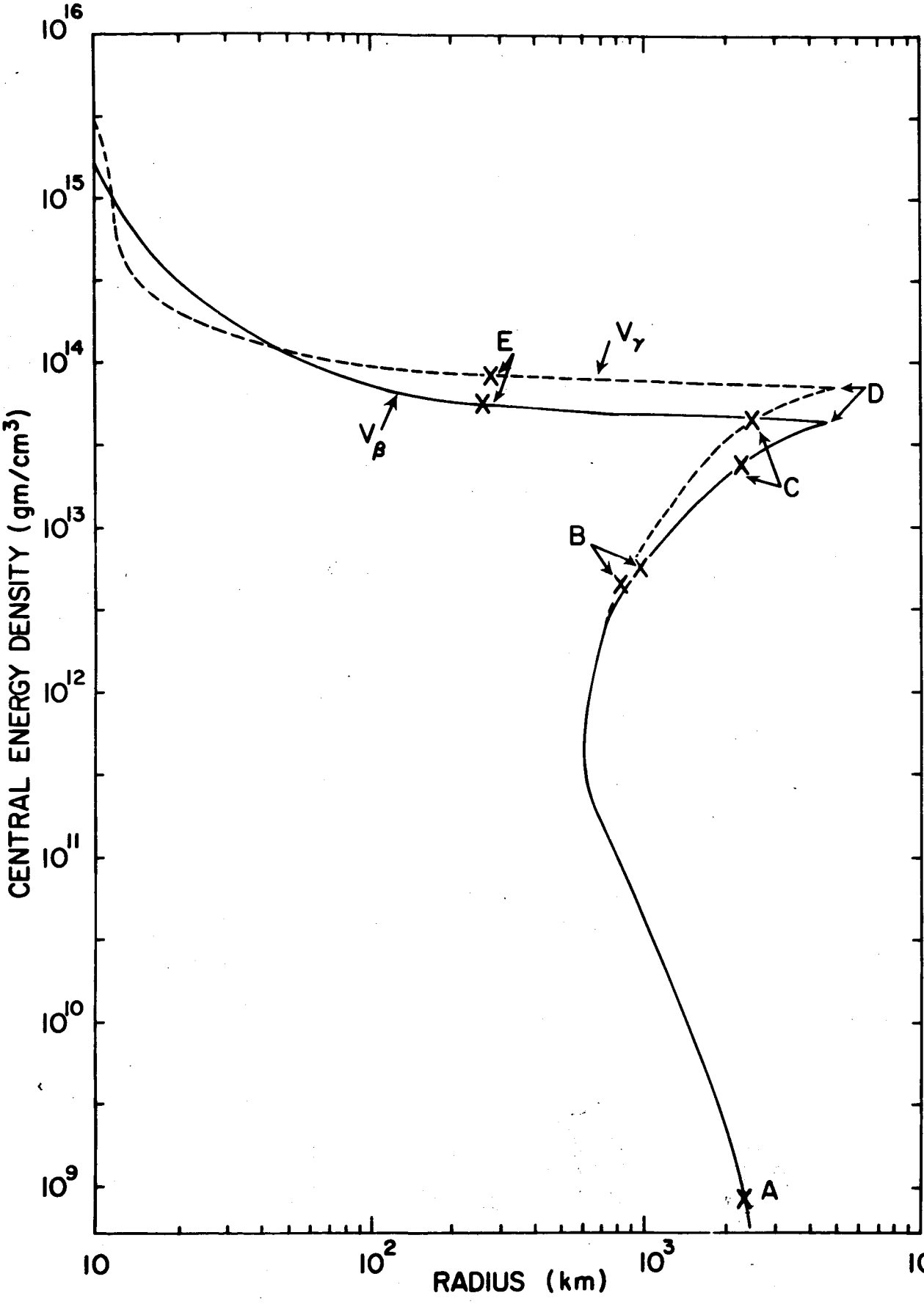
CENTRAL ENERGY DENSITY (gm/cm³)
RADIUS (km)
10¹⁶
10¹⁵
10¹⁴
10¹³
10¹²
10¹¹
10¹⁰
10⁹
10
10²
10³
10⁴
A
B
C
D
E
V_γ
V_β

Fig. 7

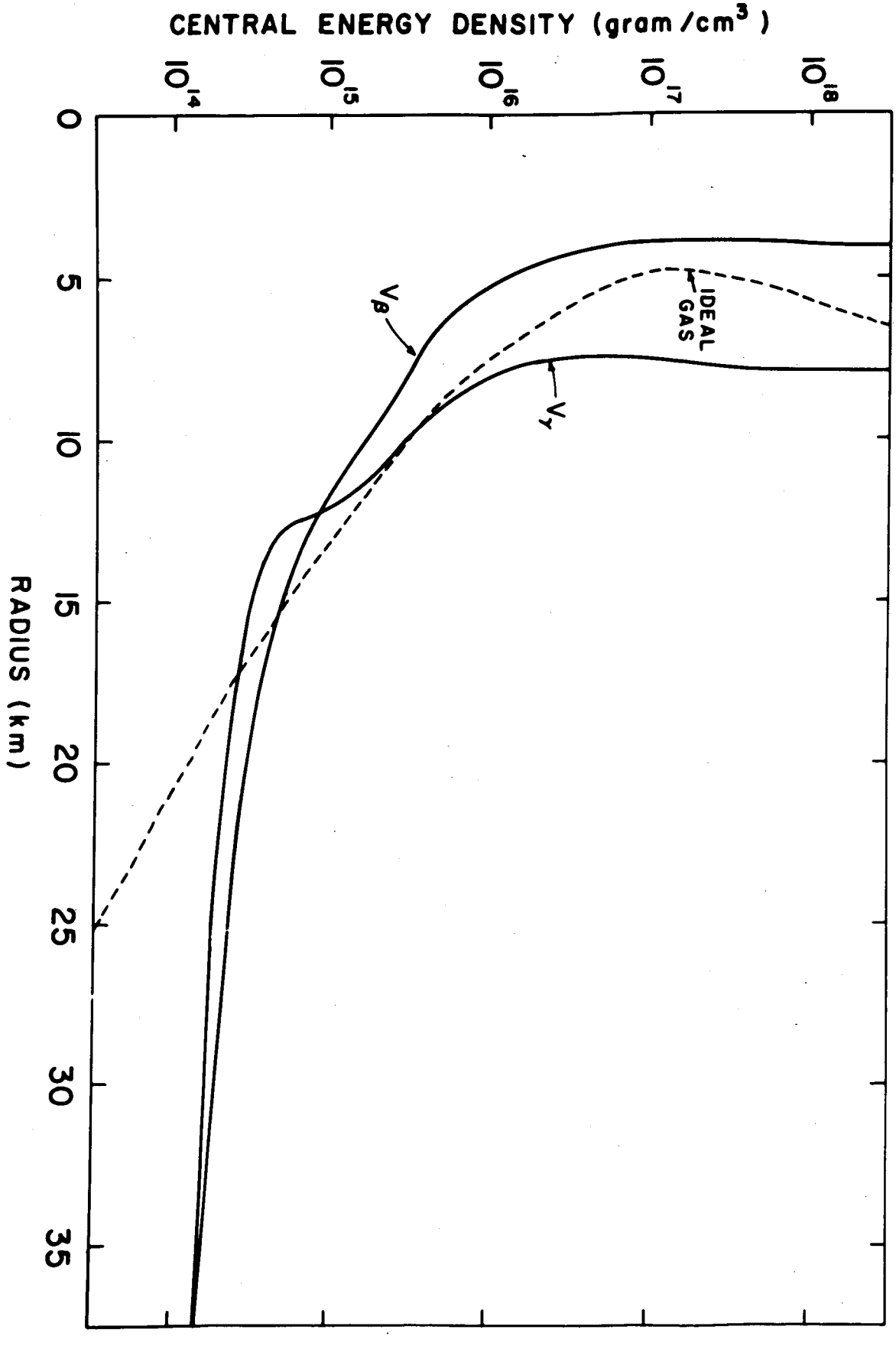
CENTRAL ENERGY DENSITY (gram/cm³)
10¹⁴
10¹⁵
10¹⁶
10¹⁷
10¹⁸
0
5
10
15
20
25
30
35
RADIUS (km)
V_β
V_γ
IDEAL GAS

Fig. 8

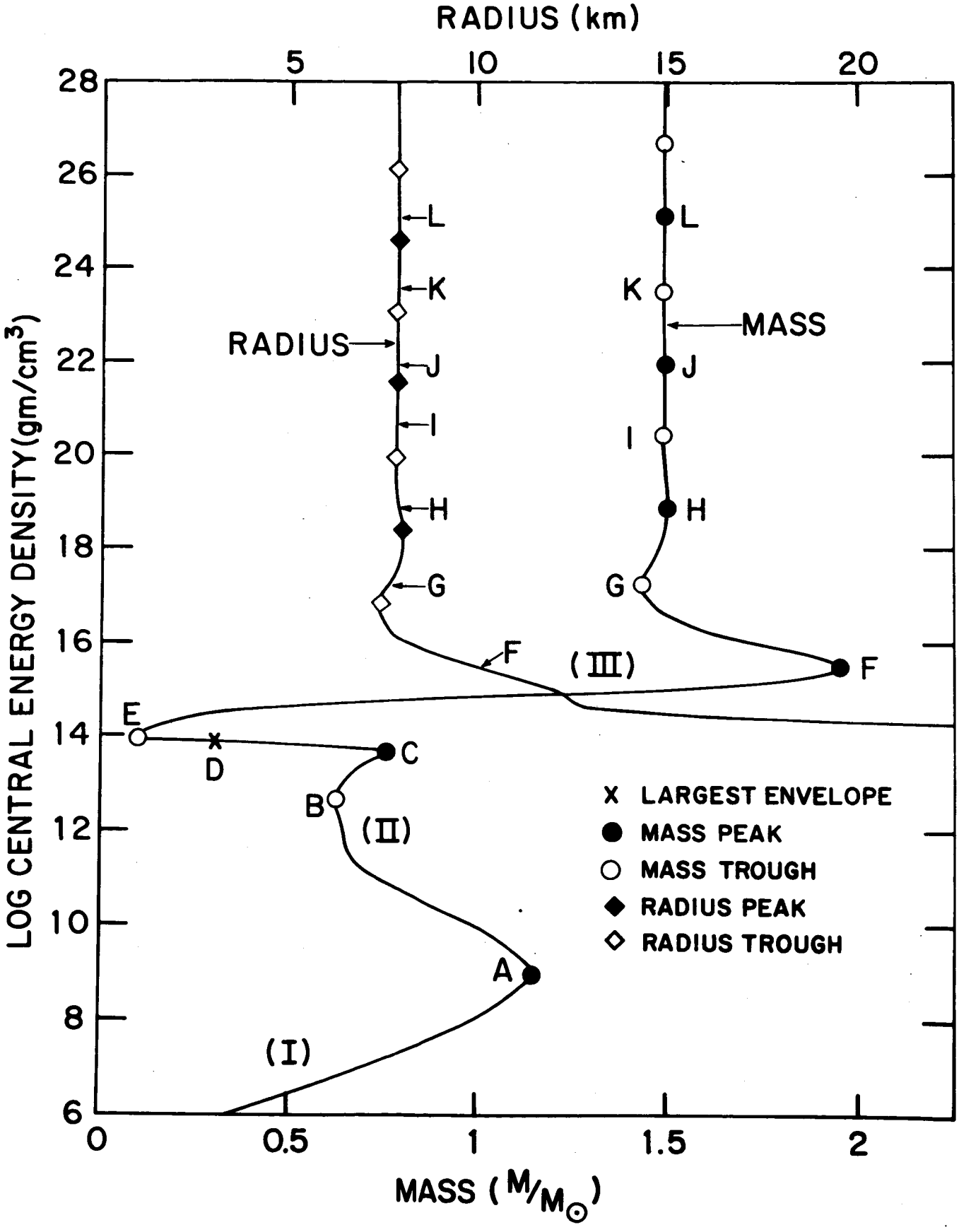
RADIUS (km)
5
10
15
20
28
26
24
22
20
18
16
14
12
10
8
6
LOG CENTRAL ENERGY DENSITY(gm/cm³)
0
0.5
1
1.5
2
MASS (M/M⊙)
RADIUS
MASS
L
K
J
I
H
G
F
E
D
C
B
A
(I)
(II)
(III)
X LARGEST ENVELOPE
MASS PEAK
MASS TROUGH
RADIUS PEAK
RADIUS TROUGH

Fig. 9

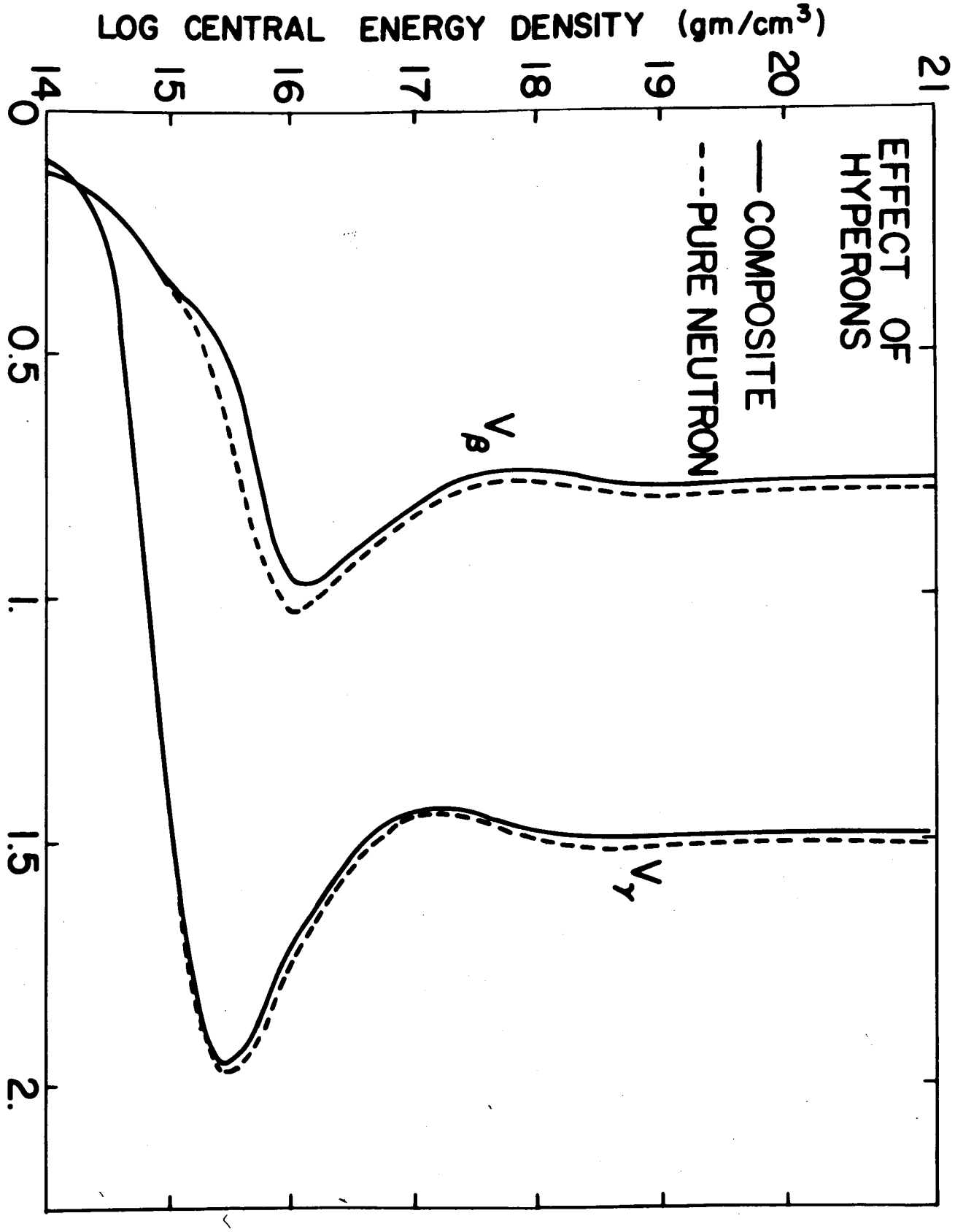
LOG CENTRAL ENERGY DENSITY (gm/cm³)
14
15
16
17
18
19
20
21
0
0.5
1.
1.5
2.
MASS (M/M⊙)
EFFECT OF HYPERONS
—COMPOSITE
---PURE NEUTRON
V_B
V_Y

Fig. 10

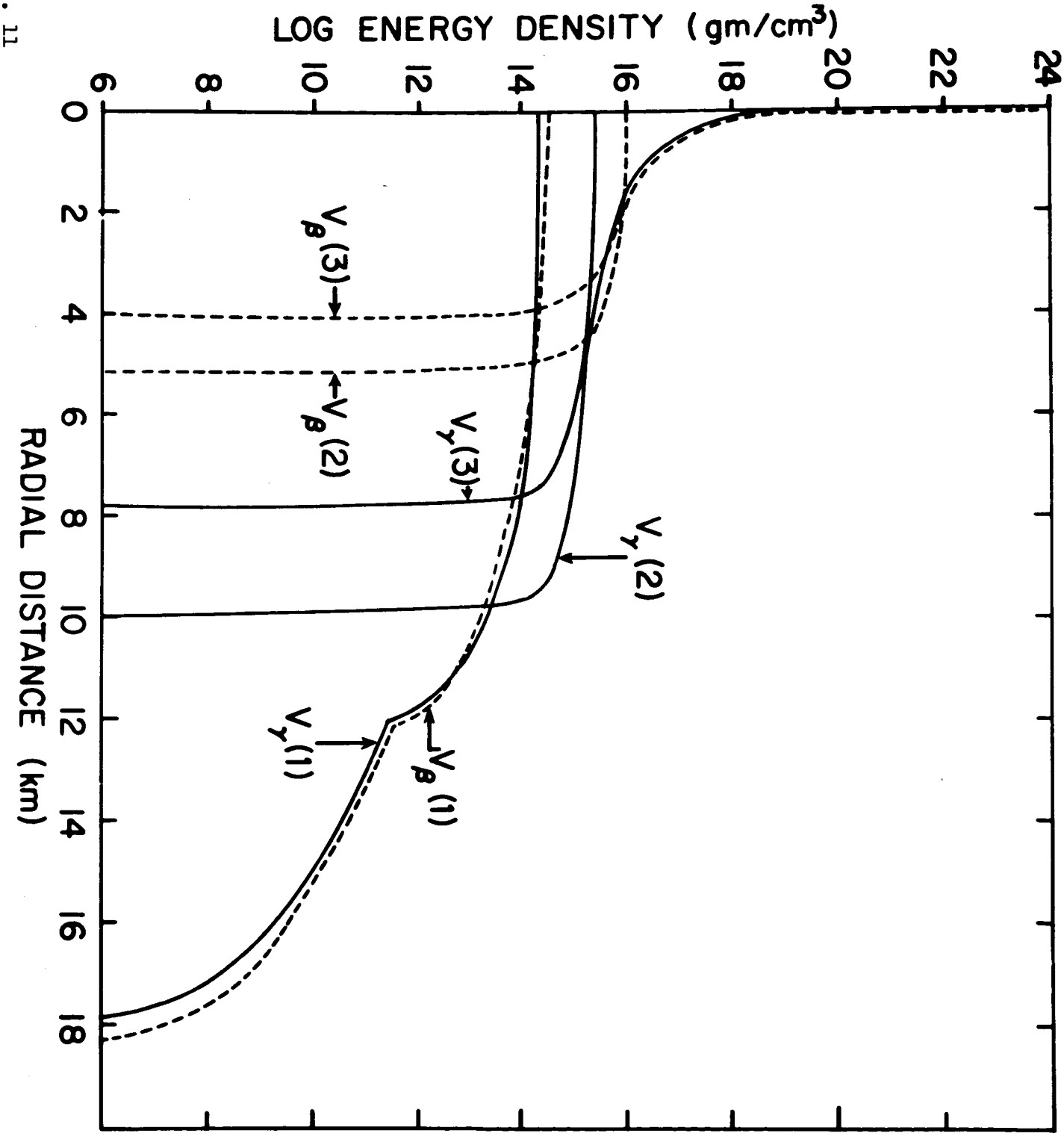
LOG ENERGY DENSITY (gm/cm³)
6
8
10
12
14
16
18
20
22
24
RADIAL DISTANCE (km)
0
2
4
6
8
10
12
14
16
18
V_β(3)
V_β(2)
V_r(3)
V_r(2)
V_r(1)
V_β(1)

Fig. 11

10. COOLING AND DETECTABILITY OF NEUTRON STARS

Sachiko Tsuruta
Smithsonian Astrophysical Observatory, Cambridge, Mass.;
Physics Department, Columbia University, New York, N.Y.;
and Institute for Space Studies,
Goddard Space Flight Center, NASA, New York, N.Y.

and

A.G.W. Cameron
Institute for Space Studies,
Goddard Space Flight Center, NASA
New York, New York

ABSTRACT

Surface properties, temperature effects, cooling behavior, and observability of neutron stars have been studied. For this purpose the opacity of the surface layers is calculated both for a pure iron and a pure magnesium composition. It is found that the non-degenerate layers are only a few meters thick and in no case exceed 1% of the stellar radius. The star cools mainly through neutrino emission when $T \geq 1 \sim 4 \times 10^8$ °K, but at lower temperatures the cooling is primarily through electromagnetic radiation. The neutrino cooling mechanisms included were the neutrino plasma process, the URCA process, and the neutrino bremsstrahlung process. The cooling behavior is quite complicated. The rate of cooling generally depends on mass, nuclear potential, and surface composition, among which the dependence on mass is the most significant. It will be hard to observe low mass neutron stars due to fast cooling rates. However,

medium and high mass stars should still have temperatures exceeding about 2×10^6 °K on the surface for times of the order of 10^3 to 10^5 years. Hence it should not be impossible to observe massive neutron stars relatively close to us, if there is no x-ray emission of larger flux coming from the surrounding region.

INTRODUCTION

From studies of nucleosynthesis and stellar evolution it appears likely that the remnants of some supernova explosions will probably contain a central core of highly condensed matter of the order of nuclear density whose main composition is neutrons, and of surrounding envelopes of ejected material which are expanding continuously (Arnett 1966, Cameron 1959 a, b, 1965a, Chiu 1964, Colgate and White 1965, Zwicky 1938, 1939, 1958). The central core, which may become as hot as $\sim 10^{11}$ °K at the peak, will cool down to $\sim 10^9$ °K within $\sim 10^{-5}$ sec or so (Chiu 1964), due to the extremely high rates of neutrino cooling. Whether the remnant, if a stable neutron star, will ever be detectable depends critically on the cooling behavior of the neutron star itself and on physical conditions in the ejected envelope.

When the first, crude, information on the recently

discovered galactic x-ray sources became available (Bowyer, Byram, Chubb and Friedman 1964 a, Giacconi, Gursky, Paolini and Rossi 1962, 1963, Fisher and Meyerott 1964), it was tempting to identify these x-ray sources with neutron stars, for a neutron star of photospheric temperature $T_e \sim 10^6$ to 10^7 ^oK would emit soft x-rays with peak near $30 \sim 3$Å if it can be regarded as a black body. The first series of cooling calculations showed that neutron stars of this range of temperature can be sufficiently luminous and last sufficiently long to be consistant with the early observational data (Chiu and Salpeter 1964, Morton 1964, Tsuruta 1964). In the meantime, possible cooling mechanisms have been reexamined and some faster cooling mechanisms have been proposed (Bahcall and Wolf 1965 a, c, Finzi 1965a, Tsuruta and Cameron 1965 a). The results of our latest calculations (whose details are given in this paper) indicate that a neutron star with $T_e \sim 10^7$ ^oK will cool too fast, 1 day to 10 years (for models of different mass), to be detected as x-ray sources, but that if $T_e \sim 2 \times 10^6$ ^oK, the medium and high mass stars will last sufficiently long for detection ($\sim 10^{3\sim5}$ years). The conclusion is that the cooling rate alone does not exclude the possibility that some neutron stars will be detectable, provided that the thermal soft x-ray emission exceeds the nonthermal background from the ejected envelope.

If we look at a bare neutron star in a vacuum, there would be several characteristic features which could be checked. For instance, a neutron star (of radius ~ 10 km) should appear to be a point source, and the x-ray spectrum from it should approximate that of blackbody radiation. A lunar occultation measurement conducted by Boyer, Byram, Chubb and Friedman (1964 b) showed that the source in the Crab Nebula has a diameter of about one light year. Clark (1965) and others reported that the same source emits a significant x-ray flux in ~ 30 kev region, which is inconsistant with the spectrum of a blackbody radiation from a surface of a few million degrees. The MIT and American Science and Engineering group and the Livermore group reported that the spectrum of the strongest x-ray source in Scorpius is inconsistent with the hypothesis of blackbody radiation (Giacconi, Gursky and Waters 1965, Chodil, Jopson, Mark, Seward and Swift 1965). These observational results seem to indicate that the observed x-rays from some sources do not consist alone of blackbody radiation from a neutron star. However, we cannot conclude that these results are evidence against the existence of neutron stars.

One of us (Cameron 1965 b) suggested that a possible model of an x-ray source may be a vibrating neutron star with an associated magnetosphere and surrounding hot

gas clouds. (Also, see Finzi 1965 b). The central neutron core may emit thermal x-rays and the surrounding area may emit non-thermal x-rays (either synchrotron radiation or bremsstrahlung). The question of whether the observed x-rays are thermal, non-thermal, or a mixture will require more extensive observations. Some of the recent experiments quoted above only suggest that the thermal component is not the main contribution to the observed x-rays, and that the effects from the surrounding envelopes are dominant. The problem of whether we can distinguish between the thermal component from the neutron star and the non-thermal components from the surrounding area will be considered in the last section of this paper. As long as there is a possibility that neutron stars are related to the galactic x-ray source, directly or indirectly, the study of neutron stars will continue to be of astronomical importance, as well as of fundamental importance in general relativistic physics.

In our earlier paper (Tsuruta and Cameron 1966) properties of neutron stars which are independent of temperature were studied. Here we discuss some thermal properties of these neutron stars. For this purpose six typical models have been chosen from our first paper. Three of these are

based on the V_β type of nuclear potential, and the other three are based on the V_γ type of potential. The different types of potential correspond to different assumptions about the possible nuclear forces which will govern the interactions between the constituent baryons. Among the three models for each type of potential, one is of low mass at the low density base of the principal mass peak, one is half-way up the peak, and the other is near the top of the peak. The characteristic properties of these models are listed in Table 1. Each model is designated by its potential type and approximate mass value. It has been suggested that a model with density $\rho > 8\ \rho_{nucl}$ (ρ_{nucl} is the nuclear density=3.7×10^{14} gm/cm^3) is unreliable (Bahcall and Wolf 1965 a, b) due to the uncertainty in high energy physics. Our model (V_β, $1M_\odot$) is denser than this critical limit. However, all other models lie roughly within the limit of validity and the general conclusions deduced from these models are expected to be reasonably reliable.

Typical models of quite different mass value and nuclear potential have been chosen in order to avoid as far as possible the danger of drawing general conclusions from limited assumptions. The main approach was, therefore, to set upper and lower limits which define the range where the most probable models of neutron stars would lie.

In the following sections the surface properties of neutron stars will be studied first, the cooling and related calculations will be presented, and finally the problem of detectability will be discussed.

ENVELOPE STRUCTURE EQUATIONS

The structure equations for the outer layers of a neutron star are:

$$\frac{dP_r}{dr} = -\frac{[P_r/c^2 + \rho(r)]G(4\pi r^3 P_r/c^2 + M_r)}{r(r-2M_r G/c^2)} \tag{1}$$

$$\frac{dM_r}{dr} = 4\pi r^2 \rho(r) \tag{2}$$

For radiative equilibrium or electron conduction:

$$\frac{dT_r}{dr} = -\frac{3}{4\,ac}\,\frac{\kappa(r)\,\rho(r)}{T_r^3}\,\frac{L}{4\pi r^2} \tag{3}$$

For convective equilibrium:

$$\frac{dT_r}{dr} = \left(1-\frac{1}{\Gamma}\right)\frac{T_r}{P_r}\,\frac{dP_r}{dr} \tag{4}$$

where M_r, T_r, P_r, $\rho(r)$ and $\kappa(r)$ are the mass, temperature, pressure, density and opacity at a distance r from the center, L is the total luminosity of the star, G is the constant of gravitation, a is Stefan's radiation constant, c is the velocity of light, and Γ is the ratio of the specific heats c_p/c_v. The assumption was made that the star is spherically symmetric and in hydrostatic equilibrium and that there is no

energy generation or sinks in the envelope. The general relativistic expressions are used in the hydrostatic equations (1) and (2) because the general relativistic effects are quite important even near the surface for some of the denser stars (Tsuruta and Cameron 1966).

Near the surface, the above equations are more easily integrated in electronic computers if they are expressed in logarithmic form, and it is better to use pressure as an independent variable because the pressure gradient is quite high near the photosphere of neutron stars. Then Eqs. (1)-(3) can be expressed as:

$$\frac{d(\ell n r)}{d(\ell n P_r)} = - \exp\ (\ell n P_r + \ell n A - \ell n B - \ell n G - \ell n D) \tag{5}$$

$$\frac{d(\ell n M_r)}{d(\ell n P_r} = - \exp\ (3\ \ell n r - \ell n M_r + \ell n\left(\frac{4\pi}{G}\right) + \ell n \rho(r) + \ell n P_r + \ell n A - \ell n B - \ell n D) \tag{6}$$

$$\frac{d(\ell n T_r)}{d(\ell n P_r} = \exp\ [\ell n(3/16\pi acG) + \ell n\ (r) + \ell n\, P(r) + \ell n L - 4\ell n T - \ell n r + \ell n P_r + \ell n A - \ell n B - \ell n D] \tag{7}$$

where

$$A = \exp\ (\ell n r) - \exp\ (\ell n 2 + \ell n M_r - 2\ell n c + \ell n G)$$

$$B = \exp\ (\ell n \rho(r)) + \exp\ (\ell n P_r - 2\ell n c) \tag{8}$$

$$D = \exp\ (\ell n M_r) + \exp\ (\ell n 4\pi + 3\ell n r + \ell n P_r - 2\ell n c)$$

The equation of state in non-degenerate layers is

$$P = \left(\frac{1}{\mu_e} + \frac{1}{\mu_{ion}}\right)\frac{\mathcal{R}\rho T}{H} + \frac{1}{3}\,a\,T^4 \tag{9}$$

where the first term is the gas pressure and the last term is the radiation pressure. In degenerate envelopes, all pressures except the degenerate pressure of electrons are negligible and the following equation for degenerate electron gases is applicable:

$$P=A\,f(\chi); \qquad \rho = n\mu_e H = B\,\chi^3, \qquad \chi = P_F/m_e c$$

$$f(\chi)=\chi(2\chi^2-3)\,(\chi^2+1)^{\frac{1}{2}}+3\,\sinh^{-1}\chi$$

$$A=\pi m_e^4 c^5/(3h^3) = 6.01\times10^{22}, \quad B=8\pi m_e^3 c^3 \mu_e H/3h^3 = 9.82\times10^5 \mu_e. \tag{10}$$

μ_e and μ_{ion} are defined as

$$\mu_e = \left[\sum_{\mathcal{R}} A_{\mathcal{R}}\, n(A_{\mathcal{R}}, Z_{\mathcal{R}})\right] \Big/ \left[\sum_i Z_i\, n(A_i, Z_i)\right]$$

$$\mu_{ion} = \left[\sum_{\mathcal{R}} A_{\mathcal{R}}\, n(A_{\mathcal{R}}, Z_{\mathcal{R}})\right] \Big/ \left[\sum_i n(A_i, Z_i)\right] \tag{11}$$

where $n(A_i, Z_i)$ is the number density of the nucleus i of mass number A_i and atomic number Z_i, H is the proton mass, and the remaining notation is conventional. The equilibrium composition of matter as found by Tsuruta and Cameron (1965b) was used. In the envelopes of neutron stars the equation of state is relatively simple as shown above, but the behavior of the opacity is quite complicated. For this reason, the opacity is treated separately in the next section. Generally,

great care has to be taken in evaluating Γ if the envelopes are in convective equilibrium. However, as is shown later, convection appears to play no role in neutron stars.

To obtain a proper boundary condition at the surface, it was assumed that the ordinary theory of stellar atmospheres would apply in the atmospheric layers above the surface of neutron stars, provided that general relativity effects are correctly taken into account in some of the denser models. The surface of the star is defined as the point where the actual temperature is equal to the effective temperature T_e (the temperature of the black body which would radiate the same flux as the star itself). Then the total luminosity of the star L is expressed as

$$L = 4\pi\sigma R^2 T_e^4 \quad , \tag{12}$$

σ is Stefan's constant.

If we assume that the opacity is independent of both height and wave length in the atmosphere but that it has the constant value determined at the photosphere, the theory of radiative transfer in stellar atmospheres leads us to the following simple relation:

$$P_{ph} = \int_0^{\tau_s} \frac{g(P_{ph}, \rho_{ph})}{\kappa(\rho_{ph}, T_e)}\, d\tau = \frac{2}{3}\,\frac{g(P_{ph}, \rho_{ph})}{\kappa(\rho_{ph}, T_e)} \tag{13}$$

where τ_s is the optical depth at the surface, (ρ_{ph}, T_e) is the

opacity at the photosphere and the general relativistic form of $g(P_{ph}, \rho_{ph})$ is:

$$g = \frac{GM}{R^2}\left(\frac{P_{ph}}{\rho_{ph} c^2} + 1\right)\left(1 + \frac{4\pi R^3 P_{ph}}{Mc^2}\right)\left(1 - \frac{2GM}{Rc^2}\right)^{-1}. \tag{14}$$

The subscript ph stands for the value of the respective variable at the photosphere. Noting that the mass content and the thickness of the atmosphere of neutron stars are negligible, the radius and the gravitational mass of the cold models of neutron stars can be used for R and M above. Then equations (9), (13) and (14) evaluated at the photosphere give us sufficient boundary conditions at the surface of a neutron star of surface temperature T_e.

OPACITY

The total opacity κ in a neutron star can be expressed as

$$\frac{1}{\kappa} = \frac{1}{\kappa_R} + \frac{1}{\kappa_c} \tag{15}$$

where κ_R and κ_c are the radiative and conductive opacity, respectively. Radiative opacity is due to the various processes of atomic and molecular absorption, emission, and scattering of radiation in which electrons play the major role. The relative importance of these processes depends strongly on the temperature-density combination. For instance, in matter of high temperature and of relatively low

density, electron scattering is dominant, while in the region of intermediate density and temperature the various photo-electric effects are the most important. In degenerate matter of high density, electron conduction is the most efficient mechanism. The major processes of atomic absorption are the bound-free, free-free, and bound-bound processes. Excited electrons emit photons in the inverse processes. The scattering processes are Thomson scattering if $T \leq 5 \times 10^8$ ^{o}K and Compton scattering for higher temperatures.

The opacity generally depends on density and temperature in quite a complicated way. In recent years, various extensive tables based on detailed computations have been published which give the absorption coefficient for many different compositions and for a large number of points in the temperature-density diagram. The most accurate method of obtaining opacities at present appears to be through use of the computer code for opacities constructed by A.N.Cox and his colleagues of the Los Alamos Scientific Laboratory (Cox, 1961), which includes most of the possible major processes contributing to opacity, and this code was kindly made available for our calculations. It includes bound-free and free-free abosrption, electron scattering (both Thomson and Compton scattering), negative ion absorption

and electron conduction. The bound-free absorption depends on the equilibrium number of electrons which are bound in the various atomic states. When the ionization of one element is completed, no more bound-free absorption due to that element can occur. For high densities the effect of degeneracy is taken into account in all but the electron scattering term. At low densities and low temperatures not all electrons are ionized. An ionization code was used in conjunction with the opacity code in these regions to calculate the degree of ionization, the partial pressure of electrons, and the number of free electrons in the opacity calculations.

At temperatures above about 5×10^7 ^{o}K, almost all elements are ionized. The existing tables are used to obtain absorption cross sections for various kinds of processes. The electron scattering term is obtained for the non-degenerate case, and pair production of electrons and positrons is not considered. Therefore, the opacity is independent of density but dependent on temperature in the high temperature region where Compton scattering is dominant. Different approximations are applied for different degrees of degeneracy to evaluate the conductive opacity.

Values of the opacity were calculated for a pure iron

composition and a pure magnesium composition, in the range of temperature from $10^{3.7}$ ^{o}K to 10^{10} ^{o}K, and of density from $10^{-4.3}$ gm/cm^3 to 10^{14} gm/cm^3. The reason for these particular choices of composition is explained in the next section. Opacities at densities higher than 10^{14} gm/cm^3 have not been included because degeneracy sets in at densities far below this. Calculations at temperatures higher than 10^{10} ^{o}K has not been carried out because the assumptions of nondegenerate electron scattering and no electron-positron pair creation cause serious errors there. Also, neutron stars of temperature higher than this are of no interest to us because they would cool too quickly. The case $T_e < 10^{3.7}$ ^{o}K and $\rho < 10^{-4.3}$ gm/cm^3 was not included because the opacity code did not work in these low temperature, low density regions.

Results obtained are plotted in Figure 1. The solid curves represent the opacity of iron 56 as a function of density at different temperatures, while the dashed curves represent the same for magnesium 24. The opacity shows quite a complicated dependence on density and temperature in the region $\rho \leq 10^{6}$ gm/cm^3 and $T \leq 10^{8}$ ^{o}K, where the transition from electron scattering or electron conduction to bound-free opacity occurs. The almost straight horizontal lines for $T \geq 10^{9}$ ^{o}K and $\rho \leq 10^{6}$ gm/cm^3 are due to Compton scattering. The almost straight lines of negative slope in the region

of high density are an indication that electron conduction is the dominant factor in the transport of energy there. We can assume that degeneracy starts as soon as the opacity in Figure 1 starts to follow one of these straight negatively sloping lines. The opacities ($\ln\kappa$) thus obtained have been stored as an input deck of cards in the form of a two-dimentional table corresponding to given $\ln T$ and $\ln\rho$ combinations, for later use.

The results from the opacity code calculations were checked in the various asymptotic regions of density and temperature, using simpler, analytic approximations. In the region where photoelectric effects are dominant, the Kramers opacity formulae (see, for instance, Schwarzschild 1958) were used. The opacity due to electron scattering was checked through the equations given by Sampson (1959). In order to check the opacity in the region of electron conduction the relations in Schatzman (1958) were used. The agreement was quite satisfactory. It turned out that the neglect of degeneracy and electron-positron pair creation in the formulae for electron scattering in Cox's opacity code causes no serious errors in the problem of neutron stars.

ENVELOPES AND THEIR CHARACTERISTICS

A computing program has been prepared for the 7094 computer which carries out the surface integrations and other related computations automatically. The program was constructed so that the equation of state automatically switched over from Equation (9) to (10) as soon as the point was reached where these two became equal. The surface boundary values were calculated through the subroutine for the atmosphere whenever a new set of values of radius R, mass M and photospheric temperature T_e of the star were given. The interval of integration $\Delta \ln P$ was automatically adjusted so that the change of every variable was kept smaller than a suitable preassigned limit. For a given ln T and ln ρ combination the corresponding opacity ($\ln\varkappa$) was obtained by linear interpolation in the input opacity table. The surface boundary values of two typical models of stable neutron stars (V_β, 0.6 $M_\odot$) and (V_γ, 2 $M_\odot$) with a pure iron atmosphere are shown in Table 2.

To determine the temperature distribution in a typical neutron star envelope, the integration was first carried out from the photosphere down to the point where $\rho=10^{14}$ gm/cm^3, for a representative model of M=1 $M_\odot$ and R=10 km. This was repeated at several different surface temperatures. The results are shown in Table 3. The temperatures at different

densities are listed in terms of the given surface temperature T_e. T_b and ρ_b are the temperature and density where degeneracy starts (where equation (9) gives the same pressure as equation (10)). Degeneracy starts at about $\rho_b=10^6$ gm/cm^3 when $T_e\sim10^7$ ^oK. But when the surface has cooled down to about 10^6 ^oK, degeneracy sets in at $\rho_b=10^4$ gm/cm^3. A significant result is that even after the degeneracy boundary has been passed, the temperature still continues to go up as we go inwards. The fractional rise in temperature as the density increases from 10^6 to 10^9 gm/cm^3 is about 10% when $T_e=7.7\times10^5$ ^oK, but at $T_e=10^7$ ^oK the temperature at the point $\rho=10^9$ gm/cm^3 is about 3 times that at $\rho=10^6$ gm/cm^3. As we go in toward the center from the point with $\rho=10^9$ gm/cm^3 to $\rho=10^{12}$ gm/cm^3, the fractional rise in temperature is about 0.5% for $T_e=10^6$ ^oK and about 3% for $T_e=10^7$ ^oK. The table shows that the temperature gradient is completely negligible for density higher than about 10^{12} gm/cm^3. The conclusion is that the temperature gradient is very high in the outermost thin non-degenerate layers; the temperature continues to rise as we go through the degenerate outer layers of heavy ions and electrons, but the inner neutron core (with $\rho\gtrsim 10^{12}$ gm/cm^3) is isothermal even for the models of the hottest neutron stars. Hence, the core temperature T_c (which

is also the central temperature of the star) can be defined as that temperature where $\rho=10^{12}$ gm/cm^3.

The central temperatures are plotted against surface temperatures in Figure 2. The solid curves are for Fe and the dashed curves are for Mg atmospheres. Curves drawn for three models of the V_ν type are marked by the corresponding mass. Similar but simpler calculations were made by Chiu and Salpeter (1964) and Morton (1964). Their central temperature was defined to be the temperature where the degeneracy sets in (our T_b), but we have noted that the temperature continues to rise considerably as we go inwards passing the degeneracy boundary ($T_c \rangle T_b$). Therefore, our central temperature should be higher than their values in general. However, in high temperature regions where the electron scattering is the most important mechanism for the opacity, they used the constant value $\kappa \sim 0.2$ cm^2/gm, Thomson scattering opacity, while the Compton scattering included in Cox's code which we used lowers the opacity from the constant value of Thomson scattering. This, in effect, lowers our values of central temperature. These two causes of discrepancy compensate one another and there is good general agreement among our results and their results for $T_c \rangle 10^9$ ^oK. We see in Figure 2 that the central temperature is somewhat lower for Mg than Fe at the

same surface temperature. This is due to the fact that somewhat lower opacities are associated with Mg than Fe as is revealed in Figure 1. For some of the coolest neutron stars ($T_e \sim 10^4$ ^oK) the central temperature is only about 10 times the surface temperature, while for hot models (of $T_e \sim 10^7$ ^oK) the core is about 100 times as hot as the surface. In any case, however, the ratio of the central temperature to the surface temperature is quite small as compared with that of ordinary stars.

To examine the region near the surface more in detail, temperature is plotted against distance from the photosphere as measured inward in Figure 3. Each curve is marked by the surface temperature. The model with one solar mass and 10 km radius is used to illustrate the general behavior of the surface properties. The crosses marked by $\chi=2.5$ represents points where the degeneracy starts. This criterion for degeneracy is derived from the fact that the kinetic energy of a non-relativistic fermion (about 3/5 of the Fermi energy E_F) and the thermal energy of a free particle with no internal degrees of freedom (3kT/2) should be equal at the boundary between the non-degenerate and degenerate layers. The result of the present calculations shows that even for the hottest models degeneracy starts before we go inward by 100

meters from the surface and that the non-degenerate layers are less than 1% in thickness for even the hottest models. The mass contained in the non-degenerate envelopes is practically zero. In our previous paper (Tsuruta and Cameron 1966) it is seen that the amount of mass contained even in the inner degenerate electron-ion envelopes is very small compared to the total stellar mass. These results more than justify our previous assumption of constant mass and radius in the atmospheric calculations and also the neglect of non-degenerate layers in determining the total mass and radius of the star in our previous paper (Tsuruta and Cameron 1966). Hot neutron stars with $T_e \sim 10^7$ °K have non-degenerate envelopes of about 10~20 meters thick but when the surface temperature falls to about a million degrees the thickness of the non-degenerate layers becomes only about a meter or so. A typical neutron star with the sun's mass, 10 km radius, and 6.7×10^6 °K at the surface (with $\sim 100 L_\odot$) is shown to have non-degenerate envelopes of 3~4 meters.

The density profile near the surface is plotted in Figure 4 for the same model. The distance from the surface is now shown in centimeters. Within about a meter (0.01% of the radius) from the photosphere, the density rises to about 10^5 gm/cm^3 when $T_e \sim 10^6$ °K and to about $10^{2.5}$ gm/cm^3 for

hotter stars (T_e=1.6x10^7 ^oK). In the photosphere the density rises within a thickness of 10 cm by a factor of about 100 for typical models (T_e~10^6 ^oK). In any case a sharp drop of density from the central value (10^{14} ~10^{15} gm/cm^3) to the photospheric value (0.01~1 gm/cm^3) occurs only at the very edge of the star.

The distribution of density, temperature and degree of degeneracy E_F/kT within the thin layers about 10 meters from the surface are numerically shown in Table 4 at several interesting values of surface temperature. On comparing this table with the previous one, we see that the degeneracy criterion used in these two tables agrees well with each other.

The conclusion according to the present calculation is that neutron stars of about 10^3 times solar luminosity are as hot as 10^7 ^oK at the surface and about 10$^{9\sim10}$ ^oK in the interior, those which are as luminous as the sun (in the x-ray region) are about 1~2x10^6 ^oK at the surface and about 10$^{8\sim9}$ ^oK in the interior, and that by the time they cool down to the point where T_c~10$^{6\sim7}$ ^oK and T_e~10^5 ^oK they are too faint to be detected (L~10^{-5} $L_\odot$). In our previous papers (Tsuruta and Cameron 1965b, 1966) it was shown that the composition of the surface layers changes sharply from layer to

layer. Starting from the boundary between the neutron core and the degenerate electron-ion envelopes the composition changes from more neutron-rich heavy nuclei to less neutron-rich ones as we go outwards. In the outermost non-degenerate layers with $\rho<10^6$ gm/cm^3, the main equilibrium composition should be ordinary iron group nuclei. This is why iron was chosen in our opacity calculations.

A possible change of surface composition can occur if a diffusion process is present. The diffusion process can become quite efficient in the presence of very small density scale heights and large gravity effects, as is the case in the atmospheres of neutron stars. Rough estimates of the effect of diffusion on the surface composition of neutron stars were made by Chiu and Salpeter (1964). Their conclusion is that some lighter elements such as Mg, O and Ne can be present on the surface of neutron stars. This is why not only Fe but also Mg was selected in our opacity and atmospheric calculations earlier. The change of composition will not occur if convective mass motions in non-degenerate layers cause efficient mixing of elements. In this case the original statistical equilibrium composition of iron will be maintained. However, convection appears to play no important role in neutron star problems since

the temperature gradients in our model atmospheres are all subadiabatic. At the present time, the effect of the diffusion is not known. However, the difference between our results for Fe and Mg compositions is relatively small. This indicates that the uncertainty of surface composition due to the effect of diffusion will not cause any serious errors in our results presented in this paper. We will see that the uncertainties due to other effects are far greater.

ENERGY CONTENT OF A NEUTRON STAR

If we assume that a neutron star belongs to the end state of a thermonuclear evolution, there can be no energy generation within it. Any stable neutron star is already so dense that gravitational potential energy due to contraction is not available. Even though the matter is highly degenerate, the only contribution to the total energy of a stationary neutron star comes from the small tail of the Fermi distribution function of the particles which constitute the star. The heat capacity of a nearly zero-temperature ideal Fermi gas was derived by Chandrasekhar (1957). Using his result, the total thermal energy of a neutron star was found to be

$$U=\left[\int_0^R \sum_i \left(\frac{\pi^2\hbar^2}{m_i c^2}\right)\left(\frac{(\chi_i^2+1)^{1/2}}{\chi_i^2}\right) n_i 4\pi r^2 dr\right] T^2 \qquad (16)$$

where $\chi_i = P_i^F/(m_i c)$

m_i, P_i^F and n_i are the mass, Fermi momentum and number density of the i^{th} particle, R is the stellar radius and T is the temperature of the isothermal core. The summation was taken over all the baryons and leptons present in each layer dr. The total energy was calculated as a function of temperature for our models. The results are shown in Tables 5 - 10. It is seen that as the surface temperature of a star decreases from about 5×10^7 ^oK to 10^4 ^oK the energy content of the star decreases from about 10^{50} ergs to 10^{40} ergs, although the precise value depends on the type of model in question.

In the above derivation the nuclear interaction between particles was neglected. The presence of nuclear forces will modify the heat capacity by an amount which typically can be of the order of factor 2, according to rough estimates which we have made. We did not take such modifications into account in making the actual cooling calculations, because the uncertainties arising from other sources are far greater.

NEUTRINO LUMINOSITY

The conserved vector current theory of weak interactions predicts that neutrino-antineutrino pairs can be radiated in quantum electrodynamic processes as well as electromagnetic

radiation. Even though the probability for the neutrino radiation is enormously small, it plays an extremely important role in some stages of stellar evolution because of the fact that the neutrino mean free path is so large that it can escape even from a dense star with hardly any interaction, while electromagnetic radiation can only diffuse out very slowly from the interior to the surface. Various different neutrino processes possible in a stellar interior have been examined. Consequently, the following three processes have been found to be the most important in the problem of neutron stars.

(1) Neutrino pair emission from the plasma process:

(17) $$\gamma(\text{plasmon}) \rightarrow \nu_e + \bar{\nu}_e$$

These neutrinos arise from the decay of plasmons in the degenerate electron gas in the interior of the neutron star. The rates are given by (Adams, Ruderman and Woo 1963, Inman and Ruderman 1964):

(18)
$$Q_{pl}\ (\text{ergs/cm}^3\text{-sec}) = 1.228\times10^{22}\left(\frac{\hbar\omega_o}{m_e c^2}\right)^9 F(\chi)$$

where
$$F(\chi)=\sum_{n=1}^{\infty}\frac{K_2(n\chi)}{n\chi} \quad \text{or}$$

$$\chi^3 F(\chi)=2\zeta(3)+\tfrac{1}{2}\chi^2\ell n\chi-\tfrac{1}{4}(2\ell n2+1)\chi^2+\chi^4\frac{\ell n\chi}{96}$$

$$-\frac{1}{96}\left(\ell n\ 2-\tfrac{1}{4}+\ell n\ 2\pi-\frac{\zeta'(2)}{\zeta(2)}\right)\chi^4 \qquad \text{for } \chi<2\pi$$

$$\zeta(3)=\sum_{n=1}^{\infty}\left(\frac{1}{n^3}\right);\ \zeta(2)=\sum_{n=1}^{\infty}\left(\frac{1}{n^2}\right)=\frac{\pi^2}{6}\ ;\ -\zeta'(2)=\sum_{n=1}^{\infty}\frac{\ell nn}{n^2}$$

$$\chi=\frac{\hbar\omega_o}{kT},\quad \omega_o^2=4\pi e^2\int d^3\bar{P}\,\frac{f(\bar{P})}{E_P}\left(1-\tfrac{1}{3}\frac{\bar{P}^2}{E_p^2}\right)\cong 4e^2P_F{}^3/(3\pi\ E_F)$$

$$E_F = (P_F^2 + m_e^2)^{\frac{1}{2}}, \qquad P_F = (3\pi^2 n_e)^{1/3}$$

for relativistic degenerate electrons. (In the last three equations the units are $\hbar = c = 1$.) Then the neutrino luminosity due to the plasma process is

$$L_\nu^{p\ell} = \int_o^R Q_{p\ell}\, 4\pi r^2 dr \quad \text{(ergs/sec)} \tag{19}$$

To evaluate the above integral, a table listing $F(\chi)$ as a function of χ and the interpolation subroutine were used. The plasma neutrino emission rates have been calculated as a function of temperature and electron number density and are shown in Figure 5.

(2) The URCA process (the beta process and its inverse process): In the interior of a neutron star it can be represented by reactions such as:

$$n + n \rightarrow n + p + e^- + \bar{\nu}_e \tag{20a}$$

$$n + n \rightarrow n + p + \mu^- + \bar{\nu}_\mu \tag{20b}$$

$$n + p + e^- \rightarrow n + n + \nu_e \tag{20c}$$

$$n + p + \mu^- \rightarrow n + n + \nu_\mu \tag{20d}$$

The approximate formulas for the rates of these processes

for a neutron star of uniform density distribution have been derived by Bahcall and Wolf (1965c). We applied their results to our neutron star models. The neutrino luminosity due to the URCA process can then be given by

$$L_\nu^{URCA} = \int_o^R 10^{20}(1+F)T_9^8\ (\rho/\rho_{nucl})^{2/3}\ 4\pi r^2\ dr \quad \text{(ergs/sec)}$$

$$(21)\quad F = P_F(\mu)/\ P_F(e) = [1-2.25(\rho_{nucl}/\rho)^{4/3}]^{1/2} \quad \text{for } \rho > 1.8\rho_{nucl}$$

$$= 0 \quad \text{for} \quad \rho < 1.8\ \rho_{nucl}$$

where ρ is the density of the neutron star matter, ρ_{nucl} is the density of nuclear matter ($= 3.7 \times 10^{14}$ gm/cm^3), T_9 is the stellar temperature in units of 10^9°K, $P_F(i)$ is the Fermi momentum of the i^{th} species.

(3) The neutrino bremsstrahlung process: In the interior of a neutron star it can be symbolically expressed as

$$(22)\qquad e^- + (\text{baryon})^{\pm} \rightarrow e^- + (\text{baryon})^{\pm} + \nu_e + \bar{\nu}_e$$

The neutrino pairs are emitted when electrons scatter from positive or negative baryons in the interior of the neutron star. Ruderman and Festa (private communication) have kindly provided us with the following approximate preliminary expression for this process:

$$(23) \quad Q_B(\text{ergs/gm-sec}) = 10^6 Z^2 \frac{n_z}{n} (T_9)^6 \text{ for } E_F >> mc^2$$

where Z is the effective charge of the electron scattering centers, n_z is the number density of such centers, and n we take here to be the baryon number density. Ruderman and Festa have suggested that there may be proton clustering in neutron star interiors in the presence of very large numbers of neutrons, so that the effective charge of a scattering center might be 2. However, for some of the massive neutron stars in which the density exceeds about 10^{15} gm/cm^3 there will also be a large number of Σ^- hyperons, which may hinder the clustering process. In such a case, we have chosen to take the effective charge of a scattering center to be 1 and to count as the scattering centers both the protons and the Σ^- hyperons. The possible error caused by the uncertainty due to the different interpretation of the scattering centers and the effective charge is in any case negligible in our present problem. The neutrino luminosity due to the bremsstrahlung process is

$$(24) \quad L_\nu^B = \int_0^R Q_B \rho \, 4\pi r^2 \, dr \text{ (ergs/sec)} .$$

The total luminosity is obtained by adding all the contributions

(25) $$L = L_{ph} + L_{\nu}^{p\ell} + L_{\nu}^{URCA} + L_{\nu}^{B} \quad .$$

L_{ph} is the photon luminosity defined by (12).
The results are shown in Tables 5-10. To visualize the contributions of different processes, the three different neutrino luminosities and photon luminosity, together with the total energy, are plotted against the central temperature for the model (V_{γ}, $1.1M_{\odot}$) and shown in Figure 6. At higher temperatures the URCA process and the plasma neutrino process compete with each other but the URCA process is always the most important. At lower temperatures the URCA process competes with the bremsstrahlung process but the plasma process becomes unimportant. At sufficiently low temperatures the bremsstrahlung process predominates over other neutrino processes. The point where the bremsstrahlung rate begins to exceed the URCA rates depends on the stellar mass. For massive stars, this switching occurs at $3\sim8 \times 10^{9}{}^{o}K$, but for low mass stars the switching temperature is $\sim 5 \times 10^{7}{}^{o}K$. Neutrino cooling of any kind becomes too small as compared with the photon cooling when the temperature becomes lower than about $1\sim4 \times 10^{8}{}^{o}K$. Hence, the bremsstrahlung process never becomes important in sufficiently low mass stars ($M \sim 0.2M_{\odot}$).

In the above luminosity calculations we assumed that all neutrino processes not included here are unimportant in neutron stars. Bahcall and Wolf (1965a,c) have raised the question of neutrino cooling from pion decays in neutron star interiors. Such pion decays can occur only if pions should have a small effective mass in the presence of a largely neutron gas. Both Bahcall and Ruderman, as well as others, have indicated to us (private communication) their expectation that, under the conditions in which pions may be present in a neutron star, there will be a predominantly repulsive interaction between the pions and the neutrons. This would raise, rather than lower, the effective mass of the pions, and make it very unlikely that pions will be present in the interiors of neutron stars.

COOLING TIMES

The cooling time τ is computed from the various theoretical data of the last sections and from the following relation:

$$\tau = - \int_{U_1}^{U_2} \frac{dU}{L(U)} \qquad (26)$$

where U is the total energy content of a star and L(U) is the total luminosity, $L_{ph} + \Sigma L_{\nu}$, expressed as a function of U. If the above integration is carried out from the initial energy U_1 to the final energy U_2, τ gives the time interval during which the star has cooled from a higher temperature T_1 where the total energy is U_1 to a lower temperature T_2 where the total energy is U_2. The moment at which a supernova explodes has been defined as the starting point for counting the age of a neutron star.

The results are tabulated in Tables 5 through 10. An important parameter which characterizes the cooling behaviour is the ratio of the central temperature to the surface temperature, a typical value of which is about 100 for a neutron star. Hence we defined α as the ratio of the central temperature to the surface temperature in units of 100, and the values of α for each model at different temperatures are listed in the same tables. We see that this ratio is a sensitive function of mass, temperature, composition and nuclear potential. With increase in mass, α decreases. With increase in temperature, α increases. For the models of the same mass, temperature and nuclear potential, the value of α for Fe models is somewhat larger than that for Mg models.

We see that the detailed behavior of cooling is different for each different type of model and that this difference comes mainly through the sensitive dependence of α on the different kind of model.

Figure 7 shows the cooling curves of our six models with iron atmospheres (solid curves correspond to V_β type and dashed curves to V_γ type models). The point at which the neutrino cooling rate and the photon cooling rate become equal is shown by a cross for each curve. The figure shows that for the same nuclear potential, the neutron stars of lower mass cool faster than those of larger mass up to an age of about 10^6 years, but after that the heavier neutron stars cool somewhat faster.

The complicated effect of the nuclear potential is observed when we compare the curves of the models of the same temperature and mass but of different nuclear potential. To see better the effects of different composition, cooling curves for the same types of model of the same masses but of different compositions are shown in Figure 8. Solid curves represent models with iron atmospheres and dashed curves those with Mg atmospheres. We see that in the region where the neutrino cooling predominates over the photon cooling

the cooling rates of Fe models are somewhat faster than the cooling rates of Mg models, but that the reverse situation is noted in the region where the photon cooling is the main cooling mechanism. This is easily explained if we note that the neutrino cooling and the total energy content of the star depend on the internal temperature while the photon cooling is a function of the surface temperature and that the opacity of Mg atmospheres is somewhat lower than the opacity of Fe atmospheres.

We see in these figures that the models with $T_e \gtrsim 10^7$ °K cool too fast for observation, while the strong absorption of x-rays from a neutron star by interstellar gases makes it very difficult for us to observe neutron stars with $T_e < 10^6$ °K. The star's luminosity itself is already low at $T_e \sim 10^6$ °K (Table 2). Hence the most important range of temperature of neutron stars from the point of view of observation is $10^7 > T_e > 10^6$ °K, and this portion of the curves is enlarged in Figure 9. A neutron star will be only about 1 day to 10 years old when $T_e \sim 10^7$ °K depending on its mass value, nuclear potential and surface composition, but it will take about 2×10^3 to 3×10^5 years before it will cool down to $\sim 10^6$ °K. We note that the effect of mass on cooling time is

the most drastic. The dependence of cooling on the different possible kinds of nuclear potential and composition is by no means negligible when we need detailed theoretical information, but this uncertainty is relatively small as compared with the mass effect. By comparing our present results with the original calculations (Tsuruta 1964) where only the plasma process was taken into account as the neutrino cooling mechanism, we note that the faster rates of cooling by the URCA process and the bremsstrahlung process cause some important effects on the cooling behavior at higher temperatures ($T_e \gtrsim 2\times10^6$ °K), but no significant change is observed when $T_e < 2\times10^6$ °K.

OBSERVATIONAL PROBLEMS

If a neutron star emits radiation as a black body, the wavelength λ_{max} giving the maximum intensity in the spectrum is given by

$$\lambda_{max}(\mathrm{cm}) = hc/(4.9651kT_e) = 0.2918/T_e(^{\circ}\mathrm{K}) \quad . \tag{27}$$

This simple relation indicates that when $T_e \sim 10^6$ to 10^7 °K the maximum comes in the soft x-ray region, $30 \gtrsim \lambda_{max} \gtrsim 3$Å, while this maximum shifts to the ultraviolet region when T_e

falls to around 10^5 - 10^4 °K. From Table 2 we see that a neutron star with $T_e > 10^6$ °K has $L > L_\odot$ ($L_\odot$ is the luminosity of the sun), while $L \sim 10^{-5}\ L_\odot$ to $10^{-9}\ L_\odot$ when $T_e \sim 10^5$ to 10^4 °K. Also it takes about 10^3 to 4×10^5 years before a neutron star cools down to $T_e \sim 10^6$ °K. That is, a neutron star can last sufficiently long to allow our observation in the x-ray regions even though it will be too faint to be seen optically.

Until recently the observation of x-rays from outer space has been prevented due to the fact that the earth's atmosphere is strongly opaque to radiation in the x-ray regions. However, interstellar gases are practically transparent to x-rays of, say, $\lambda \lesssim 30\text{Å}$ (the precise value of the upper limit to the wavelength depends on the distance between us and the x-ray emitter). The above considerations lead us to the conclusion that some of the neutron stars which are sufficiently close to us and which are not surrounded by x-ray emitting gas clouds should be observable as x-ray sources.

Since it became possible to send x-ray detectors above the earth's atmosphere, at least 10 galactic x-ray sources have been discovered (Bowyer, Byram, Chubb and Friedman 1964a,

1964b, 1965, Giacconi, Gursky, Paolini and Rossi 1962, 1963, Fisher and Meyerott 1964). Two major sources which were discovered first which are best known are Sco XR 1, the strongest x-ray source in the constellation Scorpio, and Tau XR 1, a somewhat weaker source near the center of the Crab Nebula. We use the notation of Bowyer, Byram, Chubb and Friedman (1965) to designate x-ray sources. A possible association of the strongest Scorpius source and the North Polar Spur, the nebular remains of a supernova explosion which was supposed to have occurred about 50,000 to 100,000 years ago at a distance of about 30 parsecs away (Brown, Davies and Hazzard 1960), has been suggested, but otherwise there is no nebulosity or peculiar star in the vicinity of Sco XR 1. The Crab Nebula is believed to be the remnant of a supernova explosion which occurred in 1054 AD about 1100 parsecs away from us. The angular size of the Sco XR 1 was determined to be less than 7 minutes of arc (Oda, Clark, Garmire, Wada, Ciacconi, Gursky and Waters 1965), while the size of the x-ray source in the Crab Nebula was measured to be about 1 light year in diameter through the lunar occultation experiment (Bowyer, Byram, Chubb and Friedman 1964b), less than half the size of the optical nebula in the Crab,

while the optical nebula is about two to three times smaller than the radio size. The flux of Sco XR 1 is about 10^{-7} ergs/cm^2 -sec and that of the Tau XR 1 is about 10^{-8} ergs/cm^2 -sec. The intensity of other sources is about the same as that of the source in the Crab Nebula.

All of the x-ray sources, except the Scorpius source, lie close to the galactic plane and within 90^{o} of the galactic center. This distribution resembles that of galactic novae. From this and other evidence it has been suggested that the probable origins of the x-ray sources are supernova outbursts (Bowyer, Byram, Chubb and Friedman 1965, Burbidge, Gould and Tucker 1965, Cameron 1965b,c, Morrison and Sartori 1965, Oda 1965, Hayakawa and Matsuoka 1964, Finzi 1965). Indeed there is no evidence against this assumption. Many important supernovas have not been identified with x-ray sources of strength comparable with that of the Scorpius source or the source in the Crab Nebula. This is easily explained if we note that these supernovas are far more distant from us than the Crab Nebula or the North Polar Spur. Most of the discovered x-ray sources are not identified with known radio or optical objects. This is also no contradiction to the supernova hypothesis if we note the possibility that some of the x-ray production mech-

anisms will have much longer lifetime than that of the optical or radio emissions.

As mentioned already, we believe that a remnant of a supernova explosion consists of a central condensed core in the form of a neutron star and of surrounding hot gas clouds in the form of expanding envelopes. How can we observe this complex assembly of matter? As far as the central core of neutrons is concerned there will be no hope of observation except as the emitter of soft x-rays in the narrow range of about 30 to 3Å, because a hotter neutron star of $T_e > 10^7$ °K (corresponding to x-rays of < 3Å) will cool too fast (within less than a day to 10 years) and a cooler neutron star of $T_e < 10^6$ °K (corresponding to x-rays of > 30Å) will be too faint to be detected due to the strong interstellar absorption and the faintness of the star itself. The situation is more complicated in the expanding envelopes.

Due to the complex nature of a supernova remnant, the observed x-rays can be due to non-thermal radiation from the hot gas clouds, the thermal radiation from the neutron star, or a mixture of both. The question of whether the thermal component can be singled out from the non-thermal component in the case both are present can be determined if the relative

strength of each component is known. In order to make some sensible predictions of the possible nature of some of the x-ray sources and their relation to neutron stars, we will discuss Sco XR 1 and Tau XR 1. The data on other sources are still too scarce for this purpose. If we know the distance d and the photon luminosity L of a neutron star, the flux F of the thermal component of x-rays reaching the region just above our atmosphere is found from

$$F = L / (4\pi d^2) \quad . \tag{28}$$

If we accept the tentative association of the North Polar Spur and Sco XR 1, the distance and the age of the neutron star in Scorpius are known. Taking surface temperatures of 1 or 2×10^6 ^oK, consistent with the soft x-ray fluxes measured by Friedman's group, the photon luminosity of the star can also be predicted. The results for our six models are shown in Table 11. The age of the star τ has been taken from our results in the previous section (Figures 7-9). If both the North Polar Spur and the x-ray source in Scorpius are indeed the remnants of a supernova explosion about 30 parsecs away and about $10^{4\sim5}$ years ago, the low mass models of $M \lesssim 0.3 M_\odot$ should be excluded because they are too young. However, some

massive models are sufficiently old to support this hypothesis. The flux of x-rays from a massive neutron star is also comparable with the observed x-ray flux from the Scorpius source. The result shown in Table 11 gives rise to a possibility that the observed x-rays from the Scorpius source may have a predictable amount of thermal component, if it contains a massive neutron star of about $1 \sim 2M_{\odot}$. The spectral measurements of Sco XR 1 were reported to be inconsistent with the picture of pure black-body radiation. This may suggest that the nonthermal component from the surrounding hot gas dominates over the thermal component from the neutron star sufficiently to obscure the black-body spectrum. However, because of the relatively strong flux from the neutron star as calculated above, the thermal component in this source may be identified, if the remnant star is massive enough, and if longer wavelength detectors can be used which are more sensitive to the peak of the thermal spectrum.

Next, consider the source in the Crab Nebula. Here, τ = 910 years and we get the present temperature and luminosity from the results in the previous sections. The distance is about 1100 parsecs. From this information, the thermal component of the x-ray flux from a neutron star in the Crab Nebula can be obtained. The results are shown in Table 12,

for various models of different mass, nuclear potential and surface composition. We see that, with the exception of the particular model of V_γ type, Mg composition and about 2 solar masses, the flux is less than about 1/4 of the observed x-ray flux from Tau XR 1. The large size of about one light year already indicated that the major source of the x-rays from the Crab Nebula is not thermal emission from a neutron star. The theoretical calculation also supports this view. If a neutron star exists in the x-ray source, it will not be identified if the flux from the neutron star is too weak, as compared with that from the surrounding region.

We are indebted to Mr. B. Sackaroff for assistance with the opacity calculations which involved the use of some parts of the Los Alamos opacity code in regions of temperature and density for which the entire code does not work.

REFERENCES

Adams, J.B., Ruderman, M.A., and Woo, C.H. 1963. Phys. Rev., 129, 1383.

Arnett, W.D. 1966. Thesis, Yale University.

Bahcall, J.N. and Wolf, R.A. 1965a. Phys. Rev. Lett., 14, 343.

_____ 1965b. Phys. Rev., 140, B1445.

_____ 1965c. Phys. Rev., 140, B1452.

Bowyer, S., Byram, E.T., Chubb, T.A., and Friedman, H. 1964a. Nature, 201, 1307.

_____ 1964b. Science, 146, 912.

_____ 1965. Science, 147, 394.

Brown, R.H., Davies, R.D., and Hazzard, C. 1960. Observatory, 80, 191.

Burbidge, G.R., Gould, R.J., and Tucker, W.H. 1965. Phys. Rev. Lett., 14, 289.

Cameron, A.G.W. 1959a. Astrophys. J., 129, 676.

_____ 1959b. Astrophys. J., 130, 884.

_____ 1965a. Lecture notes at Yale University.

_____ 1965b. Nature, 205, 787.

_____ 1965c. Nature, 206, 1342.

Chandrasekhar, S. 1957. An introduction to the study of stellar structure (Dover, New York).

Chodil, G., Jopson, R.C., Mark, H., Seward, F.D., and Swift, C.D. 1965.

Phys. Rev. Lett., 15, 605.

Chiu, H.Y. 1964. Annals of Phys., 26, 364.

Chiu, H.Y. and Salpeter, E.E. 1964. Phys. Rev. Lett., 12, 413.

Clark, G.W. 1965. Phys. Rev. Lett., 14, 91.

Colgate, S.A. and White, R.H. 1965. to be published.

Cox, A.N. 1961. preprint.

Finzi, A. 1965a. Phys. Rev., 137, B472.

_____ 1965b. Phys. Rev. Lett., 15, 599.

Fisher, P.C. and Meyerott, A.J. 1964. Astrophys. J., 139, 123.

Giacconi, R., Gursky, H., Paolini, F.R., and Rossi, B.B. 1962.
Phys. Rev. Lett., 9, 439.

_____ 1963. Phys. Rev. Lett., 11, 530.

Giacconi, R., Gursky, H., and Waters, J.R. 1965. Nature, 207, 572.

Hayakawa, S. and Matsuoka, M. 1964. Prog. Theor. Phys.,
Suppl. 30, 204.

Inman, C.L. and Ruderman, M.A. 1964. Astrophys. J., 140, 1025.

Morrison, P. and Sartori, L. 1965. Phys. Rev. Lett., 14, 771.

Morton, D.C. 1964. Nature, 201, 1308.

Oda, M. 1965. Presented at the Cosmic Ray Conference of IUPAP,
London.

Oda, M., Clark, G., Garmire, G., Wada, M., Giacconi, R., Gursky, H.,
and Waters, J. 1965. Nature, 205, 554.

Sampson, D.H. 1959. Astrophys. J., 129, 734.

Schatzman, E. 1958. White Dwarfs (North-Holland Publishing Co., Amsterdam).

Schwarzschild, M. 1958. Structure and evolution of the stars (Princeton University Press, Princeton).

Tsuruta, S. 1964. Thesis, Columbia University (unpublished).

Tsuruta, S. and Cameron, A.G.W. 1965a. Nature, 207, 364.

_____ 1965b. Can. J. Phys., 43, 2056.

Tsuruta, S. and Cameron, A.G.W. 1966. to be published.

Zwicky, F. 1938. Astrophys. J., 88, 522.

_____ 1939. Phys. Rev., 55, 726.

_____ 1958. Handbuch der Physik (Springer-Verlag, Berlin). 51, 776.

TABLE CAPTIONS

Table 1: Characteristics of our six chosen models. The models are identified by the type of nuclear interaction V_β or V_γ and their approximate mass in solar mass units. ρ_m^c is the central density in cgs units, $M/M_\odot$ is the mass in solar mass units, R is the stellar radius in km, and PC is the central pressure in relativistic units $\left(PC = \frac{P(\text{dynes/cm}^2)}{6.46 \times 10^{36}}\right)$.

Table 2: Photospheric properties of typical neutron stars (V_β, $0.6M_\odot$) and (V_γ, $2M_\odot$) at different surface temperatures T_e. L_{ph} is the photon luminosity, ρ_{ph}, P_{ph} and $\varkappa_{ph}$ are the photospheric density, pressure and opacity, respectively, and λ^o_{max} is the maximum wavelength without red shift correction.

Table 3: Atmospheric temperature distribution of neutron star models with $M = 1M_\odot$ and R = 10 km. The temperature T at a specified ρ, and the temperature T_b and density ρ_b where the degeneracy starts are listed as a function of surface temperature T_e.

Table 4: (Models with $M = 1M_\odot$, R = 10 km) Temperature and density distribution near the surface at different depths (R-r) at given surface temperature T_e. The point where $E_F/kT = 2.5$ indicates the thickness of the non-degenerate envelopes.

Table 5: The characteristics of the hot neutron star model (V_γ, $2M_\odot$) with the Fe and Mg atmospheres. (T_e and T_c are the surface and core temperatures, L_{ph} is the photon luminosity, ΣL_ν is the total neutrino luminosity, $\alpha = \left(\frac{T_c}{T_e} \right) 10^{-2}$, U is the internal energy and τ is the cooling time.)

Table 6: The characteristics of the hot neutron star model (V_γ, $1.1M_\odot$) with the Fe and Mg atmospheres. (The notation is that used in Table 5.)

Table 7: The characteristics of the hot neutron star model (V_γ, $0.2M_\odot$) with the Fe and Mg atmospheres. (The notation is that used in Table 5.)

Table 8: The characteristics of the hot neutron star model (V_β, $1.0M_\odot$) with Fe atmospheres. (The notation is that used in Table 5.)

Table 9: The characteristics of the hot neutron star model (V_β, $0.6M_\odot$) with Fe atmospheres. (The notation is that used in Table 5.)

Table 10: The characteristics of the hot neutron star model (V_β, $0.2M_\odot$) with Fe atmospheres. (The notation is that used in Table 5.)

Table 11: The observational problem of Sco XR1. (T_e is the surface temperature, L_{ph} is the photon luminosity. τ is the age of the neutron star of the given temperature and FLUX is the flux of the thermal component of the x-rays from a neutron star in Sco XR1, 30 parsecs away to be observed above the earth's atmosphere.)

Table 12: The observational problem of Tau XR1. (T_e is the surface temperature of the neutron star of age 910 years, L_{ph} is the photon luminosity of the neutron star of the given temperature, and FLUX is the flux of the thermal component of x-rays from the neutron star.)

TABLE 1

Model (Notation)	ρ_m^c (gm/cm^3)	$M/M_\odot$	R (km)	PC
V_γ, $0.2M_\odot$	2.33×10^{14}	0.2003	17.78	5×10^{-4}
V_γ, $1.1M_\odot$	6.89×10^{14}	1.074	12.33	0.01
V_γ, $2M_\odot$	2.17×10^{15}	1.953	9.939	0.2
V_β, $0.2M_\odot$	3.26×10^{14}	0.1996	18.21	7×10^{-4}
V_β, $0.6M_\odot$	3.55×10^{15}	0.5927	7.159	0.06
V_β, $1M_\odot$	8.26×10^{15}	0.9663	5.184	0.7

TABLE 2

T_e	MODEL V_β, $0.6M_\odot$				MODEL V_γ, $2M_\odot$				λ^o_{max}
(^oK)	$L_{ph}/L_\odot$	Log ρ_{ph} (gm/cm^3)	P_{ph} ($dynes/cm^2$)	Log κ_{ph} (cm^2/gm)	$L_{ph}/L_\odot$	Log ρ_{ph} (gm/cm^3)	P_{ph} ($dynes/cm^2$)	Log κ_{ph} (cm^2/gm)	(Å)
5×10^7	6.036×10^5	-0.476	6.69×10^{14}	-0.6959	1.1604×10^6	-0.096	1.61×10^{15}	-0.5897	0.584
2×10^7	1.544×10^4	-0.5934	2.04×10^{14}	-0.1804	2.978×10^4	-0.236	4.65×10^{14}	-0.0513	1.459
10^7	9.65×10^2	-0.602	1.00×10^{14}	0.1295	1.86×10^3	-0.292	2.05×10^{14}	0.3054	2.918
5×10^6	6.036×10^1	-1.021	1.91×10^{13}	0.8494	1.1604×10^2	-0.721	3.81×10^{13}	1.0352	5.836
2×10^6	1.544	-1.116	6.13×10^{12}	1.3425	2.978	-0.784	1.32×10^{13}	1.4966	14.59
10^6	9.65×10^{-2}	-1.119	3.04×10^{12}	1.6465	0.186	-0.760	6.98×10^{12}	1.7727	29.18
5×10^5	6.036×10^{-3}	-1.247	1.14×10^{12}	2.0745	1.1604×10^{-2}	-0.902	2.52×10^{12}	2.2158	58.36
2×10^5	1.544×10^{-4}	-1.768	1.37×10^{11}	2.9945	2.978×10^{-4}	-1.476	2.68×10^{11}	3.1886	145.9
10^5	9.65×10^{-6}	-1.956	4.43×10^{10}	3.4834	1.86×10^{-5}	-1.678	8.41×10^{10}	3.6916	291.8
5×10^4	6.036×10^{-7}	-1.987	2.07×10^{10}	3.8143	1.1604×10^{-6}	-1.743	3.62×10^{10}	4.0576	583.6
2×10^4	1.544×10^{-8}	-1.949	9.01×10^9	4.1752	2.978×10^{-8}	-1.697	1.61×10^{10}	4.4094	1459
10^4	9.65×10^{-10}	-1.849	5.69×10^9	4.3750	1.86×10^{-9}	-1.376	1.69×10^{10}	4.3882	2918
6×10^3	1.251×10^{-10}	-1.062	2.09×10^{10}	3.8094					5836

TABLE 3

SURFACE TEMPERATURE	INTERNAL TEMPERATURE T (^{o}K)				T_b (^{o}K)	ρ_b
T_e (^{o}K)	$\rho=10^6$ gm/cm^3	$\rho=10^9$ gm/cm^3	$\rho=10^{12}$ gm/cm^3	$\rho=10^{14}$ gm/cm^3		(gm/cm^3)
1.6×10^7	9.08×10^8	3.47×10^9	3.65×10^9	3.65×10^9	1.4×10^9	4.3×10^6
1.2×10^7	6.86×10^8	2.34×10^9	2.425×10^9	2.425×10^9	7.7×10^8	1.5×10^6
1×10^7	5.92×10^8	1.825×10^9	1.88×10^9	1.88×10^9	5.92×10^8	1×10^6
9.4×10^6	5.75×10^8	1.68×10^9	1.73×10^9	1.73×10^9	4.8×10^8	5.4×10^5
6.7×10^6	4.51×10^8	1.10×10^9	1.125×10^9	1.125×10^9	2.6×10^8	1.4×10^5
5.1×10^6	3.79×10^8	8.09×10^8	8.21×10^8	8.21×10^8	1.5×10^8	6.2×10^4
4.3×10^6	3.395×10^8	6.765×10^8	6.83×10^8	6.83×10^8	1.03×10^8	4.8×10^4
3×10^6	2.64×10^8	4.62×10^8	4.64×10^8	4.64×10^8	7.6×10^7	4×10^4
1×10^6	9.61×10^7	1.12×10^8	1.125×10^8	1.125×10^8	3.5×10^7	10^4
7.7×10^5	6.5×10^7	7.18×10^7	7.35×10^8	7.35×10^8	2.3×10^7	4.2×10^3

TABLE 4

(R-r) (meters)	$T_e = 7.7 \times 10^5$ °K			$T_e = 3 \times 10^6$ °K			$T_e = 6.7 \times 10^6$ °K			$T_e = 1.6 \times 10^7$ °K		
	(gm/cm^3) log ρ	(°K) log T	E_F/kT	log ρ	log T	E_F/kT	log ρ	log T	E_F/kT	log ρ	log T	E_F/kT
0	-1.176	5.887	0.039	-1.095	6.477	0.0114	-0.854	6.826	0.0074	-0.605	7.204	0.0045
0.1	0.614	6.48	0.166									
0.2	2.317	7.002	0.63	1.55	7.23	0.118						
0.3	3.275	7.261	1.53									
0.4	3.888	7.432	2.765	2.637	7.565	0.284						
0.5	4.201	7.509	3.59				2.28	7.714	0.118	1.576	7.794	0.0332
0.6	4.430	7.561	4.61	3.337	7.734	0.564						
1	4.930	7.661	7.66	4.286	7.931	1.564	3.42	7.97	0.376	2.558	8.028	0.0865
2	5.49	7.73	15.7	5.315	8.210	3.935	4.628	8.284	1.165	3.567	8.339	0.203
3				5.69	8.32	5.43	5.317	8.463	2.215	4.166	8.505	0.348
4				5.92	8.40	6.38	5.710	8.576	3.14	4.638	8.623	0.539
5	5.89	7.80	24.3	6.09	8.45	7.42	5.939	8.638	3.865	5.004	8.709	0.770
6							6.106	8.680	4.52	5.312	8.783	1.054
7				6.23	8.50	8.32						
8							6.27	8.74	5.04	5.784	8.902	1.673
10	6.463	7.835	55	6.54	8.55	11.75	6.474	8.782	6.265	6.15	8.996	2.34

TABLE 5

T_e (°K)	Log L_{ph} (ergs/sec)	Log ΣL_ν (ergs/sec)		Log T_c (°K)		$\alpha = \left(\frac{T_c}{T_e}\right) 10^{-2}$		Log U (ergs)		Log τ (years)	
		Fe	Mg	Fe	Mg	Fe	Mg	Fe	Mg	Fe	Mg
5×10^7	39.6432	47.39		10.1265		2.67		50.26		-5.21	-4.34
2×10^7	38.0514	42.25	41.48	9.5177	9.4181	1.65	1.31	49.02	48.76	-1.43	-0.57
10^7	36.8474	39.39	38.19	9.1047	8.9791	1.27	0.955	48.19	47.87	1.09	1.66
5×10^6	35.6432	37.01	35.77	8.7666	8.5777	1.165	0.756	47.49	47.08	2.89	3.34
2×10^6	34.0515	34.01	33.34	8.2938	8.1520	0.986	0.710	46.51	46.25	4.50	4.55
10^6	32.8474	31.49	30.99	7.8299	7.7550	0.750	0.570	45.61	45.49	5.43	5.25
5×10^5	31.6432	28.63	28.01	7.3814	7.2794	0.480	0.3808	44.74	44.49	5.96	5.76
2×10^5	30.0515	24.71	34.34	6.7035	6.6704	0.253	0.2341	43.37	43.28	6.41	6.23
10^5	28.8474			6.2647	6.2157	0.184	0.1641	42.51	42.41	6.73	6.60
5×10^4	27.6433			5.7925	5.6951	0.124	0.0994	41.51	41.29	7.00	6.94
2×10^4	26.0515			5.1716	5.0180	0.0743	0.0521	40.29	40.01	7.61	7.29
10^4	24.8474			4.5990		0.0398					

TABLE 6

T_e (°K)	Log L_{ph} (ergs/sec)	Log ΣL_ν (ergs/sec)		Log T_c (°K)		$\alpha = \left(\frac{T_c}{T_e}\right) 10^{-2}$		Log U (ergs)		Log τ (years)	
		Fe	Mg	Fe	Mg	Fe	Mg	Fe	Mg	Fe	Mg
5×10^7	39.8303	50.34		10.5407		6.945		50.88			
2×10^7	38.2385	44.41	43.65	9.7534	9.6952	2.836	2.480	49.31	49.21	-3.48	-2.91
10^7	37.0344	41.01	40.13	9.3347	9.2319	2.160	1.702	48.59	48.29	-0.74	0.18
5×10^6	35.8303	37.79	36.77	8.9533	8.8007	1.798	1.261	47.73	47.46	1.63	2.68
2×10^6	34.2386	34.75	33.31	8.5282	8.3253	1.686	1.059	46.84	46.47	4.08	4.63
10^6	33.0345	32.11	31.38	8.1178	8.0160	1.310	1.038	46.08	45.82	5.55	5.36
5×10^5	31.8304	29.01	28.37	7.6389	7.5400	0.871	0.693	45.09	44.89	6.08	5.89
2×10^5	30.2386	25.25	24.79	7.0080	6.9460	0.4408	0.4415	43.83	43.71	6.62	6.44
10^5	29.0345			6.5192	6.4775	0.3306	0.3000	42.84	42.75	6.96	6.77
5×10^4	27.8304			6.0681	6.0036	0.2340	0.2019	41.91	41.81	7.26	7.07
2×10^4	26.2387			5.4366	5.3218	0.1364	0.1050	40.69	40.49	7.59	7.43
10^4	25.0345			4.9261		0.0844		39.71		7.88	
6×10^3	24.1472			4.5167		0.0548		38.88		8.07	

TABLE 7

T_e (°K)	Log L_{ph} (ergs/sec)	Log ΣL_ν (ergs/sec)		Log T_c (°K)		$\alpha = \left(\frac{T_c}{T_e}\right) 10^{-2}$		Log U (ergs)		Log τ (years)	
		Fe	Mg	Fe	Mg	Fe	Mg	Fe	Mg	Fe	Mg
2×10^7	38.5563	48.78		10.2662		9.225		49.98		-5.8	
10^7	37.3552	44.51	44.01	9.7377	9.6770	5.458	4.750	48.91	48.77	-4.2	-3.35
5×10^6	36.1481	41.29	40.58	9.3197	9.2165	4.174	3.288	48.08	47.87	-1.19	-0.67
2×10^6	34.5564	37.38	36.01	8.8358	8.6595	3.424	2.281	47.12	46.76	1.68	2.60
10^6	33.3523	34.98	33.29	8.5162	8.3141	3.281	2.061	46.51	46.12	3.65	4.48
5×10^5	32.1481	31.74	30.79	8.1029	8.0004	2.536	2.000	45.74	45.51	5.59	5.61
2×10^5	30.5564	27.21	26.23	7.4816	7.3745	1.516	1.1828	44.44	44.25	6.72	6.23
10^5	29.3523	23.82	23.53	6.9866	6.9282	0.972	0.8495	43.41	43.26	7.11	6.76
5×10^4	28.1482			6.5045	6.4596	0.6398	0.576	42.51	42.37	7.41	7.19
2×10^4	26.5564			5.8944	5.8106	0.3921	0.3234	41.26	41.12	7.80	7.68
10^4	25.3523			5.4193		0.2621		40.33		8.08	
6×10^3	24.4649			5.0643		0.1937		39.61		8.28	

TABLE 8

T_e ($^\circ$K)	Log L_{ph} (ergs/sec)	Log ΣL_ν (ergs/sec)	Log T_c ($^\circ$K)	$\alpha = \left(\frac{T_c}{T_e}\right) 10^{-2}$	Log U (ergs)	Log τ (years)
5×10^7	39.0778	45.86	10.0189	2.039	49.48	-4.26
2×10^7	37.4861	41.25	9.4351	1.361	48.51	-1.10
10^7	36.2819	38.91	9.0348	1.083	47.51	0.615
5×10^6	35.0778	36.98	8.7037	1.011	46.84	2.10
2×10^6	33.4861	34.03	8.2153	0.821	45.84	4.08
10^6	32.2820	31.03	7.7379	0.546	44.88	5.16
5×10^5	31.0779	28.38	7.2934	0.393	44.01	5.78
2×10^5	29.4861		6.6211	0.209	42.71	6.25
10^5	28.2820		6.1785	0.156	41.78	6.54
5×10^4	27.0779		5.7030	0.101	40.86	6.81
2×10^4	25.4862		5.0704	0.0589	39.61	7.19

T A B L E 9

T_e (°K)	Log L_{ph} (ergs/sec)	Log ΣL_ν (ergs/sec)	Log T_c (°K)	$\alpha = \left(\frac{T_c}{T_e}\right) 10^{-2}$	Log U (ergs)	Log τ (years)
5×10^7	39.3581	48.76	10.4016	6.35	50.24	-6.5
2×10^7	37.7663	43.15	9.6815	2.40	48.74	-2.49
10^7	36.5622	39.51	9.2635	1.831	47.88	0.03
5×10^6	35.3581	37.56	8.8957	1.571	47.17	1.73
2×10^6	33.7664	35.01	8.4669	1.463	46.30	3.54
10^6	32.5623	32.58	8.0372	1.089	45.51	4.93
5×10^5	31.3582	29.65	7.5651	0.736	44.60	5.86
2×10^5	29.7664	25.81	6.9072	0.4046	43.26	6.51
10^5	28.5623		6.4444	0.2783	42.30	6.85
5×10^4	27.3582		5.9847	0.193	41.35	7.14
2×10^4	25.7665		5.3599	0.1144	40.10	7.49
10^4	24.5624		4.8191	0.0659	39.03	7.74
6×10^3	23.6750		4.4320	0.0451	38.30	7.95

TABLE 10

T_e (^oK)	Log L_{ph} (ergs/sec)	Log ΣL_ν (ergs/sec)	Log T_c (^oK)	$\alpha = \left(\frac{T_c}{T_e}\right) 10^{-2}$	Log U (ergs)	Log τ (years)
2×10^7	38.5772	48.73	10.2798	9.53	50.01	-6.99
10^7	37.3731	44.61	9.7459	5.56	48.91	-4.07
5×10^6	36.1690	41.30	9.3277	4.253	48.12	-1.39
2×10^6	34.5772	37.48	8.8417	3.472	47.12	1.30
10^6	33.3731	34.99	8.5226	3.331	46.50	3.38
5×10^5	32.1690	31.70	8.1107	2.579	45.68	5.36
2×10^5	30.5773	27.10	7.4900	1.546	44.40	6.70
10^5	29.3731	24.00	6.9971	0.975	43.44	7.09
5×10^4	28.1690		6.5122	0.650	42.50	7.39
2×10^4	26.5773		5.9057	0.4026	41.26	7.74
10^4	25.3732		5.4286	0.2681	40.51	8.01
6×10^3	24.4858		5.0769	0.199	39.60	8.20

TABLE 11

T_e			(V_γ, $0.2M_\odot$)	(V_γ, $1.1M_\odot$)	(V_γ, $2M_\odot$)	(V_β, $0.2M_\odot$)	(V_β, $0.6M_\odot$)	(V_β, $1M_\odot$)
2×10^6 °K	Log L_{ph} (ergs/sec)		34.5564	34.2386	34,0515	34.5772	33.7664	33.4861
	FLUX (ergs/cm²-sec)		3.33×10^{-7}	2.2×10^{-7}	1.03×10^{-7}	3.49×10^{-7}	5.4×10^{-8}	2.835×10^{-8}
	Log τ (years)	Fe	1.68	4.20	4.5	1.38	3.5	4.1
		Mg	2.60	4.65	4.55			
1×10^6 °K	Log L_{ph} (ergs/sec)		33.3523	33.0345	32.8474	33.3731	32.5623	32.28 20
	FLUX (ergs/cm²-sec)		2.08×10^{-8}	1.0×10^{-8}	6.5×10^{-9}	2.18×10^{-8}	3.376×10^{-9}	1.763×10^{-9}
	Log τ (years)	Fe	3.65	5.55	5.45	3.35	4.95	5.15
		Mg	4.48	5.36	5.25			

TABLE 12

		(V_γ, 0.2$M_\odot$)	(V_γ, 1.1$M_\odot$)	(V_γ, 2$M_\odot$)	(V_β, 0.2$M_\odot$)	(V_β, 0.6$M_\odot$)	(V_β, 1$M_\odot$)
Log T_e (^oK)	Fe	6.11	6.500	6.660	6.05	6.4	6.51
	Mg	6.254	6.655	6.785			
L_{ph} (ergs/sec)	Fe	7.024×10^{33}	1.087×10^{35}	3.06×10^{35}	3.742×10^{33}	1.454×10^{34}	2.10×10^{34}
	Mg	2.334×10^{34}	4.101×10^{35}	9.69×10^{35}			
FLUX (ergs/cm^2-sec)	Fe	4.85×10^{-11}	7.499×10^{-10}	2.12×10^{-9}	2.583×10^{-11}	1.003×10^{-10}	1.449×10^{-10}
	Mg	1.609×10^{-10}	2.828×10^{-9}	6.7×10^{-9}			

FIGURE CAPTIONS

Figure 1: The opacity in cm^2/gm as a function of density in gm/cm^3, at different temperatures, calculated by the use of Cox's opacity code and an ionization code. Solid curves are for iron and dashed curves are for magnesium.

Figure 2: Central temperature as a function of surface temperature for models of nuclear potential V_γ with different mass values. Solid curves are for iron and dashed curves are for magnesium.

Figure 3: Temperature distribution near the surface of a neutron star. The temperature is plotted against the distance from the photosphere in meters for a model of one solar mass, 10 km radius, and with various different values of the surface temperature T_e. The borders between the degenerate layers and non-degenerate layers are shown by crosses.

Figure 4: Density distribution near the surface of a neutron star. The density is plotted against the distance from the photosphere in cm for a model of one solar mass, 10 km, and with various different values of the surface temperature.

Figure 5: Energy loss rates due to neutrino pair emission from plasma in erg/cm^3-sec shown as a function of electron number

density in cm^{-3} at different temperatures.

Figure 6: Neutrino and photon luminosities and total internal energy of a neutron star model of 1.1 solar mass and of the V_γ type nuclear potential are shown as functions of the core temperature of the star. The neutrino luminosity L_ν due to the plasma process, the URCA process and the bremsstrahlung process are shown separately. The photon luminosity for the Mg atmosphere and the Fe atmosphere are also shown separately.

Figure 7: Cooling curves for the six typical neutron star models with iron atmospheres. Surface temperatures are plotted as functions of time in years. Solid curves represent the models with the V_β type nuclear potential and the dashed curves represent the models with the V_γ type potential. Different models are identified by their mass values and the type of the potential. The points where the major cooling mechanism shifts from the neutrino emission to the photon emission are indicated by the crosses.

Figure 8: The effect of composition on cooling curves. Surface temperatures of models of the V_γ type potential and with different mass values are plotted as functions of time in years for iron atmospheres (solid curves) and magnesium

atmospheres (dashed curves).

Figure 9: Cooling curves for models with iron atmospheres in the most interesting region for observation are shown in detail.

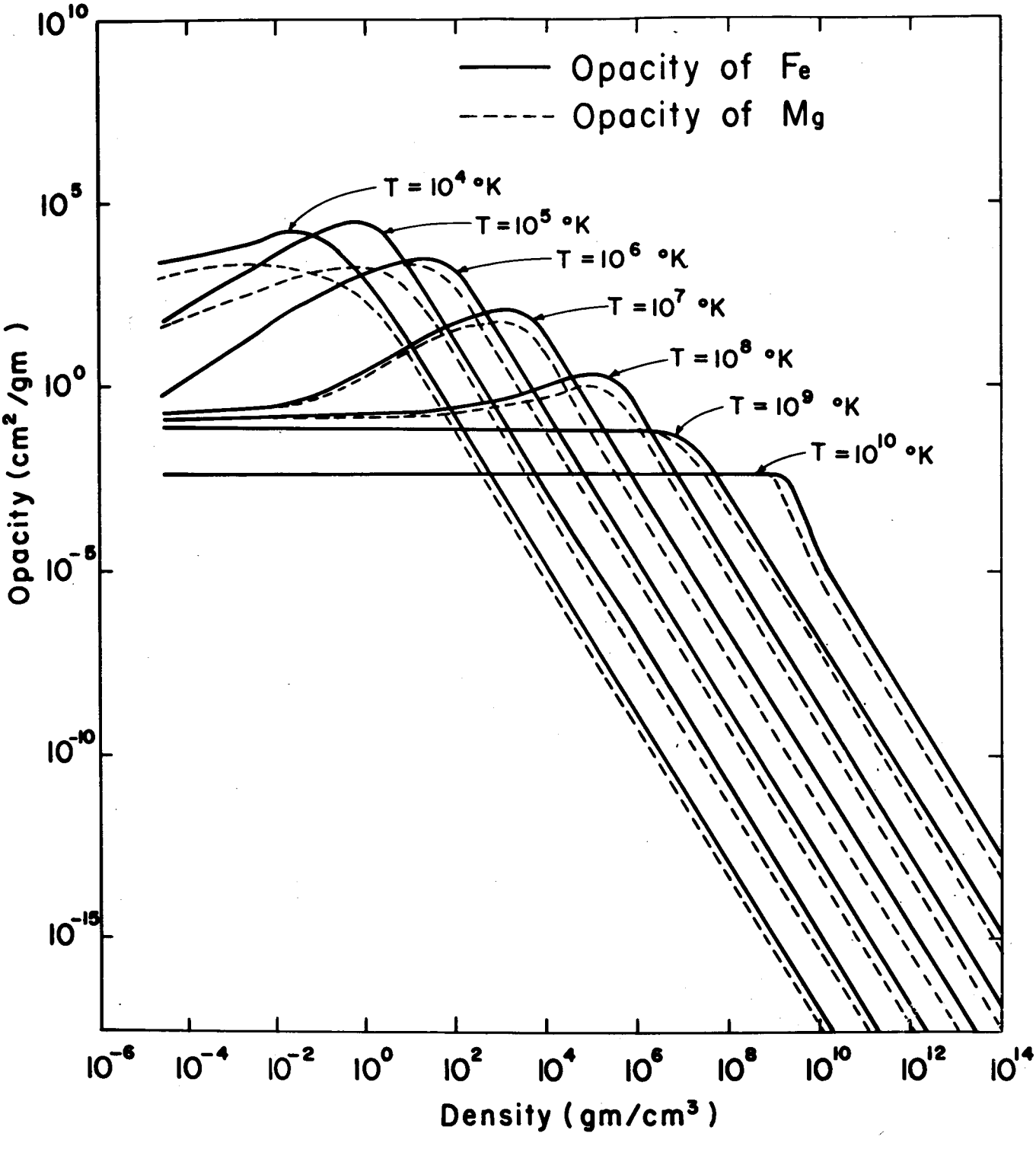
Opacity of Fe
Opacity of Mg
T = 10^4 °K
T = 10^5 °K
T = 10^6 °K
T = 10^7 °K
T = 10^8 °K
T = 10^9 °K
T = 10^10 °K
Opacity (cm^2/gm)
Density (gm/cm^3)
10^10
10^5
10^0
10^-5
10^-10
10^-15
10^-6
10^-4
10^-2
10^0
10^2
10^4
10^6
10^8
10^10
10^12
10^14

Figure 1

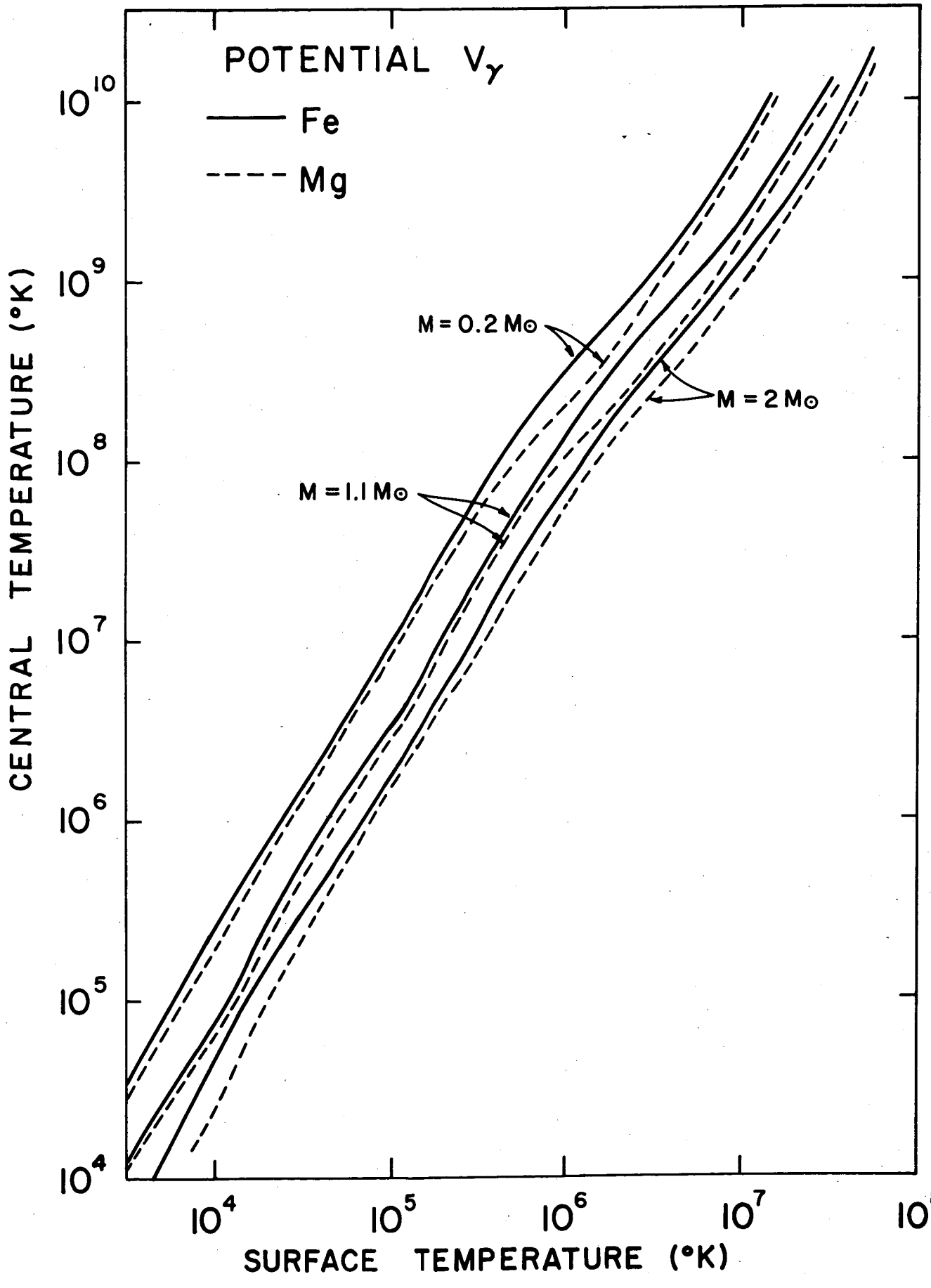
POTENTIAL V_γ
Fe
Mg
M = 0.2 M⊙
M = 2 M⊙
M = 1.1 M⊙
CENTRAL TEMPERATURE (°K)
SURFACE TEMPERATURE (°K)
10^{10}
10^9
10^8
10^7
10^6
10^5
10^4
10^4
10^5
10^6
10^7
10^8

Figure 2

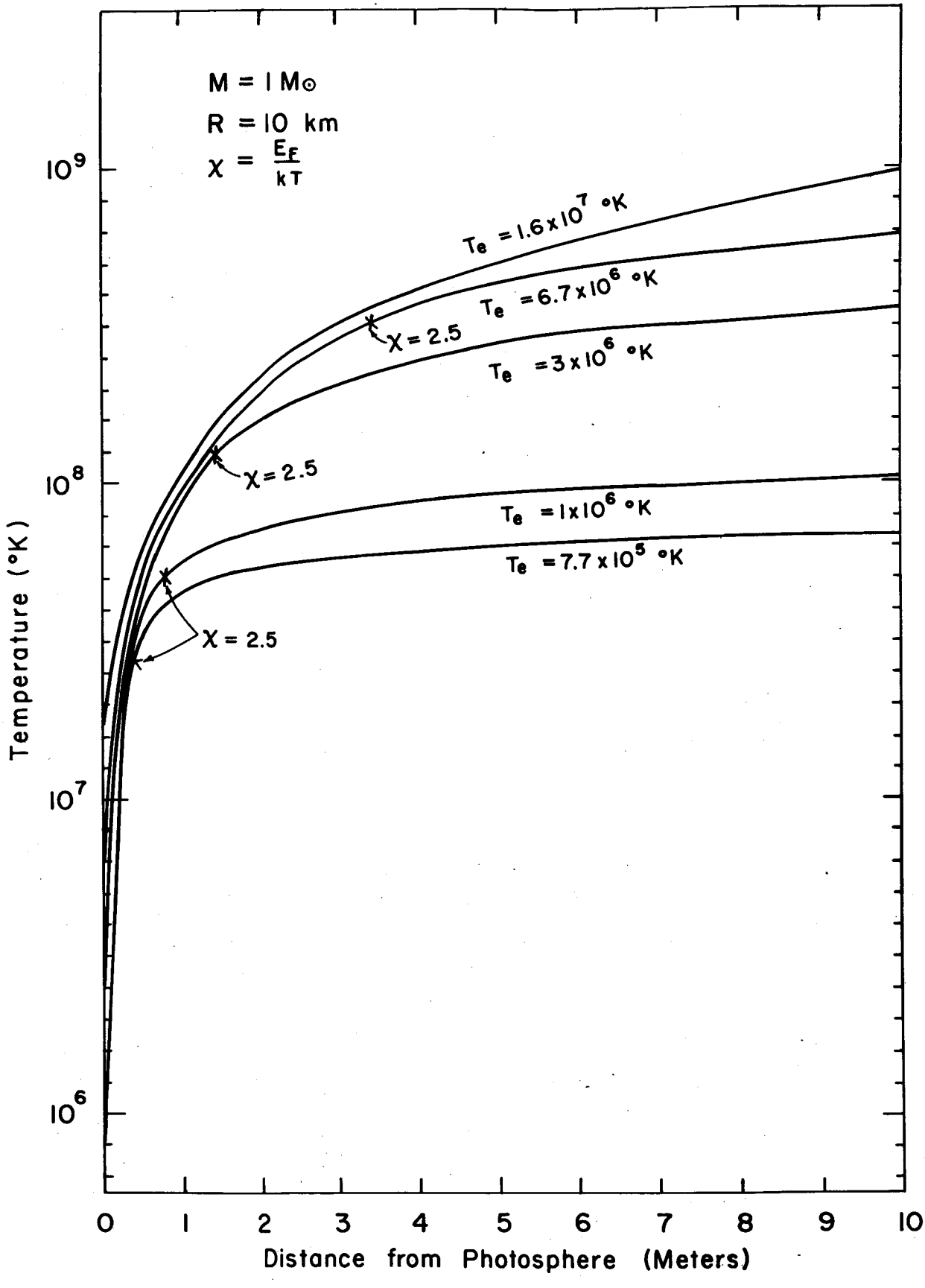
M = 1 M⊙
R = 10 km
χ = E_F / kT
Te = 1.6x10^7 °K
Te = 6.7x10^6 °K
Te = 3x10^6 °K
Te = 1x10^6 °K
Te = 7.7x10^5 °K
χ = 2.5
χ = 2.5
χ = 2.5
Temperature (°K)
10^9
10^8
10^7
10^6
0
1
2
3
4
5
6
7
8
9
10
Distance from Photosphere (Meters)

Figure 3

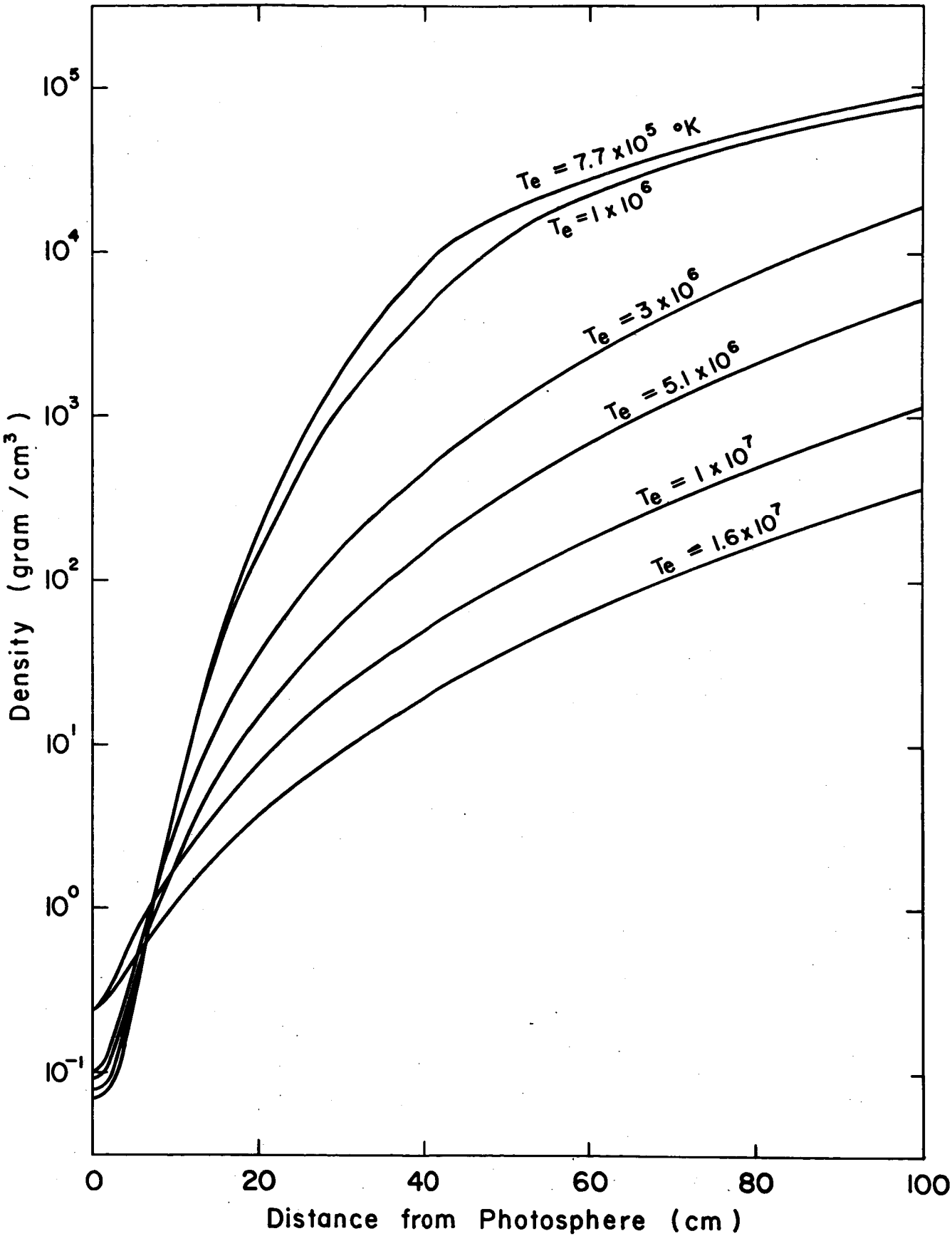
Density (gram / cm³)
10⁵
10⁴
10³
10²
10¹
10⁰
10⁻¹
Te = 7.7 x 10⁵ °K
Te = 1 x 10⁶
Te = 3 x 10⁶
Te = 5.1 x 10⁶
Te = 1 x 10⁷
Te = 1.6 x 10⁷
0
20
40
60
80
100
Distance from Photosphere (cm)

Figure 4

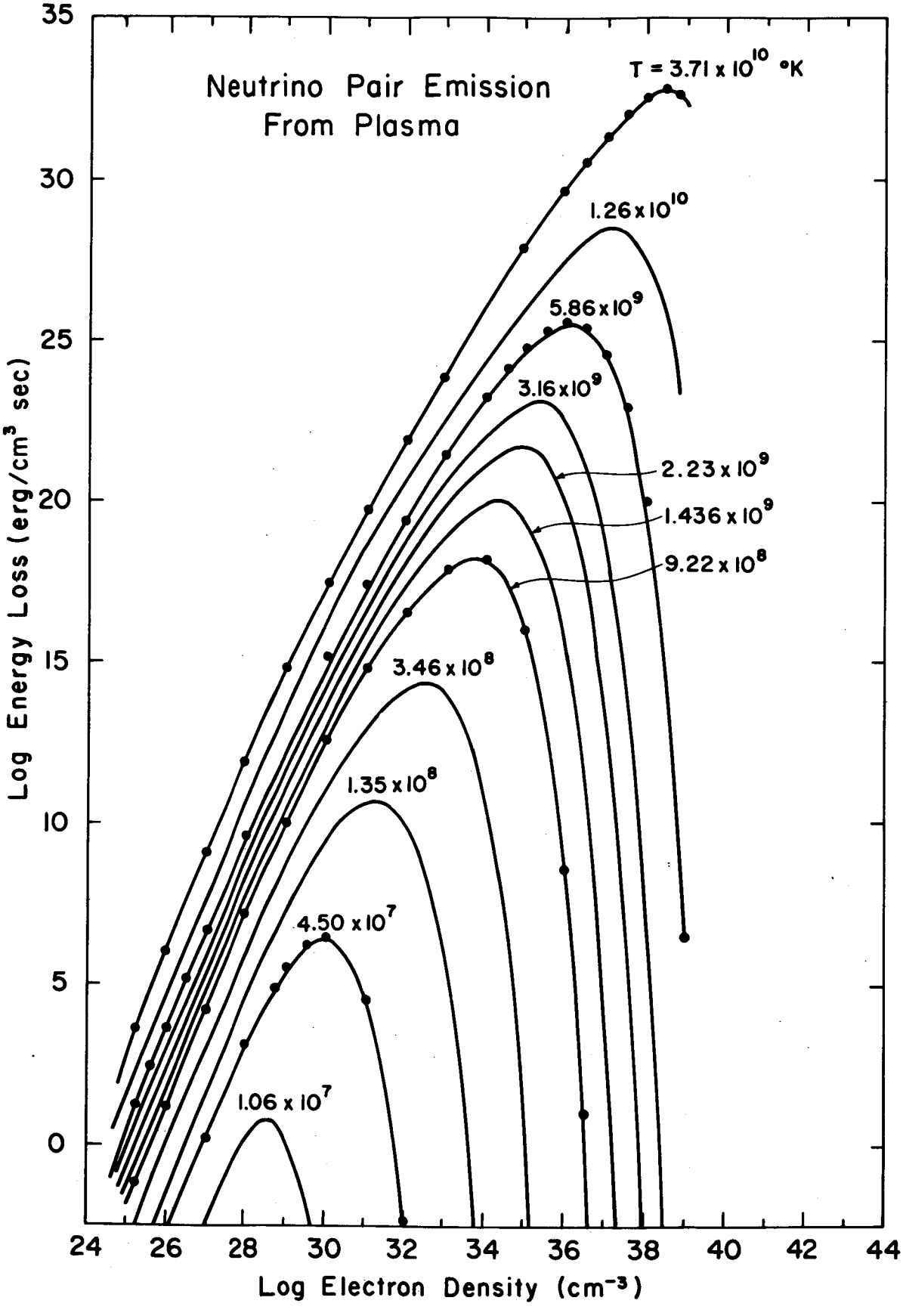
Neutrino Pair Emission
From Plasma
T = 3.71 x 10^10 °K
1.26 x 10^10
5.86 x 10^9
3.16 x 10^9
2.23 x 10^9
1.436 x 10^9
9.22 x 10^8
3.46 x 10^8
1.35 x 10^8
4.50 x 10^7
1.06 x 10^7
Log Energy Loss (erg/cm^3 sec)
Log Electron Density (cm^-3)
35
30
25
20
15
10
5
0
24
26
28
30
32
34
36
38
40
42
44

Figure 5

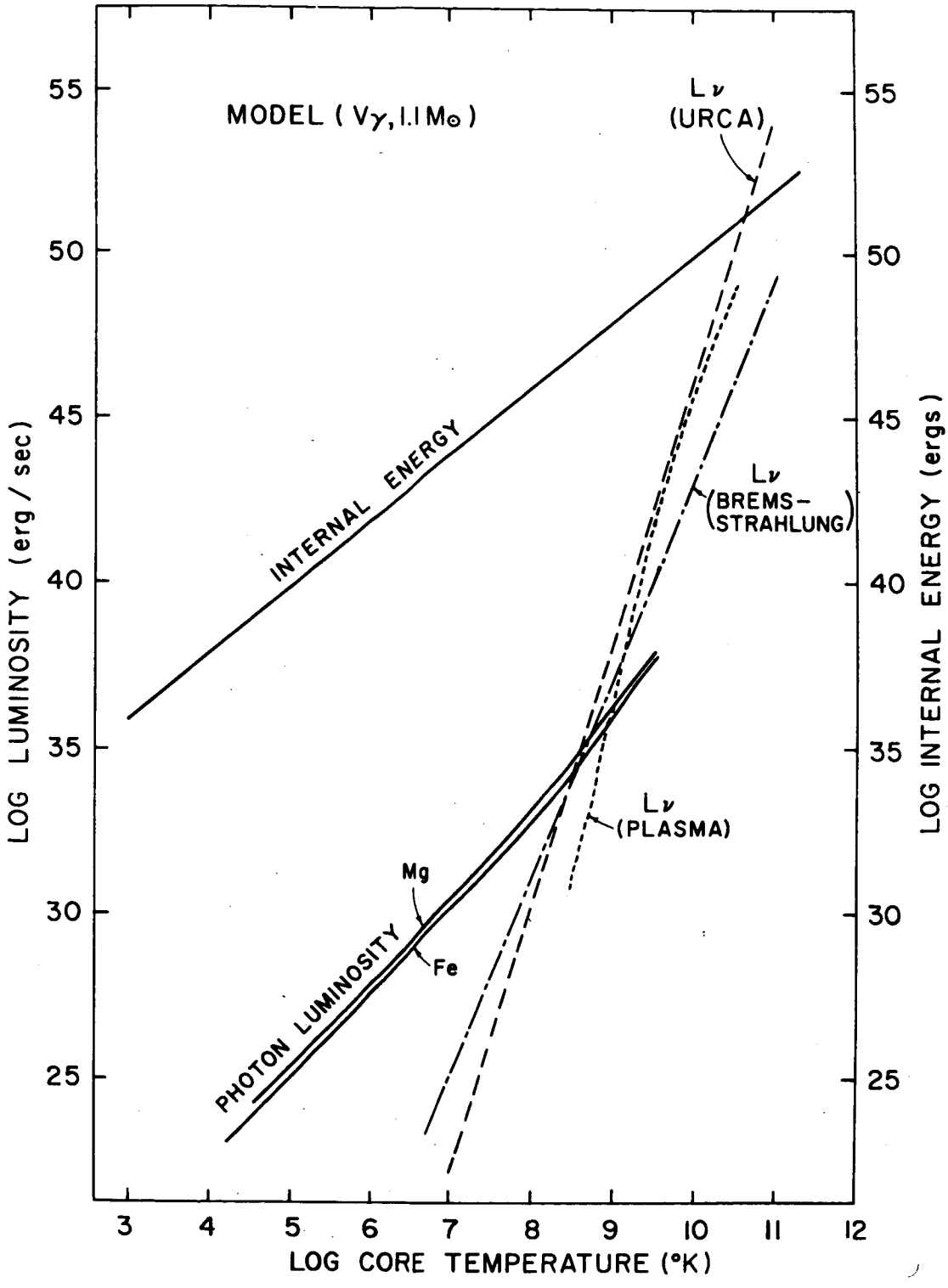
MODEL (Vγ, 1.1 M⊙)
Lν (URCA)
INTERNAL ENERGY
Lν (BREMS-STRAHLUNG)
Lν (PLASMA)
Mg
Fe
PHOTON LUMINOSITY
LOG LUMINOSITY (erg / sec)
LOG INTERNAL ENERGY (ergs)
LOG CORE TEMPERATURE (°K)
55
50
45
40
35
30
25
3
4
5
6
7
8
9
10
11
12

Figure 6

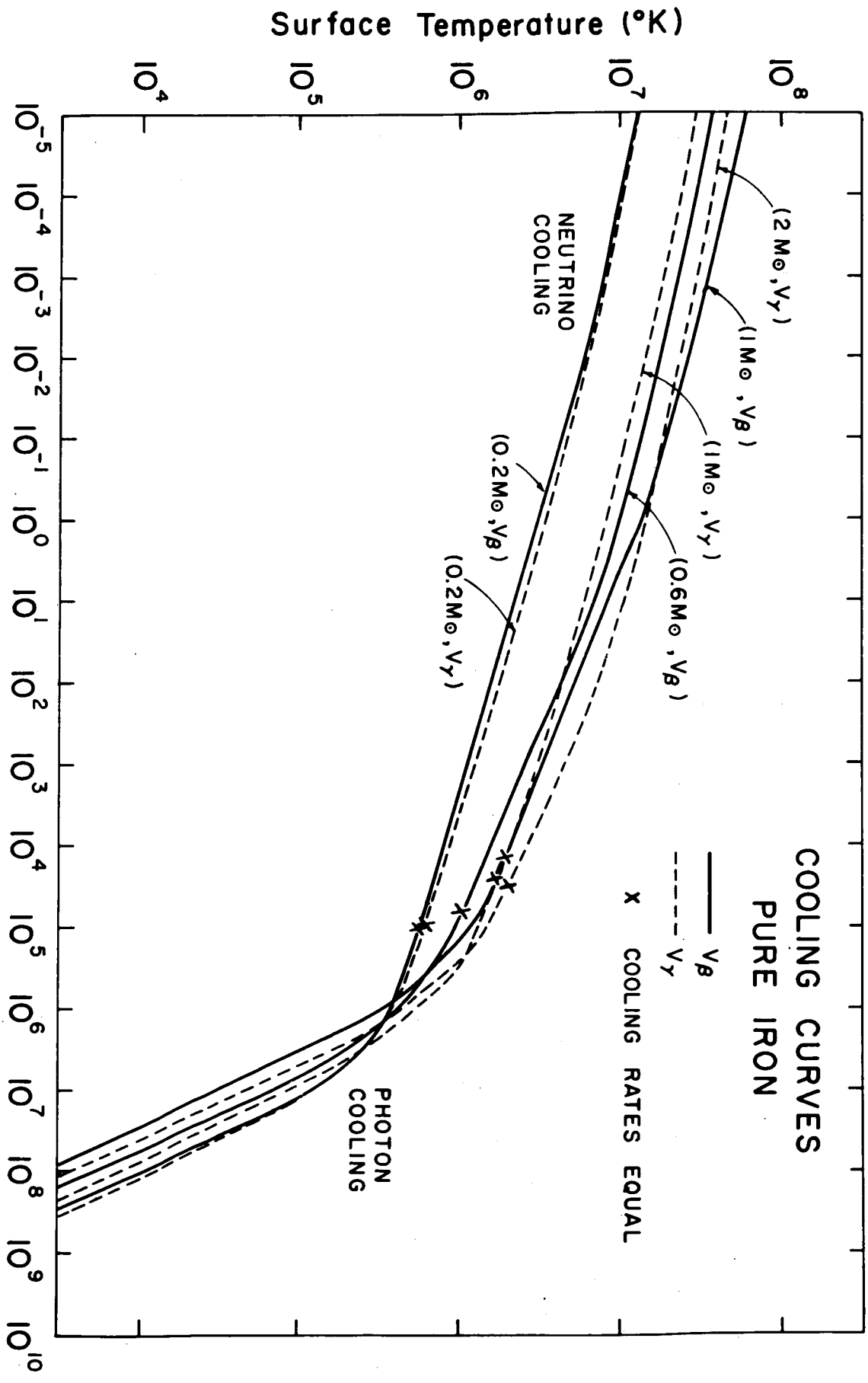
Surface Temperature (°K)
10^8
10^7
10^6
10^5
10^4
Time (years)
10^{-5} 10^{-4} 10^{-3} 10^{-2} 10^{-1} 10^0 10^1 10^2 10^3 10^4 10^5 10^6 10^7 10^8 10^9 10^{10}
COOLING CURVES
PURE IRON
V_β
V_γ
x COOLING RATES EQUAL
NEUTRINO COOLING
PHOTON COOLING
(2 M⊙, V_γ)
(1M⊙, V_β)
(1M⊙, V_γ)
(0.6M⊙, V_β)
(0.2M⊙, V_β)
(0.2M⊙, V_γ)

Figure 7

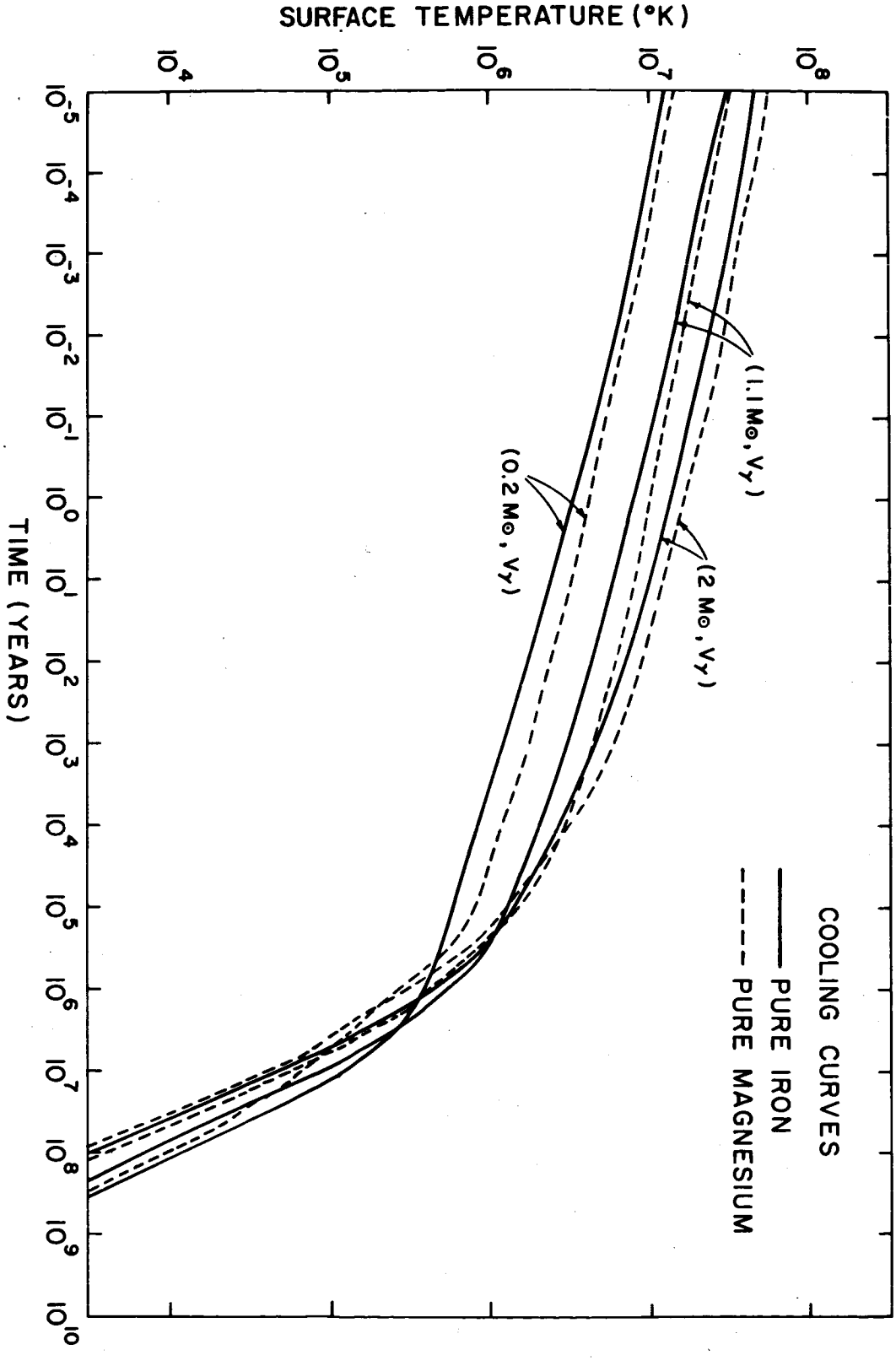
SURFACE TEMPERATURE (°K)
10^4
10^5
10^6
10^7
10^8
TIME (YEARS)
10^{-5}
10^{-4}
10^{-3}
10^{-2}
10^{-1}
10^0
10^1
10^2
10^3
10^4
10^5
10^6
10^7
10^8
10^9
10^{10}
(1.1 M⊙, Vγ)
(0.2 M⊙, Vγ)
(2 M⊙, Vγ)
COOLING CURVES
PURE IRON
PURE MAGNESIUM

Figure 8

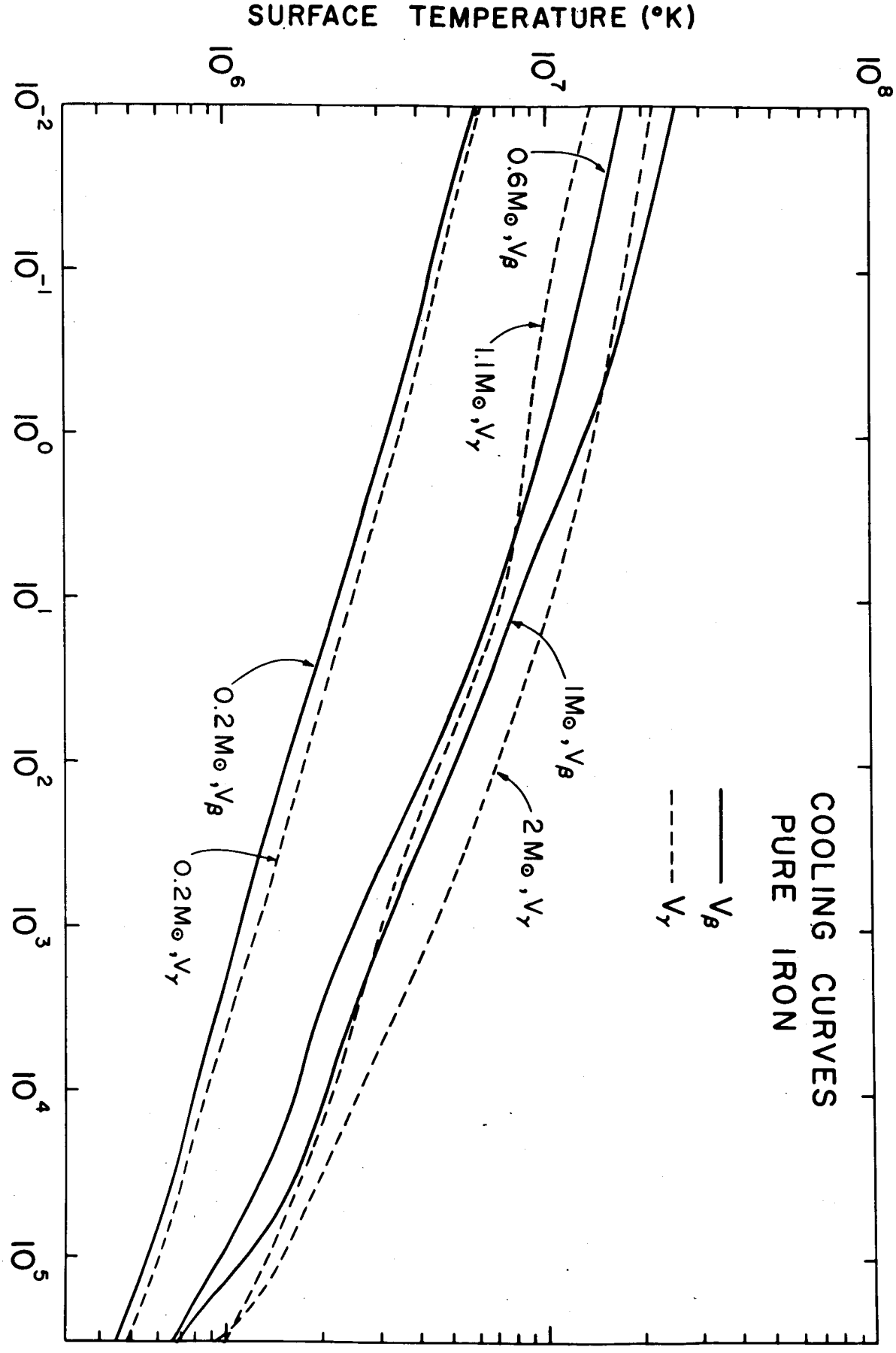
SURFACE TEMPERATURE (°K)
10^6
10^7
10^8
10^{-2}
10^{-1}
10^0
10^1
10^2
10^3
10^4
10^5
TIME (YEARS)
0.6M⊙, V_β
1.1M⊙, V_γ
1M⊙, V_β
2M⊙, V_γ
0.2M⊙, V_β
0.2M⊙, V_γ
COOLING CURVES
PURE IRON
V_β
V_γ

Figure 9

11. Vibrations of Neutron Stars.

Possible Magnetospheric Phenomena associated with Neutron Stars

WITH the discovery of X-ray sources in the sky[1,2], speculation has arisen that they might be associated with neutron or hyperon stars formed during the internal collapse which triggers off supernova explosions (probably of type I). Rates of cooling of neutron star models have been calculated by Morton[3], Chiu and Salpeter[4,5], and Tsuruta[6]. It appears (J. Bahcall, personal communication) that the importance of the early cooling by emission of neutrinos from the 'Urca' process has been underestimated in the foregoing investigations. With rough allowance for this effect, the calculations of Miss Tsuruta indicate that a neutron star will rapidly cool to 3 or 4 × 10^6 °K, but that after 10^5 years its surface temperature will still be about 2 × 10^6 °K.

During the earlier part of 1964 evidence unfavourable to the neutron star hypothesis for X-ray sources accumulated. Thus Bowyer, Byram, Chubb and Friedman[7] showed from a lunar occultation measurement that the diameter of the X-ray source associated with the Crab Nebula is about one light year, and there appeared to be a deficiency of soft X-rays from it. At the symposium on "Neutron Stars and Celestial X-ray Sources", held at the Goddard Institute for Space Studies during March 1964, Giacconi and Friedman both reported crude spectral estimates which suggested that the strongest X-ray source, in Scorpius, if thermal, would have a temperature of about 1 or 2 × 10^7 °K—much too hot to be interpreted as a neutron star.

Many more measurements were reported at the second Texas Conference on Relativistic Astrophysics in December 1964. Friedman, for example, reported that the soft X-ray flux from both the Crab Nebula and the Scorpius source has been greatly underestimated; his newer determination of the equivalent thermal temperature of the Scorpius source was 2 × 10^6 °K. He also reported that ten X-ray sources had now been identified and that these formed a distribution flattened toward the galactic plane. Also at the December 1964 Texas Conference Giacconi reported that the angular diameter of the Scorpius source is less than 8 min of arc. However, Clark, at the same Conference, reported that the Crab Nebula emitted a significant flux of ~30 keV X-rays, consistent with the synchrotron emission picture of Woltjer[8]. Fisher, again at the second Texas Conference, reported that the X-ray energy spectrum from the Scorpius source contained too large a flux of higher energy X-rays to be consistent with a pure thermal spectrum of 2 × 10^6 °K.

It is the purpose of the present communication to suggest that the discrete X-ray sources may be neutron stars with an associated magnetosphere. The X-ray spectrum would thus consist of a thermal component emitted from the photosphere and a non-thermal synchrotron component emitted by trapped electrons accelerated in the magnetosphere.

Magnetic fields are commonly associated with stars. Woltjer[8] has pointed out that neutron stars may contain magnetic fields with strengths up to ~ 10^{14} gauss, which would be formed during the compression of matter which forms the neutron star. This compression occurs during the hydrodynamic collapse of a pre-supernova star. Colgate and White[9] have found that a degenerate neutron core starts to build up in such a collapse, and additional matter descending on this core releases large amounts of gravitational potential energy. The deposition of this energy forms a strong shock wave which ejects the outer layers of the star. We must expect that the internal magnetic lines of force would be drawn radially outward in this explosion. However, the rotation of the remaining neutron star would twist the lines of force in the inner region so that they would have to reconnect to form a self-contained magnetosphere.

The surface temperature of a neutron star is comparable with the kinetic temperature in the solar corona, but its radius is orders of magnitude less than that of the Sun. Hence the stellar wind associated with a neutron star will be negligibly small compared with the solar wind, according to the hydrodynamic model for coronal expansion[10], unless much higher kinetic temperatures are produced in a corona around the neutron star. It should not be ruled out that the mechanism to be discussed here might produce these higher kinetic temperatures, in which case there could also be a bremsstrahlung component in the X-ray emission. The heating of the solar corona appears to be produced by generation of acoustic, gravity and hydromagnetic waves by turbulence in the convective layers below the solar photosphere. It is clear that no similar convective region can exist in a neutron star[6].

However, the neutron star is capable of storing gravitational potential energy in the form of radial oscillations. Such oscillations will have a period in the millisecond range (F. J. Dyson, personal communication). The shock wave which ejects matter in the supernova explosion will eject only the outer layers; the inner layers will be accelerated outward by the shock but will fall back on to the neutron star. It seems likely that a substantial amount of energy may thus be stored in the resulting radial oscillations. The gravitational binding energy of a neutron star is a sensitive function of the mass[6], but it may typically amount to several per cent of the rest mass energy. Hence it may be possible to store ~ 10^{52} ergs as vibrational energy in such a star. This is 5 or 6 orders of magnitude greater than the thermal energy content of a neutron star at the end of the initial rapid neutrino cooling stage[6].

The radial oscillations will generate hydromagnetic waves at parts of the magnetic field which emerge from the photosphere at some angle to the normal. These waves will traverse the magnetosphere and can accelerate electrons. If this picture holds for the Crab Nebula, then evidently the electrons escape from the magnetosphere into the radial magnetic field system of the surrounding expanding envelope. The electrons will initially emit X-rays by the synchrotron process, but their synchrotron lifetime for X-ray emission is only about one year[6]. This would account for the observation that the region of X-ray emission in the Crab Nebula is smaller than the region of optical synchrotron emission.

If these considerations are correct, it is evident that many other non-thermal phenomena will be associated with the mechanical energy of vibration of neutron stars, and hence that extensive theoretical investigations of such phenomena may be rewarding.

A. G. W. CAMERON

Institute for Space Studies,
Goddard Space Flight Center,
National Aeronautics and Space Administration,
New York, N.Y.

[1] Giacconi, R., Gursky, H., Paolini, F. R., and Rossi, B. B., *Phys. Rev. Letters*, **9**, 439 (1962).
[2] Bowyer, S., Byram, E. T., Chubb, T. A., and Friedman, H., *Nature*, **201**, 1307 (1964).
[3] Morton, D. C., *Astrophys. J.*, **140**, 460 (1964).
[4] Chiu, H. Y., *Ann. Phys.*, **26**, 364 (1964).
[5] Chiu, H. Y., and Salpeter, E. E., *Phys. Rev. Letters*, **12**, 412 (1964).
[6] Tsuruta, S., thesis, Columbia University (1964).
[7] Bowyer, S., Byram, E. T., Chubb, T. A., and Friedman, H., *Science*, **146** 912 (1964).
[8] Woltjer, L., *Astrophys. J.*, **140**, 1309 (1964).
[9] Colgate, S. A., and White, R. H. (to be published).
[10] Parker, E. N., *Interplanetary Dynamical Processes* (Interscience Pub. New York, 1963).

Oscillation Periods of Neutron Stars

THE recent discovery[1-4] of celestial X-ray sources prompted various authors[5-12] to propose possible production mechanisms of these X-rays. In an earlier communication, one of us[12] suggested that some of the X-ray emission might be associated with the mechanical energy of radial oscillations of neutron stars. To investigate such a possibility, precise knowledge of the oscillation periods is important. The investigation of the possible effect of nuclear forces on such periods is interesting in itself. This communication presents some results of such work.

It is well known that general relativity is important in such condensed bodies as neutron stars. Therefore, the circular frequency for purely radial oscillations in general relativity, as given by Chandrasekhar[13-15] (the final corrected expression), was used in our calculations. Three types of nuclear forces were chosen for use in the equation of state. One, designated 'Skyrme', is a three-body nuclear potential[16]. The other two are neutron–neutron potentials derived by Levinger and Simmons[17], and are designated V_β and V_γ potentials. The case of non-interacting fermions was also considered for comparison. The models with zero interactions are designated 'ideal' gas models, and the others with the three types of nuclear forces are called the 'Skyrme', V_β and V_γ type models, respectively. The properties of these models are more fully described in a thesis[11], and will be published in due course.

The periods for the four kinds of models are shown as a function of the stellar gravitational mass in Fig. 1; the periods are expressed in milliseconds and the masses are expressed in solar mass units. The broad horizontal portion of each curve corresponds to a series of stable neutron star models. The 'Skyrme'-type stars have periods of 0·2–0·3 msec and the V_γ type stars have periods of 0·4–0·5 msec in the stable region. The typical periods of the V_β type models are about 0·3 msec when the stars are massive, but for less-massive models the periods are about 1 msec. The periods for ideal gas models vary rapidly with mass, decreasing with increasing mass to about 0·8 msec. Estimates of oscillation periods that can be obtained from the classical equations (order of msec)[18] are especially good for the ideal gas models. However, our present results show that we must resort to calculations of the exact general relativistic expressions to obtain more detailed quantitative information.

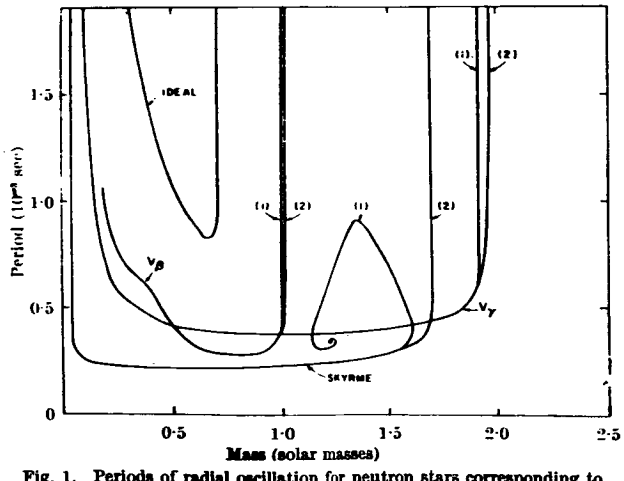

Fig. 1. Periods of radial oscillation for neutron stars corresponding to four equations of state. The branches marked (1) represent equations of state limited so that the pressure does not exceed one third of the proper energy density; branches marked (2) are limited so that the pressure does not exceed the proper energy density

In a suitable equation of state the pressure is not allowed to increase without limit as the density increases, so that either the restriction $p \leqslant \varepsilon/3$ or $p \leqslant \varepsilon$ must be imposed. The periods were calculated for both restrictions on the equations of state and are shown in Fig. 1. The curves denoted by (1) represent the models with the limit $p \leqslant \varepsilon/3$ and those by (2) with $p \leqslant \varepsilon$. The difference is negligible over the major portion of the stable region because these restrictions become applicable only near the massive end of the stability region for some of the equations of state used.

The square of frequency ω^2 is positive in a stable region, becomes zero at the point of instability, and is negative in the region of instability[13-15]. The period approaches infinity at the boundaries of the stable region (one or both ends of the curves in Fig. 1). The curve of the 'Skyrme'-type models with $p \leqslant \varepsilon/3$, however, fails to show this singularity at the massive end. Instead of going to infinity (that is, $\omega^2 = 0$), the period approaches a finite value, as infinite central density is approached, after a number of damped oscillations. For this particular model, instability never sets in at the high-density limit. All other models chosen for this investigation, however, show a singularity at the point of the major mass maximum.

The behaviour on the low-mass side is more complicated. In order to obtain more quantitative information in this region we must include electrons in our configuration. All present models have a pure neutron configuration. Therefore, all curves in Fig. 1 are terminated near 0·2 solar masses.

In order to single out the effect of nuclear forces on the periods, the following period normalization may be used. The normalization factor, τ_n, is defined as:

$$\tau_n = 2\pi/\omega_n,$$

where:

$$\omega_n^2 = AGMR^{-3}\left[3\Gamma - 4 - 3GMc^{-2}R^{-1}\left(\frac{10}{7}\Gamma - 1\right)\right]. \qquad (1)$$

The formula for ω_n^2 is the expression obtained for a homogenous fluid sphere with a constant Γ and constant energy density, if one expands the formula[5] for ω^2, subject to the condition $2GM/c^2R < 1$. The third term in the expression is therefore the general relativistic effect (this expression is quite general and may be used for any range of mass), and the general relativistic effect on the periods is accounted for in this way. The factor A is a correction which accounts for the departure from homogeneity, and Γ is the ratio of specific heats.

In Fig. 2, the normalized periods, τ/τ_n (with $\Gamma = 5/3$ and $A = 1$), are plotted versus stellar mass. We note that the effects of nuclear forces are shown more clearly in this figure. Near ordinary nuclear densities the 'Skyrme'-type potential has the largest attractive term, which decreases the pressure at a given density, the V_γ type has an attractive term of intermediate magnitude, and the V_β type has the least attractive term. One conclusion to be drawn from Fig. 2 is that an attractive force tends to decrease the oscillation periods.

The calculations presented here are intended only to illustrate the importance of nuclear interaction corrections to the equation of state. It seems likely that neutron star vibration periods will be less than would be calculated for a gas of non-interacting particles. If thermal emission

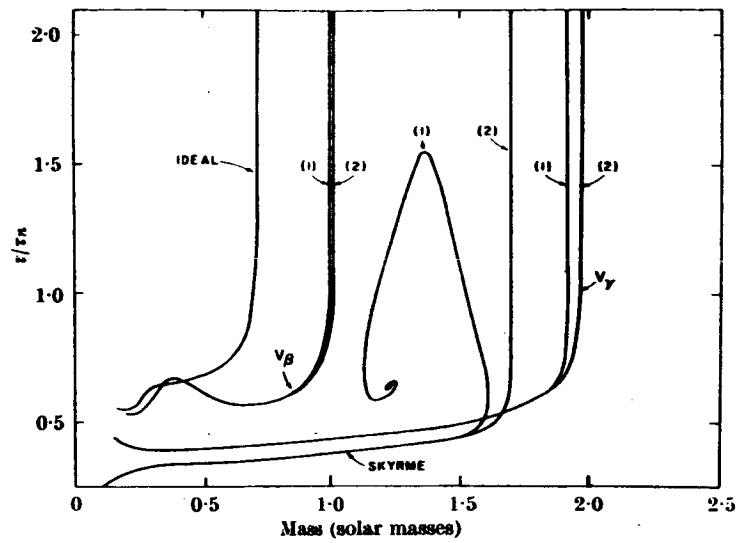

Fig. 2. Periods of radial oscillation of neutron stars with four equations of state relative to the normalization factor τ_n defined in equation 1. The branches marked (1) and (2) are as defined for Fig. 1

in the soft X-ray region should be detected from such objects, then it will become desirable to attempt to detect and measure vibration periods. With some additional indication of the mass or radius of such objects, these periods will then give information about the nuclear forces in the interiors of neutron stars.

SACHIKO TSURUTA
JAMES P. WRIGHT
Smithsonian Astrophysical Observatory,
Cambridge, Massachusetts.
A. G. W. CAMERON
Institute for Space Studies,
Goddard Space Flight Center,
National Aeronautics and Space Administration,
New York.

[1] Giacconi, R., Gursky, H., Paolini, F. R., and Rossi, B. B., *Phys. Rev. Letters*, **9**, 439 (1962).
[2] Giacconi, R., Gursky, H., Paolini, F. R., and Rossi, B. B., *Phys. Rev. Letters*, **11**, 530 (1963).
[3] Bowyer, S., Byram, E. T., Chubb, T. A., and Friedman, H., *Nature*, **201**, 1307 (1964).
[4] Fisher, P. C., and Meyerott, A. F., *Astrophys. J.*, **139**, 123 (1964).
[5] Chiu, H. Y., and Salpeter, E. E., *Phys. Rev. Letters*, **12**, 412 (1964).
[6] Morton, D. C., *Nature*, **201**, 1308 (1964).
[7] Misner, C. W., and Zapolsky, H. S., *Phys. Rev. Letters*, **12**, 635 (1964).
[8] Finzi, A., *Astrophys. J.*, **139**, 1398 (1964).
[9] Morrison, P., Second Texas Symp. on Relativistic Astrophysics, Austin, 1964 (to be published).
[10] Burbidge, G. R., Gould, R. T., and Tucker, W. H., *Phys. Rev. Letters*, **14**, 289 (1965).
[11] Tsuruta, S., thesis, Columbia Univ. (1964).
[12] Cameron, A. G. W., *Nature*, **205**, 787 (1965).
[13] Chandrasekhar, S., *Astrophys. J.*, **140**, 417 (1964).
[14] Chandrasekhar, S., *Phys. Rev. Letters*, **12**, 114 (1964).
[15] Chandrasekhar, S., *Phys. Rev. Letters*, **12**, 437 (1964).
[16] Skyrme, T. H. R., *Nuclear Phys.*, **9**, 615 (1959).
[17] Levinger, J. S., and Simmons, L. M., *Phys. Rev.*, **124**, 916 (1961).
[18] Rosseland, S., *The Pulsation Theory of Variable Stars* (Clarendon Press, Oxford, 1949).

Table [redacted]1

Neutron Star Models

Potential	M/M_o	R(km)	ρ_o(gm/cm^3)	ε_o(gm/cm^3)	c
V_β	0.34	5.7	8.7×10^{14}	9.2×10^{14}	4.0
V_β	0.62	7.0	3.8×10^{15}	4.0×10^{15}	6.0
V_β	0.89	11.7	6.2×10^{15}	7.1×10^{15}	9.2
V_γ	0.33	11.2	3.3×10^{14}	3.4×10^{14}	3.0
V_γ	1.07	12.3	6.9×10^{14}	7.4×10^{14}	6.0
V_γ	1.80	14.1	1.4×10^{15}	1.6×10^{15}	10.0

2. Vibrating Neutron Stars (C. J. Hansen)

As pointed out previously, there exist a whole catalogue of statically stable neutron star configurations, not all of which are stable against radial oscillations. Chandrasekhar (1964a,b,c) has derived the necessary criteria for establishing whether a spherically symmetric configuration is dynamically stable based on an analysis of its normal modes of radial oscillation.* For this purpose he defines the Lagrangian trial function

$$\xi(r,t) = \xi_o(r)\, e^{i\omega t} \qquad (2)$$

where $\xi(r,t)$ measures the radial displacement of a particle from its equilibrium position. Given $\xi_o(r)$ the eigenfrequencies ω are found from a complex of expressions involving the properties of the static configuration and $\xi_o(r)$. The $\xi_o(r)$ which minimizes ω^2

*See also Misner and Zapolsky (1964). Wheeler et al. (1965) have derived Chandrasekhar's results using a different approach.

describes the fundamental mode of oscillation. A sufficient condition for the occurrence of instability is that ω^2 be negative, i.e. $\xi(r,t)$ will contain an exponentially increasing or decreasing factor. We shall consider the fundamental mode only, with the warning that stars that are stable in that mode need not be stable in higher modes.

Tsuruta, et al. (1966) and Misner and Zapolsky (1964) have found that these considerations clarify the structure of the curve of mass versus central density of Figure 5, page 315. Restricting ourselves to the major peaks around $\rho_c \simeq 10^{15}$ gm/cm^3 and 10^{16} gm/cm^3, stars which are stable against radial oscillations in the fundamental mode are to be found only on the low density side of the peaks. As soon as the critical mass is reached, ω^2 goes to zero and then turns negative for higher densities. This behavior is shown in Figure 10, page 394, also page 398, in which oscillation periods P for V_β and V_γ models are plotted against mass.* Note that as the critical mass is approached the period increases suddenly implying that $\omega = 2\pi/P$ tends to zero. Similarly as the mass decreases towards the trough of ρ_c versus M ($\rho_c \sim 10^{14}$-10^{15} gm/cm^3) the same effect occurs.

The form of the trial function yielding the lowest eigenmode for stars of mass less than critical is**

---

*The numerals (1) and (2) refer to limitations on the equation of state: (1) for $p \leq \varepsilon c^2/3$ and (2) for $p \leq \varepsilon c^2$. For V_γ and V_β potentials (1) or (2) make little difference in P except near the critical mass.

**A. G. W. Cameron informs me that preliminary calculations of Mock at Columbia University indicate that actual dynamic models of oscillating neutron stars do not show as simple a displacement form as this one but that the vibrational structure is much more complicated. However, the calculations of Meltzer and Thorne (to be published) agree with Tsuruta's.

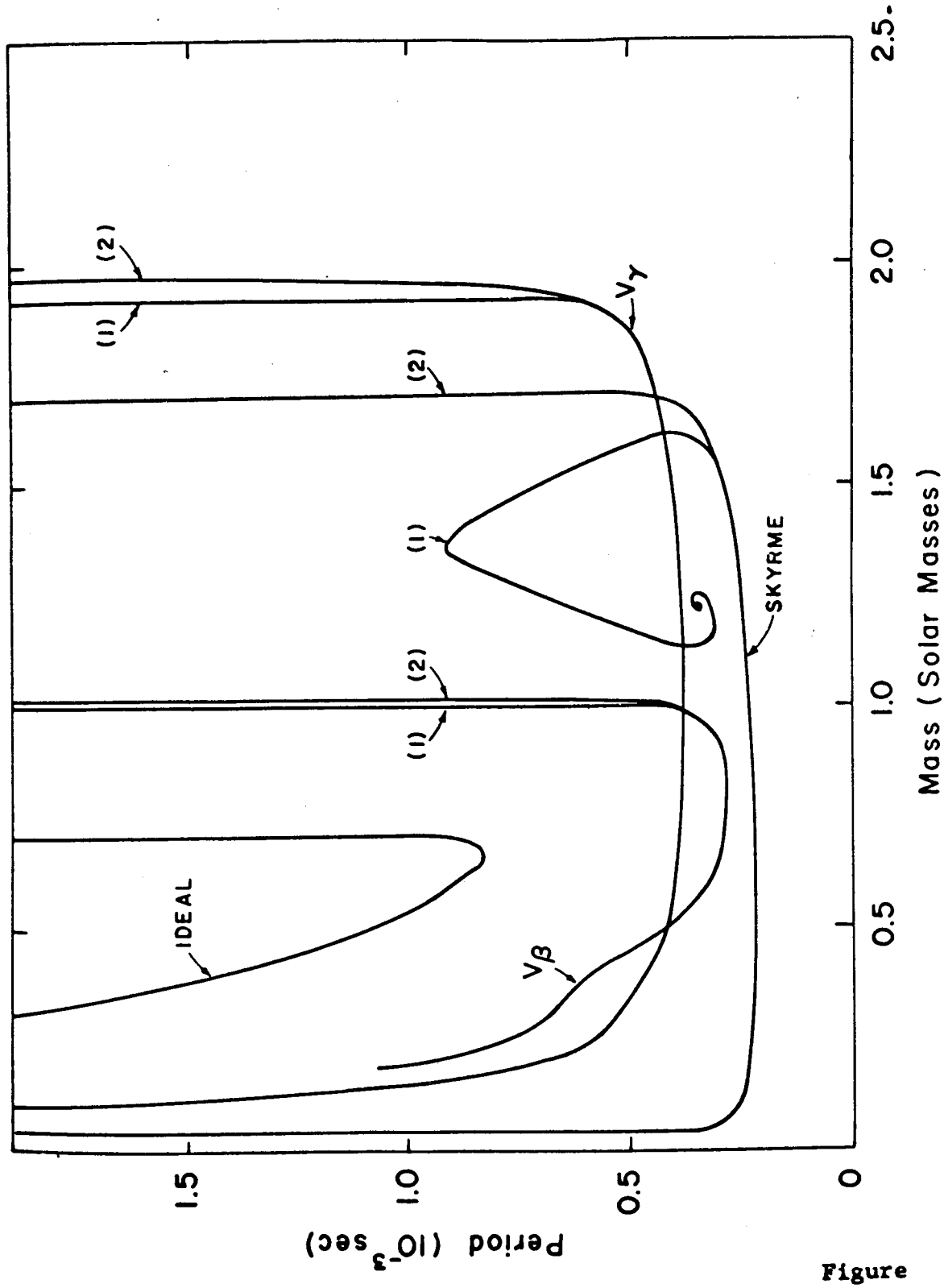
Period (10^{-3} sec)
1.5
1.0
0.5
0
Mass (Solar Masses)
0.5
1.0
1.5
2.0
2.5
IDEAL
SKYRME
V_β
V_γ
(1)
(2)
(1)
(2)
(1)
(2)
(1)
(2)

Figure 1

$$\xi_o(r) \simeq \frac{\delta r}{r_o} \simeq \text{constant} \qquad (3)$$

where δr is the radial displacement of a particle from its equilibrium position r_o. Hence, $\delta r(r_o,t) \simeq r_o \xi_o e^{i\omega t}$, where ξ_o is a constant. The star executes a simple "breathing" motion with every particle moving in phase and being displaced by an amount proportional to its equilibrium radius.

This behavior allows a very simple computation of the total vibrational energy of the object. Since all particles pass through their equilibrium positions at the same time, then the total vibrational energy (excluding general relativistic effects) is just the kinetic energy summed over all particles at that time. That is,

$$E_{VIB} = \int_o^R \frac{1}{2} \rho v^2 \, 4\pi r_o^2 \, dr_o$$

where v is the velocity of a mass element $4\pi r_o^2 \rho dr_o$. The particle's position, as a function of time, is $r = (1 + \xi_o e^{i\omega t}) r_o$ so that $v^2 = \xi_o^2 \omega^2 r_o^2$. Hence,

$$E_{VIB} \simeq 2\pi\omega^2 \, \xi_o^2 \int_o^R \rho r^4 dr \, . \qquad (4)$$

The approximate sign of (4) is stressed since vibrational characteristics of the star are sensitive functions of the properties of its outer portions. These properties are not accurately known. This equation also neglects higher vibrational modes which tend to increase E_{VIB}.

Based on the density distributions kindly furnished by Miss Tsuruta [redacted], and new calculations of vibrational periods of these models, I have computed E_{VIB}/ξ_o^2 for all models studied. Values are listed in Table [redacted]2 along with the frequencies. These models have been chosen such that none lie so near the critical mass that low frequencies limit the amount of energy that they can store.

Table [redacted]2

Vibrational Models

Model (mass)	ω(radians/sec)	E_{VIB}/ξ_o^2(ergs)	$f(\text{ergs}/T_9^2)$
V_β (0.34)	1.0×10^4	9.6×10^{51}	4.2×10^{47}
V_β (0.62)	1.96×10^4	3.3×10^{52}	2.5×10^{47}
V_β (0.89)	2.09×10^4	4.4×10^{52}	2.1×10^{47}
V_γ (0.33)	1.23×10^4	2.3×10^{52}	5.9×10^{47}
V_γ (1.07)	1.67×10^4	1.7×10^{53}	1.05×10^{48}
V_γ (1.80)	1.23×10^4	1.4×10^{53}	1.1×10^{48}

In order to compute the thermal energy of the star we use the results given in Appendix I for the total energy of a degenerate Fermi gas. The kinetic energy (total energy minus rest mass energy) is

$$E\ (\text{kinetic}) \simeq \frac{\pi m^4 c^5}{3h^3}\, k(x) \left[1 + \frac{4\pi^2}{\beta^2} \frac{(3x^2+1)(x^2+1)^{1/2} - (2x^2+1)}{x^3 k(x)}\right]$$

where

$$x = \left(\frac{3h^3\rho}{8\pi m_o^4 c^3}\right)^{1/3}, \qquad \beta = \frac{mc^2}{kT}$$

and k(x) is some function of x. The first term in brackets is the kinetic energy for a zero temperature gas. The second term is the contribution from temperature. Hence, the thermal energy is

$$E_{TH} \simeq \frac{4}{3}\pi^3 \frac{m_o^2 c (kT)^2}{h^3} \frac{(3x^2+1)(x^2+1)^{1/2} - (2x^2+1)}{x} .$$

For a neutron medium at neutron star densities this yields

$$E_{TH} \simeq 2.5 \times 10^{24}\ T_9^2\ \rho^{-2/3}\ \text{ergs/gm.}$$

Since a neutron star is essentially isothermal over most of its volume, the total thermal energy is

$$E_{TH} \simeq 3 \times 10^{25}\ T_9^2 \int_o^R \rho^{1/3} r^2 dr\ \text{ergs.} \qquad (5a)$$

with R in cm. and ρ in gm/cm^3. For a given model this is written as

$$E_{TH}(T_9) \simeq f\ T_9^2 \qquad (5b)$$

with f listed in Table 2 for all models.

C. Neutrino Losses from Neutron Stars

Some of the ways in which neutron stars can lose energy by neutrino emission are discussed in Chapter 6. The important

processes are plasmon decay and neutrino bremsstrahlung. Except for comparison with mechanisms still to be derived, these will be discussed no further.

1. The Modified URCA Process

Under conditions of thermodynamic equilibrium the composition of neutron star interiors is made up primarily of neutrons, protons, electrons and, if the density is high enough, heavy baryons. This is illustrated in Figure 3 of Chapter 5 for temperatures in the range $0 \leq T_9 \lesssim 10$. The conditions that the chemical potentials of the constituents must satisfy for equilibrium are derived in Section E of that chapter. These conditions impose strict limitations on what neutrino producing reactions can take place in the medium. We first consider reactions involving neutrons, protons and electrons.

For equilibrium,

$$\mu_n = \mu_p + \mu_e \qquad (6)$$

where the μ's are the chemical potentials for neutron, proton and electron in that order. For densities greater than $\sim 2 \times 10^{14}$ gm/cm^3 and temperatures less than $T_9 \sim 10$ these particles are degenerate so that one can sensibly talk about the Fermi energy $E_F = \mu - mc^2$. In these terms, the probability of finding an unoccupied state at or below the Fermi energy is $\sim \exp - E_F/kT$. For protons in an equilibrium mixture at $\rho \approx 3 \times 10^{14}$ gm/cm^3 and $T_9 \simeq 1$, this factor is $\sim 10^{-4}$ (see Figure 4 of Chapter 6). The same factor for neutrons or electrons under the same conditions is considerably less. Therefore any reaction that requires one of these particles to

be formed in a final state with an energy less than its Fermi energy will be strongly inhibited.

As an example, consider the electron decay of the neutron. In order that the decay take place with any rapidity, the momenta of all particles except the antineutrino must lie near their Fermi momenta P_F. If this is the case the antineutrino energy is of the order kT which is the approximate allowable spread of particle energies around their Fermi levels. Momentum is not conserved for these conditions since

$$\Delta P = P_F(n) - P_F(p) - P_F(e) \gg kT/c \ .$$

For example, when $\rho \sim 4 \times 10^{14}$ gm/cm^3, $T_9 = 1$, $kT \sim 0.1$ MeV we have $P_F(n) \simeq 400$ MeV/c, $P_F(n) \simeq P_F(e) \simeq 70$ MeV/c, or $\Delta P \simeq 250$ MeV/c which is much larger than kT/c. Hence, if the decay is to conserve both momentum and energy, exit particles must be produced with momenta less than their Fermi momenta and the rates for these decays are strongly inhibited.

These considerations led Chiu and Salpeter (1964) to suggest what they call the "modified URCA" process in which two neutrons collide at the top of the neutron Fermi sea and one of them decays into a proton, electron and antineutrino. The momenta of the initial neutrons can be so arranged as to conserve both energy and momentum and still have the proton and electron momenta be near their respective Fermi momenta. Consider, then,

$$(n,n) \rightarrow (n,p,e,\bar{\nu}) \ , \qquad (7a)$$

and its inverse

$$(n,p,e) \rightarrow (n,n,\nu) \ . \qquad (7b)$$

Even though these reactions involve six particles interacting strongly and weakly, they are very rapid under the conditions of thermodynamic or near thermodynamic equilibrium at very high densities. Before computing the neutrino loss rates for (7 a and b) we first consider a medium at zero temperature which is undergoing rapid fluctuations in density.

If the equilibrium condition (6) is satisfied at zero temperature, reactions (7 a and b) can take place but only zero energy neutrinos can be emitted. Suppose, though, the density of the equilibrium mixture is changed so suddenly that the composition remains unaltered. Is the relation (6) changed? In order to answer this we consider the special case of the oscillating neutron star in which all particles experience displacements of the form

$$\delta r = r_o \, \xi_o \sin \omega t \qquad (8)$$

where r_o is the equilibrium radial position and ξ_o is a constant small compared to unity. If the equilibrium density at r_o is ρ_o then ρ varies as

$$\rho = \rho_o(1 + \xi_o \sin \omega t)^{-3} \simeq \rho_o(1 - 3\xi_o \sin \omega t) \ . \qquad (9)$$

Similarly, each of the number densities varies as

$$N_i \simeq N_{io}(1 - 3\xi_o \sin \omega t) \qquad (10)$$

where i labels the particle. For degenerate conditions the number density of a Fermi gas is related to the chemical potential by

$$N_i = a_i(\mu_i^2 - m_i^2c^4)^{3/2}$$

where a_i is a constant. The change in number density is then

$$\Delta N_i \simeq -3N_{io}\xi_o \sin \omega t \simeq 3a_i(\mu_i^2 - m_i^2c^4)^{1/2}\mu_i\Delta\mu_i$$

where $\Delta\mu_i$ is the corresponding change in μ_i. In order to measure the deviation of $\mu_n-\mu_p-\mu_e$ from zero we define

$$\delta = |\mu_n-\mu_p-\mu_e| = |\mu_{no}+\Delta\mu_n-\mu_{po}-\Delta\mu_p-\mu_{eo}-\Delta\mu_e|$$

$$= |\Delta\mu_n-\Delta\mu_p-\Delta\mu_e| \ . \qquad (11)$$

The last step follows from the equality $\mu_{no} = \mu_{po}+\mu_{eo}$ at equilibrium. With a little algebra this becomes

$$\delta \simeq \xi_o|\sin \omega t| \left| \frac{\mu_{no}^2-m_n^2c^4}{\mu_{no}} - \frac{\mu_{po}^2-m_p^2c^4}{\mu_{po}} - \frac{\mu_{eo}^2-m_e^2c^4}{\mu_{eo}} \right|$$

For $E_{FO}(n) \ll m_nc^2$, $E_{FO}(p) \ll m_pc^2$, and $E_{FO}(e) \simeq \mu_{eo}$ we have,*

$$\delta \simeq \xi_o|\sin \omega t| \ |2E_F(n) - 2E_F(p) - E_F(e)| \ . \qquad (12)$$

---

*Finzi (1966) has given this expression for δ but includes a spurious factor of three (K. Thorne, private communication). As will be pointed out later this error introduces an incorrect factor of 3^8 in Finzi's neutrino loss rate. He has used his results to try to show that the vibrational energy can account for the distinctive shape of supernova light curves. This error invalidates his argument. In any case, Morrison and Sartori (1966) have probably found the correct mechanism for the light curve.

At a density of $\rho \sim 4 \times 10^{14}$ gm/cm^3, $E_F(n) \simeq E_F(e) \simeq 70$ MeV., and $E_F(p) \simeq 3$ MeV., so that $\delta \simeq 60\, \xi_0 |\sin \omega t|$ MeV.

Since δ is not identically zero, thermodynamic equilibrium no longer exists and the modified URCA process can take place. The rate of the reaction (for reasonable values of ξ_0) will be shown not to be so fast as to violate the restriction that the composition cannot change markedly over many oscillation cycles.

The "thermal" URCA process is derived from the smearing of Fermi levels by temperature effect. The "oscillating" URCA process is caused by shifting of the Fermi levels.

2. Calculation of the Rates

A number of authors* have calculated either thermal or oscillating URCA rates, but not both. Before discussing their results we shall compute a combined thermal and oscillating rate in a rather simple fashion. This is improved by taking into account the more sophisticated results of the above authors.

For the reaction $(n,n) \rightarrow (n,p,e,\bar{\nu})$ we consider the simplest Feynman diagram describing the scattering of two neutrons mediated by a single π^0 meson, followed by an electron decay of a virtual neutron. (We shall ignore exchange diagrams or diagrams containing charged mesons.) The four-momenta shown in the figure label the

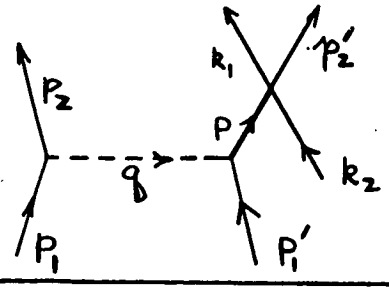

* Chiu and Salpeter (1964), Finzi (1965), Ellis (1965) and Bahcall and Wolf (1965 a,b and c) for thermal losses, and Finzi (1966) and Thorne (to be published) for oscillating URCA losses.

particles as follows:

$$k_1 \rightarrow e^-$$

$$k_2 \rightarrow \text{incident neutrino (i.e., exit antineutrino)}$$

$$p_1, p_1', p, p_2 \rightarrow \text{neutrons}$$

$$p_2' \rightarrow \text{proton}$$

$$q \rightarrow \pi^0 .$$

The Feynman rules for the weak vertex, associated γ-matrices, etc., are reviewed in ~~Appendix II~~ Chapter 6. For each strong vertex we insert a factor $gi\gamma_5$ for the pseudoscalar meson where g is the strong coupling constant $g^2/4\pi \simeq 14$. The virtual meson line contributes a propagator $i/(q^2-m_\pi^2)$ and the virtual neutron contributes $(\gamma\cdot p+m)/(p^2-m^2)$. The matrix element is

$$M = \bar{u}(k_1)\gamma^\mu(1-\gamma_5)u(k_2)\bar{u}(p_2')\gamma_\mu(1-\gamma_5)\frac{\gamma\cdot p+m}{p^2-m^2}$$

$$\times \gamma_5 g u(p_1')\frac{1}{q^2-m_\pi^2}\bar{u}(p_2)\gamma_5 g u(p_1)G/2^{1/2}$$

The neutron and proton masses are taken equal to m, G is the weak coupling constant and the u's are appropriate wave functions.

Using the methods of ~~Appendix II~~ Chapter 6 for summing final spins and averaging initial spins we find

$$M^2 = \frac{2^2 g^4 G^2}{m^4 m_e m_\nu}\frac{1}{(p^2-m^2)^2}\frac{1}{(q^2-m_\pi^2)^2}\Big[(m^2-p_1\cdot p_2)p_1'\cdot k_2$$

$$+ p_1'\cdot(p_1-p_2)k_2\cdot(p_1-p_2)\Big]p_2'\cdot k_1(m^2-p_1\cdot p_2) ,$$

where

$$q = p_1 - p_2, \quad p = q + p_1' = p_1 - p_2 + p_1' .$$

The electron mass is set to zero.

The neutrino loss rate per incident neutron pair with momenta p_1, p_1' is

$$E_\nu \sigma v = \iiiint M^2 \frac{m^4 m_e m_\nu}{(2\pi)^{12}} \frac{E_\nu}{E_2 E_2' E_e E_\nu E_1 E_1'} \quad x$$

$$x\ (1 - S(p_2))(1-S(p_2'))(1-S(k_1))(2\pi)^4\ \delta^4(p_2+k_1+k_2+p_2'$$

$$- p_1-p_1')\ d^3k_1 d^3k_2 d^3p_2' d^3p_2 \quad .$$

The factors (1-S) account for the unoccupied portions of phase space into which the exit particles may enter with S being the Fermi-Dirac distribution function

$$S = [1 + \exp \beta(E-\mu)]^{-1}$$

and

$$\beta = 1/kT .$$

The total loss rate L is the integral over the distributions of initial neutrons so that

$$L = \int \int E_\nu \sigma v\ S(p_1)S(p_1')\ \frac{d^3p_1 d^3p_1'}{(2\pi)^6}$$

This yields an 18 dimensional integral. However, the kinematics of the reaction allow for considerable simplification. Bahcall and Wolf (1964 b and c) have pointed out that degeneracy

effects permit only very restricted portions of phase space to contribute to the integral. If both initial and final neutrons are located near the top of the neutron Fermi sea, the vector momenta of these particles must form a rough equilateral triangle as shown below.

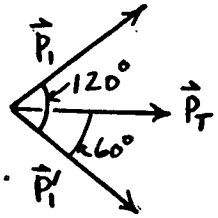

Before

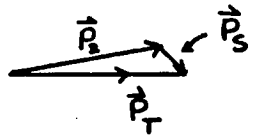

After

The vectors $\vec{p}_T$ and $\vec{p}_S$ are given by

$$\vec{p}_T = \vec{p}_1 + \vec{p}_1' = \vec{p}_2 + \vec{p}_S = \vec{p}_2 + \vec{p}_2' + \vec{k}_1 + \vec{k}_2$$

The length of $\vec{p}_S$ is much smaller than $\vec{p}_2$ or $\vec{p}_T$ and can vary only in an extremely small region because $\vec{p}_2$ and $\vec{p}_T$ are nearly equal and colinear. Vector configurations which do not conform to the above diagram involve either initial particles that come from sparsely inhabited regions of phase space or exit particles that must enter densely inhabited regions. Little leeway is allowed. Therefore M^2 can be evaluated for the above configuration and removed from the integral. To do this conveniently, we define M'^2 and P by

$$M'^2 = \frac{m^4 m_e m_\nu M^2}{(2\pi)^{14} E_2 E_2' E_e E_\nu E_1 E_1'}$$

and,

$$P = \int E_\nu \, S(p_1)S(p_1')(1-S(p_2))(1-S(p_2'))(1-S(k_1))E_\nu$$

$$\delta^4(p_2+k_1+k_2+p_2'-p_1-p_1') \quad d^3p_1 d^3p_2 d^3p_1' d^3p_2' d^3k_1 d^3k_2 \qquad (13)$$

with

$$L = M'^2 P \ .$$

From the numerical values of the Fermi momenta and energies of particles at thermodynamic equilibrium and the vector configuration it can be shown that,

$$p_1 \cdot p_2 = E_1 E_2 - \vec{p}_1 \cdot \vec{p}_2 \simeq \mu_n^2$$

$$p_1 \cdot p_1' \simeq \mu_n^2$$

$$p_1' \cdot k_2 \simeq E_\nu \mu_n$$

$$p_2' \cdot k_1 \simeq \mu_e m \simeq E_e m$$

$$p^2 - m^2 \simeq 2[m^2 - \mu_n^2] \simeq - 4E_F(n)\, m$$

$$q^2 - m_\pi^2 \simeq - 4\, E_F(n)\, m \ .$$

The second term in brackets of M^2 is small compared to the first. Hence, we find that

$$M'^2 \simeq \frac{1}{2^4} \frac{g^4 G^2}{(2\pi)^{14}} \frac{1}{m^4} \frac{1}{E_F^2(n)} \ .$$

The phase space integral P, as will be shown, is given by

$$P \simeq \frac{(4\pi)^5}{2} (kT)^8 \, m^4 \, P_F(p) P_F^2(e) \, I \qquad (14)$$

where I is a function of the ratio of δ of (II-19) over kT. For the special case of the thermal URCA rate ($\delta = 0$), Bahcall and Wolf (1965 b,c) give $I \simeq 903$. In those papers they also give the following approximate expressions for equilibrium Fermi energies and momenta for densities $\rho \lesssim 2\rho_N$ (ρ_N = nuclear density $\simeq$ 3.7×10^{14} gm/cm^3):

$$E_F(n) \simeq E_F(e) \simeq 70 \, (\rho/\rho_N)^{2/3} \text{ MeV} \qquad (15a)$$

$$E_F(p) \simeq 3 \, (\rho/\rho_N)^{4/3} \text{ MeV} \qquad (15b)$$

$$P_F(n) \simeq 400 \, (\rho/\rho_N)^{1/3} \text{ MeV/c} \qquad (15c)$$

$$P_F(e) \simeq P_F(p) \simeq 70 \, (\rho/\rho_N)^{2/3} \text{ MeV/c} \, . \qquad (15d)$$

Inserting these into $L = M'^2 P$ we find the thermal URCA rate,

$$L_{TH} \simeq 3 \times 10^{20} \, (\rho/\rho_N)^{2/3} \, T_9^8 \text{ ergs/cm}^3\text{-sec.}$$

Bahcall and Wolf's result, based on an entirely different method of computation of the matrix element, is

$$L_{TH}(B\text{-}W) \simeq 5 \times 10^{19} \, (\rho/\rho_N)^{2/3} \, T_9^8 \text{ ergs/cm}^3\text{-sec}, \qquad (16)$$

or only a factor of six lower than mine. Their matrix element will be used here because it is based on nucleon-nucleon scattering

data and the independent particle model of Gomes, et al. (1958) which is more realistic than a simple single pion exchange model.

The method for computing the phase space integral will also be taken from Bahcall and Wolf except for important modifications which make it possible to compute the total URCA rate.

The integrand of P is negligible except in those regions of phase space where all the particle momenta are within kT of their Fermi energies. Therefore consider the "important" region where

$$|p_S| + |p_1 - p_1'| < |p_2| < |p_1 + p_1'| - |p_S| \qquad (17a)$$

and

$$|p_1| > |p_S| \ . \qquad (17b)$$

The angular part of P is separated out by defining

$$A = \prod_i \int \delta^3(\vec{K}\ (\text{final}) - \vec{K}\ (\text{initial}))\ d\Omega_i$$

where the product is over all particles and $\vec{K}$ (final and initial) are the vector directions of final and initial states. Bahcall and Wolf show that

$$A = (4\pi)^5\ (2p_1 p_2 p_1')^{-1} \ .$$

After doing the integration over the neutrino momentum with the aid of the last remaining delta function we define the new variables

$$x_1 = \beta(E_1 - \mu_n)$$

$$x_2 = \beta(E_1' - \mu_n)$$

$$x_3 = -\beta(E_2 - \mu_n)$$

$$x_4 = -\beta(E_e - \mu_e)$$

$$x_5 = -\beta(E_p - \mu_p)$$

and

$$\Delta = \beta(\mu_n - \mu_p - \mu_e) = \delta/kT \quad . \tag{18}$$

Furthermore, we note that for protons and neutrons $pdp = EdE \simeq mdE$, and $p_e^2\, dp_e \simeq P_F^2(e)\, dp_e$ over the "important" region. Finally, putting everything together we have

$$P = \frac{(4\pi)^5}{2\beta^8} m^4 P_F(p) P_F^2(e) \int_{-\infty}^{\infty} dx_1 \int_{-\infty}^{\infty} dx_2 \int_{-\infty}^{\infty} dx_3 \int_{-\infty}^{\infty} dx_4 \int_{-(x_1+x_2+x_3+x_4+\Delta)}^{\infty} dx_5$$

$$\left[\sum_{i=1}^{5} x_i + \Delta\right]^3 \prod_{i=1}^{5} (1+\exp x_i)^{-1} \quad . \tag{19}$$

The limits are taken from $-\infty$ to $+\infty$ for all integrals except x_5 (corresponding to the proton). This procedure allows a maximum possible additive error in the integral of $\sim \exp - E_F(p)/kT$ providing $\delta \lesssim E_F(p)$. Since $kT \ll E_F(p)$ for all cases to be studied, the error is negligible.

The integral in ([19]) was called I in ([14]). For $\delta = 0$ ($\Delta = 0$) Bahcall and Wolf find

$$I = \frac{11,513}{120,960}\,\pi^8 \simeq 903 \ .$$

Thus, if we define the ratio

$$P'(\Delta) = \frac{I(\Delta)}{I(\Delta=0)} \ ,$$

then the general expression for the modified URCA loss rate is, using (16),

$$L(\Delta,T_9) = 5 \times 10^{19}\,(\rho/\rho_N)^{2/3}\,T_9^8\,P'(\Delta)\ \text{ergs/cm}^3\text{-sec} \qquad (20)$$

for the reaction $(n,n) \rightarrow (n,p,e,\bar{\nu})$.

The integral $P'(\Delta)$ has been evaluated. ~~in Appendix VI and its behavior for $\Delta \geq 0$ is shown in Figure AVI-1.~~ For $\Delta \gtrsim 160$,

$$P'(\Delta) \simeq 1.65 \times 10^{-7}\,\Delta^8 \ . \qquad (21)$$

Therefore, as kT tends to zero the temperature cancels in (20) and the oscillating URCA rate is obtained,

$$L_{VIB}(T_9=0,\delta) = 0.74 \times 10^7\,(\rho_N/\rho)^{1/3}\,\delta^8\ \text{erg/gm-sec} \ , \qquad (22)$$

where $\delta = \mu_n - \mu_p - \mu_e$ (in MeV.) must be greater than zero.* If $\delta < 0$ then $\mu_n < \mu_p + \mu_e$ and no neutrons can decay.

The inverse reaction $(n,p,e) \rightarrow (n,n,\nu)$ can be shown to have the same matrix element and phase space integral as the above except that Δ is replaced by $-\Delta$. Hence, the total loss rate is

---

*Finzi (1966, with corrections) and Meltzer and Thorne (to be published) have derived the zero temperature rates and their results are in good agreement with (22).

$$L(\Delta,T_9) = 5 \times 10^{19} \, (\rho/\rho_N)^{2/3} \, T_9^8 [P'(\Delta)+P'(-\Delta)] \text{ ergs/cm}^3\text{-sec} \quad (23)$$

Since $P'(\Delta)$ increases very rapidly as Δ increases there is little error in replacing $P'(-\Delta)$ by $1/P'(\Delta)$ and computing the absolute value of Δ only. As either δ or T_9 approach zero the correct limits are still obtained.

3. Other Reactions

Besides the neutron scattering reaction there are a number of other possible neutrino producing mechanisms involving the other constituents of the medium. The most important of these occurs in the density $\sim 7 \times 10^{14}$ to 4×10^{15} gm/cm^3 where muons make their appearance (see Figure 3 of Chapter 5). Their presence implies the existence of the reaction

$$(n,n) \rightarrow (n,p,\mu^-,\bar{\nu}_\mu)$$

and its inverse. The analysis of the rate follows that of the analogous electron case. It is a simple matter to show that the total rate of (23) becomes

$$L(\Delta_e,\Delta_\mu,T_9) = 5 \times 10^{19} \, (\rho/\rho_N)^{2/3} \, T_9^8 \left\{P'(\Delta_e) + 1/P'(\Delta_e)\right.$$

$$\left. + [P'(\Delta_\mu) + 1/P'(\Delta_\mu)] \, P_F^2(\mu)/P_F^2(e)\right\} \text{ ergs/cm}^3\text{-sec}, \quad (24)$$

where $P_F(\mu)$ is the muon Fermi momentum and

$$\Delta_e = |\mu_n - \mu_p - \mu_e|$$

$$\Delta_\mu = |\mu_n - \mu_p - \mu_\mu|$$

Reactions involving antiparticles (including positrons) go very slowly because at equilibrium their concentrations are negligible (see Section E, Chapter 5).

Bahcall and Wolf (1965c) have considered the reaction

$$\pi^- + n \rightarrow n + e^- \text{ (or } \mu^-) + \bar{\nu} ,$$

and its inverse. In that paper they find that the loss rate for this reaction greatly exceeds that of the modified URCA process based on their estimate of π^- concentrations in the medium. However, this view has since been discarded as Bahcall (and M. A. Ruderman), in a communication to Tsuruta and Cameron (1966), no longer believe pions are present except at very high densities. This is consistent with the results of Chapter 5 in which pions do not appear until $\sim 10^{17}$ gm/cm^3.

We shall also exclude reactions involving the heavy baryons for the following reasons: the magnitude phase space integrals for reactions such as

$$\Lambda^0 + \Lambda^0 \rightarrow \Lambda^0 + p + e + \bar{\nu}$$

or

$$\Sigma^- + \Sigma^- \rightarrow n + e + \bar{\nu}$$

should not be too different from the nucleon-nucleon interactions. It is also expected that the strong couplings are about the same.* This leaves the weak decay to be examined.

---

*See for example, the Λ^0-proton scattering cross sections given in Alexander et al. (1964) which have the same order of magnitude as nucleon-nucleon.

Following the analysis of Jackson (in Fulton, 1963, p. 263 ff.) we write the electron decay rate of a baryon in the form

$$\lambda = g F M$$

where F is a laboratory phase space integral, M is the mass of the decaying baryon and g is an effective weak coupling constant which measures the inherent strength of the decay. We want to compare g for neutron decay with the g's for the decays of the most abundant heavy baryons in the mixture, i.e. Λ^0 and Σ^-,

$$\Lambda^0 \rightarrow p + e + \bar{\nu} \; (\lambda \simeq 3.3 \times 10^6 \text{ sec}^{-1})$$

and

$$\Sigma^- \rightarrow n + e + \bar{\nu} \; (\lambda \simeq 0.9 \times 10^7 \text{ sec}^{-1}) \; .$$

Using the expressions for F given by Jackson we find

$$g \; (n \rightarrow p + e + \bar{\nu}) = 5.4 \times 10^{-10}$$

$$\frac{g \; (\Lambda^0 \rightarrow p + e + \bar{\nu})}{g \; (n \rightarrow p + e + \bar{\nu})} \simeq 0.1$$

and

$$\frac{g \; (\Sigma^- \rightarrow n + e + \bar{\nu})}{g \; (n \rightarrow p + e + \bar{\nu})} \simeq 0.06 \; ,$$

with a average weak decay inhibition of ~ 0.1. From these figures we infer that the heavy baryon reactions are probably slower than the nucleonic--or at least that the inclusion of the former cannot change the total rate by more than a factor of two.

This is certainly within the limits of error for the calculation as a whole.

4. Loss Rates During Vibration

Having established expressions for the URCA loss rates as functions of Δ and temperature we compute their behavior for sinusoidal radial variations in a neutron star.

The radial displacement of a particle during the vibration is

$$\delta r = r_\rho \xi_o \sin \omega t \qquad (25)$$

with the density varying as

$$\rho = \rho_o (1 + \xi_o \sin \omega t)^{-3} . \qquad (26)$$

A rough estimate for δ was given by (12) where for $\rho \sim 4 \times 10^{14}$ gm/cm^3, δ (max) $\simeq 60\ \xi_o$ MeV. In order that the expressions for the URCA rates derived previously be valid δ should be less than $E_F(p)$. This sets an approximate upper limit of 0.05 on the value of ξ_o that can be used when $\rho \simeq 4 \times 10^{14}$ gm/cm^3. At higher densities this restriction can be somewhat relaxed since $E_F(p)$ increases rapidly with density. Similarly the highest temperature that can be used is $\sim 10^{10}$ °K corresponding to the point at which protons start to become non-degenerate.

Equation (12) is not accurate enough to calculate δ as a function of ρ since L goes as δ^8. Therefore the degenerate expression for μ versus ρ is used.

Figure 3 shows how L (excluding muons) varies over one cycle of compression and expansion at a density of $\rho = 4.6 \times 10^{14}$ gm/cm^3

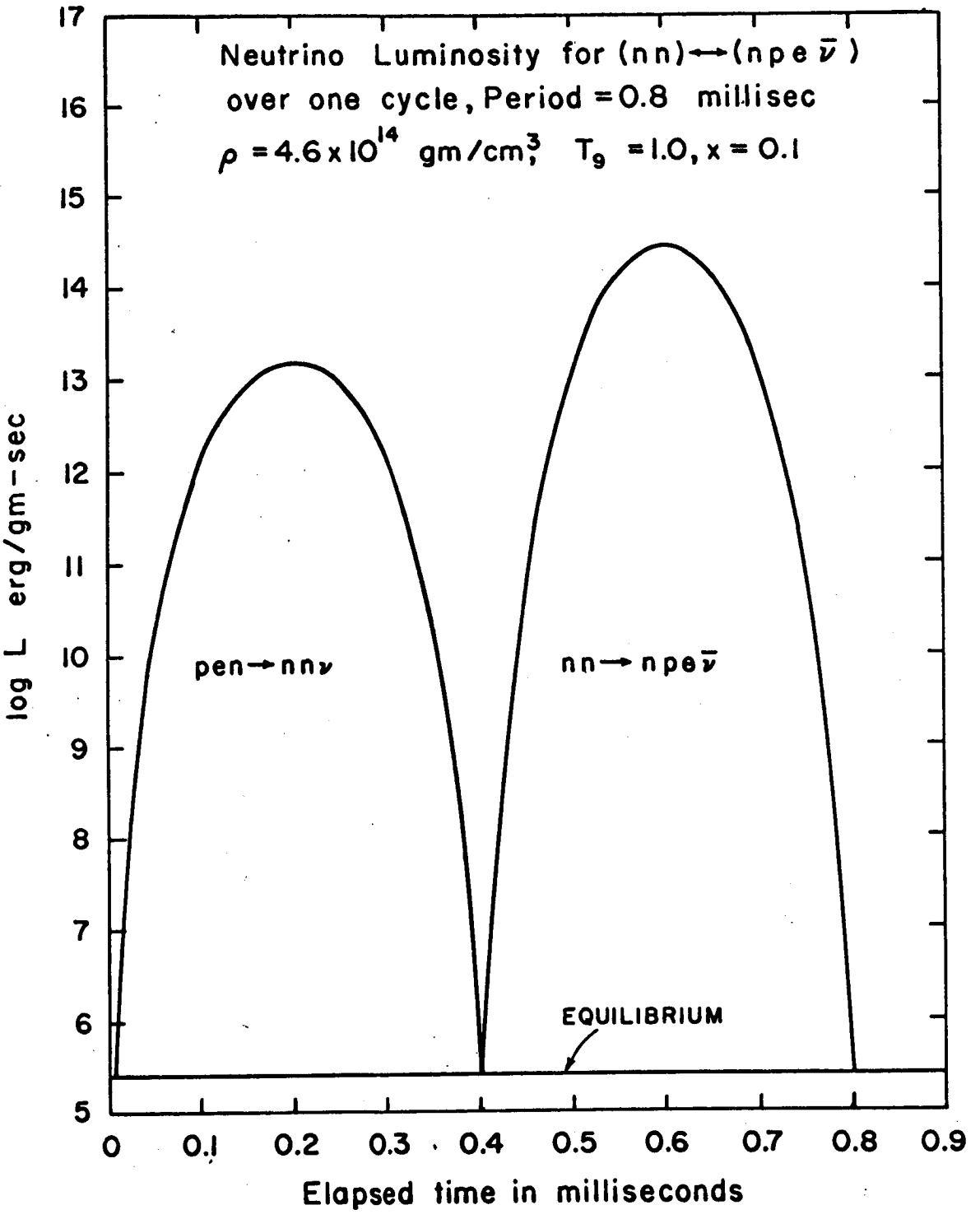
Neutrino Luminosity for (nn)↔(npe$\bar{\nu}$)
over one cycle, Period = 0.8 millisec
$\rho = 4.6 \times 10^{14}$ gm/cm^3; $T_9 = 1.0$, x = 0.1
pen→nnν
nn→npe$\bar{\nu}$
EQUILIBRIUM
log L erg/gm-sec
Elapsed time in milliseconds
17
16
15
14
13
12
11
10
9
8
7
6
5
0
0.1
0.2
0.3
0.4
0.5
0.6
0.7
0.8
0.9

Figure 3

and a temperature of $T_9 = 1$. The period of the cycle is 0.8 millisec. with an overly large amplitude of $\xi_0 = 0.1$ which is called x in the figure. Due to the large variation of L with time, L is plotted logarithmically which makes the curve deceptive. On a linear scale L is sharply cusped at the turning points of the motion. The line labeled "equilibrium" is the loss rate for the thermal URCA process only.

The disparity in the heights of L at the points of maximum compression and expansion is due to the different percentage change in ρ at these points. This means that there is a net shift in composition to more protons. For the case shown the mean life for a neutron against decay is $\tau \sim 10^3$ sec. which is a relatively short time. However, the value of ξ_0 is larger than is used for actual calculation. A more reasonable value of $\xi_0 = 0.01$ yields $\tau \sim 100$ years. An investigation of the net change in composition over times ~ 1000 years indicate that the number of neutrons converted to protons has little effect on the outcome of the vibrational damping calculation. If anything, complete neglect of composition change tends to overestimate the rate of damping.

The loss rate, integrated over as many cycles as take place in one second, is shown in Figure 4 as a function of density for several values of ξ_0 (=x) and T_9 equal to zero and unity. The humped appearance of the curves is due to the relative changes in the chemical potentials as the density varies.

A convenient expression for the time integrated L derived from numeric calculations is

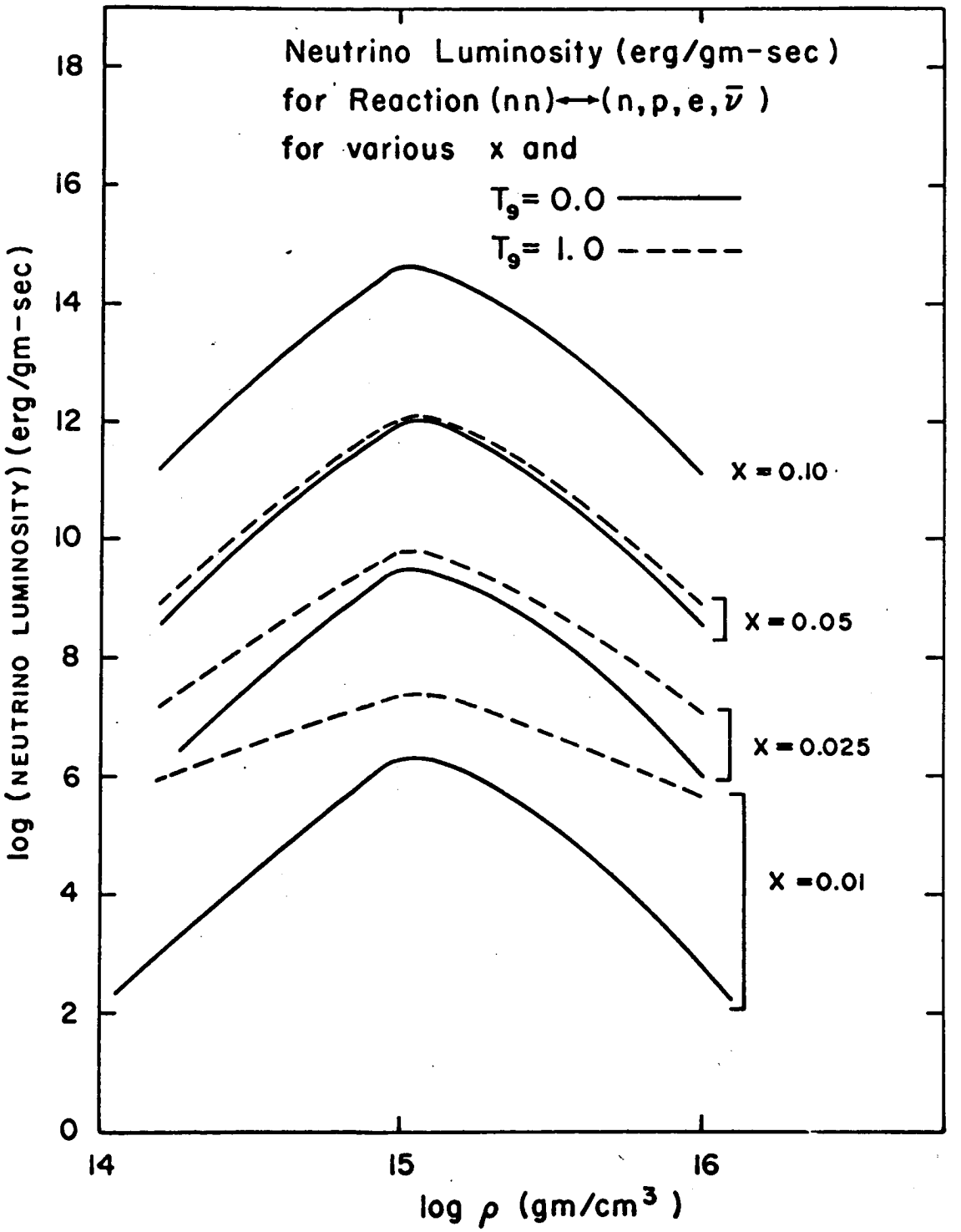
Neutrino Luminosity (erg/gm-sec)
for Reaction (nn)↔(n,p,e,$\bar{\nu}$)
for various x and
T_9= 0.0
T_9= 1.0
X = 0.10
X = 0.05
X = 0.025
X = 0.01
log (NEUTRINO LUMINOSITY) (erg/gm-sec)
log ρ (gm/cm^3)
0
2
4
6
8
10
12
14
16
18
14
15
16

Figure 4

$$L = \frac{5\times10^{19}}{6} (\rho/\rho_N)^{2/3} T_9^8 [\ell_c+\ell_e+\ell_{eq}] \text{ ergs/cm}^3\text{-sec} \qquad (23a)$$

where

$$\ell_c = P'(\Delta_e) + 1/P'(\Delta_e) + [P'(\Delta_\mu)+1/P'(\Delta_\mu)]\ P_F^2(\mu)/P_F^2(e) \qquad (23b)$$

with Δ_e and Δ_μ computed at the maximum point of compression. The quantity ℓ_e corresponds to ℓ_c with everything computed at maximum expansion. The last term

$$\ell_{eq} = 8(1 + P_F^2(\mu)/P_F^2(e)) \ . \qquad (23c)$$

5. Comparison With Other Rates

Table 3 gives a short comparison of the modified URCA loss rate with the combined rates due to the mechanisms of pair annihilation, plasmon decay and the photoneutrino process. (L^o is the combined rate.) Not included is neutrino bremsstrahlung which may be larger than the rest of the rates when the temperature is below $T_9 \simeq 1$ and if ξ_o is much smaller than 0.01. These rates are not dependent on the shifting of Fermi levels due to density changes, but, for a given density, depend only on temperature. The temperature for the table is $T_9 = 1$ and $\xi_o = 0.01$.

Table 3

Comparison of Rates

ρ (gm/cm^3)	L^o (erg/gm-sec)	L (URCA)
10^{14}	1.2×10^{3}	5×10^{5}
10^{15}	3.5×10^{-2}	2.5×10^{7}
10^{16}	1.2×10^{-2}	5×10^{5}

If ξ_0 is less than 0.01 some of the competing rates may become important but their neglect does not alter the conclusions reached.*

D. Vibrational and Thermal Damping

The total modified URCA loss rate is obtained by integrating (23) over the volume of the star, i.e.,

$$L(\xi_0, T_9) = 4\pi \int_0^R L(r, \xi_0, T_9) r^2 dr \quad \text{erg/sec.} \tag{27}$$

$E_{VIB}(\xi_0, \omega)$, L_γ and $E_{TH}(T_9)$ are given by (4) and (5) and approximations to the effective temperature and photon luminosity.

Because $L(\xi_0, T_9)$ is a complicated function of vibrational amplitude and temperature it is difficult to see how this energy loss decreases both E_{VIB} and E_{TH}. Initially we shall treat vibrational and thermal losses separately by considering the limits of zero temperature and zero amplitude.

1. Vibrational Damping

Let $L_{VIB}(\xi_0)$ be the neutrino luminosity at zero temperature. The rate of decrease of vibrational energy is then

$$\frac{dE_{VIB}(t)}{dt} = - L_{VIB}(\xi_0) \tag{28}$$

Since E_{VIB} is proportional to ξ_0^2 and L_{VIB} goes as δ^8 which in

---

*

turn goes approximately as ξ_o^8 (equation II-20) it is easy to show that

$$E_{VIB}(t) \simeq E_{VIB}(0)\,[1 + aE_{VIB}^3(0)t]^{-1/3}. \qquad (29)$$

The quantity a depends only on the particular neutron star model and is proportional to the loss rate. These results are very encouraging. The cube root dependence of E_{VIB} on "a" appreciably reduces the effect of any error in the luminosity calculations of Section C. The luminosity is then

$$L_{VIB}(t) \simeq \frac{a\,E_{VIB}^4(t)}{3} \text{ ergs/sec}, \qquad (30)$$

by substitution of (29) in (28).

Figure 5 shows the vibrational histories of all the models studied. The initial value of ξ_o is 0.05. We note that even though vibrational energies decrease very rapidly with time, yet after one thousand years have elapsed (3×10^{11} sec.) there are still more than 10^{47} ergs stored for V_β models and more than 10^{48} ergs stored for V_γ models. As will be shown, these energies are, for the most part, sufficiently large to account for the present day photon luminosity of the Crab Nebula.

2. Thermal Damping

Let $L_{TH}(T_9)$ be the neutrino luminosity for no vibration ($\xi_o = 0$). The rate of decrease of thermal energy is then,

$$\frac{dE_{TH}(t)}{dt} = -L_{TH}(T_9) - L_\gamma . \qquad (31)$$

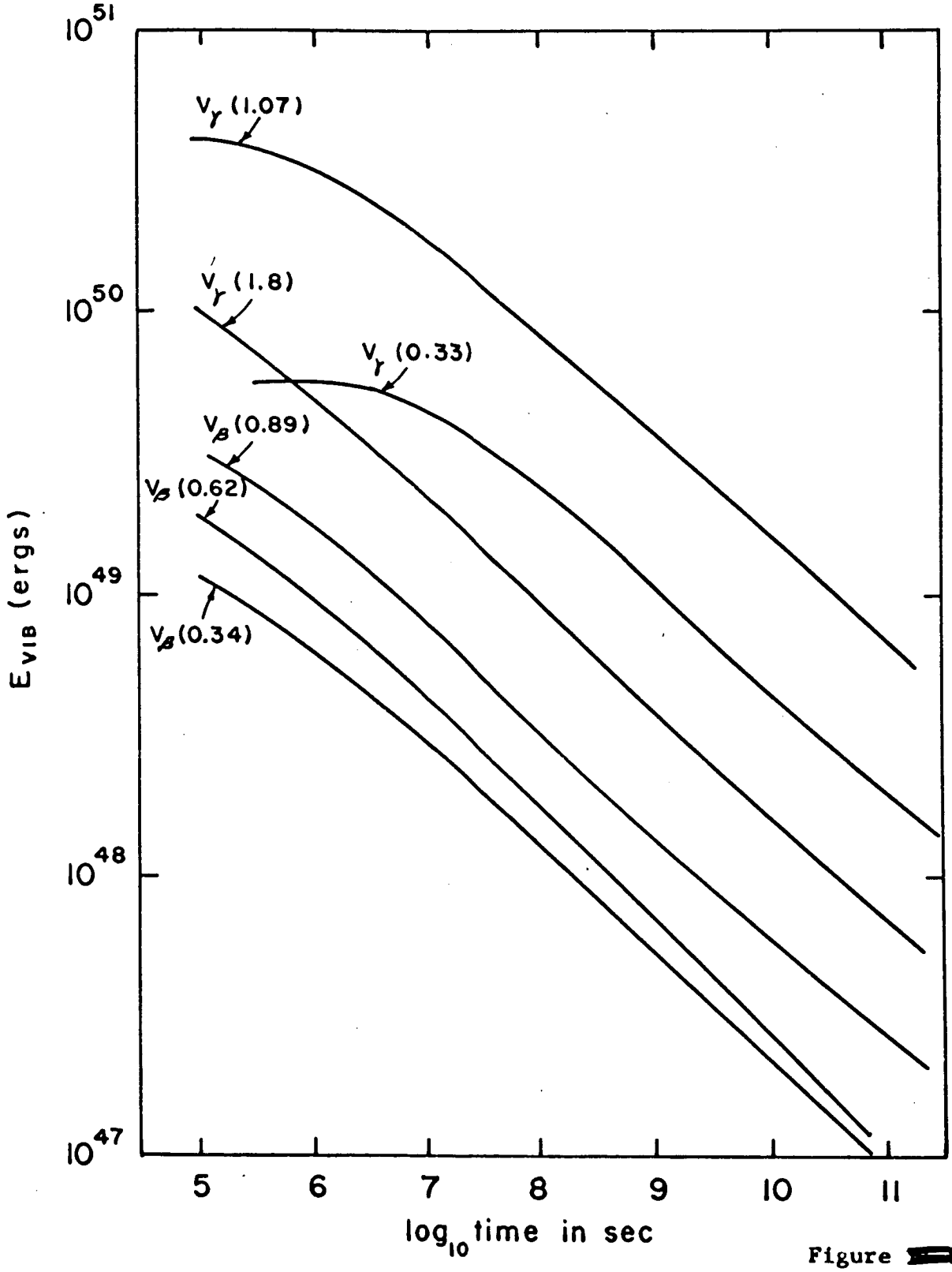
10^{51}
10^{50}
10^{49}
10^{48}
10^{47}
E_{VIB} (ergs)
V_γ (1.07)
V_γ (1.8)
V_γ (0.33)
V_β (0.89)
V_β (0.62)
V_β (0.34)
5
6
7
8
9
10
11
$\log_{10}$ time in sec

Figure 5

If L_γ is much less than L_{TH}, then it can be shown that

$$E_{TH}(t) \simeq E_{TH}(0)\,[1 + bE_{TH}^{3}(0)t]^{-1/3}\,, \qquad (32)$$

$$T_e(t) \simeq T_e(0)\,[1 + gT_e^{9}(0)t]^{-1/9}, \qquad (33)$$

and

$$L_{TH}(t) \propto b\,\frac{E_{TH}^{4}(t)}{3} \text{ ergs/sec.} \qquad (34)$$

$E_{TH}(t)$ and $E_{VIB}(t)$ have the same dependence on luminosity.

A sample cooling curve is shown in Figure 6 for V_γ (1.07) with an initial temperature of $T_9 = 1$. Also shown are vibrational energy histories for the same model with two different initial values of ξ_0. The shape of the curves are typical of all models and show that regardless of the initial conditions the curves (for E_{VIB} or E_{TH}) merge together after a suitable time has elapsed. This is in agreement with the functional forms of (32) and (29).

The behavior of T_e with time for V_γ (1.07) is illustrated in Figure 7. Also shown is an approximate relation between T_e and T_9. At 3×10^{10} sec. the effective surface temperature of V_γ (1.07) is $\sim 4 \times 10^{6}$ °K. The maximum blackbody wavelength corresponding to this temperature is

$$\lambda_{max}(\text{cm.}) = 0.2918/T_e(^\circ\text{K}) \simeq 10^{-7} \text{ cm.} = 10 \text{ Å} \qquad (35)$$

which is in the soft x-ray region.

A compilation of the survey results is given in Table 4 where the quantities a, b and g are listed for all models. Also

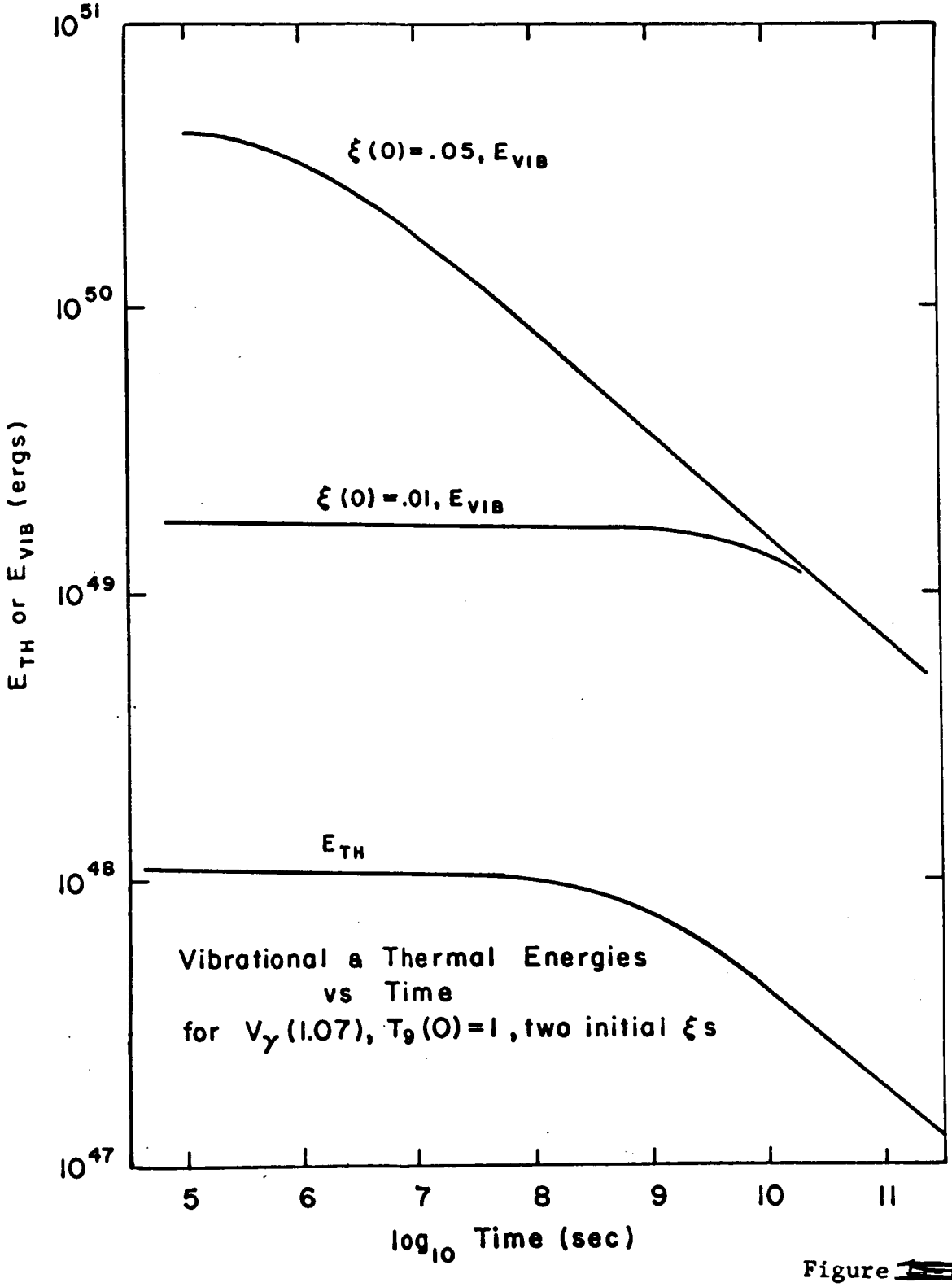
10^{51}
10^{50}
10^{49}
10^{48}
10^{47}
E_{TH} or E_{VIB} (ergs)
$\xi(0)=.05, E_{VIB}$
$\xi(0)=.01, E_{VIB}$
E_{TH}
Vibrational & Thermal Energies
vs Time
for $V_\gamma(1.07)$, $T_9(0)=1$, two initial ξs
5
6
7
8
9
10
11
$\log_{10}$ Time (sec)

Figure 6

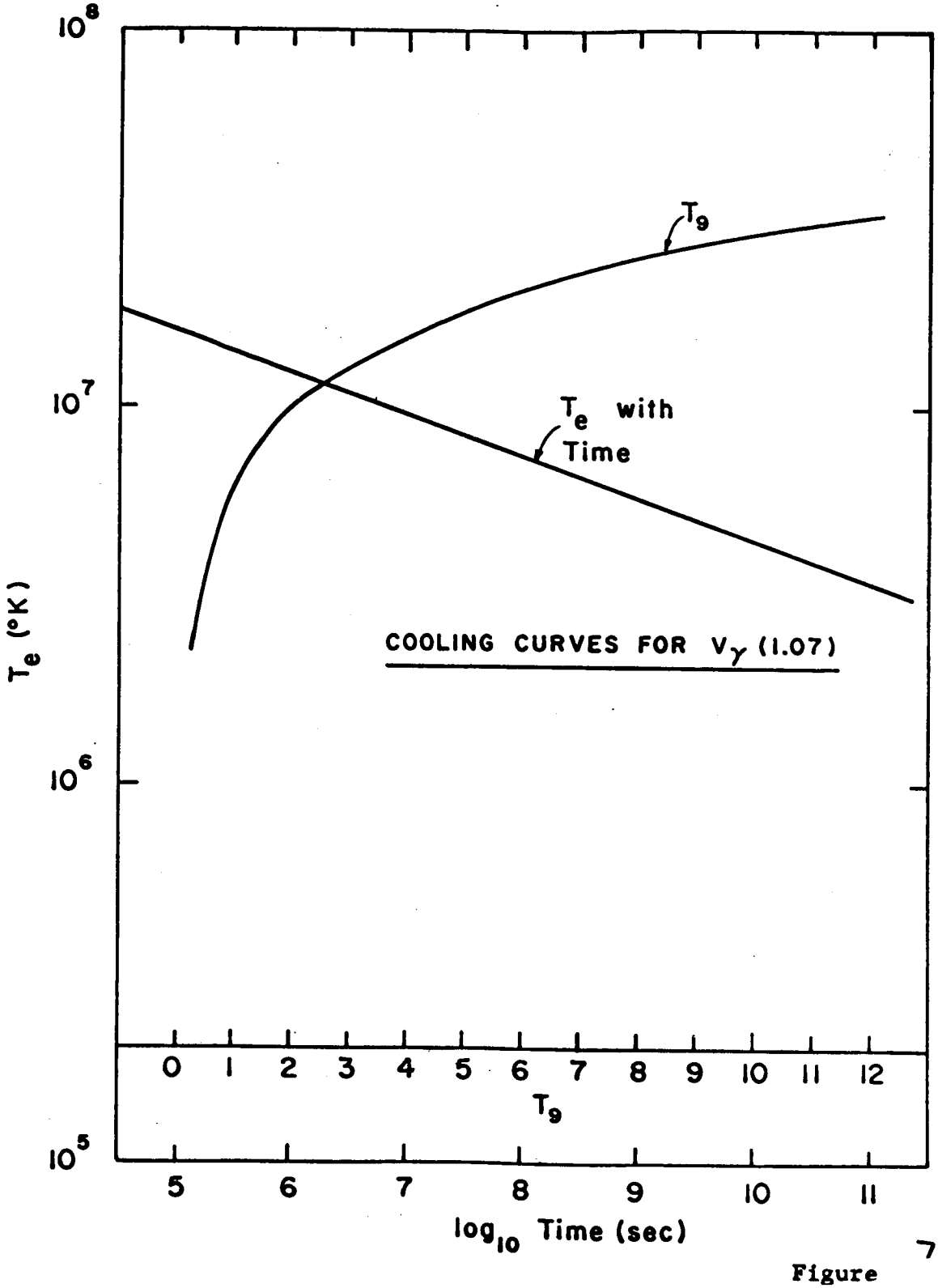
10^8
10^7
10^6
10^5
T_e (°K)
T_9
T_e with Time
COOLING CURVES FOR V_γ (1.07)
0 1 2 3 4 5 6 7 8 9 10 11 12
T_9
5 6 7 8 9 10 11
$\log_{10}$ Time (sec)

Figure 7

listed are the elapsed times τ for which the forms for $T_e(t)$ and $E_{TH}(t)$ of (II-37) and (II-38) become invalid. At times longer than τ the photospheric photon luminosity L_γ exceeds L_{TH} regardless of initial T_9. T_e^o is the photospheric temperature at τ.

Table [redacted]-4

Survey Results

Model	a (ergs^{-3}sec^{-1})	b (ergs^{-3}sec^{-1})	g (deg^{-9}sec^{-1})	T_e^o(^{o}K)	τ(sec)
$V_\gamma(1,8)$	0.92×10^{-155}	1.66×10^{-153}	1.1×10^{-8}	6×10^6	3×10^{10}
$V_\gamma(1.07)$	1.2×10^{-158}	1.53×10^{-153}	1.8×10^{-8}	2.5×10^6	4×10^{11}
$V_\gamma(0.325)$	4.5×10^{-157}	6.3×10^{-153}	3.5×10^{-8}	1×10^6	4×10^{12}
$V_\beta(0.887)$	2.3×10^{-154}	4.1×10^{-151}	1.3×10^{-8}	5×10^6	5×10^{10}
$V_\beta(0.621)$	1.2×10^{-153}	2×10^{-151}	1.9×10^{-8}	4×10^6	5×10^{11}
$V_\beta(0.34)$	4×10^{-153}	2×10^{-152}	2.6×10^{-8}	1.7×10^6	8×10^{11}

3. Vibrational and Thermal Coupling

In the more realistic case in which the neutron star is vibrating but has a non-zero initial temperature the analysis is more difficult. There appears to be no known way to decide how the combined thermal and oscillating URCA losses are divided between damping of the thermal and vibrational energies. An extreme view is to assume that half of the energy loss $L(\xi_o,T_9)$ reduces E_{VIB} and the other half E_{TH}, but for reasonable values of ξ_o and T_9 $L(\xi_o,T_9=0) \gg L(\xi_o=0,T_9)$ so this penalizes E_{TH} and causes E_{VIB} to decrease more slowly than expected. We shall then

take a more conservative view with regard to E_{VIB} and assume that $L(\xi_o, T_9)$ can be broken up into the sum of two terms,

$$L(\xi_o, T_9) \simeq L'(\xi_o) + L'(T_9) , \qquad (36)$$

with

$$\frac{dE_{VIB}}{dt} = - L'(\xi_o) \qquad (37)$$

and

$$\frac{dE_{TH}}{dt} = - L'(T_9) - L_\gamma . \qquad (38)$$

Among the possible choices for $L'(\xi_o)$ and $L'(T_9)$ are

$$L'(\xi_o) = L(\xi_o, T_9) - L(\xi_o=0, T_9) \qquad (39a)$$

and

$$L'(T_9) = L(\xi_o=0, T_9) \qquad (39b)$$

or,

$$L'(T_9) = L(\xi_o, T_9) - L(\xi_o, T_9=0) \qquad (40a)$$

and,

$$L'(\xi_o) = L(\xi_o, T_9=0) . \qquad (40b)$$

Equations (37) and (38) were solved for each of the above schemes. E_{TH} and E_{VIB} changed by no more than 20% after elapsed times of ~ 1000 years from the values that the pure thermal or vibrating cases gave.

Another scheme, suggested by Thorne (private communication) is to take account of the following: for every URCA reaction not

all of the energy is given to the neutrino but some fraction of the total reaction energy is deposited as thermal motion of the final particles. Thus, there is a feedback effect in which some of the vibrational energy is converted into heat. If in analogy to beta decay we assume that roughly half of $L(\xi_o, T_9)$ is so converted, then in the same notation as sections 1 and 2 we have

$$\frac{dE_{VIB}}{dt} = - L_{VIB}$$

and,

$$\frac{dE_{TH}}{dt} = - L_{TH} + \frac{1}{2} L(\xi_o, T_9) - L_\gamma$$

$$= \frac{1}{2} (L_{VIB} - L_{TH}) - L_\gamma .$$

For L_{VIB} initially greater than L_{TH} the thermal energy increases with time until the temperature reaches the point where $L_{TH} \simeq L_{VIB}$. Thereafter, the temperature decreases at such a rate that this equality is maintained. In terms of T_e the effect is to maintain the surface luminosity at higher values than without coupling between vibration and temperature. There is no difference in E_{VIB}.

The effect on T_e is shown in Figure 8 for V_γ (1.07) with $\xi_o(0) = 0.1$ and $T_9(0) = 1$. We see that for times greater than $\sim$ 100 years T_e is enhanced by about 30% compared with no feedback values. This corresponds to an enhancement of the blackbody luminosity of only a factor of two. In order to attain even this enhancement a very large initial amplitude is required.

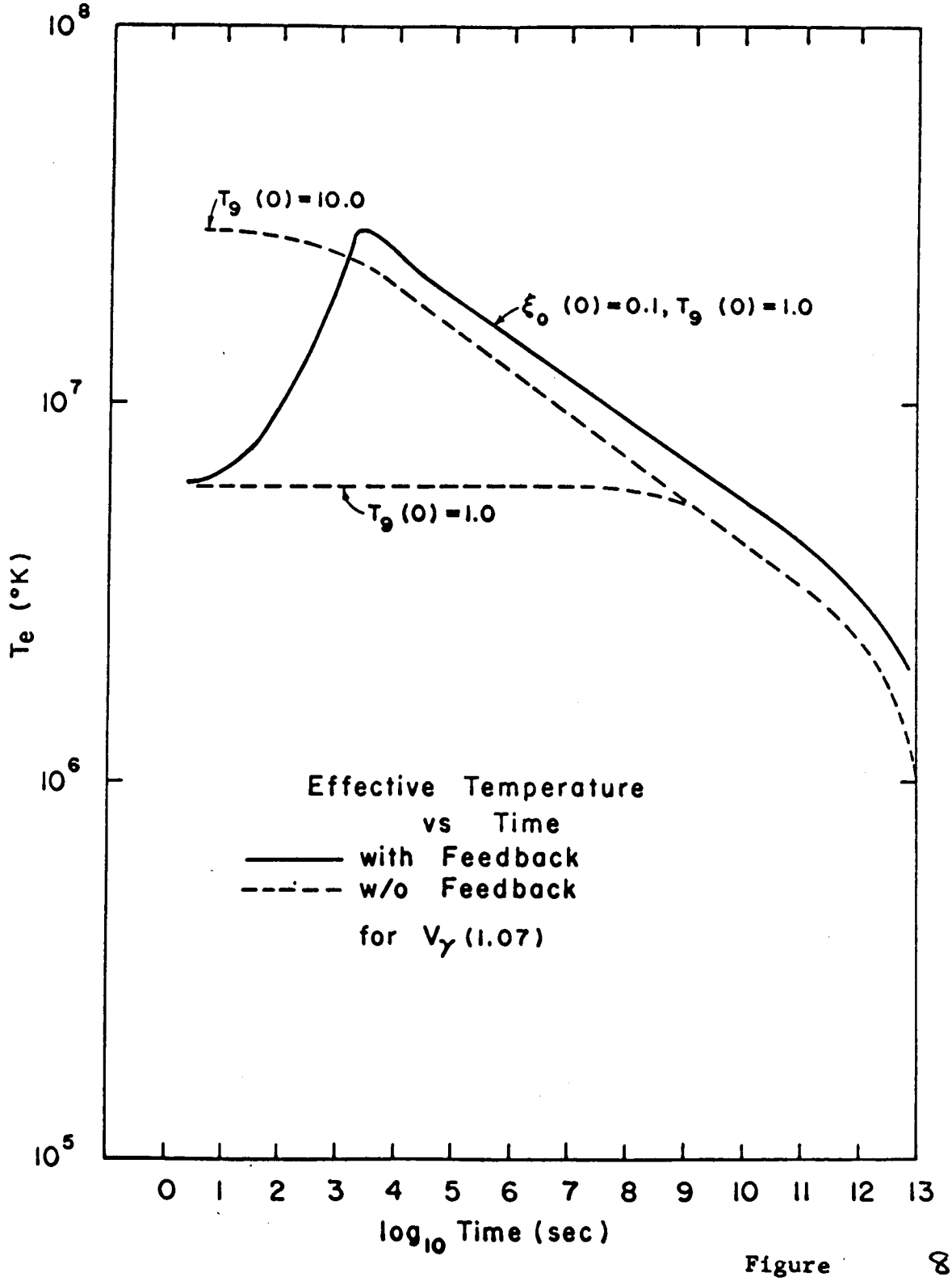
10^8
10^7
10^6
10^5
T_e (°K)
T_9 (0) = 10.0
ξ_0 (0) = 0.1, T_9 (0) = 1.0
T_9 (0) = 1.0
Effective Temperature
vs Time
with Feedback
w/o Feedback
for V_γ (1.07)
0 1 2 3 4 5 6 7 8 9 10 11 12 13
$\log_{10}$ Time (sec)

Figure 8

References

Abramowitz, M., Stegun, I. A. (1964), Handbook of Mathematical Functions, Nat. Bureau of Standards, Applied Mathematics Series No. 55, U. S. Dept. of Commerce.

Adams, J. B., Ruderman, M. A., and Woo, C. H. (1963), Phys. Rev. 129, 1383.

Alexander, A., et al. (1964), Phys. Rev. Letters 13, 484.

Ambartsumyan, V. A. and Saakyan, G. S. (1960), Soviet Astronomy 4, 187.

_____ (1962a), Soviet Astronomy 5, 601.

_____ (1962b), Soviet Astronomy 5, 779.

Arnett, W. D. (1966), Yale University Thesis.

Ajzenberg-Selove, F. (1960), Nuclear Spectroscopy, Part B (Academic Press: N.Y.).

Baade, W. and Zwicky, F. (1938), Ap. J. 88, 411.

Bahcall, J. N. (1962a), Phys. Rev. 126, 1143.

_____ (1964a), Ap. J. 139, 318.

Bahcall, J. N. and Wolf, R. A. (1965a), Ap. J. 142, 1254.

_____ (1965b), Phys. Rev. 140B (B1445).

_____ (1965c), Phys. Rev. 140B (B1452).

Bethe, H. A. (1937), Rev. Mod. Phys. 9, 69.

Bjorken, J. D. and Drell, S. D. (1964), Relativistic Quantum Mechanics (McGraw Hill Book Co.: N.Y.).

Blatt, J. M. and Weisskopf, V. F. (1952), Theoretical Nuclear Physics (J. Wiley and Sons: N.Y.).

Bowyer, S., Byram, E. T., Chubb, T. A., and Friedman, H. (1964a), Nature 201, 1307.

_____ (1964b), Science 146, 912.

_____ (1965), Science 147, 394.

Brown, R. H., Davies, R. D. and Hazzard, C. (1960), Observatory 80, 191.

Buchdahl, H. A. (1959), Phys. Rev. 116, 1027.

B^2FH, Burbidge, E. M., Burbidge, G. R., Fowler, W. A., and Hoyle, F. (1957), Rev. Mod. Phys. 29, 547.

Cameron, A. G. W. (1957a), Can. Jour. Phys. 35, 1021.

_____ (1957b), Can. Jour. Phys. 35, 666.

_____ (1959a), Ap. J. 130, 452.

_____ (1959b), The Approach to Nuclear Statistical Equilibrium, Chalk River (Ontario) Report PD-313.

_____ (1959c), Can. Jour. Phys. 37, 322.

_____ (1959d), Ap. J. 130, 884.

_____ (1963a), Nuclear Astrophysics, Yale University Lecture Notes.

_____ (1965), Nature 205, 787.

Cameron, A. G. W. and Elkin, R. M. (1965), Can. Jour. Phys. 43, 1288.

Cameron, A. G. W., Lazar, N. H., Schmitt, H. W. (1963b), Chapter V. M. in Fast Neutron Physics, Part II, Experiments and Theory (Edited by J. B. Marion and J. L. Fowler: Interscience Publ.: N.Y.).

Chandrasekhar, S. (1939), An Introduction to the Study of Stellar Structure (Dover Publ. Inc.).

_____ (1964a), Phys. Rev. Letters 12, 114.

_____ (1964b), Phys. Rev. Letters 12, 437.

_____ (1964c), Ap. J. 140, 417.

Chiu, H-Y., (1961a), Phys. Rev. 123, 1040.

_____ (1964), Proceedings of the Conference on Stellar Evolution held at the Institute for Space Studies, Goddard Space Flight Center, N.Y. (in preparation).

Chiu, H-Y, and Morrison, P. (1960), Phys. Rev. Letters 5, 573.

Chiu, H-Y, and Salpeter, E. E. (1964), Phys. Rev. Letters 12, 413.

Chiu, H-Y, and Stabler R. C. (1961), Phys. Rev. 122, 1317.

Colgate, S. A., Grasberger, W. H., and White (1961), The Dynamics of a Supernova Explosion, UCRL-6471 of Lawrence Radiation Lab.

_____ (1964), UCRL-7777.

Ellis, D. G. (1965), Phys. Rev. 139, B754.

Feenberg, E., and Trigg, G. (1950), Rev. Mod. Phys. 22, 399.

Fermi, E. (1950), Nuclear Physics, Revised Ed. (University of Chicago Press: Chicago, Ill.).

Feynmann, R. P., Gell-Mann, M. (1958), Phys. Rev. 109, 193.

Finzi, A. (1965), Phys. Rev. 137, B472.

_____ (1966), Phys. Rev. Letters 15, 599.

Fisher, P. C. and Meyerott, A. J. (1964), Ap. J. 139, 123.

Fowler, W. A. and Hoyle, F. (1964), Ap. J. Supplement 91.

Fulton, A. (1962), Elementary Particles and Field Theory, Brandeis Summer Institute, (Benjamin Inc.: N.Y.).

Gamow, G. and Schönberg, M. (1941), Phys. Rev. 59, 539.

Gell-Mann, M. (1961), Phys. Rev. Letters 6, 70.

Giacconi, R., Gursky, H., Paoline, F. R., Rossi, B. B. (1962), Phys. Rev. Letters 9, 439.

_____ (1963), Phys. Rev. Letters 11, 530.

Gilbert, A., Chen, F. S., Cameron, A. G. W. (1965a), Can. Jour. Phys. 43, 1248.

Gilbert, A., Cameron, A. G. W. (1965b), Can. Jour. Phys. 43, 1446.

Gleit, C. E., Tang, C-W., Coryell, C. D. (1963), Beta Decay Transition Probabilities, An Addendum to Nuclear Data Sheets.

Gomes, L. C., Walecka, J. D., Weisskopf, V. F. (1958), Annals of Phys. 3, 241.

Gould, R. J. (1965), Phys. Rev. Letters 15, 577.

Hamada, T. and Salpeter, E. E. (1961), Ap. J. 134, 683.

Harrison, B. K., Wakano, M., Wheeler, J. A. (1958), in Onzieme Conseil de Physique, Solvay, La Structure et l'evolution de l'univers (Brussels: Stoops).

Harrison, E. R. (1966), Ap. J. 142, 1643.

Hayakawa, S., Matsuoka, M., Sugimoto, D. (1966), Space Science Reviews 5, 109.

Hayashi, C., Hoshi, R., Sugimoto, D. (1962), Supplement of Prog. of Theoretical Physics 22.

Hoyle, F. (1946), Mon. Nat. Roy. Astro. Soc. 106, 336.

Hughes, D. H., Magurno, B. A., Brussel, M. K. (1960), BNL-325.

Inman, C., and Ruderman, M. A. (1964), Ap. J. 140, 1025.

_____ (1966), Ap. J. 143, 284.

Källén, G. (1964), Elementary Particle Physics (Addison-Wesley Pub. Co.: Reading, Mass.).

Keill, J. M.D. (MDCCLXIX), An Introduction to the True Astronomy, 6th Ed. (Buckland, et al.: London).

König, L. A., Mattauch, J. H. E., and Wapstra, A. H. (1962), Nuclear Phys. 31, 18.

Landau, L. D. (1932), Phys. Zs. Sowjetunion 1, 285.

Landau, L. D. and Lifshitz, E. M. (1958), Statistical Physics, (Addison-Wesley Pub, Co. Inc.: Reading, Mass.).

Levine, M. (1963), Thesis, Calif. Inst. of Tech.

Levinger, J. S. and Simmons, L. M. (1961), Phys. Rev. 124, 916.

Matinyan, S. and Tajlosani (1962), JETP 14, 1195.

Misner, C. W. and Zapolsky, H. S. (1964), Phys. Rev. Letters 12, 635.

Morrison, P. and Sartori, L. (1966), (submitted to Ap. J.).

Morton, D. C. (1964), Ap. J. 140, 460.

Oppenheimer, J. R. and Volkoff, G. (1939), Phys. Rev. 5, 374.

Peterson, V., and Bahcall, J. N. (1963), Ap. J. 138, 437.

Pontecorvo, B. (1959), JETP 9, 1148.

Preston, M. A. (1962), Physics of the Nucleus (Addison-Wesley Pub. Co., Inc.: Reading, Mass.).

Ritus, V. I. (1962), JETP 14, 915.

Rosenberg, L. (1963), Phys. Rev. 129, 2786.

Rosenfeld, A. H., Barbaro-Galtieri, A., Barkas, W. H., Bastien, P. L., Kirz, J., and Roos, M. (1964), Rev. Mod. Phys. 36, 977 (See also Rev. Mod. Phys. 37, 633 (1965)).

Saakyan, G. S. (1963), Sov. Astron. 7, 60.

Salpeter, E. E. (1961), Ap. J. 134, 669.

Skyrme, T. H. R. (1959), Nuclear Phys. 9, 615.

Tolman, R. C. (1934), Relativity, Thermodynamics and Cosmology (Oxford: Clarendon Press).

_____ (1939), Phys. Rev. 55, 364.

Tooper, R. F. (1964), Ap. J. 140, 434.

Truran, J. W. (1966), Thesis, Yale University (see also, Can. Jour. Phys. 44, 563 (1966)).

Tsuruta, S. (1964), Thesis, Columbia University.

Tsuruta, S., Wright, J. P. and Cameron, A. G. W. (1966), Nature 206, 1137.

Van Hieu, N. and Shabalin, E. (1963), JETP 17, 681.

von Weizsacker, C. F. (1935), Zeit. fur Physik 96, 431.

Wheeler, J. A., Harrison, B. K., Thorne, K. S., Wakano, M. (1965), Gravitational Theory and Gravitational Collapse (University of Chicago Press: Chicago, Ill.).

Woltjer, L. (1964), Ap. J. 140, 1309.

Zeldovich, Ya. B. (1962), JETP 14, 1143.

Zwicky, F. (1938), Ap. J. 88, 522.

_____ (1939), Phys. Rev. 55, 726.

The Rotation of Neutron Stars

by

Sachiko Tsuruta
Smithsonian Astrophysical Observatory
Cambridge, Mass.

and

A.G.W. Cameron
Institute for Space Studies, Goddard Space
Flight Center, NASA, New York, N. Y.

and

Belfer Graduate School of Science, Yeshiva
University, New York, N. Y.

This discussion is prompted by some calculations of Zee and Wheeler concerning energy loss by gravitational radiation from the quadrupole oscillations of a neutron star. Zee and Wheeler[1] estimate a half-life for radiation of the quadrupole vibrational energy of the order of seconds. Meltzer and Thorne[1] have further suggested that if the neutron star is rotating, the rotational flattening will provide a coupling between the purely radial oscillations of the star and the quadrupole oscillations, in which the radial vibrational energy will be drained away through the quadrupole mode with a half-life of about a day even with very moderate rotational flattening. Since energy

storage in radial vibrations has been suggested as a reservoir giving rise to x-rays from the circumstellar regions of neutron stars by synchrotron and bremsstrahlung mechanisms[2], it is of interest to examine the degree to which rotational flattening may be expected to persist after formation of a neutron star in a supernova implosion.

Recent hydrodynamical calculations on the supernova collapse problem by W. D. Arnett (ref. 3 and personal communication) show that the collapse of a star of several solar masses will leave a remnant in the range 0.5 - 2 solar masses, the uncertainty partially representing differences in starting conditions and partially representing the approximations which have so far been made in handling the equation of state during the collapse. We have recently shown that the maximum stable mass of a neutron star probably lies in the range 1 - 2 solar masses.[4,5] It may readily be shown that if a star ~ 10 solar masses is rotating on the verge of rotational instability at the equator while on the main sequence (as is usually observed to be the case), and if it continues to rotate rigidly (owing to magnetic and turbulent viscosity) after evolving to the red giant phase, then the central one solar mass will rotate at much less than the verge of rotational instability after being suddenly

compressed to neutron star dimensions with local conservation of angular momentum. This consideration is strengthened if one includes the effects of angular momentum loss accompanying mass loss in the red giant phase, but it is weakened to the extent that turbulence and magnetic fields may not be able to maintain rigid rotation of the core with the envelope in the red giant phase. For complete generality we discuss the case of a fast-rotating neutron star remnant.

Hoyle, Narlikar, and Wheeler[6] have suggested that the remnant of a supernova explosion will be a rapidly-rotating flattened disk. If the disk is very thin, the implication is that the hydrodynamic time scale of the collapse will be lengthened and the gravitational potential energy release will be less localized. Hence energy transfer by neutrino diffusion will be very inefficient and Arnett's calculations would then suggest that a strong shock wave is not formed to eject the outer envelope. Thus the disk will be very massive, and if there is outward transport of angular momentum and inward transport of mass as a result of turbulence, the central part of the disk is likely to collapse through its Schwarzschild radius, thus precluding the possibility of long-term storage of energy.

It must also be enquired as to whether a very flat disk may not be unstable to deformation into a Jacobi ellipsoid with three unequal axes, thus forming a mass quadrupole. A related question has been investigated by Roberts[7], who found that a rapidly spinning polytrope will deform into a Jacobi ellipsoid if the polytropic index is less than about unity. We have assigned rough effective polytropic indices to our models of neutron stars[5] by comparing the ratio of central to mean densities for our models with those for polytropes. The results are shown in Figure 1.

The two model sequences shown in Figure 1 represent two different expressions for the nuclear interaction potential which enters the equation of state used in the construction of the models. The correct model sequence may well lie between these two. It may be seen that the effective polytropic index of the models in the vicinity of one solar mass is indeed near or below unity. Hence there is a good chance that neutron stars can deform into Jacobi ellipsoids if they are spinning rapidly enough. The resulting mass quadrupole can emit gravitational radiation, and this will slow the spin rate until the ellipsoid relaxes to a spheroid. Chin has shown that the characteristic time for this is of the order of a second.[8]

We now consider the slowing of the spin of a neutron star due to loss of angular momentum when an external magnetic field exerts a torque on mass which is flowing away in the form of a stellar wind. The stellar wind is likely to arise from the heating of a corona around the neutron star by shock waves and hydromagnetic waves generated by the radial vibrations;[2,9] its expansion will be assisted by radiation pressure due to the high surface temperature at the photosphere. The outflowing plasma will tend to pull the magnetic field radially away from the star, and the rotation will tend to wrap the field lines into a spiral. The following calculation of angular momentum loss is similar in principle to one previously carried out by Schatzman[10] in connection with the sun.

We may expect that close to the neutron star the magnetic field causes the corona to corotate with the star, but at large distances the corona rotates slower and the field is wrapped into a tight spiral. The condition of corotation may be expected to break down at roughly that distance r such that the radius of curvature of the field lines is also r. The Coriolis pressure gradient on the gas $2\rho v\omega$ will be approximately equal to the magnetic tension:

$$2\rho v\omega = B^2/4\pi r, \qquad (1)$$

where ρ is the gas density, v is the expansion velocity, ω is the angular velocity of the neutron star, and B is the magnetic field. We take the mass flow f through any spherical surface concentric with the star to be constant:

$$f = 4\pi\rho r^2 v = \text{constant}$$

If we designate physical quantities at the neutron star surface by subscripts zero, then

$$\frac{\rho v}{\rho_o v_o} = \left(\frac{r_o}{r}\right)^2$$

For the radial magnetic field

$$\frac{B}{B_o} = \left(\frac{r_o}{r}\right)^2$$

Hence from equation (1) we obtain

$$r^3 = \frac{B_o^2}{8\pi} \frac{r_o^2}{\rho_o v_o \omega}$$

Let the angular momentum of the neutron star be

$$L = KMr_o^2 \omega$$

where M is the stellar mass.

The rate of loss of angular momentum is

$$\frac{dL}{dt} = - fr^2\omega = KMr_o^2 \frac{d\omega}{dt}$$

The solution to this equation is

$$\omega_i^{2/3} - \omega^{2/3} = bt,$$

where t is the time required for the angular velocity to be reduced from an initial value ω_i to a smaller value ω, and

$$b = \frac{2}{3} \frac{f^{1/3}}{KM} \left[\frac{B_o^2 r_o}{2}\right]^{2/3}$$

Hence the time required to remove the initial angular momentum is

$$t = \frac{3KM\omega_i^{2/3}}{2^{1/3} f^{1/3} B_o^{4/3} r_o^{2/3}} \qquad (2)$$

Let us estimate some reasonable values of the quantities in connection with equation (2). We take as rough values for a neutron star $M = 2 \times 10^{33}$ gm., $r_o = 10^6$ cm., and $K = 0.2$. The Kepler orbital velocity at the surface is $(GM/r_o^3)^{1/2} = 1.15 \times 10^4$, so we take $\omega_i = 10^4$ radians/sec. The initial rotational energy is $\frac{1}{2} KMr_o^2\omega^2 = 2 \times 10^{52}$ ergs. This must be dissipated during the slowing of the spin; let us suppose this energy goes into mass loss in order to get a crude estimate of f. The resulting mass ejection is roughly $Kr_o^3\omega^2/2G \approx 10^{32}$ grams. Hence $f \approx 10^{32}/t$, and equation (2) becomes

$$t \approx 3 \times 10^{31}/B_o^2 \qquad (3)$$

Now Woltjer[11] has estimated that a neutron star is

likely to be formed with a magnetic field B_o of the order of 10^{14} to 10^{16} gauss. If this is correct, then from equation (3) we find that the spin of a neutron star is likely to be eliminated on a time scale of seconds.

Thus we conclude that there is no assurance that rotational flattening of a neutron star will be responsible for eliminating radial vibrational energy by providing a coupling to the quadrupole oscillation mode. Furthermore, it appears that rotational energy storage in a neutron star is most unlikely to provide a reservoir which can lead to energetic radiation processes for very long after the star is formed. More careful detailed considerations of all of these processes are needed.

References

[1] Wheeler, J.A., preprint of chapter for Annual Review of Astronomy and Astrophysics, 4 (1966).

[2] Cameron, A.G.W., Nature, 205, 787 (1965).

[3] Arnett, W.D., Can. J. Phys., in press (1966).

[4] Tsuruta, S., and Cameron, A.G.W., Nature, 207, 364 (1965).

[5] Tsuruta, S., and Cameron, A.G.W., Can. J. Phys., in press (1966).

[6] Hoyle, F., Narlikar, J.V., and Wheeler, J.A., Nature, 203, 914 (1964).

[7] Roberts, P.H., Astrophys. J., 137, 1129 (1963).

[8] Chin, C.W., Phys. Rev., 139, B761 (1965).

[9] Cameron, A.G.W., Nature, 206, 1342 (1965).

[10] Schatzman, E., Ann. d'Astrophys., 25, 18 (1962).

[11] Woltjer, L., Astrophys. J., 140, 1309 (1964).

Figure Caption

Figure 1. Plot of the ratio of the central to the mean proper energy density for the Tsuruta-Cameron neutron star model sequences characterized by the Levinger-Simmons potentials V_β and V_γ. Also given are the ratios of central to mean densities for various polytropic indices n. The shaded region below n = 1 will be unstable to deformation into Jacobi ellipsoids.

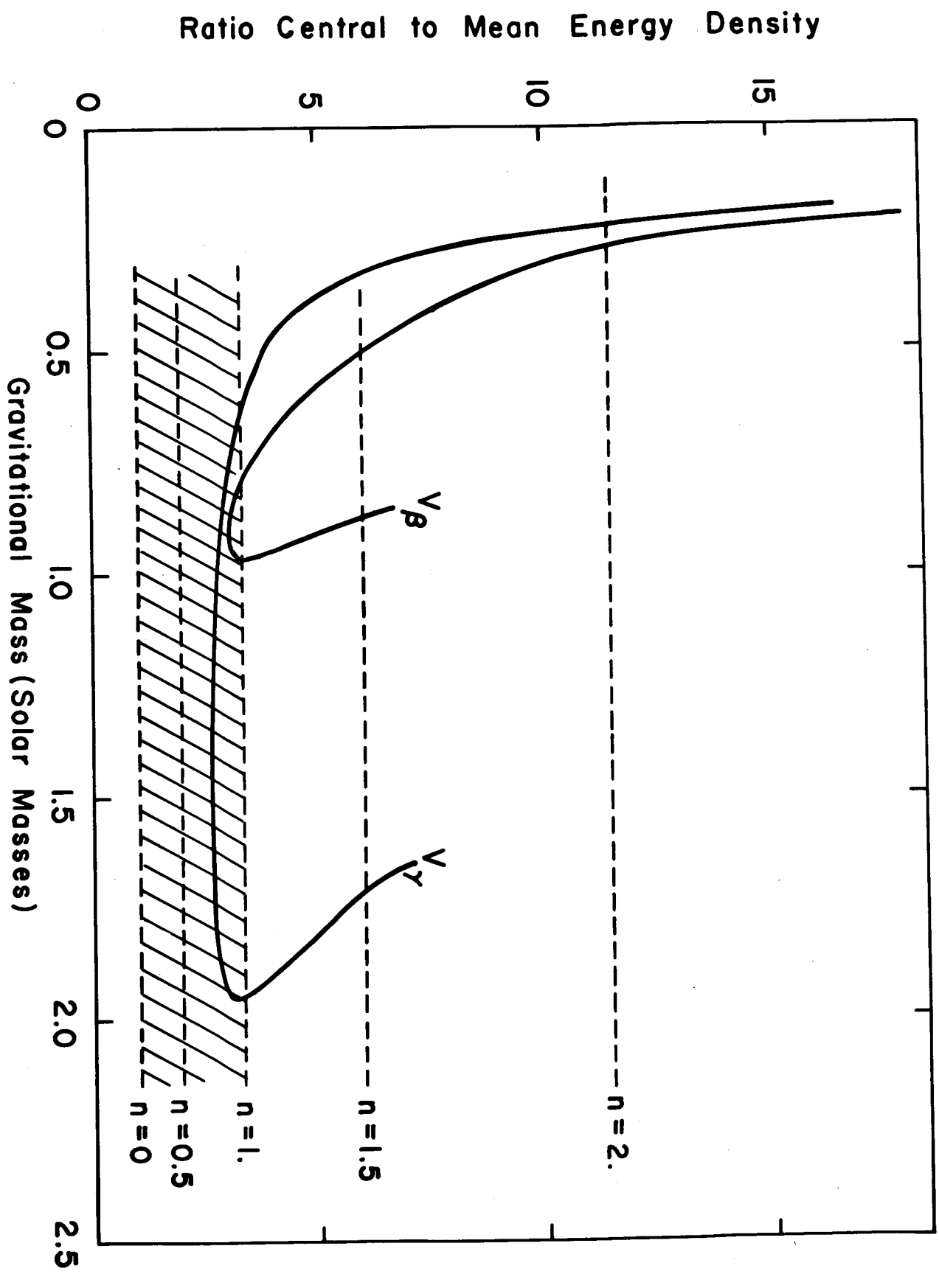
Ratio Central to Mean Energy Density
0
5
10
15
0
0.5
1.0
1.5
2.0
2.5
Gravitational Mass (Solar Masses)
V_β
V_γ
n=0
n=0.5
n=1.
n=1.5
n=2.

Cosmic Ray Production by Vibrating Neutron Stars

I HAVE recently pointed out[1] that a vibrating neutron star, which is expected to be formed as a remnant of the explosion of a Type I supernova, may store up to 10^{51} or 10^{52} ergs as mechanical energy of vibration. This energy may be dissipated by various non-thermal mechanisms. If a magnetic field is embedded in the neutron star, then the vibrations will produce hydromagnetic waves which travel along the field lines, and these will be capable of accelerating charged particles to high energies by transit[2] and stochastic[3] acceleration processes. There is a possibility that the synchrotron radiation of X-rays from the Crab Nebula results from acceleration processes of this type, where the accelerated electrons have been able to diffuse into the outer expanding envelope. Such a diffusion is rendered easier if there should be a corona produced around the neutron star, which expands to form a stellar wind, thus drawing radially outward the magnetic lines of force. Such coronal heating may arise from shocks produced by the vibrations in the atmosphere[1] or by electromagnetic interaction between the magnetic field and the surrounding plasma (Manley, O., private communication).

If electrons can be accelerated to high energies in this way, then it should also be possible to accelerate ions in the vibrating magnetic field. This leads naturally to the hypothesis that vibrating neutron stars may be some of the principal injectors of high energy cosmic rays into the galaxy. Some aspects of this hypothesis are discussed in this communication.

The ions which would be accelerated to cosmic ray energies by vibrating neutron stars should certainly include those ions composing the corona. The corona should have the same composition as the photosphere of the neutron star, and if the corona is hot enough to expand in the form of a stellar wind, then the composition of the photosphere may change with time. Hence one test of this cosmic ray acceleration process is that the composition of the heavy cosmic ray primaries should be consistent with the changing abundances in the neutron star photosphere.

The abundances of cosmic ray primaries with $Z > 2$ are shown in Fig. 1. The abundances are based on measurements by Waddington[4,5] and by the Naval Research Laboratory group[6]. Also shown in Fig. 1 are the relative abundances of the elements with $Z > 2$ in

the Sun and solar system. These abundances are based partly on solar spectroscopy[7], partly on meteorite analysis[7], and partly on rocket measurements of solar cosmic rays[8]. Both distributions are normalized to oxygen, and the abundances have been plotted as a function of mass number by spreading the abundances for each charge number over the principal isotopes of that element. Since the cosmic ray abundances have been strongly affected by spallation processes, this treatment produces a reasonably smooth abundance plot. The solar system abundances have been treated in the same way in order to facilitate comparison.

The differences between these two curves are striking. It appears that the cosmic ray abundance data cannot be obtained by accelerating particles with the relative abundances corresponding to solar composition, with modification by spallation, since there is a relative deficiency of cosmic ray nuclei in the vicinity of silicon and sulphur. On the other hand, it appears possible to account for the cosmic ray distribution if the products of three processes of nucleosynthesis form the material which is accelerated. These processes are:

(1) *Helium-burning.* Helium-burning thermonuclear reactions produce as products carbon-12 and oxygen-16. The relative abundances to be expected for these two products are unknown since these depend on the reduced α-particle width of the 7·12 MeV level of oxygen-16, which has not yet been measured.

(2) *Carbon-burning.* The products of the nuclear reactions of carbon-12 with itself are primarily neon-20, sodium-23 and magnesium-24. The relative abundances of these products which I found for a relatively slow process of carbon-burning[9] are shown near the bottom of Fig. 1. A significant abundance tail at higher mass numbers would be added if the carbon-burning occurred at somewhat higher temperatures, such as those in the supernova shock wave which traversed the outer layers of the supernova and ejected them into space.

(3) *The iron equilibrium peak.* When matter is heated to the vicinity of 3×10^9 °K or higher, the nuclei will rearrange themselves into the vicinity of the iron peak, where the binding energy per nucleon is a maximum. There is a distinct iron peak in the solar abundance data which shows the results of this process.

The heavy cosmic ray primaries appear to be composed principally of products of these three processes of nucleosynthesis, with subsequent modification by spallation. It appears that the nuclei have traversed about 3 or 4 g/cm^2 of material, presumably mostly hydrogen; but it is not clear how much of this matter was in the source and how much in the interstellar medium.

The evolution in the immediate presupernova stage of a star of not very great mass has been investigated by

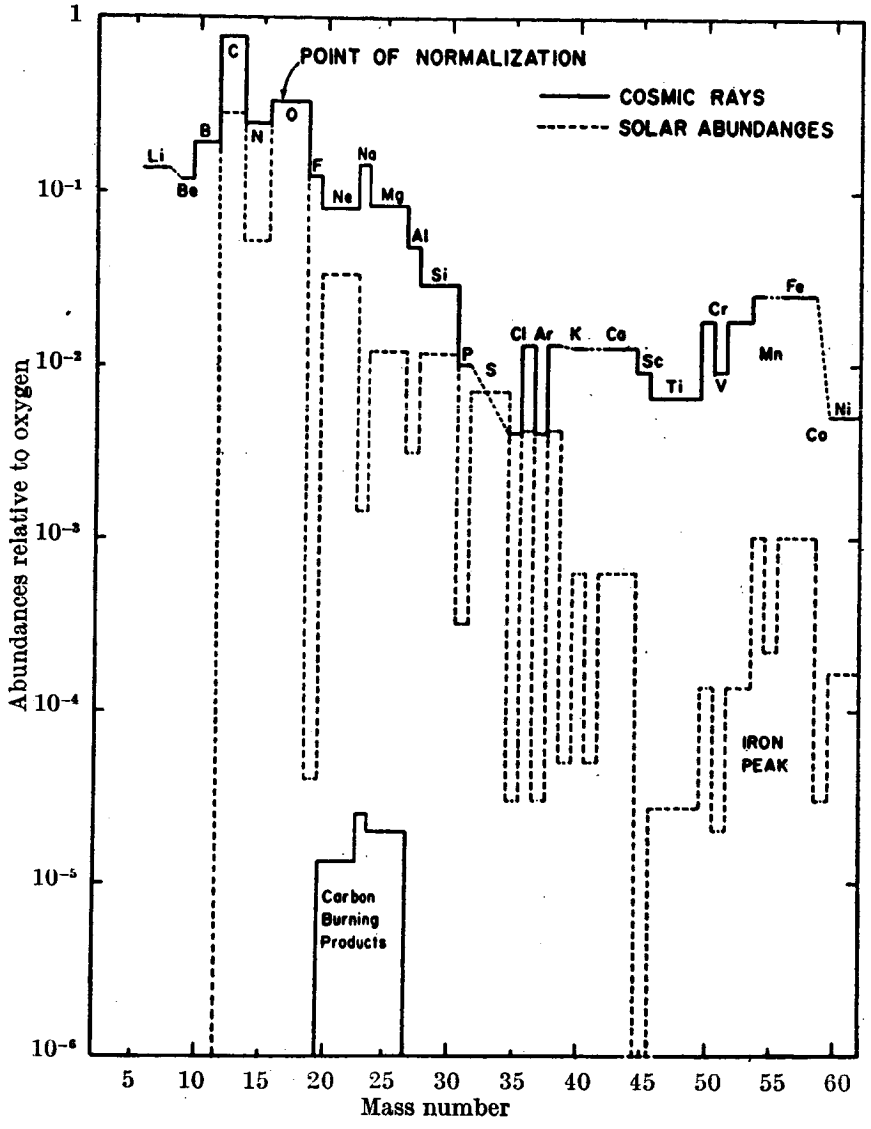

Fig. 1. Abundances in cosmic rays and in the solar system of elements with $Z > 2$. The heavier cosmic ray data are sparse, and some charges are missing. These gaps are bridged by dashed segments connecting the sections of the solid line. Shown near the bottom is the pattern of abundances formed in the carbon-burning process

Chiu[10,11]. Following the process of helium-burning in the core, such stars become highly degenerate at their centres, and the emission of neutrino pairs prevents the temperature from rising rapidly until the mass of the core is near the Chandrasekhar limit, so that contraction becomes very rapid. Then carbon or oxygen burning will commence, but this will lead to an even stronger density concentration towards the centre. The supernova collapse is triggered when the high Fermi level of the electrons at the centre starts converting nuclei into neutrons.

Colgate and White[12] have shown that, during the collapse, a degenerate neutron core will be formed at the centre of the configuration. The material continuing to rain down on this core will produce very high temperatures and cause the formation of a shock wave. The shock

wave will then traverse the outer layers, heating and ejecting them. Not all the material will be ejected to infinity; some of it will fall back and it is this material which we suspect will set up radial oscillations in the neutron star remnant.

In the interior of the neutron star ordinary nuclei will not exist. Near the surface, temperatures of 3×10^9 °K or higher will persist for times of 10^5 sec or longer. Under these conditions the material will be processed into the vicinity of the iron peak[13]. Nearer the surface the temperature will be insufficient for this to occur. Chiu and Salpeter[14] have shown that hydrogen and helium on the surface will be destroyed by inward diffusion, and that carbon will be destroyed to a considerable extent, but still heavier ions to a negligible extent.

Hence we see that even if the layer initially composing the neutron star surface contains only light elements, the final layer is likely to contain carbon, oxygen, carbon-burning products, and the iron peak. The high density at which helium-burning would occur in the surface will favour the formation of carbon relative to oxygen, as is observed in the cosmic rays. Because the temperature will fall rapidly in the envelope beyond the thermal conduction central plateau, the intermediate stage consisting of silicon and sulphur will have only small abundances, and this region will not be built up by nuclear reactions accompanying diffusion.

Thus we see that if the outer layers of the neutron star are peeled off by a stellar wind, the corona is likely to be initially composed of carbon and oxygen, later of the products of carbon-burning, and eventually of iron peak nuclei. Hence the neutron star cosmic ray acceleration hypothesis seems not inconsistent with our knowledge of the structure of a neutron star and of the processes of nucleosynthesis.

The bulk of the cosmic rays consists, not of nuclei with $Z > 2$, but of protons and α-particles. It is evident that under the conditions described here these could not be accelerated in the immediate vicinity of a neutron star. However, in the present picture in which the neutron star has a stellar wind which draws the magnetic field out in the radial direction, hydromagnetic waves may be able to progress from the vicinity of the neutron star out into the expanding ejected envelope. Such a model would seem appropriate for the Crab Nebula, and the hydromagnetic waves would then have an opportunity to accelerate protons and α-particles in the envelope. But protons and α-particles would also be the principal products accelerated in the supernova hydrodynamic hypothesis of Colgate and Johnson[15].

For many years supernova remnants have seemed likely sources for the acceleration of cosmic rays. Arguments toward this end have been based on the obvious

availability of large amounts of energy and of the presence of energetic particles as revealed by synchrotron emission. However, specific models for the acceleration process have been lacking. It is hoped that the present model will serve as a basis for further quantitative investigations.

A. G. W. CAMERON

Institute for Space Studies,
Goddard Space Flight Center,
National Aeronautics and Space Administration,
New York.

[1] Cameron, A. G. W., *Nature*, **205**, 787 (1965).
[2] Shen, C. S., *Astrophys. J.*, **141**, 1091 (1965).
[3] Sturrock, P. A. (in preparation).
[4] Waddington, C. J., in *Progress in Nuclear Physics*, **8**, 3 (Pergamon Press, Oxford, 1960).
[5] Waddington, C. J., *Proc. Intern. Conf. Cosmic Rays and the Earth Storm, J. Phys. Soc.* (Japan), **17**, Supp. A III, 63 (1962).
[6] O'Dell, F. W., Shapiro, M. M., and Stiller, B., *Proc. Intern. Conf. Cosmic Rays and the Earth Storm, J. Phys. Soc.* (Japan), **17**, Supp. A III, 23 (1962).
[7] Cameron, A. G. W., "Nuclear Astrophysics", notes of lectures at Yale University (1963).
[8] Gaustad, J. E., *Astrophys. J.*, **139**, 406 (1964).
[9] Cameron, A. G. W., *Astrophys. J.*, **130**, 429 (1959).
[10] Chiu, H. Y., in *Stellar Evolution*, edit. by Stein, R. F., and Cameron, A. G. W. (Plenum Press, in the press, 1965).
[11] Chiu, H. Y., in the proceedings of the Conference on Nucleosynthesis (to be published).
[12] Colgate, S. A., and White, R. H. (in preparation).
[13] Gilbert, A., Truran, J. W., and Cameron, A. G. W. (in preparation).
[14] Chiu, H. Y., and Salpeter, E. E., *Phys. Rev. Letters*, **12**, 412 (1964).
[15] Colgate, S. A., and Johnson, M. H., *Phys. Rev. Letters*, **5**, 235 (1960).